THE PHYSICS AND CHEMISTRY OF SOLIDS

AN INTERNATIONAL JOURNAL

VOLUME 22 1961

Editor-in-Chief HARVEY BROOKS *Cambridge, Mass.*

Associate Editors
H. B. G. CASIMIR *Eindhoven*
G. J. DIENES *Brookhaven*
JACQUES FRIEDEL *Paris*
E. M. LIFSHITZ *Moscow*

Editorial Advisory Board

U.S.A.
E. N. Adams, Pittsburg
D. Alpert, Illinois
L. Apker, Schenectady
J. Bardeen, Illinois
D. S. Billington, Oak Ridge
R. G. Breckenridge, Cleveland
Leo Brewer, Berkeley, Calif.
E. Burstein, Penn.
J. A. Burton, New Jersey
N. Cabrera, Virginia
G. C. Danielson, Iowa
I. Estermann, Washington, D.C.
J. C. Fisher, Schenectady
F. Herman, Princeton
Conyers Herring, New Jersey
A. R. von Hippel, Cambridge, Mass
J. H. Hollomon, Schenectady
W. V. Houston, Houston
H. B. Huntington, Troy
H. M. James, Purdue
C. Kittel, Berkeley, Calif.
W. Kohn, La Jolla, Calif.
J. A. Krumhansl, Ithaca
A. W. Lawson, Chicago
H. W. Leverenz, Princeton
O. T. Marzke, Pittsburgh
B. T. Matthias, New Jersey
L. R. Maxwell, Silver Spring
Joseph E. Mayer, La Jolla, Calif.
E.W.Montroll, Yorktown Heights N.Y.
David Pines, Illinois
George T. Rado, Washington, D.C.
H. Reiss, Canoga Park, Calif.
J. R. Reitz, Cleveland
A. Rose, Princeton
O. C. Simpson, Argonne
R. Smoluchowski, Princeton
F. H. Spedding, Iowa
D. Turnbull, Schenectady
J. H. Van Vleck, Cambridge, Mass.
B. E. Warren, Cambridge, Mass.
Eugene P. Wigner, Princeton
B. H. Zimm, Schenectady

Canada
R. E. Burgess, Vancouver
D. K. C. MacDonald, Ottawa
W. B. Pearson, Ottawa

United Kingdom
A. Charlesby, Shrivenham, Berks.
W. J. Dunning, Bristol
F. C. Frank, Bristol
H. K. Henisch, Reading
H. Jones, London
J. W. Mitchell, Bristol
A. B. Pippard, Cambridge
M. H. L. Pryce, Bristol
R. A. Smith, Sheffield
K. W. H. Stevens, Nottingham
F. C. Tompkins, London

France
E. F. Bertaut, Grenoble
A. Guinier, Orsay
Louis Néel, Grenoble
Louis Weil, Grenoble

Germany
M. Born, Bad Pyrmont
Ulrich Dehlinger, Stuttgart
R. Hilsch, Göttingen
G. Leibfried, Aachen
E. Mollwo, Erlangen
H. Pick, Stuttgart
H. Welker, Erlangen

Italy
F. G. Fumi, Pavia

Czechoslovakia
J. Tauc, Praha

Japan
Toshinosuke Muto, Tokyo

The Netherlands
A. Michels, Amsterdam
G. W. Rathenau, Amsterdam

Sweden
J. O. Linde, Stockholm
Per-Olov Löwdin, Uppsala

Switzerland
G. Busch, Zurich
P. Scherrer, Zurich

U.S.S.R.
G. S. Zhdanov, Moscow

PERGAMON PRESS NEW YORK · LONDON · PARIS · LOS ANGELES

Vol. 22
1961

THE PHYSICS AND CHEMISTRY OF SOLIDS

AN INTERNATIONAL JOURNAL

VOLUME 22 1961

Editor-in-Chief HARVEY BROOKS *Cambridge, Mass.*

Associate Editors
H. B. G. CASIMIR *Eindhoven*
G. J. DIENES *Brookhaven*
JACQUES FRIEDEL *Paris*
E. M. LIFSHITZ *Moscow*

Editorial Advisory Board

U.S.A.
E. N. Adams, Pittsburg
D. Alpert, Illinois
L. Apker, Schenectady
J. Bardeen, Illinois
D. S. Billington, Oak Ridge
R. G. Breckenridge, Cleveland
Leo Brewer, Berkeley, Calif.
E. Burstein, Penn.
J. A. Burton, New Jersey
N. Cabrera, Virginia
G. C. Danielson, Iowa
I. Estermann, Washington, D.C.
J. C. Fisher, Schenectady
F. Herman, Princeton
Conyers Herring, New Jersey
A. R. von Hippel, Cambridge, Mass
J. H. Hollomon, Schenectady
W. V. Houston, Houston
H. B. Huntington, Troy
H. M. James, Purdue
C. Kittel, Berkeley, Calif.
W. Kohn, La Jolla, Calif.
J. A. Krumhansl, Ithaca
A. W. Lawson, Chicago
H. W. Leverenz, Princeton
O. T. Marzke, Pittsburgh
B. T. Matthias, New Jersey
L. R. Maxwell, Silver Spring
Joseph E. Mayer, La Jolla, Calif.
E.W.Montroll, Yorktown Heights N.Y.
David Pines, Illinois
George T. Rado, Washington, D.C.
H. Reiss, Canoga Park, Calif.
J. R. Reitz, Cleveland
A. Rose, Princeton
O. C. Simpson, Argonne
R. Smoluchowski, Princeton
F. H. Spedding, Iowa
D. Turnbull, Schenectady
J. H. Van Vleck, Cambridge, Mass.
B. E. Warren, Cambridge, Mass.
Eugene P. Wigner, Princeton
B. H. Zimm, Schenectady

Canada
R. E. Burgess, Vancouver
D. K. C. MacDonald, Ottawa
W. B. Pearson, Ottawa

United Kingdom
A. Charlesby, Shrivenham, Berks.
W. J. Dunning, Bristol
F. C. Frank, Bristol
H. K. Henisch, Reading
H. Jones, London
J. W. Mitchell, Bristol
A. B. Pippard, Cambridge
M. H. L. Pryce, Bristol
R. A. Smith, Sheffield
K. W. H. Stevens, Nottingham
F. C. Tompkins, London

France
E. F. Bertaut, Grenoble
A. Guinier, Orsay
Louis Néel, Grenoble
Louis Weil, Grenoble

Germany
M. Born, Bad Pyrmont
Ulrich Dehlinger, Stuttgart
R. Hilsch, Göttingen
G. Leibfried, Aachen
E. Mollwo, Erlangen
H. Pick, Stuttgart
H. Welker, Erlangen

Italy
F. G. Fumi, Pavia

Czechoslovakia
J. Tauc, Praha

Japan
Toshinosuke Muto, Tokyo

The Netherlands
A. Michels, Amsterdam
G. W. Rathenau, Amsterdam

Sweden
J. O. Linde, Stockholm
Per-Olov Löwdin, Uppsala

Switzerland
G. Busch, Zurich
P. Scherrer, Zurich

U.S.S.R.
G. S. Zhdanov, Moscow

PERGAMON PRESS NEW YORK · LONDON · PARIS · LOS ANGELES

Vol. 22
1961

CONTENTS

	Page
A. Rose: Introductory remarks—Photoconductivity in perspective	1
S. M. Ryvkin: Kinetics of impurity photoconductivity	5
B. R. Holeman and C. Hilsum: Photoconductivity in semi-insulating gallium arsenide	19
J. Franks and P. N. Keating: The measurements of defect states in CdS	25
V. S. Vavilov, E. N. Lotkova and A. F. Plotnikov: Photoconductivity and infra-red absorption in silicon irradiated by neutrons	31
Y. E. Pokrovsky and K. J. Svistunova: Recombination processes in silicon doped with Ga, In and Sb	39
V. G. Alexeeva, S. G. Kalashnikov, I. V. Karpova and E. G. Landsberg: Recombination properties of manganese and gold in germanium	45
G. Cheroff, J. Heer and S. Triebwasser: Trapping and recombination measurement by a light modulation technique	51
G. Ascarelli and S. Rodriguez: Recombination of electrons and donors in semiconductors	57
J. J. Hopfield: On the energy dependence of the absorption constant and photoconductivity near a direct band gap	63
K. Kobayashi and T. Tomiki: Temperature dependence of the fundamental absorption tail of KCl and of the absorption due to bromine ions in KCl	73
I. Imai: Experimental study of exciton absorption in PbI_2	81
E. F. Gross and B. V. Novikov: The fine structure of the spectral curves of photoconductivity and luminescence excitation and its correlation to the exciton absorption spectrum	87
F. C. Brown, T. Masumi and H. H. Tippins: Fine structure in the absorption edge of the silver halides	101
R. E. Halsted, M. R. Lorenz and B. Segall: Band edge emission properties of CdTe	109
T. S. Moss: Unusual photoconductive effects	117
K. W. Böer: Field inhomogeneities in CdS single crystals	123
R. Williams: High electric fields in CdS	129
F. Stöckmann: Zur Sättigung von Photoströmen in starken elektrischen Feldern	135
J. Zucker and E. M. Conwell: The recombination of hot carriers in germanium—Experimental	141

Page

E. M. CONWELL and J. ZUCKER: The recombination of hot carriers—Theoretical . . 149

B. K. RIDLEY and T. B. WATKINS: Negative resistance and high electric field capture rates in semiconductors 155

G. S. PICUS: Recombination processes in far infrared photoconductors . . . 159

H. D. ADAMS, W. J. BEYEN and R. L. PETRITZ: Photoconductivity research on Cu–Ge . 167

R. H. BUBE, H. E. MACDONALD and J. BLANC: Photo-Hall effects in photoconductors . 173

A. B. FOWLER: Photo-Hall effect in CdSe sintered photoconductors 181

M. A. LAMPERT: The role of injecting contacts in photoconductors 189

W. RUPPEL: Electron injection and extraction in CdS crystals 199

L. HEIJNE: Contact influence on the photoconductivity of lead oxide 207

I. BROSER, R. BROSER–WARMINSKY, G. KLIPPING, R. RASS and H.-J. SCHULZ: Photoleitung und Lumineszenz von II–VI-Verbindungen bei tiefen Temperaturen. . 213

H. MITSUHASHI: Structures of photoconductivity spectra and related phenomena of cadmium sulphide 223

G. HEILAND: Photoconductivity of zinc oxide as a surface phenomenon 227

R. S. TITLE: Use of paramagnetic resonance to detect optical processes in photoconductors 235

E. H. PUTLEY: Impurity photoconductivity in *N*-type InSb 241

W. ENGELER, H. LEVINSTEIN and C. STANNARD JR.: Photoconductivity in *P*-type indium antimonide with deep acceptor impurities 249

G. RUPPRECHT: The capture of holes in deep lying acceptor levels in gold-doped germanium 255

R. L. WILLIAMS: Carrier lifetimes in *N*-type gold-doped germanium 261

R. S. LEVITT and A. HONIG: Low temperature electron trapping lifetimes and extrinsic photoconductivity in *N*-type silicon doped with shallow impurities 269

A. MANY, M. SIMHONY, S. Z. WEISZ and J. LEVINSON: Studies of photoconductivity in iodine single crystals 285

C. R. KANNEWURF and R. J. CASHMAN: Optical absorption and photoconductivity in germanium selenide 293

H. FEDDERS, M. HUNGER and F. LÜTY: A comprehensive study of a simple photoconductive phosphor 299

H. KANZAKI, T. NINOMIYA and K. KIDO: Photoconductivity in zone-refined KCl . . 309

M. ONUKI and H. OHKURA: Pulse and steady photoconductivities of colored alkali halides 317

C. J. DELBECQ: Hole photoconductivity in KBr crystals containing Br_2^- molecule ions 323

Vol. 2
1961

Page

Y. NAKAI and K. TEEGARDEN: Photoconductivity in RbI and KI 327

G. KUWABARA and K. AOYAGI: Photoconductivity of some alkali halide crystals in the fundamental absorption range 333

J. KOMMANDEUR: Photoconductivity in organic single crystals 339

A. SMITH and D. DUTTON: Photoconductivity and the external photoelectric effect in PbS 351

W. E. SPICER: The production of pairs in semiconductors by low energy electrons . 365

R. E. BURGESS: Some topics in the fluctuations of photo-processes in solids 371

P. T. LANDSBERG and D. A. EVANS: A unified statistical approach to recombination–generation noise in semiconductors 379

L. J. NEURINGER and W. BERNARD: Generation–recombination noise and capture cross-sections in *p*-type gold-doped germanium 385

F. M. KLAASSEN, K. M. VAN VLIET and J. R. FASSETT: Generation–recombination noise in various photoconductive semiconductors 391

D. W. GOODWIN: The noise power spectrum of *p*-type indium antimonide . . . 401

ol. 22
1961

AUTHOR INDEX

Adams, H. D., 167
Alexeeva, V. G., 45
Aoyagi, K., 333
Ascarelli, G., 57

Bernard, W., 385
Beyen, W. J., 167
Blanc, J., 173
Böer, K. W., 123
Broser, I., 213
Broser, R., 213
Brown, F. C., 101
Bube, R. H., 173
Burgess, R. E., 371

Cashman, R. J., 293
Cheroff, G., 51
Conwell, E. M., 141, 149

Delbecq, C. J., 323
Dutton, D., 351

Engeler, W., 249
Evans, D. A., 379

Fassett, J. R., 391
Fedders, H., 299
Fowler, A. B., 181
Franks, J., 25

Goodwin, D. W., 401
Gross, E. F., 87

Halstead, R. E., 109
Heer, J., 51
Heiland, G., 227
Heijne, L., 207
Hilsum, C., 19
Holeman, B. R., 19
Honig, A., 269
Hopfield, J. J., 63
Hunger, M., 299

Imai, I., 81

Kalashnikov, S. G., 45
Kannewurf, C. R., 293
Kanzaki, H., 309
Karpova, I. V., 45
Keating, P. N., 25
Kido, K., 309
Klaassen, F. M., 391
Klipping, G., 213
Kobayashi, K., 73
Kommandeur, J., 339
Kuwabara, G., 333

Lampert, M. A., 189
Landsberg, E. G., 45
Landsberg, P. T., 379
Levinson, J., 285
Levinstein, H., 249
Levitt, R. S., 269
Lorenz, M. R., 109
Lotkova, E. N., 31
Lüty, F., 299

MacDonald, H. E., 173
Many, A., 285
Masumi, T., 101
Mitsuhashi, H., 223
Moss, T. S., 117

Nakai, Y., 327
Neuringer, L. J., 385
Ninomiya, T., 309
Novikov, B. V., 87

Ohkura, H., 317
Onuki, M., 317

Petritz, R. L., 167
Picus, G. S., 159
Plotnikov, A. F., 31
Pokrovsky, Y. E., 39
Putley, E. H., 241

Rass, R., 213
Ridley, B. K., 155
Rodriguez, S., 57
Rose, A., 1
Ruppel, W., 199
Rupprecht, G., 255
Ryvkin, S. M., 5

Schulz, H.-J., 213
Segall, B., 109
Simhony, M., 285
Smith, A., 351
Spicer, W. E., 365
Stannard, C. Jr., 249
Stöckmann, F., 135
Svistunova, K. J., 39

Teegarden, K., 327
Tippins, H. H., 101
Title, R. S., 235
Tomiki, T., 73
Triebwasser, S., 51

Van Vliet, K. M., 391
Vavilov, V. S., 31

Watkins, T. B., 155
Weisz, S. Z., 285
Williams, R., 129
Williams, R. L., 261

Zucker, J., 141, 149

Vol. 2
1961

J. Phys. Chem. Solids Pergamon Press 1961. Vol. 22, pp. 1–4. Printed in Great Britain.

PHOTOCONDUCTIVITY IN PERSPECTIVE

A. ROSE

R.C.A. Laboratories, Radio Corporation of America, Princeton, N.J.

ol. 22
1961

WHILE photoconductivity dates back almost a hundred years, it is only in the last decade that a simple phenomenological framework has been developed and utilized successfully to characterize the properties of photoconductors. The developments of the last decade have, in fact, been successful enough to shift some of the effort from a direct study of photoconductivity to the use of photoconductivity as a tool for the analysis of the defect structure of solids. It has been successful enough also to open the way for more refined considerations of the photoconductive process itself. These ideas can be made more definite by reviewing the state of the art. To do so, I am choosing to resolve the field of photoconductivity along five major dimensions: optical excitation, recombination, contact phenomena, transport properties and noise.

Optical excitation

The density of photo-excited carriers is given by the product of a rate of excitation and a lifetime. The lifetime will be discussed under the heading of recombination. The rate of excitation is given in its simplest form by the rate of incidence of photons. This is not only the simplest concept, it is also the one most commonly observed. When strongly absorbed light ($h\nu >$ band gap) is incident on a solid, it is a safe approximation to regard each incident photon as creating a free electron and a free hole. If the photon energy is many times larger than that of the band gap, as in the use of X-rays, there is good evidence that a single photon gives rise to many free pairs, in particular a number equal to the photon energy divided by an energy several times that of the forbidden gap.

At the other extreme, if the photon energy is appreciably less than the band-gap energy a variety of possibilities may occur: absorption by electrons from one bound state to another without the production of free carriers; absorption by bound electrons to produce free electrons; absorption by bound holes to produce free holes; and, of course, absorption by free carriers to produce "hot" carriers. Very often, but not always, the dominant mode of absorption can be identified from independent knowledge of the solid such as the density of impurity states, conductivity, and location of the Fermi level. I need only mention that there has been frequent evidence of the simultaneous excitation of free electrons and holes from bound states giving rise to simultaneous excitation and quenching effects and to excitation across the forbidden gap with less than band-gap energy.

The most outstanding gap in our knowledge is the computation of optical absorption cross-sections of defect states from first principles. Such computations must await a satisfactory theory for electronic wave functions in deep-lying defect states. Empirical values for these cross-sections have been observed to be in the neighborhood of atomic dimensions.

For photon energies just below the band-gap energy, absorption by excitons is highly probable. About this we will hear more during the Conference. The same is true for the shape and origin of the fundamental absorption edge. Absorption by excitons can still give rise, in negligibly short times, to free pairs by thermal dissociation. At lower temperatures (or higher exciton binding energy) the significant parameters characterizing the life of an exciton are still under study both experimentally and analytically. A number of Russian publications, for example, have argued that optical excitation of CdS via excitons leads to non-linear current versus light curves.

Recent work showing quantum absorption effects of millimeter radiation is particularly significant in bridging the gap between clearly quantum and clearly classical optical processes.

Recombination

The most prolific source of variety amongst photoconductors stems from the array of recombination processes that go to determine the lifetime of a free carrier as well as the response time of the photoconductor. The literature is well studded with analyses valid for many of the special cases encountered in practice. There have been, as well, a number of reasonably generalized analyses of recombination. I do not know of any significant differences amongst the conclusions of these several analyses nor of any significant outstanding puzzles. The choice of analysis is largely a matter of taste. I will confine myself here to a few general remarks.

First, the great variety of effects is in large part a reflection of the extreme sensitivity of recombination rates to minute concentrations of defect states. Almost without exception, the dominant mode of recombination is via radiationless transitions into localized defect states. (There is evidence that under some conditions InSb and GaAs are notable exceptions.) The densities of these states need only exceed the free-carrier density (often as low as $10^6/cm^3$) to have significant effects like removing the degeneracy between electron and hole lifetime, or the degeneracy between lifetime and response time.

The decoupling of life time from response time has clarified a large area of research with insulating photoconductors in which the two time constants showed no obvious relation. Since the life time depends on recombination states and the response time on trapping states, there is meaning to making a clear conceptual separation between the two categories such as has been done by the definition of demarcation levels. Experimentally, the interpretation of response times in terms of trapping-state densities has frequently yielded trap densities ranging from $10^{17}/cm^3$ within a few tenths of a volt from the band edge to about $10^{14}/cm^3$ at about a volt removed from the band edge. In powders, evaporated layers, and polycrystalline samples, the distribution in energy is, as might be expected, a reasonably smooth continuum. In single crystals, high concentrations of states are more likely to be observed at discrete energy levels. However, even here the photoconductive response data are sufficiently incisive to reveal a low continuous background density of states in the presence of a few highly peaked densities.

A number of once puzzling phenomena such as supralinearity, sublinearity, quenching by infrared or by heat, sensitization and negative photoconductivity are now readily understandable in terms of the phenomenological analyses of recombination involving two or more types of recombination centers. Further, the identification of three broad ranges of capture cross-sections: capture by attractive Coulomb centers ($\sim 10^{-12}/cm^2$), capture by neutral centers ($\sim 10^{-15}/cm^2$), and capture by repulsive Coulomb centers ($\sim 10^{-20}/cm^2$) has readily accounted for the enormous range of photosensitivities.

What is still missing in the understanding of recombination is the chemical identification of trapping and recombination states in the higher band-gap materials. Also missing is a detailed description of the capture processes. This is particularly true for the deeper-lying states.

Contact phenomena

Much of the early work on photoconductors of the diamond and alkali halide type was done with blocking contacts—that is, contacts that supplied a negligible flow of carriers to the volume of the sample. These materials acted like simple vacuum photo-cells in that a single photon gave rise at most to a single electron charge in the measuring circuit.

The recent work with sensitive photoconductors has, on the other hand, emphasized the need for ohmic contacts, that is, contacts that can supply more carriers to the sample than are needed to support the volume currents. The concept is that of a reservoir of carriers at the contact continuously trying to enter the volume of the sample, and, for the most part, continuously rejected. Such contacts are needed to observe Ohm's law currents and are needed also to permit many electrons to pass through the photoconductor for each absorbed photon, and hence to observe high photoconductive gain.

Once having ohmic contacts and the attendant concept of a reservoir of carriers, one naturally inquires what keeps the reservoir from injecting a significant excess of carriers into the volume of the photoconductor. The answer or answers are not at all obvious. In fact, it *is* true that the reservoir *does* inject a significant density of excess carriers into the photoconductor only at a voltage

sufficiently high that the density of space-charge-injected carriers exceeds the density of the volume-excited carriers already present. The analysis of the interplay of these ohmic and space-charge-limited currents has led to two far reaching conclusions. On the technological side, a simple expression for the maximum gain–bandwidth product achievable with any photoconductor was developed: Gain $\times$ bandwidth $= M \times$ (dielectric relaxation time)$^{-1}$.

A key factor (M) in this expression is the ratio of recombination states to trapping states in the neighborhood of the steady-state Fermi level. For this reason, the expression becomes a useful tool for the determination of the densities and character of states as a function of energy depth from the band edge. Finally, the expression depends upon a clear distinction between life time and response time, trapping centers and recombination centers, ohmic and space-charge-limited current flow, and thermal equilibrium and steady-state Fermi levels. In this sense, the expression helps to clarify and to anchor the significance of these several concepts.

The state of the art is characterized here, again, by a firm grasp of the phenomenological role of contacts but only a loose understanding of the physics and chemistry that takes place when two dissimilar materials are joined. We know that high work function materials usually make blocking contacts to n-type photoconductors and low work function materials usually make ohmic contact. This is not always the case and certainly we have no confidence in deriving quantitatively the contact properties from the work functions of the two materials. As long as the separate work functions are determined in part by surface dipole layers that can change on contact, we cannot expect a close correlation between work functions and contact properties.

There is further reason to expect hazardous results from the contact of two dissimilar materials. We know, for example, that chlorine incorporated substitutionally in CdS is an excellent donor. Yet, if chlorine could be incorporated interstitially it should be an acceptor close to, or inside of, the valence band. Indium incorporated substitutionally in germanium is an acceptor. Yet, from the relative work functions of indium and germanium, indium should tend to make good ohmic contact to n-type germanium. In both these examples, and similar ones that could be cited, the electrical character of an impurity depends strongly on its immediate surround. It would seem that when a foreign atom is brought to the surface of a material, there would be a high degree of ambiguity between its substitutional and interstitial character. In fact, one would expect that there would be a continuous gamut of sites depending on the local atomic geometry of the surface.

Finally, the knowledge of surface states on high band-gap materials is all but absent. We need to know their density, their distribution in energy, their chemical character and their rate of fall-off as one penetrates the surface.

Transport

The low-field behavior of photocurrents in solids is reasonable well understood. To a good approximation, photo-carriers can be treated as if they were thermally generated carriers subject to the same types of scattering by the lattice, by charged and neutral impurities, and by the opposite sign of carrier.

What is very poorly understood is the high-field behavior of carriers. Here I am thinking particularly of the criterion for breakdown by impact ionization and the dependence of mobility on electric field in the pre-breakdown region. It is a strange inversion of reasonable expectations to find what little understanding of impact ionization there exists coming from very high band-gap ionic solids on the one hand and very low band-gap semi-conductors on the other hand. The intermediate range of band gaps covering some 2–4 volts and including such well-known materials as CdS, ZnS, ZnO, CdSe and other metal sulphides and oxides, have been all but ignored as materials for exploring the quantitative aspects of impact ionization. It is a strange inversion because these materials are clearly better suited to experiment than the semi-conductors or ionic solids. They are insulators at room temperature, their carrier densities can be reversibly varied by photoexcitation, the art of making ohmic or blocking contacts is reasonably well developed and some of them have a built-in monitor for detection of minute fractions of high energy carriers in the form of electroluminescence. Part of the experimental problem stems from the difficulty of distinguishing impact ionization currents from space-charge-

limited currents, double-injection currents and field emission currents.

On the analytic side, in spite of the many discussions of high-field behavior, we still do not know the all-important mean-free-paths for energy loss by energetic carriers, nor do we know the form of the momentum and energy distribution of carriers near breakdown field strengths. Admittedly, these are difficult problems.

Noise

A proportionately small fraction of the workers in the field of photoconductivity have concerned themselves with noise analyses and measurements. This is perhaps unfortunate since noise measurement can be a subtle monitor of internal electronic processes. The attainment of simple–shot noise currents in a photoconductor, for example, is one of the most sensitive tests for an ohmic contact.

It would be helpful, it seems to me, in spreading the popularity of noise, if the analysts would lean over backwards to make their concepts and conclusions understandable to the many experimentalists to whom the mathematical language of noise analysis is not familiar.

One of the simplest questions to ask is whether a photoconductor is a substantially noiseless transducer of photon currents into photocurrents. A vacuum photomultiplier, for example, is such a substantially noiseless transducer. This means that the ratio of average current to root-mean-square fluctuation in current (the signal to noise ratio) at the output is closely equal to the same ratio applied to the fraction of incident photons giving rise to photoemission. The same statement can be made for photoconductors. The departure from a noiseless transducer should not exceed a factor of two providing noiseless (that is, ohmic) contacts are used and the photoconductor is homogeneous. If the response time of the photoconductor is equal to the lifetime of free carriers, the signal to noise ratio of the photocurrent reproduces that of the photon current up to a frequency given by $f = (2\pi \times \text{lifetime})^{-1}$. If, on the other hand, the presence of shallow traps causes the response time of the photoconductor to exceed the lifetime of a free carrier, the upper frequency limit is reduced to $f = (2\pi \times \text{response time})^{-1}$. It is as if a low-pass filter had been inserted in the system. The low frequency part of the noise spectrum is substantially unaffected by the introduction of traps. The high frequency tail of the spectrum, that is, beyond the frequency set by the response time of the photoconductor, now contains components reflecting the thermal exchange of carriers between conduction band and traps. Unfortunately, these high frequency components are not a particularly sensitive measure of either the energy depth or the density of traps. They reflect only the time required for an electron to be captured into a set of trapping states, and thereby are a measure of the product of the trap density and their capture cross-section. A series of measurements over a range of locations of the steady-state Fermi level can show evidence of the Fermi level sweeping through a high local density of traps.

Evidence that trapping has only a small effect on noise comes for example from the photoconductive television camera tube known as the Vidicon. Here the ratio of trapped to free carriers is of the order of 10^8. Yet the signal to noise in the transmitted picture is close to that to be expected from the stream of photons incident on the tube.

The outstanding problems I have cited in this brief review appear not to be peculiar to photoconductivity. They concern the intimate physics and chemistry of defect states and of the contacts between dissimilar materials; they concern also the high-field behavior of carriers and the transport properties of excitons. These are problems whose solutions will be derived not from photoconductivity alone but from many fields of study.

Vol. 22
1961

J. Phys. Chem. Solids Pergamon Press 1961. Vol. 22, pp. 5–17. Printed in Great Britain.

KINETICS OF IMPURITY PHOTOCONDUCTIVITY

S. M. RYVKIN

Ioffe Physico-Technical Institute, Academy of Sciences of the USSR, Leningrad, USSR

IN RECENT years, problems associated with impurity photoconductivity have acquired an increasing interest because of the possibility of applying this phenomenon for the investigation of local electronic states in the forbidden band of semiconductors, and particularly of their interaction with the exciting radiation. The investigation of the properties of local levels is also of importance for the elucidation of the mechanism of intrinsic photoconductivity, since the centers yielding carriers of the extrinsic photoconductivity, when excited in the extrinsic region, will act as trapping centers responsible for the recombination of non-equilibrium carriers in the intrinsic excitation region. Besides, the quantities characterizing the properties of these local centers, in particular the cross-sections for the trapping of free carriers in the centers, are essentially the same for the two cases of extrinsic and intrinsic excitation. Below are presented the results of the investigation of the impurity photoconductivity kinetics and of the impurity photoelectromagnetic effect carried out recently at our Laboratory.

1. KINETICS OF IMPURITY PHOTOCONDUCTIVITY FOR THE CASE OF CARRIER EXCITATION FOR LOCAL LEVELS OF ONE TYPE[1]

Consider a semiconductor having local levels of one type only with density M in the forbidden band. Let the concentration of electrons on these levels be m_0 in the dark. Suppose, further, that the M-levels are located in the upper half of the band and hence are connected with the conduction band mainly through thermal transitions.* Now illuminating such a semiconductor with monochromatic light of a wavelength providing only for the transition of electrons from the local M-levels to the conduction band will result in the generation of unipolar extrinsic photoconductivity.† The diagram of electronic transitions in this case will be as shown in Fig. 1, where transition I corresponds to radiation-induced generation of carriers

* The dark concentration in the conduction band may be determined not only by the thermal transitions between the M-levels and the C-band, but also, for example, by the presence of donors which are completely ionized in the temperature region discussed and hence are not considered here. It may be noted that the case of local levels located in the lower half of the forbidden band may be treated in a similar way.

† It should be stressed that the extrinsic excitation may also result in bipolar non-equilibrium conduction because of:

(a) additional thermal ejection from the band into a level providing optical transitions into another band and

(b) double optical transitions.

The criteria of unipolarity for these two cases may be derived from the obvious condition $\Delta n/\Delta p \gg 1$.

If additional thermal ejection takes place, the unipolarity condition acquires the following form:

$$m_0^2/MP_{VM} \gg 1. \tag{1.2}$$

Thus, the following requirements should be met to obtain unipolar conduction.

(1) The levels should lie as far away as possible from the band thermal transitions from which result bipolar conduction (i.e. P_{VM} should be small).

(2) The occupancy of the levels should be as high as possible (i.e. $m_0/M \approx 1$).

It may be shown that in the case of double optical excitation the actual degree of unipolarity at low excitation levels will be determined by the condition:

$$\Delta n/\Delta p = \frac{q_1\gamma_1 m_0^2}{q_2\gamma_2(M-m_0)^2} \tag{1.3}$$

where q_1 and q_2 are the photon capture cross-sections for optical transitions I and II, respectively, and γ_1 and γ_2 are the recombination coefficients for the corresponding backward transitions.

Thus, in this particular case, the condition of unipolarity will be:

$$\frac{q_1\gamma_2 m_0^2}{q_2\gamma_1(M-m_0)^2} \gg 1. \tag{1.4}$$

from the M-levels, transition II accounts for recombination, and transition III represents thermal ejection into the conduction band.

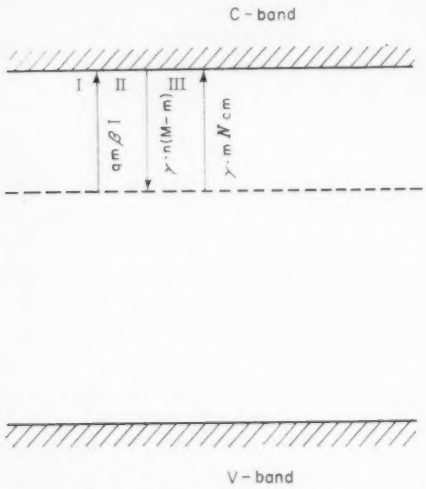

FIG. 1. Diagram of transitions.

The kinetic equation corresponding to the diagram of transitions of Fig. 1 may be written as follows:

$$\frac{dn}{dt} = mq\beta J - \gamma n(M-m) + \gamma m N_{CM}. \quad (1.1)$$

q—cross-section for photon capture by electron at M-level;
$m = m_0 - \Delta m$—electron concentration at M-level;
β—quantum efficiency assumed below to be unity;
J—light intensity;
γ—recombination coefficient;
$n = n_0 + \Delta n$—electron concentration in conduction band;
n_0—dark concentration of electrons in conduction band;
$N_{CM} = N_C \exp(-\Delta E_M/kT)$—effective density of states in C-band reduced to level of M-centers[2];
N_C—density of states in conduction band;
ΔE_M—distance of impurity level from bottom of conduction band;
Δm, Δn—changes of electron concentration at M-levels and C-band, respectively, on illumination with light intensity of J.

Equation (1.1) should be supplemented with the condition of neutrality, which in the case considered takes the following form:

$$\Delta n = \Delta m. \quad (1.5)$$

Using the condition of neutrality (1.5), expression (1.1) may be written down as follows:

$$d\Delta n/dt = (m_0 - \Delta n)qJ - \gamma \Delta n(N_{CM} + M - m_0 + n_0 + \Delta n). \quad (1.6)$$

Equation (1.6) shows that the intensity of generation decreases in time with the increasing non-equilibrium concentration as the local centers become exhausted. This is a distinctive feature of the extrinsic photoconductivity as compared with the intrinsic photoconduction for which the probability of generation does not change at illumination intensities realizable in practice.

Let us write equation (1.6) in the following form*

$$\frac{d\Delta n}{dt} = m_0 qJ - \frac{\Delta n}{\tau_{\text{mom}}} \quad (1.7)$$

where

$$\tau_{\text{mom}} = [\gamma(M - m_0 + N_{CM} + n_0 + \Delta n) + qJ]^{-1} \quad (1.8)$$

may be regarded as the momentary relaxation time.[2]†

The values of equilibrium concentrations n_0 and m_0 in (1.8) are related to one another by $m_0 = M/(N_{CM}/n_0 + 1)$, and hence τ_{mom} may be also written as:

$$\tau_{\text{mom}} = \left\{\gamma\left[(n_0 + N_{CM})\left(1 + \frac{MN_{CM}}{(n_0 + N_{CM})^2}\right) + \Delta n\right] + qJ\right\}^{-1}. \quad (1.9)$$

* The corresponding expressions for decay on removal of illumination may be obtained from (1.7) and (1.8) by setting $J = 0$.

† It should be noted that in contrast to the case of intrinsic excitation where τ_{mom} corresponds to the lifetime of non-equilibrium carriers and is determined by recombination processes, in the case of extrinsic excitation this quantity depends also upon the processes of generation (term qJ).

Vol. 2
1961

The momentary relaxation time depends in a complicated way upon light intensity and time through terms $\gamma\Delta n$ and qJ. It should be stressed, however, that the difference between the reciprocals of τ_{mom} for the cases of rise and decay, taken at equal concentrations Δn, will always be qJ. Thus the rise of the extrinsic photoconductivity will always take place faster than its decay, and this symmetry will be the more pronounced the higher the light intensity.*

In the case of the excitation of a semiconductor by rectangular light pulses, the solutions of equation (1.6) for rise (Δn_r) upon illumination and decay (Δn_d) on removal of light will be:†

$$\Delta n_r = Ath(\gamma At+B)-C, \tag{1.10}$$

where

$$A = \sqrt{(c^2+mqJ/\gamma)}; \quad B = \tfrac{1}{2}\ln(1+2C/\Delta n_{\text{st}});$$

$$C = \tfrac{1}{2}(N_{CM}+M-m_0+n_0+qJ/\gamma);$$

and

$$\Delta n_d = \frac{\Delta n_{\text{st}}\exp(-t/\tau_d)}{1+\gamma\Delta n_{\text{st}}\tau_p[1-\exp(-t/\tau_d)]}, \tag{1.11}$$

where

$$\tau_d = [\gamma(N_{CM}+M-m_0+n_0)]^{-1}.$$

The steady-state concentration of non-equilibrium carriers is

$$\Delta n_{\text{st}} = \tfrac{1}{2}(N_{CM}+M+n_0-m_0+qJ/\gamma) \times\left\{\sqrt{\left[1+\frac{4m_0qJ}{\gamma(N_{CM}+M-m_0+n_0+qJ/\gamma)^2}\right]}-1\right\} \tag{1.12}$$

Consider the dependence of the steady-state concentration on light intensity. Taking into account that both at low and high light intensities

$$\frac{4m_0qJ}{\gamma(N_{CM}+M-m_0+n_0+qJ/\gamma)^2} \ll 1,$$

we obtain that at low intensities:

$$\Delta n_{\text{st}} = \frac{m_0qJ}{\gamma(N_{CM}+M-m_0+n_0)}, \tag{1.13}$$

whereas at high light intensities

$$\Delta n_{\text{st}} \simeq m_0. \tag{1.14}$$

Thus, the photocurrent versus light curve of the extrinsic photoconduction at low light levels will be linear, achieving saturation at high light levels. The latter may be readily explained by the fact that at sufficiently high light intensities practically all electrons can be excited by light into the C-band from the impurity centers. Such a saturation of the photocurrent versus light characteristic caused by exhaustion of the impurity centers represents also a distinctive feature of the extrinsic photoconductivity as compared with the intrinsic effect, where it does not appear at excitation intensities normally in use.

By way of an illustration, Fig. 2 shows calculated photocurrent versus light curves characterizing extrinsic photoconduction, which are plotted on a

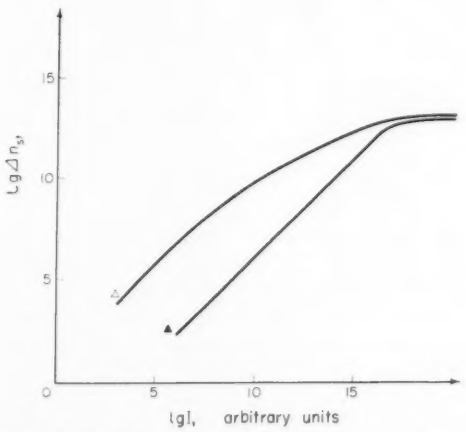

FIG. 2. Dependence of steady-state concentration on light intensity. △ $T = 77°$K ▲ $T = 190°$K. Curves in Figs. 2, 3, and 4 drawn for $\triangle E_M = 0{\cdot}2$ eV; $M = 10^{12}$ cm^{-3}; $g/\gamma = 5\times10^{-4}$ sec/cm; $M-m_0 = n_0$.

* Asymmetry in the nonlinear case is observed also in intrinsic photoconduction. However, in impurity photoconductivity it is determined by kinetics of excitation rather than by recombination.

† It should be noted that the magnitude of the extrinsic photoconductivity $\Delta\sigma$ may in our case be directly related to the concentration of non-equilibrium carriers as $\Delta\sigma = e\mu_e\Delta n$ where e and μ_e are the charge and mobility of an electron, respectively. Therefore we will use in our treatment below the concentration of non-equilibrium carriers Δn.

log–log scale and drawn for a particular case for two temperatures.

In view of the evident complexity of the above formulae depicting the relaxation of the extrinsic photoconductivity in a general case, it may be expedient to consider some particular cases revealing the peculiarities of the impurity photoconductivity kinetics.

Equation (1.6) may be linearized, and its solutions will be exponentials if

$$N_{CM}+M-m_0+n_0 \gg \Delta n, \qquad (1.15)$$

corresponding to a constant τ_{mom} [(cf. (1.7) and (1.8)].

Condition (1.15) is met in the following two particular cases.

(1) Low excitation level: $n \gg \Delta n$, corresponding to low light intensities J.

$$\tau_r = [\gamma(N_{CM}+M+n_0)+Jq]^{-1} \qquad (1.18)$$

$$\tau_d = [\gamma(N_{CM}+M+n_0)]^{-1} \qquad (1.19)$$

As seen from formulae (1.16) through (1.19), the time constant for rise τ_r is always smaller than the decay time constant τ_d, resulting in an asymmetry of the relaxation curves which becomes particularly pronounced at high light levels. In the case of low illumination, where the condition $\gamma(N_{CM}+M-m_0+n_0) \gg qJ$ is met, the time constants for rise and decay do not differ appreciably.

The above mentioned peculiarities of the kinetics of the impurity photoconductivity are clearly revealed in Fig. 3 showing relaxation curves for the cases of high and low light levels.

Relations (1.16) and (1.17), or (1.18) and (1.19),

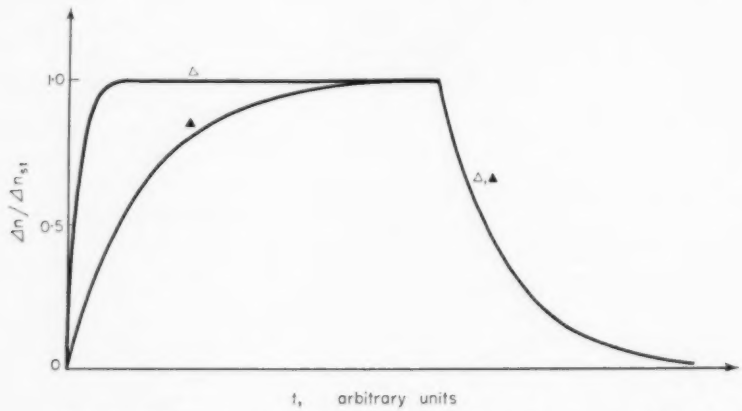

FIG. 3. Photoconductivity relaxation curves for the case of excitation by rectangular light pulses.
$T = 77°\text{K}$. $J_\triangle/J_\blacktriangle = 150$.

(2) Low occupancy of the local centers: $M \gg m_0 \gg \Delta n$. In this case, condition (1.15) will be satisfied at any light intensities.

Under these circumstances the expressions for τ_r and τ_d derived for the cases of low excitation levels and low occupancies of the local centers, respectively, will be as follows:

$$\tau_r = [\gamma(N_{CM}+M-m_0+n_0)+qJ]^{-1} \qquad (1.16)$$

$$\tau_d = [\gamma(N_{CM}+M-m_0+n_0)]^{-1} \qquad (1.17)$$

derived above permit one to determine certain parameters of the impurity centers; in particular, the cross-section for photon capture by an electron on an impurity center q, and the recombination constant γ.

Indeed, by determining the decay time constant and knowing the quantities n_0, $M-m_0$ and N_{CM}, we obtain γ from formula (1.17) or (1.19). On the other hand, the difference between the reciprocals of the rise and decay time constants is related with light intensity through a simple formula:

Vol. 2
1961

$$\frac{1}{\tau_r} - \frac{1}{\tau_d} = qJ. \tag{1.20}$$

Hence the dependence of this difference upon light intensity will represent a straight line with a slope determining q. As mentioned above, in the general case the difference between the reciprocals of τ_{mom} for rise and decay taken at the same concentration Δn will always be qJ. This is illustrated by the curves in Fig. 4, where are graphically

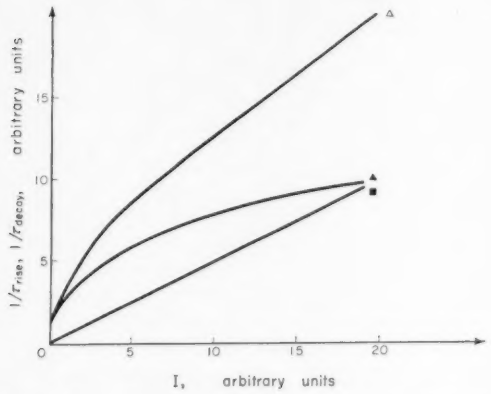

FIG. 4. Dependence of relaxation time constants on light intensity ($\triangle n = \triangle n_{st}$). $T = 77°$K. $\triangle$ $1/\tau_d$. $\blacktriangle$ $1/\tau_r$). $\blacksquare = 1/\tau_r - 1/\tau_d$

shown the calculated relationships between the reciprocals of the momentary relaxation times for rise and decay and light intensity, as well as the dependence of the difference between these quantities upon light intensity representing a straight line from the slope of which q may be found.

By using the above feature of the difference between the reciprocals of τ_{mom}, one may determine the cross-section for photon capture by an electron on an impurity center for the general case. Indeed, the relation

$$\frac{1}{\tau^r_{\text{mom}}} - \frac{1}{\tau^d_{\text{mom}}} = qJ, \tag{1.21}$$

where τ^r_{mom} and τ^d_{mom} are the momentary relaxation times for rise and decay, respectively, will always hold for equal Δn on the curve of rise and decay.

On the other hand, using relationships

$$\tau^r_{\text{mom}} = \frac{\Delta n}{m_0 qJ - d\Delta n/dt} \tag{1.22}$$

$$\tau^d_{\text{mom}} = -\frac{\Delta n}{d\Delta n/dt} \tag{1.23}$$

for equal Δn yields:

$$\frac{1}{\tau^r_{\text{mom}}} - \frac{1}{\tau^d_{\text{mom}}} = \frac{1}{\Delta n}\left[m_0 qJ - \left(\frac{d\Delta n}{dt}\right)_r + \left(\frac{d\Delta n}{dt}\right)_d\right].$$

Taking into account that $m_0 qJ = (d\Delta n/dt)^{\text{or}}_r$ represents essentially the original slope of the rise curve, we obtain finally:

$$q = \frac{1}{J\Delta n'}\left[\left(\frac{d\Delta n}{dt}\right)^{\text{or}}_r - \left(\frac{d\Delta n}{dt}\right)^{\Delta n'}_r + \left(\frac{d\Delta n}{dt}\right)^{\Delta n'}_d\right], \tag{1.24}$$

where $\Delta n'$ is the concentration of non-equilibrium carriers at those points on the relaxation curves for which the calculation is being carried out.

Thus the problem of finding q becomes reduced to the determination of three slopes (Fig. 5): an original slope on the rise curve α_1 and two slopes α_2 and α_3 at the chosen concentration $\Delta n'$ on the rise and decay curves, respectively.*

In practice it is convenient to choose $\Delta n' = \Delta n_{\text{st}}$ (where Δn_{st} is the steady-state concentration at a given light intensity) as the concentration at which q is to be determined. Since $(d\Delta n/dt)^{\Delta n' = \Delta n_{\text{st}}} = 0$ in this case, relation (1.24) is simplified to:

$$q = \frac{1}{J\Delta n_{\text{st}}}\left[\left(\frac{d\Delta n}{dt}\right)^{\text{or}}_r + \left(\frac{d\Delta n}{dt}\right)^{\Delta n_{\text{st}}}_d\right]. \tag{1.26}$$

In this case, the determination of q requires

* It should be noted that q may be determined from the measurement of the photoconductive yield from

$$q\left(\frac{d\Delta n/dt}{M_0 qJ}\right)^{\text{or}}_r \tag{1.25}$$

However in this case one should know not only the light intensity but the equilibrium concentration of electrons on the impurity center as well.

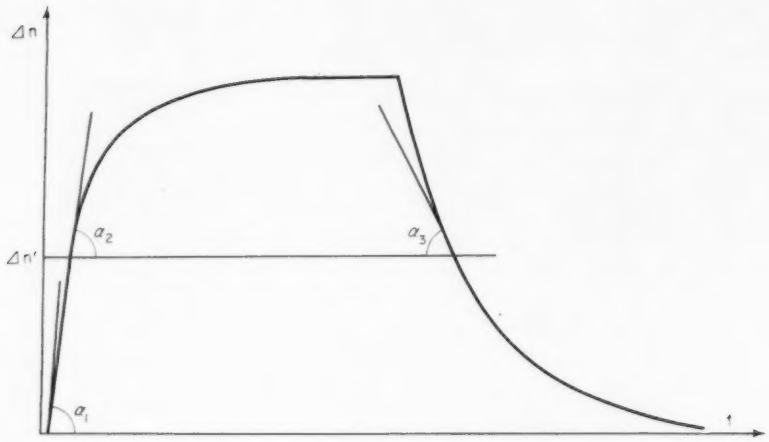

FIG. 5.

only knowing the original slopes of the rise and decay curves.*

The above considerations have been used to interpret the results of the investigation of the impurity photoconductivity kinetics on n-type Ge with radiation-induced defects produced by γ-rays from Co^{60} and by fast electrons (2·5 MeV).[3] A series of parameters of the radiation-induced levels have been determined, including the cross-section for photon capture by an electron at the level $E_c - 0{\cdot}2$ eV, which has been found to be 4×10^{-16} cm, and the recombination coefficient γ.

2. INDUCED PHOTOSENSITIVITY. CHARGE EXCHANGE OF IMPURITY CENTERS

In the foregoing Section we have considered the impurity photoconductivity induced by optical excitation of equilibrium carriers. If, however, a level is not filled at equilibrium, it may generate impurity photoconductivity only due to its filling by non-equilibrium carriers, produced as a result of a preliminary or simultaneous excitation of the crystal by the light of a shorter wavelength (causing transitions into the band from deeper-lying filled levels or from the filled band).

The impurity photoconductivity of such a type induced by continuous illumination in the intrinsic region (referred to hereafter as intrinsic illumination) represents a general phenomenon possessing a number of peculiarities.

The induced photoconductivity has been observed both in insulating photoconductors (CdS, CdSe, CdTe, Sb_2Se_3 etc.)[4–7], and in compensated germanium (Ge with copper and radiation-induced defects).

Figure 6 shows the spectral response of the photocurrent in CdTe at $T = 77°K$ under different conditions. The curve marked by solid triangles ▲

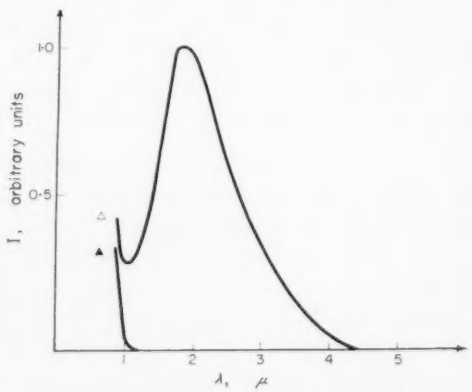

FIG. 6. Spectral response of photoconductivity in CdSe. △ Without preliminary intrinsic illumination. ■ Upon preliminary intrinsic illumination.

* We have not touched here upon the question of the effect of the trapping centers on the relaxation of the impurity photoconduction, which, as may be shown, considerably affects the results of the determination of parameters from the relaxation curves. This problem is considered elsewhere.

Vol. 2
1961

has been obtained without preliminary illumination and shows zero photosensitivity in the long wavelength region. However if the sample has been preliminarily illuminated with light in the intrinsic absorption region (after which it has been kept in the dark for a long time), an appreciable photoconductivity is revealed beginning at $\sim 4\mu$(Δ-curve).

Figure 7 illustrates the time dependence of the induced photoconductivity at $\lambda = 2\mu$ in (a) CdTe and (b) CdSe following a preliminary intrinsic illumination.

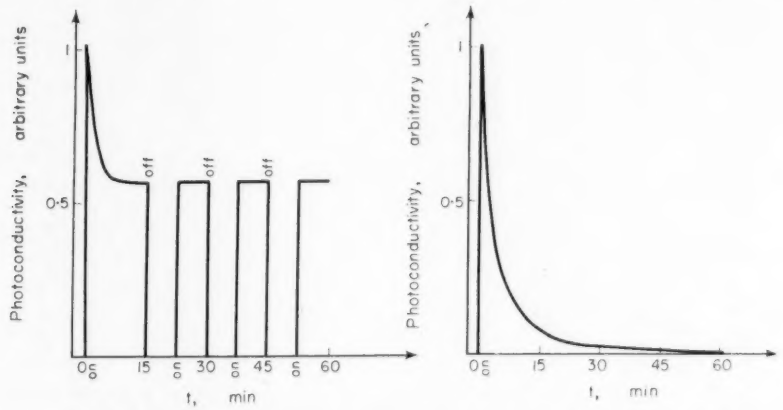

FIG. 7. Relaxation of induced photoconductivity in (a) CdTe and (b) CdSe.

It is seen that upon illumination with long wavelength light the relaxation curve acquires the shape of a "burst", with the current in CdSe dropping to zero in a comparatively short period of time; whereas in CdTe (and in CdS as well) a quasi-steady excited state persists for a long time, characterized by a sensitivity of the crystal in the long wavelength region which does not depend on time, to a first approximation. When in this state, the rise and decay of the photocurrent on illumination and after its removal approach an exponential law and take place during comparatively short times (about several milliseconds). The observed character of the induced photoconductivity in substances of the CdS group may be explained by considering the following band diagram. In the forbidden band of a crystal there are trapping centers with a density M which are empty while in the dark and which become filled with electrons when excited in the intrinsic region. Holes from the valence band are trapped by recombination centers S. Light in the region 2–6μ excites electrons from the M-levels into the conduction band. The electrons in the band may later on either undergo recombination (i.e. become captured in the S-levels), or return to the M-levels. The relation between the probabilities for these two processes may be different, and in the limiting cases it corresponds to a single or multiple trapping where optical excitation plays the role of thermal ejection. Increasing at first, the photoconductivity begins to decrease as the intensity of the carrier generation drops, which is associated with the emptying of the M-levels.

If the recombination is constant and secondary trapping in the M-levels is of low intensity, the photoconductivity drops in a comparatively short time [Fig. 7(b)]. If, however, the intensity of recombination decreases with time (due to the decrease of hole concentration on the centers of recombination), repeated trapping begins to prevail, and photoconduction may persist for quite a long time, with electronic transitions taking place practically only between the C-band and the M-levels (a quasi-steady excited state). Under these conditions all relationships valid for the case of one level (Section 1) may be applied to the relaxation of the photoconductivity.

In Fig. 8(a) are shown the relationships between the time constants of rise τ_r and decay τ_d, and the

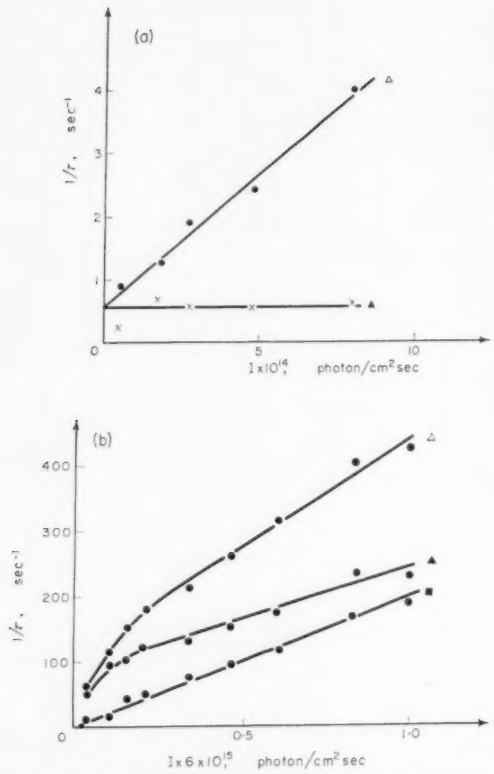

FIG. 8. Experimental relationships for photoconductivity rise and decay time constants in (a) CdS and (b) CdTe. △ $1/\tau_r$. ▲ $1/\tau_d$. ■ $1/\tau_r - 1/\tau_d$.

light intensity at $\lambda = 2\mu$. The same relations for an n-type specimen of CdTe are graphically presented in Fig. 8(b).

The graphs indicate that the relationships of kinetics found are in a good agreement with the theory elaborated. The magnitudes of the cross-sections for photon capture in an impurity center have been found to be:

CdS, $E_c - 0{\cdot}3$ eV level: $q = 3 \times 10^{-15}$ cm²;
CdTe, $E_c - 0{\cdot}33$ eV level: $q = 2 \times 10^{-15}$ cm²;
CdTe, $E_v - 0{\cdot}30$ eV level: $q = 2 \times 10^{-15}$ cm².

The knowledge of the electron concentration on the local level permitted calculation of the coefficient of absorption in the infra-red ($\lambda = 2\mu$) $\kappa = qm$, which for CdS specimens constitutes 3×10^{-6} cm^{-1}, a too low value to be measured directly by optical means.

The investigation of the kinetics of the induced photoconductivity in copper-doped germanium has been carried out on specimens with different degrees of compensation. The simplest relationships have been obtained in the case of unipolar impurity photoconduction in specimens with equilibrium occupation of local levels shown in Fig. 9 (the spectral response of such a specimen is presented in the same figure).

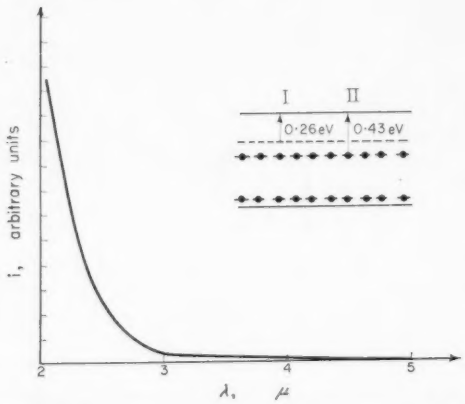

FIG. 9. Spectral response of photoconductivity and the band diagram of level occupation in Cu-doped Ge specimen.

A preliminary illumination at $\sim 3\mu$ (transition II) resulted in a partial charge exchange of local centers associated with the filling of the $E_c - 0{\cdot}26$ eV level and production of unoccupied levels at $E_c - 0{\cdot}43$ eV. This has been accompanied by the appearance of an appreciable photosensitivity in the 4μ region due to transitions I. The kinetics of this induced photoconductivity reveal a clearly pronounced "burst"-type character with an exponential dropping branch. The corresponding relaxation curves at different intensities of long wavelength illumination are given in Fig. 10.

3. PECULIARITIES OF IMPURITY PHOTOCONDUCTIVITY RELAXATION WHEN LOCAL LEVELS OF SEVERAL TYPES ARE PRESENT

When local levels of more than one type are

Vol. 22
1961

present in the forbidden band, as well as in the case of multipli-charged centers, the relationships governing the impurity photoconduction become

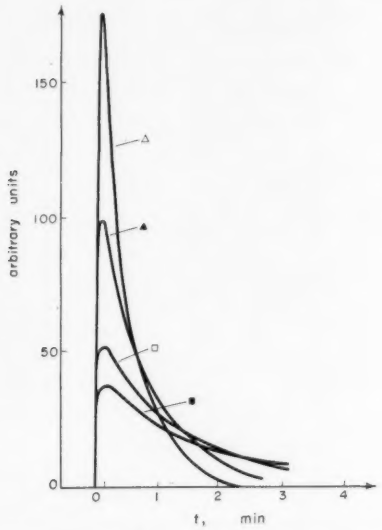

FIG. 10. "Bursts" of photoconduction in optical excitation from the $E_c-0{\cdot}26$ eV level in Cu-doped Ge at different light intensities.

△ J = 100 per cent □ J = 25 per cent
▲ J = 60 per cent ■ J = 20 per cent.

very complicated due to the possibility of optical generation simultaneously from several levels, and also because of the important role played by their mutual influence in the processes of recombination and trapping of the carriers.

The case of a large equilibrium conductivity, when all sufficiently deep levels responsible for photoconduction are completely filled, is the simplest for interpretation. Under these conditions, the photoconduction from multipli-charged centers (at low excitation levels) is essentially similar to the case of photoconduction from a single isolated level (Section 1); and the relationships governing the impurity photoconduction in the presence of independent levels are of the simplest form possible. It may be shown that in this case the levels will act independently from one another and the corresponding relaxation curve will be represented by a sum of exponentials associated with these levels:

$$\Delta n = \sum_{k=1}^{r} \frac{m_k q_k J}{\gamma_k n_0}[1 - \exp(-\gamma_k n_0 t)],$$

where r is the actual number of the level types involved.

Measuring the characteristics of individual components of the curve permits one to determine the cross-sections for the capture of carriers and the absorption coefficient for each of the levels just as this has been outlined in Section 1.

The relaxation of the impurity photoconduction in the case where part of the levels remain unfilled in the dark or filled to only a small extent proceeds in a considerably more complicated way. The role of mutual influence of the levels considered becomes very important.

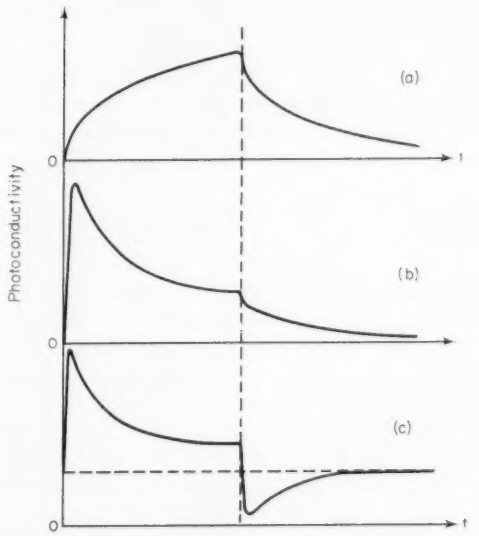

FIG. 11. Calculated relaxation curves of impurity photoconductivity for the case of excitation from two levels.

Illumination results in a redistribution of carriers between different levels in accordance with the magnitudes of their cross-sections for capture and optical ionization, that is, in a charge exchange of the levels as compared with equilibrium conditions.

The corresponding calculations show that the

relaxation curves under these conditions may not only exhibit a monotone character, but reveal extrema as well—see Figs. 11(b) and (c). (Curves in Fig. 11 have been calculated for two levels.)

Investigating the relaxation under such conditions permits one to obtain detailed data concerning the mechanism of the processes and the parameters of the levels responsible for photoconduction.

4. METHOD OF LONG-WAVE PROBING OF LOCAL LEVELS

Data usually obtained in the investigation of photoconduction kinetics may be satisfactorily interpreted only in the simplest cases. When levels of more than one type are present in the forbidden band, as well as in the case of "nonlinear" processes, solving the corresponding kinetic equations presents practically insurmountable difficulties, and selecting an adequate model becomes ambiguous to a considerable degree.

Such a situation is explained in the first place by insufficient information which may be gained from the experimental investigation of the relaxation curves. Indeed, the results of such an investigation may amount only to the determination of the time dependence of the concentration of free carriers in the band [i.e. $n(t)$ and $dn/dt(t)$], whereas the concentrations of carriers in bound states filling local levels in the forbidden band remain beyond possibility of measurement. It is obvious that if we succeeded in broadening experimental capabilities so as to include the concentration of not only free but also of bound carriers [i.e. $m(t)$ and $dm/dt(t)$] into the number of measured quantities, this would drastically reduce the mathematical difficulties encountered through transformation of differential equations into algebraic ones, and by reducing the number of unknowns.

Such a possibility may be provided by the so-called long-wave probing method[8] consisting essentially in the following. In order to determine the concentration of the carriers filling a local level, one may make use of the fact that the intensity of generation of the impurity photo-effect from this level, g, (determined by the original slope of the curve characterizing the photoconduction rise upon illumination) is directly proportional to the concentration of carriers on this level:

$$g = mqJ \qquad (4.1)$$

Since the quantity qJ may be readily determined by any of the above mentioned methods (see Section 1), measuring q (or the magnitude of the signal upon illumination with a long-wave light pulse having a duration much shorter than the rise time of the impurity photoconductivity) yields directly the concentration of the carriers on the level.* Now as the duration of the probing

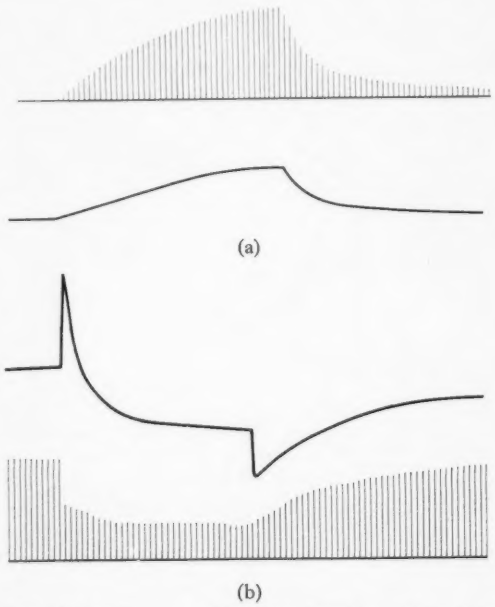

FIG. 12. Oscillograms of local level probing. (a) Probing of the $E_c-0{\cdot}3$ eV level in CdS during intrinsic photoconductivity relaxation. (b) Probing of the same level during quenching of intrinsic photoconductivity.

pulse may be taken sufficiently short, and the duty ratio adequately small, the illumination by probing pulses will not materially affect the processes being investigated.

By way of illustration, Fig. 12(a) presents oscillograms obtained with a dual-trace oscillograph and showing the probing of the level

* Another possibility for the measurement of the concentration of carriers in bound states consists in investigating impurity absorption of light. It is known, however, that the magnitude of absorption in the extrinsic region is rather small and depends not only on the concentration of bound carriers, which is of interest for us, but upon other rivalling absorption mechanisms as well. Hence this method would be of little use.

Vol. 22
1961

$E_c-0{\cdot}3$ eV in a single crystal of CdS in the course of photoconductive relaxation caused by illumination in the wavelength region near the edge of intrinsic absorption ($\lambda = 0{\cdot}52\mu$); the lower curve gives the photoconductivity versus time relationship [i.e. $n(t)$]. Probing has been done by long-wave light pulses ($\lambda = 2\mu$). The envelope of the amplitudes of the pulse "fence" (the upper curve) represents (when taken in the corresponding scale) the time dependence of the concentration of nonequilibrium carriers on this level [i.e. $m(t)$.]

Figure 12(b) shows an oscillogram of the kinetics of photoconduction quenching in CdS with illumination by long-wave quenching light ($\lambda = 0{\cdot}9\mu$) and upon its removal (the upper curve), as well as the variation of electron concentration on the $E_c-0{\cdot}3$ eV level during this process (lower curve). The results indicate that in the course of quenching the levels $E_c-0{\cdot}3$ eV act as centers of the 1st class.[9]

Figure 13 presents the dependence of the steady-state intrinsic photoconductivity in CdS (Δ) and

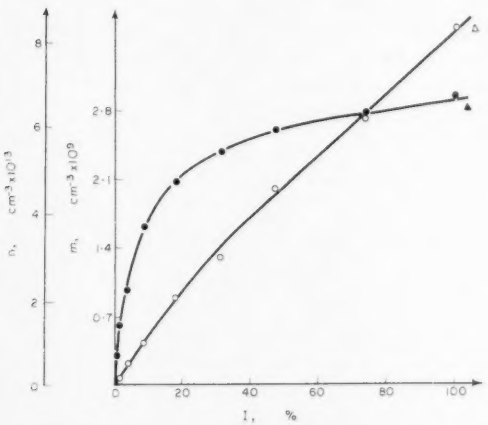

FIG. 13. Dependence of steady-state concentration of electrons in C-band (n) and on $E_c-0{\cdot}3$ eV level (m) in CdS on light intensity.

the simultaneously obtained dependence of the electron concentration on the $E_c-0{\cdot}3$ eV level (▲) upon light intensity. The first one approaches a linear relationship, whereas the second dependence tends to reveal saturation. Assuming the $E_c-0{\cdot}3$ eV level to be a trapping level, one may deduce the concentration of the corresponding carriers from the curve.

In cases where continuous illumination with probing pulses interferes with the process under investigation, one may use a single probing pulse shifted in phase with respect to the beginning of the process concerned.

In the case of several local levels being present, the concentration of carriers on them is calculated in a more complicated way.

For example, the concentration m_2 for the second level from the band edge may be determined by the formula:

$$m_2 = \frac{g(\lambda_2)}{q_2(\lambda_2)} - \frac{q_1(\lambda_2)}{q_1(\lambda_1)} m_1, \qquad (4.2)$$

where

m_1 and m_2 are carrier concentrations on the first (shallow) and second (deeper) levels, respectively,

g is the original slope upon illumination at wavelength λ_2,

q_2 is the cross-section for photon capture by electrons on the second level,

$q_1(\lambda_1)$ and $q_1(\lambda_2)$ are the cross-sections for photon capture by electrons on the first level at wavelengths λ_1 and λ_2 respectively.

5. NON-STEADY-STATE UNIPOLAR PHOTOELECTROMAGNETIC EFFECT

In conclusion, consider the problem of diffusion of non-equilibrium current carriers in a magnetic field under unipolar extrinsic excitation. Both the steady-state and non-steady-state photoelectromagnetic effects of Kikoin–Noskov associated, as is well known, with ambipolar diffusion of electrons and holes have been studied in detail. A major pre-condition for the existence of this effect is a simultaneous generation of electrons and holes by light, that is, bipolar photoconduction. In the case of unipolar photoconductivity (extrinsic excitation) this phenomenon will disappear.

Indeed, the diffusion current of non-equilibrium carriers in the steady state is balanced accurately by the conduction current which equals the first both in magnitude and in what concerns the energy of the component charges. Thus, the flow of charge carriers will not deviate under the action

of the magnetic field, and hence there will be no photoelectromagnetic effect.*

However, the photoelectromagnetic effect may be revealed also with extrinsic excitation, if the observation is carried out in the non-steady state. In this case, as the light is turned on, a diffusion current of non-equilibrium charge carriers appears, which is unbalanced since the charges have not yet displaced so as to produce an electric field.

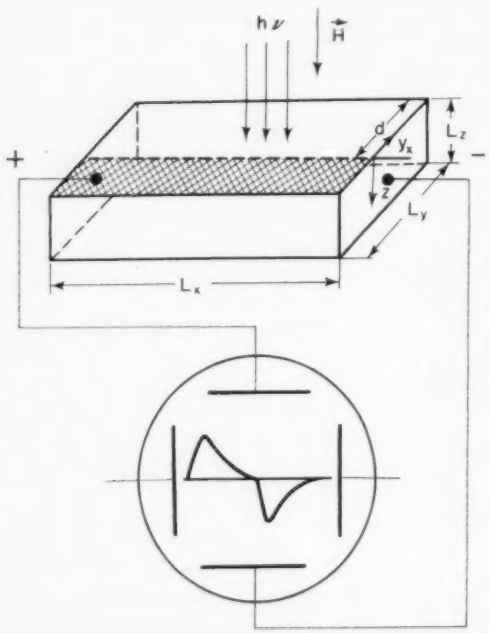

FIG. 14. Diagrams for the calculation and measurement of the photoelectromagnetic effect.

The unbalanced diffusion flow of non-equilibrium carriers will be displaced by the magnetic field producing the photoelectromagnetic effect. Upon illumination, a reversed current of space charge "resolution", and hence a reversed photoelectromagnetic e.m.f., will build up.

It is obvious that the higher the absorption coefficient the higher will be the photoelectromagnetic e.m.f. However this will take place only as long as the reciprocal of the absorption coefficient exceeds the Debye screening length. As soon as this relation is reversed, the dependence on the absorption coefficient disappears. Unfortunately, the absorption coefficient of light in the extrinsic region is not sufficiently high, being as a rule considerably below the reciprocal of the Debye length. To avoid this difficulty, it is expedient to illuminate only one part of the specimen uniformly in volume ($y > 0$) leaving the other part ($y < 0$) in the dark (Fig. 14). At the boundary between these regions, one may expect a build-up of a substantial concentration gradient determined by the light intensity and screening length and not by the magnitude of the absorption coefficient.

When working out a problem, one should select a specific model of a semiconductor, In the present work, the model shown in Fig. 1 has been accepted.

Assuming that the specimen is illuminated at $t = 0$ by a light of constant intensity (a step), and that the inequalities d, $(L_y - d) \gg x^{-1}$ hold, one may obtain the following expressions for the photoelectromagnetic e.m.f. and the short-circuit current taking a low injection level and a weak magnetic field:

$$E_x = \frac{\tilde{\mu}H}{c}\frac{4\pi eD}{\epsilon L_y}\Delta n_{st}\cdot\tau \times \frac{\{[(1/\tau - 1/\tau_\sigma)t - 1]\exp(-t/\tau_\sigma) - \exp(-t/\tau)\}}{(1-\tau/\tau_\sigma)^2} \tag{5.1}$$

$$J_{short} = -\frac{\tilde{\mu}H}{c}eDL_z\Delta n_{st}\frac{\exp(-t/\tau_\sigma) - \exp(-t/\tau)}{1-\tau/\tau_\sigma}, \tag{5.2}$$

where $\tilde{\mu}$, μ are the Hall and ordinary mobility of the current carriers, $\tau_\sigma = \epsilon/4\pi\sigma$, $\sigma = e\mu n_0$, n_0 the equilibrium concentration of current carriers, and Δn_{st} is the steady-state concentration of photoelectrons at $t \to \infty$ in the neutral part of the illuminated region; t is the time,

$$\tau = [\gamma(N_{CM} + n_0 + M - m_0)]^{-1},$$

and x the reciprocal of the Debye length.

* In the case of bipolar conduction, the photoelectromagnetic effect will take place under the same conditions, since the vanishing of the total current in the direction of illumination is achieved here because of equal flows of electrons and holes, each of which is other than zero.

Vol. 2
1961

Figure 15 shows the time dependence of the photoelectromagnetic e.m.f. for different t to τ_σ ratios.

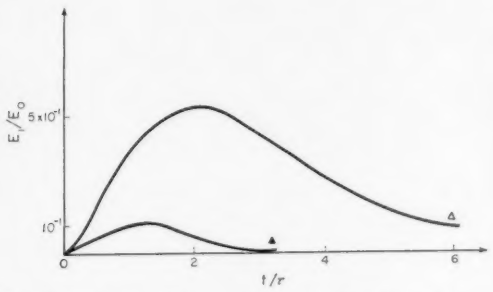

FIG. 15. Time dependence of the unipolar photoelectromagnetic e.m.f. for different τ to τ_σ ratios.
$\triangle$ $\tau = \tau_\sigma$. $\blacktriangle$ $\tau = 2\tau_\sigma$.

Evaluate the absolute magnitude of the effect (short-circuit current) at the following possible values of parameters:

$$L_x = 1 \text{ cm}; \quad L_z = L_y = 0{\cdot}1 \text{ cm}; \quad \epsilon = 16;$$

$$\frac{\mu H}{c} = 1; \quad \Delta n = n_0; \quad J_0 m_0 q = 10^{15} \text{ cm}^{-3}.$$

In accordance with the above formula, the maximum value of the current will be (at $\tau = \tau_\sigma$):

$$J_{\text{short}}^{\max} = L_z \frac{\mu H}{c} \frac{kT}{e} \frac{\Delta n_{\text{st}}}{n_0 \tau} \frac{\epsilon}{4\pi} \approx 4{\cdot}10^{-10} \text{ A}.$$

If the mobility $\mu = 10^3$ cm^2/V sec, the resistance of the specimen will be $R = 10^7\ \Omega$. Thus the signal which may be obtained from across the load resistor R_l providing short-circuit operating conditions $R_l \approx 0{\cdot}3R$ is $V = J_{\text{short}}^{\max} R_l \approx 10^{-3}$ V, which may be measured.

Experiments in this direction are being carried out.

REFERENCES

1. RYVKIN S. M., PARITSKY L. G., HANSEVAROV R. Y. and YAROSHETSKY I. D., *Solid-State Phys.* (*USSR*) **3,** 252 (1961).
2. RYVKIN S. M., *Semiconductors in Science and Technology* (*USSR*) Vol. II (1958).
3. RYVKIN S. M., HANSEVAROV R. Y. and YAROCHETSKY I. D., *Solid-State Phys.* (*USSR*). In Press.
4. LAMBE J. and KLICK C. C., *Phys. Rev.* **98,** 905 (1955).
5. ARKADYEVA E. N., PARITSKY L. G. and RYVKIN S. M., *Solid-State Phys.* (*USSR*) **2,** 1161 (1960).
6. ARKADYEVA E. N. and RYVKIN S. M., *Solid-State Phys.* (*USSR*) **2,** No. 8 (1960).
7. ARKADYEVA E. N., KOSYMOVA R. S. and RYVKIN S. M., *Solid-State Phys.* (*USSR*) **3,** No. 8 (1961).
8. PARITSKY L. G. and RYVKIN S. M., *Solid-State Phys.* (*USSR*) **3,** No. 8 (1961).
9. ROSE A., *Phys. Rev.* **97,** 322 (1955).

BLANK
PAGE

Vol. 2
1961

J. Phys. Chem. Solids Pergamon Press 1961. Vol. 22, pp. 19–24. Printed in Great Britain.

PHOTOCONDUCTIVITY IN SEMI-INSULATING GALLIUM ARSENIDE

B. R. HOLEMAN and C. HILSUM

Services Electronics Research Laboratory, Baldock, Herts., England

Abstract—The photoconductive (PC) and photoelectromagnetic (PEM) effects have been measured for a number of specimens of semi-insulating gallium arsenide (resistivity greater than 10^5 Ω/cm). The results enable both majority and minority carrier lifetimes to be determined and some values are given. In the small signal region, the lifetimes are found to be only slightly dependent on intensity of illumination, indicating an essentially linear relationship between intensity of illumination and photo-signal. For specimens at room temperature, the two lifetimes are of the same order of magnitude, which shows that trapping effects are small. A check on these measurements can be obtained in principle from a measurement of photoconductive decay time constants.

The photoconductive spectral response shows a tail on the long wavelength side of the absorption edge extending to approximately 2 μ. This has been ascribed to a level lying deep in the band gap with a threshold energy for photoconductivity of 0·63 eV.

1. INTRODUCTION

PREVIOUS work in this laboratory[1] has shown that it is possible to measure the very short carrier lifetimes found in semi-conducting GaAs by a determination of the photoconductive (PC) and photoelectromagnetic (PEM) effects at a known intensity of illumination, together with a photoconductive spectral response. This method enables both majority and minority carrier lifetimes to be determined, and can be used even when trapping effects are large. A similar technique has now been applied to semi-insulating GaAs.[2] Changes were necessary in the experimental technique to accommodate the high specimen resistance encountered, and the rapid variation of this resistance with temperature. The results show that trapping effects in semi-insulating GaAs are smaller than in semi-conducting GaAs, and that the lifetimes are slightly dependent on the light intensity.

2. EXPERIMENTAL TECHNIQUES

A. *Measurement of* PC *and* PEM *effects*

For the experiments on semi-conducting samples of GaAs, the light was modulated at 800 c/s and the PC and PEM open-circuit voltages were measured using a tuned amplifier. This method was not suitable for semi-insulating samples, as tuned amplifiers with sufficiently high input impedance were not available. A d.c. method was therefore adopted which enabled the PC and PEM voltages and the Hall voltage to be measured in the same apparatus. The circuit is shown in Fig. 1. The electrometers* had an input impedance of 10^{13} Ω on the "HI" terminal, which was at least two orders of magnitude greater than the highest probe impedances encountered. The "LO"

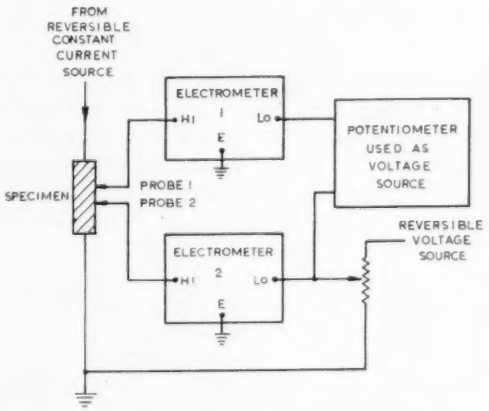

FIG. 1. Circuit used for d.c. measurements.

* "Vibron" Electronics Instruments Ltd., Richmond, Surrey, England.

terminal was isolated from earth, which allowed the instrument to be used as a null detector. With this circuit, a probe-to-probe voltage of 1 V could be measured to 1 mV, giving a higher accuracy than a direct measure of the probe voltages. The Hall coefficient of the specimen was deduced from the voltage swing of a single probe on applying a reversible magnetic field.

It has been found[2] that consistent measurements of Hall coefficient and mobility can be made only after the specimen has been heated to at least 100°C under high vacuum, and when this vacuum is maintained during subsequent measurements. This technique was used for PC, PEM and R_H measurements. As the resistivity of semi-insulating GaAs varies rapidly with temperature, the specimen jig was surrounded by a liquid jacket kept at constant temperature. Light from a calibrated tungsten filament lamp was restricted to a narrow band centred on 0·645μ by a series of filters, and was focused on the sample through a glass window. Great care was taken to exclude all other light during measurement.

B. *Spectral response of photoconductivity*

Light from a tungsten lamp was modulated at 800 c/s and passed through a Leiss double monochromator. The monochromatic radiation obtained was focused on the specimen by an optical system that did not alter the distribution of radiation over the specimen surface if the slit width of the spectrometer was altered. The short-circuit current signal from the GaAs specimen was compared with the signal from a germanium detector of unit quantum efficiency over the relevant wavelength range. For both the GaAs specimen and the Ge detector the signal was amplified by an 800 c/s tuned amplifier and presented on a potentiometric recorder.

C. *Photoconductive decay measurement*

Time constants for PC decay in GaAs can range from 10^{-7} sec to at least several milliseconds, and therefore a versatile apparatus is required. Previous workers have obtained light pulses from high speed turbine-driven rotating mirrors[3] or by using multiple reflections from a hexagonal mirror[4]. The apparatus described briefly here combines the sharp rise and fall times of these methods with a large degree of flexibility and comparatively low mirror rotational speeds.

Multiple reflections are obtained between a fixed plane mirror and a rotating plane mirror (Fig. 2). The whole system can be represented by a single reflection from a mirror rotating n-times

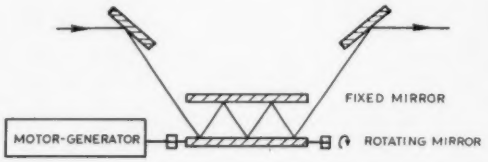

FIG. 2. Arrangement of rotating mirror.

as fast as the rotating mirror, where n is the number of reflections on the rotating mirror. This mirror was driven by a feedback motor-generator enabling any desired speed up to 6000 rev/min to be obtained. In practice n can be varied between 4 and 15 giving effective rotational speeds up to 90,000 rev/min.

The light source was a high intensity $1\frac{3}{4}$ kW Xenon arc lamp which was chosen because of its high light output between 0·8 and 0·9μ. The optical system is shown in Fig. 3. The ellipsoidal mirror on which is focused an image of S_1 enables a rectangular pulse of light to be obtained at the specimen, as light falls on the specimen for the whole time that the image of S_1 falls on the ellipsoidal mirror. In this way a pulse-length to rise-time ratio of up to 100 to 1 is obtained.

The photo-voltage was amplified by an amplifier of 10 Mc/s bandwidth and displayed on an oscilloscope. For semi-insulating specimens the noise level was generally sufficiently low for a clear trace to be obtained. In this case the decay trace was measured by a trace comparison method in which a synthesized signal consisting of the sum of up to three exponential RC decays was compared with the specimen signal (Fig. 4). When the noise level is too high for this technique a sampling method can be used in which the specimen signal is sampled for 1μ sec during each pulse, and the sampled signal is integrated by a long-time-constant RC network. The sampling point is then swept slowly through the specimen pulse and the integrator output is plotted on a X–Y recorder

Vol. 22
1961

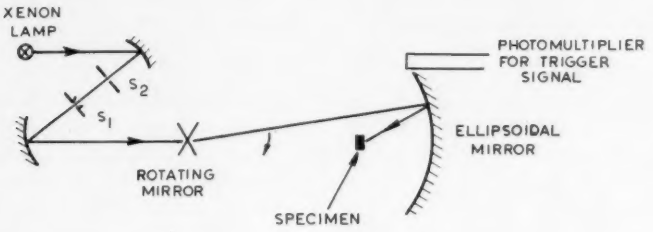

S_1 – VERTICAL SLIT IMAGED ON ELLIPSOIDAL MIRROR.
S_2 – HORIZONTAL SLIT IMAGED ON ROTATING MIRROR AND ON SPECIMEN.
FOCI OF ELLIPSE AT ROTATING MIRROR AND AT SPECIMEN.

FIG. 3. Optical path through light-pulse apparatus.

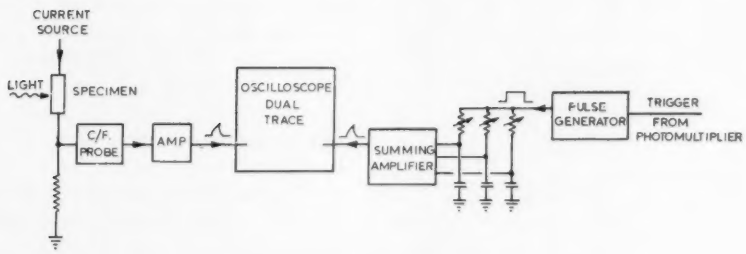

FIG. 4. Circuit for decay comparison.

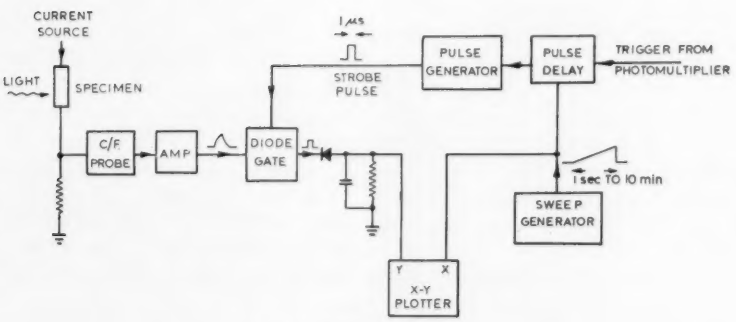

FIG. 5. Sampling circuit.

(Fig. 5). This method can easily improve the signal to noise ratio by a factor of a hundred.

3. RESULTS

A. *Lifetime*

The carrier lifetimes measured from the PC and PEM effects are tabulated in Table 1. For

Table 1

Specimen	Light intensity (photons/cm^2)	Carrier lifetime τ_n($\times 10^8$ sec)	τ_p($\times 10^8$ sec)	No. of carriers (n/cm^3)
1	$2{\cdot}3\times10^{13}$	3·4	3·0	2×10^7
1	$3{\cdot}8\times10^{11}$	12	9·5	2×10^7
2	$1{\cdot}5\times10^{12}$	5·2	8·0	$3{\cdot}2\times10^6$
2	$8{\cdot}1\times10^{10}$	20	80	$3{\cdot}2\times10^6$
3	$1{\cdot}4\times10^{12}$	6·0	9·0	$8{\cdot}6\times10^6$
4	$7{\cdot}8\times10^{10}$	20	15	$2{\cdot}7\times10^6$
5	$2{\cdot}5\times10^{13}$	0·5	0·17	$3{\cdot}4\times10^6$
5	$2{\cdot}4\times10^{12}$	0·8	0·65	$3{\cdot}4\times10^6$
5	$1{\cdot}3\times10^{11}$	3·1	1·2	$3{\cdot}4\times10^6$
6	$5{\cdot}5\times10^{11}$	2·6	0·7	$9{\cdot}4\times10^6$
6	$2{\cdot}1\times10^{12}$	3·6	2·7	$9{\cdot}4\times10^6$

comparison, in semi-conducting GaAs the lifetimes range from a majority carrier lifetime of 10^{-6} sec and a minority carrier lifetime of 10^{-9} sec to a majority carrier lifetime of 10^{-4} sec and a minority carrier lifetime of 10^{-12} sec. The ratio of the majority to minority carrier lifetimes gives an indication of the amount of trapping in a particular specimen, and in semi-conducting GaAs this ratio varies between 10^3 and 10^8. In semi-insulating GaAs this ratio is much closer to unity, and is never greater than 10, indicating that there is much less carrier trapping in this material than in semiconducting GaAs.

The mean of the two carrier lifetimes will be approximately the lifetime of carriers in trap-free material, and this is seen to vary from 3×10^{-9} to 5×10^{-7} sec, the longest mean lifetimes being obtained in the materials with the lowest electron concentration.

The lifetimes are a function of light intensity, giving a decreasing lifetime at increasing intensity of illumination. This results in a non-linear relationship between photosignal and light intensity, the photoconductive voltage (V_{PC}) increasing as light intensity (I) according to the relationship

$$V_{PC} = (I)^m$$

where m varies between 0·6 and 1·0. For monomolecular recombination, m should be 1·0 and for bimolecular recombination m should be 0·5. For sample 5, m was measured as 0·65 when the radiation was unmodulated, and became 1·0 when the radiation was modulated at 800 c/s. The photoconductive decay contained long time constant components of appreciable magnitude and these are probably affecting the d.c. measurement.

In semi-conducting GaAs agreement was obtained between the majority carrier lifetime as measured by PC, PEM, and the photoconductive decay time constant. In semi-insulating GaAs the shortest decay time constants observed are not less than a microsecond, irrespective of whether the full Xenon lamp spectrum or only that part of the spectrum which was fully absorbed was used whereas the majority carrier lifetimes measured by the PC, PEM method are at least an order of magnitude shorter. No explanation of this discrepancy is offered here, but theoretical calculations[5] show that deep levels which need not be trap levels can give rise to long time constant decays of appreciable magnitude. The presence of deep levels in semi-insulating GaAs has been shown by BUBE[6] by measurements of thermally stimulated currents.

B. *Spectral response*

The simplest way to measure the spectral response of a specimen is to keep the spectrometer slit-width constant and to vary the wavelength. This results in a rapidly decreasing light output from the spectrometer as the wavelength is decreased below 0·9μ, and if the value of m in the photoconductive voltage–light intensity relationship is not unity, but is less than one, an apparently increasing spectral response is measured as the wavelength is reduced. In such specimens, the spectral response must be measured at constant photon density, and then a uniform, or slowly varying response, is observed as the wavelength is reduced. The spectral response of a specimen from the absorption edge to shorter wavelengths is required as a measure of the surface conditions in calculating the carrier lifetime.

Vol. 22
1961

All semi-insulating samples show a response extending beyond the absorption edge to about 2μ. The signal in this region is linear with light intensity. This response has been analysed for a number of n-type specimens and is found to obey a relationship of the form of:

$$\text{Response} = (h\nu - E)^{5/2}$$

where E is $0{\cdot}63 \pm 0{\cdot}01$ eV (Fig. 6).

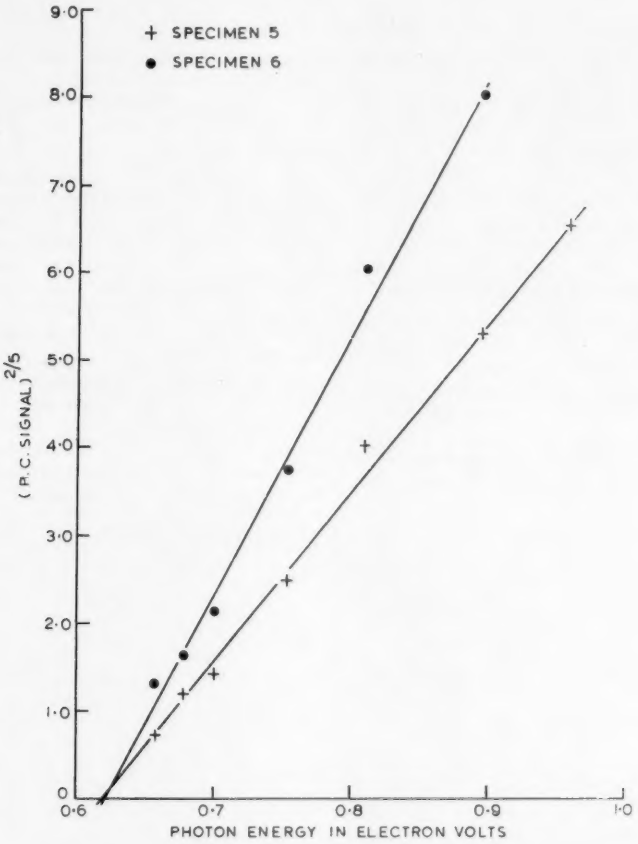

FIG. 6. Long wavelength photoconductive tail response in semi-insulating GaAs.

CONCLUSIONS

The methods developed for measuring carrier lifetime and associated photoeffects in semi-conducting GaAs have been extended to semi-insulating GaAs. Carrier lifetimes of 10^{-7} sec are found, and trapping effects are smaller than in semi-conducting GaAs. The photoconductive spectral response has a long wavelength tail with a threshold energy of 0·63 eV in n-type material.

Acknowledgements—The authors are glad to acknowledge the assistance of Miss B. TAYLOR in these measurements, and Mr. W. HARDING for the supply of material. Permission to publish has been given by the Admiralty.

REFERENCES

1. HILSUM C. and HOLEMAN B. R., *Proceedings of the International Conference on Semiconductor Physics, Prague*, 1960.

2. GOOCH C. H., HILSUM C. and HOLEMAN B. R., *Proceedings of the International Conference on Semiconducting Compounds, Schenectady* 1961.
3. BRIXNER B., *Rev. Sci. Instrum.* **30,** 1041 (1959).
4. GARBUNY M., VOGL T. P. and HANSON J. R., *Rev. Sci Instrum.* **28,** 826 (1957).
5. VAN ROOSBROECK W., *Bell Syst. Tech. J.* **39,** 515 (1960).
6. BUBE R. H., *J. Appl. Phys.* **31,** 315 (1960).

DISCUSSION

A. R. BEATTIE: In the large signal region, the lifetime may be expected to vary with number of excess carriers so that the lifetime will vary not only with photon flux but also with magnetic field, since the magnetic field increases the surface number of excess carriers. Work on large signal PEM effect will shortly be published.

B. R. HOLEMAN: In the experiments, the photon flux was kept as low as possible in an attempt to avoid high field effects. The surface conductivity change will be larger than the specimen conductivity change of about 1 per cent, as strongly absorbed light had to be used.

M. GREENE: Since the holes and electrons ultimately recombine via traps, why should the majority and minority lifetimes be different?

B. R. HOLEMAN: A trap is not necessarily a recombination centre; the effect of a trap is to remove numbers of one particular carrier from the relevant band, and thus prevent them from taking part in recombination, giving different majority and minority carrier lifetimes. See also Ref. (1).

R. H. BUBE: Thermally stimulated current data obtained by us on high resistivity GaAs crystals from the Services Electronics Research Laboratory indicate traps with depth about 0·6 eV and densities of 10^{14}–10^{15} cm^{-3}. Similar traps are found in a variety of other high resistivity GaAs crystals.

M. A. LAMPERT: For those samples which are near intrinsic (by "accident"), the assumed impurity level, 0·63 eV from a band edge (invoked to explain the photoconductivity tail), should reveal itself very dramatically in a one-carrier space-charge limited current experiment via the usual trap-filled-limit current rise (room temperature experiment). A trap density as low as 10^{10}–$10^{11}/cm^3$ would easily show up in this way.

B. R. HOLEMAN: Measurements of space-charge limited currents have been made on a number of specimens of semi-insulating GaAs, and show a trap density which varies over a wide range from specimen to specimen.* Measurements have not yet been made on specimens used for photoconductivity.

* ALLEN J. W., *Nature, Lond.* **189,** 297 (1961).

J. Phys. Chem. Solids Pergamon Press 1961. Vol. 22, pp. 25–29. Printed in Great Britain.

THE MEASUREMENTS OF DEFECT STATES IN CdS

J. FRANKS and P. N. KEATING

A.E.I. Research Laboratory, Harlow, Essex, England

Abstract—In the analysis of thermoluminescence and thermoconductivity curves the capture cross-sections, S, of traps are generally taken to be independent of temperature or to vary according to an inverse square law. The analysis is extended for the case of no retrapping to allow the trapping cross-section to depend on the temperature according to a simple power law T^{-a}. A single thermoluminescence heating run is sufficient to obtain S, a, and the trap depth E. Similar considerations apply to thermoconductivity provided the recombination lifetime is not strongly temperature dependent. If trapping states are filled at low temperature in the dark by applying a voltage above that corresponding to the trap's filled limit, it is shown that under certain conditions the analysis applies independently of retrapping or recombination lifetime. The results of thermoconductivity measurements on a copper-doped CdS crystal containing trapping centres for which $a \approx -\frac{5}{2}$ are discussed.

INTRODUCTION

THE CORRELATION of defect states in the forbidden band with crystal imperfections and impurities is essential to the understanding of many of the electrical and optical properties of CdS. In a study of these effects, the degree of perfection of the crystals is important. Considerable advances have been made in the control of crystal growth from the vapour phase.[1] Recent work has shown that the growth of CdS crystals of some specific habits depends on the nature of the substrate as well as on temperature and atmosphere.[2]

The detection of trace impurities in CdS, however, still leaves much to be desired, especially as regards anionic impurities, of which oxygen presents particular difficulties. In addition, small deviations from stoichiometry can have a profound effect on the electronic properties;[3] direct measurements of such deviations appear at present to be virtually impossible.

Although the identification of defect centres with particular impurities and imperfections can therefore not be very complete, some parameters relating to these centres, such as their depth and capture cross-sections, have been extensively investigated. Optical and electrical techniques have been developed to examine centres of different types, but the interpretation of results is still often open to controversy, especially in the fields of thermoluminescence and thermoconductivity.

THERMOLUMINESCENCE

In the absence of retrapping, use is made of the relation between intensity of emission, I, at a temperature T and the energy, E, of a level below the conduction band:[4]

$$I = n_0 N_c S v \exp\left\{-E/kT - \int_{T_0}^{T} \frac{N_c S v}{\beta} \times \exp\left(-E/kT\right) dT\right\} \quad (1)$$

where n_0 is the number of trapped electrons at the lowest temperature T_0, N_c is the effective density of states in the conduction band, S is the capture cross-section of the traps at level E, v is the thermal velocity of the electrons and β is the heating rate.

The derivation is based on the fact that for most phosphors the recombination lifetime τ is sufficiently short for the rate of change of electrons in the conduction band dn_c/dt to be negligible with respect to n_c/τ under normal experimental conditions.

In applying equation (1), the product $N_c S v$ is often taken to be independent of temperature[5–7] implying that S varies as T^{-2}, since $N_c v$ may be taken to vary as T^2; in other analyses, S is taken to be independent of temperature[8, 9]. It has been shown that S may depend strongly on temperature,[10] however, so that it would appear more

realistic to allow S to vary according to a power law T^{-a}, or

$$N_c S v = BT^b, \qquad (2)$$

where B is a constant, and $b = 2-a$.

On substituting (2) in (1), evaluating the integral by an asymptotic series and expressing the constant factor under the integral in terms of the peak temperature T_g,

$$\frac{B}{\beta} = \left(\frac{b}{T_g^{(b+1)}} + \frac{E}{kT_g^{(b+2)}}\right) \exp(E/kT_g), \qquad (3)$$

equation (1) becomes

$$-\ln I/I_0 \sim E/kT - b \ln T + (T/T_g)^{(b+2)} \times \left(1+\frac{bkT_g}{E}\right)(1-\Delta)\exp(E/kT_g - E/kT) \qquad (4)$$

where $I_0 = n_0 B$ and $\Delta = (b+2)kT/E$. The error involved is less than 3 per cent if $E/kT_g > 10$.

Applying equation (4) to the two cases of half intensity of the peak, a relationship is obtained between trap depth, half-peak temperatures T_1 and T_2, and peak temperatures T_g ($T_1 < T_g < T_2$), such that

$$\frac{kT_g}{E} \sim \alpha(1{\cdot}2\gamma - 0{\cdot}54) + 5{\cdot}5 \times 10^{-3} - \left(\frac{\gamma - 0{\cdot}75}{2}\right)^2, \qquad (5)$$

where

$$\alpha = \alpha_1 + \alpha_2, \quad \gamma = \alpha_2/\alpha_1, \quad \alpha_1 = (T_g - T_1)/T_g,$$

and

$$\alpha_2 = (T_2 - T_g)/T_g.$$

This expression, which is used to obtain E, is accurate to within 5 per cent over the range of experimental interest with E/kT_g between 10 and 35, and γ between 0·75 and 0·9. The value of a can be read from plots of E/kT_g against γ, and finally B, and hence S, is obtained using equation (3).

If retrapping occurs, the value of E can be shown not to be greatly altered, but S will be affected.[11]

A similar analysis can be applied to thermoconductivity curves, provided the recombination lifetime τ varies only slowly with temperature; the thermoconductivity is

$$\sigma = \tau e \mu I, \qquad (6)$$

where μ is the electron mobility.

A variation of τ with temperature will change the values of α and γ, and hence introduce an error in the value of E if equation (5) is used. The temperature dependence of τ could be obtained by comparing the shapes of thermoluminescence and thermoconductivity curves due to electrons released from the same level.

CHARGED THERMOCONDUCTIVITY

In thermoluminescence and thermoconductivity measurements, whereby electron distributions are changed by irradiation so that holes are introduced in deep levels, recombinations can occur which are not detected by either methods. With a sufficiently thin crystal, it is possible, however, to fill trapping levels systematically by applying at low temperature a voltage exceeding that corresponding to the trap filled limit. These levels will in general remain filled until the temperature is raised sufficiently for the electrons to escape into the conduction band. The crystal is of course negatively charged during the process.

If a potential is applied across the crystal, thermoconductivity curves are obtained, which depend on an average time t_c spent by the electrons in the conduction band before reaching the anode instead of on the recombination lifetime. The analysis is simplified if electrons are prevented from entering at the cathode while the traps are being emptied. If ohmic electrodes are used, the voltage applied during the thermoconductivity measurements must be below the trap filled limit. A higher voltage can be permitted if the specimen is provided with an ohmic and a blocking electrode, the ohmic electrode acting as cathode during the trap filling stage and the blocking electrode as cathode during the heating stage.

If the applied potential, V, is large compared with the variation in potential through the crystal due to the trapped charge, a crystal of thickness d, containing a uniform distribution of traps, on average

$$t_c = d^2/2\mu V. \qquad (7)$$

For a 10μ-thick CdS crystal with 10 V applied, $t_c = 5 \times 10^{-10}$ sec if $\mu = 100$ cm^2/V sec. For a trapping cross-section of 10^{-15} cm^2, retrapping becomes appreciable only if the trap density exceeds 10^{17} centres/cm^3, so that in general it does not appear necessary to take retrapping into account.

Also $dn_c/dt \ll n_c/t_c$ so that RANDALL and WILKINS'[4] relation can again be used.

The charged thermoconductivity curve should therefore be given by

$$\sigma = e\mu t_c I \tag{8}$$

and if the simple expression (7) for t_c is substituted, the thermoconductivity is given by

$$\sigma = e\, d^2 I/2V \tag{9}$$

so that in this case the multiplying factor is independent of temperature and an analysis similar to that for the thermoluminescence curves applies. No account has been taken, however, of the effect of the applied and space-charge field on the apparent depths of the traps. A comparison of curves under charged and neutral conditions could yield information on this aspect.

DESCRIPTION OF APPARATUS

The apparatus [Fig. 1(a)] is designed to allow thermoluminescence and thermoconductivity recordings to be taken simultaneously. The crystal is mounted on a glass plate between two indium electrodes in the specimen holder [Fig. 1(b)]. The temperature is measured with two copper–constantan thermocouples in contact with the electrodes. The inner vessel is flushed with nitrogen, and a very slow gas flow is maintained throughout the experiment, the pressure being sufficient to prevent liquid nitrogen entering the crystal chamber.

To ensure that the specimen is efficiently cooled at the start of the experiment, the top is opened to allow the liquid from the Dewar to rise round the specimen chamber (as shown on the diagram). Before the heater is switched on, the liquid is expelled again by closing the tap, so that thermal coupling between specimen and coolant is minimized.

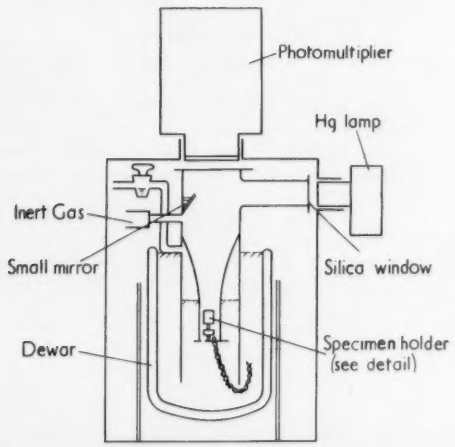

FIG. 1(a). Thermoluminescence–thermoconductivity apparatus.

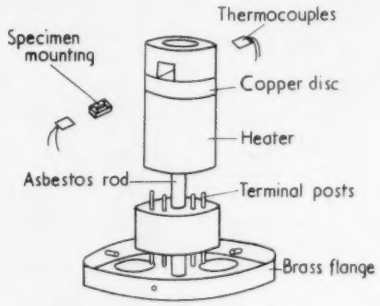

FIG. 1(b). Specimen holder.

The heater supply circuit includes an automatically driven Variac, the heating rate is linear to within 5 per cent between 95 and 350°K and can be varied from 0·1–3°C/sec. Light from the specimen is collected by an E.M.I. 9558 photomultiplier, the output of which is fed to a recorder. Thermoconductivity curves are taken at a potential of about 5 V, and the amplified output recorded.

THERMOCONDUCTIVITY MEASUREMENTS

Thermoconductivity measurements have been made on a plate crystal of CdS, grown by the method of FOCHS[1] and doped with 4×10^{-5} molar fraction of copper. The doping was effected by firing the crystal embedded in CdS powder containing $Cu(NO_3)_2$ at 700°C for 2 hr in an atmosphere of H_2S. The luminescent emission from this specimen was insufficient to allow an analysis of the thermoluminescence curve to be made.

To check the consistency of the results, measurements were made at a number of different heating rates and in each case the peak was analysed by the method[11] outlined above. These results are listed in Table 1.

The main reason for the variations appears to

be the error involved in the temperature measurement. The method is quite sensitive to such errors although not to the same extent as those methods in which a relation is required between $1/T_g$ and other parameters, as β is varied in a series of runs (e.g. Refs. 9 and 12).

With a mean value of $E = 0{\cdot}053$ eV, the value of $a \approx -\frac{5}{2}$, so that S increases with temperatures as $T^{\frac{1}{2}}$, and has an absolute value of 2×10^{-21} $(T/100)^{\frac{1}{2}}$, taking $m^* = 0{\cdot}16m$.[13]

The method allows the capture cross-section at room temperature to be calculated from curves obtained at various temperatures, provided a simple power law is obeyed. In any case, the power law expression can be used to establish the nature of the centre, and then a more appropriate law could be applied to individual cases.

Table 1

°C/sec	T_g(°K)	T_1(°K)	T_2(°K)	α	γ	E(eV)
0·49	100·5	87·5	115	0·274	1·12	0·046
0·64	104·5	92	118	0·249	1·08	0·054
1·1	105	93·5	119	0·243	1·20	0·052
1·2	106	92·5	120	0·259	1·00	0·057

DISCUSSION OF RESULTS

The example taken shows that a may differ considerably from the values of 0 and 2 which are generally assumed. Admittedly the variation in τ with temperature could not be estimated because the equipment was not sufficiently sensitive to obtain a useful thermoluminescence curve with this specimen. Also, the computed curves had to be extrapolated because of the small capture cross-section of the centre and hence the low value of E/kT_g (approx. 6). However, the small value for the capture cross-section and the increase of cross-sections with temperature are consistent with the behaviour of a capturing centre exhibiting coulombic repulsion.[14, 15]

In this case the trapping centre may be complex; a singly charged donor would be expected to exhibit coulombic attraction and to have a much larger trapping cross-section; for such a centre a value $E/kT_g \sim 30$ is often found.

REFERENCES

1. Fochs P. D., *J. Appl. Phys.* **31,** 1733 (1960).
2. Fochs P. D. and Lunn B., to be published.
3. Bube R. H. and Barton L. A., *RCA Review* **20,** 564 (1959).
4. Randall J. T. and Wilkins M. F. H., *Proc. Roy. Soc.* A**184,** 366 (1945).
5. Booth A. H., *Canad. J. Chem.* **32,** 214 (1954).
6. Garlick G. F. J. and Gibson A. F., *Proc. Phys. Soc. Lond.* A**60,** 574 (1948).
7. Grossweiner L. I., *J. Appl. Phys.* **24,** 1306 (1933).
8. Bube R. H., *Photoconductivity in Solids*, p. 293. John Wiley, New York (1960).
9. Haering R. R. and Adams E. N., *Phys. Rev.* **117,** 451 (1960).
10. Lax M., *Phys. Rev.* **119,** 1502 (1960).
11. Keating P. N., to be published in *Proc. Phys. Soc. Lond.*
12. Hoogenstraaten W., *Philips Res. Rep.* **13,** 515 (1958).
13. Piper W. W. and Halsted R. E., *Proceedings International Conference on Semiconductor Physics, Prague* (1960) p. 1046.
14. Gummel H. and Lax M., *Ann. Phys., New York* **2,** 28 (1957).
15. Kalasnikov S. G., *Proceedings International Conference on Semiconductor Physics, Prague* (1960) p. 241.

DISCUSSION

H. A. Klasens: The author assumes for analysis of glow curves a fixed trap depth. A distribution of trap depths would lead to quite different results. A spread in depths can be found from the initial slope of "decayed glow curves". Have such measurements been made?

J. Franks: The theory developed so far applies to

traps of a single depth. The analysis of glow curves has therefore been restricted to isolated peaks, or to peaks which would be resolved by partial emptying techniques.

F. C. BROWN: How do you justify the neglect of retrapping in the analysis of your glow curves?

J. FRANKS: If extensive retrapping occurs, the error introduced in E is small, but the value obtained for the capture cross-section becomes unreliable because, in the determination of E, the effect of retrapping is largely compensated by a change in the apparent capture cross-section.*

* KEATING P. N., *Proc. Phys. Soc. Lond.* to be published.

ol. 22
961

BLANK
PAGE

Vol. 22
1961

J. Phys. Chem. Solids Pergamon Press 1961. Vol. 22, pp. 31–38. Printed in Great Britain.

PHOTOCONDUCTIVITY AND INFRA-RED ABSORPTION IN SILICON IRRADIATED BY NEUTRONS

V. S. VAVILOV, E. N. LOTKOVA and A. F. PLOTNIKOV

P.N. Lebedev Institute of Physics, Academy of Sciences, Moscow, USSR

Abstract—The infra-red absorption and photoconductivity of silicon single crystals irradiated by neutrons were investigated in *p*-type samples. Absorption bands at 1·8 μ, 4·1 μ, 5·9 μ and weaker bands at 3·5 μ and 3·7 μ were found. In *n*-type silicon a band was observed near 1·8 μ along with a band near 3·7 μ which at low temperature was resolved into two at 3·5 μ and 3·7 μ, and a band at 5·5 μ. The photoconductivity spectra in *p*-type crystals correspond to energy levels situated at 100°K near

$$E_v + 0{\cdot}3 \text{ eV } (4{\cdot}1\ \mu)$$
$$E_v + 0{\cdot}33 \text{ eV } (3{\cdot}8\ \mu)$$
$$E_v + 0{\cdot}38 \text{ eV } (3{\cdot}3\ \mu)$$
$$E_v + 0{\cdot}45 \text{ eV } (2{\cdot}8\ \mu)$$

and two levels in the upper part of the forbidden gap:

$$E_c - 0{\cdot}4 \text{ eV } (1{\cdot}62\ \mu)$$
$$E_c - 0{\cdot}16 \text{ eV } (1{\cdot}23\ \mu).$$

The investigation of the kinetics of photoconductivity has made it possible to determine the hole capture cross-section for some of the radiation defects, energy levels.

INTRODUCTION

DATA on energy level positions and other properties of defects formed in silicon single crystals as a result of neutron and electron bombardment were obtained by several authors by electrical measurements,[1, 2] by the investigation of the recombination capture phenomena,[2, 3] and also by the measurements of optical absorption and photoconductivity spectra[4]. Work in the latter direction was also carried out by us at P.N. Lebedev Institute of Physics of the Academy of Sciences of the USSR with the aim of further clarifying the nature of radiation damage. In addition to spectral response measurements, the kinetics of impurity photoconductivity were investigated for several energy levels.

Measurements were made at temperatures between 18°K and 300°K. The method used for transmission measurements is described in Ref. (5).

The condition necessary for the observation of absorption bands corresponding to the electron transitions from the valence band to the level is that the number of empty states is large enough, i.e. the level is weakly populated by electrons at equilibrium. For bands corresponding to the transitions into the conduction band, the inverse condition must be fulfilled. The same considerations are valid for photoconductivity spectra. They can be used as an argument to prove that the analysed part of the extrinsic photoconductivity spectrum is due to volume photoionization and not to the centres on the surface of the crystal. The Fermi level position was determined by Hall effect measurements.

1. THE ABSORPTION IN *n*-TYPE SILICON

The single crystal samples initially had a resistivity $\rho_0 \simeq 0{\cdot}03 \div 0{,}04\ \Omega/\text{cm}$ and contained phosphorus. The fast neutron integral flux ϕ was between 3×10^{17} and 6×10^{17} n/cm^2. Cadmium foils were used as a shield from slow neutrons. In all samples, the carrier concentration decreased and the transmission beyond the fundamental band edge increased accordingly. As cited in the earlier works, a broad band not separated from the fundamental absorption edge appeared, and

also the well-known maximum at 1·8 μ. The absorption bands were found also at 3·7 μ and 5·5 μ. At temperatures lower than 100°K, the 3·7 μ band was resolved into two bands at 3·5 μ and 3·7 μ. Typical transmission spectra for the n-type crystal before and after irradiation are shown in Fig. 1.

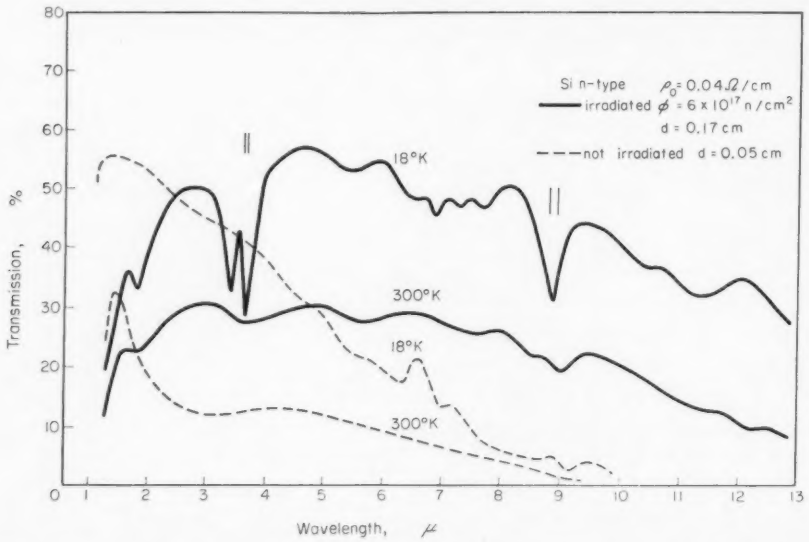

FIG. 1. The transmission spectrum of an n-type silicon sample, $\rho_0 \simeq 0{\cdot}04\ \Omega$/cm, irradiated by 6×10^{17} neutrons/cm^2.

2. THE ABSORPTION IN p-TYPE SILICON

In the spectra of p-type samples containing boron as the acceptor impurity and having initial resistivity $\rho_0 \simeq 0{\cdot}09\ \Omega$/cm at 300°K, bands at 1·8 μ; 3·5 μ; 3·7 μ; 4·1 μ and 5·9 μ, apparently directly connected with radiation damage, were observed. Besides this, in the 6–8 μ region, there were bands not connected with irradiation[6] and near 9 μ there was the well-known band due to oxygen. The intensity of this band decreased after neutron irradiation. In Fig. 2, a part of the p-type silicon absorption spectrum is shown, measured at the temperature 18°K after irradiation by $6{\cdot}10^{17}$ neutrons/cm^2 (fast neutrons with average energy near to 1 MeV).

3. PHOTOCONDUCTIVITY SPECTRA IN p-TYPE SILICON

The photoconductivity spectra measurements were made at a temperature near 100°K with a spectrometer arrangement consisting of an IKS–12 prism monochromator with a mirror focusing unit. The scattered light was eliminated by germanium or silicon filters. As compared with the FAN and RAMDAS experiment, much lower integral neutron fluxes were used (10^{13}–10^{15} n/cm^2).[7] A typical photo-response spectrum of a crystal irradiated by a flux $\phi \simeq 10^{14}$ n/cm^2 is shown in Fig. 3(a).

The spectrum of this sample and also all the spectra of the irradiated p-type crystals having the Fermi level at the experimental conditions at 0·1 ÷ 0·25 eV from the valence band, show a maximum of rather unusual form between 0·3 and 0·35 eV (4·1–3·6 μ). The spectra of this type were observed for samples with initial resistivities

$\rho = 10\ \Omega$/cm, $\phi = 10^{14}$ and 10^{15} n/cm^2
$\rho = 40\ \Omega$/cm, $\phi = 10^{14}$ n/cm^2
$\rho = 100\ \Omega$/cm, $\phi = 10^{13}$ and 10^{14} n/cm^2.

Figure 3(a) shows the positions of levels in the lower half of the forbidden gap, corresponding to the results of the experiment.

Figure 3(b) shows, in semi-logarithmic scale, the photoconductivity spectrum typical for p-type

Vol. 2
1961

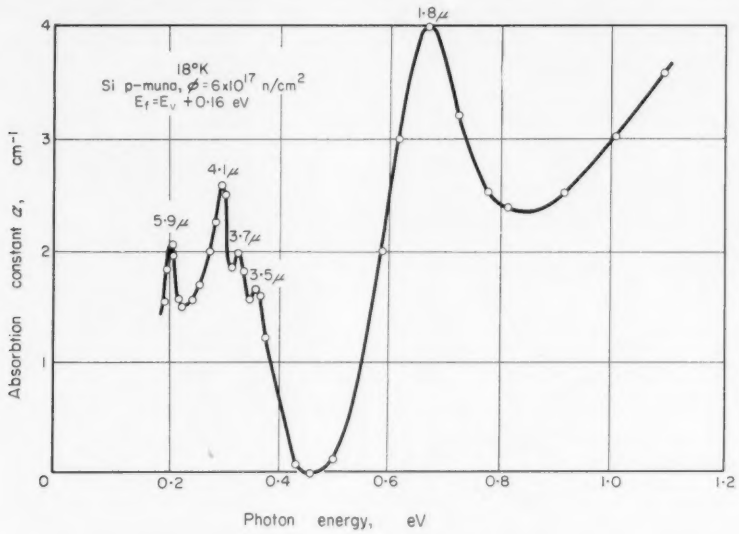

FIG. 2. The absorption spectrum of a p-type silicon sample; $\rho_0 \simeq 0{\cdot}09\ \Omega$/cm, irradiated by 6×10^{17} neutrons/cm^2. Fermi level position $E_f \simeq E_v + 0{\cdot}16$ eV. Measurements at 18°K.

samples having the Fermi level between $E_v+0{\cdot}3$ and $E_v+0{\cdot}33$ eV. Spectra of this type were measured for crystals with initial values of ρ:

$\rho = 40\ \Omega$/cm, $\phi = 10^{15}$ and 10^{16} n/cm^2
$\rho = 100\ \Omega$/cm, $\phi = 10^{15}$ n/cm^2.

In this case there is no maximum and in its place a more usual "step" corresponding to a photoionization energy of 0·33 eV is seen.

As it is known from the experiments with irradiated germanium crystals, extrinsic photoconductivity may result from the photoionization of centres on the crystal surface. We think that the data of Fig. 4 show that the effects observed in our experiments result from the photoionization in the volume of samples. As was shown in the case when the Fermi level in the irradiated sample lies at 0·36 eV from the valence band, the part of spectrum due to the two lower levels of defects disappears. The same argument shows positively that the levels are situated in the lower half of the forbidden gap. Control experiments with samples of varying dimensions and with bars of p-type silicon having an n-type layer made by phosphorus diffusion over the entire surface except at the ends gave the same photoconductivity spectra.

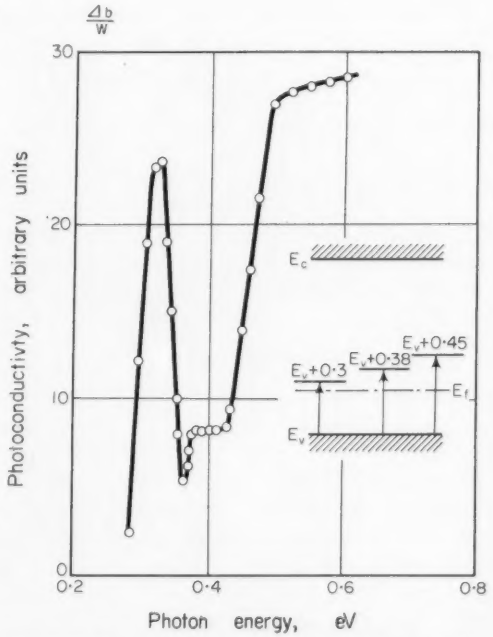

FIG. 3(a). Photoconductivity spectrum in p-type silicon irradiated by 10^{14} neutrons/cm^2. Measurements at 100°K; $E_f = E_v + 0{\cdot}25$ eV.

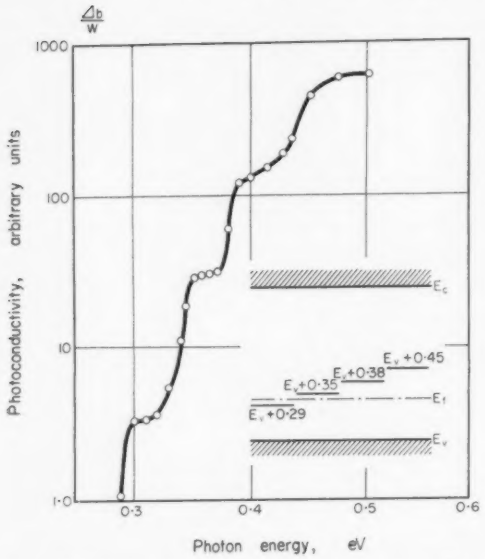

FIG. 3(b). Photoconductivity spectrum in p-type silicon irradiated by 10^{15} neutrons/cm^2. Measured at 100°K; $E_f = E_v + 0{\cdot}32$ eV.

The last of the photoconductivity spectra given in Fig. 5, in the photon energy range between 0·4 and 1 eV, shows that in the upper half of the forbidden gap, near $E_c - 0{\cdot}4$ eV and $E_c - 0{\cdot}16$ eV, there are two more energy levels.

3. THE KINETICS OF IMPURITY PHOTOCONDUCTIVITY

The study of photoconductivity kinetics in the samples, spectra of which were given in the above, made it possible to determine the capture cross-section of holes σ_p by the centres with levels at

$$E_v + 0{\cdot}3 \text{ eV};\ E_v + 0{\cdot}38 \text{ eV};\ E_v + 0{\cdot}45 \text{ eV}.^{(8)}$$

At 100°K, the samples had high resistivity. The equilibrium concentration of holes p_0 did not exceed 8×10^8 cm^{-3} at $E_f \simeq E_v + 0{\cdot}25$ eV. Thus, the initial concentration of holes at the defect level practically coincides with the centres' concentration and the thermal exchange can be neglected. The kinetics of photoconductivity is described by the equation

$$\frac{d\Delta p}{dt} = (m_0 + \Delta p)\beta q J - \gamma \Delta p\,(P_{vm} + M_0 - m_0 + \Delta p + p_v), \quad (1)$$

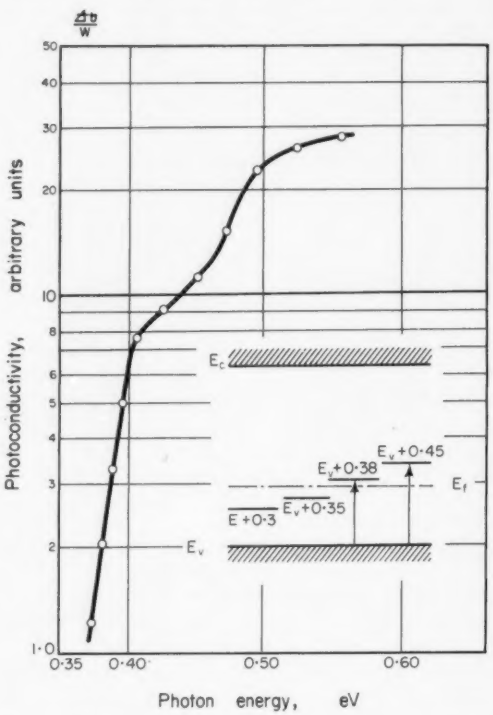

FIG. 4. Photoconductivity spectrum in p-type silicon irradiated by 10^{16} neutrons/cm^2. Measurement at 100°K; $E_f = E_v + 0{\cdot}36$ eV.

where

m_0 is the initial concentration of holes at the level M, equal to the concentration of centres M_0;

Δp is the excess hole concentration;

q is the photon absorption cross-section for the transition to the level M;

β is the quantum yield taken to be unity;

γ is the recombination coefficient:

$\gamma = 1/\sigma_p V$ where V is the holes' thermal velocity;

p_{vm} is the hole concentration reduced to the M-level;

$$p_{vm} = p \exp\left(-\frac{\Delta E_m}{kT}\right).$$

The solution of this equation in the case of excitation by a rectangular light pulse, for the increase of hole concentration Δp_H and for the

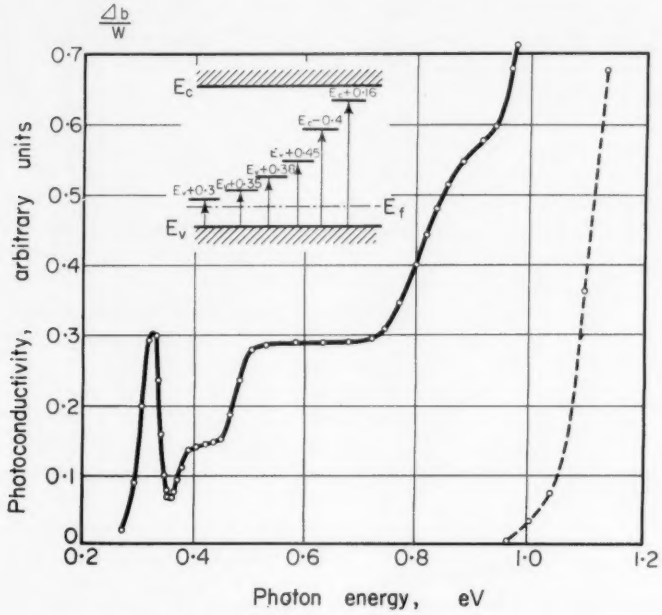

FIG. 5. Photoconductivity spectrum in p-type silicon irradiated by 10^{14} neutrons/cm^2 in the photon energy region up to 1 eV. Measurement at 100°K. Dotted line: photoconductivity before irradiation.

decrease after the excitation is over, Δp_c is

$$\Delta p_H = \frac{A \tanh \alpha t}{1+\beta \tanh \alpha t}, \tag{2}$$

where

$$A = \frac{2m_0 qJ}{\gamma\left(p_0+\frac{qJ}{\gamma}\right)\sqrt{\left(1+\frac{4m_0 qJ}{\gamma(p_0+qJ/\gamma)^2}\right)}}, \tag{2a}$$

$$B = \frac{P+\frac{qJ}{\gamma}}{\left(p_0+\frac{qJ}{\gamma}\right)\sqrt{\left(1+\frac{4m_0 q\ J}{\gamma(p_0+qJ/\gamma)^2}\right)}}, \tag{2b}$$

$$\alpha = \frac{\gamma\left(p_0+\frac{qJ}{\gamma}\right)\sqrt{\left(1+\frac{4m_0 qJ}{\gamma(p_0+qJ/\gamma)^2}\right)}}{2}, \tag{2c}$$

$$\Delta p_c = \frac{\Delta p_{ct}\exp(-\gamma p_0 t)}{1+\frac{\Delta p_{ct}}{p_0}[1-\exp(-\gamma p_0 t)]}, \tag{3}$$

and the stationary value of the hole concentration increase

$$\Delta p_{ct} = \frac{1}{2}\left(p_0+\frac{qJ}{\gamma}\right)\left[\sqrt{\left(1+\frac{4m_0 qJ}{\gamma(p_0+qJ/\gamma)^2}\right)}-1\right] \tag{3a}$$

For the condition $\Delta p_{ct} \ll m_0$, which is fulfilled in our case, the initial slopes of the curves

$$\frac{d\Delta p_H}{dt} \text{ and } -\frac{d\Delta p_c}{dt}$$

are equal, and

$$\frac{d\Delta p_H}{dt} = -\frac{d\Delta p_c}{dt} = m_0 qJ. \tag{4}$$

If the excess concentration of holes Δp is small enough, i.e. $\Delta p \ll p_0$, the formulae given are simplified and the expressions for Δp_H and Δp_c become exponential functions of time.[9]

In our experiments, however, the expressions (1–4) in their general form had to be used.

One can analyse an oscillographic record of the decrease of photoconductivity, $\Delta p_c = f(t)$; if the stationary excess concentration Δp_{ct} and the initial slope of the curve are known, one can compare the computed dependence with experiment.

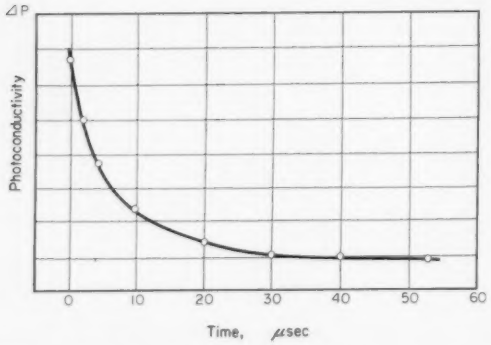

FIG. 6. The relaxation of extrinsic photoconductivity due to electron transitions to the level: $E_v+0{\cdot}3$ eV. Solid line: experiment; dots are computed by choosing the appropriate γ value.

For instance, dots in Fig. 6 were computed by choosing appropriate γ-values. In the case of coincidence with experiment, the value of hole capture cross-section $\sigma_p = v^{-1}\gamma^{-1}$ was found.

Our measurements gave the following values of σ_p with the error of $\pm$ 50 per cent.

Level:	$E_v+0{\cdot}3$ eV	$E_v+0{\cdot}38$ eV	$E_v+0{\cdot}45$ eV
σ_p (cm^2)	3×10^{-14}	7×10^{-17}	10^{-17}

DISCUSSION

Comparing the system of defect levels in silicon irradiated by electrons, based mostly on electrical measurements and shown on the left side of Fig. 7, with a similar system constructed from the data of optical experiments, i.e. absorption and photoconductivity spectra, one can see a rather good correspondence; one has to add that the right side of the picture is based mostly on neutron irradiated samples. There is a good correspondence between the results of FAN and RAMDAS and our results for absorption, with exception of the following two facts.

(a) The presence of weak absorption bands in p-type crystals at 3·5 μ and 3·7 μ in our experiments.

(b) The presence of the 1·8 μ band not only in irradiated samples, but also in unirradiated n-type silicon at 100°K.

The first fact cannot be explained by n-type inversion layers on the surface or by the existence of n-type inclusions in the volume; moreover, the absorption data are confirmed by photoconductivity spectra.

As it is seen from Fig. 7, the positions of deep levels determined optically or by electrical measurements (Hall effect, recombination experiments) generally coincide. The levels $E_v+0{\cdot}3$ eV and $E_c-0{\cdot}16$ eV are a good example.

However, the investigation of photoconductivity indicates the existence of a number of centres with other photoionization energies. This is a result of the greater sensitivity of photoelectric experiments.

The final identification of the nature of defect levels, of course, requires further experimental work.

A tentative explanation of the maximum in the 0·3–0·35 eV region for p-type samples as suggested by SMIRNOV, is that the uncontrolled gold impurity recombination level situated at $E_v+0{\cdot}35$ eV probably reduces the photoconductivity after the photon energy exceeds 0·35 eV when the concentration of defects is small enough. If the number of defects increases sufficiently with irradiation dose, the minimum induced by gold disappears.

According to our experiment, the hole capture cross-section for the level $E_v+0{\cdot}3$ eV in p-type silicon

$$\sigma_p \simeq 3\times10^{-14}\ \text{cm}^2.$$

This may be compared with the value given by WERTHEIM[2] for the level at the same position in n-type silicon:

$$8\times10^{-13}\ \text{cm}^2.$$

This larger cross-section may be due to the

Vol. 22
1961

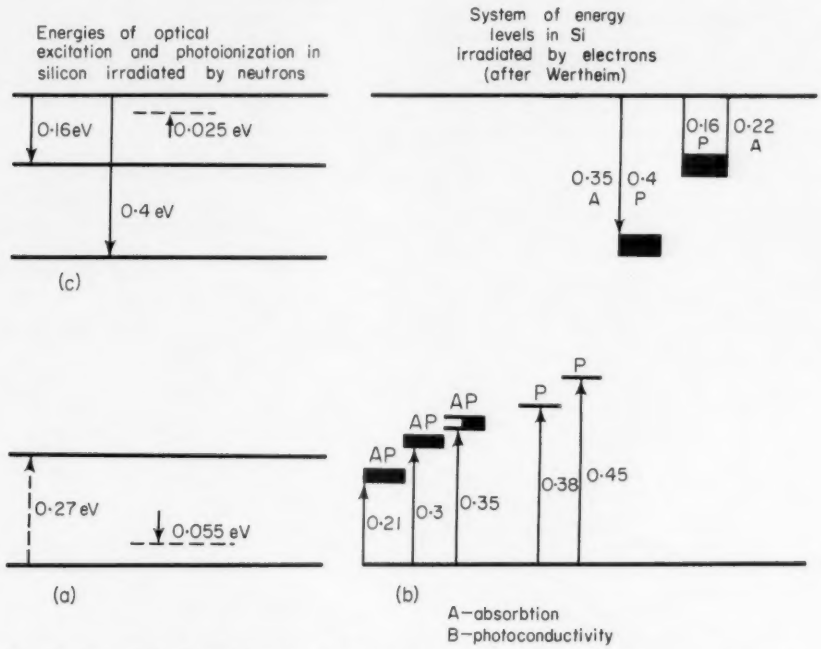

FIG. 7. Energy level positions in silicon irradiated by fast electrons (determined by electrical measurements). Energies of optical excitation and photoionization in silicon irradiated by neutrons.

A—absorption measurements. P—photoconductivity.

coulomb interaction, or the temperature dependence of the cross-section.

Our data on the existence of the 1·8 μ absorption band in n-type samples with the Fermi level near $E_c - 0{\cdot}15$ eV do not agree with the interpretation of KLEIN[1] who attributed this band to transitions from the level at $E_v + 0{\cdot}16$ eV to the excited state level near $E_v - 0{\cdot}3$ eV.

We feel that a clear picture of radiation damage in silicon will require further experiments, particularly the experiments with dislocation-free and oxygen-free samples.

Acknowledgements—The authors express their sincere gratitude to B. M. VUL, N. N. SOBOLEV, S. M. RYVKIN and L. S. SMIRNOV for the discussion of the results and L. SMIRNOVA for Hall effect measurements.

REFERENCES

1. KLEIN C., *J. Appl. Phys.* **30,** 1222 (1959).
2. WERTHEIM G., *J. Appl. Phys.* **30,** 1166 (1959).
3. GALKIN G. N., RYTOVA N. S. and VAVILOV V. S., *Zh. Fiz. Te. Tekh.* **2,** 2025 (1960).
4. FAN H. and RAMDAS A., *J. Appl. Phys.* **30,** 1127 (1959).
5. LOTKOVA E. N. and FRADKOV A. B., *P.t.e.* No. 1 (1961).
6. VAVILOV V. S., *Zh. Fiz. Te. Tekh.* **2,** 374 (1960).
7. VAVILOV V. S. and PLOTNIKOV A. F., *Zh. Fiz. Te. Tekh.* (1961), in press.
8. PLOTNIKOV A. F., VAVILOV V. S. and SNURNOV L. S. *Zh. Fiz. Te. Tekh.* (1961), in press.
9. RYVKIN S. M., *Semi-conductors in Science and Engineering*, No. 2 (1958).

DISCUSSION

I. T. STEINBERGER: Were there any differences in the photoconductivity excitation spectrum observed if the time sequence of the measurement was changed, i.e. from the long wavelengths to the short ones or *vice versa*?

V. S. VAVILOV: There was no difference. Moreover, there was no difference between the shapes of spectra at 9 c/s and those obtained with unmodulated light.

G. F. J. GARLICK: (1) What temperature was reached

by the silicon crystals during neutron irradiation? (2) It would be interesting to use short wavelength excitation of specimens with high Fermi level to empty levels below the latter and then to explore transitions into the levels to see whether the resulting photoconduction spectrum shows sharp peaks, as it does in specimens with lower Fermi levels.

V. S. VAVILOV: (1) The temperature during irradiation did not exceed 50°C. (2) We plan to do the experiment mentioned by you since it may give the data necessary for the explanation of the peak observed.

H. Y. FAN: In the spectral photoconductivity curve which shows peaks, is the photo-response normalized for constant intensity of *incident* radiation or for a constant number of *absorbed* photons? In the former procedure, variations in the curve may result simply from the variations of transmission. When normalized for constant number of absorbed photons, the curve would be expected to show steps rather than sharp peaks and valleys, unless sharp variations of some competing, non-photoconductive absorption are present.

V. S. VAVILOV: The curves are normalized to *incident* light. However, control experiments on transmission have definitely shown that in the region of the unusual minimum there are no appreciable absorption or reflection peaks which could produce the effect mentioned by you.

Vol. 22
1961

J. Phys. Chem. Solids Pergamon Press 1961. Vol. 22, pp. 39–43. Printed in Great Britain.

RECOMBINATION PROCESSES IN SILICON DOPED WITH Ga, In AND Sb

Y. E. POKROVSKY and K. J. SVISTUNOVA

Institute of Radio and Electronics, Academy of Sciences, Moscow, USSR

Abstract—The temperature and concentration dependence is studied of the excess charge carrier's lifetime in Si doped with Ga, In and Sb. The elements listed do not show any significant influence on the recombination rate of the minority carriers. Trapping is observed in In-doped *n*-type silicon due to the hole capture by negatively charged In centers. The hole capture cross-section is equal approximately to 2×10^{-16} cm^2 at 80°K and is but weakly temperature dependent. The electron capture cross-section of neutral In centers is 4×10^{-22} cm^2 at 80°K and increases with decreasing temperature. Recombination radiation accompanying the electron capture by In atoms is studied quantitatively; the capture cross-section is shown to be determined by radiative transitions.

THE RECOMBINATION processes in silicon doped with the elements of Groups III and V are of great interest, since the elements in question possess but one energy level in the forbidden region. Therefore the interpretation of the experimental results may be expected to be especially simple in this case. In this paper we report the data on the influence of Ga, In and Sb on the recombination of excess carriers in silicon.

The monocrystalline silicon samples were pulled and doped by floating zone technique. The impurity concentration was measured by Hall effect in the temperature range 50°–500°K. In the same range, photoconductivity decay measurements were done using both intrinsic and extrinsic excitation.

The lifetime in Si doped with Ga, In and Sb decreases slightly with decreasing temperature and is practically independent on the doping impurity concentration in a large range of its values. The presence of such a concentration plateau means that the minority carriers capture cross-sections of Ga, In and Sb are small and the recombination rate is determined by some other imperfections which are present in the samples in constant amount. The relevant data for the *n*-type silicon samples doped with both In and Sb are shown in Table 1. It is seen that at 300°K all the samples are characterized by the same lifetime value, independent on the doping impurity concentration. Yet on lowering the temperature the photoconductivity decay time τ increases exponentially (see Fig. 1). The activation energy for this process is close to 0·16 eV, corresponding to the In ionization energy.[1] When the temperature becomes lower than 100°K, the exponential growth of τ is replaced by a weak temperature dependence.

This type of the τ temperature dependence is due to a great difference between the electrons' and holes' capture cross-sections of In. When the excess charge carriers of both signs are introduced, the holes are captured quickly by negatively charged In ions. The electron capture cross-section of neutral In atoms is small and the excess conductivity decay rate is controlled by the hole emission from In into the valence band, with subsequent pair recombination via some other centers. When the temperature is low enough and the thermal ionization of In is insignificant, it is the rate of electron capture by neutral In atoms that determines the excess conductivity decay time constant. Thus the In provides trapping in *n*-type silicon, practically all the excess conductivity being due to excess electrons.

To explain the experimental results quantitatively, the excess conductivity decay was considered in *n*-type silicon containing indium and

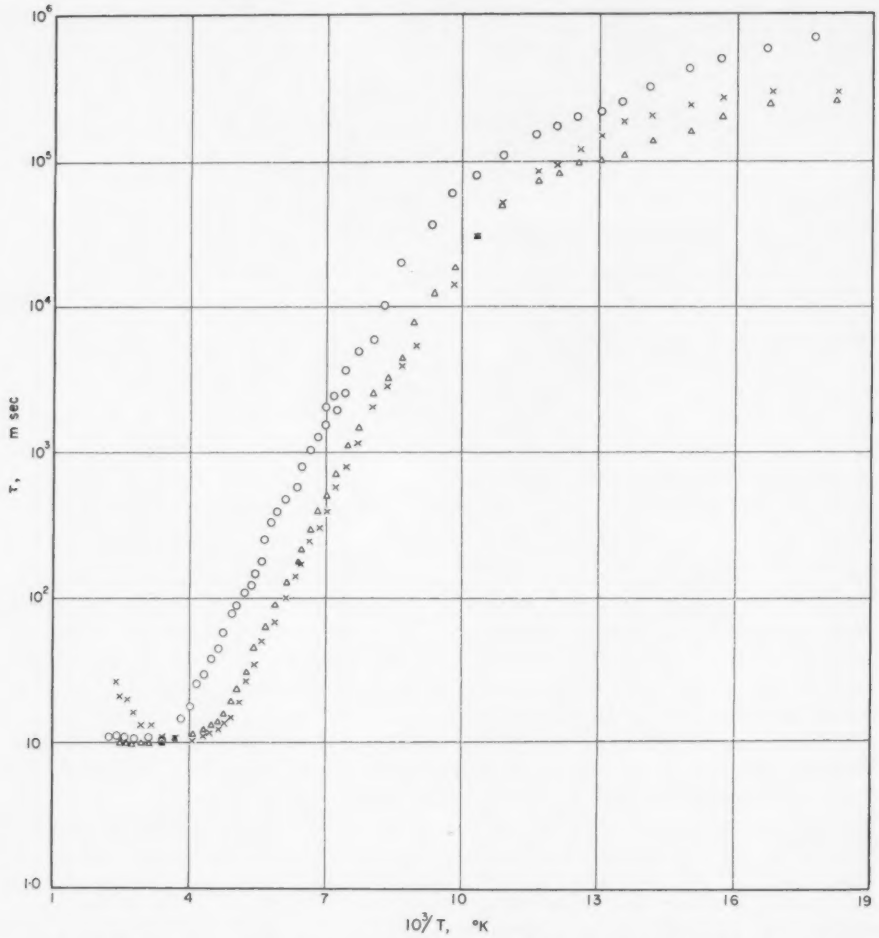

FIG. 1. Temperature dependence of the photoconductivity decay time in silicon doped with both In and Sb. × △—sample 9-*B*, —sample 26-*B*, ○—sample 27-*B*.

some other recombination centers.[2] The calculations show that at relatively high temperatures

$$\tau = \tau_{po}\left(1+\frac{N_t}{P_1^t}\right), \qquad (1)$$

where N_t is the In concentration, P_1^t is the hole concentration when the Fermi level coincides with the In level, and τ_{po} is the lifetime of holes in heavily doped n-type silicon. This relation fits well to the experimental data if $\tau_{po} = 1\times10^{-5}$ sec and P_1^t is calculated with $E_t - E_v = 0{\cdot}16$ eV and assuming that the density of states mass is approximately equal to m_0.

At the other limiting case of low temperatures, another relation is applicable:

$$\tau = \frac{1}{S_n^t v n_0}. \qquad (2)$$

Here v is the mean electron thermal velocity; n_0, the equilibrium electron concentration; and S_n^t the electron capture cross-section of the neutral In atom. The corresponding S_n^t versus temperature

Vol. 22
1961

curve calculated from the data of Fig. 1 is shown in Fig. 2. In course of the calculation, m_e was taken equal to m_0. The value of S_n^t at 80°K is 4×10^{-22} cm^2 and increases on cooling. Though its temperature dependence for all the three samples is satisfactorily described by the T^{-3} law (the straight line in Fig. 2), we do not think it is yet possible to obtain the exact temperature dependence, since the temperature range in question is rather small.

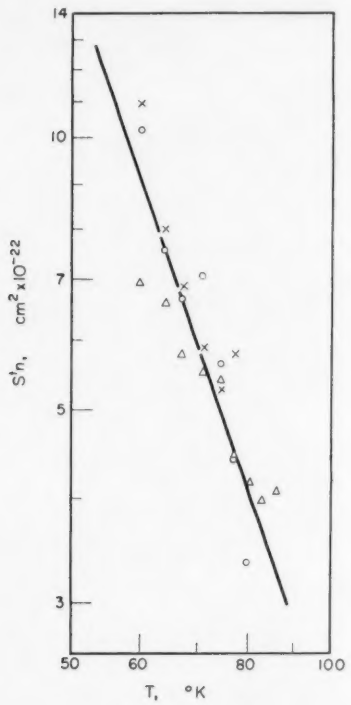

FIG. 2. Temperature dependence of the electron capture cross-sections of In atoms. ×—sample 9-*B*, △—sample 26-*B*, ○—sample 27-*B*.

To make clear the nature of elementary processes governing the S_n^t value, the quantitative study was carried through of the recombination radiation accompanying the electron transitions from the conduction band to the neutral In atoms. Such a radiation had been observed by HAYNES and WESTPHAL[3]; yet it had not been made clear to what extent the radiative transitions determine the recombination rate.

The recombination radiation was studied for the two samples at 80°K. The monochromator was used to generate the electron–hole pairs. The intrinsic excitation was used and there was no light in the frequency range where the recombination radiation was being observed. The image of the sample was focussed on the entrance slit of the spectrometer. The image of the exit spectrometer slit was focussed on the PbS photo-resistor registering the recombination radiation.

The spectral distribution of recombination radiation is shown in Fig. 3. The radiation maximum corresponds to the photon energy of 0·97 eV—in satisfactory agreement with the value given up in the electron transition from the conduction band to the indium atom.

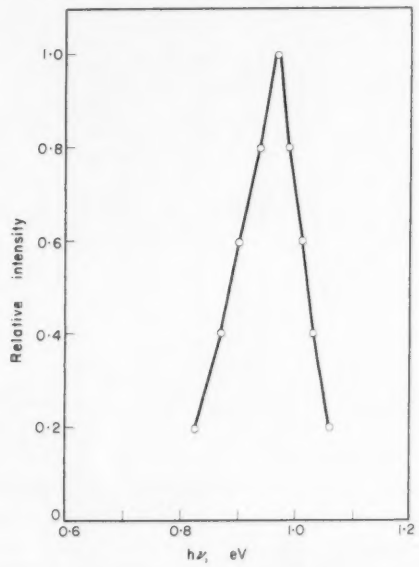

FIG. 3. Spectral distribution of the recombination radiation.

The recombination radiation intensity was measured to determine the quantitative relation between the number of emitted photons and the number of recombination acts. To this end, the nichrome band was placed into the cryostat instead of the sample. The band was current-heated and had the dimensions and the form of the sample. Its temperature was measured by the thermocouple. The band radiation had been calibrated

beforehand by the black-body radiation. The band temperature was regulated so as to make the signal from band radiation equal to that of the recombination radiation. The optical geometry having been the same in both cases, the recombination radiation intensity from the unit sample area, I, was equal to that of the band radiation in the given spectral range. It could, therefore, be easily calculated.

The number of recombination acts per unit time was determined experimentally. The recombination radiation intensity was calculated under the assumption that every recombination act is accompanied by a single photon emission and the radiation is isotropic. The reflection at the sample surface was taken account of in calculations.[4] The measured (I) and calculated (I_0) intensities of the recombination radiation are given in Table 2. It is seen that practically all the capture acts proceed via the photon emission. Thus the electron capture cross-section of neutral In atoms is governed by radiative transitions.

The hole capture cross-section, S_p^t, of negatively charged In centers was estimated by the extrinsic photoconductivity decay in p-type silicon. The samples were illuminated by short pulses through the germanium filter. The samples contained, besides In, some residual shallow acceptors in the concentration from 10^{12} to 10^{13} cm^{-3} determining the hole concentration p_0 at low temperatures. In this case, the extrinsic photoconductivity decay time constant, τ, was given by the simple relation:

$$\tau = \frac{1}{S_p^t v p_0} \tag{3}$$

From equation (3), the hole capture cross-sections of In were calculated for different samples, having different values of N_t and p_0, under the assumption that $m_h = m_0$. S_p^t turned out approximately equal to 2×10^{-16} cm^2 at 80°K and was but weakly temperature dependent.

Thus the hole capture cross-section exceeds that of electrons by almost six orders of magnitude. Such a big difference may be understood. Really, the hole is captured by a negatively charged In ion. In this case, the capture cross-section may be controlled by the phonon cascade process[5] which explains the large cross-sections of deep traps. The electron is captured by a neutral indium atom and the energy of about 1 eV has to be given up. In this case, for the cascade process to be possible a sufficient number of excited states is necessary. It may happen that there are not enough levels in a potential well due to the polarization of the neutral center. According to the experiments discussed above, here the dominant

Table 1

Sample number	9-*B*	26-*B*	27-*B*
Indium concentration (cm^{-3})	$1{\cdot}4 \times 10^{15}$	$4{\cdot}5 \times 10^{15}$	6×10^{16}
Electron concentration at $T = 300$°K (cm^{-3})	$5{\cdot}8 \times 10^{15}$	$2{\cdot}3 \times 10^{16}$	$2{\cdot}7 \times 10^{16}$
τ at $T = 300$°K (μ sec)	11	11	10

Table 2

Sample number	26-*B*	27-*B*
Calculated intensity I_0 (W/cm^2)	$1{\cdot}25 \times 10^{-5}$	$4{\cdot}4 \times 10^{-6}$
Observed intensity I(W/cm^2)	$1{\cdot}10 \times 10^{-5}$	$4{\cdot}3 \times 10^{-6}$

Vol. 2
1961

process is the radiative transition. The theoretical estimate made by BONCH-BRUEVICH[6] shows that radiative transitions may really happen often enough to explain the experimental data.

Acknowledgement—The authors wish to thank Professor S. G. KALASHNIKOV for a constant interest in their work and for a discussion of results.

REFERENCES

1. BURTON J. A., *Physica* **20,** 845 (1959).
2. POKROVSKY J. E. and SVISTUNOVA K. J., *Solid State Phys.* **3,** 757 (1961).
3. HAYNES J. R. and WESTPHAL W. C., *Phys. Rev.* **101,** 1676 (1956).
4. BRIGGS H. B., *Phys. Rev.* **77,** 287 (1950).
5. LAX M., *Phys. Rev.* **119,** 1502 (1960).
6. BONCH-BRUEVICH V. L., private communication.

DISCUSSION

M. G. A. BERNARD: Have you any evidence that the radiative capture of In atoms for electrons is phonon assisted?

S. G. KALASHNIKOV: From the experiments described, one can only conclude that within the experimental error, the energy released turns into radiation energy.

A. ROSE: Is it possible that the very small capture cross-section for electrons ($10^{-21}/cm^2$) means that the In capturing center is negatively charged?

S. G. KALASHNIKOV: According to the generally accepted model of Group III elements in silicon, indium can take on only a single electronic charge and therefore must be neutral when it is capturing an electron.

BLANK
PAGE

Vol. 2
1961

J. Phys. Chem. Solids Pergamon Press 1961. Vol. 22, pp. 45–50. Printed in Great Britain.

RECOMBINATION PROPERTIES OF MANGANESE AND GOLD IN GERMANIUM

V. G. ALEXEEVA, S. G. KALASHNIKOV, I. V. KARPOVA and E. G. LANDSBERG

Institute of Radio and Electronics, Academy of Sciences, Moscow, U.S.S.R.

Abstract—Measurements are made of the photoelectromagnetic effect and photoconductivity in *n*- and *p*-type Ge doped with Au and Mn in the temperature range ~ 330–90°K. The Au capture coefficients at 300°K are found to be: $\alpha_n^0 = 5\times10^{-10}$, $\alpha_n^- = 2\times10^{-9}$, $\alpha_p^= = 1\times10^{-7}$ (cm³/sec); while for Mn one obtains: $\alpha_n^0 = 2\times10^{-9}$, $\alpha_n^- = 4\times10^{-10}$, $\alpha^= = 6\times10^{-10}$ (cm³/sec). The $\alpha^=$ temperature dependence is of the form T^{-n}, where $n = 3{\cdot}5$ for Au and 4·5 for Mn. α_n^0 and α_n for Mn, as well as α_n^0 for Au, are but weakly temperature dependent. The α-values obtained are in agreement with the analyses of the trapping phenomena in *n*-type samples. The experimental results are discussed and compared with the data given by other authors.

INTRODUCTION

THE RECOMBINATION properties of gold atoms in Ge have been studied recently by various authors.[1–4] Some data on Mn in Ge are given in Refs. (3–5). Yet the information obtained up till now is not complete enough. Thus the capture coefficients* α_n^0 of Au, given in Refs. (1) and (2), differ by more than two orders of magnitude; the temperature dependence as well is not known for all the coefficients. In the Mn case, there are quantitative data on one of the coefficients only.[3] Therefore we continued studying the recombination properties of gold and manganese in germanium in more detail.

EXPERIMENT

The lifetimes were measured by photoelectromagnetic (τ_{PEM}), photoconductivity (τ_{PC}), and by the ratio methods (τ_C). The measurements were made under the following conditions.

(1) The Hall angles were small enough.

(2) The one-dimensional case: the length of the illuminated region was much more than the diffusion length; the contact regions were shaded; and the width of the sample was much more than its thickness.

(3) The linear recombination law. This was checked by independence of τ on the light intensity.

(4) The surface generation of pairs. The diffusion length in all the samples in the whole temperature range was considerably more than the Debye length as well as the light penetration length. The generation rate was determined by comparing the τ_{PEM}, τ_{PC} and τ_C values in the absence of trapping. The concentration of gold was varied from 3×10^{13} to $1{\cdot}1\times10^{15}$ cm^{-3}, and of manganese from 5×10^{13} to $1{\cdot}1\times10^{15}$ cm^{-3}.

No significant trapping was observed in the *p*-type samples. Therefore the lifetime in this case was measured by the ratio method. The *n*-type samples showed strong trapping at low temperatures; therefore τ_{PEM} and τ_{PC} were measured. The unimportance of surface recombination was checked by a special device in a vacuum cryostat, allowing the introduction of the dry nitrogen into the sample container. The recombination was ascribed to bulk effects when the PEM and PC signals were the same both *in vacuo* and in nitrogen atmosphere.

The mobility of majority carriers was obtained in all cases by Hall and resistivity measurements. The majority to minority mobilities' ratio was taken from Ref. (6). No difference was made between the Hall and drift mobilities.

The samples were cut out of the ingots

* The capture coefficient is defined as the capture cross-section times the thermal velocity. The lower index shows the type of the carrier captured; the upper one, the charge state of the center before the capture.

perpendicular to the growth direction [111]. The gold used had a purity of 99·99 per cent and was taken from two different sources. The results were the same for different sources. The manganese purity was the same as that of gold. Dislocation density in the crystals used, as determined by etch pits, was of the order of 10–10^3 cm^{-2}.

p-TYPE

The typical lifetime versus temperature curves for the two *p*-type samples containing gold and manganese are shown in Fig. 1. The presence

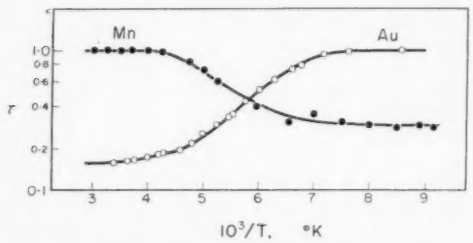

FIG. 1. The lifetime temperature dependence in *p*-type samples. ○—gold (in units of the low temperature τ values). ●—manganese (in units of the high temperature τ value).

of the two plateaus is characteristic. The lifetime values at each of them are inversely proportional to the Au (or Mn) concentration, N_t, this showing that the effect is really due to the impurities under study.

The data obtained are in good agreement with the model of recombination through the two energy levels. The presence of the two plateaus on the curves of Fig. 1 means that for Mn the coefficients α_n^0 and α_n^- are but weakly temperature dependent. The same is true for the α_n^0 in the Au case. The α_n^- temperature dependence for Au cannot be obtained reliably since the high temperature plateau is observed only in the small temperature range. The capture coefficients are determined from the relations:

$$\tau_{no1} = (\alpha_n^0 N_t)^{-1}, \quad \tau_{no2} = (\alpha_n^- N_t)^{-1}, \qquad (1)$$

where τ_{no1} and τ_{no2} are the lifetime values corresponding respectively to the low- and high-temperature plateaus. The data obtained are shown in Tables 1 and 2.

Our value of α_n^0 for Au is in satisfactory agreement with the data of Ref. (2) and is about 10^3 times less than that given in Ref.(1) Our α_n^- value (at 300°K) coincides exactly with the result of Ref. (2); it agrees also with the value obtained in Ref. (1) at 90°K if account is taken of the temperature dependence observed there.

Table 1. *Gold*

Capture coefficient	Temperature (°K)	Value (cm^3 sec^{-1} ×10^9)	Temperature dependence
α_n^0	90	0·5	~ constant
α_n^-	300	2	—
$\alpha_p^=$	300	100	$T^{-3.5}$

Table 2. *Manganese*

Capture coefficient	Temperature (°K)	Value (cm^3 sec^{-1} ×10^9)	Temperature dependence
α_n^0	90	2	~ constant
α_n^-	300	0·4	~ constant
$\alpha_p^=$	300	0·6	$T^{-4.5}$

The solid curves in Fig. 1 are the theoretical ones. In calculating them, use was made of the experimental τ_{no1} and τ_{no2} values as well as of the equilibrium hole concentration, p_0. The curves have as parameters the energy of the first Au (Mn) acceptor level and the statistical weight ratio, g_0/g_1, for this level in the empty and occupied states. For Au, we take $g_0/g_1 = 8{\cdot}5$[9], the energy level being determined by fitting the theoretical curve to the experimental data. For the six crystals investigated, the level values lie in the range 0·14–0·15 eV. For Mn, both parameters are varied; the results are quite consistent with the level value of 0·15 eV. The values thus obtained are in satisfactory agreement with the data on the lowest Au and Mn acceptor levels given in the literature[5]. The results just described are given in more detail elsewhere[7,8]

n-TYPE

Figure 2 shows the τ_{PEM} and τ_{PC} versus temperature curves for one of the samples containing

Vol. 22
1961

gold. The curves for Mn are analogous. In both cases, τ_{PEM} and τ_{PC} being equal at room and higher temperatures become significantly different on lowering the temperature. This shows that strong trapping of minority carriers (holes) comes into play. On raising Au (or Mn) concentration the difference between τ_{PEM} and τ_{PC} increases, that

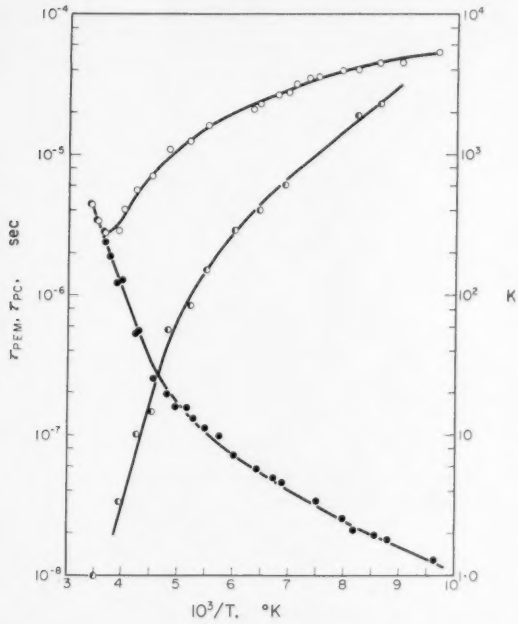

FIG. 2. The temperature dependence of τ_{PEM}(●), τ_{PC}(○) and the trapping factor $k = \tau_{PC}/\tau_{PEM}$(◐) n-type gold-doped sample, $N_t = 3\times10^{13}$ cm^{-3}, $n_0 = 1{\cdot}7\times10^{14}$ cm^{-3}. The solid k-curve is calculated (see text).

is the trapping becomes stronger, and at the same time τ_{PEM} is reduced. This means that Au and Mn atoms act simultaneously as trapping centers and as recombination centers.

The results obtained are consistent with the concept that both recombination and trapping are due mainly to a single level, namely the second acceptor level ($E_c - E_t = 0{\cdot}20$ eV for Au, $E_c - E_t = 0{\cdot}37$ eV for Mn). It is known that τ_{PEM} does not depend on trapping and coincides with the lifetime of the Hall–Shockley–Read theory for the small trap concentration [see, for instance, Ref. (10).] This means that in the low temperature part of the Fig. 2 we have

$$\tau_{PEM} = (\alpha_p^{=} N_t)^{-1}. \tag{2}$$

For Mn, this relation holds practically already at room temperature (and lower). This makes it possible to obtain the coefficients $\alpha_p^{=}$ and to determine their temperature dependence. The data thus

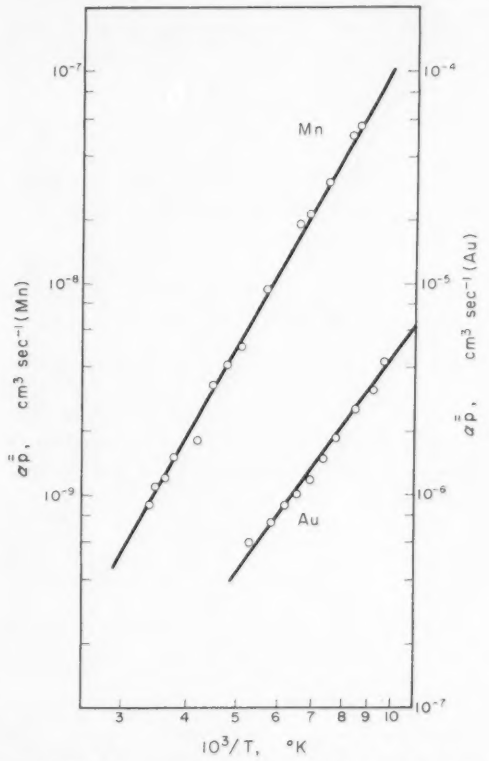

FIG. 3. The temperature dependence of $\alpha_p^{=}$ in the gold-doped ($N_t = 5\times10^{14}$ cm^{-3}, $n_0 = 1{\cdot}3\times10^{15}$ cm^{-3}) and manganese-doped ($N_t = 3{\cdot}7\times10^{14}$ cm^{-3}, $n_0 = 8{\cdot}5\times10^{14}$ cm^{-3}) samples.

obtained are shown in the Fig. 3 for one of the Mn-doped samples and one of the Au-doped samples. In both cases, the temperature dependence fits the T^{-n} law. The average values of n and of $\alpha_p^{=}$ at 300°K, obtained on 7 Au-doped samples and on 4 samples containing Mn, are listed in Tables 1 and 2. The $\alpha_p^{=}$ value for gold is in good agreement with the data of Ref. (2) (300°K) and is consistent with the data of Ref. (1) (90°K).

To see if the α-values obtained are consistent with the observed trapping phenomena, we made a detailed camparison of the τ_{PEM} and τ_{PC} data, similar to that which had been done in Ref. (11). To this end, we studied the temperature dependence of the trapping factor

$$k \equiv \tau_{PC}/\tau_p \cong \tau_{PC}/\tau_{PEM}.$$

Using the results of Ref. (12) one easily obtains for the n-type samples:

$$k = 1+\frac{b}{b+1}\frac{\delta P_t}{\delta p}, \qquad (3)$$

where $b = \mu_n/\mu_p$, δp_t and δp are the added concentrations of trapped and free holes. On the other hand,

$$\frac{\delta p_t}{\delta p} = N_t \frac{\alpha_p^{=} f - \alpha_n^{-}(1-f)}{\alpha_p^{=}(p_0+p_1)+\alpha_n^{-}[n_0+n_1+N_t(1-f)]}, \qquad (4)$$

where f is the equilibrium electron occupation number of the level in question and the other symbols have their usual meaning in the Hall–Shockley–Read statistics. This relation reduces to a simple form for Au and Mn in Ge at lower temperatures:

$$\frac{\delta p_t}{\delta p} = \frac{N_t}{n_0}\cdot\frac{\alpha_p^{=}}{\alpha_n^{-}} f^2. \qquad (5)$$

Now the function $\alpha_p^{=}(T)$ is known from the PEM measurements and the quantities N_t and n_0 are measured directly. Besides that in the Mn case $f \cong 1$ in all the temperature range in question. Therefore, fitting the theoretical k-curves to the experimental data, the α_n^{-} can be determined. Such a comparison is shown in the Fig. 4 for the two Mn-doped samples. For both samples, we obtain $\alpha_n^{-} = 2\times10^{-10}\,\mathrm{cm^3\,sec^{-1}}$. We consider this to be in satisfactory agreement with the value $4\times10^{-10}\,\mathrm{cm^3\,sec^{-1}}$ obtained from the p-type measurements, since the experimental errors in determining the generation rate (PEM) and the mobilities' temperature dependence might be considerable.

For Au-doped samples, the α_n^{-} temperature dependence could not be determined reliably from p-type measurements. Therefore it was obtained from the low temperature part of the k-curve, the $\alpha_p^{=}(T)$ function being known. The $f(T)$ values were determined from the high temperature part of the τ_{PEM}-curve. Then it was possible to get the $k(T)$ curve in the whole temperature range. Fig. 3 shows the comparison of such a curve with the experimental data for one of the samples. In this case, too, the α_n^{-} value extrapolated to 300°K is consistent with the p-type measurements up to the experimental error.

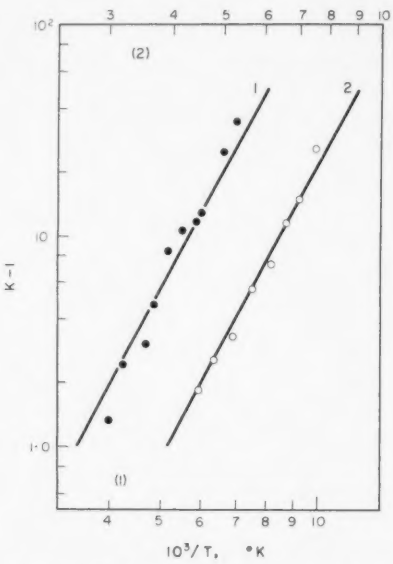

FIG. 4. Trapping factor k vs. temperature for the two Mn-doped n-type samples. (1) $N_t = 1{\cdot}0\times10^{15}\,\mathrm{cm^{-3}}$, $n_0 = 2{\cdot}3\times10^{15}\,\mathrm{cm^{-3}}$; (2) $N_t = 6{\cdot}5\times10^{14}\,\mathrm{cm^{-3}}$, $n_0 = 1{\cdot}5\times10^{15}\,\mathrm{cm^{-3}}$. The solid curves are calculated (see text).

DISCUSSION

It is interesting to discuss the results from the point of view of the mechanism of elementary capture processes. Consider first the $\alpha_p^{=}$ and α_n^{o}.

The $\alpha_n^{=}$ are most likely determined by the LAX's phonon cascade process[13], leading to very large capture cross-sections. In the α_n^{o} case, this is *a priori* not so clear since the polarization forces may not provide the sufficient number of excited states.* Comparing the magnitudes of $\alpha_p^{=}$ and α_n^{o}, one sees that α_n^{o} for gold being considerably

* This was pointed out by BONCH-BRUEVICH (private communication).

Vol. 22
1961

smaller than α_p^- is yet large enough and corresponds to the cross-section $S_n^0 \sim 10^{-16}$ cm^2. For Mn, α_n^0 is of the same order of magnitude and is even bigger than α_p^- (at 300°K). These results are consistent with the view that in this case the α_n^0 processes proceed via the phonon cascade as well.

For gold, the α_p^- temperature dependence follows the $T^{-\hbar}$ law. This agrees with the theory of LAX. The value of n is in good agreement with the maximum theoretical value (for the capture coefficients) $n = 3{\cdot}5$. Yet for Mn the experimental value of n is somewhat larger.

The temperature dependence of α_n^0 is somewhat weaker than that expected theoretically. However, it is possible that weak temperature dependences might be slightly distorted by errors in the mobility values.

Of special interest is the comparison of α_n^0 and α_n^- values. Once the usual scheme of Au and Mn charge states in Ge is assumed, we might expect α_n^- to be several orders of magnitude less than α_n^0, since in view of the Coulomb barrier there would be no cascade process, and beside that, the electron transport to the center would be hampered. Yet the experiment shows that both in gold-doped and in manganese-doped samples α_n^0 and α_n^- are of the same order of magnitude; in the Au case α_n^- even exceeds α_n^0. Moreover, for Mn at 300°K α_n^- is approximately equal to $\alpha^=$ in spite of that in the last case the cascade process is surely possible. The weak α_n^- temperature dependence also gives no indications as to the significant role of the Coulomb barrier.* Therefore, we are led to the conclusion that the capture processes in the presence of the Coulomb barrier are not fully explained as yet.

REFERENCES

1. JOHNSON L. and LEVINSTEIN H., *Phys. Rev.* **117,** 1191 (1960).
2. GLINCHUK K. D., MISELYUK E. G. and FORTUNATOVA N. N., *Solid-State Phys.* (*U.S.S.R.*) **1,** 1345 (1959); MISELYUK E. G. and GLINCHUK K. D., *International Conference on Semiconductors, Prague* (1960).
3. RUPPRECHT G., *International Conference on Semiconductors,* Prague (1960).
4. NEURINGER L. I. and BERNARD W., *Phys. Rev. Letters* **6,** 455 (1961).
5. NEWMAN R. and TYLER W. W., *Solid-State Physics,* Vol. 8, p. 50. Academic Press, New York (1959).
6. PRINCE M., *Phys. Rev.* **92,** 681 (1953).
7. ALEKSEEVA V. G., KARPOVA I. V. and KALASHNIKOV S. G., *Solid-State Phys.* (*U.S.S.R.*) **3,** 964 (1961).
8. LANDSBERG E. G. and KALASHNIKOV S. G., *Solid-State Phys.* (*U.S.S.R.*) **3,** 1566 (1961).
9. DEBYE P. P., KLEIN C. A. and RUPPRECHT G., Bull. Amer. Phys. Soc. **5,** 62 (1960).
10. ROOSBROECK W. V., *Phys. Rev.* **119,** 636 (1960).
11. KALASHNIKOV S. G. and MOROSOV G. I., *Solid-State Phys.* (*U.S.S.R.*) **2,** 1813 (1960).
12. ZITTER R. N., *Phys. Rev.* **112,** 852 (1958); MIRONOV A. G., *Solid-State Phys.* (*U.S.S.R.*) **1,** 525 (1959).
13. LAX M., *J. Phys. Chem. Solids* **8,** 66 (1959); *Phys. Rev.* **119,** 1502 (1960).
14. BONCH-BRUEVICH V. L., *Solid-State Phys. Suppl.* (*U.S.S.R.*), 182 (1959).

* The weak temperature dependence of the capture coefficients of this type may be due to tunnelling.[14]

DISCUSSION

T. E. HARTMAN: Since only one change of ambient atmosphere was introduced to check the effects of surface recombination, it is possible that the surface potential has been moved to the other side of the maximum in the S vs. surface potential curve and that surface recombination effects are present.

S. G. KALASHNIKOV: This seems to me quite improbable because we changed the pressure of the gas and the results were the same.

G. C. DOUSMANIS: Could the extent of difference in trapping between the p- and n-type cases be obscured by the different mobilities and their different temperature dependence? The Landau level structures could effect the results differently in the warped surface and the ellipsoidal energy surfaces, especially if high fields are used at the lower temperature range.

S. G. KALASHNIKOV: We used the experimental data for mobilities given in the literature. Possible inaccuracies in mobility values cannot account for difference in trapping in p- and n-type samples which is very large.

R. L. WILLIAMS: For gold-doped germanium:

(a) Did you observe an exponential temperature dependence for the cross-section as observed by JOHNSON and LEVINSTEIN?

(b) Over what temperature range was the $T^{-3{\cdot}5}$ cross-section temperature dependence observed?

S. G. KALASHNIKOV: (a) We could not obtain the

temperature dependence of S_n^- directly because the plateau of the τ vs. $10^3/T$ curve (Fig. 1) which corresponds to this cross-section was observed only near room temperature.

(b) The $T^{-3\cdot5}$ temperature dependence was observed from about 200°K to liquid nitrogen temperature.

M. G. A. BERNARD: How were Au and Mn atoms introduced into the germanium lattice and what is the dislocation content?

S. G. KALASHNIKOV: Au and Mn were introduced into the melt. The dislocation density was about 10^2 cm^{-2} or less.

Vol. 22
1961

J. Phys. Chem. Solids Pergamon Press 1961. Vol. 22, pp. 51–55. Printed in Great Britain.

TRAPPING AND RECOMBINATION MEASUREMENT BY A LIGHT MODULATION TECHNIQUE

G. CHEROFF, J. HEER and S. TRIEBWASSER

International Business Machines Corporation, Thomas J. Watson Research Center, Yorktown Heights, New York

Abstract—A technique is described by which recombination lifetime may be resolved from trapping effects. Analysis is shown by which trap capture and release times may be measured as well as density and energy level of trapping levels. It is shown that superlinearity in CdSe sintered layers arises not from "activation", as described in currently held models of variation of recombination time with light level, but rather is associated with increase of mobility with light level.

1. INTRODUCTION

BOTH from a practical and academic standpoint, it has long been recognized that trapping, sensitivity and time of response are intimately related in photoconductive processes. In particular, for the simple case of a single current carrier (electrons in CdSe), the conductivity may be written:

$$\sigma = e\mu\tau_r(\alpha I)\beta \tag{1}$$

where e is the charge on the electron, μ the electron mobility, τ_r the recombination lifetime of electrons, α the optical absorbtion coefficient, I the light intensity and β the quantum efficiency. Response time is defined by the differential equation:

$$\frac{dn}{dt} = -\frac{n}{\tau_0} \tag{2}$$

where n is the density of electrons in the conduction band and τ_0 the response time. Equation (2) should determine n for at least a short time interval after the exciting radiation is turned off. ROSE[1] pointed out that τ_0 is related to τ_r by:

$$\tau_0 = \tau_r\left(1+\frac{DkT}{n}\right), \tag{3}$$

where D is the density of carriers at the quasi Fermi level (Q.F.L.).* Theories directed at explaining the super- sub- and linear dependence of σ on I have concentrated on models that result in assignment of responsibility for these variations to τ_r. Unfortunately measurements of τ_r thus far reported have been indirect. For example, if μ, α and β are known, τ_r can be found from equation (1). The difficulties are obvious. If there were no traps, or if DkT/n were very small, then equation (2) could be used. This relation predicts exponential variation of n with time, a behavior generally observed either for very small time intervals or very high light intensities. As a matter of fact, NIEKISCH[2] used equations (2) and (3) and an a.c. light method to measure D as a function of the depth below the conduction band.† We have extended NIEKISCH's technique to show how examination of the a.c. response as a function of frequency can yield trapping times, recombination lifetime and trap concentrations.

2. THEORY

In NIEKISCH's earlier work[2] two assumptions were necessary: (a) τ_r is independent of light level and (b) mobility is independent of light level. In general if these assumptions were valid, conductance vs. light intensity curves would be linear—a condition rarely seen in a photoconductor. In fact, a good deal of effort has been directed at finding models to explain the wide variety of

* BROZER and WARMINSKY give a detailed statistical argument supporting equation (3). It can also be shown quite simply that for traps all well above the Q.F.L., $\tau = \tau_r(1+h/n)$, where h = number of trapped electrons per unit volume.

† The relations between noise measurements and response to sinusoidal variations of light are discussed in Ref. 2.

slopes of log σ vs. log I plots observed. In addition, BUBB and MACDONALD[3] showed recently that μ also varies with light level. This has been confirmed by FOWLER[4] in this laboratory on samples similar to those on which our experiments were performed. It is important to unravel the various factors that contribute to the observed photoconductive response.

The model under examination is that shown in Fig. 1. It is assumed that the single trapping

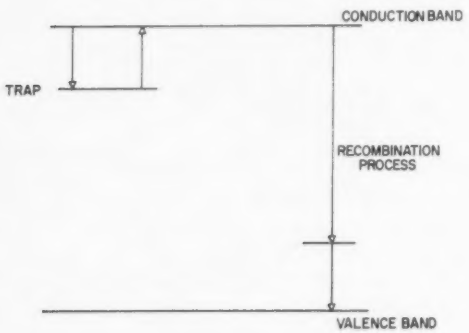

FIG. 1. Transitions considered in this treatment.

level is in contact with the conduction band (C.B.), but not the valence band. In addition, it is assumed that the dependence of recombination rate on the density of trapped electrons is a higher order effect—i.e. the recombination rate for small signal theory depends only on n. Using the SHOCKLEY–READ[5] relation for this case, the differential equation governing both conduction electrons and trapped electrons can be written:

$$\frac{dn}{dt} = -f(n) - \frac{dh}{dt} + F \tag{4}$$

$$\frac{dh}{dt} = -hN_cSv\exp(-E/kT) + n(H-h)Sv \tag{5}$$

where:

$f(n)$ describes the dependence of recombination on n,

h, the density of trapped electrons,

F, the electron generation rate via optical excitation,

N_c, the effective density of states in the C.B.,

S, the capture cross-section of the traps for electrons,

v, the average thermal velocity of electrons in the C.B.,

H, the density of traps at a depth E,

E, the depth of the trap below the conduction band.

If now we assume an incremental change in F of δF and write $F = F_0 + \delta F$, $n = n_0 + \delta n$, $h = h_0 + \delta h$, then equations (4) and (5) become to first order:

$$\frac{d(n_0)}{dt} + \frac{d(\delta n)}{dt} = -f(n_0) - \delta n f'(n_0) - \frac{dh_0}{dt} - \frac{d(\delta h)}{dt} + F_0 + \delta F \tag{6}$$

$$\frac{dh_0}{dt} + \frac{d(\delta h)}{dt} = -h_0N_cSv\exp(-E/kT) - \delta hN_cSv\exp(-E/kT) + n_0(H-h_0)Sv + \delta n(H-h_0)Sv - n_0\delta hSv. \tag{7}$$

If all the zero subscripted quantities represent steady state values, then

$$\frac{dn_0}{dt} = \frac{dh_0}{dt} = 0 \text{ and } f(n_0) = F_0$$

also,

$$h_0N_cSv\exp(-E/kT) = n_0(H-h_0)Sv \tag{8}$$

Now letting,

$$\begin{aligned} \delta F &= F_1\exp(i\omega t) \\ \delta n &= n_1\exp(i\omega t) \\ \delta h &= h_1\exp(i\omega t) \end{aligned} \tag{9}$$

and taking relations (9) into account, it follows directly

$$n_1 = \frac{F_1}{\omega_0 + i\omega[1+\omega_2/(\omega_1+i\omega)]} \tag{10}$$

where

$$\omega_0 = f'(n_0),\quad \omega_1 = \left(\frac{n_0}{h_0}\right)HSv,\quad \omega_2 = (H-h_0)Sv \tag{11}$$

In the simple case that $f(n_0) = n_0/\tau_r$, and τ_r is independent of n_0, $\omega_0 = 1/\tau_r$. In the case that the trap is well above the Q.F.L., ω_1 represents the trap release frequency, and ω_2 represents the

Vol. 2
1961

trapping rate. When there are many trapping levels the term $\omega_2/(\omega_1+i\omega)$ in the denominator of (10) is replaced by a summation of appropriate ω's, or for the continuous distribution case by an integral.

The cases previously described in the literature deal with ω_1 and $\omega_2 \gg \omega_0$. Then if measurements are carried out at frequencies below ω_1 and ω_2 where $\omega \ll \omega_1$, equation (10) reduces to:

$$n_1 = \frac{F_1}{\omega_0+i\omega[1+(\omega_2/\omega_1)]}. \tag{12}$$

For the case of a trap well above the Q.F.L., $(H-h_0) \approx H$ and $\omega_2'/\omega_1 = h_0/n_0$. The behavior described by equation (3) is predicted; i.e. a photoconductor with a response time of $\tau_0 = \tau_r[1+(h_0/n_0)]$. This is the case treated originally by NIEKISCH. In a more recent publication,[5] he extended the work to larger ω, $(\omega > \omega_1)$, but assumed that τ_r and the electron mobility were not a function of n. The results we have found are at variance with those predicted by NIEKISCH from his assumptions with respect to the variation of n_1 with frequency.

3. EXPERIMENTAL RESULTS

The measurements reported were made on sintered CdSe doped with 100 p.p.m. Cu. The Cu was added in the form of $CuCl_2$. In addition, $CdCl_2$ was used as a flux so that the Cl content of the samples was not controlled. Measurements of impedance vs. frequency were made to look for barrier relaxation effects. In the frequency range and light levels of interest in this experiment no relaxation effects were observed. In addition, preliminary examination of a Cu-doped CdSe single crystal gave the same qualitative results as those reported here.

The sample thickness was large compared with an absorption length. The effect of the non-uniform distribution of carriers on the quantitative results can be calculated, and has been included in the stated results. Measurements have been made over a wide range of wavelengths—all of which showed the same qualitative behavior. Actual data shown here are either taken from an unfiltered neon lamp or with monochromatic light at 6000 Å. The neon lamp is a handy source for CdSe since its spectrum matches the CdSe response reasonably well and it has the added advantage that it can be easily modulated.

There are several cases of interest. The simplest is that in which $\omega_0 \gg \omega_1$ and ω_2, and $\omega_2/\omega_1 \ll 1$. This will be the case for very deep traps or traps located below the Q.F.L. Effectively in such a case the traps do not contribute to the dynamic response and equation (12) reduces to

$$n_1 = \frac{F_1}{\omega_0+i\omega} \tag{13}$$

and the normalized amplitude R becomes

$$R = \frac{n_1(\omega \gg \omega_0)}{n_1(\omega \ll \omega_0)} = \frac{F_1/i\omega}{F_1/\omega_0} = \frac{\omega_0}{i\omega}. \tag{14}$$

When R is plotted as a function of $1/\omega$, it is obvious that the slope gives ω_0. Fig. 2 shows three such

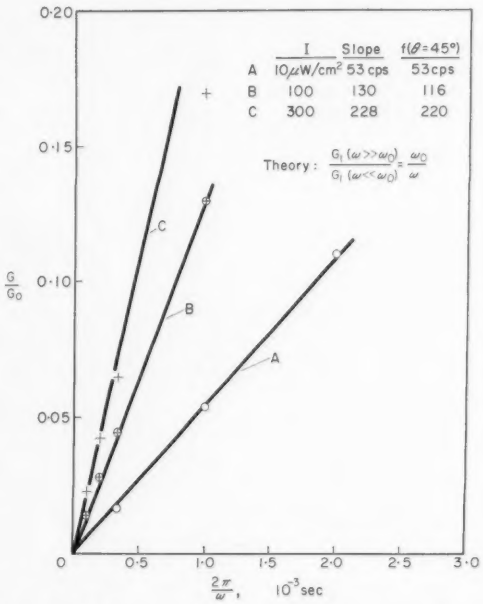

FIG. 2. $G_1(\omega \gg \omega_0)/G_1(\omega \ll \omega_0)$ vs. ω. $G_1 \propto n_1$. It can be shown that the fact that n_1 actually varies with depth of penetration of the light leads to a slope of $[\tau_r(I_0)]^{-1}$ where $\tau_r(I)$ is defined by $n(I)/\tau_r(I) = f(n)$.

plots for three different light intensities. In addition, when $\omega = \omega_0$, a phase shift of 45° between n_1 and F is observed according to equation (13). The agreement is excellent.

A more interesting case is one in which $\omega_2/\omega_1 > 1$, and ω_1 and $\omega_2 \geqslant \omega_0$. In this case, if the magnitude of the inequality is large, two ($n_1 \propto 1/\omega$) regions are observed, one following equation (14) and the other giving a slope of $\omega_0(1+\omega_2/\omega_1)^{-1}$. If the frequencies are not very well separated, the two regions are not resolved and only the former is observed at $\omega \gg \omega_2$. A more typical plot is shown in Fig. 3. For a case such as this, the relative phase between n_1 and F_1 is most sensitive to the exact values of ω_0, ω_1 and ω_2 and H, but the results are tentative and will not be reported at this time.

On the other hand, $\tau_r(I_0)$, the value of τ_r for small attenuation, can be found from exploration of G_1 at high frequencies (as in Fig. 2). It can be shown that

$$\frac{dG}{dI_0} = e\mu(I_0)\tau_r(I_0), \tag{15}$$

where G is the conductance per square, I_0 the

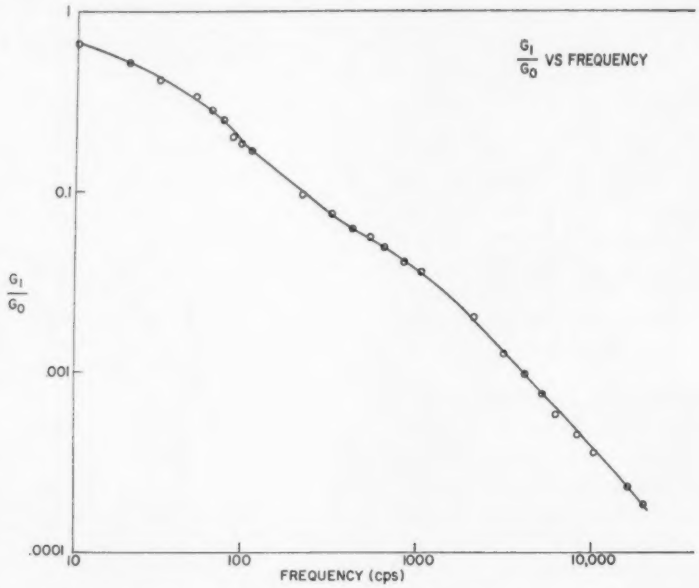

FIG. 3. G_1/G_0 vs. f for the Q.F.L. 0·3 eV below the C.B. $I = 0{\cdot}6\ \mu\text{W/cm}^2$.

ω_2. Because the conductance

$$G_1 = \int_0^{z_0} n_1 e\mu\, dz$$

(an integration performed over the sample thickness) is the experimentally observed quantity, no simple phase relationship can be expressed except for the simple case where ω_0 is widely separated from ω_1 and ω_2. For this case, internal consistency with the model is observed. (See Fig. 2.) Work is in progress on many samples including single crystals which will lead to values for ω_1, incident photon flux and $\mu(I_0)$ is the mobility for the case of small attenuation (or that near the surface of the photoconductor). Fig. 4 shows dG/dI_0 and $\tau_r(I_0)$ for two different samples. The G vs. I_0 data show a superlinear region at the lower light intensity. We must conclude that the observed non-linear behavior is associated with a variation of mobility with light intensity, not with "activation" described in terms of recombination passing from "fast" to "slow" recombination centers. In the region of slow variation of μ, where we have Hall mobility data,[4] the results agree; i.e. inserting measured μ and assuming

Vol. 2
1961

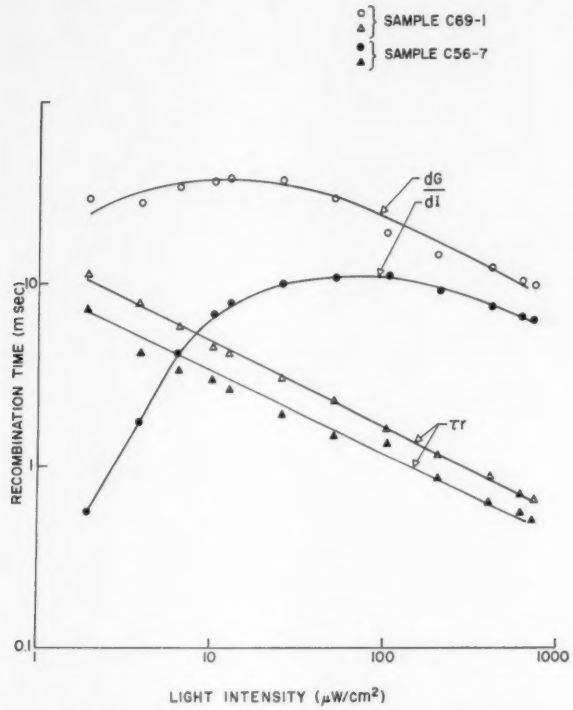

FIG. 4. dG/dI_0 and $\tau_r(I_0)$ for two different samples.

a quantum efficiency of one, agreement with equation (15) is found.

4. CONCLUSIONS

Since variation of photoconductance with light intensity has been explained in terms of variation of recombination lifetime, it is important to measure this quantity independently. A method has been described by which τ_r can be found directly. From the results found it is concluded that current models of photoconductor "activation" are incomplete.

Acknowledgements—We wish to thank R. CHANG and F. HOCHBERG for assistance in some of the measurements reported here.

REFERENCES

1. ROSE A., *RCA Rev.* **12,** 363 (1951); BROSER I. and WARMINSKY R., *Ann. Phys. Leipzig* (6), **16,** 361 (1955).
2. NIEKISCH E. A., *Ann. Phys. Leipzig* (6), **15,** 279, 288 (1955); VAN VLIET K. M., BLOK J., RIS C. and STEKETEE J., *Physica* **22,** 723 (1956) and VAN VLIET K. M. and BLOK J., *Physica* **22,** 525 (1956).
3. BUBE R. H. and MACDONALD H. E., *Phys. Rev.* **12,** 473 (1961).
4. FOWLER A. B., *International Conference on Photoconductivity, New York* (1961).
5. SHOCKLEY W. and READ W. T., *Phys. Rev.* **87,** 835 (1952).

DISCUSSION

Van der MAESEN: You reported changes in mobility and in lifetime as functions of intensity. Due to what mechanism in your experiments were the changes in μ occurring?

S. TRIEBWASSER: This question is dealt with at length in papers.*

*Pp. 173 and 181 of this issue.

BLANK
PAGE

Vol. 22
1961

J. Phys. Chem. Solids Pergamon Press 1961. Vol. 22, pp. 57–62. Printed in Great Britain.

RECOMBINATION OF ELECTRONS AND DONORS IN SEMICONDUCTORS†

G. ASCARELLI

Department of Physics, University of Illinois, Urbana, Illinois

and

S. RODRIGUEZ

Department of Physics, Purdue University, Lafayette, Indiana

Abstract—A description is given of a calculation of the recombination of electrons in the conduction band of a semiconductor with ionized donor impurities. The process which we assume consists in the initial capture of the electron in an excited state of the donor center followed by a transition to the ground state. This mechanism is most effective in the case in which all transitions are accompanied with emission or absorption of phonons.

The results obtained are compared with earlier theoretical calculations and with experiments. The agreement between the present theory and experiment is reasonably good and is displayed in Fig. 1.

IT IS the purpose of this paper to review some theoretical calculations and the experimental data regarding the processes of recombination of conduction electrons with donor centers in semiconductors.

Calculations of the recombination cross-section of electrons and donors in germanium and silicon have been made by GUMMEL and LAX[1] and by SCLAR and BURSTEIN[2]. In the first of these calculations, the direct recombination of an electron in the conduction band and a ionized donor is considered to occur with the emission of a phonon. The final state of the electron is the ground state of the impurity center. The interaction between the electron and the phonon field is described by means of the deformation potential E_1.

The result of this work can be expressed in terms of a cross-section for the recombination process given by the equation

$$\sigma_p = \frac{256\pi E_1^2 \hbar^5 c_s^3}{\rho a^{*6} E_i^5 kT}. \tag{1}$$

Here c_s is the longitudinal sound velocity, ρ the density of the semiconductor, $\hbar$ is Planck's constant divided by 2π, k is Boltzmann's constant, and T the temperature. The quantities a^* and E_i are the effective Bohr radius and the ionization energy of the ground state of the donor center. They are given by

$$a^* = \frac{K\hbar^2}{m^* e^2}, \tag{2}$$

and

$$E_i = \frac{m^* e^4}{2\hbar^2 K^2}. \tag{3}$$

K is the dielectric constant and m^* an effective mass which describes the response of the electron to external forces in the presence of the crystal potential.

SCLAR and BURSTEIN[2] obtained the cross-section for direct recombination of electrons with ionized impurities accompanied by the emission of a single infra-red photon by scaling the known result for hydrogen,[3] taking into account the effective mass and the dielectric constant of the lattice. Their result is:

$$\sigma_0 = 1{\cdot}71 \times 10^{-18} K^{1/2} \left(\frac{m}{m^*}\right) \frac{E_i(\text{eV})}{T} \text{ cm}^2, \tag{4}$$

† This work has been supported by the Air Force Office of Scientific Research.

where E_i (eV) is the ionization energy of the donor expressed in electron volts.

The temperature dependence and the magnitude of the cross-section calculated either by SCLAR and BURSTEIN or by GUMMEL and LAX are in disagreement with the experimental result shown in Fig. 1.

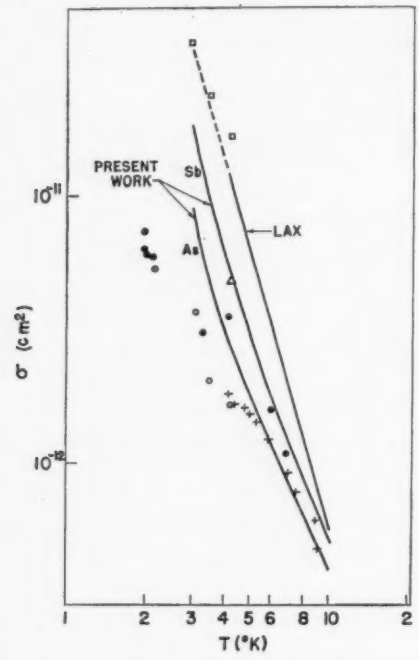

FIG. 1. The result of our calculation, Ref. 7, is shown as a solid line for both As and Sb donors in germanium. A hydrogen model of the impurity was used. LAX's calculation, Ref. 5, is also shown. It has been multiplied by a factor 9·5 to account for the 4 valleys of the conduction band of germanium and a factor 2·38 to correct for the dielectric constant of the material, 16 rather than 12 as used in Ref. 5. This last correction is probably over estimated. The experimental points are:
+ n–WLB 28–6 (Ref. 9); Δ n–WLB 28–6 (Ref. 10);
□ BTL−1 (Ref. 10); O As LL2 (Ref. 10);
● Ref. 5. Fig. 7.

SCLAR and BURSTEIN[2] also calculated the rate of impact recombination by scaling the result obtained for atomic hydrogen[4] and by using the principle of detailed balance. Again the rate of impact recombination is much too small to account for the experimental result. It might become the leading recombination mechanism for densities of the order of 10^{12} or 10^{13} carriers/cm^3, but there is no experimental evidence to support this point of view.

For germanium, taking $E_1 = 20$ eV, $c_s = 5 \times 10^5$ cm/sec, $\rho = 5{\cdot}36$ gm/cm^3, and $K = 16$, we find $a^* = 38{\cdot}5$ Å and $E_i = 1{\cdot}17 \times 10^{-2}$ eV. At 4°K, $\sigma_p = 5{\cdot}4 \times 10^{-15}$ cm^2 and $\sigma_0 = 4{\cdot}15 \times 10^{-19}$ cm^2.

LAX[5] introduced a new approach to the problem when he realized the importance that the capture of an electron in an excited state should have in the recombination process. LAX described the excited states of the donor as a continuum and studied the diffusion of an electron from an excited state into a tightly bound state. This approach is similar to that used by THOMSON[6] to describe the recombination process in a low pressure gaseous discharge. LAX's idea is that if an electron looses sufficient energy in a collision with a phonon when it is in the vicinity of an impurity, it will be captured in a bound orbit. If the binding energy of this excited state is larger than $3/2\ kT$, our electron will continue loosing energy until it is finally captured in the ground state. If we call R the distance from the ionized center of the point at which the electron experiences an energy loosing collision, λ the electron mean-free-path for a collision with the emission of a phonon and $3/2\ kT$ the average thermal energy, the radius R_0 of a sphere that limits the region in space where electrons that emit a phonon will be eventually captured by the ionized center is

$$\frac{e^2}{KR_0} = \frac{3}{2kT}. \tag{5}$$

The probability for an electron crossing a sphere of radius R to experience an energy loosing collision is $4/3\ R/\lambda$, so that the capture cross-section in a sphere of radius R_0 is

$$\sigma = (\pi R_0^2)\left(\frac{4}{3}\frac{R_0}{\lambda}\right). \tag{6}$$

Besides the energy loosing collisions, there are also those in which an electron that is bound in an orbit whose radius is $R < R_0$ gains energy and is excited into an orbit whose radius $R > R_0$ and finally returns into the conduction band. LAX's calculation considers the influence of both types of

Vol. 2
1961

collisions that can take place along an electron orbit. They provide an effective mechanism for the diffusion of the electron towards more tightly bound states. In Fig. 1, we display the result of LAX's work multiplied by a factor 4 to take into account the four valleys of the conduction band of germanium and another factor $(16/12)^3$ to consider the effect of the dielectric constant of germanium which is 16 rather than 12 as used in Ref. 5.*

We wish to present the result of a simple calculation which appears to give good agreement with the available experimental data.

Our model envisages the recombination of an electron with a donor as follows: initially the electron is captured in an excited state, j, with the emission of a single phonon. The average capture cross-section associated with this process is designated by $\sigma_c(j)$. Subsequently the electron can either experience a transition to a lower lying state, again with the emission of a phonon, or it can be excited back into the conduction band. In view of the much smaller density of states, the electron in a state j has a small probability of making a transition into a higher excited states as compared to that of being excited into the conduction band. We will call sticking probability S_j, the probability for an electron that has been initially captured in an excited state j to remain bound to the impurity center rather than being excited into the conduction band. The total recombination probability is σ

$$\sigma = \sum_j \sigma_c(j) S_j.$$

Throughout this calculation we assume spherical effective masses and that the electron–donor system can be described by a hydrogenic model.[8] Each excited state, j, of the system is represented by the quantum numbers (n,l,m) that correspond to the usual assignment of quantum numbers for the eigenstates of the hydrogen atom. S-states will be denoted by their principal quantum number, n, only.

The rate of capture of electrons into a donor state j is:

$$\nu_j = V(N_A+n) \int_{E_c}^{\infty} d\epsilon\, n(\epsilon) f(\epsilon)\, v\, \sigma_c(j\epsilon) \quad (7)$$

$$\equiv V(N_A+n) n \langle v \rangle\, \sigma_c(j). \quad (7a)$$

$\sigma_c(j\epsilon)$ is the cross-section for the capture of an electron with velocity v and energy ϵ in a state j, $f(\epsilon)$ is the Fermi distribution, E_c is the energy of the electron at the bottom of the conduction band and V the volume of the crystal. The second equality defines the average cross-section, $\sigma_c(j)$, for the capture of an electron in a state j. N_A and N_D are the concentrations of acceptors and donors respectively.

The number of electrons excited per unit time from the state j into the conduction band is:

$$\nu_j' = V N_D^{(j)} \beta_j. \quad (8)$$

In thermal equilibrium, we must have $\nu_j = \nu_j'$. β_j is the probability per unit time for an electron in the state j to be excited into the conduction band. The quantity $N_D^{(j)}$ is equal to the number of donors per unit volume that have an electron in the jth state. From equations (7) and (8) using the condition of detailed balance, we obtain

$$\sigma_c(j) = \frac{N_D f_j \beta_j}{n_\infty (N_A + n_\infty) \langle v \rangle}. \quad (9)$$

where f_j is the probability that the state j is occupied and n_∞ is the density of electrons in the conduction band when the system is in thermal equilibrium. The latter quantity is given by:

$$n_\infty = N_c \exp \frac{\xi - E_c}{kT}, \quad (10)$$

with

$$N_c = 2 \left(\frac{m^* kT}{2\pi\hbar^2} \right)^{3/2}. \quad (11)$$

The quantity ξ is the Fermi energy. After some simple transformations, we get

$$\sigma_c(j) = \frac{\pi^2 \hbar^3 \beta_j}{m^* (kT)^2} \exp \left(\frac{I_j}{kT} \right) \quad (12)$$

I_j is the ionization energy of the jth state.

$$I_j = E_c - E_j \quad (13)$$

* To correct LAX's calculation assuming that the recombination cross-section varies as K^3 is an over estimate being that the mean-free-path, λ, is such that an electron must loose at least an energy $(e^2/2KR_0)$. λ is thus a function of K.

To estimate $\sigma_c(j)$, we must assume a detailed mechanism that is responsible for the capture of the electron in the excited state. We assumed that this mechanism is a process in which a single phonon is emitted.

In the deformation potential approximation, β_j can be obtained in a straightforward manner using the Born approximation. For the states of the electron in the conduction band, we use Coulomb wave functions rather than plane waves. More details are given in Ref. 7.

The second step in the work consists in the computation of the sticking probability S_n. If $w_{jj'}$ is the transition probability per unit time that an electron will make a transition from state j to state j', the probability that an electron, that is in state j, will be excited into the conduction band is approximately, (see Ref. 7)

$$p_j^{(1)} = \beta_j \left[\sum_{j' \neq j} w_{jj'} + \beta_j \right]^{-1} \tag{14}$$

and

$$S_j + P_j = 1. \tag{15}$$

The transition probability with emission of a phonon, for the transition between $n-s$ states is:

$$w_{n'n} = \frac{64 E_1^2 \hbar^4 c_s^3}{\pi \rho a^{*8} E_i^5} \frac{(n'n)}{(n-n')^5 (n+n')^3} \times \left[1 - \exp - \frac{\hbar \omega_{nn'}}{kT} \right]^{-1} \tag{16}$$

where $n' < n$ and

$$\hbar \omega_{nn'} = E_i \left(\frac{1}{n'^2} - \frac{1}{n^2} \right). \tag{17}$$

We have considered only transitions between s-states as these are much more probable than transitions between states of other symmetries.

We have calculated S_n for different values of n. We used the value of E_i given by equation (3) except for the ground state where we used the experimental value for each donor. $E_n = E_i/n^2$ with E_i obtained from equation (3); a^* is given by equation (2). In view of the dependence of the ionization energy on the donor impurity, w_{nl} will depend on the type of donor. The importance of the different terms that contribute σ is shown in Fig. 2 for $T = 4°K$ for the case of Sb donors in Ge. S_n is also shown for As donors.

We can now attempt to take into account, in first approximation, the actual band structure of germanium.

If we assume that the transition probability of an electron, that is in the αth ($\alpha = 1,2,3,4$) minimum of the conduction band, to the donor bound level made out of Bloch functions of the α'th minimum is the same whether α is equal to α' or not, then the recombination cross-section in a multi-valleyed semiconductor is:

$$(\sigma)_{\substack{\text{multi} \\ \text{valley}}} = (\sigma)_{\text{spherical}} \times (\text{number of valleys}) \tag{18}$$

In the case of germanium, we have four valleys. The result of our calculation for a simple band multiplied by 4 is plotted in Fig. 1, together with the experimental results available. The temperature dependence of the cross-section we calculated agrees with LAX's at temperatures below 4°K. This is due to the fact that at low temperatures more excited states contribute to the capture cross-section and the energy loss per collision is still small ($m^* c_s^2 < kT$) so that diffusion theory is a good description of events. At higher temperatures, the discrete character of the excited states of the ionized center are important and there is a large disagreement between the temperature dependence of the recombination cross-section predicted by both theories. At low temperatures ($m^* c_s^2 > kT$) both approaches should again diverge in view of the large fractionary energy loss of the electrons.

We may now attempt to speculate on how the recombination cross-section should change in the case of hot electrons.

Another process begins to compete with the ionization of an electron in an excited state of a donor: impact ionization.

The capture cross-section should then be calculated in two cases:

(a) capture with emission of a phonon $(\sigma_c)_T$ (in which case the calculation presented in this paper should be modified to take into account the hot electron distribution),

(b) capture by means of an Auger process $(\sigma_c)_I$. The ionization mechanism corresponding to this type of capture will profoundly influence S_j when the applied electric field is varied.

Vol. 2
1961

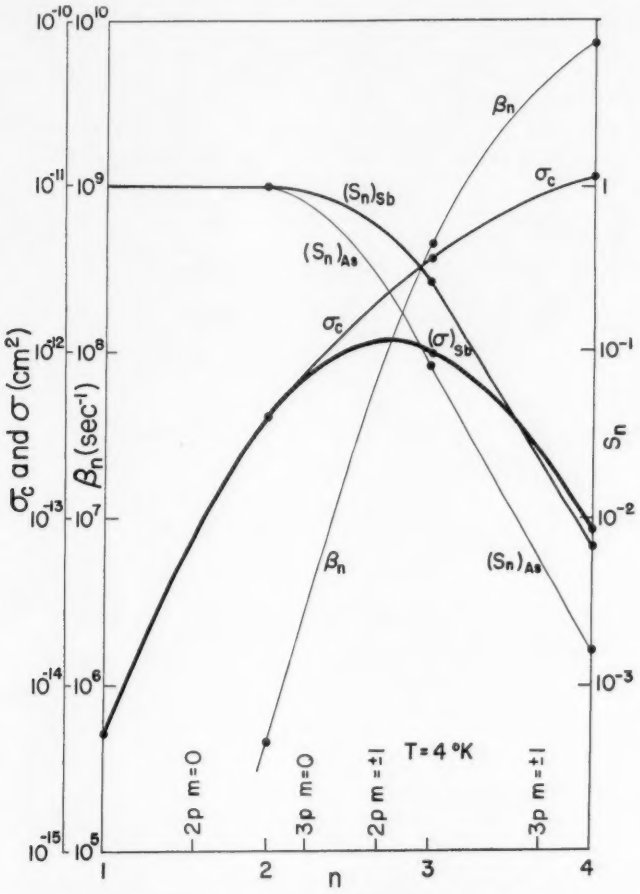

FIG. 2. Example of the result of our calculation for different bound states at 4°K. The sticking probability is given for both Sb and As donors. The experimental bound states as well as the values of n in our simple hydrogen model are shown in abcissa.

If we call γ_j the average probability of impact ionization of an electron in the jth bound state of the donor, we have

$$(\beta_j)_I = \gamma_j n, \tag{19}$$

$$S_j = \frac{\sum_{j' \neq j} w_{jj'}}{\beta_j + n\gamma_j + \sum_{j' \neq j} w_{jj'}}, \tag{20}$$

$$\sigma = \sum_j [(\sigma_c(j))_T + (\sigma_c(j))_I] \frac{\sum_{j' \neq j} w_{jj'}}{\beta_j + n\gamma_{j'} + \sum_{j' \neq j} w_{jj'}} \tag{21}$$

Two simple cases can be envisaged:

(a) $\sum_{j' \neq j} w_{jj'} \ll \beta_j \ll n\gamma_j$ and $(\sigma_c)_T \ll (\sigma_c)_I$

(b) $\sum_{j' \neq j} w_{j'j} \ll n\gamma_j \ll \beta_j$ and $(\sigma_c)_I \ll (\sigma_c)_T$.

Since σ_c is proportional to the corresponding probability of ionization, we see that both in case (a) and in case (b) the rate of disappearance of electrons from the conduction band will appear to be bi-molecular. It will be difficult to recognize the importance of an Auger recombination on the

basis of the rate of disappearance of electrons from the conduction band.

In the calculation of the recombination process by means of the mechanism described in this paper, it is easy to take into account hot electron effects. The electron distribution used in calculating σ_c should be changed from a Fermi to a hot electron distribution.

In the Auger process instead, the effect of the electric field will be much more important because it determines the number of electrons that have an energy sufficient to ionize an electron in the state j, i.e. γ_j.

REFERENCES

1. GUMMEL H. and LAX M., *Phys. Rev.* **97,** 1463 (1955); *Ann. Phys. New York* **2,** 28 (1957).
2. SCLAR N. and BURSTEIN E., *Phys. Rev.* **98,** 1757 (1955).
3. BETHE H. A. and SALPETER E., *Quantum Mechanics of One- and Two-Electron Atoms.* Academic Press, New York (1957).
4. MOTT N. F. and MASSEY H. S. W., *The Theory of Atomic Collisions* (2nd Ed.), p. 247. Clarendon Press, Oxford (1949).
5. LAX M., *Phys. Rev.* **119,** 1502 (1960).
6. THOMSON J. J., *Phil. Mag.* **47,** 337 (1924).
7. ASCARELLI G. and RODRIGUEZ S., *Phys. Rev.*, to be published.
8. KOHN W., *Solid State Physics*, (F. Seitz and D. Turnbull, editors). Vol. 5, p. 258. Academic Press, New York (1955).
9. KOENIG S. H., *Phys. Rev.* **110,** 988 (1958).
10. ASCARELLI G. and BROWN S. C., *Phys. Rev.* **120,** 1615 (1960).

Vol. 2
1961

J. Phys. Chem. Solids Pergamon Press 1961. Vol. 22, pp. 63–72. Printed in Great Britain.

ON THE ENERGY DEPENDENCE OF THE ABSORPTION CONSTANT AND PHOTOCONDUCTIVITY NEAR A DIRECT BAND GAP

J. J. HOPFIELD

Bell Telephone Laboratories, Inc., Murray Hill, New Jersey

Abstract—The absorption of light by a crystal in a spectral region in which direct excitons are observed can best be described as the creation of some (generally complicated) final state by an optical transition through an intermediate exciton state. The energy of the intermediate states determine the absorption line positions, but it is the final states which determine the line shape and are of interest in photoconductivity. A formalism is developed which expresses the absorption line shape in terms of an energy-dependent line width, whose form depends on the final states. This point of view is used to discuss some exciton line shape and photoconductivity experiments in CdS and Cu_2O.

1. INTRODUCTION

THE CALCULATION of the photoconductive response of a crystal to light of a given energy can be divided into two parts. The first is the problem of what changes are made in the crystal electronic states by the fundamental process which causes the absorption of the light. The second is the calculation of the change in conductivity due to the generation of these changes in the crystal electronic states. The present work concerns the first of these problems for crystals having a direct band gap in the energy region in which exciton absorption lines occur.

Section 2 is devoted to the form and interpretation of the absorption constant in the vicinity of an isolated exciton. In Section 3 the form of some particular absorption lines is discussed as an aid to understanding the meaning of the formalism. Section 4 contains a brief discussion of the application of this interpretation of the absorption constant to photoconductivity, with the example of Cu_2O discussed in detail. In Section 5, a reminder is given that the superposition of absorption constants due to different processes or different excitons is not always additive, and an example in which this nonadditivity might have already been observed is presented.

2. THE ONE-EXCITON WEAK COUPLING LINE SHAPE

We will consider an idealized system in which the exciton absorption lines are well enough separated that each can be considered individually. It will be initially supposed for simplicity that the exciton under consideration is formed from nondegenerate bands. In the one-exciton approximation, the electronic energy band structure of the crystal consists of a point (the ground state) and an exciton band as shown in Fig. 1(a). There are in addition phonon states in the crystal, and a coupling between the excitons and phonons. There is an optical matrix element of the light between the crystal ground state and the $k = 0$ exciton state. Phonon coupling between the crystal ground state and the exciton states plays a negligible role, and will be omitted.

With no phonon interactions in a perfect crystal, such a model would yield for the imaginary part of the dielectric constant a δ-function at E_0, whose oscillator strength we assume to be f_0.

By supposition, the ground state of the crystal with an arbitrary number of phonons is an exact eigenstate of our problem. Let such a state be denoted by ϕ_i, having energy E_i, where i is an index referring to the phonon coordinates. Let ψ_f be an

exact eigenstate of the crystal when one exciton is present. These states have energy E_f. The subscript f is understood to label the exciton wave vector and all phonon coordinates. For an initial state i, the oscillator strength at energy E is then

$$f_i(E) = f_o \sum_f |\langle\psi_{io}|\psi_f\rangle|^2 \delta(E+E_i E_f), \qquad (1)$$

where state ψ_{io} (not an eigenstate) is the state obtained by creating an exciton of wave number zero keeping the phonons present in state ϕ_i.

The factor f_o represents the oscillator strength of the transition $\phi_i \to \psi_i$. The other two factors simply project this oscillator strength on the eigenstate f having an energy $E+E_f$.

It is convenient to take the Fourier transform of (1). This yields:

$$f_i(E) = \frac{f_o}{2\pi\hbar} \int_{-\infty}^{\infty} \langle\psi_{io}|\psi_f\rangle \langle \exp(iE_f t/\hbar)\psi_f| \times \exp[-i(E_i+E)t/\hbar]\psi_{io}\, dt\rangle. \qquad (2)$$

Making use of the fact that ψ_f is an exact eigenstate, E_f can be replaced by the Hamiltonian H, and the sum of f performed to yield:

$$f_i(E) = \frac{f_o}{2\pi\hbar} \int_{-\infty}^{\infty} \langle\psi_{io}| \exp[i(H-E_i-E)t/\hbar]|\psi_{io}\rangle\, dt \qquad (3)$$

or alternatively,

$$f_i(E) = \frac{f_r}{\pi\hbar} \operatorname{Re} \int_0^{\infty} \langle\psi_{io}|\exp[-i(H-E_i-E)t/\hbar]| \times \psi_{io}\rangle\, dt \qquad (4)$$

where by Re is meant the real part of the integral. A similar form was derived by TOYAZAWA[1].

To solve (4), it is necessary to find the solution of

$$(H-E_i-E)\chi = ih\frac{d\chi}{\partial t} \qquad (5)$$

for $\chi = \psi_{io}$ at $t = 0$. Only the weak-coupling problem is tractable in general. For the weak-coupling problem, an adequate solution to this problem is the Wigner–Weisskopf solution.[2] Let ψ_{ik} represent the set of bare exciton and phonon states, of which one is of course ψ_{io}. The solution to this problem is then:

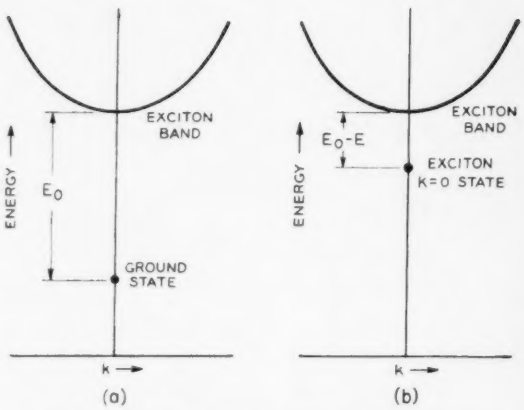

FIG. 1(a). $E(k)$ for the crystal electronic states in the one exciton problem. (b). The $E(k)$ for the exciton states of the New Hamiltonian $\mathscr{H}$ for calculation of the line width at energy E. The exciton $\boldsymbol{k} = 0$ state has been removed from its band, while all other states are unmodified.

$$f_i(E) = \left(\frac{f_o}{\pi}\right) \frac{\Gamma_i(E)}{[E-E_o-\Gamma_r(E)]^2+[\Gamma_i(E)]^2} \qquad (6)$$

where Γ_r and Γ_i are in turn given by

$$\Gamma_r + i\Gamma_i = \sum_{\substack{k,i \\ i'k\neq io}} \frac{|\langle\chi_{io}|H|\chi' k\rangle|^2}{E_{i'k}-E-E_{io}+i\epsilon} \qquad (7)$$

$$\lim \epsilon \to 0$$

For the expectation value of $f(E)$ at a given temperature, it is of course necessary to average over a thermal distribution of initial states i.

When the absorption constant is due to a single exciton, (6) and (7) are a special case of a more general weak-coupling result. Let the exciton be scattered by anything whatsoever, into other exciton states, into free electron hole pairs, or any other final state. The energy dependent width and level shift is then given by the solution to the following problem. Define a new Hamiltonian $\mathscr{H}$, identical to H except that the $\boldsymbol{k} = 0$ exciton state is assigned an energy lowered by (E_o-E). The real part of $\Gamma(E)$ is simply the energy shift of the $\boldsymbol{k} = 0$ exciton state due to the perturbation. Γ_i is

Vol. 22
1961

$\hbar^{-1}$ times the rate of amplitude decay of the $\boldsymbol{k} = 0$ exciton state under $\mathscr{H}$, or $(2\hbar)^{-1}$ times the transition rate out of the $\boldsymbol{k} = 0$ state under the action of $\mathscr{H}$. The exciton energy levels for $\mathscr{H}$ are shown in Fig. 1(b).

It is important from the point of view of photoconductivity to note that the electronic states which should be considered as being generated in the optical absorption process are also the final states of the $\mathscr{H}$ problem.

In most problems, the type of observations made are not sufficiently sensitive to detect the *changes* in Γ_r. For practical purposes, $E_0+\Gamma_r(E)$ can be replaced by the observed energy of the maximum of the imaginary part of the dielectric constant.

For most physical problems, the nature of the real final states makes $d\Gamma(E)/dE$ less than 1. In such a case, the center of an absorption line will appear Lorentzian, while the wings may not.

The simplest application of (6) and (7) lies in the area of lattice vibrations. Equations (6) and (7) apply equally well, of course, to optical mode vibrations. Consider a simple model of the lattice absorption of a polar crystal. Assume that there is no second-order dipole moment, but that anharmonic forces are present. Then the imaginary part of the dielectric constant should be very nearly Lorentzian near the Restrahl frequency. The width of the absorption Lorentzian is given by (7) with $E = \hbar\omega_{\text{transverse optical}}$, and is provided by anharmonic phonon scattering. Away from the Restrahl frequency, the absorption constant (really, always, the imaginary part of the dielectric constant) will still be given by (6), but Γ_i can be neglected in the denominator. At energies such that the two-phonon density of states is large, $\Gamma_i(E)$ will also be large. The "combination bands" are thus also given by (6), when Γ is calculated as the solution to the $\mathscr{H}$ problem. The advantage of (6) and (7) is that they treat resonance and off-resonance energies at the same time.

Actually, (6) and (7) applied to lattice absorption do not give the complete answer, because of the initial supposition that the coupling between the crystal states having no excitons and the crystal states in the presence of excitons could be neglected. This supposition is not satisfactory when $\Gamma(E)$ is to be calculated at distances away from e_0 comparable with E_0, as is desired for the calculation of combination bands in lattice vibrations. For the absorption due to excitons, however, $\Gamma(E)$ is important only in energy regions for which $|E-E_0| \ll E_0$. The neglect of the phonon coupling between crystal states having no excitons and crystal states with excitons present is completely analogous to approximating the actual imaginary part of the dielectric constant of a damped harmonic oscillator

$$\epsilon_i = \frac{A\omega}{(\omega^2-\omega_0^2)^2+4\omega^2\Gamma^2} \tag{8}$$

by

$$\epsilon_i \approx \frac{A/4\omega_0}{(\omega-\omega_0)^2+\Gamma^2} \tag{9}$$

a procedure well justified for $|\omega-\omega_0| \ll \omega_0$.

3. THE FORM OF $\Gamma(E)$ FOR A TYPICAL EXCITON

Figure (2) shows the experimental forms of $\Gamma(E)$ for the $n = 1$ exciton state in CdS formed from an electron in the conduction band and a hole in the top valence band at 77°K. $\Gamma(E)$ is plotted versus $E-E_0$, the amount of energy by which the $\boldsymbol{k} = 0$ state is suppressed in Fig. 1(b).

For the exciton band of lowest energy, $\Gamma(E)$ will generally be characterized, like the data in Fig. 2, by a rapid drop-off for small E. The reason for this is clear when reference is made to Fig. 1(b). For $E_0-E > 0$, phonons must be found to supply energy E_0-E. For $E_0-E > kT$, $\Gamma(E)$ will tend to drop exponentially with decreasing E. Analogy might be made between Fig. 1(b) and the energy level of a donor below a conduction band. $\Gamma(E)$ is exactly analogous to the rate at which the donor state ionizes, which tends (under suitable approximations) to decrease exponentially with binding energy.

At least a part of the detailed structure of $\Gamma(E)$ can be quantitatively understood. At 77°K there are still a few longitudinal optical phonons around, having an energy of $0{\cdot}038_5$ eV. These scatter the exciton quite strongly, and, of course, give rise to a $\Gamma(E)$ which has a threshold at $E+\hbar\omega_l = E_0$. The experiments of THOMAS *et al.*[3] showed that $\Gamma(E)$ behaves like a function of energy multiplied by $\exp(-\hbar\omega_l/kT)$ (over the energy range between $E-E_0 = 0{\cdot}038_5$ eV and $E-E_0 \approx -0{\cdot}018$ eV) as would be expected for such a process. DIETZ *et al.*

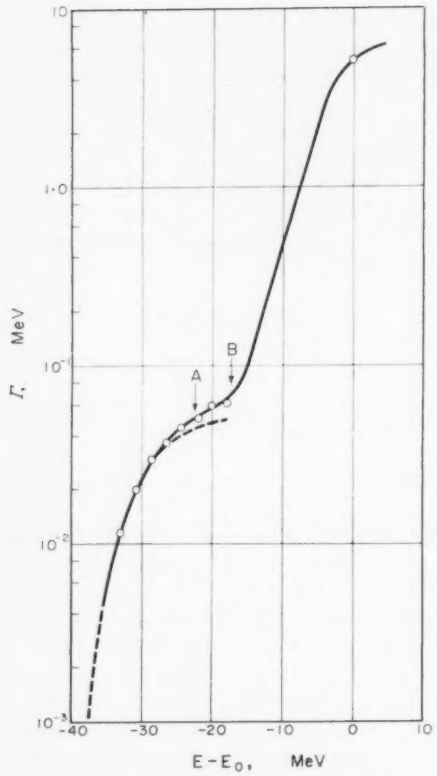

FIG. 2. The experimental form of $\Gamma(E)$ for the lowest exciton state in CdS at 77°K. Energies are measured in electron millivolts from the exciton line. The data below -18 is from the absorption spectrum measured by THOMAS *et al.*[3]. The point at the exciton energy was measured in reflection by THOMAS and HOPFIELD[4]. The region between -5 and -15 was filled in by a temperature extrapolation of measurements by DUTTON[5], and is only qualitatively correct due to the difficulty of extrapolation. The dashed line represents the theoretical form of $\Gamma(E)$ for intraband optical phonon absorption. The point of possible onset of intraband optical mode scattering is indicated by the arrows.

have observed similar behavior in ZnO. The calculated form of $\Gamma(E)$, according to the expression given in Ref. (4) is shown in Fig. 2 by the dashed line.

At higher energies, more processes which involve the absorption of a longitudinal optical phonon become possible. At the threshold marked A, scattering of the $n = 1$ exciton state of the top valence band into the $n = 1$ state of the second valence band becomes energetically possible. At the threshold B, intra-exciton band scattering becomes possible from the $1S$ state of the top valence band to the $2S$ and $2P$ states of the top valence band.

The sharp rise in $\Gamma(E)$ above $E-E_o = -20$ is probably due to acoustic two phonon processes. When E_o-E approaches kT, but $kT \ll \hbar\omega_l$, these processes would be expected to become important. In CdS, two phonon acoustic mode scattering by the piezoelectric effect is probably the most important mechanism of scattering at 77°K in the energy range from -10 to $+20$ meV. For $E_o-E > -kT$, it is easy to find phonon combinations which will conserve energy, and the sharp rise in $\Gamma(E)$ will flatten off. For $E \approx E_o$, $\Gamma(E)$ will in general increase slowly, varying only algebraically with energy.

Single phonon acoustic mode scattering does not give an appreciable contribution to $\Gamma(E)$ over at least the range covered in Fig. 2. The process is energetically possible when $E-E_o > -\frac{1}{2}\mathcal{M}MU^2$, where M is the total mass of the exciton and U the velocity of sound. The density of states for the process near $E = E_o$ is extremely small. In CdS, the two-phonon acoustic phonon–exciton intraband scattering is large because of piezoelectric coupling to the electron and hole. Piezoelectric scattering, however, does not contribute to one-phonon intraband scattering of excitons.

Over the energy range from the optical phonon threshold to $E-E_0$ equal to 10 or 20 meV, what is generated by the optical absorption is essentially always the $n = 1$ exciton state. Different energies in this range, however, do correspond to the generation of excitons having different kinetic energies.

The form of $\Gamma(E)$ shown was to a great extent influenced by the fact that the lowest energy exciton state was investigated. All higher exciton bands can make transitions by single acoustic mode phonon emission to lower energy exciton bands. For such transitions, $\Gamma(E)$ would be much more nearly constant in the vicinity of the exciton energy.

MOSER and UHRBACH's rule[7] of the form of an optical absorption edge is a high-temperature rule[3] involving many phonons. The exciton–phonon interaction cannot in such a case be considered as weak, and the formalism of Section 2

Vol. 22
1961

is not applicable. Nonetheless, the simple picture of the ionization rate of a single depressed level of Fig. 1(b) gives at least a plausible explanation for an exponential dependence of $\Gamma(E)$ on $\exp[-E_o-E/kT]$, and perhaps a qualitative description of MOSER and UHRBACH's rule in the case of excitons.

4. THE CONSEQUENCES OF THE ENERGY-DEPENDENT WIDTH IN PHOTOCONDUCTIVITY MEASUREMENTS

In order that the excitons produce photoconductivity, it is of course necessary to somehow break up the exciton to get free charge carriers. How this takes place (thermal ionization, the giving up of a carrier to a charged impurity, etc.) is of great interest in photoconductive research, but is not our present concern. We will assume only that some process of breakup is possible, and that, given an exciton of energy S, there will be some $P(S)$ probability per unit time that this exciton will yield a free charge carrier by some process. (Such a function will, in general, not depend very strongly on S.) In the general case, $P(S)$ will also depend on the spatial position of the exciton if inhomogeneities or surfaces are present. We also assume that the crystal is sufficiently pure that the absorption of the light is due to excitons and band-to-band processes, and not due to impurity centers.

Consider now the absorption in the immediate vicinity of an exciton absorption line. Over a narrow energy region which contains the absorption line peak, $\Gamma(E)$ and the processes which control it will be nearly constant. Thus the exciton final state after absorption will be (in terms of energy and wave vector distribution) almost independent of the photon energy. The only large physical difference between the exciton final state for $E = E_o$ (the absorption peak) and, for example, $E = \pm\,\Gamma(E_o)$ (the absorption half-power points) is the spatial distribution of the generated excitons. In the immediate vicinity of an exciton absorption peak, the photoconductive response will therefore be given by $R = f(\alpha)$ where $f(\alpha)$ is a function only of the absorption constant, α, for a given crystal, temperature, intensity, and experimental geometry, $f(\alpha)$ is the solution to the following problem at $E = E_o$. "The final state excitons have a kinetic energy and exciton band distribution which can be calculated if the contributions to $\Gamma(E_o)$ are understood. If the same distribution in states is given a spatial distribution $N_o \exp(-\alpha x)$, what is the photoconductive response?"

The calculation of $f(\alpha)$ is of course extremely difficult. We wish only to emphasize that the study of the photoconductive response in the immediate vicinity of the exciton absorption lines is a study chiefly of $f(\alpha)$, the effect of inhomogeneous spatial generation, on the photoconductive response. Whether $f(\alpha)$ has maxima, minima, or no structure at all in this energy region is determined only by the inhomogeneities of the problem.

For energies farther from E_o, $\Gamma(E)$ can change from its value $\Gamma(E_o)$. Such a change is normally accompanied by a change in "final state" for the $\mathscr{H}$ problem. Such a change will also in general change $P(S)$, and the photoconductive response will therefore be altered.

There would seem, therefore, to be two types of analysis of experiments which could yield particularly useful information about the photoconductive process. The first is the study, near a single absorption line, of $f(\alpha)$. The second is the comparison, at a constant level of α, of the photoconductive response for different energies. This experiment would reveal the dependence of the photoconductive response on the final states of the exciton after absorption. In the one-exciton band problem, for example, this might yield the dependence of $P(S)$ on the exciton kinetic energy.

The dependence of the photoconductive response on α can be well illustrated by comparing the work of APFEL and PORTIS[8] on the photoconductivity of Cu_2O with the experimental work of NIKITINE[9] and his collaborators on the absorption spectrum of Cu_2O.

ELLIOTT[10] has pointed out that the large low temperature line width of the $n = 2$ and higher exciton states compared to the line width of the $n = 1$ (forbidden) absorption line is probably due to the emission of a longitudinal optical phonon in the transition.

$$2P_{k=0} \rightarrow 1S_k + \text{optical phonon}_{-k}.$$

The $1S$–$2P$ energy separation is about 8 times the energy of an optical phonon, so the process is quite feasible. Strong support is given to this argument by the experiments of ZVEREV, *et al.*[11] who measured the temperature dependence of

the $2P$-state line width. The measured temperature fits reasonably well the form $\Gamma(E_{2P}) = A \coth \hbar\omega_0/2kT$ expected for such a process, for $\hbar\omega_0 = 95\ \text{cm}^{-1}$. There is a known longitudinal optical phonon having an energy of about $100\ \text{cm}^{-1}$. (ZVEREV *et al.* interpreted their results rather differently.)

The generated final state after the absorption of light anywhere in the yellow exciton series is thus a $1S$ exciton having kinetic energy $(E-E_{1S}-\hbar\omega_l)$ where E_{1S} is the energy of the $\boldsymbol{k} = 0$ $1S$ exciton. (Actually, there are two slightly split $1S$ states, a singlet and a triplet, but this is unimportant.) In the energy region near E_{2P}, (say $\pm$ 20 mV), the fractional change in the kinetic energy of the $1S$ exciton generated is negligible. Over this energy region, the final states are essentially constant, and have a kinetic energy very nearly equal to $E_{2P}-E_{1S}$.

The absorption continuum in Cu_2O, which starts at low temperatures near the energy of the $1S$ state, has been studied in detail by NIKITINE[9] and interpreted by ELLIOTT[12] on the basis of transitions via higher bands to the $1S$ exciton states with phonon emission at low temperature (and, of course, with both emission and absorption at high temperatures). The energy of the phonon is small (the phonon actually seems to have the same energy as the phonon involved in the $2P$ exciton decay), so that in the neighborhood of $E \approx E_{2P}$, the final state is again a $1S$ exciton having kinetic energy $E_{2P}-E_{1S}$. The phonon energy in this case has been measured to be $10^4\ \text{cm}^{-1}$.

The absorption spectrum for Cu_2O at 4·2° is shown in Fig. 3(a). (The absorption spectrum at 100° is qualitatively similar.) The continuum and the exciton $2P$-state have, at $E = E_{2P}$, similar contributions to the absorption constant. The photoconductivity of polycrystalline Cu_2O as measured by APFEL and PORTIS is shown in Figs. 3(b) and 3(c). Two different types of experiments were done, whose difference we will not attempt to describe or interpret.

APFEL and PORTIS noted that the exciton $2P$- and $3P$-states were visible in the photoconductive spectrum, and suggest that there was a photoconductive effect specifically associated with excitons. From the point of view we have adopted, the optical absorption process in Cu_2O always

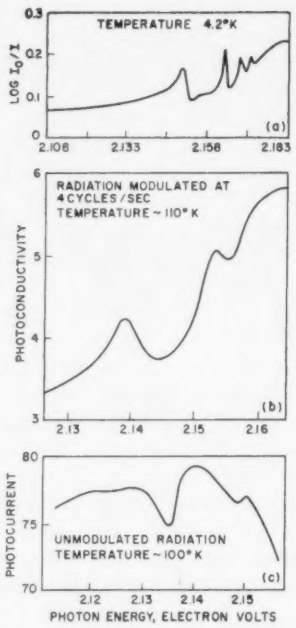

FIG. 3(a). The absorption spectrum of Cu_2O in the region of the yellow exciton series (after NIKITINE *et al.*[9]). This data should be shifted 0·010 eV to the left to compensate for the temperature shift between 4°K and 100°K. (b) and (c). Two observed forms of the photoconductivity of Cu_2O in the region of the yellow excitons at about 100°K (after APFEL and PORTIS[8]).

generates excitons, energetic $1S$ excitons, over the range of energy shown in Fig. 3, and the photoconductive response in this narrow energy region should be very nearly a function of the absorption constant alone.

It is clear in the comparison of Figs. 3(a) and 3(b) that the absorption constant and the photoconductive response have the same form, and that the photoconductive response is a function only of α is quite plausible. Unfortunately there are at present no published absorption data available at the temperature at which they performed their experiment, and a quantitative determination of the relation between α and the photoconductive response cannot be made.

A comparison of Figs. 3(a) and 3(c) is more distressing. APFEL and PORTIS have characterized their data as having here valleys in the positions of the exciton absorption peaks, and have suggested

Vol. 22
1961

that the excitons have some peculiar properties not associated with the background photoconductivity. A more reasonable explanation in the light of the previous discussion would be that the photoconductive response is a function of α, but that it increases for small α, reaches a maximum near $\alpha = 150$ cm^{-1}, and declines again for α larger than this. Since the background absorption due to the indirect processes has a value of about 150 cm^{-1} at the exciton $n = 2$ peak, the increase in absorption at the $2P$ peak would then decrease the photoconductive response. A detailed inspection of the photoconductive response shows that this explanation is at least qualitatively tenable. In the absence of absorption constant data, we will compare directly Fig. 3(b), for which the photoconductive response increases monotonically with α, and Fig. 3(c), for which there is a maximum in the response for $\alpha = 200$ (i.e. for the α which happens to occur. among other places, at about 2·14 eV). In Fig. 3(b), the photoconductive response at the far right of the figure is greater than that at the $n = 2$ exciton peak and increasing. For Fig. 3(c), one would predict that the photoconductive response at the far right should therefore be less than that at the $n = 2$ valley and decreasing, because α is larger than the value at which the photoconductive response has its maximum. Other qualitative comparisons of Figs. 3(b) and 3(c) also indicate that Fig. 3(c) seems consistent with a photoconductive response which is a function of α only.

We do not wish to go into the details of the experimental difference between the experiments which produced curves 3(b) and 3(c), or their interpretation. It should be added, however, that in order to obtain a photoconductive response which has a maximum for a given value of α, a characteristic length of α^{-1} should exist in the problem. In the experiments of Fig. 3(c), such a length would be about 50μ. Two possibilities for such a characteristic length specifically arise from the experimental geometry, the electrode separation (100μ) and the mean crystallite diameter (also 100μ).

5. THE SUPERPOSITION OF ABSORPTION CONSTANTS

It might be off-hand assumed that if equation (6) is a valid expression for the absorption constant due to one exciton, one could simply superpose expressions like (6) to obtain the effect of all exciton and continuum states. Unfortunately, this is not universally valid.

Consider the following system. State $|0\rangle$ (to be regarded as photon) is coupled to discrete state $|1\rangle$ and $|2\rangle$. For simplicity, $E_1, E_2 \neq E_0$. These discrete states are in turn coupled to a continuum of final states $|f\rangle$. The rate of decay of state $|0\rangle$ is then given simply by:

$$W_0 = \frac{2\pi}{\hbar}\left|\frac{H_{01}H_{1f}}{E_0-E_1}+\frac{H_{02}H_{2f}}{E_0-E_2}\right|^2 \rho_f, \qquad (10)$$

where ρ_f is the density of states (i) at energy E_0. This transition rate is analogous to an absorption constant.

If state (1) were coupled to a continuum of final states (f') and state to a different continuum of final states (f^2), the result would be

$$W_0 = \frac{2\pi}{\hbar}\left\{\left|\frac{H_{01}H_{1f}}{E_0-E_{f'}}\right|^2 \rho_{f'}+\left|\frac{H_{02}H_{2f}}{E_0-E_{f''}}\right|^2 \rho_{f''}\right\}. \qquad (11)$$

Each of the two terms in (11) is analogous to (10) for a single level, and the absorptions are additive. From the comparison of (10) and (11), one sees that the absorption constant due to two different exciton intermediate states will not be additive in energy regions in which both (1) each intermediate state considered separately would produce comparable absorption constants, and (2) the final states which dominate the "width" of each exciton at the energy under consideration are not disjoint.

The form of (10) indicates that when $H_{01}H_{1f}$ and $H_{02}H_{2f}$ have complex phases which do not differ by 90°, an interference effect between transitions via state $|1\rangle$ and state $|2\rangle$ will occur. Under these circumstances, absorption constants are not additive. For the two cases $E_0-E_1 < 0$ and $E_0-E_1 > 0$, the relative signs of the one part of the compound matrix element with respect to the other is different. This effect results in an asymmetry of the absorption "due to state (1)". When the damping due to states (f) is included, which introduces an imaginary term in the energy denominators of (10), it is found that, regardless of the phase of $H_{01}H_{0f}$ and $H_{02}H_{2f}$ an interference effect results, and the absorptions "due to state (1)" and "due to state (2)" are not additive.

Cu_2O in the energy region of the yellow exciton series seems to present an example of a system in

which the interference between optical transitions plays an observable part in determining the energy dependence of the absorption spectrum. The shape of the $n = 2$ and $n = 3$ exciton lines are both quite asymmetric. ZVEREV, *et al.*[11] have interpreted this result on the basis of acoustic phonon intra-exciton band scattering and TOYAZAWA's theory of the shape of absorption lines. As was pointed out in Section 3, it is much more likely that optical mode scattering involving interband scattering is the dominant source of line width. ELLIOTT suggested that a rapid variation of the scattering matrix element for the $2P \rightarrow 1S$ optical mode transition might lead to an asymmetry. Indeed, a rapid change with wave vector of this scattering matrix element would lead to a $\Gamma(E)$ which would *not* be nearly constant at the exciton energy, and an asymmetric line would result. It is a bit difficult to believe, however, that the matrix element changes rapidly enough to cause the observed asymmetry.

A simpler explanation of the asymmetry of the $n = 2$ yellow exciton line can be based on the qualitative conclusions of equations (10) and (11). It is known that the $n = 2$ absorption line lies on top of a continuum due to something else, and that the $n = 2$ line peak absorption coefficient is comparable to the continuum absorption at the exciton energy. Thus the first criterion for non-additive absorption constants is met.

It is believed that the continuum on which the $n = 2$ state lies is, at low temperatures, due to the absorption of light via a virtual transition to a higher band, producing as a final state a $1S$ exciton and an optical phonon of about 100 cm^{-1}. It is suggested that the width of the $n = 2$ state is due to transitions to the $1S$ state with the emission of a phonon of about 100 cm^{-1} also. Suppose that, at least part of the time, the phonons associated with the $2P \rightarrow 1S$ decay and the phonons associated with continuum belong to the same branch of the lattice vibration spectrum. The final states for the two processes will not then be disjoint, and the second criterion for the observation of non-additivity of absorption constants will be met.

If the phonons associated with the two processes are indeed always the same, it can easily be shown that the absorption constant *away from the center of the line* is given in this case by

$$\alpha(E) = \left| |\alpha_1(E)|^{\frac{1}{2}} \frac{|E - E_{2P}|}{E_{2P} - E} + e^{i\theta} |\alpha_2(E)|^{\frac{1}{2}} \right|^2,$$

where $\alpha_1(E)$ is the absorption constant which would exist for the $2P$ exciton state if the continuum absorption could not be excited via a higher band, $\alpha_2(E)$ the absorption constant which would be present if the $2P$ exciton state did not exist, and θ a phase factor. The change in sign of the first term in between $E < E_{2P}$ and $E > E_{2P}$ will in general introduce an asymmetry in $\alpha(E)$ about E_{2P}, even when $\alpha_1(E)$ and $\alpha_2(E)$ were symmetric about E_{2P}.

It is thus possible that the $n = 2$ and $n = 3$ P states of the yellow series in Cu_2O have line shapes that would be symmetric (and presumably nearly Lorentzian) except for the existence of the continuous background. A nonadditivity of absorption constants can reasonably explain the observed large asymmetry.

6. CONCLUSION

A formalism for understanding exciton line shapes in weak coupling was presented. The formalism treats the tails and the center of the absorption line on the same basis, and emphasizes the question of what is actually produced in the absorption process.

The photoconductive response is dependent on what is produced and where it is produced in the absorption process. The former depends explicitly only on the energy of the incident photon; the latter depends explicitly only on the absorption constant. The spectral dependence of photoconductivity can give information about both subjects. Unfortunately the absorption constant itself depends upon the energy of the incident light. In order to understand the spectral dependence in the exciton region, it is in general necessary to understand the absorption process and its final states. As was shown in the case of Cu_2O, to assume that, because the absorption constant shows a peak, one is observing the real generation (rather than the virtual generation) of that exciton is not correct.

The simplest method of obtaining real information about the photoconductive response due to excitons would be to measure the response near an exciton absorption line. If the exciton belongs to the series corresponding to the smallest band gap, it is fairly certain, at low temperatures, that

Vol. 2
1961

excitons would be generated, (although perhaps not the exciton which corresponds to the energy of the photon). This could then be compared with the photoconductive response at an energy in the continuum, where free electron–hole pairs are generated. It would be important to make such a comparison at energies chosen such that the continuum and the exciton have the same absorption coefficient *in the crystal being measured.*

A simple method of measuring the specific effect on the photoconductivity on absorption constant would be to measure the absorption constant and photoconductive response in a single sample in the vicinity of a single absorption peak. In this case, what is actually generated would be relatively constant over a small energy interval, while the absorption constant would change rapidly over this same small interval.

Finally, an example was given in Cu_2O where the absorption coefficients due to two different processes are not additive because the final states for these two processes are not disjoint. This non-additivity may explain the asymmetry of the $n = 2$ exciton line in the yellow exciton series of Cu_2O.

Acknowledgements—The author is indebted to A. R. HUTSON for information on piezoelectric effects in CdS, and to S. NIKITINE and his co-workers for discussions of the properties of Cu_2O.

REFERENCES

1. TOYOZAWA Y., *Progr. Theor. Phys. Osaka* **20,** 53 (1958); **19,** 214 (1958).
2. See, for example, HEITLER W., *The Quantum Theory of Radiation*, p. 164. Clarendon Press, Oxford (1954).
3. THOMAS D. G., HOPFIELD J. J. and POWER M., *Phys. Rev.* **119,** 570 (1960).
4. THOMAS D. G. and HOPFIELD J. J., *Phys. Rev.* **116,** 573 (1959).
5. DUTTON D., *Phys. Rev.* **112,** 785 (1958).
6. DIETZ R. E., HOPFIELD J. J. and THOMAS D. G. *J. Appl. Phys.* in press.
7. MOSER F. and URBACH F., *Phys. Rev.* **102,** 1519 (1956).
8. APFEL J. H. and PORTIS A. M., *J. Phys. Chem. Solids* **15,** 33 (1960).
9. NIKITINE S., GRUN J. B. and SIESKIND M., *J. Phys. Chem. Solids* **17,** 292 (1961); NIKITINE S. and REISS R., *J. Phys. Chem. Solids* **16,** 237 (1960).
10. ELLIOTT R. J., *Proceedings of International Conference on Semiconductor Physics, Prague*, 1960, pp. 408–410. Czechoslovak Academy of Sciences, Prague (1961).
11. ZVEREV L. P., NOSKOV M. M. and SHUR M. YA., *Sov. Phys.–Solid State* **2,** 2357 (1961) (Amer, Inst. Phys. translation).
12. ELLIOTT R. J. (to be published).

DISCUSSION

P. T. LANDSBERG: I take it that Uhrbach's rule is purely empirical, and I wonder if you would care to state it for us.

J. J. HOPFIELD: Uhrbach's rule states that the low energy absorption tail of the fundamental absorption edge behaves like:

$$\alpha = A \exp[-\gamma(E_o - E)/kT]$$

where A, γ, and E_o are experimental constants.

P. T. LANDSBERG: Is this rule supposed to hold for $E < E_o$ and $E > E_o$?

J. J. HOPFIELD: Uhrbach's rule holds experimentally only for $E < E_o$. The behavior of $\Gamma(E)$ is quite different for $E < E_o$ and for $E > E_o$, where it is not necessary that phonons supply energy.

E. BURSTEIN: Can you give a physical interpretation of Uhrbach's rule?

J. J. HOPFIELD: The rate of generation of free carriers across the band gap E_o at temperature T is given by:

$$R = \text{const} \times \exp(-E_o/kT).$$

The presence of a photon of energy E simply has the effect of reducing the energy which needs to be supplied by the lattice from E_o to $(E_o - E)$. Thus the rate of generation of pairs due to the presence of a photon is:

$$R = \text{const} \times \exp[-(E_o - E)/kT].$$

This rate of generation is proportional to the absorption constant, so a qualitative interpretation of Urbach's rule results (but with $\gamma = 1$).

M. LAMPERT: In what way are polaron effects (particularly low-temperature, temperature-independent polaron effects) included in your calculation?

J. J. HOPFIELD: At the band edge, polaron effects (for zero temperature) renormalize the bandgap, particle masses, and electron–hole interactions, but are not specifically visible. Observed masses will refer to polaron masses, and the observed bandgap is the rigid-lattice bandgap less the electron and hole binding energies. At energies above the band edge, specific effects of the interaction of the carriers with the lattice will become observable.

M. LAMPERT: Would you expect to see a difference, at low temperatures, in the optical bandgap (free-free transitions) from the thermal bandgap, i.e. does the bandgap light absorption correspond to the creation of *unclothed* electrons and holes?

J. J. HOPFIELD: Imagine a crystal at $T = 0$ with an electron and hole each at $\boldsymbol{k} = 0$. The electron and hole are clothed in phonons. By definition of the bandgap E_o at $T = 0$, the energy of this state is E_o above the energy of the ground state. Let the electron and hole recombine. There will be emission of a photon accompanied by 0, 1, 2, etc. phonons. In weak coupling, the probability that a photon is emitted with no phonon is finite so that a finite fraction of the time, a photon of energy E_o will be emitted. At $T = 0$, the reverse process will take place but phonon absorption is impossible. The optical bandgap in absorption is therefore the same as the thermal bandgap at $T = 0$ in weak coupling.

E. BURSTEIN: Can you tell us something about the physics underlying the asymmetry in the exciton lines and also something about the nature of the phase factor?

J. J. HOPFIELD: When a transition can take place from state $|0\rangle$ to state $|f\rangle$ via two channels, the transition amplitudes for the two channels must be added and squared to find the net rate. The transition amplitude via a single channel changes sign as one goes through resonance. The square of the sum of the amplitudes will not then be symmetric around a resonant frequency. In the present problem, the phase factor (although in principle calculable from the Hamiltonian) is introduced because the relative phase of the two channels is not known.

Vol. 22
1961

J. Phys. Chem. Solids Pergamon Press 1961. Vol. 22, pp. 73–79. Printed in Great Britain.

TEMPERATURE DEPENDENCE OF THE FUNDAMENTAL ABSORPTION TAIL OF KCl AND OF THE ABSORPTION DUE TO BROMINE IONS IN KCl

K. KOBAYASHI

Institute for Solid State Physics, University of Tokyo, Tokyo, Japan

and

T. TOMIKI

Department of Physics, Tohôku University, Sendai, Japan

Abstract—Optical absorption in the fundamental absorption tail of specially purified KCl and that due to bromine ions in KCl were measured between room temperature and 196°C. The latter was estimated from the difference between the fundamental absorption tails of pure KCl and KCl with bromine of which the concentration was $1{\cdot}3 \times 10^{-4}$ mole fraction. Measured absorption coefficients were corrected by considering the errors due to the finite band width of the spectrometer. The fundamental absorption tail of KCl was found to be represented by the Urbach rule with $\sigma = 0{\cdot}80 \pm 0{\cdot}02$ and $h\nu_0 = 7{\cdot}76 \pm 0{\cdot}10$ eV. The long wavelength side of the bromine absorption was describable by the same rule where $\sigma = 0{\cdot}51 \pm 0{\cdot}03$ and $h\nu_0 = 7{\cdot}35 \pm 0{\cdot}15$ eV.

1. INTRODUCTION

ABSORPTION coefficients of some ionic crystals in their fundamental absorption tails have been known to change exponentially with photon energy and with temperature. This behavior has been known as the Urbach rule and was first found by URBACH[1] in silver bromide. For alkali halides, MARTIENSSEN[2] has made measurements of the absorption tail in pure KBr, and HAUPT[3] in pure KI, and they have found that these tails can be described fairly well by the Urbach rule over a very wide range of temperature and absorption coefficient. The tails of these crystals are believed to be due to exciton absorption so that their results have given important information on the exciton picture in alkali halides.

The purpose of this study is two-fold. Firstly, no work relating to the Urbach rule has been made on the fundamental absorption tail of KCl, the most typical substance among potassium halides. As has been reported in our previous paper,[4] we have succeeded in preparing pure KCl with a clean fundamental absorption tail by eliminating impurity bromine ions which are present in fairly large amount in crystals commonly used. Therefore, it is interesting to investigate the fundamental absorption tail of such pure KCl. Secondly studies on the absorption tails made so far are on pure alkali halides and the observed exciton absorptions are due to halide ions surrounded by alkali ions and halide ions of the same kind. If one changes the environment around a halide ion in whose optical excitation one is interested, by replacing the surrounding halide ions with another halide, and compares its absorption with that of the pure crystal, one may obtain some new information on excitons in alkali halides because of the effect of a local change of lattice constant and electronic configuration. In a previous paper,[4] we found an absorption band due to bromine ions present in very small concentrations in KCl at the tail of the fundamental absorption of the host crystal. Therefore it would be worthwhile to study this band more thoroughly.

In the present paper, we shall report results of the measurements of absorption coefficients in the long wavelength tail of the fundamental absorptions of pure KCl and KCl containing $1{\cdot}3 \times 10^{-4}$ mole fraction of bromine at several different temperatures. The fundamental absorption tail of

KCl is obtained from measurements on the former crystal. The absorption due to bromine is estimated from the results of both crystals. We find that both the fundamental absorption tail of pure KCl and the long wavelength side of the absorption due to bromine in KCl can be described fairly well by the Urbach rule.

2. MEASUREMENTS AND RESULTS

KCl–aK–1,[4] the KCl crystal used in this study as a pure crystal with clean fundamental absorption tail, was prepared from purified bicarbonate and hydrochloric acid by the method which has been developed by us[4] and it contains bromine ions of 9×10^{-6} mole fraction and divalent metallic ion impurities of 1×10^{15} per cm^3. KCl–bK–1,[4] the KCl crystal in which bromine absorption is investigated, contains bromine ions of $1{\cdot}3\times10^{-4}$ mole fraction and divalent metallic ion impurities of 4×10^{15} per cm^3. Hydroxyl ions in a concentration of 2×10^{15} per cm^3[4] were found in both crystals.

Optical transmission in the absorption tails of both crystals was measured by a vacuum ultraviolet spectrometer with a band pass of about 2 mμ at 26°, 56°, 100°, 147° and 196°C. In determining absorption coefficients from transmission measurements, it is necessary to take into account the light losses due to scattering at the surface and in the volume of the crystal, as well as specular reflection losses at the surface. We have shown in Ref. 4, however, that the scattering correction is negligible in these crystals and that the absorption coefficient can be estimated fairly well from the observed transmittance and reflectivity calculated from the refractive index.

It has been pointed out by MOSER and URBACH[5] that an appreciable error might be introduced into a determination of an absorption coefficient, K, as a result of using a finite band width in a measurement of a transmission where an absorption coefficient changes markedly with a wavelength, λ. Their analysis shows that if a band width is finite and an absorption coefficient is represented by $K = K_1\exp(-b\lambda)$, where K_1 and b are constants, an absorption coefficient calculated from a measured transmittance of a crystal with certain thickness must be different from that of a crystal of different thickness. Only an observed absorption coefficient satisfying the condition $Kd = 1$ is a true absorption coefficient of a crystal with a thickness d.

Figure 1 is an example of the present measurements of absorption coefficients in the tails of KCl–aK–1 and KCl–bK–1 at 56°C. They were calculated from the measured transmittances of the crystals with different thicknesses and the refractive indices. One may readily see that the observed absorption coefficients are always higher for the crystal with smaller d. This is the tendency which can be derived from the analysis by MOSER and URBACH[5]. Double circles in this figure are the points where Kd is unity. These points are well represented by straight lines in log K versus photon energy plots as indicated by dashed lines. This exponential behavior of the absorption coefficient with photon energy may indicate that the analysis by MOSER and URBACH is applicable to the present observed values, since the exponential behavior may hold for photon energy as well as for wavelength if the range of wavelength is small. Therefore, the points at $Kd = 1$ are the absorption coefficients free from errors due to the finite band width, and the dashed lines may be the true absorption tails of both crystals.

Measurements on crystals with different thicknesses at other temperatures have also indicated the same features as described above. Fig. 2 shows the true absorption tails of pure KCl (KCl–aK–1) at five different temperatures. Fig. 3 shows the photon energies corresponding to constant absorption coefficient in the curves in Fig. 2 as a function of temperature. Their extrapolations are found to cross one another at zero degrees Kelvin.

From Figs. 2 and 3, it may be found that the fundamental absorption tail of KCl can be represented by the Urbach rule:

$$K = K_0\exp\left[-\frac{\sigma(h\nu_0-h\nu)}{kT}\right], \qquad (1)$$

where K_0 and σ are constants, $h\nu$ the photon energy at K and T, and $h\nu_0$ the extrapolated photon energy at zero degrees Kelvin. Taking into account the errors due to the measurements, we found that $h\nu_0$ is $7{\cdot}76 \pm 0{\cdot}10$ eV and σ is $0{\cdot}80 \pm 0{\cdot}02$.

The absorption due to bromine ions in KCl–bK–1 were estimated at five different temperatures by subtracting the true absorption curves of KCl–aK–1 from those of KCl–bK–1. The

Vol. 22
1961

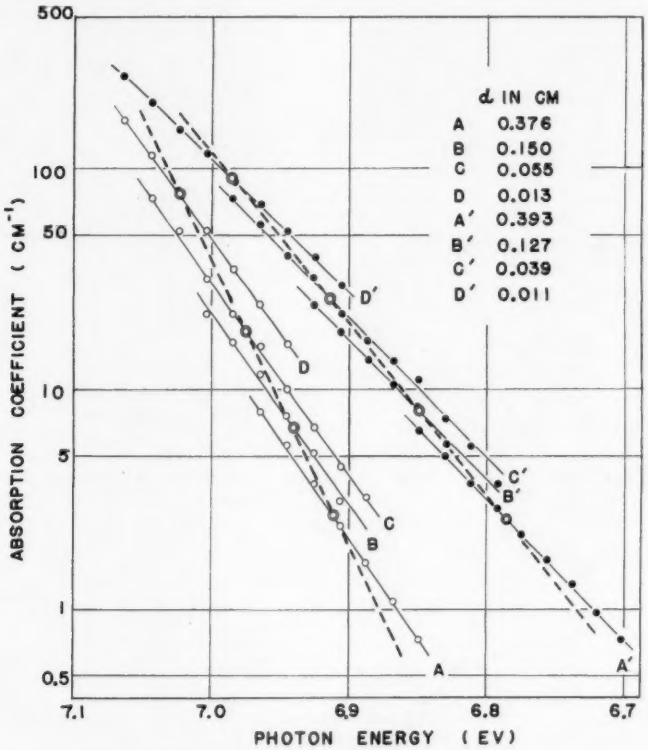

FIG. 1. Absorption spectra in the fundamental absorption tails of pure KCl (KCl–aK–1) and KCl containing bromine (KCl–bK–1) at 56°C. The open circles are the absorption coefficients calculated from the observed transmittances of KCl–aK–1 with different thicknesses, and the filled ones are those of KCl–bK–1. The dashed lines are those which connect the points where $Kd = 1$ (double circles). The thicknesses of crystals are indicated at the upper right hand of this figure.

results are shown in Fig. 4. One may note that these absorptions are due to bromine ions at concentrations of $1{\cdot}2 \times 10^{-4}$ mole fraction since the concentration of bromine in KCl–aK–1 is 9×10^{-6} and in KCl–bK–1 it is $1{\cdot}3 \times 10^{-4}$. In the low absorption coefficient region, absorption curves are linear in log K versus photon energy plots, and their slopes decrease with increasing temperature. The dashed lines are their linear extrapolations to high K value where they are found to cross one another at one point. The highest points among the observed ones are found to deviate from the linear relationship since they are the points which are close to the maxima of the absorption bands.[4] Fig. 5 shows the photon energies corresponding to constant absorption coefficient in the curves of bromine absorption for different temperatures in Fig. 4. Their extrapolations are found to cross one another at zero degrees Kelvin.

From Figs. 4 and 5, one may find that the absorption due to bromine in KCl can be described fairly well by the Urbach rule with $h\nu_0 = 7{\cdot}35 \pm 0{\cdot}15$ eV and $\sigma = 0{\cdot}51 \pm 0{\cdot}03$ in equation (1). Since the absorptions shown in Figs 4 and 5 are due to bromine ions of $1{\cdot}2 \times 10^{-4}$ mole fraction, the magnitude of K_0 is estimated as being in the range between 3×10^9 and 2×10^8 cm^{-1}, assuming that all chlorine ions in KCl are replaced by bromine ions without an accompanying change lattice constant and that there is no interaction

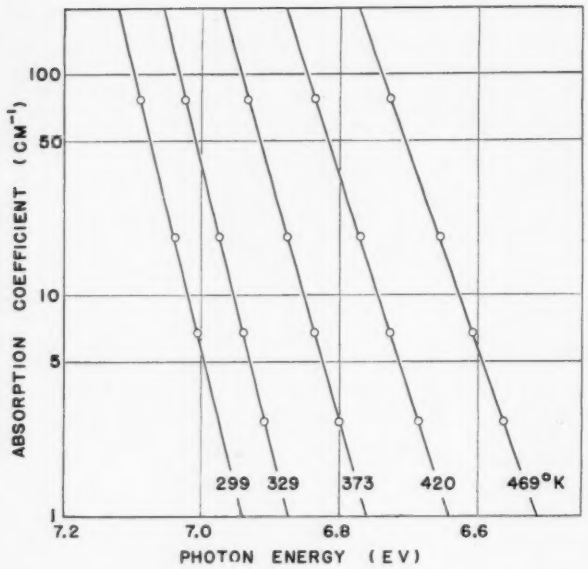

FIG. 2. Fundamental absorption tails of pure KCl at several different temperatures. The open circles are the points which satisfy the condition: $Kd = 1$, in observed absorption curves of crystals with different thicknesses. Temperatures are indicated in this figure on an absolute scale.

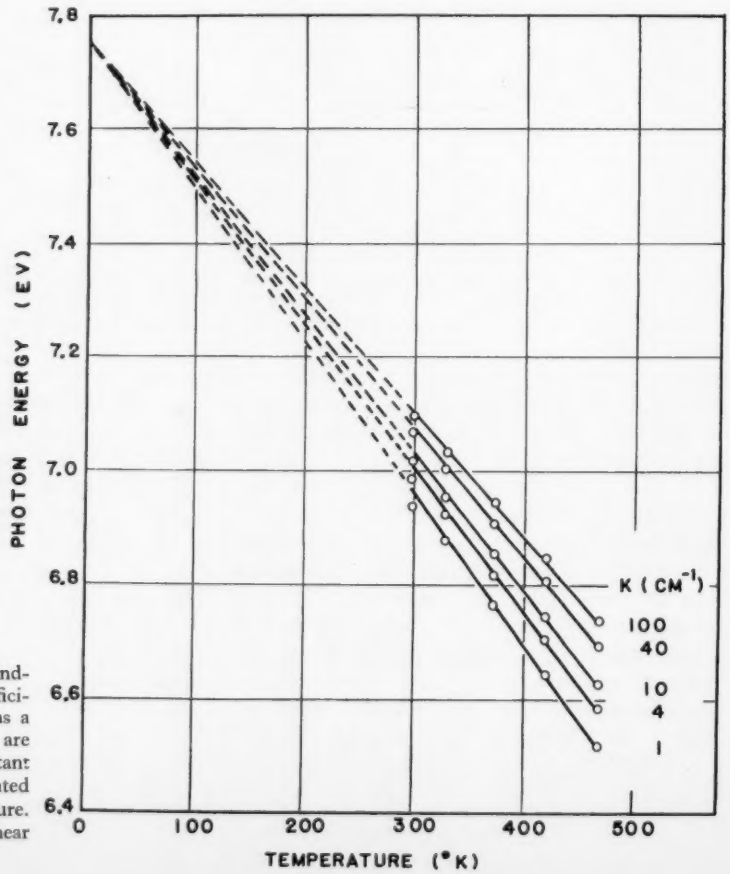

FIG. 3. Photon energies corresponding to a constant absorption coefficient in the curves in Fig. 2 as a function of temperature. They are represented by full lines for constant K of which magnitudes are indicated at the right hand side of this figure. The dashed lines are their linear extrapolations.

Vol. 22
1961

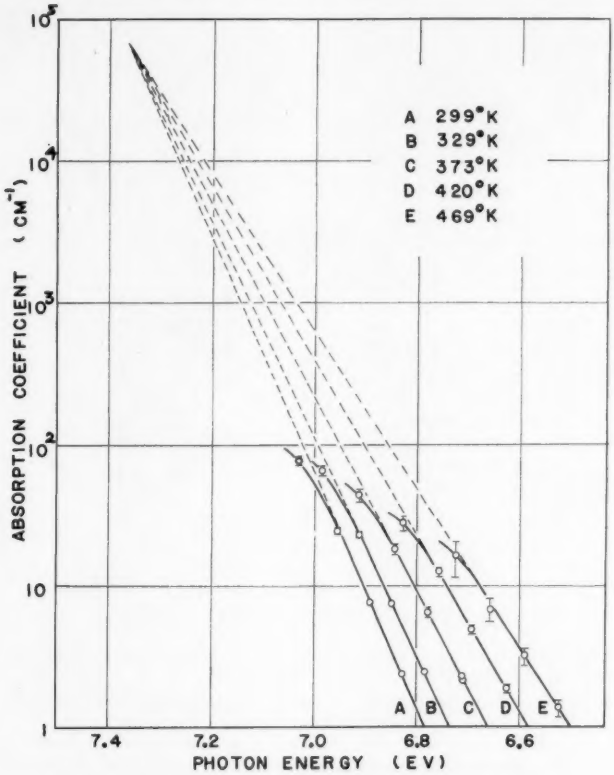

FIG. 4. Absorption spectra on the long wavelength side of the absorption band due to bromine in KCl at different temperatures (indicated in this figure on an absolute scale). The full lines are those which connect the observed absorption coefficients and the dashed ones are those extrapolated linearly to high absorption coefficient.

between bromine ions. If the lattice constant of KBr is used in the above estimation, K_0 may be smaller by about 10 per cent.

3. DISCUSSION

In present study, σ of the fundamental absorption tail of pure KCl has been determined as $0{\cdot}80 \pm 0{\cdot}02$. σ in KBr has been given by MARTIENSSEN[2] as 0·79 and in KI by HAUPT[3] as 0·82. These magnitudes are almost the same in spite of the difference in lattice constant and kind of halogen.

According to TOYOZAWA[6], σ may be represented by $C/|E_2|$ where C is an appropriate elastic constant and E_2 a constant to a quadratic term of deformation in the expression of electronic energy change as a function of deformation. Therefore, the difference of the lattice constant and the kind of halogen seems to be rather insensitive to the determination of the magnitude of $C/|E_2|$ of the exciton excitation of pure potassium halides.

It has been known that KCl and KBr make a good solid-solution. The concentration of bromine in KCl–bK–1 is as small as $1{\cdot}3 \times 10^{-4}$ mole fraction. Therefore, the bromine ions may be distributed randomly and the interaction between bromine ions through the host matrix may be negligible in this crystal. Thus the absorption due to the presence of bromine in KCl investigated in this study may be due to the isolated

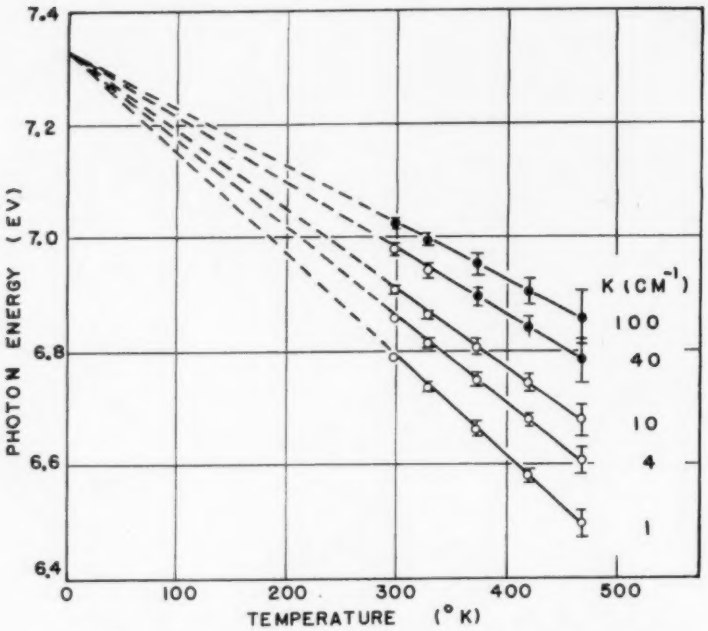

FIG. 5. Photon energies corresponding to a constant absorption coefficient in the absorption curves of bromine in KCl as a function of temperature. The open circles are taken from the observed curves in Fig. 4 and the filled ones are from the linearly extrapolated lines as indicated as dashed lines in Fig. 4. They are represented by full lines for constant K, of which magnitudes are indicated at the right hand side of this figure. The dashed lines are their linear extrapolations.

bromine ions which simply occupy the chlorine lattice sites.

The exact nature of this absorption due to bromine in KCl is not known. However, the position of the maximum of this absorption band can be estimated roughly by the assumption that the absorption is due to bromine ions themselves. The electron affinity of chlorine is 87·1 kcal, and that of bromine is 81·2 kcal;[7] the maximum of the first absorption peak of the exciton doublet of KCl is at approximately 7·52 eV at room temperature.[8] Thus the bromine absorption in KCl is expected to have its maximum at around 7·26 eV at room temperature which is not far different from 7·12 eV,[4] the observed position of the maximum. The maximum absorption coefficient of the bromine absorption in KCl, after being normalized to the case in which all chlorine ions in KCl are replaced by bromine ions, can be estimated as about 1×10^6 cm^{-1} from the maximum height of the bromine absorption in KCl–bK–1.[4] This magnitude is of an order comparable with the maximum height of the exciton absorption in KBr.[2] Therefore, it would be rather unlikely that this absorption is due to optical excitations of twelve chlorine ions at the second-nearest-neighbour sites around the bromine ion, but is very likely to be due to the bromine ions themselves.

It has been shown that the bromine absorption in KCl can be described by the Urbach rule. However, the magnitude of σ for the bromine absorption in KCl is 0·51 $\pm$ 0·03, which is far smaller than 0·79 for bromine in KBr[2] and 0·80 $\pm$ 0·02 for chlorine in KCl. The small magnitude of σ for the bromine absorption in KCl might be understood by different C and/or different E_2 from those of pure potassium halides as a result of strong distortion around the bromine ions.

Acknowledgements—We wish to thank Professor M. UETA for his allowing us to use his vacuum ultraviolet spectrometer. One of us (K.K.) is also indebted to Professors T. INUI and Y. TOYOZAWA for helpful discussions. A part of this work was supported by a Research Grant from the Ministry of Education of Japan.

REFERENCES

1. URBACH F., *Phys. Rev.* **92,** 1324 (1953).
2. MARTIENSSEN W., *J. Phys. Chem. Solids* **2,** 257 (1957).
3. HAUPT U., *Z. Phys.* **157,** 232 (1959).
4. KOBAYASHI K. and TOMIKI T., *J. Phys. Soc. Japan* **15,** 1982 (1960).
5. MOSER F. and URBACH F., *Phys. Rev.* **102,** 1519 (1956). See also Ref. 3.
6. TOYOZAWA Y., *Prog. Theor. Phys.* Suppl. **12,** 111 (1959).
7. MOTT N. F. and GURNEY R. W., *Electronic Processes in Ionic Crystals,* p. 8. Clarendon Press, Oxford (1946).
8. EBY J. E., TEEGARDEN K. J. and DUTTON D. B., *Phys. Rev.* **116,** 1099 (1959).

DISCUSSION

H. MAHR: We measured the absorption due to I^- diluted in KCl. From the slope of the exponential decay of the absorption constant at long wavelengths, we determined the constant σ of Urbach's law. Although at room temperature our value of $\sigma = 0{\cdot}49$ agrees well with the value of $\sigma = 0{\cdot}51$ found for Br^- in KCl, we noticed a strong temperature dependence of σ in the range from 80°K to 700°K. It can be explained by taking zero-point oscillations into account. For the limit of high temperatures σ approaches 0·77, very close to the value $\sigma = 0{\cdot}80$ found for pure KI, KBr and KCl.

K. KOBAYASHI: It would be interesting to measure the magnitude of σ for our case over a wider temperature range.

ol. 22
1961

BLANK
PAGE

Vol. 2
1961

J. Phys. Chem. Solids Pergamon Press 1961. Vol. 22, pp. 81–86. Printed in Great Britain.

EXPERIMENTAL STUDY OF EXCITON ABSORPTION IN PbI_2

I. IMAI*

The Institute for Solid-State Physics, The University of Tokyo, Tokyo, Japan

Abstract—The optical absorption spectra of evaporated films of PbI_2 in the region of 200–700 mμ were measured in the temperature range 298–37°K, using a Cary spectrophotometer, and at 4·2°K, using a spectrophotograph. Even at 4·2°K, the first band at 500 mμ shows rather smooth intensity distribution and does not split into hydrogen-like series lines. The general behaviour of the spectrum in PbI_2 was found to have similar characteristics to those of the Ag and Tl halides. The tail part of the longer wavelength side of the first band was measured in detail, using thicker samples, in which Urbach's rule is approximately valid. Our analysis of the spectrum of PbI_2 indicates that the exciton in PbI_2 does not resemble that of Cu_2O but is quite similar to that of the silver and thallous halides.

1. INTRODUCTION

ACCORDING to both experimental and theoretical investigations of excitons performed so far, it may be considered that two kinds of excitons, i.e. the so-called tight-binding exciton and loose-binding exciton, are relatively well understood at present.[1] The former corresponds to a small-size exciton of which the radius is smaller than the lattice constant and seems to be observed in alkali halides and similar crystals with relatively small dielectric constants.

The latter type of exciton corresponds to a large-size exciton, its radius being much larger than a lattice constant, and gives rise to hydrogen-like series line spectra as observed in Cu_2O. In theoretical studies of the tight-binding exciton, the excitation model and the transfer model have been proposed in approximate, one-electron treatments, whereas, for the loose-binding exciton, the effective-mass approximation initiated by WANNIER has been applied with fruitful results. However exciton absorption of silver and thallous halides, observed at low temperatures, seems to show characteristic behaviour between the two types of excitons mentioned above.

As for PbI_2, the absorption spectrum was first measured at room temperature by HILSCH and POHL[2], and FESEFELDT[3]. Recently, NIKITINE *et al.*[4] measured photographically the detailed behaviour of the absorption near 500 mμ in PbI_2 in the course of their systematic studies of exciton spectra of ionic crystals, and they reported several lines at liquid helium temperature subject to a hydrogen-like series formula, suggesting loose-binding exciton absorption. In order to clarify the exciton characteristics in PbI_2, the present measurement of the optical absorption spectrum of PbI_2 crystals over a wider range of wavelength was undertaken, special attention being paid to the spectrum near 500 mμ.

2. PREPARATION OF SAMPLES AND EXPERIMENTAL PROCEDURE

Samples used in our experiments were prepared in the following ways:

(1) *Vacuum-evaporated films.* These were evaporated on to fused quartz plates at room temperature. Thereafter, some of the samples were annealed at about 100°C, beyond which revaporization of the film occurred. The source materials for vaporization were pure single crystals obtained after a process of threefold repetition of the Bridgman method.

(2) *Iodized lead films.* Vacuum-evaporated Pb films on fused quartz plates were treated in an iodine atmosphere at about 120°C.

(3) *Single crystals.* Thin plates were obtained

* Paper presented by Professor T. MUTO

from blocks of single crystals prepared by the Bridgman method by cleaving along the plane perpendicular to the *c*-axis.

(4) *Single flakes.* The flakes were crystallized from a saturated aqueous solution of PbI_2.

(5) *Compressed samples.* Molten PbI_2 was compressed between two fused quartz plates or glass plates and then solidified.

X-ray diffraction patterns of some of these evaporated samples were observed using a Norelco diffraction camera. Diffracted lines from the planes perpendicular to the *c*-axis were found to be predominant, indicating that the micro-crystals in the evaporated film were preferentially oriented. Single flakes seemed to grow along a direction perpendicular to the *c*-axis, judging from the external form, and samples (5) also seemed to be crystallized in such a manner that the direction of the thickness was almost parallel to the *c*-axis.

The refractive indices of samples (1) and (2) at the Na D-line (589 mμ) and Hg green line (546 mμ) were measured by the method of Abelés and the simple Brewster angle method, respectively. The results are shown in Table 1, in which the dielectric constants at lower frequency are also described.[5] These values are larger than those of alkali halides, but nearly equal to or slightly larger than those of silver and thallous halides.[6] As seen in Table 1, the smaller refractive indices observed in the evaporated film, compared with those in the single crystal, will be ascribed to some porosity in the former sample.

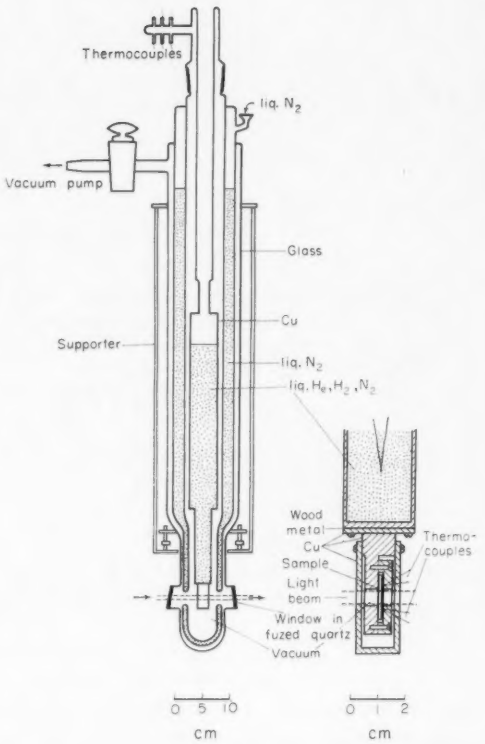

FIG. 1. Cryostat used with Cary recording spectrophotometer.

Table 1. *Refractive indices and dielectric constant of* PbI_2

	Evaporated film	Single crystal
Refractive index (Na–*D* 589 mμ)	2·84 ± 0·04	3·00 ± 0·15
Refractive index (Hg 546 mμ)	2·92 ± 0·07	3·26 ± 0·10
Dielectric constant[5] (5×10^5–10^6 c/s)	20·8	20·8

The optical absorption measurement was made with a Cary Recording Spectrophotometer Model 14*M*–50, of which the purity in wavelength at 5000 Å was at most 2 Å. Using a double Dewar as shown in Fig. 1, the sample was not immersed directly in a refrigerant. The light beam from the source passed through only the sample and two fused quartz plates used as windows. As the sample was cooled through thermal conduction in the present case, the cooling efficiency was not high, and the lowest temperature of the sample attained by using liquid helium in the inner

Vol. 22
1961

Dewar was about 37°K, as measured with calibrated copper–constantan thermocouples. In order to cool the sample to still lower temperatures, another type of cryostat was used. Here the sample itself was immersed directly in the cooling liquid, thus being kept at the temperature of the surrounding liquid. In this experiment the absorption spectra were recorded photographically, and the dispersion of the spectrograph with glass prisms was about 20 Å/mm at 5000 Å. The experimental procedure with this apparatus is quite similar to that of NIKITINE. In this case, however, the light beam passed through four layers of refrigerants and many glass walls of double Dewars which have slight curvatures. Therefore, some precautions are needed for getting accurate results in such an experimental arrangement.

3. EXPERIMENTAL RESULTS AND DISCUSSION

In Fig. 2 are shown the optical absorption curves of a vacuum-evaporated sample which was annealed at 100°C for 50 hr. The absolute values of $\log(I_0/I)$ in Fig. 2 are not accurate enough because the reflection and sample-holder loss are not corrected for, but their relative values may be considered to be correct. The result at room temperature corresponds closely to the results of the older measurements,[2, 3] but a shoulder at 500 mμ, which can be noticed in the present result, was missed completely in the older data. With decreasing temperatures of the sample, several peaks make their appearance in the absorption curves and, particularly, the first absorption band at 500 mμ grows up most strikingly. It is near this band that NIKITINE found hydrogen-like absorption lines. In Fig. 2, however, we cannot find such series line absorptions even at the lowest temperature attained. The behaviour of the curves at longer wavelengths than the first band should contain interference effects on account of the small thickness of the sample. Judging from the result shown in Fig. 6, the sample should be quite transparent in this wavelength region.

Figure 3 depicts the first band and its neigh-

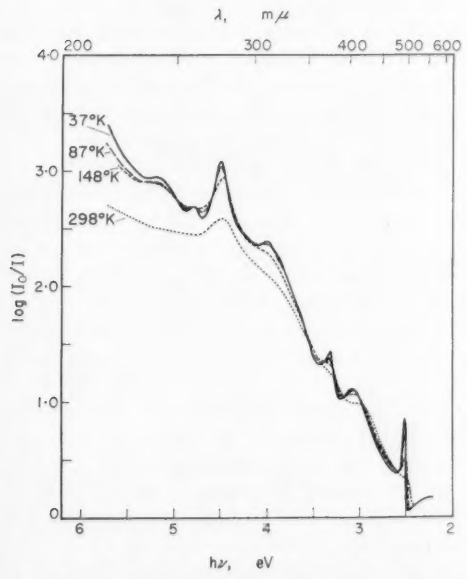

FIG. 2. The optical absorption spectrum of PbI_2. The film (sample No. 42_8) was evaporated on to a fused quartz plate at room temperature and after that it was annealed for 50 hr at about 100°C. The thickness of the film was 500 Å.

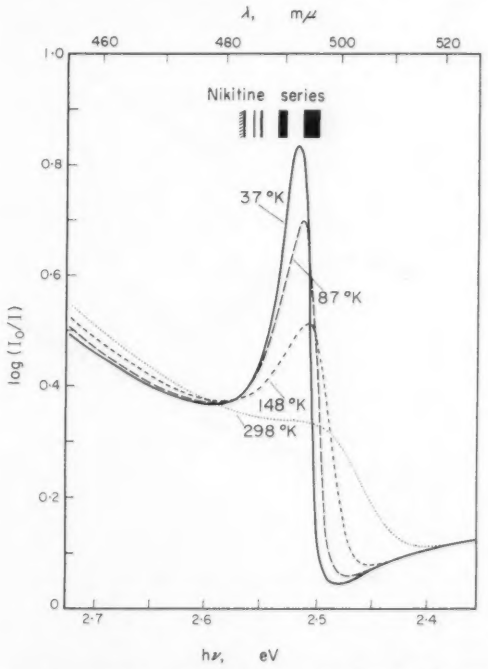

FIG. 3. Details of the curves near the first band in Fig. 2. The lines observed photographically by NIKITINE *et al.*[4] are also shown.

bourhood at various temperatures on an enlarged scale. The absorption lines observed at 4·2°K by NIKITINE are also described in the figure. The spectral curves in Fig. 3 show quite smooth behaviour and there is no trace of the band splitting into series lines in contradistinction to the results of NIKITINE. However, NIKITINE has found the hydrogen-like series lines in the absorption spectrum of a compact thin film at 4·2°K. In the present experiment, the sample used was annealed in order to remove as many lattice defects as possible, whereas the temperature of the sample is not as low (37°K) as that in NIKITINE's experiment. There might be a possibility that the band in Fig. 3 eventually splits into several sharp lines at still lower temperatures, for example at liquid helium temperature.

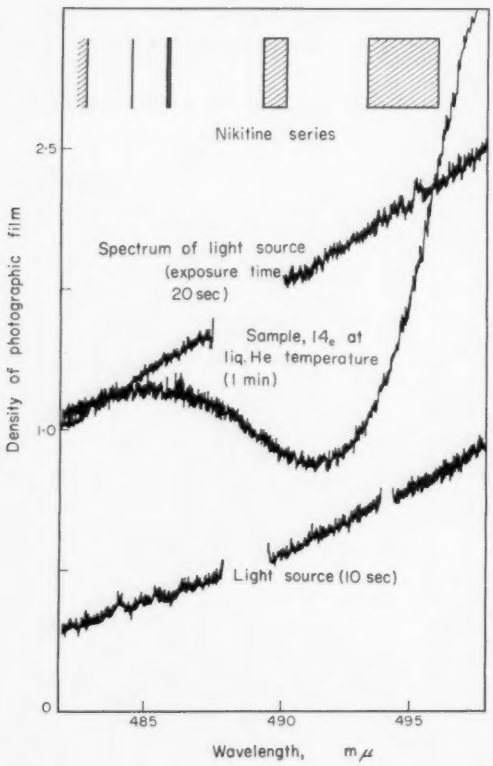

FIG. 4. The microphotometer recordings of the photographic films obtained using the cryostat in which the sample was directly immersed in the liquid helium. The lines observed by NIKITINE[4] are also shown.

In order to cool the sample to liquid helium temperature, another type of cryostat, which is quite similar to that used by NIKITINE, was constructed, the sample being directly immersed in the liquid helium. The method of detection of light absorption in the sample was photographic as in NIKITINE's experiment. For detecting any structure in the absorption spectrum, very high characteristic constants, say $\gamma \sim 3$, are given to the photographic film. In Fig. 4 the microphotometer recordings of the photographic film obtained in such experiment are reproduced together with the spectrum of a tungsten lamp used as a light source. However, the result in Fig. 4 shows characteristics quite similar to those in Fig. 3 and no pronounced structure in the absorption band appeared. The experiment was repeated using a number of samples prepared by method (1) as well as (2), but the first band at 500 mμ always appeared as a single band without series line structure.*

Judging from the appearance of the absorption spectrum over a wider range of wavelength, it can be inferred that a continuous absorption is superposed onto the observed several peaks. Such a state of affairs has been already found in the materials with higher dielectric constant such as the silver[8] and thallous[9] halides. In order to obtain the contribution of the first band alone, therefore, the underlying continuous absorption should be subtracted from the observed data. The position of the peak of the first band obtained by such a subtraction procedure shifts toward the higher energy side with decreasing temperature as shown in Fig. 5. The shift at higher temperature shows a linear variation with temperature, its rate of change being about $1{\cdot}5 \times 10^{-4}$ eV/degree, but at lower temperatures it has a tendency to saturate. The absorption area, i.e. half-width times peak absorption constant, of the first band is found to be nearly independent of temperature. From the absorption area thus obtained, the oscillator strength is estimated to be $\sim 0{\cdot}001$, which is compared with $\sim 0{\cdot}24$ (KI)[10], $\sim 0{\cdot}05$ (AgCl), $\sim 0{\cdot}01$ (AgBr), $\sim 0{\cdot}01$ (TlCl)[9] and $\sim 10^{-6}$ (Cu_2O)[11].

Whether the first band is actually intrinsic to

* Our previous analysis[7] of the first band had various kinds of ambiguities and the discussions based on such analysis were not conclusive.

Vol. 22 1961

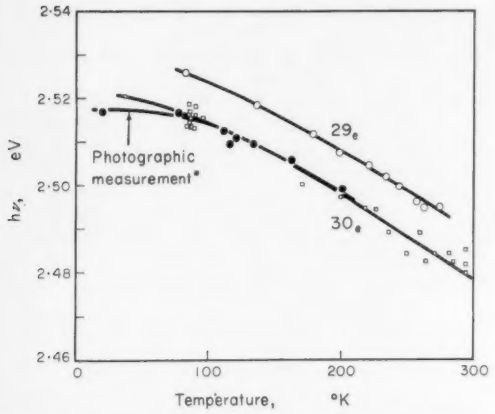

FIG. 5. Temperature shift of the peak of the first absorption band of PbI_2. Samples 29_e and 30_e were prepared by the vacuum evaporation method. *Previous results.[12]

PbI_2 or not was examined experimentally by using the various kinds of samples. The experimental results indicate that the first band is not so structure-sensitive, but corresponds to intrinsic absorption in the PbI_2 crystal itself.

It is interesting to investigate the spectrum in the range of lower absorption constants, using thicker samples such as (3), (4) and (5). The experiments were performed mainly at room temperature and some of them at liquid nitrogen temperature. The experimental results are described in Fig. 6 together with the results obtained for the thin samples prepared by vacuum-evaporation. Fig. 6 indicates, in the long wavelength tail of the first band, that PbI_2 becomes quite transparent and that the behaviour of the absorption constant seems to be approximately represented by Urbach's rule, i.e.

$$\alpha = \alpha_0 \exp\left(-\sigma\frac{h\nu_0 - h\nu}{kT}\right).$$

From the results at room temperature and liquid nitrogen temperature, the various parameters in Urbach's rule are determined to be roughly $\sigma \sim 1{\cdot}3$, $h\nu_0 \sim 2{\cdot}525$ eV and $\alpha_0 \sim 10^6$ cm^{-1}, respectively.

Some preliminary experiments on the photoconductivity of PbI_2 at room temperature was attempted. With increasing photon energy, the induced current increases at first and, after reaching a maximum, decreases. The decrease of the current will presumably be due to the fact that the light absorbing layer becomes very thin.

It is interesting to estimate the energy required to transfer an electron from an I^- ion to the nearest neighbour Pb^{++} ion, using a simple, Born-cycle method. The result is 2·3 eV in comparison with the observed value of 2·52 eV corresponding to the first band.

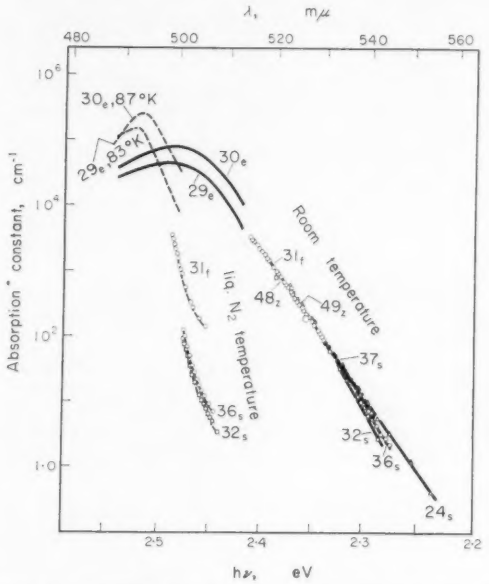

FIG. 6. Absorption tail on the longer wavelength side of the first band of PbI_2. Samples 24_s, 32_s, 36_s, and 37_s were prepared by method (3); sample 31_f, by method (4); samples 48_z and 49_z, by method (5); samples 29_e and 30_e, by method (1). ⊙ is the point measured by ZAHNER and DRICKAMER[13].

In conclusion, all the experimental evidence described above indicates that the exciton corresponding to the first band of PbI_2 seems to have a resemblance to that of the silver and thallous halides rather than cuprous oxide: namely, it will be of an intermediate type between the loose-binding exciton observed in Cu_2O and the tight-binding exciton in alkali halides.

Acknowledgements—The author is very grateful to Professor T. MUTO and Professor K. ISHIGURO for introducing him to the exciton problem and for many encouraging discussions. The many helpful discussions

with Professor T. USUI and Professor G. KUWABARA are also highly appreciated.

REFERENCES

1. MUTO T., *Progr. Theor. Phys. Osaka.* Suppl. **12,** 1 (1959).
2. HILSCH R. and POHL P. W., *Z. Phys.* **48,** 384 (1928).
3. FESEFELDT H., *Z. Phys.* **64,** 741 (1930).
4. NIKITINE S., *C.R. Acad. Sci. Paris* **240,** 64 (1955); *Phil. Mag.* **4,** 1 (1959); NIKITINE S., BURCKEL J., BIELLMANN J. and REISS R., *C.R. Acad. Sci. Paris* **251,** 935 (1960).
5. EUCKEN A. and BÖCHNER A., *Z. Phys. Chem.* (B) **27,** 321 (1934); ROBERTS S., *Phys. Rev.* **76,** 1215 (1949).
6. MOTT N. F. and GURNEY R. W., *Electronic Processes in Ionic Crystals,* p. 12. Clarendon Press, Oxford (1940).
7. IMAI I. and ISHIGURO K., *Prog. Theor. Phys. Osaka.* Suppl. **12,** 179 (1959).
8. OKAMOTO Y., *Nachr. Akad. Wiss. Göttingen* **14,** 277 (1956); TUTIHASI S., *Phys. Rev.* **105,** 882 (1957).
9. TUTIHASI S., *J. Phys. Chem. Solids* **12,** 344 (1960); ZINNGREBE H., *Z. Phys.* **154,** 495 (1959); YANAGI T. (presented at Annual Meetings of the Physical Society of Japan in 1959 and 1960).
10. TOYOZAWA Y., *Progr. Theor. Phys. Osaka* Suppl. **12,** 111 (1959).
11. NIKITINE S., GRUN J. B. and SIESKIND M., *J. Phys. Chem. Solids* **17,** 292 (1961).
12. IMAI I. and ISHIGURO K., *Progr. Theor. Phys. Osaka.* Suppl. **12,** 174 (1959).
13. ZAHNER J. C. and DRICKAMER H. G., *J. Phys. Chem. Solids* **11,** 92 (1959).

DISCUSSION

E. BURSTEIN: Do you have any explanation for the difference between the present results and those of NIKITINE?

T. MUTO: First, the difference between the present results and those of NIKITINE might be ascribed to different amounts of crystal imperfections involved in the sample. As a matter of fact, IMAI had carefully produced his samples by various methods. Secondly, in the photographic measurement the sample was immersed directly in liquid helium and the light beam passed through four layers of refrigerant and many glass walls of DEWARS which have slight curvatures. Therefore, some precautions are needed for getting accurate results in such an experimental arrangement. I am afraid such precautions might not have been taken into account in NIKITINE's experimental observation.

J. Phys. Chem. Solids Pergamon Press 1961. Vol. 22, pp. 87–100. Printed in Great Britain.

THE FINE STRUCTURE OF THE SPECTRAL CURVES OF PHOTOCONDUCTIVITY AND LUMINESCENCE EXCITATION AND ITS CORRELATION TO THE EXCITON ABSORPTION SPECTRUM

E. F. GROSS and B. V. NOVIKOV

Abstract—The exciton fine structure of the fundamental absorption edge in semiconductor crystals was examined. It was observed that substances having such a structure are fairly strong photoconductors. This fact leads to the conclusion that there is a correlation between the exciton absorption lines and the shape of the photoconductivity curve.

Crystals with well-known structures of the absorption edge (CdS, Cu_2O, HgI_2, PbI_2 and GaSe) were chosen for investigation. A fine structure of the spectral curves of photoconductivity, corresponding to exciton absorption lines, was discovered in all the investigated crystals at low temperatures. Its properties in a CdS single crystal were studied in detail. It turned out that either the maxima (first type of crystals) or the minima (second type of crystals) on the photocurrent curves could correspond to the exciton absorption lines. By means of proper treatment crystals can be converted from one type into another and vice versa.

The coincidence of photocurrent and absorption maxima is considered as a consequence of exciton participation in giving rise to photocurrent. Possible mechanisms of exciton participation in creating charge carriers are discussed.

On the spectral curve of luminescence excitation of CdS crystals at low temperatures, a fine structure related to the exciton spectrum is also observed. Either maxima or minima on the excitation spectral curve coincide with the exciton absorption lines.

ol. 22
961

In 1931 FRENKEL[1], for the first time, suggested a hypothesis concerning non-photoconductive excitation in a crystal lattice. This excitation, capable of migrating through the crystal, was called an exciton.

FRENKEL's ideas found further development in the theoretical works of WANNIER[2], MOTT[3], HELLER and MARCUS[4], PEKAR[5, 6] and others. Later, both theoreticians and experimentalists applied the hypothesis of the exciton in connection with attempts to explain various phenomena. Thus, for instance, the well-known wide absorption peaks in alkali halide crystals were identified with excitation, by means of light, of excitons in these crystals. The concept of the exciton was also referred to in connection with migration of energy in luminescence processes.[7] In essence, the concept of the exciton (under the name of "energy migration") was used by VAVILOV for the explanation of some phenomena of luminescence in liquids. The role of the exciton as an energy carrier was taken into account when explaining a number of experimental facts in the phenomena of external and internal photoeffects. It was shown in a number of very interesting and important researches of APKER and his collaborators[8] that a whole series of peculiarities in the phenomenon of photoemission becomes clear, if one assumes the participation of the exciton in these phenomena.

As a result of a whole series of experiments, carried out for the purpose of studying photoconductivity in Cu_2O crystals, ZHUZE and RIVKIN[9] came to the conclusion that the role of the exciton in the phenomenon of photoconductivity is essential. However, the problem of whether such a quasi-particle really existed in crystals remained to be proved. Confirmation of the actual existence of such a particle in crystals was obtained further from another quarter—that of optical phenomena. Proceeding from the experimental results of

ZHUZE and RIVKIN, research on optical absorption at low temperatures in Cu_2O crystals was undertaken by one of the authors (E.G.) in 1950. These investigations resulted in the discovery of a hydrogen-like series of narrow lines on the absorption edge of the crystal.[10] This series of lines was interpreted[10] as the optical exciton spectrum in the Cu_2O crystal.

This investigation, proceeding from the exciton concept, gave an interpretation of the coefficients of the hydrogen-like series,[10] and revealed their relation to the reduced effective mass of the exciton (the effective masses of electron and hole), Rydberg's constant, and crystal refractive index, on the one hand, and the energy of exciton photodissociation, on the other. Further studies[11] as well as detailed electro-optical[12] and magneto-optical[13] investigations of the Cu_2O absorption spectrum confirmed the correctness of its exciton interpretation.

The existence of the hydrogen-like series on a Cu_2O absorption edge was independently discovered also in the experiments of HAYASHI[14].* In further investigations, carried out in different laboratories, the complex structure of the absorption edge was observed in a number of other crystals. This phenomenon, which reveals itself with particular distinctness in Cu_2O, is a general property of crystal lattices. At present, there are no doubts that this structure is the exciton optical spectrum of the crystals.

As will be seen further, the complex structure on the absorption edge turned out to be closely connected with the photoelectric phenomena in crystals. First of all, it was noticed[17] that all crystals with a complex absorption edge structure are strong photoconductors, e.g. Cu_2O, CdS, CdSe, ZnS, HgI_2, PbI_2, AgI and others. All these materials at low temperatures reveal narrow and strong lines at the absorption edge; these lines should be connected with the formation of excitons. Besides, the fact that these groups of exciton lines are disposed in that part of the spectrum where the maximum photoconductivity is usually observed, draws attention to itself.

Side by side with crystals in which a clear exciton spectrum with strong lines is observed, there are crystals which do not reveal the absorption edge structure, e.g. MoO_3, Bi_2O_3, V_2O_5, As_2S_3, PbO (the yellow form) and others. It was noticed that in such crystals photoconductivity is either not observed at all or is of a very low value.

The correlation between the exciton lines and photoeffect displays itself particularly clearly in the case of the red and yellow modifications of HgI_2 crystals.[18] In the red modification, there are exciton lines and a strong photoeffect; in the yellow modification, the exciton lines are absent and the photoeffect is extremely weak. This fact is particularly convincing, as the correlation between the exciton lines and the photoconduction value is observed here on one and the same material.

A detailed study of the spectral photosensitivity of crystals, in the absorption spectra of which lines connected with excitons are observed, is of great importance for clearing up the role of excitons in photoconductivity. The discovery of photosensitivity peaks coinciding with exciton absorption lines would be direct proof that formation of excitons at light absorption leads to the appearance of charge carriers. The first experiments in this direction were undertaken by us together with KAPLIANSKI in 1955 on CdS and HgI_2 crystals.[19] Both these materials are strong photoconductors and have a rich structure in absorption. At present, the absorption edge spectrum of CdS[20–22] has been studied in particular detail. The theoretical investigations of BIRMAN[23] and HOPFIELD[24] made it possible to classify the intensive exciton lines into three groups, *A*, *B* and *C*, each of which corresponds to the transition to exciton levels from one of the valence bands.

Investigations on the spectral distribution of photocurrents in monocrystal CdS were carried out at $T = 77°K$ and $4°K$ with polarized light.[25] A monochromator of a relatively high dispersion was used for the investigations. The width of the slit varied within the limits from 0·5 Å to 5 Å. The

* In this paper,[14] however, HAYASHI does not give any interpretation of the hydrogen-like series coefficients, and does not relate the hydrogen-like Cu_2O spectrum with the exciton. After the publication of our paper on the exciton spectrum,[10] HAYASHI and KATSUKI in a later article[15] subscribed to our interpretation of the hydrogen-like Cu_2O spectrum only in the case of the green series. The Cu_2O yellow series is attributed by them to the polaron, and in a recent 1959 publication[16] HAYASHI again stresses this conception.

One cannot agree with the Japanese authors' latter interpretation of the Cu_2O yellow series as a polaron spectrum, because such an explanation is at variance with experimental facts.

Vol. 2
1961

thickness of the CdS samples (and all other substances investigated by us) was chosen with the aim in mind that all the light in the spectral region of the exciton lines was fully absorbed by the crystal.

About 80 monocrystal samples, grown in different ways, were investigated. At low temperatures the spectral photocurrent curves of all the investigated crystals reveal clear peaks in the spectral range of exciton absorption lines. The shape of the photocurrent curves and its character of correlation with the absorption lines make it possible to divide the large variety of obtained curves into two types.

In certain samples (conventionally attributed to the "first" type), the photocurrent maxima (peaks) correspond to the absorption lines on the spectral distribution curve and coincide in position with them.

In other samples (the "second" type), the spectral photocurrent curve differs greatly from the curve for crystals of the first type: in this case, the absorption lines coincide in position with the photocurrent minima (dips). The spectral photocurrent curves, for crystals of both types, depend considerably upon the orientation of the crystal with respect to the direction of propagation and polarization of the incident light.

In Fig. 1 characteristic spectral photocurrent curves obtained on two samples belonging to different types are shown, for example. The curves were obtained for different polarizations of incident light.

In the long-wave part of the curve of first-type crystals (Fig. 1a and b, curves 1) there are a number of clearly defined peaks. The first of them, $\lambda = 4870$ Å, is polarized with the electric vector $E \perp C$. This peak, according to position and polarization coincides with the most intensive long-wave absorption line in the crystal CdS observed at $T = 77°$K. The remaining photocurrent peaks (some of which, apparently, are only partially polarized) are located near $\lambda = 4840$ Å, 4795 Å, 4730 Å and 4660 Å. These peaks also correspond to the intensive absorption lines, the position of which is shown in Fig. 1. Both long-wave photocurrent peaks 4870 Å and 4840 Å are rather narrow, their half-width is 6–8 Å.

In Fig. 1 it is seen that the photocurrent curve of first-type crystals looks like a wide, smooth

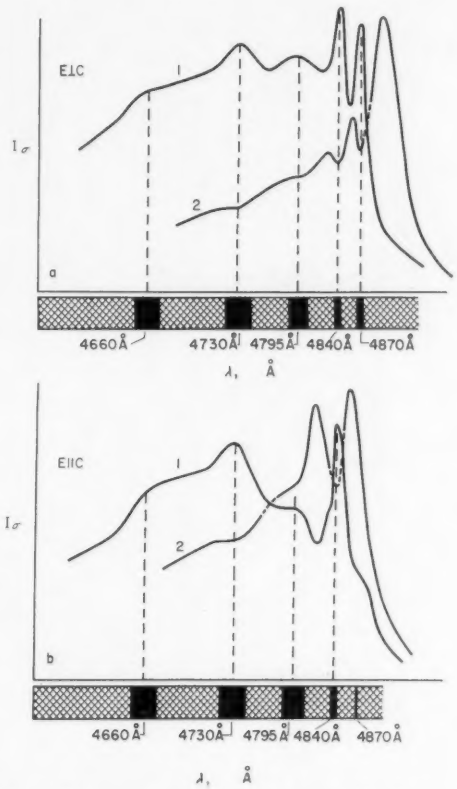

FIG. 1. Curves of spectral photocurrent distribution of two types (1 and 2) of CdS crystals in polarized light.

maximum ("background") with protruding peaks above it. The relative value of peaks and background, on which these peaks are located, may greatly differ in various samples. In some samples, the peaks make a comparatively small edition to the strong background (curves a_3b_3 in Fig. 2), whereas in others it is the other way round: the largest part of sensitivity is concentrated in the peaks (curves a_2b_2 in Fig. 2). It is noteworthy that an increase of the background leads to a decrease of the relative value of peaks, i.e. the background is not simply added to the peaks, but, in a way, absorbs them.[26]

In second-type crystals (Figs. 1a and b, curves 2), the steep rise of the photocurrent for both polarizations begins at noticeably larger wavelengths in comparison with the already described first-type crystals. An essential difference in the

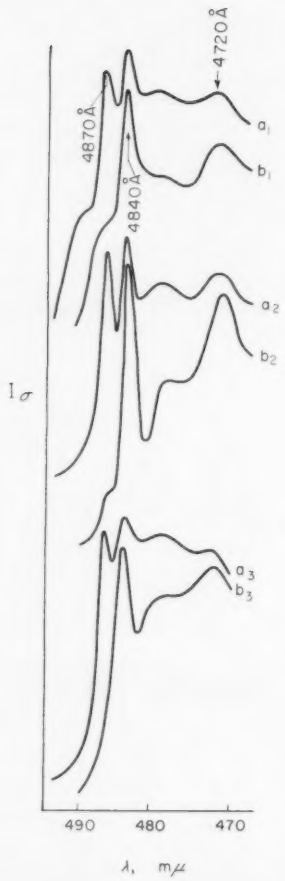

FIG. 2. Curves of spectral photocurrent distribution in three CdS crystals at $T = 77°K$. *a*—$E \perp C$; *b*—$E \| C$.

crystals of both type is observed also in the short-wave part of the curves. The second-type crystals have a steeper short-wave drop of the photocurrent curve, where a distinct structure consisting of narrow peaks and dips is observed. The narrow minima (with half-width 6–8 Å) correspond to absorption lines $\lambda = 4870$ Å and 4840 Å, and the wider ones are located near absorption lines $\lambda = 4795$ Å and 4730 Å. In certain samples, a minimum is also seen near line $\lambda = 4660$ Å. It is of essential importance that in second-type crystals the minima (dips) and not the maxima (peaks) on the photocurrent curve correspond to the absorption lines. This is also a significant difference between the two types of crystals.

As is the case in the first-type crystals, the relative depth and clarity of the photocurrent minima may differ from sample to sample, and, sometimes, may differ also in different parts of one and the same crystal.

Investigations of second-type crystals with polarized light reveal a strong dependence of the long-wave part of the photoconductivity curve upon the polarization of the incident light.

The dip on the photocurrent curve (Fig. 1a, curve 2), connected with line 4870 Å, is present only in component $E \perp C$, and is absent in component $E \| C$; this is due to the strong polarization of this absorption line with $E \perp C$. It must be noted that strong photocurrent peaks near 4890 Å on curve 2 (Fig. 1a) for component $E \perp C$ do not correspond to any absorption line. The same takes place also in the case of the most long-wave and intensive peak near 4860 Å for component $E \| C$ (Fig. 1b, curve 2). Other peaks on the photocurrent curves of second-type crystals (Figs. 1a and b, curve 2) do not have any correspondence with absorption lines either. These peaks, the position of which, by the way, considerably changes from sample to sample, are closely connected with the depth of the minima (dip) on the photocurrent curves of second-type crystals. These peaks apparently are caused by the side parts ("wings") of the absorption line shape, the central parts of which coincide with the dips of the photocurrent curve. Thus, the situation here is analogous to the phenomenon of self-reversion of the atomic spectral lines, when on the shape of the emission line there sometimes also appear two side peaks, which change their position according to the conditions of the experiment. In this respect, the above-mentioned peaks on the photocurrent curve of a second-type crystal must be regarded as "false" peaks, which should not correspond to the absorption lines, and, therefore, no definite physical sense should be ascribed to them.

Such a self-reversion of the peak on the spectral curve of the photoemission of coloured alkali-halide crystals was observed under certain conditions by APKER and TAFT[8].

At room temperature the difference between first- and second-type crystals still remains. Further, we shall consider the connection between

Vol. 22
1961

these groups and the conditions under which crystals pass over from one type to the other.

Our following observations are testimony to the fact that the absorption lines are correctly compared with the narrow photocurrent peaks (in cases of first-type crystals) and narrow dips (in second-type crystals).[25]

By orienting the optical axis of the crystal perpendicular to the rotation axis and parallel to the electric vector of the polarizer, it is possible (as is known) to observe in an extraordinary ray an intensification of absorption line 4870 Å when increasing the angle ($\angle EC$) between the crystal axis and electric vector of the incident light.[21]

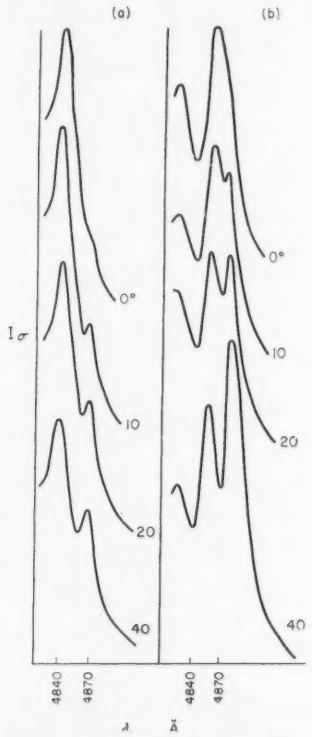

FIG. 3. Influence of rotation of a CdS crystal upon the shape of spectral curves of photocurrent distribution. *a*—for first-type crystals; *b*—for second-type crystals.

As it is seen in Fig. 3, an increase of the angle between E and C from 0° to 40° in first-type crystals leads to the appearance of a peak on the photocurrent curve in the same place as absorption line 4870 Å.

When the angle ($\angle EC$) is increased, the peak increases and the whole curve approaches the shape characteristics of $E \perp C$.

In Fig. 3b, the behaviour of the long-wave part of the photocurrent spectral curve for second-type crystals at an analogous rotation of the crystal is presented. In these crystals, on increasing the angle between E and C on the long-wave drop of the photocurrent curve (on the drop of the "false" peak), a dip, which rapidly increases with the increase of the angle, appears in the same place as absorption line 4870 Å. As a result of this, there appears on the photocurrent curve a second "false" peak, which shifts in the direction of the larger wavelengths and grows in size while rotating the crystal.

At large angles, the shape of the curve approaches the curve characteristic of $E \perp C$ in second-type crystals also.

It is known that when lowering the temperature to 4°K the absorption edge of CdS crystals and the lines located near it shift in the short-wave direction. The spectral photocurrent curves also shift in the same direction. The narrow long-wave photocurrent peaks in first-type crystals at $T =$ 4°K become yet narrower and take up a position near $\lambda = 4853$ Å and 4823 Å, (i.e. they are displaced from their positions at $T = 77°$ by 17 Å) Fig. 12b. It is possible to observe also at 4°K a photocurrent peak at 4808 Å. In second-type crystals, the photocurrent dips are located at the same wavelengths. The wide, short-wave photocurrent peaks (dips) undergo a somewhat smaller temperature shift.

The insufficient dispersion of the monochromator did not enable us so far to reveal the photocurrent peaks' fine structure which is connected with the existence of longitudinal and transverse excitons[27] in CdS crystals. According to the theoretical conception of PEKAR and DYKMAN[28], the longitudinal exciton waves must give rise to a photocurrent several times stronger than in the case of transverse ones.

A cooling to 4°K considerably influences the general shape of the spectral photocurrent curve (see further).

A question naturally arises whether the discovered phenomenon (the fine structure of the

photoconductivity curve) is a general one for all crystals with an exciton spectrum. The most interesting substance from this point of view was Cu_2O, where the exciton absorption spectrum is observed especially clearly. Indeed, the experiments carried out in the Soviet Union (GROSS and PASTERNJAK[29] and in the United States (APFEL and PORTIS[30]) proved that on the Cu_2O photocurrent curve, in the yellow and green parts of the spectrum, photocurrent peaks are observed. They form two hydrogen-like series, which exactly correspond to the yellow and green series of the exciton in Cu_2O (see Fig. 4). At the same time, the shape of the photoconductivity curve reflects all the peculiarities of the absorption-edge structure.

A similar conformity between the fine absorption structures and photoconductivity has now been discovered in a large number of substances. Nearly simultaneously with CdS, these phenomena were discovered by us in a crystal of red modification of HgI_2. Investigations were carried out on a number of single HgI_2 crystals in polarized light. The most typical curves are presented in Fig. 5. A comparison of the absorption spectra data[18, 31] reveals that on the photocurrent curve, in the case of $E \perp C$, the dips at $\lambda = 5330$ Å and 4930 Å coincide with the absorption lines. According to our terminology, this curve belongs to the second type of crystal. Apparently, the dips on photocurrent curve for the case of the extraordinary ray ($E \| C$) should also be compared with the absorption lines. Absorption line $\lambda = 5330$ Å is polarized with $E \perp C$ and, therefore, only the structure on the photocurrent curve for the ordinary ray should correspond to it. The narrow photocurrent peak in component $E \| C$, situated near line 5330 Å, we think, should not be connected with the absorption line. This peak (its position differs from sample to sample) is, apparently, a false peak typical of second-type crystals, as is the case in CdS. It must be noted that in some crystals in component $E \perp C$, the photocurrent peak may correspond to absorption line $\lambda = 5330$ Å (first type of crystal).

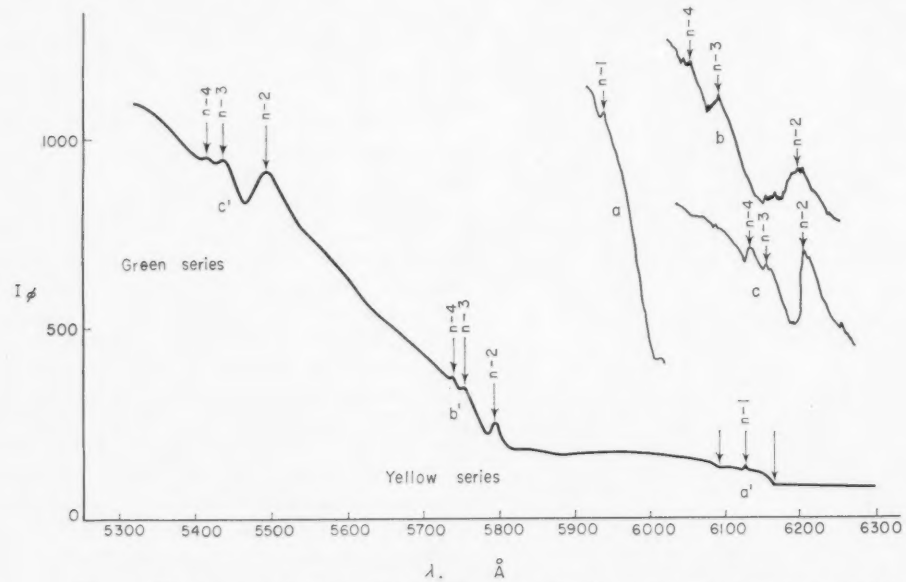

FIG. 4. The spectral photocurrent dependence of a Cu_2O crystal. The tension of applied electric field $E = 750$ V/cm, $T = 77°K$ (curves a', b', c').

Original curves of a fine-structure of spectral photocurrent dependence of a Cu_2O crystal. $T = 77°K$. *a*—region of first step, $E = 1{\cdot}5$ kV/cm; *b*—region of exciton yellow series, $E = 750$ V/cm; *c*—region of exciton green series, $E = 750$ V/cm (After GROSS and PASTERNJAK).

Side by side with the red modification, the

Vol. 22
1961

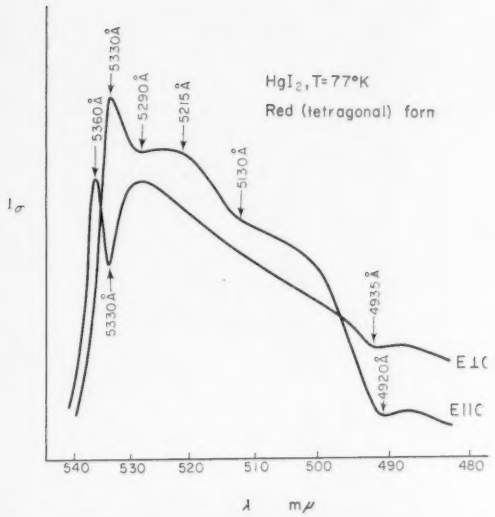

FIG. 5. Spectral photocurrent dependence of a HgI_2 crystal (red modification) at $T = 77°K$ in polarized light.

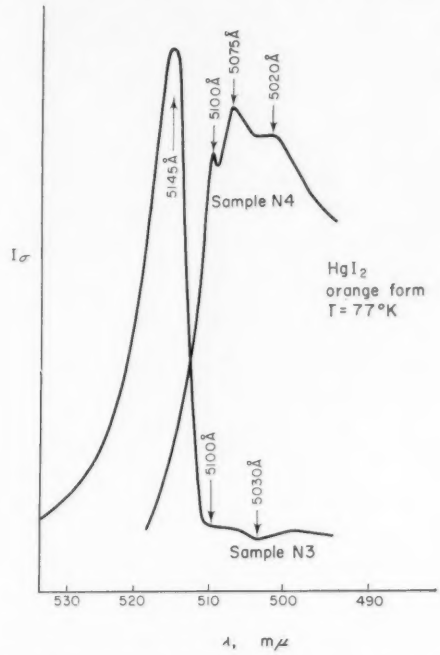

FIG. 6. Spectral photocurrent dependence in a HgI_2 crystal (orange modification) at $T = 77°K$.

orange modification of HgI_2 also has a strong photoconductivity. At $T = 77°K$ in the long-wave part of the spectral photocurrent curves of these crystals, a structure is also observed, the extremes of which may be compared with the absorption lines discovered in this material by SIESKIND and his collaborators.[32] In Fig. 6, two most typical spectral photocurrent curves for two different HgI_2 crystals of orange modification are presented.

In single crystals of PbI_2 and GaSe, the structure of the absorption edge is particularly simple. Thus, in PbI_2 at $T = 77°K$, a wide band with $\lambda = 4950$ Å as the centre[18, 33] is observed; in GaSe, at the same temperature, we may observe a strong line near 4900 Å and a wide, weak band at 5870–5800 Å.[34] The simplicity of the absorption structure in these substances makes it possible to observe, with great obviousness and conviction, the phenomenon which was for the first time discovered by us with CdS: the absorption lines manifest themselves as photocurrent peaks in first-type crystals, and as dips on the spectral photocurrent curves in second-type crystals. This phenomenon for PbI_2 and GaSe crystals is illustrated in Figs. 7 and 8.

We have discovered a rich structure of photocurrent curves in polycrystalline films of AgI. Fig. 9 gives the photocurrent curves for the cubic (a) and hexagonal (b) modifications of this substance. A comparison of obtained results with published data on adsorption[35] shows that the dips on the photocurrent curves coincide with the absorption lines in both AgI modifications.

The discovered correlation, in a large number of substances, between the structure of the spectral photoconductivity curves and the line structure of the absorption edge, we think, shows a possibility of using photoconductivity as a spectral method for investigating energy levels in a crystal. The investigation of energy absorption levels by means of the photoconductivity method does away with the difficulties connected with the size, surface conditions, and the thickness of the samples. It is well known that the preparation of very thin single crystals, for investigating their absorption spectrum, presents considerable difficulties. The necessity of a registering apparatus falls away. This fact is very important when investigating those parts of the spectrum which are difficult of

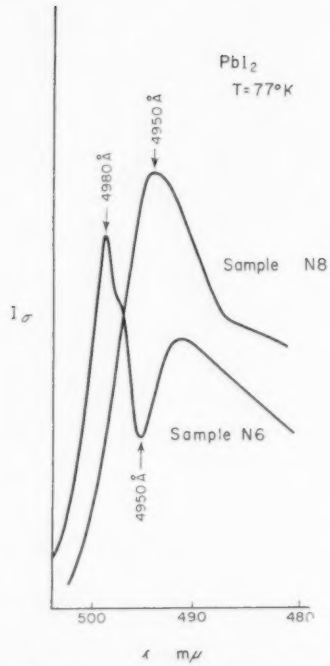

FIG. 7. Spectral photocurrent dependence in a PbI_2 crystal at $T = 77°K$. The crystal optic axis is perpendicular to the sample surface.

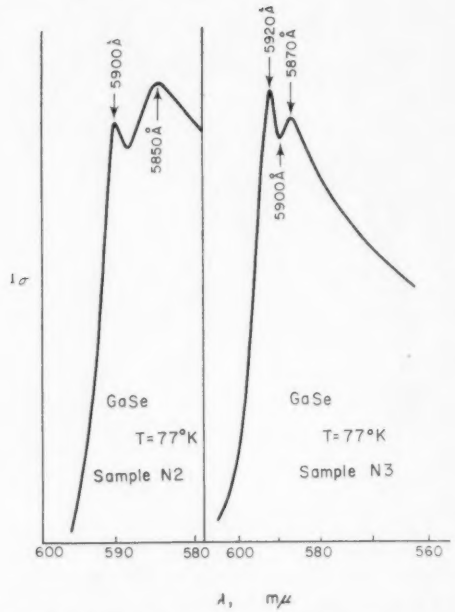

FIG. 8. Spectral photocurrent dependence in a GaSe crystal at $T = 77°K$. The crystal optic axis is perpendicular to the sample surface.

access. As our investigations show, photoconductivity spectra in some cases are more "sensitive" than the absorption spectra. Thus, in CdS, a number of photocurrent peaks were discovered considerably earlier than the corresponding lines in absorption.

Thus, the observations described show that the absorption lines are closely connected with the structure of the spectral photocurrent curves, and can promote both an increase of the photocurrent (in the case of peaks) and its decrease (in the case of dips). It is of particular interest to find out under what conditions the absorption lines manifest themselves in the spectral distribution of photocurrent as peaks, and under what conditions as dips. One of the experiments carried out in this direction was the thermal treatment of CdS crystals with different cooling conditions (annealing and tempering).

CdS crystals were heated in a furnace at $T =$ 400–500°C during 1–1½ hr, and then quickly cooled to room temperature or, more often, to the temperature of liquid nitrogen (tempering). In cases of annealing, the crystals, heated during the same period of time, were slowly cooled (approximately 10–12 hr) to room temperature. The spectral photocurrent curves were investigated both before and after the described thermal treatment at $T = 77°K$.

First-type crystals, where the absorption lines correspond to the photocurrent peaks, essentially changed the general shape of the spectral photocurrent distribution after being subjected to tempering. From the long-wave side there appeared a wide, clear peak; from the short-wave side, a redistribution of photocurrent values took place in such a way that the dips on the photo-current curve now corresponded to the absorption lines. Such a transition took place with greater certitude at quicker cooling to $T = 77°K$. Tempering did not produce any considerable effect upon second-type crystals.

Furthermore we established that first-type crystals after annealing retained the shape of their spectral curves which they had before the thermal treatment. (After annealing, in some cases, the

Vol. 22
1961

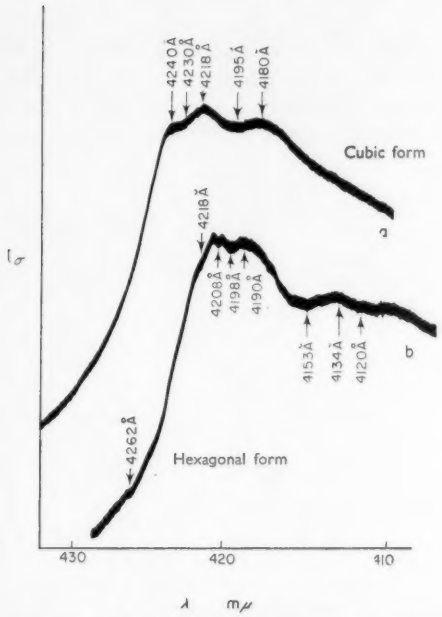

FIG. 9. Spectral photocurrent dependence in AgI polycrystalline films. *a*—cubic modification; *b*—hexagonal modification (original curves).

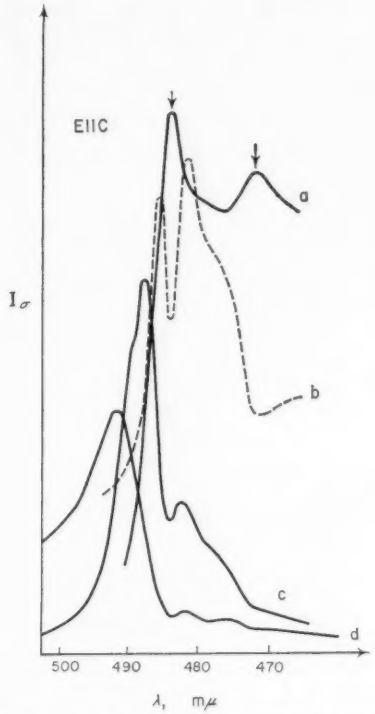

FIG. 10. Spectral curves of photocurrent distribution (in relative units for each curve) of a CdS crystal after different surface treatments at $T = 77°K$.

a—non-treated crystal (the peaks marked by arrows coincide with absorption lines);
b—after a short polishing on wet silk;
c—after polishing with chromium oxide on silk;
d—after grinding with fine emery powder.

peaks on the photocurrent curve became clearer.) In second-type crystals after annealing, the spectral photocurrent curves changed and took the shape characteristic of first-type crystals. Thus, annealing transferred second-type crystals into first-type crystals.

The process of transferring CdS crystals from one type into another is quite reversible. We managed to transfer a first-type crystal, after tempering, into a second-type crystal and then, by means of annealing, to transfer it back to its original state.

Besides annealing and tempering, we investigated the influence of a mechanical treatment of the surface of CdS crystals upon the structure of their photocurrent curves.[36] It was possible to presume that the influence of defects located on the surface would be particularly essential. The absorption coefficient in the exciton lines and background is quite considerable (more than $10^5\,cm^{-1}$) and, consequently, the excitons and free-current carriers arise in the immediate proximity of the surface.

In Fig. 10 are shown the spectral photocurrent curves of a crystal which originally belonged to the first type (Fig. 10a) after different mechanical treatments of the surface. The treatment of the sample surfaces was carried out in the following sequence: polishing on the surface of wet silk (Fig. 10b); polishing on silk with chromium oxide (Fig. 10c); and grinding with fine emery powder (Fig. 10d). An examination of the results obtained makes it possible to mention the following regularities.

(1). Already after a slight treatment of the surface, the photocurrent peaks (curve a) self-reverse, forming dips (curve b, Fig. 10).

(2). The long-wave false peak widens and shifts

in the direction of the long waves (curves b, c, d, Fig. 10) when increasing the degree of surface treatment.

It must be noted that with the increase of degree of surface treatment the general photosensitivity of the samples also falls considerably.*

on it) produces a strong influence on the shape of the structure of the photocurrent curves in the region of the Cu_2O exciton series.[37] The photoconductivity peaks shift and its hydrogenic nature is broken (Fig. 11). However, the relatively small value of photocurrent peaks in relation to back-

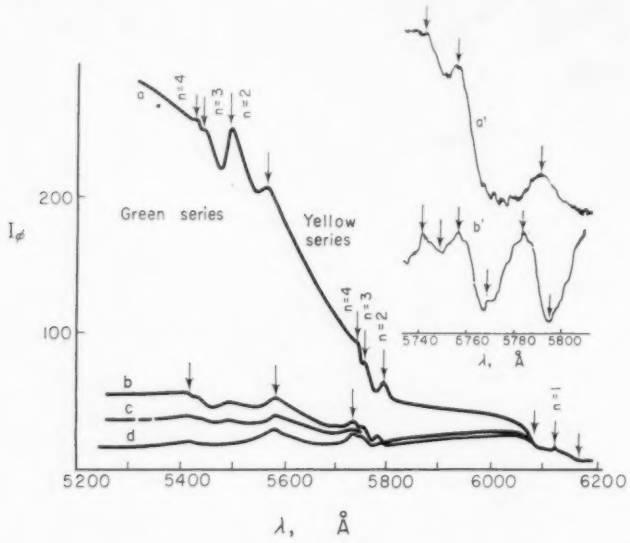

FIG. 11. Spectral photoconductivity distribution of a Cu_2O sample at $T = 77°K$. Sample thickness—400μ.

a—natural surface;

b—after etching in HNO_3 (a similar curve, but with a washed-out fine-structure, is obtained after polishing);

c—after a 20 min annealing at 150°C in air;

d—after oxygen photosorption on the annealed surface.

Shift of the photocurrent fine-structure peaks in the region of yellow exciton series after surface treatment. (Original curves.)

a'—natural surface;

b'—after etching in HNO_3

(After GROSS and PASTERNJAK[37].)

In the case of Cu_2O crystals, a mechanical treatment of the surface (and also etching of the surface and absorption of water and spirit molecules ground does not enable us here to observe the phenomenon as clearly as in CdS.

We established that in the course of time changes take place with the photocurrent curves of some CdS crystals; these changes remind one of those that are caused by a mechanical treatment of the surface. First-type crystals pass over into second type. A sharp drop of sensitivity in the short-wave part of photocurrent curves takes place in second-type crystals. This is connected

* In our first experiments,[19] when the fact of the existence of two types of CdS crystals had not yet been established, we tried to explain the phenomenon of self-reversion of photocurrent peaks by the difference of absorption coefficients in ordinary and extraordinary rays. On the basis of the facts set forth, this explanation was rejected as erroneous.

Vol. 2
1961

apparently with the deterioration of the surface condition.

An interesting phenomenon is observed at a considerable cooling (to 4°K) of CdS crystals which at $T = 77$°K belonged to the second type.

An account was given above concerning the observed facts relating to the phenomena of photoconductivity. We find it of some interest to compare them with the phenomena of luminescence, as it is known that both these groups of phenomena

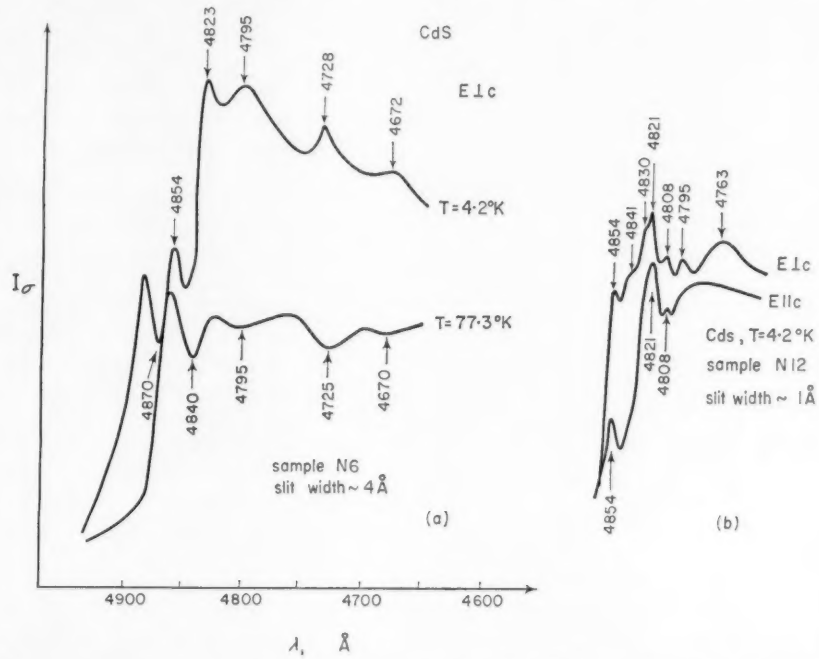

FIG. 12. Spectral photocurrent dependence in a CdS crystal at $T = 77$°K and 4°K in polarized light.

An increase of sensitivity takes place in the short-wave part of the curves in relation to the long-wave part. Simultaneously, the long-wave false peak becomes less clear. However, the photocurrent peaks in these crystals at $T = 4$°K correspond to the absorption lines (at $T = 4$°K) as was the case at $T = 77$°K.

In some crystals, a cooling to 4°K causes a considerable change of the correlation between the photocurrent curves and absorption lines. The crystal which at $T = 77$°K belonged to the second type (the photocurrent dips coincide with the absorption peaks), at $T = 4$°K passes over into the first type (the photocurrent peaks coincide with the absorption lines). The spectral photocurrent curves of such a crystal for $T = 77$°K and $T = 4$°K are given in Fig. 12a.

are often correlated. It turned out that when studying the spectra of luminescence excitation of CdS crystals (at $T = 77$°K), a connection between luminescence and exciton absorption lines is also revealed. As is the case on the curves of spectral distribution of photoconductivity excitation, on the curves of luminescence excitations we observe peaks also, which coincide with the exciton absorption lines. This phenomenon has also been observed by DUTTON[38] and by BROUDE *et al.*[39].

Recently,[40] it was established that CdS crystals, according to the excitation curves of edge emission (green) luminescence, may be divided, chiefly, into two kinds (Fig. 13, curves 4 and 5). In first-type crystals, the peaks on the excitation curves coincide with the exciton absorption lines; and in second-type crystals, the dips coincide with the

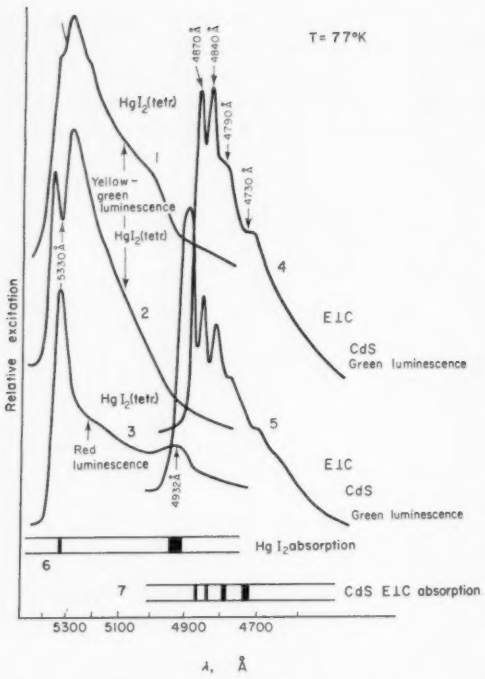

FIG. 13. Luminescence excitation spectra of CdS and HgI_2 crystals at $T = 77°K$. (After GROSS *et al.*[40].)

exciton absorption lines. These two kinds of crystals are closely connected and first-type crystals can be transferred into second-type crystals by means of thermal treatment. Thus, an evident parallelism between the phenomena of photoconductivity is observed here.

Similar phenomena in luminescence were discovered in HgI_2 and PbI_2 crystals. In HgI_2 crystals (red modification), the excitation spectra both of the yellow-green and red luminescence were studied on one and the same sample.[41] The excitation spectra of these luminescence bands differ considerably. If in the case of the excitation spectrum of red luminescence the peaks coincide with the absorption lines ($\lambda = 5330$ Å and 4930 Å), in the excitation spectrum of the yellow-red luminescence, the dips correspond to the absorption lines (Fig. 13, curves 1, 2 and 3). A surface treatment considerably influences the shape of the exciton curves of yellow-green luminescence; the excitation curves of red luminescence do not noticeably change.

The appearance of photocurrent peaks in crystals where the light in the region of fundamental absorption is absorbed completely by the crystal is testimony to the existence of two mechanisms of photocurrent origination. One of them—the usual one—is connected with the direct formation of free electrons and holes. The second one is connected with light absorption in the lines. The trustworthy fact that the absorption lines appertain to the exciton speaks in favour of the assumption that this second creation mechanism of free carriers has, as an intermediate stage, a neutral particle—the exciton.

Two principal processes of origination of free charges through the exciton state are conceived.

(1). Dissociation of the exciton by thermal oscillation of the lattice. However, the comparatively considerable binding energy of the exciton makes this process hardly probable. Besides, from this point of view, it would be very difficult to explain the phenomenon (which is experimentally observed) of transition of photocurrent peaks to dips at thermal treatment of CdS crystals. Furthermore, this process should have had a significant temperature dependence, which, however, is not experimentally observed either in the peaks or the background.*

(2). An interaction of the exciton either with an impurity centre, a defect or other excitons. This process provides for a transfer of the exciton energy to the electron of the impurity centre or defect as a result of a "collision of the second kind".[9] We consider this mechanism of photocurrent origination more probable than the first one for the explanation of the phenomena observed by us. The proposed mechanism includes in itself, as an obligatory fact, the movement of the exciton. Therefore, the existence of peaks on the photocurrent curve should then be considered as proof in favour of exciton migration in the crystal lattice.

If we accept this mechanism of origination of photocurrent peaks, it must explain the origination of dips on the spectral photoconductivity curve. We assume that the defects in the crystal lattice play here a considerable role. Indeed, the defects are sure to impede the movement of the exciton and stimulate its "premature" non-photoactive

* It is possible that in individual cases this mechanism plays a certain role in the phenomena studied by us, but not a leading one.

Vol. 22
1961

annihilation. This makes it difficult for the exciton to migrate to those centres, to interact with them and to create free-charge carriers. It is natural to assume that the maximum number of such defects will be near the surface. This, we think, may explain the specific shape of the photoconductivity curves with dips.

The high coefficient in the absorption peak of the exciton lines leads to the origination of excitons chiefly in the thin layer of the crystal in the immediate proximity of the surface. At a large concentration of these defects, the annihilation of excitons will be maximum for spectral regions with the highest absorption coefficient (centre of absorption line). The excitons formed by the outer parts ("wings") of the absorption lines will originate in the depth of the crystal, where the concentration of defects is less than near the surface. This must lead to the self-reversion of the exciton photocurrent peak on the photoconductivity curve. This causes the formation of dips and false peaks in second-type crystals.

The results of our experiments with thermal treatment and grinding of crystals then receive a natural explanation from the latter point of view. It is known that both at tempering and grinding a large number of defects appear in the crystals. It is not surprising that after these treatments first-type crystals pass over to second-type crystals.

It is natural to assume that annealing "heals" the defective parts of the crystals and therefore the concentration of excitons that take part in the origination of a photo-current after annealing again increases and photocurrent peaks appear again on the places of exciton lines.

As we have already mentioned earlier, the spectral photoconductivity curves of the crystals investigated at low temperatures are made up of two parts: photocurrent peaks and structureless background. This phenomenon, apparently, is in conformity with the spectrum on the edge of the fundamental absorption, consisting of exciton lines and a continuous background. A rise of the background in photoconductivity takes place, apparently, simultaneously with the increase of the background in absorption. This is seen, for instance, from our investigations with evaporated CdS films.[26] It must be particularly noted that the intensity of the background on the photoconductivity curves in relation to the peaks changes not only from sample to sample but, to a greater degree, from substance to substance. Thus, for instance, in a Cu_2O crystal the height of the peak above the background is so slight that their detection presented certain experimental difficulties. At the same time, in CdS crystals, the exciton peaks usually stand out boldly. This shows that the contribution of excitons to photoconductivity may differ greatly from substance to substance.

The photoelectric effectiveness (the quantum yield) in the lines and background are probably different. This is an indication of the different nature of these phenomena. We think that the existence of a background on the photoconductivity curve is connected with the direct formation of free-charge carriers by means of light, i.e. by the ordinary (usually considered) mechanism.

However, one must keep in mind that the primary formation by light of the electron and hole may lead to the formation of excitons as a secondary phenomenon. We think it is natural to assume that a recombination of the electron and hole may take place through the intermediate formation of an exciton, and that probably a direct annihilation of the electron and hole is hardly even possible. The free electron and hole when meeting at first form the exciton in different excitation states, and then annihilate from exciton levels either with emission of light or without radiation. Thus one can assume two ways of exciton formation in a crystal under the effect of light—direct and indirect (through the free electron and hole).[42] Excitons formed in such an indirect way can also cause a photocurrent as a result of collisions with impurity centres or phonons. If this phenomenon actually takes place, then the exciton photoconductivity component may be found not only in peaks but also in a continuous background.

Acknowledgements—The authors are grateful to Professor S. M. Rivkin (Physico-Technical Institute, Leningrad) and Professor R. Rompe (Institüt für Strahlungsquellen, Berlin) for the possibility of experimentation with crystals grown in their laboratories.

REFERENCES

1. Frenkel J., *Phys. Rev.* **37,** 1276 (1931).
2. Wannier G. H., *Phys. Rev.* **52,** 191 (1937).
3. Mott N. F., *Proc. Roy. Soc.* **167,** 384 (1938).

4. HELLER W. R. and MARCUS A., *Phys. Rev.* **84,** 808 (1951).
5. PEKAR S. I., *J. Exp. Theor. Phys.* (*USSR*) **33,** 1022 (1957); **38,** 522 (1958).
6. PEKAR S. I., *J. Phys. Chem. Solids* **5,** 11 (1958).
7. FANO U., *Phys. Rev.* **58,** 544 (1950).
8. APKER L. and TAFT E. A., *Phys. Rev.* **79,** 964 (1950); **81,** 698 (1951); **82,** 814 (1951).
9. ZHUZE V. P. and RYVKIN S. M., *Dokl. Akad. Nauk. SSSR* **77,** 241 (1951); *Isv. Akad. Nauk. SSSR* ser. fiz. **16,** No. 1 (1952).
10. GROSS E. F. and KARRYEV N. A., *Dokl. Akad. Nauk. SSSR* **84,** 261, 471 (1952).
11. GROSS E. F. and ZAKHARCHENJA B. P., *Dokl. Akad. Nauk. SSSR* **90,** 745 (1953).
12. GROSS E. F., ZAKHARCHENJA B. P. and REINOV N. M. *Dokl. Akad. Nauk SSSR* **97,** 57 (1954).
13. GROSS E. F., ZAKHARCHENJA B. P and REINOV N. M. *Dokl. Akad. Nauk. SSSR* **99,** 527 (1954); GROSS E. F. and ZAKHARCHENJA B. P., *J. Tech. Phys.* (*USSR*) **27,** 1940 (1957).
14. HAYASHI M., *J. Fac. Sci. Hokkaido Univ.* **11,** 4 107 (1952).
15. HAYASHI M. and KATSUKI K. J., *J. Phys. Soc. Japan* **7,** 599 No. 6 (1952).
16. HAYASHI M., *Progr. Theor. Phys. Osaka* Suppl. **12,** 160 (1959).
17. GROSS E. F. and BELLE M. L., *J. Tech. Phys.* (*USSR*) **25,** 948 (1955).
18. GROSS E. F. and KAPLIANSKI A. A., *J. Tech. Phys.* (*USSR*) **25,** No. 9, No. 12 (1955).
19. GROSS E. F., KAPLIANSKI A. A. and NOVIKOV B. V., *J. Tech. Phys.* (*USSR*) **26,** 697, 913 (1956); *Dokl. Akad. Nauk SSSR* **110,** 761 (1956).
20. HOPFIELD J. J. and THOMAS D. G., *Phys. Rev.* **116,** 573 (1959).
21. GROSS E. F. and JACOBSON M. A., *Dokl. Akad. Nauk. SSSR* **102,** No. 3 (1955).
22. GROSS E. F. and RASBIRIN B. V., *J. Tech. Phys.* (*USSR*) **27,** No. 6 (1957); *J. Tech. Phys.* (*USSR*) **27,** No. 9 (1957); **28,** No. 2 (1958).
23. BIRMAN J. L., *Phys. Rev.* **114,** 1491 (1959); **115,** 1493 (1960).
24. HOPFIELD J. J., *J. Phys. Chem. Solids* **10,** 110 (1959).
25. GROSS E. F. and NOVIKOV B. V., *J. Tech. Phys. USSR* **28,** 782 (1958); *Solid State Phys.* (*USSR*) **1,** 357 (1959).
26. GROSS E. F. and NOVIKOV B. V., *Solid State Phys.* (*USSR*) **3,** 1249 (1961).
27. GROSS E. F., *Proceedings International Conference on Semiconductor Physics, Prague* 1960, p. 407; *Czech. J. Phys.* B.**11,** No. 7 (1961); HOPFIELD J. J. and THOMAS D. G., *J. Phys. Chem. Solids* **12,** 276 (1960).
28. DIKMAN I. M. and PEKAR S. I., *J. Exp. Theor. Phys.* (*USSR*) **37,** No. 2, 510 (1959).
29. GROSS E. F. and PASTERNJAK I., *Solid State Phys.* (*USSR*) **1,** 162 (1959).
30. APFEL J. H., *J. Phys. Chem. Solids* **8,** 193 (1959); APFEL J. H. and PORTIS A. M., *J. Phys. Chem. Solids* **15,** 33 (1960).
31. NIKITINE S., SIESKIND M., COUTURE L. and PERNY G., *C.R. Acad. Sci. Paris* **238,** 1786 (1954); SIESKIND M. and NIKITINE S., *C.R. Acad. Sci. Paris* **245,** 659 (1957).
32. SIESKIND M., MICHEL P. and GRUN J. B., *J. Chem. Phys.* **56,** No. 10 (1959).
33. NIKITINE S., *Phil. Mag.* **1,** 1 (1959).
34. GROSS E. F., NOVIKOV B. V., RASBIRIN B. S. and SUSLINA L. G., *Opt. i Spectr.* (*USSR*) **6,** 569 (1959).
35. PERNY G., *J. Chim. Phys.* **55,** 650 1958); MAIER G. and WAIDELICH W., *Z. Naturf.* **13a,** 562 (1958).
36. GROSS E. F. and NOVIKOV B. V., *Solid State Phys.* (*USSR*) **1,** 1882 (1959).
37. GROSS E. F. and PASTERNJAK I., *Solid State Phys.* (*USSR*) **1,** 837 (1959).
38. DUTTON D., *J. Phys. Chem. Solids* **6,** 101 (1958).
39. BROUDE V. L., EREMENKO V. V. and MEDVEDEV V. S., *J. Tech. Phys.* (*USSR*) **28,** 2263 (1958).
40. GROSS E. F., RASBIRIN B. S. and SHEKHMAMETJEV R. I., *Solid State Phys.* (*USSR*) **3,** No. 12 (1961), to be published.
41. GROSS E. F. and SHEKHMAMETJEV R. I., *Solid State Phys.* (*USSR*) **3,** 889 (1961).
42. GROSS E. F., *Vest. Akad. Nauk. SSSR* **10,** 11 (1958).

Vol. 22
1961

J. Phys. Chem. Solids Pergamon Press 1961. Vol. 22, pp. 101–107. Printed in Great Britain.

FINE STRUCTURE IN THE ABSORPTION EDGE OF THE SILVER HALIDES*

F. C. BROWN, T. MASUMI and H. H. TIPPINS

Department of Physics, University of Illinois, Urbana, Illinois

Abstract—The results of new optical absorption measurements on pure AgCl and AgBr will be reported and compared with the wavelength dependence of photoconductivity in these materials. Detailed structure consisting of low-level absorption tails and several shoulders has been found at various temperatures down to 4·2°K. The data will be analysed in terms of indirect optical transitons together with a plausible band structure and vibration spectrum.

1. INTRODUCTION

THE CHARACTERISTIC absorption of AgCl and AgBr has been investigated by several workers. For example, OKAMOTO[1] and TUTIHASI[2] have made point by point measurements on both thick and thin crystals down to 20°K. The absorption constant begins to rise in the visible or near ultraviolet and increases to values in excess of 10^5 cm^{-1} in the vicinity of 250 $m\mu$. One notes a remarkable similarity between the observed structure in the ultraviolet for AgCl and for an alkali halide like NaCl.[3] There seems little doubt that the first strong absorption peak in AgCl, which shows the characteristic chlorine doublet,[4] is due to a direct exciton process associated with an electron on a halogen ion. Unlike the alkali halides, however, the silver halides have a relatively low-level absorption which extends to long wavelengths near the visible. Light absorbed in this region produces photoconductivity with high efficiency and is also important in connection with the photographic process.

SEITZ[5,6] and others[7] have suggested that the long wavelength absorption of the silver halides is due to indirect optical processes involving phonons to conserve wave number. It was thought that a branch of the valence band bends strongly upward in at least one direction in k-space. Indirect transitions occur between a maximum in this band not at $k = 0$ and a minimum in the conduction band at $k = 0$. There are other plausible explanations for the long wavelength absorption. For example, direct, forbidden transitions involving levels associated with the silver ion have been suggested.[8] In an attempt to decide between the various explanations it was thought important to carry out absorption measurements on pure crystals[9] with high spectral resolution down to 4·2°K. If indirect transitions are important, one expects to find structure associated with different phonon processes as reported for Ge and Si.[10–12] This is indeed found to be the case.

2. EXPERIMENTAL DETAILS

The measurements were carried out by mounting the crystals (annealed, zone-refined or otherwise purified material) in a glass–metal cryostat[13] designed so as to locate the sample at the measurement position of a Cary Model 14R recording spectrophotometer.† Under some conditions the spectrophotometer was run at its lowest scanning rate of one-half Ångstrom per second using a resolution better than 1 Å to reveal details in a sharply rising absorption edge. Because of good thermal insulation of the cryostat and a slow warming rate, it was possible to obtain some data at temperatures intermediate between the temperatures of liquid helium and liquid nitrogen.

* Supported in part by the U.S. Air Force Office of Scientific Research.

† In this instrument, the sample is located at the point of convergence of the incoming light beam and the detectors have a large light gathering geometry which tends to minimize the effects of surface scattering.

Care was taken to determine the true temperature of the crystals mounted in the cryostat. The samples were surfaced by cutting with a tungsten carbide saw followed by microtoming and polishing on a soft cloth using either a potassium cyanide or sodium thiosulfate solution. The microtome was also used to reduce the thickness of some samples to values around 100 μ.

Optical density was obtained from the recorder traces by referring to a base line extrapolated from beyond the onset of absorption. Little or no dependence of the base line on wavelength was involved. The absorption constant, K, can be obtained after correcting for multiple reflections. This was done by an iterative process which amounted to determining K from the equation:

$$T = \frac{(1-R)^2 \exp(-Kx)}{1-R^2 \exp(-2Kx)}, \qquad (1)$$

where T is the transmission of the sample, x the sample thickness and R an effective reflectivity.

3. OBSERVATIONS

The results for AgBr will be presented first since they appear less complicated, probably because of a simpler vibration spectrum. Fig. 1 shows optical density at low level traced directly from the spectrophotometer curves for a AgBr crystal 0·122 cm thick. Fig. 2 is a plot of very low level absorption taken at 4·2°K on a thick crystal after changing the slidewire of the recorder for increased sensitivity. Note that the data has a characteristic shape consisting of a shoulder following an abrupt threshold. Slight but definite structure 1 and 2 appears in the shoulder at 2·70 eV and near 2·72 eV, respectively. As the temperature is increased, a low-level tail begins to rise beyond the threshold as seen in Fig. 1. Several different crystals were investigated and this phenomena is apparently not related to impurity content. The data of Fig. 1, for example, were taken on a crystal which was multiple zone refined in halogen.[14] Parts of the ingot were spectrochemically analyzed and showed only a possible trace ($<0{\cdot}03$ parts per million) of iron.[15] Fig. 3 shows a plot of $(Kh\nu)^{1/2}$ vs. photon energy obtained from measurements on both thick and thin crystals. Here the method of plotting accents the threshold shoulders $[Kh\nu \propto (\Delta E)^{1/2}]$ but

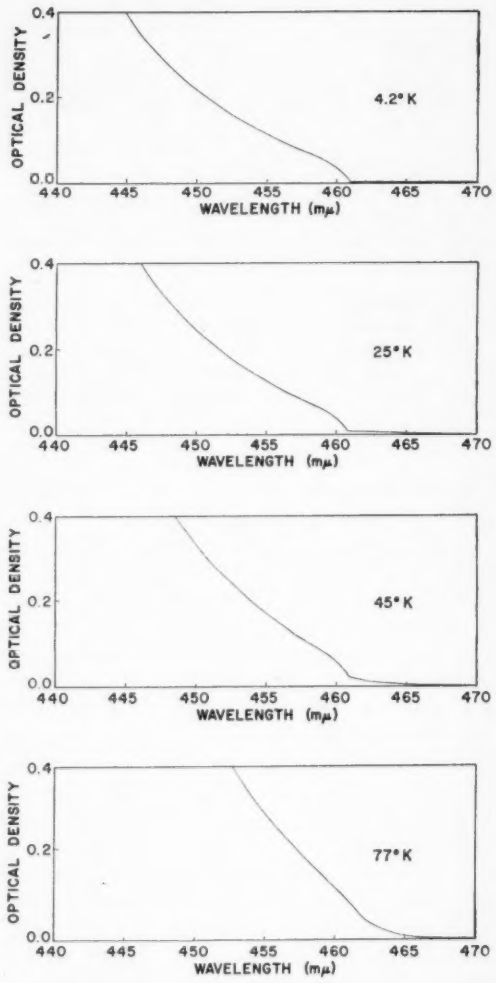

FIG. 1. Spectrophotometer tracings for a very pure AgBr crystal 0·122 cm thick at various temperatures; notice at 4·2°K the sharp threshold of absorption at 460·8 mμ and the growth of a single tail as the temperature is increased.

permits the presentation of data to a higher absorption constant, as well as a comparison with the theory of indirect-allowed band-to-band transitions $[Kh\nu \propto (\Delta E)^2]$.[10] Note the presence of a broad bump beginning near 2·84 eV in the 4·2°K data. The low-level tail of the data (Fig. 1) is apparent at 77°K and additional low level,

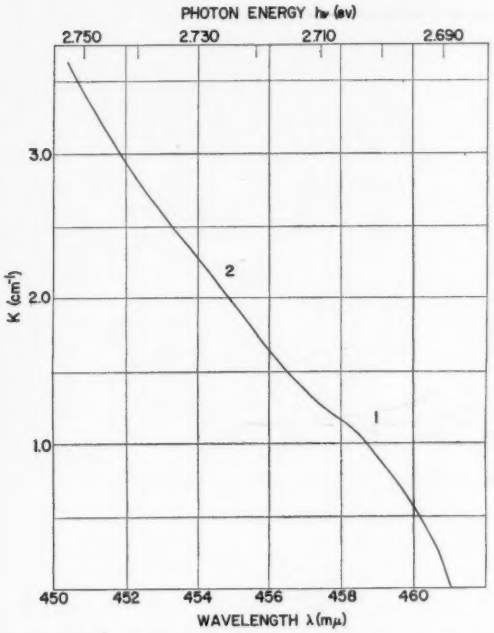

FIG. 2. Very low-level absorption in AgBr at 4·2°K showing slight structure in the basic shape near 1 and 2.

long wavelength absorption appears at higher temperatures.

Figure 4 shows optical density vs. wavelength for AgCl at various temperatures. Note that a very narrow range of wavelength is covered near the threshold of a steeply rising edge. An absorption tail increasing with temperature is again apparent and a second component is seen at higher temperatures. At 4·2°K, the first knee begins abruptly at 381 mμ (3·254 eV) and there is just the hint of a broad structure around 380·2 mμ (3·260 eV). Expansion in sensitivity comparable to Fig. 2 was not attempted. Fig. 5 shows absorption constant for AgCl to higher values on a $(Khv)^{1/2}$ basis. Definite shoulders at A and B, as well as slightly broader structure near C and D, are seen.

Figure 6 shows transient photoconductivity at 78°K and at 2°K for both AgCl and AgBr. The data were taken using a vibrating reed electrometer to record a small amount of charge released by low intensity pulses of light from a quartz prism monochromator.[16] The sample, immersed in either liquid nitrogen or pumped liquid helium, was illuminated from the side in a direction parallel to the plane of the electrodes. Unlike the absorption data, the photoresponse was observed point by point and care was taken to avoid polarization or space charge effects. The photoresponse plotted in Fig. 6 was corrected for variation in the number of incident photons with wavelength but not for absorption constant.

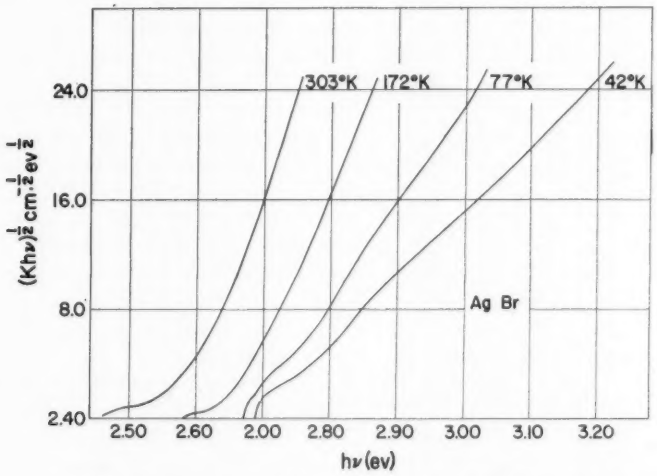

FIG. 3. $(Khv)^{1/2}$ vs. photon energy, hv, for AgBr from data taken up to higher absorption constant and temperature than Figs. 1 or 2.

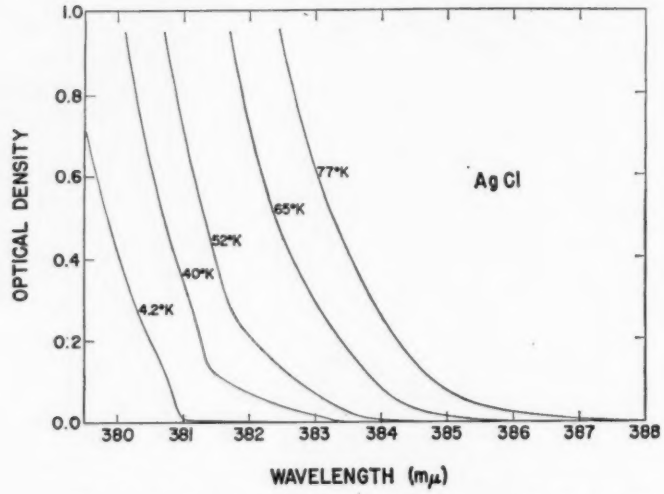

FIG. 4. Spectrophotometer tracings for a pure AgCl crystal 0·208 cm thick.

4. DISCUSSION

Some general remarks are in order before presenting an anaylsis of the absorption data. First, it is apparent that the smooth exponential behavior of K predicted by "Urbach's rule"[17] is not valid at very low temperatures (below 77°K) in the silver halides. Even at high temperatures, except at very low level, the extinction must arise because of the merging of phonon absorption and emission processes reminiscent of the situation in Ge and Si.[11,12] There is, however, a remarkable smoothing of the structure as the temperature is increased above about 65°K. (See Fig. 4.) Notice further that very low level ($K < 0{\cdot}5\ \text{cm}^{-1}$) more or less exponential tails begin to occur above this temperature at wavelengths beyond the threshold for indirect transitions. "Urbach's rule" is apparently applicable to this low level absorption at higher temperatures. An explanation has been given by DEXTER[18] who showed that the effect of temperature is to produce a tail in the density of states toward lower energy measured from a band gap. Apparently this phenomena also causes a smoothing of the exciton structure at moderate temperatures in the silver halides. The effect seems to be a little stronger in the chloride than in the bromide.

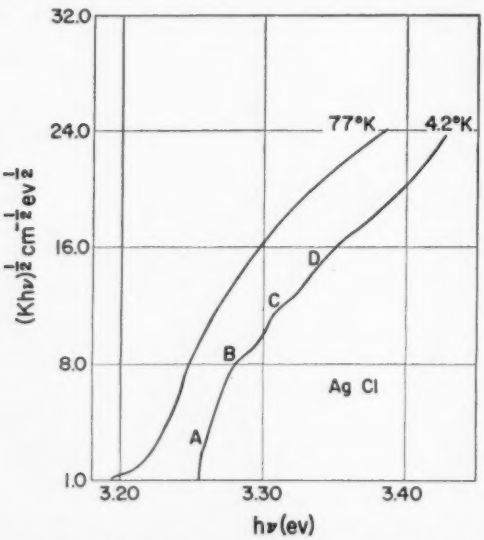

FIG. 5. $(Kh\nu)^{1/2}$ vs. photon energy, $h\nu$, for AgCl—the results of both thick and thin crystal data.

Since thermal broadening and the low level tails discussed above are not very important below 77°K, it is possible to analyze the low temperature absorption data in terms of indirect processes.[10] The band structure and vibration spectrum of the silver halides is not well known at present. However, magnetoresistance experiments[19] have

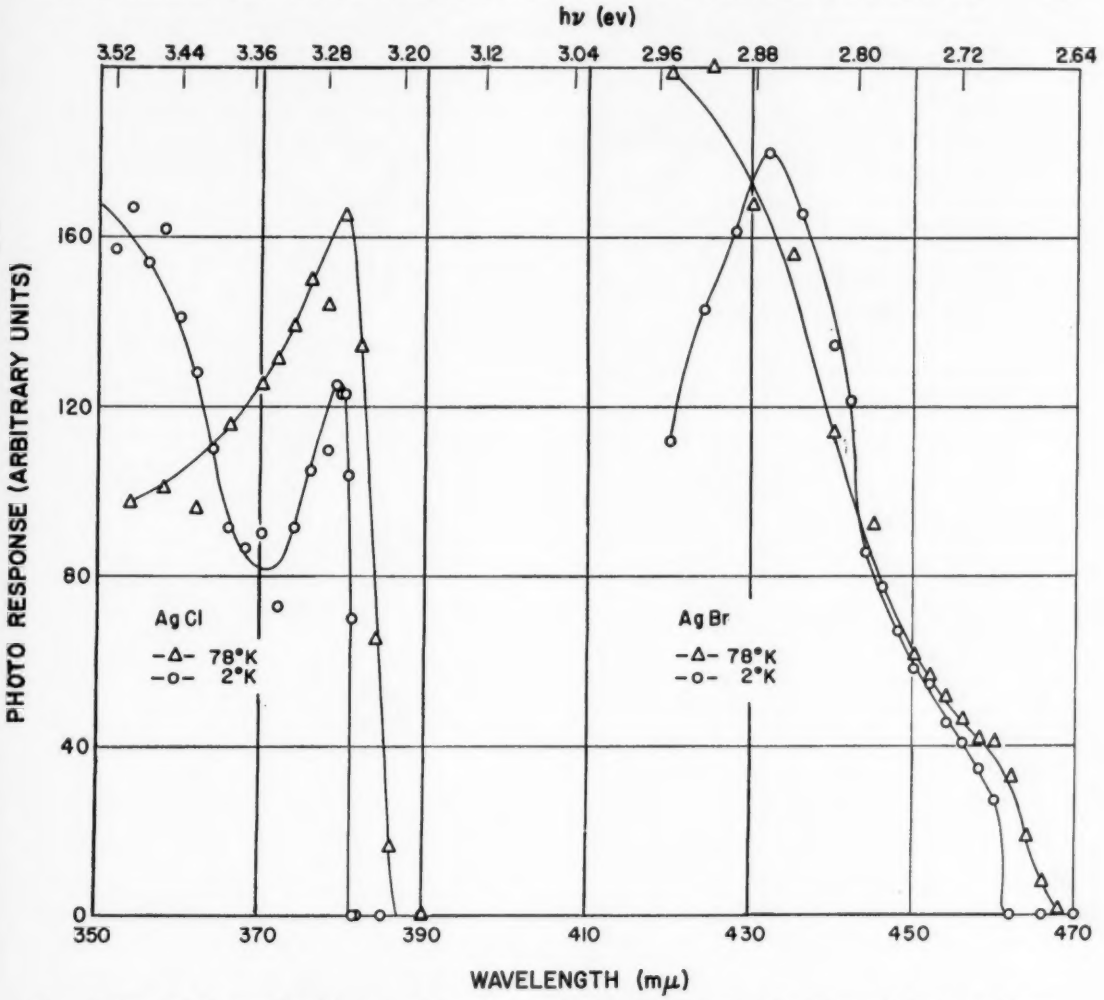

FIG. 6. Transient photoconductivity vs. wavelength near the edge for AgCl and AgBr. The vertical scale is arbitrary so that the four curves cannot be compared with one another as to magnitude. The photo-response in each case is proportional to the number of electrons collected per photon *incident*.

recently shown that the conduction band of AgBr is of nearly standard form with a minimum at $k = 0$. An analysis of the absorption data assuming indirect transitions near the center of the zone with high energy optical phonons[20] was not satisfactory. Therefore it seems plausible for both salts, that indirect transitions occur from one or more maxima in the valence band not at $k = 0$ to a minimum in the conduction band near $k = 0$ as originally suggested.[5]

Let us first discuss the simplest data, that for AgBr. There are various ways to interpret the observations but one is most plausible and internally consistent. We suggest that one fairly low energy phonon is involved toegther with a single maximum in the valence band probably at the zone boundary. An analysis of the absorption constant into components K_e and K_a' corresponding to phonon emission and absorption can be carried out as explained in Refs. (10–12). The

results are given in Table 1. Since a phonon absorption tail is missing at 4·2°K, the data for this temperature is taken to indicate the basic shape. This same shape increased by $1/[1-\exp(-\theta/T)]$ is used for the emission component $K_e(T)$ at higher temperatures.

Table 1. Threshold energies E_a and E_e for absorption and emission of a phonon of temperature θ together with the resulting energy gap E_g for AgBr *as a function of temperature*

T(°K)	E_a(eV)	E_e(eV)	θ(°K)	E_g(eV)
4·2	—	2·690	—	2·6836
25	2·677	2·690	(75)	2·6835
45	2·676	2·689	75	2·6825
77	2·670	2·683	75	2·6765

It may be that the shoulder and higher energy peak in the basic shape correspond to excitation to the $n = 1$ and $n = 2$ states of the exciton respectively. The intensity ratios more or less agree with ELLIOT's[21] estimate for indirect-allowed excitons. The observed separation is 0·13 eV which gives a reduced mass $m = 0{\cdot}27\ m_e$ from the equation:

$$\Delta E = \frac{13{\cdot}6}{\epsilon^2}\frac{m}{m_e}\left(\frac{1}{1}-\frac{1}{4}\right). \qquad (2)$$

In view of the likelihood that the hole is heavy,[22] m is close to the electron mass and is in reasonable agreement with other results[23]. We have used the optical dielectric constant $\epsilon = n^2 = 4{\cdot}6$ for AgBr since the exciton radius lies well within the limit v_i^{-1} given by HAKEN[24] but of the order of a few lattice spacings.

Excitons must dissociate with reasonable probability at the surface or at imperfections in the silver halides since the 2°K photoresponse shown in Fig. 6 begins coincident with the absorption edge. A marked increase occurs near 2·8 eV in the bromide and this might well correspond to the less strongly bound $n = 2$ exciton states. The exact shape of the exciton absorption, including the very slight structure of Fig. 2, is left unexplained.

A tentative explanation of the chloride data is as follows. The basic shape of the indirect exciton absorption includes peaks A and C of the 4·2°K data, Fig. 5.* Both a low energy, $\theta_1 = 93$°K, and a high energy $\theta_2 \simeq 250$°K phonon are involved. The lower energy phonon can be determined quite well by an analysis of the low-temperature curves before thermal broadening sets in. Results are given in Table 2. The weak absorption component

Table 2. Threshold energies E_a and E_e for absorption and emission of a phonon of temperature θ_1 together with the resulting energy gap E_g for AgCl *as a function of temperature. A second phonon $\theta_2 \simeq 250$°K may be important in the chloride but is not shown*

T(°K)	E_a(eV)	E_e(eV)	θ_1(°K)	E_g(eV)
4·2	—	3·254	—	3·246
40	3·235	3·250	93	3·242
52	3·231	3·246	93	3·238
65	3·223	3·238	87	3·230
77	3·219	3·234	87	3·226

K_{2a} lies under the "exponential" tail seen in the 77°K data (Fig. 5) and cannot readily be used to determine θ_2. Peaks B and D of Fig. 5 would correspond to the basic shape involving emission of the higher energy phonon, θ_2. The lower energy phonon is probably an acoustic phonon near the zone boundary, whereas θ_2 could belong to the optical branch.[25]

A band calculation for the silver halides would be most important in connection with the assignments made above. This might be carried out according to recent developments.[26] In addition, it would be valuable to have more information on the vibrational spectrum of these crystals.

Acknowledgements—The authors would like to express their appreciation for the suggestions and help of Dr. A. GOLD. The assistance of Mr. H. ROCKSTAD and R. SCHIMEK is also gratefully acknowledged. The help of the group at Eastman Kodak in connection with crystal preparation and analysis is much appreciated.

* If these correspond to the states $n = 1$ and $n = 2$, use of equation (2) and $\epsilon = n^2 = 4{\cdot}0$ gives $m = 0{\cdot}08\ m_e$ which is rather small. Excitation to $n = 2$ and $n = 3$ states would occur in the indirect-forbidden case. This would result in $m = 0{\cdot}4\ m_e$. The possibility of structure beyond 3·4 eV has not been investigated.

REFERENCES

1. OKAMOTO Y., *Nachr. Akad. Wiss. Göttingen*, **IIa,** No. 14, 275 (1956).
2. TUTIHASI S., *Phys. Rev.* **105,** 882 (1957).
3. EBY J. E., TEEGARDEN K. J. and DUTTON D. B., *Phys. Rev.* **116,** 1099 (1959).
4. KNOX R. S. and INCHAUSPÉ N., *Phys. Rev.* **116,** 1093 (1959).
5. SEITZ F., *Rev. Mod. Phys.* **23,** 328 (1951).
6. SEITZ F. and BROWN F. C., *International Conference on Scientific Photography, Liege* 1959, to be published.
7. KRUMHANSL J. A., in BRECKENRIDGE R. G., RUSSELL B. R. and HAHN E. E. *Photoconductivity Conference*, John Wiley, New York (1956).
8. MARTIENSSEN W., *Proceedings International Conference on Semiconductor Physics*. Czechoslovak Academy of Sciences, Prague (1961).
9. MOSER F. and URBACH F., *Phys. Rev.* **102,** 1519 (1956).
10. MCLEAN T. P., in GIBSON A. F., BURGESS R. E. and KRÖGER F. A., *Progress in Semiconductors*, Vol. 5, Heywood, London (1960).
11. MACFARLAND G. G., MCLEAN T. P., QUARINGTON J. E. and ROBERTS V., *Phys. Rev.* **108,** 1377 (1957).
12. MACFARLAND G. G., MCLEAN T. P., QUARINGTON J. E. and ROBERTS V., *Phys. Rev.* **111,** 1245 (1958).
13. HERSH H. M., *Phys. Rev.* **105,** 1158 (1957).
14. MOSER F., BURNHAM D. C. and TIPPINS H. H., *J. Appl. Phys.* **32,** 48 (1961).
15. NAIL N. R., MOSER F., GODDARD P. E. and URBACH F., *Rev. Sci. Instrum.* **28,** 275 (1957).
16. VAN HEYNINGTEN R. S. and BROWN F. C., *Phys. Rev.* **111,** 462 (1958).
17. URBACH F., *Phys. Rev.* **92,** 1324 (1953).
18. DEXTER D. L., *Nuovo Cim.*, Suppl. **VII**, No. 2, 245 (1958).
19. TIPPINS H. H., Ph.D. Thesis, University of Illinois, to be published.
20. DUMKE W. P., *Phys. Rev.* **108,** 1419 (1957).
21. ELLIOT R. J., *Phys. Rev.* **108,** 1384 (1957).
22. HANSON R. C., *J. Appl. Phys.* **31,** 210 (1960).
23. BURNHAM D. C., BROWN F. C. and KNOX R. S., *Phys. Rev.* **119,** 1560 (1960).
24. HAKEN H., *J. Phys. Chem. Solids* **8,** 166 (1959).
25. COLE H., *J. Appl. Phys.* **24,** 482 (1953).
26. BASSANI F. and KNOX R. S., private communication.

ol. 22
961

BLANK
PAGE

Vol. 22
1961

J. Phys. Chem. Solids Pergamon Press 1961. Vol. 22, pp. 109–116. Printed in Great Britain.

BAND EDGE EMISSION PROPERTIES OF CdTe*

R. E. HALSTED, M. R. LORENZ and B. SEGALL

General Electric Research Laboratory, Schenectady, New York

Abstract—Near band edge, fluorescent emission in CdTe is described. Longitudinal optical phonon spacing between emission lines is observed at 20°K. Analogous spectra in ZnS, CdS, ZnSe, CdSe and ZnTe show this to be a general rule for II–VI compounds. Emission lines of instrumentally limited width $< kT$ were observed in CdTe, ZnTe and ZnSe. In conjunction with similar prior observations in Si, CdS and SiC, one concludes that such narrow line emission must also be of general occurrence near the band edge in semiconducting materials. A preliminary investigation of the dependence of the CdTe spectra on impurity content and conductivity type, and of the influence of temperature on position and relative intensity of emission provides useful correlations to guide further study.

INTRODUCTION

At 20°K, single crystal CdTe exhibits a variety of emission "lines" of near band-gap energy in fluorescence, many occurring equally spaced in series.[1] Similar behavior has been observed in a number of semiconducting materials, suggesting the general occurrence of similar types of recombination mechanisms. In silicon, where the luminescence is best understood, three types of band-edge emission lines have been reported: (a) emission from bound and free particle recombination;[2] (b) exciton emission with phonon cooperation;[3] and (c) emission from an immobile four-particle complex formed when an exciton encounters an occupied donor or acceptor impurity level.[4,5] In compounds, the possibility of interaction between impurity and stoichiometric defects multiplies the number of possible transitions. Recent experimental investigations in SiC[6], CdS[7–11], ZnSe[12], and ZnTe[13] have achieved only a limited correlation of band edge emission with specific crystal defects. In this paper, band-edge emission spectra observed in CdTe at 20°K are described. Much more detail is observed than at higher temperatures.[14,15] Some correlations with spectra in other compounds are evident.

EXPERIMENTAL PROCEDURE

CdTe crystals can be grown from the melt by variations of the Bridgeman–Stockbarger method or from the vapor.[14,16,17]† We have employed two types of growth from the melt. Undoped crystals have been grown from high purity Cd and Te metal under controlled Cd pressure. A temperature gradient of approximately 7°C/cm was passed through stationary 150–200 g CdTe melts at about 1·5 mm/hr. Pure crystals and a limited group of crystals with 200 p.p.m added impurity have been grown by passing 15–20 g charges in pyrolytic-graphite-coated quartz ampoules through a r.f.-heated graphite sleeve at rates of 3 to 6 mm/hr. Although the tip section is often polycrystalline, the bulk of each ingot consists of a few large single crystals. For observations of band-edge emission spectra, either single crystals were cut to yield flat surfaces which were chemically polished[18] or, preferably, cleaved surfaces were employed.

Spectra have been measured in an apparatus employing a filtered high pressure mercury arc (*GE AH–6*) as an excitation source, a 30 Å/mm dispersion monochromator, and a cooled infrared-sensitive photomultiplier detector (*RCA* 7102). Samples were mounted with a CdTe powder loaded calorimeter cement on a coolable copper substrate. They were masked, except for an observation slit, with indium foil. A thermocouple secured in pressure contact with the edge of a crystal by calorimeter cement, but shielded from

* Supported in part by the Aeronautical Research Laboratory, Office of Aerospace Research, USAF and by the Aeronautical Systems Division, Air Force Systems Command, USAF.

† The authors wish to thank D. G. Thomas for a preprint of his forthcoming paper on "Excitons and Band Splittings Produced by Uniaxial Stress in CdTe".

exposure to excitation by the foil, was used for a temperature measurement.

RESULTS

Figure 1 shows an emission spectrum for an undoped CdTe crystal at 20°K. The position of the exciton absorption peak, derived from reflectance data, is shown to occur at 1·594 ± 0·001 eV. The band edge is placed by estimating an exciton binding energy of 0·012 eV. Some reduction in the apparent complexity of the emission results from the fact that series of lines separated by 0·021(3) eV are simultaneously present. It has been shown that the band-edge emission lines are separated by the longitudinal optical phonon energy for ZnS[19], ZnO[19] and CdS[8]. This relationship is confirmed for CdTe in Table 1. The band-edge emission line separation energies have also been measured in crystals of several other II–VI compounds at 20°K to ascertain the generality of this correlation. In each case, the tabulated line separation is taken from the spectrum obtained with the best resolution of phonon structure. Results from less well resolved spectra are consistent within their experimental error. The origins of the tabulated static and optical dielectric constants, ϵ_s and ϵ_o, and the transverse optical phonon energies, E_T, are given. A mean value is employed where anisotropic static dielectric constants have been measured. With the possible exception of ZnS, the correlation is excellent. Recent infrared absorption and reflectivity data for ZnS are not consistent with each other. The reflectivity curve which gives a poor correlation in Table 1 has been noted to be anomalous in shape.[20]

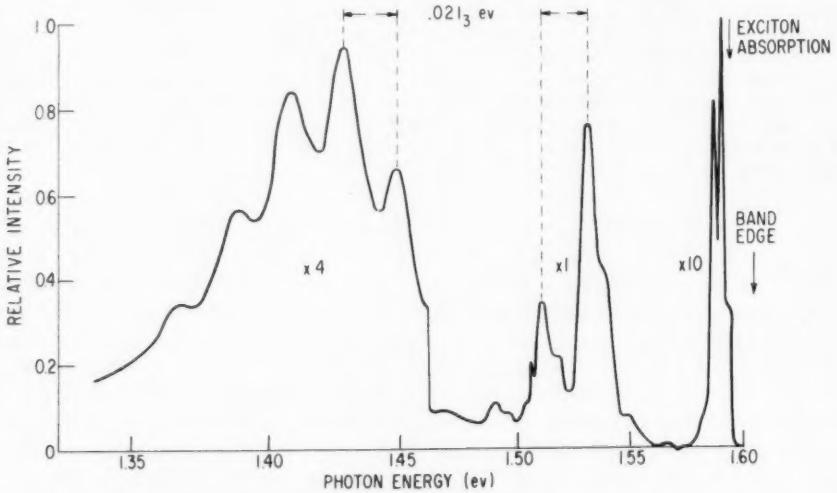

FIG. 1. Fluorescent emission spectra near the band edge in CdTe at 20°K. Series of lines separated by the $k = 0$ longitudinal optical (LO) phonon energy, 0·021(3) eV, are observed. Emission lines of width $< kT$ occur at ≈ 1·51 eV and ≈ 1·59 eV. Various portions of the emission are shown in more detail in subsequent figures.

The emission peaks immediately adjacent to the band edge are shown in more detail in Fig. 2 for samples from two boules employing the same starting materials. They have phonon satellites of the order of 1 per cent relative intensity. Of particular interest is the fact that some have a width at half-height limited by instrumental resolution but significantly $< kT (kT = 0{\cdot}002$ eV at 22° K). Others appear $\approx kT$ in width. With an increase in temperature between 20°K and 80°K the peaks shift 0·011 eV to lower energy at the same non-uniform rate as the exciton absorption

Vol. 22
1961

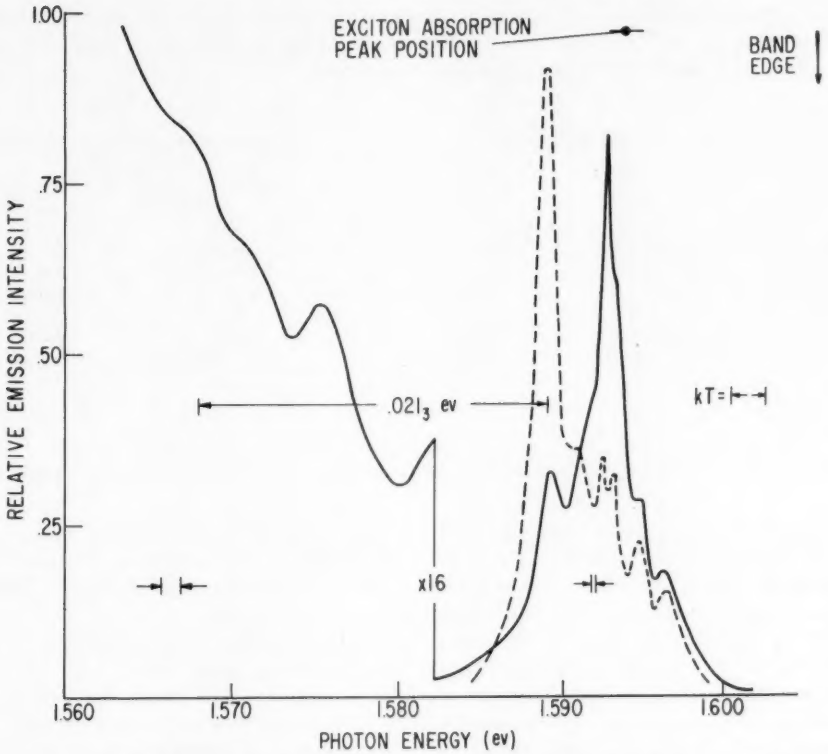

FIG. 2. Fluorescent emission near the exciton absorption peak in CdTe at 20°K for two crystals grown from the same Cd and Te. The positions of the exciton absorption peak and of the estimated band edge are indicated. Phonon spaced satellites of ≈ 1 per cent relative intensity are present. Emission lines of width $\approx kT$ and of instrumentally limited width $< kT$ are observed.

peak.[17] The intensity of the emission peaks in this group decreases with increasing temperature, the rate of decrease being greatest for the lower energy peaks. Preliminary attempts to correlate these spectra with impurity content have proved unsuccessful to date. The emission observed in this region with doped crystals has been of insufficient intensity to resolve the structure. In addition, some loss of resolution observed in doped crystals now appears due to the method of growth and possibly subject to removal by annealing.

Several types of emission processes might be anticipated in this energy region at low temperatures. Emission peaks coincident in energy with exciton absorption peaks and attributed to free exciton recombination are observed to result from band-gap excitation in CdS.[9] They could have an analog here. From transitions between donor impurity levels and the valence band, emission might be anticipated at energies a donor-level depth, $\approx 0{\cdot}02$ eV in CdTe,[14] less than band-gap energy. The width of such an emission line would be determined by the energy distribution of the holes. An immobile four-particle complex at a donor site would give peaks $< kT$ in width intermediate in energy between donor and exciton emissions.[4,5] Band-edge emission narrow with respect to kT has been independently observed in CdTe,[17] also in CdS[9] and SiC[6]. We have also observed such emission in ZnTe and ZnSe. One may therefore suspect general occurrence in semiconducting compounds of emission from

Table 1. The energy spacing observed between fluorescent emission lines in various II–VI compounds is compared with a longitudinal optical phonon energy calculated from cited reststrahl and dielectric constant data using the relation: $E_{LO} = E_T(\epsilon_s/\epsilon_o)^{1/2}$

	Transverse optical phonon energy (eV)	ϵ_s	ϵ_o	Longitudinal optical phonon energy (eV)	
				Calculated	Observed
CdTe	0·0174[21,14,16]	10·6[14,16]	7·13[21,14,16]	0·021	0·0213
CdSe	0·023[22]*	10·0[23]	7·02[24]	0·027	0·027
CdS	0·0299[8]	9·2[23]	5·24[24,25]	0·039	0·038
ZnTe	0·0236[22]*	10·1[23]	8·26[23]	0·026	0·0259
ZnSe	0·026[26]	8·1[26]	5·75[26]	0·031	0·0314
ZnS	0·034–0·038[22]* 0·048[20]	8·1[20]	5·13[25]	0·042–0·048 0·060	0·044

* The position of the absorption maximum is taken as an approximation of the resonance frequency.

immobile complexes. The above processes all should yield emission peaks shifting in energy with temperature approximately as the band gap. In fact, any complex whose electronic structure can be described in terms of the states at the edges of the valence and conduction bands (i.e. by the effective mass approximation) should show this temperature dependence. The possibility of such processes is not inconsistent with the emission observed in CdTe and provides working hypotheses for further study.

Between 1·47 and 1·56 eV in Fig. 1, two series of lines with prominent phonon spaced satellites are simultaneously present. This emission pattern from undoped CdTe is drawn on an enlarged scale in Fig. 3, curve 1. The two series are observed to be separated by 0·008 eV. Maximum emission occurs at the highest energy peak of each series. The relative intensity of the two series is strongly temperature dependent with the lower energy series becoming dominant at low temperatures. The emission shifts 0·011 eV to lower energy at 80°K. If, however, the emission of curve 1 is observed in low resolution as one set of lines, the loss of the lower energy series with increasing temperature can, over a limited temperature range, give an apparent shift to higher energy with increasing temperature. This emission pattern was found to occur, equally well resolved, at energies up to 0·02 eV greater than shown. A shift in energy was apparent between materials grown in graphite and quartz crucibles. This shift could also be produced in emission from the surface of graphite-grown CdTe by heating the specimen in oxygen.

Emission in this energy range was also examined in a series of crystals grown with 0·02 per cent added impurity. The results for several samples are also shown in Fig. 3. The emission patterns occurred with a maximum near 1·52(5) eV for samples (with conductivity types noted) containing excess Cd(n), Tl(n), Ga(n) and Al(p). Crystals containing Cd deficiency (p), Cu(p), Ag(p) and In(n) exhibited a maximum near 1·55 eV. Spectra comprised of a combination of these emission patterns were observed, the lower energy pattern becoming more pronounced with decreasing temperature. The position of these spectra varied with temperature as previously noted. In our doped samples, broad peaks were obtained although phonon structure was still evident at 20°K.

This emission appears analogous to the green edge emission of CdS. Emission is strong in both pure and doped material suggesting that a lattice defect can but may not necessarily have to be involved in the recombination center. Two factors appear to influence the position of the emission. One, resulting in a continuous shift of a well resolved emission pattern, may be due to a change in lattice constant resulting in our case from the incorporation of oxygen as an impurity. The other, resulting in two preferred positions

Vol. 22
1961

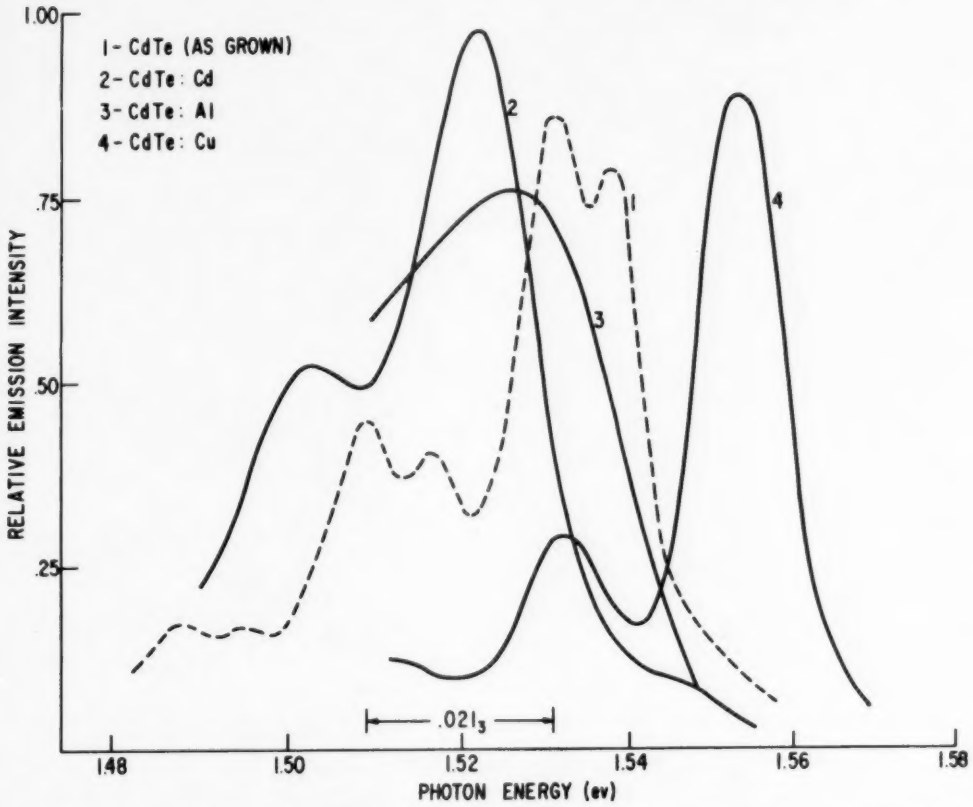

FIG. 3. 20°K fluorescent emission in CdTe believed analogous to the green "edge emission" of CdS. The spectrum for undoped CdTe (1) reveals the presence of two sets of lines with LO phonon spacing separated by 0·008 eV. The spectra for CdTe with defects or impurities added, (2)–(5), occur with maximum emission preferentially at ≈ 1·52 eV and ≈ 1·55 eV.

for the emission, was first noted as a reversible shift with stoichiometry in undoped material. A similar shift in position has been observed in ZnSe.[13] The preliminary data on doped samples show that edge emission is definitely influenced by impurities but provides no clear indication of the origin of this effect. The temperature dependence of emission energy is the same as that of the exciton absorption peak.[17]

Between 1·49 and 1·51 eV in Fig. 1, narrow emission lines are observed which are shown in more detail in Fig. 4. The emission can be $< kT$ in width at 20°K as seen in curve 1. Closely spaced structure is observed. In our undoped material the peak at 1·508 eV is dominant. Emission at 1·503 eV was strong in Ga- and In-doped samples, curves 2 and 3, and evident also in Al-doped material. Examined in more detail at 80°K, these peaks retained 50 per cent of their 20°K intensity, were unchanged in width (therefore narrower than kT), and prominent in the 80°K emission. The temperature change from 20°K to 80°K moved these peaks 5×10^{-4} eV to lower energy, 4 per cent of the change in band gap. In acceptor doped CdTe, curves 4 and 5, the peak at 1·495 eV was observed. The small temperature dependence of position of the peaks suggests that transitions within an unidentified impurity ion are involved.

Emission spectra observed below 1·48 eV are

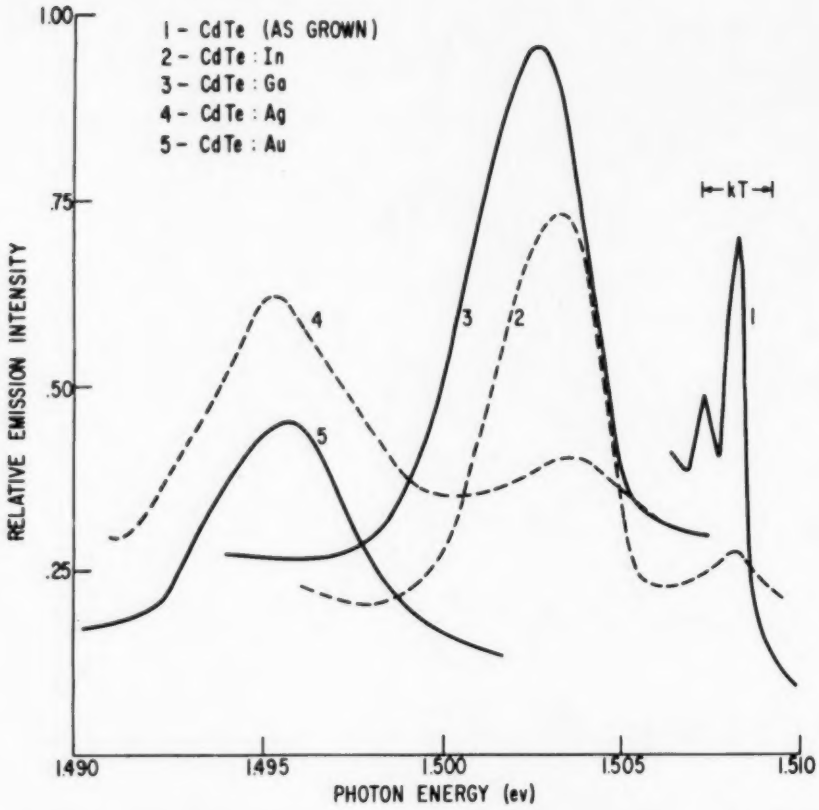

FIG. 4. Narrow emission lines occurring at 20°K in CdTe ≈ 0·1 eV from the band edge. Donor and acceptor impurity additions influence the position of the emission as shown.

shown in Fig. 5 for CdTe(n), CdTe(p), CdTe:Ag(p), CdTe:Au(p) and CdTe:Ga(n). The emission band of CdTe:Ga is representative of those observed with other donor-doped materials. These spectra are clearly dependent upon the identity of the acceptor impurity or defect. For n-type undoped CdTe (excess Cd), spectrum (1), no emission is observed in this region. For p-type undoped CdTe(2) emission centered at ≈ 1·43 eV is observed. This is attributed to Cd vacancy formation.[14] A similar emission pattern should result if the crystal compensates for donor introduction by Cd vacancy formation. Curve (3) for CdTe:Ga shows this to be the case. Curve (4) shows that Ag can introduce an impurity level 0·04 eV closer to the band edge than the 1·43 eV Cd vacancy emission. Curve (5) places a CdTe:Au emission peak below 1·32 eV, not inconsistent with the peak value of 1·26 eV previously reported.[14]

These preliminary emission results appear quite analogous to the luminescent properties of II–VI compounds of larger band gap. This encourages the expectation that the combination of optical and electrical properties of CdTe will make it a useful study material in developing an understanding of the extrinsic behavior of this class of materials.

Vol. 2
1961

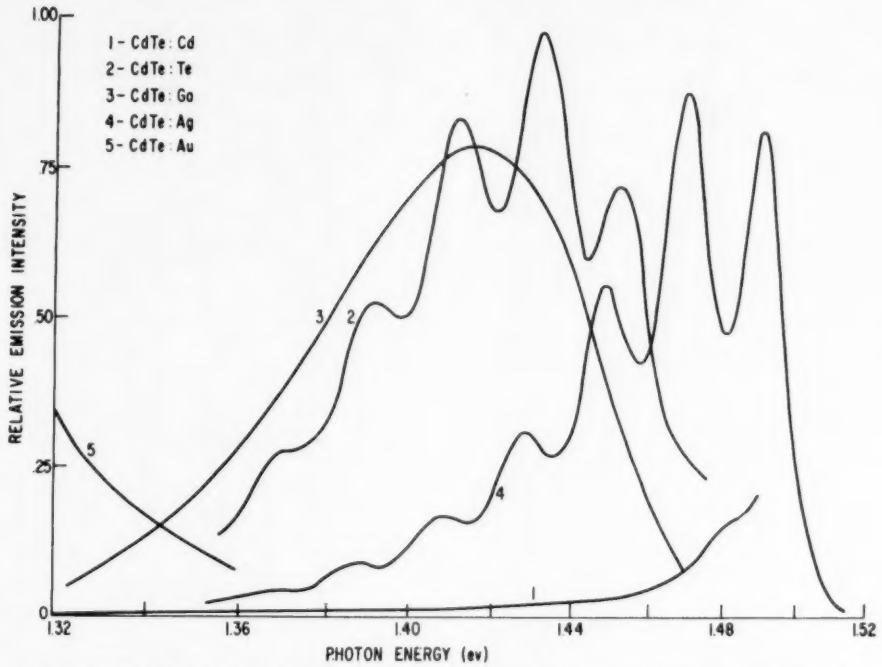

FIG. 5. Emission below 1·50 eV in CdTe is strongly dependent upon the identity of acceptor impurities or defects present as shown. CdTe:Cd(1) contains no added impurities and stoichiometric acceptors, CdTe:Ga(3) is representative of III B donor-doped material. LO phonon structure is evident in spectra (2) and (4).

Acknowledgements.—The assistance of B. B. BINKOWSKI and L. H. ESMANN in crystal growth and in obtaining emission data is gratefully acknowledged.

REFERENCES

1. HALSTED R. E., MARPLE D. T. F., LORENZ M. R. and SEGALL B., *Bull. Amer. Phys. Soc.* **6,** 148 (1961).
2. HAYNES J. R. and WESTPHAL W. C., *Phys. Rev.* **101,** 1676 (1956).
3. HAYNES J. R., LAX M. and FLOOD W. F., *J. Phys. Chem. Solids* **8,** 392 (1959).
4. HAYNES J. R., *Phys. Rev. Letters* **4,** 361 (1960).
5. LAMPERT M. A., *Phys. Rev. Letters* **1,** 450 (1958).
6. CHOYKE W. J., HAMILTON D. R. and PATRICK L., *Phys. Rev.* **117,** 1430 (1960).
7. COLLINS R. J. and HOPFIELD, J. J., *Phys. Rev.* **120,** 840 (1960).
8. COLLINS R. J., *J. Appl. Phys.* **30,** 1135 (1959).
9. THOMAS D. G. and HOPFIELD J. J., *Phys. Rev.* **116,** 573 (1959).
10. PEDROTTI L. S. and REYNOLDS D. C., *Phys. Rev.* **120,** 1664 (1960).
11. KULP B. A. and KELLEY R. H., *J. Appl. Phys.* **31,** 1057 (1960).
12. LARSON O. W., PEDROTTI L. S. and REYNOLDS D. C., *Bull. Amer. Phys. Soc.* **6,** 111 (1961).
13. HALSTED R. E. and AVEN M., *Bull. Amer. Phys. Soc.* **6,** 312 (1961).
14. DE NOBEL *Phillips Res. Repts.* **14,** 357, 430 (1959).
15. GARLICK C. F. J., *J. Phys. Chem. Solids* **8,** 449 (1959).
16. YAMADA S., *J. Phys. Soc. Japan* **15,** 1940 (1960).
17. THOMAS D. G. *J. Appl. Phys.* (Suppl.) **32,** 2298 (1961).
18. ICHIMIYA T., *et al., Solid-State Physics in Electronics and Telecommunications* Vol. 2, p. 845. Academic Press, New York (1960).
19. KRÖGER F. A. and MEYER H. J. G., *Physica* **20,** 1149 (1954).
20. MOSS T. S., *Optical Properties of Semiconductors,* p. 211. Butterworths, London (1959). Calculations from data of H. Yoshinaga, *Phys. Rev.* **100,** 753 (1955).
21. FISHER P. and FAN H., *Bull. Amer. Phys. Soc.* **4,** 409 (1959).
22. MITSUISHI A., YOSHINAGA H. and FUYITA S., *J. Phys. Soc. Japan,* **13,** 1235 (1958).

23. SHIOZAWA L. R., DEVLIN S. and YOST J. M., *Fourth Quarterly Progr. Rpt.* January, 1961 Contract AF 33 (616)–6865. Clevite Corporation, Cleveland, Ohio.
24. KOSTYSHIN M. T., *Opt. i Spekt.* **5**, 71 (1958).
25. CZYZAK S. J., BAKER W. M., CRANE R. C. and HOWE J. B., *J. Opt. Soc. Amer.* **47**, 240 (1957).
26. AVEN M., MARPLE D. T. F. and SEGALL B., *J. Appl. Phys.* (Suppl.) **32**, 2261 (1961).

Vol. 22
1961

J. Phys. Chem. Solids Pergamon Press 1961. Vol. 22, pp. 117–122. Printed in Great Britain.

UNUSUAL PHOTOCONDUCTIVE EFFECTS

T. S. MOSS

Royal Aircraft Establishment, Farnborough, Hants, England

Abstract—Two classes of effect are discussed. In the first, electrons which are already free are excited into higher energy states where they have different mobilities—in contrast to conventional photoconductive effects which are due to excitation of electrons from bound states to conducting states. Such effects can arise from transitions between different conduction bands, between magnetic levels or even within the conduction band continuum.

The second class discusses effects in metals in either the normal or superconducting state.

INTRODUCTION

THE EFFECTS to be considered can be divided into two general classes:

(1) Effects in semiconductors due to changes of mobility.

(2) Effects in metals.

Phenomena in the former class are in contrast to conventional photoeffects which occur when radiation excites electrons from bound states to states where they can move freely through the crystal and contribute to the conductivity.* In terms of the simple expression for conductivity by electrons:

$$\sigma = ne\mu, \tag{1}$$

the conventional case corresponds to an increase in conductivity

$$\Delta\sigma = \Delta ne\mu \tag{2}$$

If we have radiation induced transitions which excite free carriers from a state where they have mobility μ_1 to a state of mobility μ_2, then although the total number of carriers present is unchanged there will nevertheless be a change of conductivity given by:

$$\Delta\sigma = \Delta ne(\mu_2 - \mu_1). \tag{3}$$

If the mobility change is large, i.e. $\mu_2 \gg \mu_1$ (or even $\mu_2 \ll \mu_1$), the effect would be readily observable if values of Δn comparable to those found in normal photoconductivity could be obtained. However from the general expression

$$\Delta n = Q\tau, \tag{4}$$

we see that the magnitude will depend directly on τ, the lifetime in the new state, which may be very small except perhaps at low temperatures. Determination of values of τ may well be one of the most important outcomes of this type of experiment. Four possible ways for such photoeffects to occur will be considered separately.

Photoconductivity in metals has been ignored largely on terminological grounds. In fact, metals must have filled bands from which electrons can be excited optically into states where they can increase the conductivity—however slightly, and it will be shown that, particularly in the poor or semi-metals, effects should be observable. In addition, good metals may show effects if there are suitable energy gaps present as in the superconducting state.

TRANSITIONS BETWEEN DEGENERATE VALENCE BANDS

It is well known that in germanium and silicon the valence band is degenerate, with three distinct sub-bands, all having extrema at $k = 000$.[1] The band structure of the III–V compounds is similar; because, although theoretically there should be linear terms in k which displace the extrema, these terms appear to be very small. Absorption resulting from transitions between these sub-bands has been observed in p-type Ge by several workers.[2,3]

* This discussion is intended to cover positive holes instead of (or as well as) electrons.

The absorption arises from vertical transitions, i.e. no phonons are required. Transitions can occur from bands V_1 and V_2 to V_3 and also from V_1 to V_2. Transitions at $k = 0$ are forbidden by selection rules, but away from $k = 0$ the rule breaks down and absorption will occur. As most of the holes are normally in the heavy hole-band V_1, the main absorption will be due to transitions from V_1 to V_3—particularly at low temperatures. The spectral dependence of the photoconductivity should resemble the absorption spectrum.

The magnitude of the voltage output (ΔV) from a photoconductor is given by simple theory to be:

$$\frac{\Delta V}{V} \sim \left(\frac{Q\tau}{P}\right)\left(\frac{\mu_3-\mu_1}{\mu_1}\right), \qquad (5)$$

where

V is the steady polarizing voltage,

Q is the rate of absorption of photons,

τ is the lifetime in V_3,

P is the total number of current carriers in the dark, and μ_3 and μ_1 are the mobilities in V_3 and V_1.

There are no experimental values for μ_3, but an estimate may be obtained from impurity scattering theory.[4] For $p = 5 \times 10^{16}$ cm^{-3} for example, we find $\mu_3 = 1{\cdot}3$ m^2/V sec at liquid-air temperature, which is an order larger than the measured value of μ_1 for this purity, namely 0·12 m^2/V sec.

The photoconductivity would thus be quite marked, provided τ were reasonably large. Experimentally, however, we found the effect to be extremely small,[5] and only under limiting conditions was it possible to detect it at all. By measuring all the parameters in equation (5) except τ, it was possible to determine the latter within rather wide limits. The result gave the extremely low value:

$$\tau = 4-14 \times 10^{-12} \text{ sec at } 77°\text{K},$$

which is only some 10 or 20 times larger than the scattering time corresponding to μ_3.

PHONON ASSISTED TRANSITIONS BETWEEN BANDS IN DIFFERENT REGIONS OF k-SPACE

Most semiconductors have bands in different parts of k-space with extrema at different energy levels. In Ge for example,[1] the lowest conduction bands have ellipsoidal energy surfaces in the 111 directions with minima at 0·66 eV above the top of the valence band (at room temperature). In addition, there is a band at k 000 at 0·80 eV above the valence band, i.e. ~ 0·14 eV above the ellipsoidal energy surfaces.

It must therefore be possible to excite electrons into the k 000 band by photons of wavelength ~ 8·5 μ, provided that momentum is conserved by phonon interaction. The effective mass at k 000 is only 0·036 m_o, compared with longitudinal and transverse masses of 1·6 m_o and 0·08 m_o in the ellipsoidal bands, so that a considerable increase in mobility should occur. Data for GaSb, whose band structure resembles Ge, show that the mobility at k 000 is 8[6]–16[7] times that for the 111 band.

No evidence of this type of transition in Ge has been observed so far, but FAN[7] reported recently that n-type GaSb has a small absorption band at 0·4 eV which is tentatively attributed to transitions from the 000 or 111 minima to a minimum in the 100 direction.

Data on the main absorption edge of germanium indicate that indirect, phonon assisted, absorption gives an absorption coefficient about 100 times smaller than for vertical transitions—although the higher density of states in the 111 ellipsoids favours the non-vertical transitions. Hence it is expected that the absorption resulting from transitions between conduction bands will be rather weak.

TRANSITIONS BETWEEN MAGNETIC LANDAU LEVELS

When a magnetic field is applied to an n-type semiconductor, the continuum of levels in the conduction band coalesces into discreet Landau levels. Transitions between these levels give cyclotron resonance absorption.

If the conduction band is non-parabolic, then the effective mass will be energy dependent and the mobility will change slightly following a transition to an adjacent level.

For InSb for example, the band theory of KANE[8] gives for the E–k curves:

$$k^2P^2 = \frac{E(E+G)(E+G+\Delta)}{(E+G+2\Delta/3)} \qquad (6)$$

where

G is the energy gap,

Vol. 22
1961

Δ is the spin–orbit splitting,
P is the matrix element, and
E is measured above the bottom of the conduction band.
The Landau levels are given by:

$$E = (n+\tfrac{1}{2})\hbar\omega_o\left(\frac{G}{E+G}\right)\left(\frac{G+\Delta}{E+G+\Delta}\right) \times\left(\frac{E+G+2\Delta/3}{G+2\Delta/3}\right), \quad (7)$$

where $\omega_0 = Be/m_o^*$ is the angular cyclotron resonance frequency appropriate to m_o^*, the mass at the bottom of the conduction band.

The effective mass is given by:

$$m^* = \tfrac{1}{2}\hbar^2(dk^2/dE). \quad (8)$$

Consider n-type InSb with so few carriers that they are all in the lowest Landau level. Assume cooling to liquid-air temperatures or below, when $G = 0{\cdot}23$ eV, and a magnetic field of 38 kG which gives:

$$E(n=0) = 0{\cdot}03 \text{ eV}, \qquad E(n=1) = 0{\cdot}077 \text{ eV}$$

Thus the transition from $n = 0$ to $n = 1$ will occur at $h\nu = 0{\cdot}047$ eV or 26 μ. Taking $m_o^* = 0{\cdot}0143\, m_0$,[9] then from equation (6) the effective masses at these energy levels are:

$$m^*(n=0) = 0{\cdot}0177\, m_o, \quad m^*(n=1) = 0{\cdot}0229\, m_o.$$

Thus if the mobility in the Landau levels is inversely proportional to m^*, it will decrease by 1·3:1 following the transition.† For wavelengths $< 26\,\mu$ the change will of course be larger. The effects should thus be considerable if τ is not too small.

The scattering times estimated from the width of cyclotron resonance lines are very low, namely: 5×10^{-13} sec at room temperature,[10] increasing to $\sim 10^{-11}$ sec at liquid-helium temperature.[11] The time spent in the upper Landau level may, however, be considerably larger than this—it is unlikely to be less than the energy relaxation time discussed in the next Section.

For a circularly polarized wave, the absorption coefficient in a magnetic field is:[1]

$$K = \frac{\sigma_o/nc\epsilon_0}{1+(\omega-\omega_c)^2\tau^2}, \quad (9)$$

where n is the refractive index.

Thus at resonance the absorption is quite high. Even in very pure InSb for example, at low temperature, taking 10^{14} electrons/cm^3 and $\mu \sim 10^5$ cm^{-1}, we have $K = 100$ cm^{-1}.

TRANSITIONS IN THE CONDUCTION BAND

The free electron in the conduction band (or similarly the holes in the valence band) can absorb energy from radiation. This will increase their energy above the thermal equilibrium value appropriate to the lattice temperature, and hence change their mobility.

The main effect on the mobility in this case will be the energy dependence of the scattering time—changes in mass with energy will be ignored. Scattering with phonons will be the main process for dissipating the excess carrier energy, which will decrease with an energy relaxation time (τ_e) given by:

$$\partial E/\partial T = (E-E_o)/\tau_e,$$

where E and E_o are the actual and equilibrium carrier energies.

The phonon scattering time will be energy dependent i.e.

$$1/\tau_p \propto TE^{1/2}m^{*1/2}.$$

Now it has been shown by GUNN[12] that τ_e is considerably larger than τ_p, the relation being:

$$\tau_e/\tau_p \sim kT/m^*U^2,$$

where U is the phonon velocity.

As m^*U^2 is only 10^{-6} eV for InSb, τ_e is hundreds of times greater than τ_p even at liquid-helium temperatures.

It has been estimated from measurements of the voltage dependence of mobility[13] that for a particular specimen of very pure InSb the energy relaxation time reached $\tau_e \sim 10^{-7}$ sec at 2°K.

At low temperatures, the mobility will probably be determined by impurity scattering, giving:

$$\mu \propto E^{3/2}$$

so that

$$\Delta V/V = \Delta\mu/\mu = 3\Delta E/2E. \quad (10)$$

† Energy dependence of the scattering time is also significant, as discussed in the next Section.

Now $\Delta E = P\tau_e$,where P is the radiant power absorbed, and $E \sim NkT$, where N is the total number of electrons in the specimen. Hence for $\tau_e = 10^{-7}$ sec and $T = 2°K$:

$$\Delta V/V \sim P\tau_e/NkT \qquad (11)$$

i.e. $\Delta V/V \sim 10^4$ per watt for a small specimen. This is a very high value of responsivity—corresponding to $\sim 10^{-14}$ W for signal = Johnson noise—so the effect should be very easy to detect and may well result in an efficient long wavelength detector.[13] At short wavelengths, the absorption of material of the purity discussed above will be very low but will of course increase in proportion to carrier concentration.

PHOTOCONDUCTIVITY IN METALS

Photoconductivity in metals seems to have been considered impossible in the past simply on the grounds that metals are not semiconductors and therefore not photoconductors. Although the conduction bands in metals contain large numbers of electrons, the excitation of more electrons from lower energy valence bands must produce *some* increase in conductivity, however small. With modern techniques these effects may well be detectable—particularly in poor or semi-metals.

Let us consider a very small, but feasible, specimen of metal to be investigated, with dimensions: $0{\cdot}3 \times 0{\cdot}03 \times 10^{-4}$ cm^3. (This is roughly the size of the strips used in a metal bolometer. For photoconductive investigation, the specimen can and should be mounted on a heat conducting backing.) The resistance of such a specimen will be: $R = 10^5\rho$.

For a poor metal such as bismuth, $\rho \sim 10^{-4}\ \Omega$ cm, so that $R \sim 10\ \Omega$. For many alloys approximately the same resistivity can be obtained. It is therefore feasible to use a polarizing voltage of 1 V across the specimen.

We have:

$$\Delta V/V = \Delta R/R = \Delta N/N = Q\tau/N. \qquad (12)$$

Takin a high radiant intensity of 1 W, of which $\sim$ 10 per cent is assumed to be absorbed, giving $Q \sim 10^{18}$ photons per second, we have:

$$\Delta V = 10^{18}\tau/10^{-6}n = 10^{24}\tau/n, \qquad (13)$$

where n is the electron density .

Taking the limit as Johnson noise in 1 c/s bandwidth, i.e. $\Delta V_n = 10^{-9}$ V, we have for the signal/noise ratio:

$$S/N = 10^{33}\tau/n. \qquad (14)$$

Hence for Bi, where $n < 10^{20}$ cm^{-3}, we have

$$S/N \sim 10^{13}\tau. \qquad (15)$$

Thus even if τ is as low as 10^{-11} sec, large values of signal/noise should be obtained, and if suitable samples of bismuth can be prepared it should be possible to measure spectral sensitivity curves. Metals of resistivity $\sim 10^{-5}\ \Omega$ cm with $\sim 10^{22}$ electrons/cm^3 should give detectable photoconductivity unless the lifetimes are particularly unfavourable (i.e. $< 10^{-11}$ sec).

If lifetimes are very short it will be preferable to use the photoelectromagnetic (PEM) effect, rather than photoconductivity (PC). Consider the simple theory for a photoconductor of length X with applied field F. The photocurrent will be

$$I_{PC} = Fe\mu Q\tau/X. \qquad (16)$$

For the PEM effect the short circuit current is[1]

$$I_{PEM} = QeL\mu B/X, \qquad (17)$$

where $L = (D\tau)^{1/2}$ is the diffusion length.

Hence the ratio is:

$$I_{PEM}/I_{PC} = BL/F\tau = (B/F)(D/\tau)^{1/2}. \qquad (18)$$

This ratio thus increases as τ falls, i.e. the PEM effect is favourable when lifetimes are very short. The cross-over occurs at $I_{PEM} = I_{PC}$, i.e. when

$$\tau_c = B^2D/F^2. \qquad (19)$$

Assuming we can use $B = 1$ Weber/m^2 (i.e. 10^4 gauss) in the PEM case and fields of 100 V/m in the PC case, then the cross-over value of τ is $\tau_c \sim 10^{-8}$ for D appropriate to a mobility of 40 cm^2/V sec.

Thus for time constants much less than 1 μsec in materials of low resistance (which limit the usable electric fields) better signal/noise ratios should be obtainable from the PEM effect, particularly as there are no current noise problems in PEM work. It is probably significant that the only results so far reported for a metal are PEM measurements on bismuth.[14]

Vol. 22
1961

SUPERCONDUCTORS

Modern theories of superconductivity[15] show that in the superconducting state some of the upper energy levels in the conduction band become separated from the continuum by a small energy gap:

$$Eg \sim 4kT_S,$$

where T_S is the superconducting transition temperature. Hence for lead, where T_S is fairly high, $Eg = 2{\cdot}7 \times 10^{-3}$ eV.

It has recently been shown[16] that structures of superconductors separated by thin oxide blocking layers show tunneling effects, analogous to semiconductor Esaki diodes. The tunneling current at low applied voltages depends on the density of carriers excited thermally across the energy gap, and it has been suggested by BURSTEIN *et al.*[17] that photoexcitation of carriers across the gap should therefore produce photocurrents under low bias conditions. By cooling the junction to a temperature well below T_S the thermal excitation rate will be kept low.

The most important parameter will again be the lifetime of the carriers in the excited state. As a rough estimate, effects should be detectable if $\tau > 10^{-11}$, while if $\tau > 10^{-6}$ sec the system may make a useful detector of far infra-red radiation—the response extending to $\sim 500\,\mu$ even for the high energy gap superconductors such as lead.

For efficient operation, however, it will be necessary to reduce the reflection and increase the absorption of the superconductor. This should result from making the layers very thin,[17] i.e. < 100 Å.

REFERENCES

1. MOSS T. S., *Optical Properties of Semiconductors*, Butterworths, London (1959).
2. BRIGGS H. B. and FLETCHER R. C., *Phys. Rev.* **87,** 1130 (1952).
3. NEWMAN R. and TYLER W. W., *Phys. Rev.* **105,** 885 (1957).
4. BROOKS H., *Advanc. Electron.* **7,** 85 (1955).
5. MOSS T. S. and HAWKINS T. D. F., *Proc. Phys. Soc. Lond.* **76,** 565 (1960).
6. SAGAR A., *Conference on Semiconducting Compounds, Schenectady* (1961), published in *J. Appl. Phys.* **32,** 2073 (1961).
7. FAN H. Y., *J. Appl. Phys.* **32,** 2094 (1961).
8. KANE E. O., *J. Phys. Chem. Solids* **1,** 249 (1957).
9. SMITH S. D., MOSS T. S. and TAYLOR K. W., *J. Phys. Chem. Solids* **11,** 131 (1959).
10. BURSTEIN E., PICUS G. S. and GEBBIE H. A., *Phys. Rev.* **103,** 825 (1956).
11. LAX B. and MAVROIDES J. G., *Solid-State Phys.* **11,** 261 (1960).
12. GUNN J. G., *Progress in Semiconductors* **2,** 211 (1957).
13. ROLLIN B. V., *Proc. Phys. Soc. Lond.* **77,** 1102 (1961).
14. YOUNG T., *Phys. Rev.* **117,** 1244 (1960).
15. BARDEEN J. J., COOPER L. N. and SCHRIEFFER J. R., *Phys. Rev.* **108,** 1175 (1958).
16. GIAEVER I. and MEGERLE K., *Phys. Rev.* **122,** 1101 (1961).
17. BURSTEIN E., LANGENBERG D. N. and TAYLOR B. N., *Phys. Rev. Letters* **6,** 92 (1961).

DISCUSSION

M. A. LAMPERT: In the case of extrinsic photoconductivity there can be a continuous gradation from the conventional effect to the "unusual" effect, depending on the impurity density. For a low density of "hydrogenic" impurity levels the "conventional" effect is observed. For a high density an "unusual" effect will be observed, because of impurity band conduction via the hopping mechanism. Thus, it is not unfair, but only imprudent, to describe the "conventional" extrinsic photoconductivity as the limiting case of an infinitely large "unusual" effect.

T. S. MOSS: A legitimate view, but I prefer to regard "carriers" in impurity bands as quasi-bound electrons.

G. S. PICUS: Dr. E. LOH of our Laboratory has attempted to measure the photoconductive effect expected from excitation of an electron from the 000 minimum to the next higher conduction band in GaAs. SPITZER and WHELAN have attributed an i.r. absorption band at $2{\cdot}5\,\mu$ to this transition. So far we have not found any evidence for this effect which should be a resistance increase because of the lower mobility in the higher band.

T. S. MOSS: These effects are certain to be very small and will probably only be observable in the most favorable circumstances.

G. C. DOUSMANIS: We have been studying processes related to those discussed by Dr. Moss in that unusual photoconductive effects and bulk conductances are involved.

(a) Steady-state cyclotron resonance with circular microwaves, under broad-band optical excitation, has shown that the small negative mass branch of heavy holes in Ge yields an emissive resonance comparable in magnitude to the absorptive third harmonic of heavy holes. This emissive distribution (or population in

version along the m^- directions of k-space) is brought about in this *inverted* Landau structure by the optical excitation and collisions in the anisotropic band. The particle distribution must protrude along the (100) axes, to energies higher ($\sim 50°K$) than $T_{lattice}$ (4·2°K).

(b) A process has been theoretically considered, where in arrangements similar to (a), most of the photo-excited carriers would be thrown, for short time intervals, inside the re-entrancy (m^- region), or other parts of k-space, by additional excitations whose rise time must be shorter than the scattering time. Recently the purity of materials and increasing speed of instruments have approached the requirements of this method.

In (a) and (b) further basic information on photo-excited carriers could be obtained and for these processes improvements in material purity control seem particularly significant.

Vol. 22
1961

J. Phys. Chem. Solids Pergamon Press 1961. Vol. 22, pp. 123–128. Printed in Great Britain.

FIELD INHOMOGENEITIES IN CdS SINGLE CRYSTALS

K. W. BÖER

IV. Physikalisches Institut der Humboldt–Universität und Physikalisch–Technisches Institut der Deutschen Akademie der Wissenschaften zu Berlin

Abstract—The field and current distribution in CdS is described by a new electro-optical method. Well-known inhomogeneities, e.g. barrier layers and current channels, are confirmed. New effects, such as plasma-like inhomogeneities and kinetic effects in the breakdown region are discussed. The mechanism of the development of these effects is given.

WHEN studying the conductivity of semiconductors it is important to know the distribution of the electric field. The distributions of field and current are influenced by the sample and electrode geometry as well as by barrier layers at the electrodes, by crystal imperfections, and by non-homogenous distributions of impurities. Until now, field distributions have been measured by probe scanning, which is laborious and lengthy.[1–3] Fast changes in the field distribution can not be studied by this method; the time resolution being limited by the probe point resistance in series with the total capacity of the arrangement.

A method of visualizing the field distribution has been developed[4, 5] which makes use of the fact that electrons colliding with the top of the valence band in a high electric field may penetrate somewhat into the forbidden gap (Franz–Keldysh effect[6–8] resulting in the optical absorption edge, as a consequence, being shifted towards long wavelengths with rising field strength (Fig. 1). Consider a sample which is illuminated with monochromatic light in the absorption edge range. The absorption will be increased with increased field strength (Fig. 2). If there is a non-homogeneous field distribution, the sample will appear to be non-uniformly darkened, the degree of darkness being a direct measure of the field strength. Changes of the field distribution in time can be immediately observed and can also be photographed.

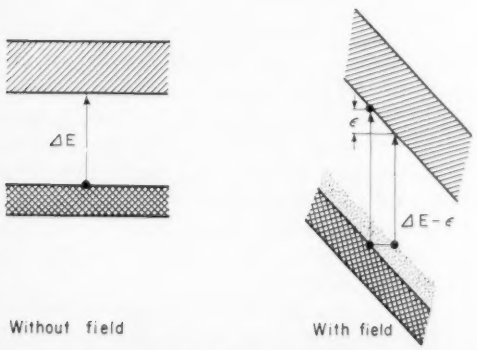

FIG. 1. Band scheme with and without electric field.

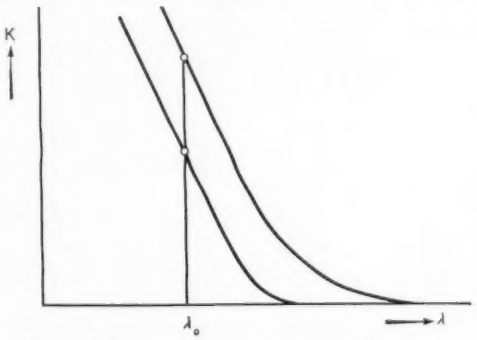

FIG. 2. Shift of the optical absorption edge.

The experiments have been carried out with CdS single crystals. Gold electrodes, displaced with respect to each other, were evaporated on two opposite crystal faces. A series resistance was used to prevent breakdown (Fig. 3).

If a high voltage is applied, the region below the cathode is darkened. One concludes that a high field-region lies below the cathode, which is also observable by probe scanning and is due to contact barrier layers.[9] This field has its maximum

value at the cathode and decreases with increasing distance from the cathode.

With higher voltages applied, a type of field inhomogeneity not previously known has been found: the region of maximum field now surrounds the cathode as a ring, the position of maximum field and the cathode being clearly separated (Fig. 4). This distortion of the electric field is quite different from that due to a barrier layer. The field has its maximum value within the crystal, viz. on the side of the "ring" far from the cathode (Fig. 5). The field distribution obtained by this method has been confirmed by probe scanning.

With the light on the field distortion is built up in about 1 sec after the voltage is applied. It decays in times of the same order after removing the voltage. The field distortion cannot be due to a local temperature rise, for it is found to be present 10 min after light and voltage have been switched off (the dark region may be seen for a moment if the light is switched on again).[4] The field distortion is observed to build up and decay with a time constant which increases with decreasing light intensity, i.e. with decreasing photoconductivity.[10]

These field inhomogeneities are, in many respects, similar to the field distribution in a low pressure gas discharge, e.g. the cathode is "wrapped up" by the glow boundary in a gas discharge and by a dark ring in an insulator; the region of maximum field is separated from the cathode in a striated discharge as well as in an insulator. We shall refer to such field distortions in insulators as plasma-like field distortions.[4, 11]

Let us assume that the field in an insulator at one point $x = x_0$ happens to be so high as to produce conduction electrons (Fig. 6). These electrons will drift to the anode giving rise to a high conductivity in the region $x > x_0$. Near x_0 a region of fixed positive space charge (ionized centres) is formed. Since the cathode does not supply enough electrons, the space charge region moves towards the cathode, and the field strength at the cathode rises. If the field strength becomes high enough so that, by field emission from the cathode, as many conduction electrons are supplied as are removed from the x_0 region, the space charge region ceases to move.

The field distortion observed must arise from

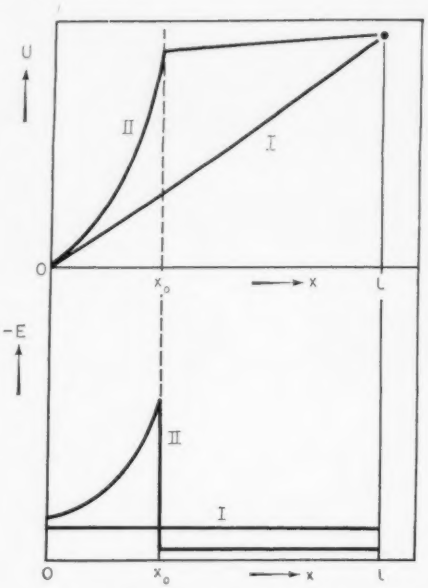

FIG. 6. Potential and field distribution before (I) and after (II) plasma-like field inhomogeneity is formed.

a double layer. The initiation of a field distortion may be understood by assuming that the concentration of conduction electrons is reduced by the electric field ("field quenching" of photoconductivity): holes are excited from activator levels into the valence band and recombine with electrons in traps or in the conduction band. Thus, the concentration of positive and of negative charge carriers is decreased, both being at first equal everywhere in the crystal. If the field strength in any volume element happens to be higher than in its neighbourhood, a further (local) decrease of the concentrations appears. Now the profile of the (mobile) negative charge $n(x)$ is displaced somewhat against the profile of positive charge $p(x)$ by the electric field, so that a double layer is formed (Fig. 7). Thus, the electric field strength rises more and more until it can produce conduction electrons. Then, the space charge region begins to move as has been described above.[11]

The local high field leading to the initiation of the field distortion may also be produced by shadowing a zone of the crystal. Owing to the local decrease of conductivity a local rise of the field strength results (Fig. 8). This means that a field distortion may be "triggered" (as a gas discharge).

Vol. 22
1961

It is possible to produce several zones of space charge in a crystal (Fig. 9).

"Naturally" generated, as well as "triggered", field distortions are found to oscillate and to move towards the anode, the "naturally" generated distortions first having migrated toward the cathode (as described above).[10] A more rapid movement is observed with increasing voltage. The current passing through the crystal is found to increase when the space charge region approaches the anode, the maximum current being reached when the region arrives at the anode. Then the space charge vanishes, a new space charge region is formed at the cathode, and a drop in current is found. This process is repeated periodically. In the current-voltage characteristic a plasma-like field distortion is indicated by a drop of current (Fig. 10). If the voltage is increased rapidly, the distortion appears at higher voltages than in the case of a slow increase, i.e. a time lag is observed, as in gas discharges.

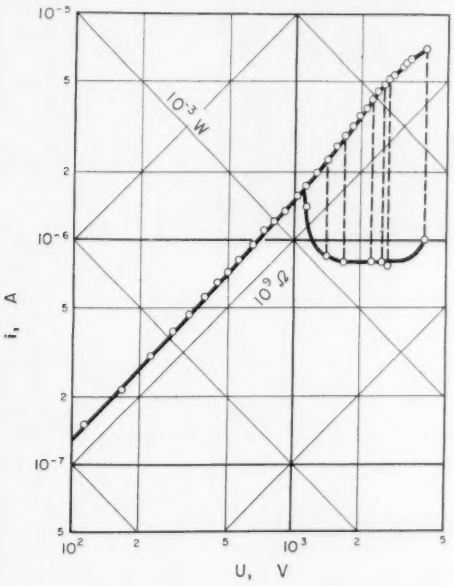

FIG. 10. Current–voltage characteristic; upper curve without, lower curve with, plasma-like field inhomogeneity.

The space charge oscillations mentioned above are accompanied by current oscillations, i.e. by a low-frequency noise component. Both the noise and the space charge oscillations are found to increase at the same rate, with increasing voltage. The shape and behaviour of the space charge regions are appreciably affected by crystal imperfections.

It follows from the presence of plasma-like space charge regions that, if a high voltage is applied to a crystal, an analysis of the field distribution is required for all meaningful discussions of field dependent phenomena.

Acknowledgements—I am indebted to Dr. U. KÜMMEL, H.-J. HÄNSCH, H. LANGE and W. WILHELM for valuable assistance in these investigations. I thank R. BOYN and H. FELDMAN for revising the English manuscript.

REFERENCES

1. SMITH R. W., *RCA Rev.* **12,** 350 (1951).
2. POPPE I., *Arbeitstagung Festkörperphysik Bd.* II. Akademie Verlag, Berlin (1954).
3. POPPE I., dissertation, Humboldt University (1954).
4. BÖER K. W., HÄNSCH H.-J. and KÜMMEL U., *Z. Phys.* **155,** 170 (1959).
5. BÖER K. W. and KÜMMEL U., *Z. Angew. Phys.* **12,** 241 (1960).
6. FRANZ W., *Z. Naturf.* **13a,** 484 (1958).
7. KELDYSCH L. V., *J. Exp. Theor. Phys.* (*USSR*) **34,** 1138 (1958).
8. KELDYSCH L. V., VAVILOV V. S. and BRICIN K. I., *Proceedings International Conference on Semiconductors, Prague* (1960) p. 824.
9. BÖER K. W. and KÜMMEL U., *Z. Phys. Chem.* **214,** 127 (1960).
10. BÖER K. W. and ROMPE R., *Ann. Phys. Leipzig* **5,** 200 (1960).
11. BÖER K. W., *Z. Phys.* **155,** 183 (1959).

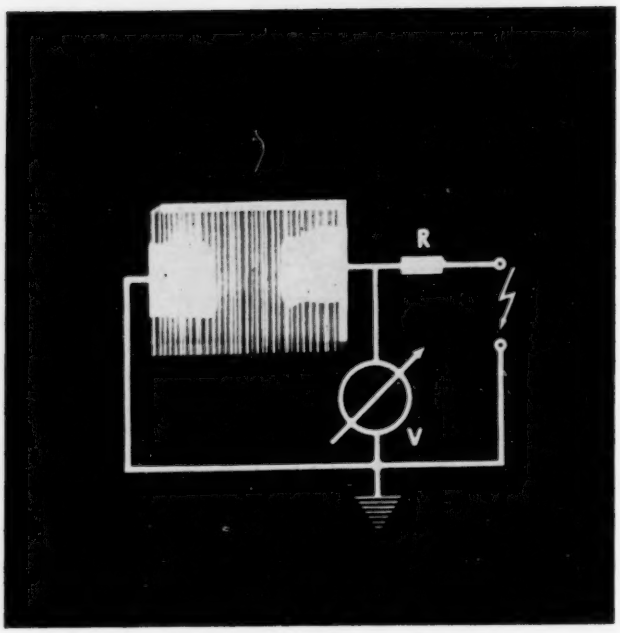

FIG. 3. Electrical arrangement.

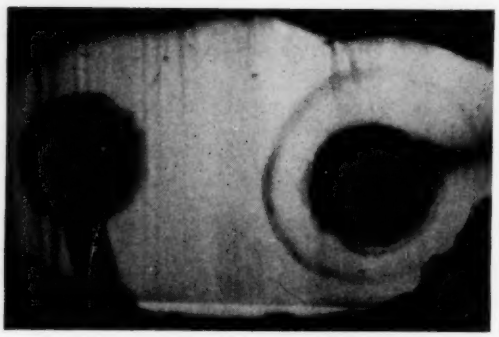

FIG. 4. "Ring" shaped region of high field strength at the cathode (right electrode).

Vol. 22
1961

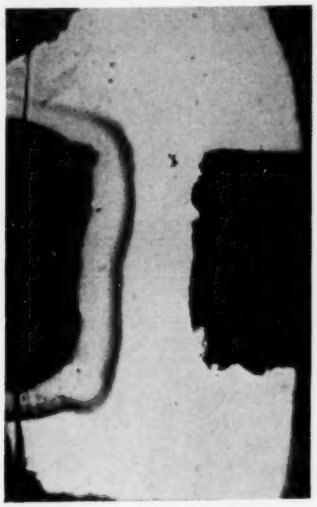

FIG. 5. Plasma-like field inhomogeneity before the cathode (left electrode).

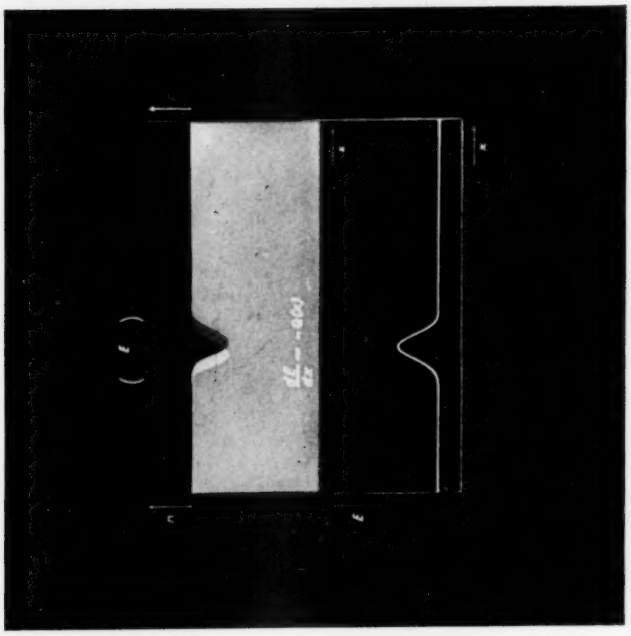

FIG. 7. "Iniation" of a double layer by "field quenching".

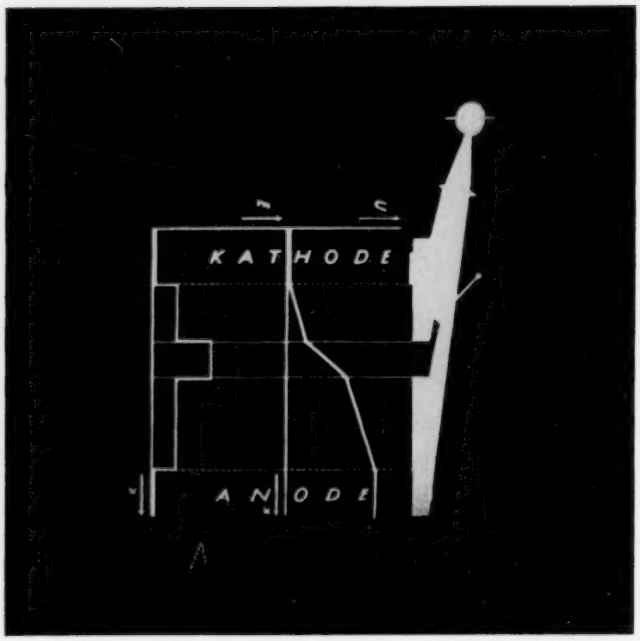

FIG. 8. "Triggering" a plasma-like field inhomogeneity in a zone of increased field strength (increased by shadowing this zone).

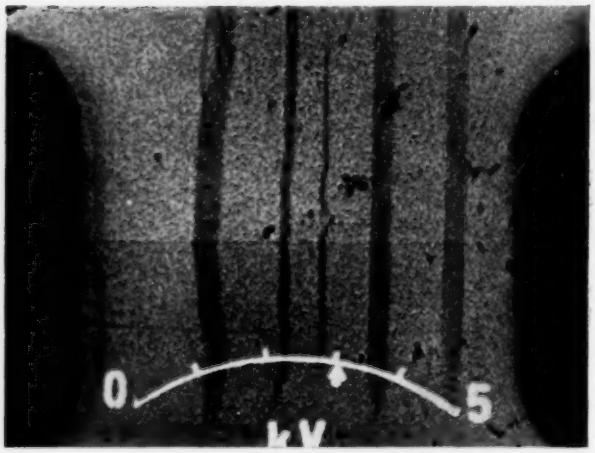

FIG. 9. Several ("triggered") zones of high field strength.

Vol. 2
1961

J. Phys. Chem. Solids Pergamon Press 1961. Vol. 22, pp. 129–133. Printed in Great Britain

HIGH ELECTRIC FIELDS IN CdS

R. WILLIAMS

RCA Laboratories, Princeton, N.J.

Abstract—A technique has been developed for measuring and studying high electric fields in CdS crystals. Fields are produced by a transparent blocking electrode in direct contact with a conducting crystal. D.C. field-effect experiments have been used to measure the magnitude of the electric field and its distribution within the crystal.

Electro-optic effects occur in fields greater than 10^5 V/cm and dielectric breakdown occurs in fields greater than 10^6 V/cm. The main electro-optic effect is a shift of the optical band edge to longer wavelengths with increasing fields. Dielectric breakdown field strengths have been measured in a variety of crystals. The mechanism of dielectric breakdown has been studied by several kinds of experiments including measurement of pre-breakdown currents as a function of field and study of the behavior of optically injected carriers as breakdown proceeds. A comparison of results with theoretical treatments of dielectric breakdown indicates that the breakdown is due to tunneling.

MEASUREMENTS of the properties of insulators in high electric fields have always been troubled by the difficulty of establishing a high field whose magnitude and distribution within the specimen are known with some confidence. In the present work a technique is evaluated for producing and measuring high fields in CdS single crystals. A description of the method is given along with the results of its application to the study of dielectric breakdown.

DESCRIPTION OF METHOD

For these experiments, the high field was produced by means of a blocking contact on highly conducting CdS crystals, using an aqueous electrolyte solution as the blocking electrode.[1, 2] The CdS crystals were *n*-type with 10^{16} to 10^{17} carriers/cm^3. When a negative bias is put on the blocking electrode, the field appears across a space charge region due to ionized donors within the crystal. The Mott–Schottky theory describes the distribution of field and potential within the space charge region.[3] In particular, the relation between the thickness, λ, of the space charge region and the applied voltage, V_2, is given by:

$$\lambda = \left(\frac{\epsilon V_2}{2\pi N e}\right)^{1/2} = 3{\cdot}6 \times 10^3 \left(\frac{V_2}{N}\right)^{1/2}, \qquad (1)$$

where ϵ = static dielectric constant = 11·6 for CdS[4],

e = electronic charge,

N = number of donors/cm^3,

λ = thickness of space charge region in cm.

Equation (1) was tested quantitatively by means of field-effect current pinch experiments with conducting CdS crystals having small dimensions. These experiments are best described with reference to Fig. 1. The crystals were vapor-grown specimens in the form of very thin ribbons several microns thick, about 1 cm long and 1 mm wide.* Their conductivity was due to halogen donors incorporated during growth. Ohmic contacts were applied to the ends and the crystal was mounted so that the center section was surrounded by the electrolyte solution which served as the field electrode. This solution was contained by a Glyptal ring in such a way that it did not come into contact with the end electrodes. D.C. field-effect measurements were made, using a constant value of V_1, usually 1·5 V, with V_1 small compared to the field electrode voltage, V_2. With the polarities shown in Fig. 1, increasing values of V_2 give successively larger values of λ within the crystal until finally the space charge region fills the entire crystal. Since there are no free carriers in the space charge region, the volume filled by the space charge region is not available for flow of the longitudinal current, i_1. Thus, changes in λ are

* The crystals were grown in this Laboratory by S. M. THOMSEN and C. BUSANOVICH.

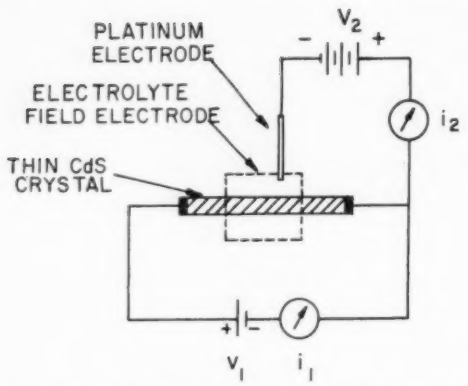

FIG. 1. Circuit and electrode arrangement for d.c. field-effect measurements.

accompanied by changes in i_1 and these changes serve as a direct measure of λ. Fig. 2 shows how i_1 changes with increasing V_2 for a typical crystal.

the measured carrier concentration, N. N was obtained for each crystal by measuring its resistivity and combining this with the reported value of 210 cm^2/V sec for the bulk electron mobility in CdS.[4] Crystal thickness was measured by viewing the thin edge under vertical illumination through a microscope having a calibrated eyepiece. Thus a theoretical value of λ is obtained for the pinch-off voltage according to equation (1). On the other hand, we recognize that the pinch-off occurs when the space charge region fills the entire crystal. Since it penetrates in toward the center of the crystal from the two opposite faces, this happens when λ is equal to one-half the thickness of the crystal. Thus equation (1) gives a theoretical value of λ at the pinch-off voltage and the experimental value of λ for this voltage is half the crystal thickness. Comparing these two quantities shows how well the equation describes the properties of the space charge region under these conditions.

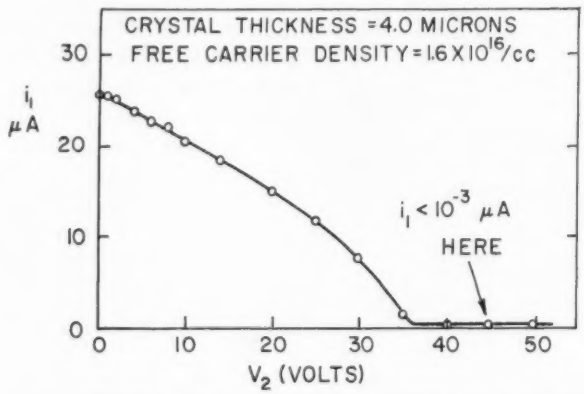

FIG. 2. Field-effect pinch-off of current flow through a CdS crystal.

The current, i_2, through the blocking contact is small compared to i_1 and is ordinarily no more than 10^{-4} times the initial value of i_1. The observed current pinch-off is reproducible, reversible and insensitive to the ionic compound in the electrolyte solution. (Ordinarily 0·1 M KCl was used).

To test equation (1), a number of crystals were chosen which were thin enough to show complete pinch-off of current flow by the field electrode as in Fig. 2. The value of V_2 at which complete pinch-off occurred was put into equation (1) along with

Since the equation also describes the field and potential within the space charge region the same comparison also indicates the extent to which these are described by theory. Table 1 compares theoretical and experimental values of λ for a number of crystals. There is overall agreement to within about 10 per cent. Errors of this magnitude may be introduced by uncertainty in the dielectric constant or in the mobility value used. Understanding the exact dependence of i_1 on V_2 for voltages below the pinch-off voltage requires detailed consideration

Table 1. *Experimental test of equation* (1) *using field-effect current pinch data from nine different crystals. All measurements made at* 25°C

Voltage for complete pinch-off of current (V)	Measured crystal resistivity (Ω-cm)	λ calc. Calculated from equation (1) (μ)	λ exp. Half measured crystal thickness (μ)	Fractional difference $\frac{\lambda_{exp.}-\lambda_{calc.}}{\lambda_{exp.}}$
11·6	2·05	1·0	1·1	+0·09
42	0·86	1·2	1·2	0
90	1·20	2·1	2·0	−0·05
35	1·92	1·7	2·0	+0·15
45	1·13	1·5	2·0	+0·25
80	1·08	1·9	2·4	+0·21
44	2·46	2·1	2·4	+0·12
140	1·23	2·6	2·4	−0·08
105	2·57	3·4	4·3	+0·21

Average value of $\frac{\lambda_{exp.}-\lambda_{calc.}}{\lambda_{exp.}} = +0{\cdot}09.$

of the specimen geometry and when this is done the results are again in good agreement with theory, assuming a uniform volume distribution of donors. This analysis, along with further experimental details, is given elsewhere.[5] It is concluded that the simple Mott–Schottky model, leading to equation (1), gives a quantitative description of λ for various voltages and therefore a quantitative description of the field. According to the model, the field is not uniform but is a linear function of distance within the space charge region, rising from zero at the inner edge to a maximum value at the surface of the crystal. This is illustrated in Fig. 3.

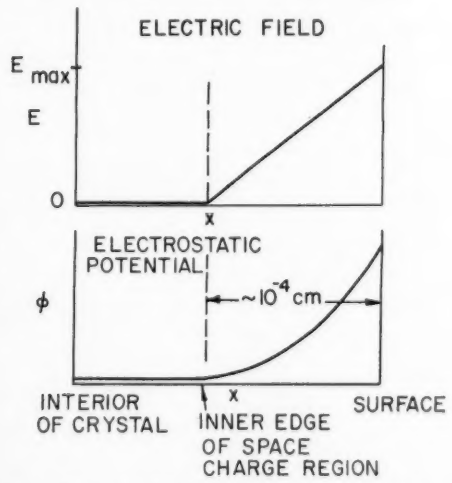

FIG. 3. Electric field and potential as a function of position within the crystal according to the Mott–Schottky model.

Deep electron traps, which are always present in CdS, can behave like donors in the field effect measurement and contribute space charge. Traps, in sufficient concentration, would destroy the agreement obtained above since the deep traps are not ordinarily ionized and contribute no free carriers for the resistivity measurement. Using the above method on less highly doped crystals, about 10^{15} deep traps per cm^3 or less were found in typical crystals. This is not sufficient to affect the present technique for crystals having free carrier concentration above 10^{16}/cm^3 such as were used above. It was observed that for crystals with much lower free carrier concentrations, about 10^{14}/cm^3, the field effect *is* dominated by deep traps. In this case the above method of obtaining field strength from data on free carrier concentration is no longer valid.

DIELECTRIC BREAKDOWN STRENGTH

The above method was used to determine the field strength at which dielectric breakdown occurs

in CdS crystals. The crystals used were thick enough that dielectric breakdown occurred before the space charge region was thick enough to fill the crystal. As above, the blocking electrode surrounded a section of the crystal with the result that the high field was directed inward at all points on the surface. Only one ohmic contact was used and breakdown was detected by measuring current through the blocking electrode as a function of applied voltage. Very small currents flow till just below the breakdown voltage where the current begins to rise rapidly with voltage. A typical pre-breakdown current is shown in Fig. 4. It is the maximum field at the surface which is shown here and which is used to specify breakdown field strengths. Breakdown is arbitrarily defined in this discussion as the field at which the current is equal to 1 μA. Breakdown field strengths were measured for many different crystals of CdS and range from about 1 to $2{\cdot}5 \times 10^6$ V/cm as shown in Fig. 5.

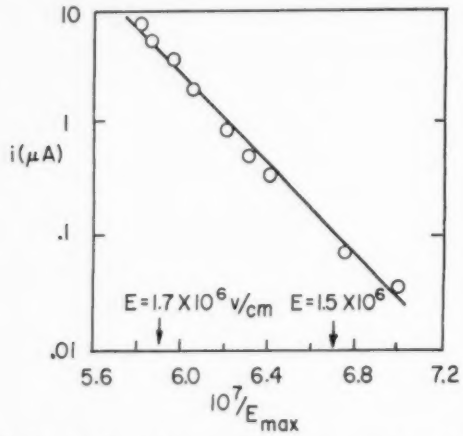

FIG. 4. Pre-breakdown current vs. reciprocal field for a CdS crystal. The maximum field at the surface is used here.

It was thought that the breakdown might be due to impact ionization and extensive experiments were carried out in an effort to observe multiplication of light-injected carriers as found in silicon and germanium.[6] Details will be reported elsewhere,[7] but the result was that no evidence could be obtained to show that injected carriers are multiplied during the breakdown process. This result, along with other experiments done during this study, leads to the conclusion that the breakdown, under these conditions, is due to internal field emission from valence band to conduction band. The following evidence for this conclusion was obtained.

(1). No multiplication of light-injected carriers takes place during breakdown.

(2). Absolute magnitudes of the breakdown field strengths are in approximate agreement with theoretical estimates based on the internal field emission mechanism.[5]

(3). Pre-breakdown currents follow the exponential dependence on field predicted by the internal field emission theory and the slope of the appropriate line is in approximate agreement with theory.[7]

(4). For fields somewhat below those necessary to give internal field emission there should be a shift of the optical absorption edge.

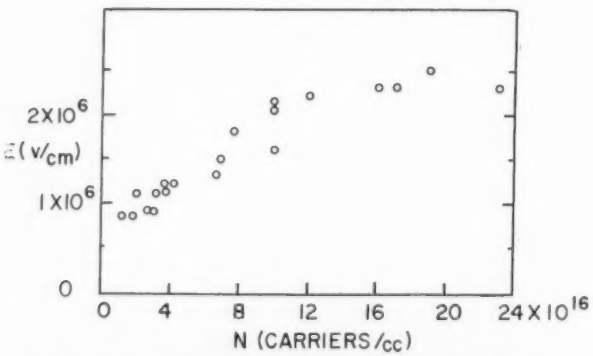

FIG. 5. Breakdown field strengths for several different crystals having different carrier concentrations.

Vol. 2
1961

Both effects may be analyzed with very similar theory.[8] Fig. 6 shows an example of the shift of the absorption edge as a function of field up to the breakdown field. Shift of the band edge (Franz effect) and internal field emission are closely related phenomena and the occurrence of the shift indicates that the fields present are not far below those required for internal field emission.

The trend of breakdown field strength with carrier concentration shown in Fig. 5 appears to be due to the fact that thicker, high field regions are present at lower carrier concentrations and tunneling occurs in a greater volume of the crystal. Since breakdown is here specified by the field required to produce a fixed value of current, this leads to lower apparent breakdown strengths in crystals with lower carrier concentrations.

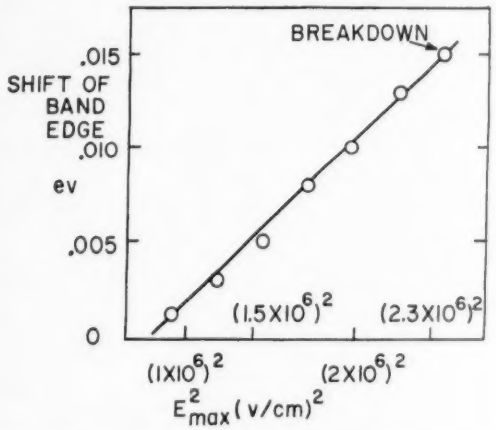

FIG. 6. Shift of the optical band edge of a CdS crystal plotted against the square of the maximum applied field.

CONCLUSIONS

Field effect measurements show that high electric fields of known magnitude may be produced by using conducting CdS crystals and electrolyte blocking contacts. The method is suited to the study of various high field effects and especially to optical effects. Dielectric breakdown field strengths have been measured in several crystals and range from 1×10^6 to $2{\cdot}5 \times 10^6$ V/cm. From a variety of evidence it appears that breakdown occurs by internal field emission.

Acknowledgement—The author is indebted to A. ROSE for many helpful suggestions and discussions.

REFERENCES

1. WILLIAMS R., *J. Chem. Phys.* **32,** 1505 (1960).
2. WILLIAMS R., *Phys. Rev.* **117,** 1487 (1960).
3. HENISCH H. K., *Rectifying Semiconductor Contacts*, p. 189. Oxford University Press, London (1957).
4. KROGER F. A., VINK H. J. and VOLGER J., *Phillips Res. Rep.* **10,** 39 (1955).
5. WILLIAMS R., *Phys. Rev.*, **123,** 1645 (1961).
6. MCKAY K. G. and MCAFEE K. B., *Phys. Rev.* **91,** 1079 (1953).
7. WILLIAMS R., *Phys. Rev.*, Feb. 1 (1962).
8. FRANZ W., *Z. Naturf.* **13a,** 484 (1958).
9. FRANZ W., *Handbuch der Physik*, Bd. 17, s. 155–263. Springer-Verlag, Berlin (1956).

BLANK
PAGE

Vol. 22
1961

J. Phys. Chem. Solids Pergamon Press 1961. Vol. 22, pp. 135–140. Printed in Great Britain.

ZUR SÄTTIGUNG VON PHOTOSTRÖMEN IN STARKEN ELEKTRISCHEN FELDERN

F. STÖCKMANN

Institut für angewandte Physik der Technischen Hochschule, Karlsruhe, Deutschland

Zusammenfassung — Durch Verallgemeinerung früherer Überlegungen wird gezeigt, dass sich im Grenzfall schwacher Anregung alle Photoleiter in vier Gruppen einteilen lassen, deren Sättigungsströme in starken elektrischen Feldern sich charakteristisch unterscheiden. Dadurch kann u.a. erklärt werden, warum bei verschiedenartigen Anwendungen von Photoleitern die maximale Ausbeute von Photoströmen ganz verschieden und geradezu typisch für die betreffende Awendung ist. Diese Einteilung der Photoleiter ist gleichwertig mit einer Einteilung aller Halbleiter in vier verschiedene Gruppen im Hinblick auf die Injektion von Ladungsträgern. Zu jeder Gruppe werden die Bedingungen dafür und allgemeine Ausdrücke für die zur Sättigung erforderliche Feldstärke und für die Grösse der Sättigungsströme angegeben, die in jedem Einzelfalle leicht ausgewertet werden können, und zwar sowohl bei stationären als auch bei nicht stationären Photoströmen. Bei Wechselanregung hängt z.B. die Sättigung der Photoströme von der Anregungsfrequenz ab.

Abstract—By generalization of earlier work it is demonstrated that in the limiting case of weak excitation all photoconductors may be divided into four groups, whose saturation currents have characteristic differences for strong electric fields. It can be explained, for instance, why for various applications of photoconductors the maximum yield of photocurrents is different and characteristic of the particular application. This grouping of the photoconductors is equivalent to the division of all semiconductors into four different categories with respect to charge carrier injection. For each group, the conditions and general expressions for the fields required for saturation and the magnitude of saturation currents are given. They can be evaluated easily in each case for steady as well as time dependent photocurrents. For the case of sinusoidal excitation, for example, the saturation of the photocurrents depends on the frequency.

1. FRÜHERE ERGEBNISSE UND FRAGESTELLUNG

In der Photoconductivity-Konferenz in Atlantic City wurde zum ersten Male gezeigt,[1] dass es vier Gruppen von Photoleitern gibt, die sich durch das Verhalten der Photoströme bei hohen Feldstärken, nämlich durch die Grösse der Sättigungsströme und die zur Sättigung erforderlichen Feldstärken charakteristisch unterscheiden. Der Beweis dafür folgt direkt aus den Kontinuitätsgleichungen für freie Elektronen und freie Defektelektronen zusammen mit der Poisson–Gleichung. Die Integrale dieses Gleichungssystems enthalten genau vier Grenzfälle, und diese entsprechen den vier Gruppen.

Die vier Gruppen lassen sich am einfachsten durch Bedingungen zwischen vier Grössen mit der Bedeutung einer Zeit charakterisieren. Zwei davon kennzeichnen den Photoleiter selbst, nämlich seine dielektrische Relaxationszeit $\tau_R = \epsilon_0\epsilon/\sigma$ (ϵ = Dielektrizitätskonstante, $\epsilon_0 = 8{,}89 \cdot 10^{-14}$ A sec/V cm, σ = elektrische Leitfähigkeit) und die Lebensdauer τ der durch die optische Anregung erzeugten freien Ladungsträger. Die beiden anderen Zeiten sind die Laufzeiten $T_{\text{maj.}}$ und $T_{\text{min.}}$ der Majoritäts- und der freien Minoritätsträger durch den Photoleiter von der einen zur anderen Elektrode. Sie hängen ausser von der Beweglichkeit μ der betreffenden Trägersorte auch von speziellen Versuchsbedingungen ab, nämlich vom Elektrodenabstand L und der angelegten Spannung U. So ist z.B. bei homogenem Potentialverlauf

$$T_{\text{maj.}} = L/\mu_{\text{maj.}} \cdot E = L^2/\mu_{\text{maj.}} \cdot U$$

($E = U/L$ = elektrische Feldstärke). Die Bedingungen für die Gruppeneinteilung sind nun einfach Grössenordnungsbeziehungen zwischen diesen vier Zeiten, wobei $T_{\text{maj.}}$ mit τ_R und $T_{\text{min.}}$ mit τ in Beziehung gesetzt wird. Eine Unterscheidung zwischen Majoritäts- und Minoritätsträgern ist nur bei Störleitern sinnvoll ($p_o \gg n_o$ oder $n_o \gg p_o$); bei Eigenleitern ($p_o \approx n_o$)* gilt darum eine andere Beziehung, die in den 2×2 Zeiten symmetrisch ist. Diese Gruppen und ihre wichtigsten Kennzeichen sind in der Tabelle 1 zusammengestellt.

Wegen mathematischer Schwierigkeiten konnten die Rechnungen nur unter einschränkenden Voraussetzungen durchgesetzt werden, nämlich nur für Photoleiter ohne jegliche Störstellen. Ferner wurden nur stationäre Photoströme diskutiert, und zwar nur im Grenzfall schwacher Bestrahlung. In der Untersuchung, über die hier berichtet wird, konnten diese Einschränkungen beseitigt werden — bis auf die letzte, die weiterhin erforderlich ist, um das Gleichungssystem linearisieren zu können. Es ergibt sich, dass die Gruppeneinteilung mit ihren wesentlichen Kennzeichen auch für Photoleiter mit Störstellen und für nichtstationäre Photoströme gilt. Die Bedingungen und Merkmale erhält man aus denen in Tabelle 1 durch einfache, physikalisch unmittelbar anschauliche Substitutionen.

2. ZUSAMMENHANG ZWISCHEN DER SÄTTIGUNG VON PHOTOSTRÖMEN UND DER INJEKTION VON LADUNGSTRÄGERN

Zuvor sei jedoch noch auf eine andere Konsequenz der früheren Überlegungen hingewiesen, die mit den entsprechenden Substitutionen ebenfalls bei den im folgenden diskutierten allgemeinen Bedingungen gültig bleiben. Photoströme werden dann gesättigt, wenn die durch eine Bestrahlung erzeugte inhomogene Konzentrationsverteilung von Ladungsträgern durch das angelegte elektrische Feld aus dem Photoleiter herausgezogen werden kann. Bei der gleichen Feldstärke wird aber auch jede andere ungleichmässige Ladungsverteilung über den ganzen Leiter hinweg "verweht", gleichgültig, welche Prozesse die Ursache für solche inhomogenen Verteilungen sind. Das ist eine direkte Folge aus den Kontinuitätsgleichungen, denn sie unterscheiden ja nicht zwischen den Mechanismen, durch die eine gegebene Trägerkonzentration erzeugt wird. Das gilt auch für eine inhomogene Konzentrationsverteilung an Kontakten, z.B. für die Gebiete erhöhter Trägerkonzentration vor nachliefernden, sog. "Ohm'schen" Kontakten, die die betreffenden Trägersorten injizieren können. Folglich sind die Bedingungen für die Sättigung von Photoströmen identisch mit denen für eine Injektion von Ladungsträgern, bei der die injizierten Träger ohne nennenswerte Verluste durch Rekombination oder Raumladungsausgleich bis zur Gegenelektrode gelangen. Die Einteilung der Photoleiter in vier Gruppen ist also äquivalent mit einer Einteilung aller Halbleiter in vier Gruppen im Hinblick auf die Injektion von Ladungsträgern (und natürlich auch im Hinblick auf eine Extraktion bei sperrenden Kontakten für die betreffende Trägerart). Die Bedingungen dafür sind in beiden Fällen dieselben, darum ist bereits in Tabelle 1 angegeben worden, welche Trägersorten bei der betreffenden Bedingung injiziert werden können. Dem Verstärkungsfaktor der Photoströme entspricht in diesem Falle (allerdings mit gewissen Einschränkungen) die maximale Stromverstärkung, die durch eine Trägerinjektion erreicht werden kann. Dieser allgemeine Zusammenhang zwischen der Sättigung von Photoströmen und der Injektion von Ladungsträgern dürfte die Erklärung für die schon alte und immer wieder bestätigte Erfahrung sein, dass eine Sättigung von Photoströmen bei derselben Feldstärke einsetzt, bei der unter sonst gleichen Versuchsbedingungen die Dunkelstromkennlinie vom Ohm'schen Gesetz abzuweichen beginnt — nur mit "neutralen" Kontakten erhält man auch bei hohen Feldstärken einen Ohm'schen Dunkelstrom.

Die maximale Ausbeute bei der Anwendung von Photoleitern hängt bekanntlich ganz auffällig davon ab, für welchen Zweck man den Photoleiter benutzt. Die Gruppeneinteilung erklärt auch diese scheinbar widersinnige Tatsache. Ein Photoleiter, der für eine bestimmte Anwendung optimal geeignet ist, muss recht einschränkende Forderungen erfüllen. Dadurch wird im allgemeinen, meistens zwar nur indirekt, eine einzige der vier Gruppen in Tabelle 1 ausgezeichnet, deren Bedingungen der Photoleiter für diesen speziellen

* p_o, n_o = Gleichgewichtskonzentrationen der Defektelektronen und der Elektronen im unbelichteten Photoleiter.

Vol. 2
1961

Tabelle 1. *Zur Gruppeneinteilung der Photoleiter*

Bedingungen für Sättigungsströme	Verstärkungsfaktor f = Gain*	Injektion von Ladungsträgern	Beispiele
Störleiter $T_{maj.} \gg \tau_R$ $T_{min.} \gg \tau$	keine Sättigung	keine Injektion	—
$T_{maj.} \gg \tau_R$ $T_{min.} \ll \tau$	$\dfrac{\mu_{maj.}+\mu_{min.}}{\mu_{min.}}$	nur Minoritätsträger	Ge u.a.
$T_{maj.} \ll \tau_R$ $T_{min.} \gg \tau$	τ/τ_R	nur Majoritätsträger	Se (?)
$T_{maj.} \ll \tau_R$ $T_{min.} \ll \tau$	2	beide Trägersorten	Isolatoren†
Eigenleiter $T_P \cdot T_n \approx \tau_R \cdot \tau$	$\approx \sqrt{(\tau/\tau_R)}$	beide Trägersorten	CdS (?)

* f = gesättigter Photostrom $J_{Sätt}$/Primärstrom = $J_{Sätt}/\frac{1}{2}$ GeL.
† Sowie *alle* Photoleiter bei grosser Feldstärke und kleinem L.

Zweck genügen muss. Damit ist auch die maximale Ausbeute bestimmt.

3. STATIONÄRE SÄTTIGUNGSSTRÖME IN EINEM PHOTOLEITER MIT STÖRSTELLEN

Die früher nur für einen idealisierten Photoleiter ohne Störstellen durchgeführten Rechnungen wurden jetzt für einen Photoleiter wiederholt, der die drei für jeden Photoleiter charakteristischen Gruppen von Störstellen enthält: Donatoren D, Akzeptoren A und Rekombinationszentren R. Das Energieschema solch eines Photoleiters und die in der Rechnung berücksichtigten Elektronenübergänge sind in Abb. 1 dargestellt. Für dieses Modell erhält man in bekannter Weise das Gleichungssystem:

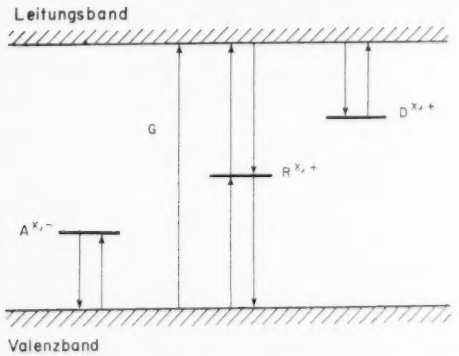

ABB. 1. Energieschema des Modells, das in der vorliegenden Arbeit diskutiert wird. In der Rechnung sind nur die eingezeichneten Elektronenübergänge berücksichtigt worden. Die speziellen Angaben über die Ladung der Störstellen (mit bzw. ohne Elektron) sind für alle Ergebnisse unwesentlich; man kann die Gleichungen aber übersichtlicher schreiben, wenn man sich auf einen bestimmten Fall festlegt.

$$\operatorname{div} i_p = \operatorname{div}(e\mu_p pE - eD_p \operatorname{grad} p) \tag{1}$$
$$= e\left(-\frac{\partial p}{\partial t} + G - r_p pR^* + \gamma_p R^+ - r_A pA^- + \gamma_A A^*\right)$$

$$\operatorname{div} i_n = \operatorname{div}(e\mu_n nE + eD_n \operatorname{grad} n) \tag{2}$$
$$= -e\left(-\frac{\partial n}{\partial t} + G - r_n nR^+ + \gamma_n R^* - r_D nD^+ + \gamma_D D^*\right)$$

$$\frac{\partial D^+}{\partial t} = -r_D nD^+ + \gamma_D D^* \tag{3}$$

$$\frac{\partial A^-}{\partial t} = -r_A pA^- + \gamma_A A^* \tag{4}$$

$$\frac{\partial R^+}{\partial t} = -r_n nR^+ + \gamma_n R^* + r_p pR^* - \gamma_p R^+ \tag{5}$$

$$\operatorname{div} E = \frac{e}{\epsilon\epsilon_0}\Big[(p-p_0)+(D^+-D_0^+)+(R_-^+R_0^+) - (n-n_0)-(A^--A_0^-)\Big]. \qquad (6)$$

Die Symbole der Störstellen bedeuten hier die betreffende Konzentration, der Index 0 bezeichnet die Gleichgewichtskonzentrationen, ein Stern* bezeichnet den neutralen Ladungszustand. G ist die Erzeugungsrate freier Träger infolge der Bestrahlung, die Grössen r und γ sind die Rekombinationskoeffizienten und die Koeffizienten für die gegenläufigen Prozesse, die thermische Wiederabspaltung. Alle übrigen Symbole haben die übliche Bedeutung.

Aus dem System Gleichung (1) bis Gleichung (6) erhält man das früher diskutierte, indem man alle Störstellenkonzentrationen gegen Null gehen lässt und, damit trotzdem eine Rekombination möglich ist, in Gleichung (1) und Gleichung (2) einen Term $r\,(pn-p_0n_0)$ für eine direkte Rekombination neu einführt.

Es erscheint völlig aussichtslos, die Lösungen dieses Systems in voller Allgemeinheit zu erhalten und zu diskutieren. Darum wurde als wesentliche Voraussetzung beibehalten, dass die Anregung G schwach ist,* dann kann das System linearisiert und vollständig integriert werden. Diese Voraussetzung ist zweifellos immer noch recht einschneidend, denn bei vielen wichtigen Photoleitern sind die Photoströme tatsächlich gross gegen die Dunkelströme. Andererseits kann man aber nur so wirklich alle Möglichkeiten untersuchen, wenigstens für einen Grenzfall, der bei jedem Photoleiter realisiert werden kann, nämlich $G \to 0$. Die weiteren Voraussetzungen der Rechnung haben auf die wesentlichen Merkmale der Gruppeneinteilungen keinen Einfluss: eindimensionaler Fall, d.h. eine Ortsabhängigkeit nur in der x-Richtung; homogene Anregung und Dotierung, d.h. G und alle Gleichgewichtskonzentrationen sind unabhängig von x ; Gültigkeit der Einsteinschen Beziehung $D = \mu \cdot kT/e$ mit Beweglichkeiten μ, die nicht von der Feldstärke abhängen.

Unter den genannten Voraussetzungen kann man für den stationären Fall (alle $\partial \ldots /\partial t = 0$) die von x abhängigen Störstellenkonzentrationen mit Hilfe der Gleichungen (3), (4) und (5) leicht aus dem linearisierten Gleichungssystem eliminieren. Die übrigen 3 Gleichungen, nämlich die Kontinuitätsgleichungen (1) und (2) sowie die Poisson-Gleichung (6) erhalten dann eine Form, die durch die einfachen Substitutionen von Tabelle 2 aus dem früher diskutierten System hervorgeht. Infolgedessen gelten mit diesen Substitutionen auch alle früheren Ergebnisse, insbesondere bleibt die Gruppeneinteilung der Halb- und Photoleiter mit all ihren wesentlichen Merkmalen unverändert gültig. Die Bedingungen für die Sättigung der Photoströme und die Verstärkungsfaktoren erhält man ohne weitere Rechnung, wenn man auch in Tabelle 1 die Substitutionen nach Tabelle 2 ausführt.

Die drei Faktoren a, b und ρ_0, die bei den Substitutionen benötigt werden, haben eine einfache physikalische Bedeutung. Wenn Δp die Konzentrationsänderung der freien Defektelektronen infolge der Anregung bedeutet und Δp_t die Konzentrationsänderung der in Akzeptoren und Rekombinationszentren gebundenen Defektelektronen, dann ist $a = (\Delta p + \Delta p_t)/\Delta p$, a ist also die gesamte Konzentrationsänderung im Verhältnis zur Änderung der Konzentration der freien Träger, b bedeutet das entsprechende Verhältnis für Elektronen, und ρ_0 ist ein effektiver Rekombinationskoeffizient, der an die Stelle des Koeffizienten r für die direkte Rekombination tritt, wenn die Rekombination tatsächlich über Rekombinationszentren verläuft (bis auf die Schreibweise ist ρ_0 identisch mit dem entsprechenden Koeffizienten beim Rekombinationsmodell von Shockley–Read, denn in Abb. 1 ist ja derselbe Rekombinationsmechanismus angenommen worden).

Da durch die Substitutionen $p_0 \cdot a$ statt p_0, usw. die Konzentrationen der freien Träger durch die gesamten Konzentrationen (d.h. freie und gebundene) ersetzt werden, sind die Substitutionen für die Beweglichkeiten μ, die Diffusionskonstanten D, die Laufzeiten T und die Relaxationszeit τ_R unmittelbar plausibel. Die Lebensdauer τ geht in einen komplizierteren Ausdruck τ_0 über, der aber auch jetzt noch die Bedeutung einer Lebenszeitdauer hat. Es ist nämlich $\Delta p \cdot a = \Delta n \cdot b = G \cdot \tau_0$ (falls alle $\partial \ldots /\partial x = 0$ sind). Ferner ist τ_0, wie früher die Zeit τ, wieder die Zeitkonstante der Photoströme bei zeitlich veränderlichen

* Diese Bedingung verlangt nicht, dass sich z.B. die Konzentration der Minoritätsträger nur um einen Betrag ändern darf, der klein gegen ihre Gleichgewichtskonzentration ist. Dann hätten alle Folgerungen nur einen sehr begrenzten Wert. Tatsächlich muss gefordert werden

$\Delta p = p - p_0 \ll p_0 + n_0$ und $\Delta n = n - n_0 \ll p_0 + n_0$.

Vol. 2 1961

Tabelle 2. Substitutionen, die die Werte von Tabelle 1 auf das Modell in Abb. 1 übertragen

Statt ist zu setzen	p_0 $p_0 \cdot a$	n_0 $n_0 \cdot b$	Δp $\Delta p \cdot a$	Δn $\Delta n \cdot b$	μ_p μ_p/a	μ_n μ_n/b
Statt ist zu setzen	τ_R τ_R	$\tau = 1/r(p_0+n_0)$ $\tau_0 = a \cdot b/\rho_0(p_0 \cdot a+n_0 \cdot b)$			T_p $T_p \cdot a$	T_n $T_n \cdot b$

$$\text{mit} \quad a = 1+\frac{A_0^* A_0^-}{p_0(A_0^*+A_0^-)}+\frac{\rho_0 R_0^*}{r_n(R_0^*+R_0^+)} = 1+a_1+a_2$$

$$b = 1+\frac{D_0^* D_0^+}{n_0(D_0^*+D_0^+)}+\frac{\rho_0 R_0^+}{r_p(R_0^*+R_0^+)} = 1+b_1+b_2$$

$$\rho_0 = \frac{(r_p r_n R_0^+ R_0^*)}{(r_p p_0 R_0^*+r_n n_0 R_0^+)}.$$

Vorgängen, allerdings jetzt nur noch, wenn sie quasistationär verlaufen.

4. ZEITLICH VERÄNDERLICHE PHOTOSTRÖME

Bei einer zeitlich veränderlichen Anregungsfunktion $G = G(t)$ in Gleichung (1) ist es zweckmässig, $G(t)$ in seine Fourierkomponenten zu zerlegen:

$$G(t) = \int_{-\infty}^{+\infty} G_\omega \, e^{i\omega t} \, d\omega,$$

das Gleichungssystem für jede Kompenente G_ω zu integrieren und die einzelnen Teillösungen zu addieren. Für ein lineares Gleichungssystem ist das bekanntlich ein völlig legales Verfahren, und es vermittelt den besten Überblick über die gesamte Lösungsmannigfaltigkeit.

Durch den Lösungsansatz

$$\Delta p_\omega(x,t) = \Delta p_\omega(x) \cdot e^{i\omega t}$$

[und entsprechend für alle anderen orts- und zeitabhängigen Grössen in Gleichung (1) bis Gleichung (6)] werden alle $\partial \ldots / \partial t$ ersetzt durch $i\omega \cdot \ldots$, und dadurch wird die Zeitabhängigkeit vorläufig ganz eliminiert. Das Gleichungssystem kann danach also genau so diskutiert werden wie das frühere zeitunabhängige System.

Für einen Photoleiter *ohne* Störstellen ist das Ergebnis recht einfach. Die Differentialgleichung für Δp_ω bzw. Δn_ω, die durch Eliminieren von ΔE_ω und Δn_ω (bzw. Δp_ω) aus Gleichungen (1), (2) und (6) folgt, unterscheidet sich von der früheren für Δp bzw. Δn wieder nur durch einfache Substitutionen*:

τ geht über in $\tau/(1+i\omega\tau)$ und τ_R geht über in $\tau_R/(1+i\omega\tau_R)$.

Mit diesen Substitutionen bleiben folglich auch alle Konsequenzen richtig, insbesondere also die Gruppeneinteilung und ihre Merkmale in Tabelle 1. Es sei jedoch darauf hingewiesen, dass infolge dieser Substitutionen sowohl die Bedingungen für die Sättigung der Photoströme als auch die Grösse der Sättigungsströme von der Frequenz ω der Wechselanregung abhängen. Vorläufige experimentelle Ergebnisse scheinen diese Vorhersage zu bestätigen.

τ und τ_R erweisen sich durch diese Substitutionen als Relaxationszeiten, darum wird auch der zeitliche Verlauf der Photoströme allein durch τ und τ_R bestimmt.

Für einen Photoleiter *mit* Störstellen nach Abb. 1 ergibt sich, dass man die vorhergehenden Ergebnisse miteinander kombinieren muss. Einerseits müssen in Tabelle 1 τ und τ_R durch die obigen Relaxationsterme ersetzt werden,

* Abgesehen von zwei Termen, die bei praktisch allen Photoleitern immer vernachlässigt werden dürfen.

andererseits müssen auch die Substitutionen nach Tabelle 2 ausgeführt werden, jedoch mit frequenzabhängigen Faktoren a_ω, b_ω und ρ_ω:

$$a_\omega = 1+\frac{a_1}{1+i\omega\tau_a}+\frac{a_2}{1+i\omega\tau_\rho}$$

$$b_\omega = 1+\frac{b_1}{1+i\omega\tau_b}+\frac{b_2}{1+i\omega\tau_\rho} \qquad (7)$$

$$\rho_\omega = \rho_0/(1+i\omega\tau_\rho)$$

mit den Kürzungen a_1, a_2, b_1, b_2 und ρ_0 wie in Tabelle 2, sowie

$$\tau_a = \frac{A_o^*}{r_p p_0(A_o^*+A_o^-)},\ \tau_b = \frac{D_o^*}{r_n n_0(D_o^*+D_o^-)},$$

$$\tau_\rho = \frac{\rho_0}{r_p r_n(R_o^*+R_o^+)}.$$

Man kann so auch diesen allgemeinen Fall auf den früher behandelten Spezialfall zurückführen.

Im einzelnen sind diese Umformungen allerdings zum Teil recht unübersichtlich. Z.B. führt die Substitution von τ durch $\tau_\omega/(1+i\omega\tau_\omega)$ mit $\tau_\omega = a_\omega b_\omega/\rho_\omega(p_o \cdot a_\omega + n_o \cdot b_\omega)$ nach Tabelle 2 und a_ω, b_ω und ρ_ω aus Gleichung (7) nach den üblichen Umformungen auf eine Summe von 5 Relaxationstermen $\tau_j/(1+i\omega\tau_j)$. Die Zeiten τ_j bestimmen also auch den zeitlichen Ablauf der elektronischen Prozesse im Photoleiter und der Photoströme. Sie hängen in komplizierter Weise von den Konzentrationen aller Störstellen im Photoleiter ab, man kann sie als Eigenwerte der Koeffizientenmatrix des Systems Gleichungen (1)–(6) berechnen. Mit den anderen bisher erwähnten Grössen von der Art einer Zeit stimmen sie nur in Sonderfällen überein. Diese Fragen sind jedoch für die Sättigung der Photoströme, die das Hauptthema der vorliegenden Arbeit bildet, nur von sekundärer Bedeutung und sollen darum hier nicht weiter diskutiert werden. Wegen genauerer Einzelheiten hierzu und auch zu den übrigen Fragen der vorliegenden Arbeit wird auf eine ausführlichere Veröffentlichung verwiesen, die in *physica status solidi* erscheinen wird.

LITERATUR

1. STÖCKMANN F., Photoconductivity Conference, p. 269. John Wiley, New York (1956); *Z. Phys.* **147,** 544 (1957).

Vol. 2
1961

J. Phys. Chem. Solids Pergamon Press 1961. Vol. 22, pp. 141–147. Printed in Great Britain.

THE RECOMBINATION OF HOT CARRIERS IN GERMANIUM—EXPERIMENTAL*

J. ZUCKER† and E. M. CONWELL

General Telephone and Electronics Laboratories, Inc., Bayside, N.Y.

Abstract—The recombination of excess hot carriers in germanium has been investigated by measuring the change in photoconductivity caused by exciting samples with 2·85 kMc microwaves up to peak fields of 10^4 V/cm. Microwave rather than d.c. pulse excitation was used, and other precautions taken, to avoid sweep-out of excess carriers. Samples whose lifetimes were determined by surface recombination and by recombination at copper impurities in the bulk were investigated in this manner. In all these samples a decreased photoconductivity was observed immediately following the microwave pulse, indicating enhanced recombination in the high field. Comparison of the experimental results with theory indicates that the cross section for electron capture of singly charged copper centers decreases with increasing speed of the carriers.

INTRODUCTION

THE application of pulses of high electric field to a germanium sample, as is done in the usual hot carrier experiment,[1] increases the average energy of the carriers during the pulse while affecting the lattice temperature very little. This provides a means for measuring the dependence of recombination rate of excess carriers on carrier energy, separating it from other dependences that change with temperature.[2] To use this means effectively, changes in carrier concentration with field other than those due to changed energy of the carriers must be eliminated. One such effect is sweepout of excess carriers at the contacts.[3] To avoid this, high-intensity microwave pulses were used for excitation rather than d.c. pulses. The frequency used, 2·85 kMc, was sufficiently low so that the velocity distribution of the carriers could follow the field.[4]

EXPERIMENTAL PROCEDURE

To determine the effect on recombination of changing the carrier energy in a given sample, the procedure used was to set up a steady photocurrent in the sample, and then measure the change in this current caused by applying a high-intensity microwave pulse. The experimental setup used is shown in Fig. 1. The sample was a 5 mm diameter single crystal cylinder with a wire 2·5 mm long and 0·25 mm in diameter ground at one end. The wire was inserted into a wave-guide sample holder, as shown in the figure, where it could be subjected to peak fields as high as 12,000 V/cm. Because the dimensions of the wire are so small that the contribution of its current to the field can be neglected, the field in the wire can be determined simply from a knowledge of the power density of the travelling waves at the location of the wire.[4] To obtain this, the average power transmitted down the wave guide is measured by means of a bridge in conjunction with a coaxial detector.[4] (See Fig. 2.)

In most of the work, the photocurrent was produced by a small tungsten filament lamp, or by light shone down a quartz light pipe inserted into the sample holder as shown in Fig. 1. More uniform illumination, obtained by having a second light source on the other side of the sample, was used for some of the measurements, but this did not make much of a difference in the results. To measure photoconductivity a small variable d.c. sweep field was supplied by a 1·5 V battery across a 1000 Ω carbon potentiometer. Oscillograms of the photocurrent through the sample were obtained by monitoring the voltage across a small resistor in

* This work was partly supported by the U.S. Signal Corps.

† A portion of this paper is based on the thesis work submitted to the Department of Physics of New York University in partial fulfilment of the requirements for the Ph.D. degree.

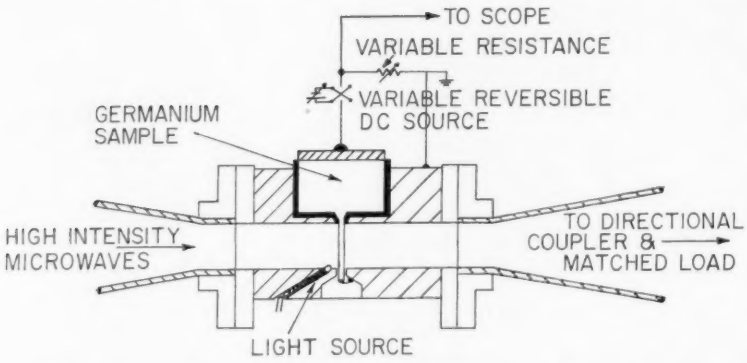

FIG. 1. Experimental setups for investigating recombination of hot carriers.

series with the sample. The block diagram of the apparatus is shown in Fig. 2, and discussed in more detail in reference 4.

The experimental procedure is best described with the aid of Fig. 3, which shows schematically the sequence of changes in conductivity. At the beginning of the time scale, the sample is unilluminated and conductivity has its thermal equilibrium value σ_{th}. Upon illumination, the conductivity increases at a rate depending on τ_{th}, the zero-field lifetime. After the photoconductivity has reached a steady value $\sigma_{th}+\delta\sigma_L$, the microwave field is applied for a time Δ, three μsec in these experiments. This causes the conductivity to drop sharply because of the decrease in carrier mobility.[1] If the recombination is energy-dependent, there will be a further and gradual change in σ during the course of the microwave pulse due to the change in carrier concentration. After the microwave field is removed, the energy distribution and mobilities return to their thermal equilibrium values in a very short time, estimated as less than 10^{-11} sec, and the conductivity returns exponentially to the value $\sigma_{th}+\delta\sigma_L$ with time constant τ_{th}, which is several microseconds or more. Thus the difference between the conduc-

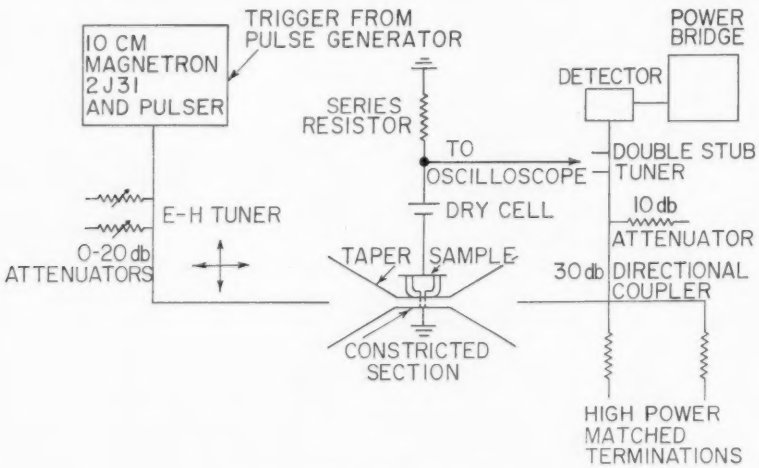

FIG. 2. Block diagram of apparatus.

Vol. 22
1961

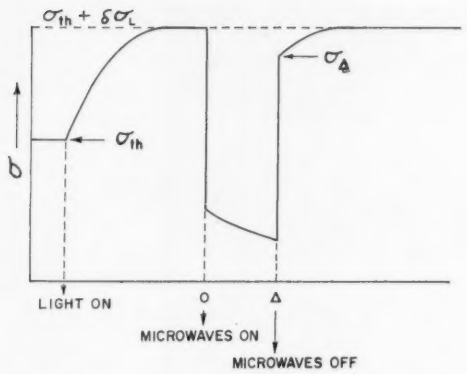

FIG. 3. Schematic representation of the changes in conductivity.

tivity σ_Δ measured directly, i.e. within $\frac{1}{2}$ microsecond, after the removal of the microwave pulse and $\sigma_{th}+\delta\sigma_L$ reflects the change in carrier concentration produced by the microwave field. Since this change clearly depends on the magnitude of the initial photoconductivity, it has been found convenient in practice to represent the effect of the field by the ratio

$$[\sigma_\Delta-(\sigma_{th}+\delta\sigma_L)]/\delta\sigma_L$$

to be denoted by m. If the trap concentration in the sample is small compared with the equilibrium majority carrier concentration, deviations of both electrons and holes from thermal equilibrium values must be equal, and the ratio m equals the ratio of the decrease (or increase) in concentration of either type of carrier produced by the microwaves to the increase produced by light.

As noted earlier, in order to interpret the changes of carrier concentration with field as due to changes in carrier energy it is necessary to eliminate injection or sweepout of carriers by d.c. sweeping field. Injection from the contacts was eliminated by using samples with one massive end, and arranging the polarity of the d.c. field so that minority carriers enter at the massive end. Sweepout of the photo-injected carriers was avoided by limiting the d.c. field $E_{\text{d.c.}}$ to values for which the range of the carriers, $\mu E_{\text{d.c.}}\tau_{th}$, where μ is the minority carrier mobility, is less than the wire length. As will be shown in the next Section, this limited the sweeping field to quite small values.

Measurements of the effect of microwave fields on the dark currents were also made with a view to checking some of the above considerations, and/or finding effects of the field on the dark carrier-concentration.[5]

Large increases in dark current after application of high microwave fields were actually found in some samples, the effect being as much as 100 per cent in one of them. Further investigation of these increases, however, showed that they occur in samples with marked bulk inhomogeneity, being the larger the more inhomogeneous the sample. Also, a great enhancement of the effect was observed in one sample after surface damage, in the form of a track, had occurred as a result of electrical breakdown. Thus, these large increases in dark current appear to be due to injection during the microwave pulse from surface or bulk inhomogeneities, and photoconductivity data were not taken on samples that showed sizeable changes in dark current after application of the microwaves.

Measurements of the type described were made on n- and p-type germanium samples with lifetimes determined by surface recombination, and also on samples with lifetimes determined by recombination at intentionally introduced copper centers. Samples of the former type included some with small surface recombination velocity s and some with large s. The small s-surfaces were produced by etching in CP4 for one minute, and the large s-surfaces were produced by etching in $HF–HNO_3$ for 15 sec. The copper doped samples were produced by plating with copper and heating in sealed quartz vials evacuated to 10^{-5} mm Hg. One sample, Cu–1, was made from germanium that was originally 2 Ω/cm n-type and which was converted to 24 Ω/cm p-type by copper diffusion at 630°C. A second sample, Cu–2, was made from a 2 Ω/cm p-type germanium sample into which copper was diffused at 560°C; the resistivity of this sample changed very little.

EXPERIMENTAL RESULTS

A typical oscillogram showing dark currents and photocurrents immediately after a microwave pulse of 6000 peak V/cm is reproduced in Fig. 4. The nearly straight lines represent the dark current, the exponential traces the photocurrent. The data

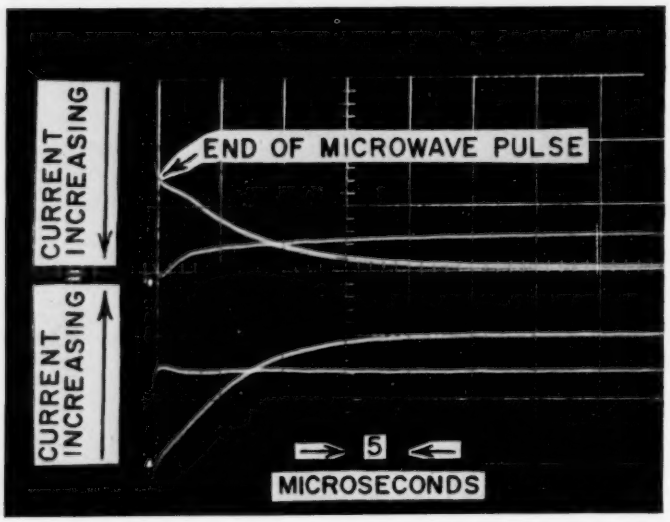

FIG. 4. Oscillogram of photocurrent (exponential traces) and dark current (straight traces) in a 5 Ω/cm *n*-type Ge sample immediately following a microwave pulse of 6000 peak V/cm. The upper pair of traces is for one direction of d.c. field, the lower pair for the opposite direction. The sample had a surface-limited lifetime of 6 μ sec.

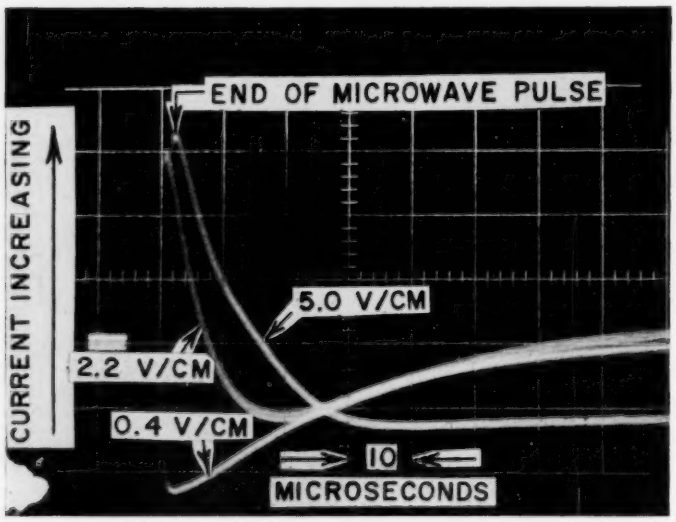

FIG. 5. Oscillogram of photocurrent in an *n*-type Ge sample after a microwave pulse of 7000 peak V/cm at d.c. sweeping fields of 0·4, 2·2 and 5·0 V/cm.

shown were taken for both directions of sweep current to show that the observed effects were not due to changes in contact injection or extraction. If this had been the case, great differences would be expected in the traces obtained in the two current directions due to the asymmetry of the contacts; such differences are not observed. The significant feature of these data is the rise in photocurrent with time after the microwave pulse, indicating that the effect of the high field was to cause a net recombination of carriers. An enhanced recombination rate in high field was, in fact, found for all of the samples measured. A small increase in dark current immediately after the pulse can also be seen on the oscillogram. This is probably due to the effect mentioned in the last Section, injection from sample inhomogeneities. It was also found that the steady-state value of photocurrent shown on the photograph was somewhat higher than the steady-state value before the pulse. This is probably due to a small temperature rise of the sample during the pulse, which increases the zero-field lifetime and therefore the photocurrent. In support of this hypothesis, it was found that after times longer than those shown on the photograph, of the order of 50 msec or more, the photocurrent decayed to its pre-pulse value.

The effects of sweepout by the d.c. field are shown in Fig. 5. To understand this, it must be noted that if the d.c. field is high enough to give noticeable sweepout of excess carriers, this sweepout will decrease during the microwave pulse because the average mobility of the carriers is decreased. Thus if there were no other changes in carrier concentration caused by the microwave field, the decreased sweepout would result in the photocurrent immediately after the microwave pulse being larger than the steady-state value. It would then of course decay to the pre-pulse steady-state value as carriers were swept out again at the normal rate. These effects are illustrated in Fig. 5, which shows photocurrent for an *n*-type germanium sample after a microwave pulse of 7000 peak V/cm at d.c. sweeping fields of 0·4, 2·2 and 5·0 V/cm. At the lowest sweep field only the change in recombination has disturbed the equilibrium carrier concentration and the photocurrent after the microwave pulse increases exponentially with the zero-field lifetime of 30 μsec. For a sweep field of 2·2 V/cm the effect of the change in sweepout is apparent and the photocurrent first decreases before increasing exponentially as did the low sweep-field trace. At a sweep field of 5 V/cm the change in photocurrent is completely determined by the decreased sweepout during the microwave pulse and the photocurrent shows a

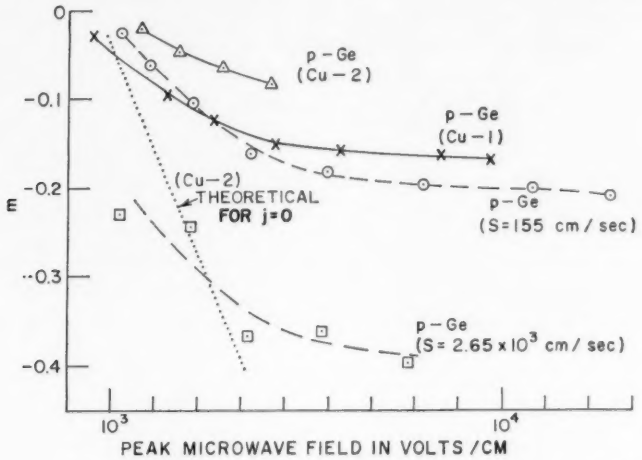

FIG. 6. Plot of the ratio m v. peak microwave field for several Ge samples. The dotted line is the theoretically calculated ratio for constant capture cross section.

monotonic decrease with time. In the interest of maximum sensitivity, experimental data on the various samples were taken at the highest d.c. fields consistent with negligible sweepout.

Data on representative samples are presented in Fig. 6 where m, the ratio of the change in photoconductivity due to the microwave field to the change in conductivity due to light alone, is plotted as a function of peak microwave field. This ratio is always negative, corresponding to the fact, noted earlier, that the microwave field caused a conductivity decrease in all samples observed.

DISCUSSION OF RESULTS

Because of its doping, at room temperature sample Cu–2 should have one level responsible for recombination, the copper level at 0·3 eV.[6, 7] The density of copper centers introduced into the sample by diffusion is about $10^{14}/\text{cm}^3$, while the hole concentration is considerably larger, about $2\times10^{15}/\text{cm}^3$, Since the traps are essentially all empty, the lifetime τ_{th} in such a sample is equal to the reciprocal of the zero-field capture rate for electrons, $1/C_n^0$. The theory developed in the previous paper[2] is applicable to this sample, and the minority carrier concentration at a time t after application of the microwave pulse is given by equation (13) of that paper:

$$n(t) = (n_{th}+g\tau_{th})[\exp(-t\langle 1/\tau\rangle)(1-1/\tau_{th} \times\langle 1/\tau_E\rangle)+1/\tau_{th}\langle 1/\tau_E\rangle],$$

where $\langle 1/\tau_E\rangle$ is the average over a microwave cycle of the high-field capture rate C_n^E. Using this equation for $n(t)$, we obtain for the ratio m defined earlier:

$$m = (1+n_{th}/g\tau_{th})\{[\exp(-\Delta\langle 1/\tau_E\rangle)-1] \times(1-1/\tau_{th}\langle 1/\tau_E\rangle)\}.$$

Since the sample is quite extrinsic, the factor multiplying the angular bracket is practically equal to unity. The quantity $1/\tau_E$ or C_n^E depends, as discussed in the previous paper, on the product of electron speed and capture cross section A_n of the traps. If some particular dependence of A_n on speed is assumed, $\langle 1/\tau_E\rangle$ can be calculated and m is completely determined for a given sample. For A_n proportional to $1/v$, C_n^E is a constant, independent of field, $1/\tau_E = 1/\tau_{th}$, and $m = 0$. The ratio m for Cu–2 has also been calculated for A_n independent of speed, and the result is shown as a dotted line on Fig. 6. The actual m for Cu–2 falls between the horizontal line for A_n proportional to $1/v$ and the dotted line for A_n constant, lying much closer to the former. We conclude that at room temperature the capture cross section for electrons of Cu-centers with a single negative charge decreases as electron speed is increased, almost as rapidly as $1/v$.

Unfortunately it is not possible to give such a quantitative interpretation of the data for any of the other samples. In the other copper-doped sample both electron and hole capture processes would be important in determining the life-time. In the samples with surface recombination predominant there are other complications. The zero-field lifetime was a function of the diffusion rate D of minority carriers as well as of S, and both of these can be expected to change with field. Theoretical calculation has shown that D for electrons in Ge will increase with increasing average speed and therefore with field. The way in which s changes with v will depend on what the surface traps are, and how their capture cross sections change with speed. As in the case of the bulk samples, in order for data such as those shown in Fig. 6 to be useful in obtaining information about the traps it is necessary to achieve a situation where capture of a single type of carrier by a single trap level determines the recombination rate. This was not attempted for the samples investigated here, and is of course much more difficult for the case of surface recombination than for bulk recombination.

Acknowledgement—It is a pleasure to acknowledge our indebtedness to Prof. A. MANY for suggesting this investigation.

REFERENCES

1. RYDER E. J. and SHOCKLEY W., *Phys. Rev.* **81,** 139 (1951).
2. CONWELL E. M. and ZUCKER J., preceding paper in this journal.
3. STOCKMANN F., *Photoconductivity Conference* (edited by BRECKENRIDGE R. G., RUSSELL B. R. and HAHN E. E.) p. 269. John Wiley, New York (1956).

4. ZUCKER J., FOWLER V. J. and CONWELL E. M., *J. Appl. Phys.* in press.
5. CONWELL E. M., *J. Phys. Chem. Solids* **17,** 342 (1961).
6. BURTON J. A. *et al.*, *J. Phys. Chem.* **57,** 853 (1953).
7. ALEXEEVA V. G., KARPOVA I. V. and KALASHNIKOV S. G., *Soviet Physics Solid State* **1,** 475 (1959).
8. FULLER C. S., *et al.*, *Phys. Rev.* **93,** 1182 (1954).

DISCUSSION

M. A. LAMPERT: Although most of the acceptors are singly ionized, in thermal equilibrium in your experiment, a certain fraction of them are neutral. Have you taken care to establish that the recombination is *not* going mainly through the neutral acceptors. Though these are fewer in number, the electron capture cross section presumably favors them—a case of a neutral cross section versus a Coulomb-repulsive one.

E. M. CONWELL: I do not know of any data on the relative size of neutral and repulsive capture cross sections for Cu centers at room temperatures. There are such data, however, for Ni and Au centers in Ge, quoted by Kalashnikov in his Prague Conference paper, and for those cases neutral and repulsive centers are within a factor 10 of each other. This would seem to provide further evidence, i.e. in addition to the voltage dependence we have found, that the Coulomb repulsion is unimportant at room temperature.

BLANK
PAGE

Vol. 2
1961

J. Phys. Chem. Solids Pergamon Press 1961. Vol. 22, pp. 149–153. Printed in Great Britain.

THE RECOMBINATION OF HOT CARRIERS —THEORETICAL*

E. M. CONWELL and J. ZUCKER

General Telephone and Electronics Laboratories Inc., Bayside, N.Y.

Abstract—To determine the dependence of capture cross sections of recombination centers on carrier speed, it is desirable to vary the average speed of the carriers while keeping lattice temperature constant. These conditions, plus the advantage of negligible sweepout of excess carriers by the field, can be obtained in high mobility semiconductors by applying short pulses of high microwave field. The kinetics of recombination in such high fields are investigated along the lines used by SHOCKLEY and READ for low fields. A relation between the change of carrier concentration in microwave field and the speed-dependence of the cross sections is obtained. This relation has been used to determine the speed-dependence of the cross section for electron capture of negatively charged copper centers in germanium, and the result is discussed.

INTRODUCTION

WHEN excess carriers are introduced into a germanium sample by light, injection at contacts, or otherwise, unless the carrier concentration is extremely high recombination is known to take place through a deep-lying energy level in the forbidden energy gap. Such levels can be provided by impurities or other defects at the surface or in the bulk. The process of recombination consists of an electron from the conduction band being captured by an empty recombination center or trap, which then captures a hole. Beyond this, details of the capture process such as how the recombining carriers dispose of their energy are not known. Some of the possible ways for the energy to be given up are by radiation or photon emission, emission of many phonons either simultaneously or in sequential fashion, or to another carrier in the form of kinetic energy. The latter process is likely to be important at high carrier concentration, but we shall not consider such high concentrations here.

The probability per unit time of an empty trap capturing an electron is the product of its capture cross section A_n for electrons and the speed v of the electron. The capture cross section A_p of a filled trap for holes can be defined similarly. The cross sections A_n and A_p can be expected to depend on the speed or energy of the carriers, the nature of this dependence being determined by the nature of the trap potential and the details of the capture process. It would be useful to measure the dependence of cross sections on speed of the carriers in order to help elucidate the nature of the capture process. Since varying the lattice temperature changes phonon abundance as well as carrier speed, measurements of recombination or lifetime as a function of temperature do not give unambiguous information about the speed-dependence. It is clearly desirable to observe recombination under conditions where carrier speed is varied but phonon abundance is not. These conditions are obtained in the typical hot carrier experiment[1] where, by applying high electric fields in short pulses with low repetition rate, the "temperature" of the carriers is substantially raised during the pulse while the lattice temperature is kept constant to within a few degrees.* Such experiments have been done with pulses of d.c. field or with pulses of microwave field. Since high d.c. fields would sweep out excess carriers rapidly, heating the carriers by pulses of microwave field is more suitable for this type of investigation.

* This work was partly supported by the U.S. Signal Corps.

* Although phonons are continually generated by the hot carriers, the phonon lifetime at room temperature is expected to be so small that no significant deviation from the thermal equilibrium distribution results.

Unless A_n and A_p are proportional to $1/v$, which is not likely to be generally true, the capture rates of electrons and holes, and therefore the recombination rate, will be changed by application of high fields. This applies to the case where the traps are at the surface as well as in the bulk. If the traps are at the surface, however, the recombination rate depends also in general on the diffusion rate of excess carriers. The diffusion rate can also be expected to depend on the average speed or "temperature" of the carriers, and this provides an additional source of field-dependence of recombination.

In what follows we shall discuss only the effect of high fields on the bulk recombination rate,† and how to extract from the measurement of the change in recombination the dependence of the cross sections on speed. Experimental observation of the predicted effects and speed-dependence of A_n for one particular case are reported in the following paper.[2]

BULK RECOMBINATION IN HIGH ELECTRIC FIELD

The model of recombination we have been considering, and will now discuss more quantitatively, is that investigated by SHOCKLEY and READ[3] under the (implicit) assumption of low electric fields. Recombination is assumed to occur through a single set of trap levels at energy ϵ_t in the forbidden gap. Actually, of course, recombination centers usually have many levels, but by careful choice of sample doping and temperature it is possible to approximate a one-level situation quite well. For simplicity we shall deal with a unit volume of material. The number of empty traps in this volume is the number of traps N_t times the probability that a trap is unoccupied, f_p. The number of conduction electrons in this volume is n. As noted earlier, the probability per unit time of an empty trap capturing an electron with speed v is vA_n. The total number of conduction electrons captured by traps per second is then $\langle vA_n \rangle N_t f_p n$, where the average of vA_n indicated is to be taken over the velocity distribution of the conduction electrons. In low electric fields this velocity distribution is, of course, a Maxwell–Boltzmann distribution at the lattice temperature θ_o. In high electric fields this is no longer the case. To emphasize the fact that the average is to be taken over the velocity distribution at the field E, a subscript E will be written after the average. It is convenient to introduce the notation

$$\langle vA_n \rangle_E N_t \equiv C_n^E \tag{1}$$

The quantity C_n^E is the average probability per unit time that an electron in the conduction band will be captured if all the traps are empty and the distribution of electron energies is that produced by a field of intensity E. With this notation, the capture rate of electrons by traps is $C_n^E f_p n$. It should be emphasized that f_p and n may not have the same values in high fields as in low fields.

When an electron is in a trap, it can either be emitted back into the conduction band or fall into the valence band. The latter event can be thought of as hole capture and its rate calculated in a quite similar way to that for electron capture. The rate for the former event, electron emission, was shown by SHOCKLEY and READ for the low-field case to be $C_n f n_1$, where f is the fraction of traps that are filled, and

$$n_1 = N_c \exp(\epsilon_t - \epsilon_c)/k\theta_o,$$

N_c being the density of states in the conduction band and $\epsilon_t - \epsilon_c$ the energy of the trap level measured from the edge of the conduction band. If f were to remain the same in high fields, this rate would be the same as for low fields because in nondegenerate samples it does not depend on the actual distribution of carriers in the conduction band. We can then write the rate of emission in high fields as $C^n f n_1$, the superscript 0 indicating that the average of vA_n is to be taken over the zero-field distribution of the carriers.

The *net* rate of capture of electrons in high fields is the difference between capture and emission rates,

$$C_n^E f_p n - C_n^0 f n_1 \tag{2}$$

It can be shown similarly that the net rate of capture of holes in high fields is

$$C_p^E f p - C_p^0 f_p p_1 \tag{3}$$

† The effect of high fields on the diffusion rate is discussed in another publication now in preparation.

where p_1, the quantity analogous to n_1, is the density of states N_v in the valence band times $\exp(\epsilon_v-\epsilon_t)/k\theta_0$.*

We shall now apply these considerations to a situation that was studied experimentally by J. ZUCKER.[2] A germanium sample is irradiated with light of intensity such that it generates g electron-hole pairs per second. With a small d.c. field applied to the sample, this gives rise to a small photocurrent. In the steady state, carrier concentrations are given by $n_o = n_{th}+g\tau_{th}$ and $p_o = p_{th}+g\tau_{th}$, the subscript th indicating the thermal equilibrium values of the quantities. At $t = 0$, and after the establishment of the steady state, a sinusoidally varying high electric field is applied to the sample. If we assume no changes in carrier concentration from surface or contact effects, to find the carrier concentration at a time t after application of the field we must solve the equations

$$\frac{dn}{dt} = -C_n^E f_p n + C_n^0 f n_1 + g \tag{4}$$

$$\frac{dp}{dt} = -C_p^E f p + C_p^0 f_p p_1 + g, \tag{5}$$

and the additional equation obtained from the conservation of charge condition:

$$\frac{d(N_t f)}{dt} = -\frac{dn}{dt} + \frac{dp}{dt} \tag{6}$$

The last equation can be integrated directly and the result used to eliminate f and f_p ($\equiv 1-f$) from the other two equations. The resulting pair of coupled differential equations is not easily integrated for the general case. We shall confine ourselves here to solving them approximately for a simple case that is quite useful. If concentration changes due to both light and field are small, and majority carrier density is large compared to the trap density, then we may neglect the changes in n and p produced by changing concentrations in the traps, and take f and f_p to be constant. The third equation then gives

$$\frac{dn}{dt} = \frac{dp}{dt}. \tag{7}$$

This means we can get the same information by solving either of the other two equations, so we shall work only with equation (4). It is informative to put this in a different form before integrating. Before the application of the high electric field, the system was in a steady state such that:

$$\frac{dn}{dt} = 0 = -C_n^0 f_p n_o + C_n^0 f n_1 + g \tag{8}$$

We can use this relation to eliminate g from (4), transforming it into

$$\frac{dn}{dt} = -C_n^E f_p n + C_n^0 f_p n_o \tag{9}$$

This says that the rate of change of n in the electric field E is given by the difference between the capture rate of electrons in zero field and the capture rate in the field E. The equation takes this simple form because by assuming constant f we have made the emission rate from the traps independent of E.

The solution of (9) that satisfies the boundary condition that at $t = 0$ $n = n_o$ is:

$$n = n_o[\exp -(t\langle C_n^E f_p\rangle_T \times (1-C_n^0/\langle C_n^E\rangle_T)+C_n^0/\langle C_n^E\rangle_T], \tag{10}$$

where the average of C_n^E, as indicated, is to be taken over a cycle of the electric field. A solution of similar form is obtained for p, with f_p replaced by f. It is interesting to note that in the limit of very long time t

$$n \xrightarrow[t\to\infty]{} (n_{th}+g\tau_{th})C_n^0/\langle C_n^E\rangle_T \tag{11a}$$

$$p \xrightarrow[t\to\infty]{} (p_{th}+g\tau_{th})C_p^0/\langle C_p^E\rangle_T \tag{11b}$$

In the absence of light ($g = 0$) this gives:

$$np \xrightarrow[t\to\infty]{} n_i^2(C_n^0C_p^0/\langle C_n^E\rangle_T\langle C_p^E\rangle_T), \tag{12}$$

where n_i is the intrinsic carrier concentration. This relation is the generalization for high alternating electric fields of the expression derived earlier for high d.c. fields.[4]

Equation (10) has been derived for a sample that has the property that recombination takes place through one set of trap levels, the concentration of these levels being small compared to the majority carrier concentration. To relate the

* These expressions have been derived in more detail by E. M. CONWELL, Ref. 4.

quantities in (10) to experimentally observable ones, it is convenient to impose the further requirement that the sample lifetime be determined by the capture rate of only one type of carrier. A sample that satisfies all these requirements is a p-type germanium sample at room temperature with resistivity of about 1Ω cm, corresponding to about 2×10^{15} holes/cm^3, and recombination taking place at copper centers present in a concentration of 10^{14}/cm^3 or less.[5, 6] In such a sample the copper levels at 0·05 eV will all be filled and the copper levels at 0·3 eV will practically all be empty. The hole concentration is high enough for the lifetime to be equal to the rate at which the negativity charged copper centers capture electrons.[5] Since C_n^0 denotes this rate, the lifetime of this sample in the absence of electric field, τ_{th}, equals $1/C_n^0$. If we denote the quantity C_n^E by $1/\tau_E$, then for such a sample we may write (10) as

$$n = n_0\,[\exp(-t\langle 1/\tau_E\rangle) \times (1-1/\tau_{th}\langle 1/\tau_E\rangle)+1/\tau_{th}\langle 1/\tau_E\rangle)] \qquad (13)$$

where n is now the minority carrier concentration.

From the form of (10) or (11) it can be anticipated that the quantity that will be determinable experimentally is $\langle C_n^E\rangle/C_n^0$. In terms of the cross section for electron capture A_n this is given by

$$\langle C_n^E\rangle/C_n^0=(1/T)\int_0^T\langle vA_n\rangle_E\,dt/\langle vA_n\rangle_0 \qquad (14)$$

where the averages are to be taken over the velocity distribution at the field indicated. If we make the assumption that the cross section is proportional to v^j, we obtain from (14):

$$\langle C_n^E\rangle/C_n^0=(1/T)\int_0^T\langle v^{j+1}\rangle_E\,dt/\langle v^{j+1}\rangle_0 \qquad (15)$$

For hot electrons in germanium it has been found that over a wide range of fields the distribution function is well approximated by a Maxwell–Boltzmann distribution.[7] Denoting the temperature of this distribution by θ_E, we obtain

$$\langle C_n^E\rangle/C_n^0=(1/T)\int_0^T(\theta_E/\theta_0)^{(j+1)/2}\,dt = \langle(\theta_E/\theta_0)^{(j+1)/2}\rangle_T \qquad (16)$$

The ratios θ_0/θ_E and $(\theta_E/\theta_0)^{1/2}$ for electrons in germanium are plotted in Fig. 1 as a function of d.c.

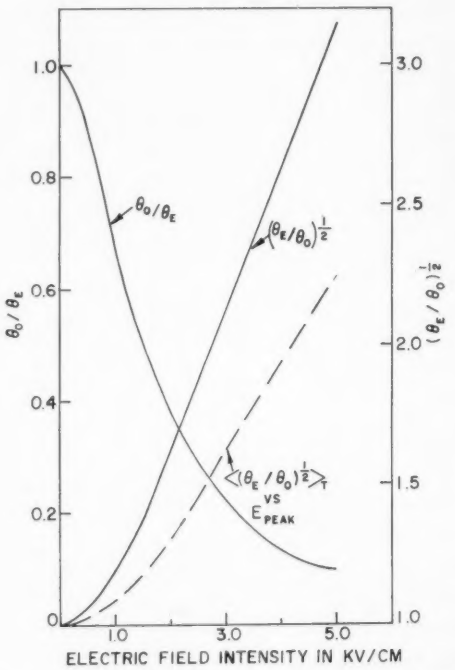

FIG. 1. (θ_0/θ_E) and $(\theta_E/\theta_0)^{1/2}$ (solid lines) as a function of electric field, and average of $(\theta_E/\theta_0)^{1/2}$ over a cycle (dashed line) as a function of peak electric field for electrons in Ge at room temperature.

field. They were obtained from a theoretical calculation of high-field mobility μ_E as a function of θ_E by correlating with each value of θ_0/θ_E the field at which the theoretically predicted value of μ_E/μ_0 is observed experimentally.[9] Of course the calculations of μ_E vs. θ_E were made for the electrons as majority carriers. Since the hole temperature in a given field does not appear to be very different from the electron temperature,[8] and carrier concentrations are not very high in the samples under consideration here, it is felt that the temperature

Vol. 22
1961

vs. field curves of Fig. 1 should provide a good approximation for this situation.

The averaging over a cycle of the electric field indicated in equation (16) has been carried out for the case of a velocity-independent cross section, i.e. $j = 0$. The resulting variation of $\langle C_n^E \rangle / C_n^0$ with peak electric field is shown by the dashed line in Fig. 1. At a peak field of 5000 v/cm it is seen that the average rate of electron capture for this case of constant cross-section is more than twice the rate in zero field. For $j > 0$ the average capture rate would increase even more rapidly with field. For j less than zero there are different situations depending on whether $j > -1$ or $j < -1$. At $j = -1$, corresponding to $1/v$ dependence of the cross section, $\langle C_n^E \rangle / C_n^0 = 1$ and there is no change in recombination rate with field, as anticipated. Thus the curves representing the variation with field of $\langle C_n^E \rangle / C_n^0$ for values of j between 0 and -1 would be between the dashed curve and the horizontal axis of Fig. 1, the increase in average speed being partly cancelled by the decrease in cross section with field. For $j < -1$, $\langle C_n^E \rangle / C_n^0$ is less than 1. The curves of $\langle C_n^E \rangle / C_n^0$ would lie below the horizontal axis of Fig. 1, the more so the larger the magnitude of j.

Application of the foregoing theory to the experimental results of J. ZUCKER has produced information on the variation in cross section with speed for a Cu-doped sample of the type described earlier. Specifically, it is found[2] that the cross section for electron capture of copper centers with a single negative charge decreases with increasing speed of the carriers. This result is rather surprising. Because of the Coulomb repulsion between the center and the electron, it has been felt that the cross section should increase rapidly with increasing speed of the carriers. Early work[9, 10] on the temperature-dependence seemed to be in agreement with these expectations, the experimentally obtained cross sections apparently increasing rapidly with increasing temperature between 100 and 300°K. On the basis of more recent theoretical and experimental work, however, KALASHNIKOV[11] states that this cross section decreases slightly when the temperature is raised. He still feels that A_n should increase with increasing speed, and therefore suggests that the observed temperature dependence is due to other factors that decrease A_n with increasing temperature. He also points out that it has been shown by BONCH-BRUEVICH that the v-dependence of A_n need not be as strong as was thought earlier, because electrons may tunnel through the Coulomb barrier.

It has been pointed out by AIGRAIN that one possibility for explaining the decrease of cross section with increasing speed is that the capture process involves multi-phonon emission. An electron with greater energy would have to emit more phonons, which would be a less probable process. Evidence that electron capture by Ni-centers in Ge involves multi-phonon emission has been found by M. BERNARD and coworkers.[12]

REFERENCES

1. RYDER E. J. and SHOCKLEY W., *Phys. Rev.* **81,** 139 (1951).
2. ZUCKER J. and CONWELL E. M., following paper in this journal.
3. SHOCKLEY W. and READ T., *Phys. Rev.* **87,** 835 (1952).
4. CONWELL E. M., *J. Phys. Chem. Solids* **17,** 342 (1961)
5. BURTON J. A. *et al.*, *J. Phys. Chem.* **57,** 853 (1953).
6. ALEXEEVA V. G., KARPOVA I. V. and KALASHNIKOV S. G., *Soviet Physics Solid State* **1,** 475 (1959).
7. REIK H. G., RISKEN H. and FINGER G., *Phys. Rev. Letters,* **5,** 423 (1960).
8. CONWELL E. M., *J. Phys. Chem. Solids* **8,** 234 (1959).
9. BAUM R. M. and BATTEY J. F., *Phys. Rev.* **98,** 923 (1955).
10. SHULMAN R. G. and WYLUDA B. J., *Phys. Rev.* **102,** 1455 (1956).
11. KALASHNIKOV S. G., *Proc. Int. Conf. Semicond. Phys.* p. 241. Czech Academy of Sciences, Prague (1961).
12. BERNARD M., MENORET M. and MENACHI H., *Proc. Int. Conf. Semicond. Phys.*, p. 256. Czech Academy of Sciences, Prague (1961).

* It is assumed that all valleys have the same temperature. This can be achieved experimentally by using a [100] orientation for the samples.

BLANK
PAGE

Vol. 2
1961

J. Phys. Chem. Solids Pergamon Press 1961. Vol. 22, pp. 155–158. Printed in Great Britain.

NEGATIVE RESISTANCE AND HIGH ELECTRIC FIELD CAPTURE RATES IN SEMICONDUCTORS

B. K. RIDLEY and T. B. WATKINS

Mullard Research Laboratories, Salfords, England

Abstract—It is pointed out that the rate of capture of electrons and holes by charged centres should depend markedly on electric field strength when this is high enough to produce hot electrons. In particular, the capture rate for an attractive centre should decrease while the rate for a repulsive centre should increase as the field rises. Each effect will alter the steady state density of carriers. For the case of repulsive centres, a decrease in carrier density will occur and the possibility of using this phenomenon to produce a negative resistance state in the semiconductor is discussed. Suitably compensated *n*-type germanium crystals containing copper, nickel or gold appear to have the requisite properties for exhibiting negative resistance at temperatures low enough for the thermal ionization rate of the centre to be small. It is pointed out that the long time constants involved in the process preclude the use of short pulse fields.

1. INTRODUCTION

THE fact that an electric field above a certain critical value can alter the equilibrium distribution of electrons over the various energy states in a semiconductor has recently given rise to speculations concerning the possibility of achieving a negative resistance region in the current–voltage characteristic (RIDLEY and WATKINS[1]). A semiconductor exhibiting a differential negative resistance will have the peculiar property of passing a smaller current when the field is increased, and this should produce a marked electrical instability if random fluctuations in the field occur slowly enough. Interesting phenomena may occur and it is of interest to enquire under what conditions a differential negative resistance can be obtained.

Naïvely, we may collect all the various energy states into groups characterized by different mobilities of the electrons or holes occupying them. For instance, in *n*-type GaSb there would be at least three groups—the central conduction band minimum at $k = 0$ characterized by mobility μ_a, the [111] minima characterized by mobility μ_b, and the majority impurity states characterized by zero mobility, or mobility μ_c if impurity conduction is important. Or again, in *n*-type Ge doped with gold the two important groups at low temperatures might be the [111] conduction band minima, mobility μ_a, and the upper gold levels, mobility μ_b. The action of the electric field will be to alter the mobilities and by raising the electronic energy change the population of the various conduction groups. If only two groups predominate the condition for a differential negative resistance is

$$\left(\frac{\mu_a-\mu_b}{\mu_a+f\mu_b}\right)\left(-\frac{F}{n_a}\frac{dn_a}{dF}\right) - \frac{F}{\mu_a+f\mu_b}\left(\frac{d\mu_a}{dF}+f\frac{d\mu_b}{dF}\right) > 1 \qquad (1)$$

where n_a and n_b are the numbers of electrons in groups a and b respectively, $f = n_b/n_a$, F is the electric field, and it is assumed that n_a+n_b remains constant. If raising the field tends to increase the population of group b it is essential that $\mu_b < \mu_a$, and we must rely on lattice scattering to make the mobilities decrease with increasing field.

An ideal case is one in which the group b states are localized for then $\mu_b = 0$. This is the case to be discussed here. The group a states are the conduction band states in *n*-type material and we will limit the discussion to electronic conduction.

Since localized states are below the conduction band in energy it may be asked how an increase in energy of the conduction electrons can lead to an increase in the population of a lower energy state. The paradox is solved if the electrons are

forced to overcome a potential barrier before being captured and this will occur whenever the localized centre is negatively charged. An increase in field means that more electrons have the necessary energy for surmounting the barrier and this results in an enhanced capture rate. If no increase in the generation rate occurs, and this supposes a constant temperature and no impact ionization, the net result is a withdrawal of conduction electrons which can lead to a differential negative resistance. Barriers of up to 0·2 eV have been observed in germanium containing copper, nickel or gold (BATTEY and BAUM[2]; SHULMAN and WYLUDA[3]; JOHNSON and LEVINSTEIN[4]).

Before going on to obtain more explicit requirements it is instructive to consider the orders of magnitude involved in changes of capture cross-section with field. For repulsive centres the cross-sections for thermal electrons are around 10^{-22} cm^2 and for attractive centres they can be as high as 10^{-12} cm^2, while for neutral centres they are of the order of 10^{-17} cm^2. For low energy electrons the effect of the charge on a centre is very large but as the electron energy increases the effect of the charge decreases until in the limit the centre appears virtually as neutral. Thus changes in cross-section with mean electron energy over five orders of magnitude seem possible especially at low temperatures. It is clear that large changes in carrier density can occur, a reduction in the case of repulsive centres and an increase in the case of attractive centres. CONWELL[5] has already pointed out that the field dependence of capture rate can be an important effect in hot electron experiments.

2. CHANGE IN CAPTURE RATE FOR REPULSIVE CENTRE

Consider the case of an extrinsic n-type semiconductor at a low temperature whose conduction electrons derive from thermal ionization of a negatively charged impurity centre. We shall suppose, for simplicity, that any other localized levels in the bulk or on the surface which may exist are separated in energy from the impurity level by several kT and that the Fermi level is near to the impurity level. This means that the other localized levels are either empty or full and do not interact significantly with the conduction band. These are the usual conditions pertaining when Hall measurements are made to determine the activation energy of the impurity level, so they are in no way unusual. Over a suitable temperature range a germanium crystal containing N gold atoms per cm^3 and about $2{\cdot}5\,N$ antimony atoms per cm^3 would fulfil these conditions (for $N \gtrsim 10^{14}$/cm^3 to swamp other impurities). The density of electrons in the conduction band would then be governed solely by the rates of transition associated with the upper gold level.

Under these conditions the rate of increase of electron density, n, in the conduction band is

$$\frac{dn}{dt} = gN^- - Bn\,N^0 \qquad (2)$$

where N^- is the density of filled levels, N^0 is the density of unfilled levels and g and B are the rates for thermal ionization and capture respectively averaged over the electron distribution and are in general field dependent. We shall assume that the thermal ionization rate, depending solely on lattice temperature as it does, is not appreciably affected by the field. At the steady state, therefore,

$$B_0 n_1 N^- - Bn\,N^0 = 0$$

where

$$n_1 = 2\left(\frac{2\pi m^* kT}{h^2}\right)^{1/2} \exp(-E_t/kT)$$

E_t is the energy of the level measured from the conduction band edge, and the suffix zero denotes thermal equilibrium (low field) values.

If Δn is the increase in electron density due to the field we obtain by putting $n = n_0 + \Delta n$, $N^- = N_0^- - \Delta n$, and $N^0 = N_0^0 + \Delta n$

$$\Delta n = \tfrac{1}{2}[\{(N_0^0 + n_0 + \gamma n_1)^2 - 4n_0 N_0^0(1-\gamma)\}^{1/2} - (N_0^0 + n_0 + \gamma n_1)] \qquad (3)$$

where

$$\gamma = \frac{B_0}{B}.$$

This may be simplified for the case when the doping is such that only about half the levels would be occupied at 0°K. The example of gold-doped germanium cited above would satisfy this condition. There is then always a substantial density of unoccupied levels available for electron capture,

Vol. 2
1961

and at temperatures below that for complete ionization of the level we can put

$$n_0 \lesssim n_1 \ll N_0^0.$$

For a repulsive centre $\gamma \leqslant 1$ so that γn_1 is also small and (3) becomes

$$\Delta n = -n_0(1-\gamma). \tag{4}$$

The potential distribution around a repulsive centre is shown schematically in Fig. 1. It may be

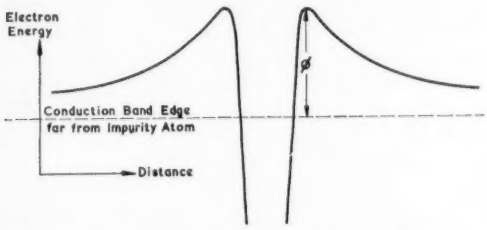

FIG. 1. Schematic diagram of potential around a negatively charged impurity centre.

thought of as the superposition of a coulomb repulsive potential and a short range attractive potential. Since the interaction between an electron and this potential field will be substantial it means that an appreciable energy variation over a free electron wavelength will occur. A rigorous estimation of the electron density near the centre, which is the operative density governing the effective rate of capture, would therefore involve the solution of the relevant Schrödinger equation, which in turn requires a knowledge of the precise potential field. We need, in fact, a refined picture of deep-level centres in semiconductors but, unfortunately, this does not exist. To avoid an impasse we will accept PEKAR'S[6] assumption that the electron density near the centre differs from the average by a factor $\exp[-\phi/kT]$ at thermal equilibrium, where ϕ is the potential barrier. If β is the capture rate of electrons which have surmounted the barrier, the effective capture rate B_0 is

$$B_0 = \beta \exp(-\phi/kT)$$

If ϕ/kT is large the main variation with field will come from the density factor. For hot electrons the distribution function changes in general from a Maxwellian to some function $f(F,\phi)$, so if the variation of β with field is neglected

$$B = \beta f(F,\phi). \tag{5}$$

3. CONDITIONS FOR NEGATIVE RESISTANCE

The conditions for negative resistance (1) becomes with $\mu_b = 0$, $n_a = n_o + \Delta n$, and $\mu_a \alpha F^p$,

$$-\frac{F}{n_0+\Delta n} \cdot \frac{d\Delta n}{dF} - p > 1$$

or, with (4) and (5) substituted

$$\frac{F}{f(F,\phi)} \frac{df(F,\phi)}{dF} - p > 1. \tag{6}$$

The most favourable case occurs when the electron temperature is high enough for excitation of optical phonons to become the dominant mechanism for scattering, for then p tends towards -1 and any increase in the capture rate will be effective. However, if the barrier is less than or of the same order as $h\omega_{opt}$ the variation of β with field becomes important and this we have neglected in (6). All measured barriers in germanium are greater than $h\omega_{opt}$ ($\sim 0{\cdot}04$ eV) so an increase of capture rate should occur in the current saturation region.

If the electron temperature is low enough for impurity scattering to be still dominant the conditions are much more formidable. An estimate can be made with the assumptions that $p = +1{\cdot}5$, the electron temperatures, $T_e = \text{constant} \times F$, and a Maxwellian distribution prevails, i.e.

$$f(F,\phi) = \exp(-\phi/kT_e).$$

The condition is

$$\phi/kT_e > 2{\cdot}5.$$

The solubilities of deep level impurities in germanium preclude concentrations much above $10^{15}/\text{cm}^3$ which means that impurity scattering will not be important when kT_e is greater than,say, $0{\cdot}025$ eV. Always assuming that the lattice temperature is low enough for $kT \lesssim 0{\cdot}02$ eV the condition becomes

$$\phi > 0{\cdot}07 \text{ eV}.$$

Observed barriers satisfy this condition. This suggests that negative resistance phenomena

should be observable over a wide range of field strengths.

As regards material, germanium, containing as impurity any one of copper, silver, gold, platinum, iron, cobalt, or nickel, and suitably doped with a shallow level donor, should be suitable.

4. DISCUSSION

It must be emphasized that these considerations apply to the steady rate. The time constants involved in transitions between repulsive impurity states and the conduction band can be of the order of seconds or even minutes at low fields and still be of the order of tens of microseconds at high fields. The use of short field pulses of about 1 μsec duration would merely show the mobility variation with field (unless the impurity concentration were high). D.C. fields are therefore desirable but heating effects must be avoided since the thermal generation rate must not increase. Heating effects can be delayed to higher fields by working at low temperatures and with high resistivity material.

Impact ionization of the deep level will destroy any negative resistance effects. An electron to produce impact ionization must not only surmount a higher barrier, since the filled centre will carry an extra negative charge, but still have sufficient energy left over to ionize. This effect should therefore occur at higher fields than those necessary to affect the capture rate, so its influence will be rather to reduce the range of fields over which negative resistance is possible than eliminate the possibility altogether.

The conditions relating to temperature and doping considered in section 2 are, of course, especially favourable but by no means essential. For instance, if over-compensation gives an excess of donors so that some occupation of donor levels occurs at very low temperatures, the effect of the change of capture rate of the repulsive centre on the population of the conduction band will be less and the conditions for negative resistance become more stringent but not necessarily impossible to meet.

5. CONCLUSIONS

When the mean conduction electron energy is less than the potential well surrounding a positively charged centre or the potential barrier surrounding a negatively charged centre the capture rate will be markedly dependent on the local density of electrons at the centre. Increasing the mean energy by applying an electric field decreases the density near positive centres and increases the density near negative centres. The capture rate for positive centres is therefore reduced while that for negative centres is increased. In this paper we have shown that the increased rate of capture for repulsive centres provides a feasible mechanism for the production of negative resistance phenomena. In materials where the high field drift velocity is limited by optical phonon emission the barrier height, ϕ, must be, preferably, several times the optical phonon energy $\hbar\omega_{opt}$. In germanium, therefore, $\phi \sim 0{\cdot}1$ eV and barriers of this amount have been observed. This suggests that far from being a marginal effect, the phenomenon of negative resistance should be readily observable.

REFERENCES

1. Ridley B. K. and Watkins T. B., *Proc. Phys. Soc. Lond.* **78,** 293 (1961).
2. Battey J. F. and Baum R. M., *Phys. Rev.* **100,** 1634 (1955).
3. Shulman R. G. and Wyluda B. J., *Phys. Rev.* **102,** 1455 (1956).
4. Johnson L. and Levinstein H., *Phys. Rev.* **117,** 1191 (1960).
5. Conwell E. M., *J. Phys. Chem. Solids* **17,** 342 (1961).
6. Pekar S. T., *Zh. eksp/Fiz. teor.* **20,** 627 (1950); Translation: *Abb. Low Phys.* **1,** 47 (1951).

Vol. 2
1961

J. Phys. Chem. Solids Pergamon Press 1961. Vol. 22, pp. 159–166. Printed in Great Britain.

RECOMBINATION PROCESSES IN FAR INFRARED PHOTOCONDUCTORS

GERALD S. PICUS

Hughes Research Laboratories, Malibu, Calif., U.S.A.

Abstract—The conductivity, photoresponse and noise in germanium doped with Zn and Cu have been measured at 4·2°K as a function of applied electric field and incident background photon flux in an effort to better understand the free carrier generation and recombination processes that determine the behavior of these materials as detectors of far infrared radiation. The I–V characteristic shows a high field breakdown similar to that observed in the dark. At intermediate values of electric field, the current varies as $I = I_0 \exp(V/_0V)$ where I_0 is proportional to the incident photon flux and V_0 is of the order of 0·25 to 0·4 of breakdown voltage. For low fields the samples are ohmic with conductivity proportional to the incident photon flux. The deviation from ohmic behavior is attributed to the increase of the free carrier recombination time as the carriers are heated by the electric field. There are indications that carrier effective temperatures depend also on the spectral distribution of the incident radiation.

1. INTRODUCTION

A NUMBER of fast, sensitive detectors of long wavelength infrared radiation have been fabricated utilizing the photoconductive effect in impurity doped semiconductor materials. These materials show striking deviations in their behavior from that based on the simple model usually invoked to explain their properties. It is found from this model that the equivalent short circuit signal and noise currents are both directly proportional to the d.c. electric field and that the noise power frequency spectrum is flat up to frequencies of the order of the reciprocal of the lifetime. Only generation recombination noise is being considered here. The current voltage characteristic of such a photoconductor is by assumption a straight line.

For zinc- and copper-doped germanium, the most striking deviations from ideal behavior occur in the case of the current–voltage characteristics and the noise. The current increases above that which would be expected for a purely ohmic element at fields as low as a tenth of a volt per centimeter and all three materials eventually show, at some critical field V_c, a very sharp increase in the current (by several orders of magnitude) with very small increase in the field. This breakdown is attributed to the impact ionization of impurity centers by energetic free carriers.[1, 2] In this region of the current–voltage curve more carriers are being produced by the internal impact ionization mechanism than by the incident external photon flux, and the photoresponse decreases sharply. This paper is concerned only with phenomena occurring at fields below breakdown.

With respect to noise, the situation is confusing in that the behavior of the short circuit noise current as a function of bias field was found to vary considerably from sample to sample and appeared to be related to the electroding technique that was used. Copper-doped germanium showed such variations to a much greater extent than did zinc-doped germanium. One feature which both materials had in common was a very large increase in the noise power output at fields just preceding the onset of breakdown. This effect was found regardless of electroding technique and polarity of the applied field.

In the hope of better understanding these phenomena, a program was undertaken to investigate the generation and recombination mechanisms of free carriers with ionized impurity centers in doped semiconductors at low temperatures. Since estimates of carrier lifetime from normal photoconductance measurements indicated values of the order of 10^{-8} to 10^{-10} sec, we did not attempt to study recombination directly by measuring the

photoconductivity decay time. Instead, the approach taken was to vary the carrier concentration in the photoconductor by varying the photon flux incident on it and to study the current–voltage characteristics, noise and photoresponse in the presence of different incident photon fluxes. The purpose of this paper is to report the results of these measurements and some considerations concerning their interpretation in terms of the generation and recombination processes occurring in these materials.

2. EXPERIMENTAL DETAILS

The zinc- and indium-doped germanium crystals used in these experiments were Czochralski pulled crystals doped in the melt. The copper-doped germanium was prepared from zone leveled starting material by diffusion of copper at temperatures in the range of 700–800°C. The properties of the individual samples will be described when the experimental results are given. Samples cut 0·125 in. square and 0·060 in. thick were electroded on two opposite 0·060 × 0·125 in. sides by one of three techniques: (1) electroplating copper; (2) electroplating nickel; or (3) alloying indium. The latter technique gave excellent results on zinc- and indium-doped germanium, but gave very erratic results with copper-doped germanium. Such alloyed contacts on copper-doped specimens gave polarity dependent current-voltage characteristics and the low temperature impedance and critical breakdown field varied over an order of magnitude for samples prepared from the same material by what was presumably the same electroding procedure. Plated electrodes were much more successful on copper-doped germanium in giving consistent values of impedance and breakdown field, although they were not reproducible with respect to noise characteristics.

The samples were soldered to the bottom of the helium reservoir in a standard metal Dewar vessel and were surrounded by helium temperature shields with aperture defining a solid angle of 0·0156 steradians. A blackbody constructed from a copper cylinder with a 14° cone cut into the end of it was mounted in the Dewar so that it completely filled the solid angle seen by the sample. By varying the temperature of this blackbody from 90°K up to about 380°K it was possible to vary the background photon flux incident on the sample by several orders of magnitude. For photoresponse measurements, the blackbody is removed and an infrared transparent window is substituted. All of the results to be presented in this paper were taken with the sample held at liquid helium temperature.

Where data is presented in this paper without any presentation of individual points, the original raw data was obtained by continuous recording techniques. Signal and noise measurements are all referred to a calibrating signal introduced into the input circuit in such a way that the recorded data can be easily interpreted to give directly the equivalent short circuit signal and noise currents corrected for the sample's dynamic impedance, which varies with the applied bias.

3. EXPERIMENTAL RESULTS

Zinc-doped germanium

A semilogarithmic plot of current versus sample voltage for zinc-doped germanium is shown in Fig. 1. The material had a room temperature resistivity of 0·4/Ωcm, corresponding to a net

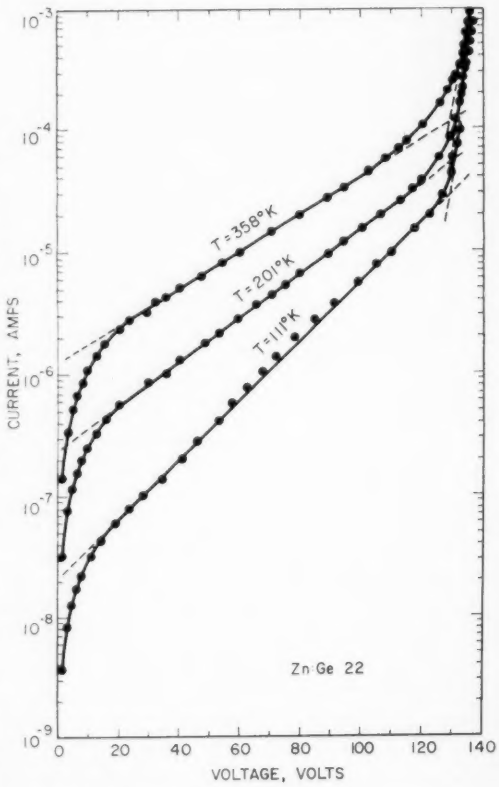

FIG. 1. Semilogarithmic plot of current versus voltage for zinc-doped germanium at three different temperatures of the illuminating blackbody.

zinc concentration of $10^{16}/cm^3$. No data is available concerning the compensating donor concentration but from experience with materials from the same source it is estimated at between 10^{13} and $10^{14}/cm^3$. For clarity, curves corresponding to only three different blackbody temperatures are shown in this figure. The current increases above that

Vol. 22
1961

corresponding to ohmic behavior at electric field intensities as low as 15 V/cm. The dependence of current on voltage is exponential from 20 V (63 V/cm) up to the onset of breakdown, which is observed in this sample at 129 V (405 V/cm). If the exponential portion of the curve is represented as $I = I_o \exp(V/V_o)$, then the parameters I_o and V_o are found to vary with the incident photon flux as indicated in Figs. 2 and 3. The photon flux was

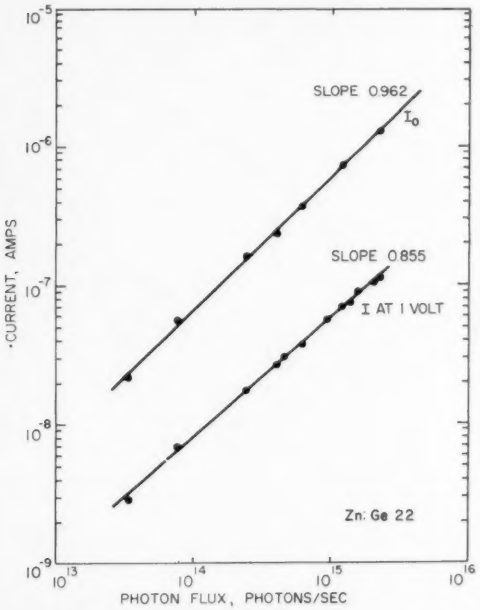

FIG. 2. Variation of coefficient I_o of exponential portion of I–V characteristic curve of zinc-doped germanium with incident photon flux.

calculated using the blackbody radiation law and assuming that the photoionization absorption of the zinc impurity centers cut off at 40 microns. Impurity concentration and sample thickness were large enough so that the sample was no more than 10 per cent transmitting at wavelengths shorter than 10 microns and even less transparent at longer wavelengths. The assumption of an opaque sample is justified within the precision of the experiments and eliminates the necessity for integration over the blackbody spectrum. The parameter I_o is found to increase linearly with the incident photon flux, within experimental error, and V_o increases logarithmically with photon flux.

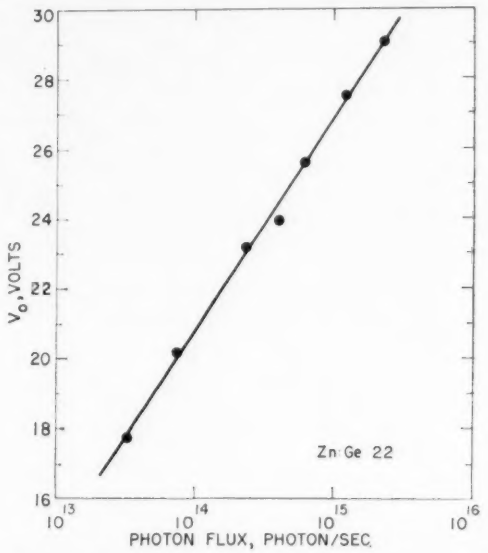

FIG. 3. Variation of the parameter V_o of exponential portion of I–V characteristic curve of zinc-doped germanium with incident photon flux.

The current at one volt bias, which for this sample is in the ohmic region, is also shown as a function of photon flux in Fig. 2 and is found to vary a little less rapidly with incident photon flux. The difference is not outside of the estimated experimental precision and both curves would probably be slightly steeper if accurate account were taken of the variation of sample absorption with wavelength.

Copper-doped germanium

The copper-doped germanium sample tested was one of a series prepared to check the effect of compensation on photoconductor properties. Of these only the one to be described here has so far been measured and it was prepared by diffusing copper into germanium that was initially 15 Ω/cm n-type and so had approximately 10^{14} compensating donor impurities per cubic centimeter.

This sample, cut to the standard 0·125 × 0·125 in. size, was electroded by plating the ends with nickel and then soldering to the nickel plate with pure indium. The current voltage characteristics for four different temperatures of the illuminating blackbody are displayed in Fig. 4. The general

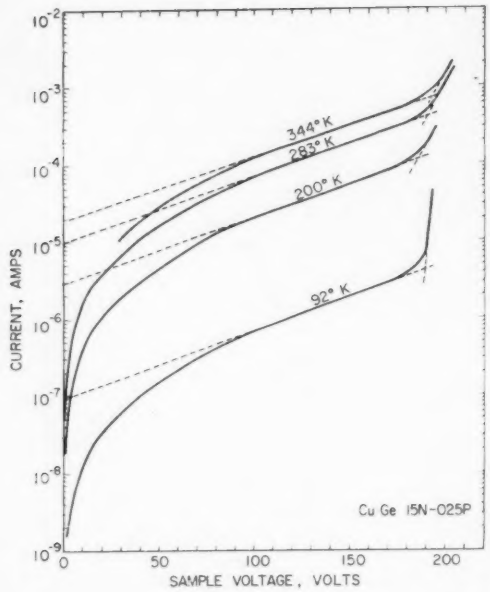

FIG. 4. Semilogarithmic plot of current versus voltage for copper-doped germanium at four different temperatures of the illuminating blackbody. The sample was prepared by diffusing copper into initially 15 Ω/cm *n*-type germanium.

character of the curves is as previously noted for the zinc-doped germanium specimen. The data for these curves was recorded on an *x–y* recorder and deviations from ohmic behavior are evident on the traces at sample voltages of 0·3 V (electric field intensities of 1 V/cm). The sample conductance in the ohmic region was found to vary linearly with the incident photon flux and the same is true for the parameter I_o. V_o was found to change by less than 10 per cent over approximately two orders of magnitude of photon flux, as compared to a factor of two for the zinc-doped germanium.

For this sample, the incident photon flux was also varied by changing the aperture in the helium temperature shield with room temperature radiation incident on the sample. The *I–V* characteristics for these two situations are shown in Figs. 5 and 6. Within experimental error, I_o changed in the ratio of the areas of the apertures, but V_o was identical for the two runs. This result leads to the speculation that the variation in V_o is only indirectly related to the magnitude of the incident photon flux and may be due to the variation in spectral distribution of the incident photons as the blackbody temperature is changed. This point is being checked in measurements on other copper-doped samples.

Figures 5 and 6 also display two other parameters of interest for these photoconductor materials: photoresponse and noise as a function of applied voltage. Both of these quantities are represented by the square of the ratio of the equivalent short circuit currents to the bias current. The curves shown are for a frequency of 1000 c/s and the passband for the noise measurement was approximately 350 c/s. This wide passband was used in order to reduce the amount of time necessary for a complete trace on the *x–y* recorder.

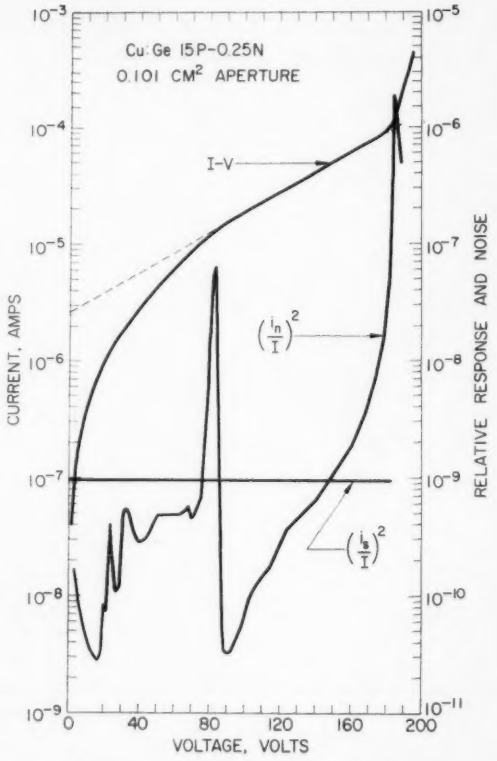

FIG. 5. Current-voltage characteristic, photoresponse and relative noise power of partially compensated copper-doped germanium as functions of applied voltage. Shield aperture was $1{\cdot}01 \times 10^{-1}$ cm².

Vol. 2
1961

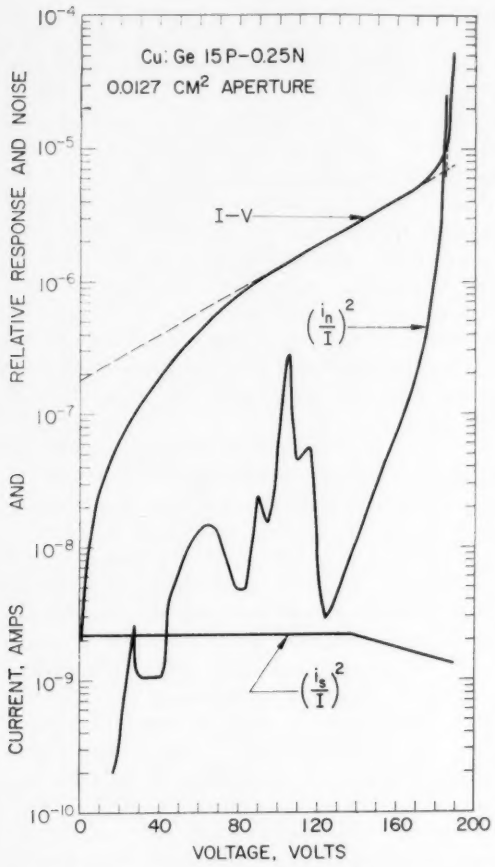

FIG. 6. Current–voltage characteristic, photoresponse and relative noise power of partially compensated copper-doped germanium as functions of applied voltage. The shield aperture was $1{\cdot}27 \times 10^{-2}$ cm² and a cooled intrinsic germanium filter preceded the sample.

The photoresponse is flat up to critical breakdown voltage in the presence of high photon flux (large aperture), but begins to fall off at $0{\cdot}7\ V_c$ when the photon flux is reduced. The widely varying noise power indicated in the figures was reproducible for a given set of operating conditions but changed drastically if polarity was reversed or if the electrodes were modified. Only the large increase in noise power immediately preceding breakdown appeared reproducibly in different samples.

DISCUSSION

Discussion of the results presented above is best presented within the framework of the simple model of impurity photoconductivity in which the recombination rate is assumed proportional to the free carrier concentration and the mean lifetime and mobility of the carriers are regarded as independent of the sample operating conditions. The kinetic equation describing the time rate of change of the number of free carriers is then:

$$\frac{dP}{dt} = G_I + G_B + G_S \exp(i\omega t) - P/\tau \qquad (1)$$

where P is the number of free carriers, G_I is the thermal equilibrium free carrier generation rate, G_B is the carrier generation rate due to the incident photon flux, $G_S \exp(i\omega t)$ is the generation rate due to a small additional photon signal which is taken as sinusoidal in time to distinguish it from the background, and τ is the mean carrier lifetime. Solution of this equation is straightforward and one finds:

$$I = \frac{eV}{Z^2}(G_B + G_I)\mu\tau$$

$$i_s = \frac{eV}{Z^2}\frac{G_S \exp[i\omega(t+\tau)]}{(1+\omega^2\tau^2)^{1/2}}\mu\tau \qquad (2)$$

$$i_n = \frac{eV}{Z^2}\frac{(\Delta f)^{1/2}}{(1+\omega^2\tau^2)^{1/2}}(G_B + G_I)^{1/2}\mu\tau$$

I is the bias current and V the sample voltage; i_s and i_n are respectively the equivalent short circuit signal and noise currents; Z is the length of the sample in the direction of current flow, which is regarded as perpendicular to the direction of incidence of the radiation. Since τ is of the order of 10^{-9} sec, $\omega\tau < 1$ at the frequencies at which measurements are usually made. The ratios of signal and noise currents to the d.c. bias current are simply:

$$\frac{i_s}{I} = \frac{G_S \exp(i\omega t)}{G_B + G_I}$$

$$\frac{i_n}{I} = \frac{2(\Delta f)^{1/2}}{(G_B + G_I)^{1/2}} \qquad (3$$

These are particularly simply related to the carrier generation rates in the photoconductor. The noise

current represented in these equations is that due solely to carrier generation and recombination.

At liquid helium temperatures the thermal equilibrium generation rate, G_I, is negligible compared to that due to the incident background photon flux. Under these conditions, the properties of these photoconductors—at least when the model above applies—are determined by the external photon flux incident on the sample and by the mobility and recombination time. The observed behavior of these materials, as reported in the previous Section, should then be explainable in terms of the dependence of carrier mobility and lifetime on photon flux and applied field.

Before attempting such a discussion it is important to ascertain that the properties observed are not due to some spurious effects. Two such possibilities that arise are heating of the sample and space charge effects. Calculations of the temperature rise to be expected for a sample mounted as in these experiments indicate that a heat input to the sample of 20 milliwatts would raise its temperature by 0·1°K. Reference to the current voltage curves will indicate that we are always operating within this limit. This is corroborated by one set of pulse measurements on zinc-doped germanium in which no deviation from the d.c. measurements was found until currents in the breakdown region were reached. It would be expected, though, that an increase in the aperture in the Dewar by a factor of more than two would lower the resistivity of the sample sufficiently that significant heating could occur before the critical breakdown field were reached. This was observed in one set of measurements made on a copper-doped germanium sample with the aperture shields removed. The exponential region did not extend to as high a field and the transition to the breakdown region was not sharp, as would be expected if the sample temperature increased significantly.

Since the ohmic resistivity at 4·2°K of the photoconductor materials used in these experiments is of the order of $10^6\ \Omega$/cm it is possible that space charge currents might be observed in them. Using Rose's[3] analysis for a trap free solid, it is found that the space charge currents become comparable with the ohmic current at voltages of 10 V. However, the ionized impurity centers in the material would act as traps for any majority carriers injected from the electrodes and only a small proportion of the injected carriers would remain free to conduct current. Such injected carriers would distribute themselves between conduction and ionized impurity states in the same ratio as do the carriers in the photoconductor, at least until the ionized impurity centers have become filled. For these photoconductors under the conditions of these experiments, the free carrier concentration is of the order of 10^9/cm^3, the ionized impurity concentration is therefore equal to the compensating impurity concentration of about 10^{14}/cm^3 and the impurity concentration is of the order of 10^{16}/cm^3. Consequently, only 10^{-7} of the injected space charge will be in conducting states and space charge currents should be negligible for all fields below breakdown.

If, then, the current–voltage characteristics of these materials are to be interpreted in terms of the properties of the free carriers, the simple model suggests that it is necessary to find some mechanism whereby the mobility or the recombination time become functions of the applied electric field and the incident photon flux. Carrier heating effects provide such a mechanism. For a sample at 4·2°K even very small electric fields can produce a considerable increase in the mean kinetic energy of the free carriers.[4] A measurement of mobility as a function of field was carried out for copper-doped germanium, but on a bridge sample which had been electroded with indium alloy contacts and which was illuminated through glass Dewar walls. (i.e. The spectral distribution of the incident radiation was confined to photons of wavelength shorter than 3·5 microns and so was quite different, and at a much lower level, than in the case of the photoconductivity measurements.) The results of this measurement, which are not regarded as too reliable, were that the mobility remained constant for fields up to about 0·9 of the critical breakdown field and then fell off at a rate slightly greater than E^{-1}. No information concerning the kinetic energy of the free carriers can be inferred from this particular dependence of mobility on field, although it is not inconsistent with neutral impurity scattering for which the collision relaxation time is independent of carrier energy. The E^{-1} mobility dependence at high fields could be attributed to polar mode lattice scattering and would then lead to the conclusion that the mean kinetic energy was of the order of 400°K.

Vol. 2
1961

Another estimate of the effective carrier temperature can be made by applying the result LAX[5] obtained in the theory of giant traps that the capture cross-section of an ionized impurity center for a free carrier varies as the inverse square of the mean kinetic energy. Assuming that mobility is independent of field, the increase in current with field in the photosensitive region of an impurity photoconductor is due to the increase of the recombination time τ. In terms of the capture cross-section σ, mean carrier velocity v, and density of ionized impurity centers, N_D, the recombination time is $\tau = (\sigma v N_D)^{-1}$ and so must vary as $T_e^{3/2}$. From the I–V characteristics one finds that τ near breakdown is approximately a factor of 20 greater than the low field ohmic value. This leads to an estimate of 32°K for the mean carrier temperature just preceding breakdown.

Aside from the order of magnitude discrepancy between these two estimates of mean carrier temperature, there are reasons to suspect the validity of either of them. BRAY,[6] in studies of the field dependence of the mobility in p-type samples of germanium at temperatures where the impurity centers are completely ionized has found good agreement between experimental results and theoretical calculations which included ionized impurity and acoustic mode scattering, but that inclusion of polar mode scattering introduced discrepancies. In addition, he found effective carrier temperatures rising to thousands of degrees, an order of magnitude greater than our highest estimate. The defect in the second estimate based on the change in the recombination time is that in the giant trap calculations of LAX, a sufficiently low density of ionized impurity centers is assumed so that it is not necessary to take into account a limit to the range of interaction of a carrier with a center due to the proximity of other centers. Despite the fact that significant carrier heating effects must be occurring, the data to date provides us with no adequate means for gaining some insight into this process.

The magnitude of the recombination time τ in the ohmic region is estimated at 10^{-9} sec for the copper- and zinc-doped samples described in this paper. A mobility of 5×10^4 cm^2/V sec, the value determined for the copper-doped sample, was used for this estimate. At fields close to breakdown τ is of the order of 2×10^{-8} sec. The general picture of a recombination time varying with the mean kinetic energy of the free carriers is not sufficient to explain the variation of V_0 with incident photon flux. This was observed most strikingly in the zinc-doped sample and appeared to a much less marked extent in the copper-doped germanium. There is the possibility that it is not the magnitude of the photon flux, but its spectral distribution which is responsible for this effect. The mean kinetic energy of the carriers will depend on the initial states to which they are excited and the rate at which they are redistributed in momentum space as a result of scattering processes. In the simple model of the photoconductors, the tacit assumption is made that the time necessary for this redistribution is small compared to mean lifetime of the carriers and that, consequently, their initial distribution in energy immediately after excitation does not influence the steady state distribution. If this assumption is given up, then it is reasonable to assume that for any given field the mean kinetic energy of the carriers will be higher as the blackbody temperature is increased, since the energy peak in the incident radiation moves to larger photon energies. It might also be expected that the relative effect of the field in heating the carriers would be diminished as their initial kinetic energy increased. This qualitatively accounts for an increase in the parameter V_0, since larger V_0 means a smaller change in τ for a given increase in voltage.

SUMMARY

The objective of this paper has been to present the results of a group of experiments which were undertaken in the hope of shedding some light on the recombination processes in impurity photoconductors. The principle finding reported here is the exponential current voltage dependence found for fields in the region where the photoresponse, i_s/I, is constant. The large current increase is attributed to a change in the recombination time of free carriers with ionized impurity centers and the most likely mechanism for this is regarded as the heating of the free carrier distribution under the influence of the applied field. Unfortunately, a quantitative comparison with existing theories of hot carriers and trapping was not possible. Some of the phenomena observed raise the possibility of the carrier distribution

depending on the spectral distribution of the incident photon flux.

Acknowledgements—The author wishes to acknowledge his indebtedness to L. TELK, E. LOH and N. KYLE for their considerable help on various portions of the experimental program described here. Thanks are also due to R. NEWMAN, E. KANE, P. KAUS and R. BRAY for valuable and interesting discussions.

REFERENCES

1. SCLAR N. and BURSTEIN E., *J. Phys. Chem. Solids* **2,** 1 (1957).
2. KOENIG S. H. and GUNTHER-MOHR G. R., *J. Phys. Chem. Solids* **2,** 268 (1957).
3. ROSE A., *Phys. Rev.* **97,** 1538 (1955).
4. GUNN J. B., *Progress in Semiconductors* **2,** 211 (1957); KOENIG S. H., *J. Phys. Chem. Solids* **8,** 227 (1959).
5. LAX M., *Phys. Rev.* **119,** 1502 (1960).
6. BRAY R. and BROWN D. M., *Bull. Amer. Phys. Soc.* **5,** 194 (1960).

Vol. 2
1961

J. Phys. Chem. Solids Pergamon Press 1961. Vol. 22, pp. 167–172. Printed in Great Britain.

PHOTOCONDUCTIVITY RESEARCH ON Cu–Ge

H. D. ADAMS, W. J. BEYEN and R. L. PETRITZ

Texas Instruments, Incorporated

Abstract—Photoconductivity and electrical phenomena associated with the 0·04 eV copper acceptor level in germanium have been examined. Experimental data giving the dependence of photosignal I_S/I, noise $I_n/I\Delta f^{1/2}$, and current on the applied electric field across the copper doped germanium filament are presented for several copper concentrations. Hall mobility and carrier concentration were measured with the sample exposed to ambient radiation. The mobility and carrier concentration data are given as a function of applied field in an effort to correlate the photoconductivity and *IE* measurements.

1. INTRODUCTION

THIS work attempts to bring together the necessary experimental data for analysis of field effects on optical processes in *p*-type germanium at low temperatures. Copper-doped germanium was chosen for study, since experimental parameters are easily controlled and the 0·04 eV acceptor level is typical of the levels of interest. Initially, only photosignal, noise, and *IE* measurements were made. An immediate discrepancy with theory[1, 2] arose in connection with the noise and current dependence on applied field. Subsequent Hall measurements with 300°K background illumination gave results which allow a degree of interpretation of the optical and electrical data; however, a theoretical analysis is, for the present, lacking.

2. SAMPLE PREPARATION

Samples of >40 Ω/cm *n*-type germanium grown with 111 crystal orientation were plated with copper and diffused at temperatures sufficient to obtain desired copper concentrations. Table 1 shows the pertinent data before and after diffusion for representative filaments.

All cold work was removed from the samples by etching in CP–4. Alloyed contacts of pure indium were used, and each sample was soldered directly to a copper block. The block was subsequently placed in intimate contact with a liquid helium heat sink for evaluation. All contacts were ohmic to within better than 1 per cent, as evidenced by four point probe measurements.

3. ELECTRICAL MEASUREMENTS*

Current vs. applied electric field

The current vs. applied-electric-field characteristic of a number of copper-doped germanium filaments at a temperature of ~ 5°K was determined. Three measurements were made on each sample listed in Table 1, two with varying amounts of ambient background radiation and a third dark measurement with the sample in thermal equilibrium at ~ 5°K. A cesium iodide window in the liquid helium Dewar was used to admit radiation in the spectral region of interest. The amount of ambient background radiation was limited by a liquid nitrogen temperature aperture. The amount of background radiation absorbed per second is designated as G_r and defined as

$$G_r = \int_0^{\lambda_0} \eta(\lambda)\epsilon_{BG}(\lambda, T_{BG}) \frac{2\pi c}{\lambda^4} [e^{ch/\lambda k T_{BG}} - 1]^{-1} \, d\lambda \tag{1}$$

and

$$\eta(\lambda) = \frac{F\alpha T_W A(1-R)(1-e^{-\alpha\chi})}{1-Re^{-\alpha\chi}} \tag{2}$$

where F is rate of incident photons for restricted aperture/rate of incident photons for 2π steradian aperture;

T_W, transmittance of the window;

* For a review of the experimental and theoretical situation of field effects in germanium, see Ref. 3.

Table 1. *Copper concentration, Hall mobility, resistivity and residual donor concentration. All measurements at* 300°K

Sample	Diffusion temperature (°C)	Copper concentration ($\times 10^{15}$ cm^{-3})	μ_H (cm^2/V/sec)	ρ (Ω/cm)	Residual donors ($\times 10^{13}$ cm^{-3})
4A	700	1·7	2900	1·3	5·5
4C	725	3·3	2600	0·72	5·5
5A	750	5·3	2400	0·49	6·9
5C	775	7·5	2400	0·35	6·9
6C	825	14·0	2000	0·22	7·0

R, reflection coefficient;
α, absorption coefficient for photons giving rise to impurity ionization based on Ref. 4 was taken as 5×10^{-16} cm^2, multiplied by the copper concentration;
x, length of sample;
A, area of sample;
T_{BG}, temperature of background;
$\epsilon_{BG}(\lambda, T)$, emissivity of background; and
λ_0, long wavelength cutoff of photons capable of ionizing 0·04 eV copper level.

For the dark measurements the samples were shielded from radiation by a liquid helium temperature cap. All samples were approximately 2 mm cubes, and current flow was perpendicular to incident radiation.

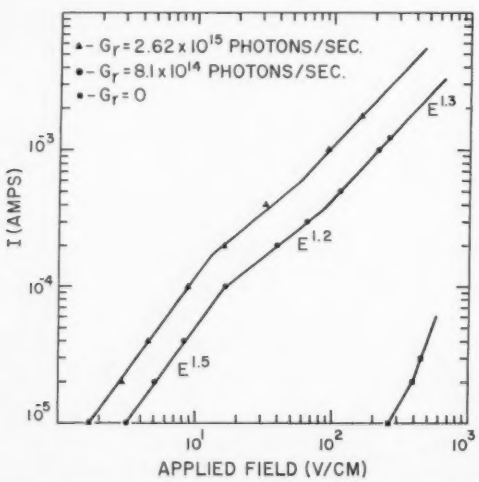

FIG. 1. Current vs. applied electric field. Sample 4A.

Detailed features of the d.c. I vs. E curves for low copper concentrations, ($< 2 \times 10^{15}$ cm^{-3}), are given in Fig. 1. No current breakdown takes place for fields as high as 200 V/cm for the light measurements. Only a few points were taken in the dark condition; however, the current starts into breakdown at 400 V/cm. There are three different field dependencies of current with no ohmic behavior observed for even the lowest fields considered.

Figure 2 illustrates the IE behavior for higher copper concentrations. ($> 7 \times 10^{15}$ cm^{-3}). It

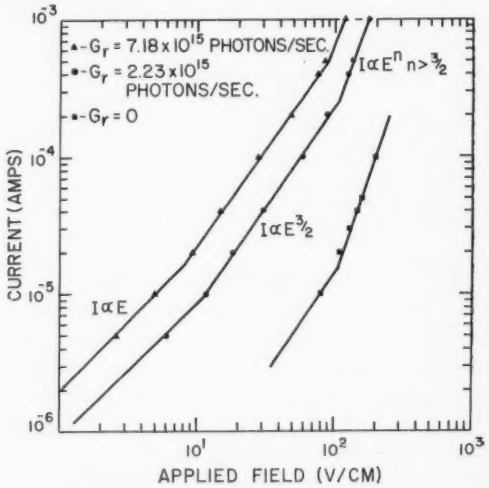

FIG. 2. Current vs. applied electric field. Sample 5C.

should be noted that the change in G_r from sample 4A to sample 5C is due only to the change in absorption coefficient, since identical background restricting apertures were used for all samples.

Vol. 22
1961

Again, three distinct regions are observed. At low fields, i.e. under 7 V/cm, the sample appears ohmic, with the current becoming at intermediate fields dependent on $E^{3/2}$ and at 100 V/cm proportional to E^n, with ~ 2. Mention should be made of possible thermal effects on the shape of the *IE* curves. If the hole concentration at constant field is assumed to be proportional to current, the curves indicate that the carrier concentration in the light condition is at least an order of magnitude greater than that at thermal equilibrium (dark case). Thus, the measurements made under light conditions involve optically rather than thermally generated carriers.

In summary, all samples exhibit three regions of current behavior with applied field in the field region explored. The current behavior is independent of background radiation excitation rate in a given sample, but varies between samples depending on the copper concentration.

Hall and resistivity measurements

Hall coefficient and resistivity were measured at $\sim 5°$K. Hall mobility and carrier concentration were calculated using the normal Ohm's law based formulae, for two samples chosen to correspond with copper concentrations having distinctly different *IE* characteristics. While there is an obvious question of the validity of the ohmic assumption in the present case, the error introduced appears to be insufficient to explain the observed behavior. The Hall samples were mounted on a copper heat sink so that one edge was exposed to ambient radiation. The experimental condition of the *IE* and photoconductivity measurements was closely reproduced for the Hall measurements in respect to copper concentration. The background excitation rate was 2×10^{16} photons/sec for both samples.

Figure 3 shows the hole concentration for the two samples as a function of applied field. In both cases the concentration increases superlinearly with applied field. Note however, that the magnitude of carrier increase is less for the more lightly doped sample and, in fact, appears to level off at a field of about 30 V/cm.

Figure 4 shows the Hall mobility vs. applied electric field. For the lower copper concentration value, sample 4AH, mobility is constant up to 6 V/cm and then becomes proportional to $E^{-1/2}$.

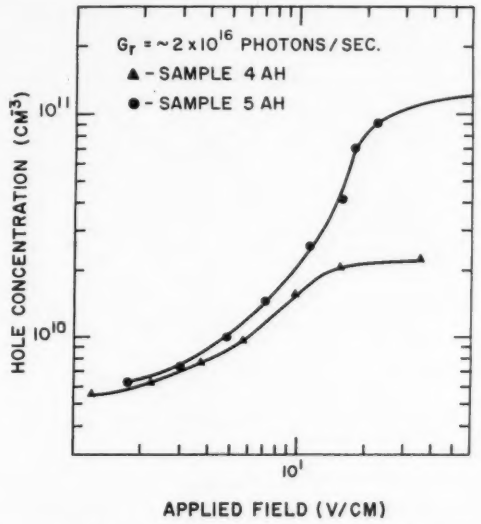

FIG. 3. Hole concentration vs. applied electric field.

Sample 5AH, with approximately 5 times the copper concentration, has a mobility which begins to deviate from a constant value at about 3 V/cm.

4. PHOTOCONDUCTIVITY MEASUREMENTS

Both blackbody photosignal and relative spectral response of the copper-doped germanium were measured with the samples at $\sim 5°$K. Figure 5 gives the relative spectral response of the 0·04 eV copper level in germanium. The data have been

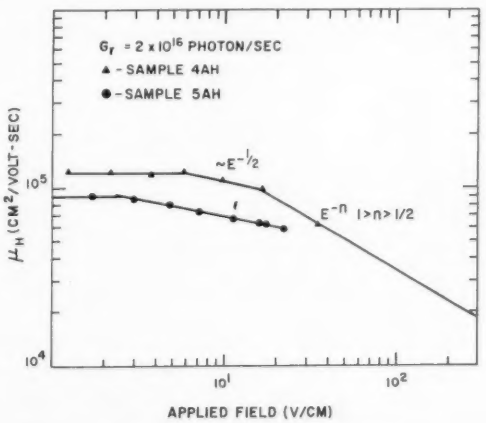

FIG. 4. Hall mobility vs. applied electric field.

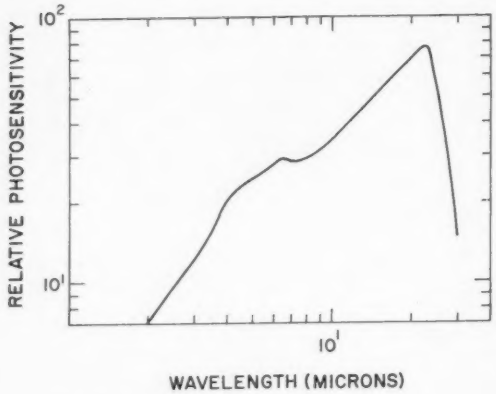

FIG. 5. Relative photosignal vs. wavelength.

smoothed but do correlate the 0·04 eV copper level.[4] The slight hump at 6·5 μ was present for all samples measured.

Dimensionless photosignal, I_s/I, and dimensionless noise, $I_n/I\Delta f^{1/2}$, were measured for the samples listed in Table 1. Mechanically chopped 500°K blackbody radiation was used to generate a small change, ΔR, in the sample resistance. The a.c. voltage appearing across a biased series load resistor may then be expressed as

$$V_s = IR_{ac}R_L/(R_{ac}+R_L)\,(\Delta R_{ac}/R_{ac})_s \qquad (3)$$

where R_L is load resistance and

R_{ac} is a.c. impedance of the sample given by

$$1/R_{ac} = 1/R_{dc}(1-V/R_{dc}\,dR_{dc}/dV) \qquad (4)$$

In terms of a constant current signal generator

$$I_s = I(\Delta R_{ac}/R_{ac})_s, \qquad (5)$$

$$I_s/I = (\Delta R_{ac}/R_{ac})_s \qquad (6)$$

Similarly, for the unit bandwidth noise when no signal radiation is incident

$$I_n/I\Delta f^{1/2} = (\Delta R_{ac}/R_{ac})_n\,1/\Delta f^{1/2} \qquad (7)$$

where Δf is noise bandwidth of the measurement equipment.

Figure 6 shows photosignal and noise vs. applied electric field with two different rates of background excitation. These data may be directly correlated with Fig. 1, since the measurements were made simultaneously. The ratios I_s/I and $I_n/I\Delta f^{1/2}$ are absolute in that all circuit parameters have been removed. G_s relates to the theoretical amount of signal radiation absorbed by the sample and is given by

$$G_s = \frac{1}{F}$$

$$\times \int_0^{\lambda_0} \eta(\lambda)\epsilon_{BB}(\lambda,T_{BB})\,\frac{2\pi c}{\lambda^4}\,[e^{ch/\lambda kT_{BB}}-1]^{-1}\,d\lambda \qquad (8)$$

where ϵ_{BB} is emissivity of blackbody and T_{BB}, temperature of blackbody.

For all copper concentrations photosignal is essentially constant with field; however, the noise decreases with increasing field, approaching at high fields the value expected from the photon fluctuation present in the incident background radiation. The JOHNSON–NYQUIST noise component is essentially due to the series load resistor and is less by an order of magnitude than any of the measured values. The noise values given in Fig. 6 were taken at 1000 c/s, a relatively flat region of the noise frequency spectrum. $I_n/I\Delta f^{1/2}$ vs. frequency at high field is given in Fig. 7; this data is typical of that taken at all fields with $1/f$ noise becoming negligible at frequencies over 100 c/s.

There is interest in the effect of copper concentration on photosignal and noise. The notation $G_r F/_\eta$ in Fig. 8 is a measure of the photon flux density at the sample, and not of the number of photons absorbed. The points given in Fig. 8 summarize the photosignal and noise measurements made on all samples of Table 1 for two background excitation rates. The noise values were taken at an applied field of 50 V/cm and a frequency of 1000 c/s.

5. DISCUSSION

The experimental investigations have established the following.

(1) The current–voltage characteristic of copper (0·04 eV acceptor level) doped germanium is a non-ohmic bulk phenomenon. Samples having the heavier doping ($> 7\times10^{15}$/cm^3) showed apparent ohmic behavior for fields less than about 10 V/cm, when exposed to 300°K radiation. The current–applied field plots for various dopings are similar in that all display superlinear dependence

Vol. 2
1961

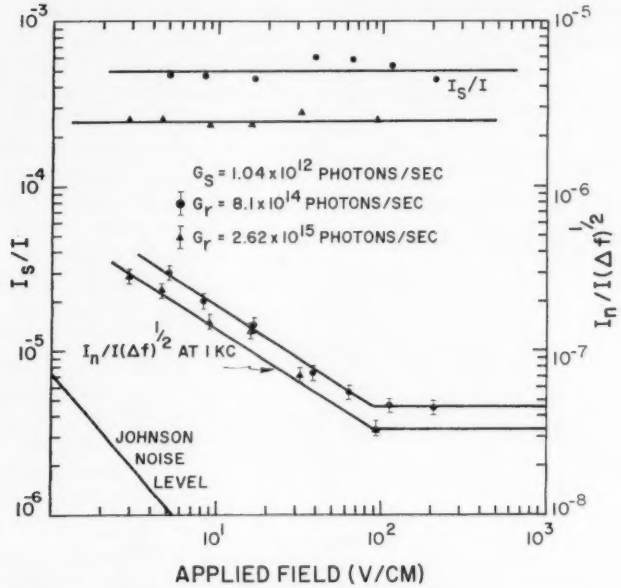

FIG. 6. Photosignal and noise vs. applied electric field. Sample 4A.

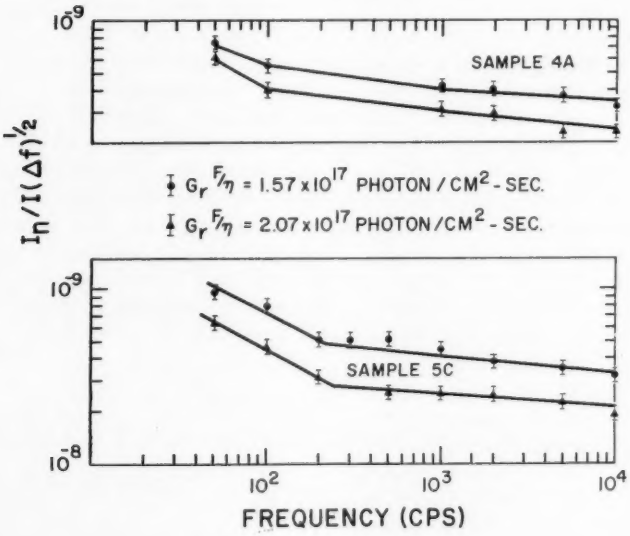

FIG. 7. Noise vs. frequency.

of current on field; however, the degree of dependence is not identical when the samples are exposed to 300°K radiation. Comparisons for the dark situation are not wholly conclusive; the data for higher fields appear to indicate similar behavior for the various dopings.

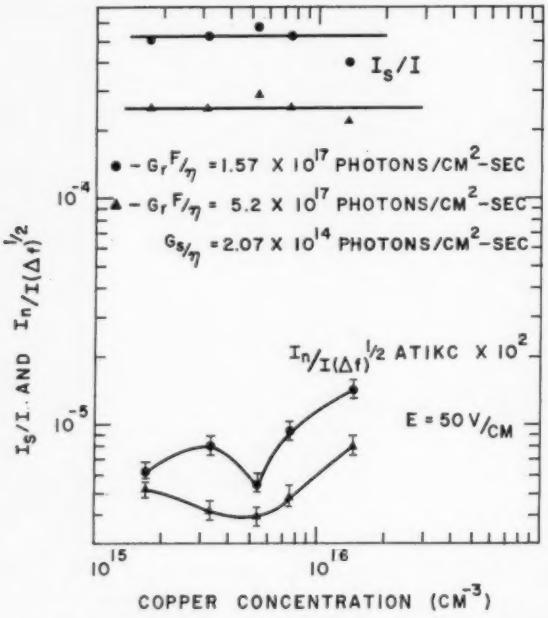

FIG. 8. Photosignal and noise vs. copper concentration.

(2) Hall data indicate apparent carrier multiplication does occur with increasing field. The effect is greater in the more heavily doped samples. Deviations in derived Hall mobility also occur, the mobility decreasing with increasing field.

(3) Dimensionless photosignal (fractional change in conductance for small irradiance) is constant with applied field. Dimensionless noise, expressed similarly, shows a contrasting behavior, decreasing approximately as E^{-n} ($\frac{1}{2} < n < 1$) for low fields. As a lower limit, at high fields the noise approaches the value dictated by photon fluctuations in the incident radiation. The measured noise in all cases was greater by at least an order of magnitude than the JOHNSON–NYQUIST component.

Several points merit detailed discussion. The apparent ohmicity of the heavier doped samples at fields less than 10 V/cm is only apparent; reference to the Hall data indicates that the effects of a decreasing mobility and a carrier multiplication process tend to offset each other in this field region. Mobility is constant for low fields for the more lightly doped samples, and as a result, the consequences of carrier multiplication are immediately exhibited by the current–applied field characteristic. Examination of the Hall data indicates that at fields below 10 V/cm, the carrier multiplication process is very similar for both sample types. At higher fields the effects of carrier multiplication are more pronounced for heavier doping.

We are not prepared, at present, to present a model for the non-ohmic behavior of copper-doped germanium but would like to mention several factors which require consideration before a mechanism could be established. First, the weighting of the Boltzmann factor is equivalent to that received by a 1·5–3 eV band-gap semiconductor at room temperature. Since space charge effects are common in this type of insulating semiconductor, they should receive consideration in the present instance. Note, however, that because of the high mobilities, resistivities for the copper-doped germanium are orders of magnitude less than for insulating semiconductors. Second, carrier lifetime, as estimated from carrier concentrations in radiation exposed samples at low fields, is approximately 10^{-8} sec. The dielectric relaxation time at zero field is one order of magnitude greater, or about 10^{-7} sec. For our samples, the transit time becomes equal to the zero field dielectric relaxation time at a field of about 50 V/cm. Third, whatever the process involved in the non-linear current–voltage characteristic of copper-doped germanium it must account for the decrease in noise with increasing field. Particularly, it must account for a non-JOHNSON–NYQUIST white noise that is well over an order of magnitude greater than generation–recombination noise induced by the radiation field at lower electric fields, but which approaches this limiting noise at higher electric field strengths.

Acknowledgements—Our thanks are due to Messrs. PAUL CUNNINGHAM and HOWARD BROWN for assistance with experimental measurements and sample preparation.

REFERENCES

1. PETRITZ R. L., *Photoconductivity Conference* (Edited by BRECKENRIDGE R. G.) p. 49. John Wiley, New York (1956).
2. VAN DER ZIEL A., *Physica* **19,** 749 (1953).
3. KOENIG S. H., *Advances in Semiconductor Science,* (Edited by BROOKS H.) p. 227. Pergamon Press, London (1959).
4. KAISER W. and FAN H. Y., *Phys. Rev.* **93,** 977 (1954).

Vol. 2
1961

J. Phys. Chem. Solids Pergamon Press 1961. Vol. 22, pp. 173–180. Printed in Great Britain.

PHOTO-HALL EFFECTS IN PHOTOCONDUCTORS*

R. H. BUBE, H. E. MACDONALD and J. BLANC

RCA Laboratories, Radio Corporation of America, Princeton, New Jersey

Abstract.—Measurements of Hall mobility as a function of light excitation intensity at room temperature have shown a dependence of Hall mobility on intensity in single crystals of CdS, CdSe, GaAs, InP, and Si. Such a variation of Hall mobility under photoexcitation can result either from (1) a change in the microscopic mobility for single-carrier conductivity, or (2) the initiation of two-carrier conductivity. The recognition of the existence of these effects through photo-Hall measurements is essential for the interpretation of photoelectronic measurements, since simple measurements of conductivity or photoconductivity usually fail to reveal them. Results involving a change in microscopic mobility through photoexcitation indicate a change in scattering associated with the neutralization of charge in centers with an effective scattering cross-section of about 10^{-10} cm^2. A number of other effects resulting from the initiation of two-carrier conductivity have also been explored.

INTRODUCTION

THE variation of Hall mobility with photoexcitation intensity has been previously reported for Ge and Si[1], CdS[2], and GaAs[3], when photoexcitation produces a change in the scattering by neutralization of charged centers. The variation of Hall mobility with photoexcitation which initiates two-carrier conductivity has been described for Ge and Si[4–6], CdS[2], and GaAs[3]. This paper summarizes results of this type and reports additional measurements which aid in the interpretation of the phenomena.

SCATTERING CROSS-SECTIONS

It has been previously pointed out[2] that the scattering cross-section of a Coulomb center is given to within a factor of order unity by the expression:

$$S = \frac{10^{-10} Z^2}{\epsilon^2} \left[\frac{300}{T}\right]^2 \text{cm}^2 \qquad (1)$$

where Z is the number of charges on the center and ϵ is the dielectric constant, regardless of whether the cross-section is calculated by simply equating the Coulomb energy to kT, from the Conwell–Weisskopf[7] equation for impurity scattering, or from the Brooks–Herring[8] equation for impurity scattering. At room temperature, therefore, with $\epsilon = 10$, $S = 10^{-12} Z^2$ cm^2.

SINGLE-CARRIER HALL EFFECT

When the conductivity is dominated by carriers of one type: the conductivity $\sigma = ne\mu$, where n is the density of free carriers, and μ their mobility; the Hall constant $R = K/ne$, where K is a constant between 1 and 2 depending on the scattering mechanism and the band structure; and the Hall mobility $\mu_H = \sigma R = K\mu$. The variation of Hall mobility with photoexcitation can be expressed:

$$\frac{d\mu_H}{dL} = \mu \frac{dK}{dL} + K \frac{d\mu}{dL}. \qquad (2)$$

The term involving the variation of K with L can be neglected for present purposes; not only is the variation less than a factor of 2 for complete changeover from impurity-dominated to phonon-dominated scattering[9], but the sign of the variation is in the wrong direction, i.e. K decreases with L under these conditions. The variation of μ with L can be illustrated by the simple case where photoexcitation raises the Fermi-level to fill positively charged centers and hence greatly reduce their scattering. Other related cases have been previously described.[2] The variation of μ

* The research reported in this paper was sponsored in part by the Office of Aerospace Research, United States Air Force.

with L can be derived from the relation:

$$\frac{1}{\mu} = \frac{300 m_e^*}{e}\left[\frac{1}{\tau_0} + v S_+ (N_+ - n_+)\right] \qquad (3)$$

where $300\, m_e^*/e$ is the proportionality factor between $1/\mu$ and $1/\tau$, τ being the time between scatterings, $v = (2kT/m_e^*)^{1/2}$ is the thermal velocity of an electron, S_+ is the scattering cross-section of the positively charged centers, N_+ is the density of imperfection centers, and n_+ is the density of electrons in imperfection centers. The proper form for the addition of mobilities is also dependent on the type of scattering dominant, but a change in this form with photoexcitation also cannot explain the observed variation of mobility, since the maximum correction factor is about 30 per cent.[9,10]

The first term on the right of equation (3) includes all scattering processes not involved in the motion of the Fermi-level through the levels described by the second term. The variation of the second term as a function of the location of the Fermi-level is given by:

$$(N_+ - n_+) = \frac{N_+}{1 + 2\exp[(E_+ - E_{fn})/kT]} \qquad (4)$$

where E_+ is the energy difference between the bottom of the conduction band and the imperfection level, and E_{fn} is the energy difference between the bottom of the conduction band and the electron Fermi-level, both positive quantities. As E_{fn} varies from much greater than E_+ to much less than E_+, $1/\mu$ passes through a single "step". The change in $1/\mu$ in this step, $\Delta(1/\mu)$, is given from equation (3) by:

$$\Delta(1/\mu) = 10^4 m_e^{*1/2} T^{1/2} S_+ N_+ \qquad (5)$$

From the variation of $1/\mu$ with E_{fn}, it is therefore possible to determine both the energy level of the scattering centers and the product of scattering cross-section and density. If the value of N_+ can be determined independently, as by knowing the density of impurities present or from the analysis of thermally stimulated current curves, a value for S_+ can be calculated.*

* Since both electrons and holes are generated by photoexcitation, the cross-section calculated corresponds to the net change in scattering caused by the capture of both electrons and holes.

TWO-CARRIER HALL EFFECT

When both carriers are making an appreciable contribution to the conductivity, the measured Hall constant R is given by:

$$R = \frac{p\mu_p^2 - n\mu_n^2}{e(p\mu_p + n\mu_n)^2} \qquad (6)$$

if we assume, as we do in the rest of this paper, that the appropriate K's may be taken equal to unity. Since for two-carrier conductivity, $\sigma = pe\mu_p + ne\mu_n$, the Hall mobility $\mu_H = \sigma R$ is given by:

$$\mu_H = \frac{p\mu_p^2 - n\mu_n^2}{p\mu_p + n\mu_n}. \qquad (7)$$

Thus μ_H goes to zero when $p\mu_p^2 = n\mu_n^2$, with R changing sign as this point is traversed.

PHOTO-HALL EFFECTS IN GALLIUM ARSENIDE

A variety of single carrier and two-carrier effects have been observed through measurements of photo-Hall effect in high-resistivity GaAs.[3,11] Fig. 1(a) shows a typical single step in $1/\mu_H$ as a function of Fermi-level position, as varied by photoexcitation, for a sample of n-type GaAs. It is shown that the experimental points can be fitted with a calculated curve derived from equations (3) and (4), if values of τ_0 and S_+N_+ are chosen properly. The value of E_+ obtained from Fig. 1(a) agrees within 0·01 eV with the value determined for a trapping level in the same sample by measurements of thermally stimulated current. Knowing the trap density from the thermally stimulated current data, a value for S_+ of 3×10^{-11} cm^2 is calculated. The data for this crystal (GaAs 58) and other crystals of CdS, CdSe, and InP are summarized in Table 1.

If band-gap radiation is used to excite high-resistivity p-type GaAs, it might be expected that a change in sign of R would occur with increasing excitation intensity, because of the higher electron mobility. Such effects have been measured and are shown in Fig. 1(c). If, however, there are many deep electron traps in p-type GaAs, band-gap radiation may merely serve to increase the hole mobility with no change in the sign of R; photo-excited electrons are trapped and remove the charge of the trapping centers. Effects of this

Vol. 2
1961

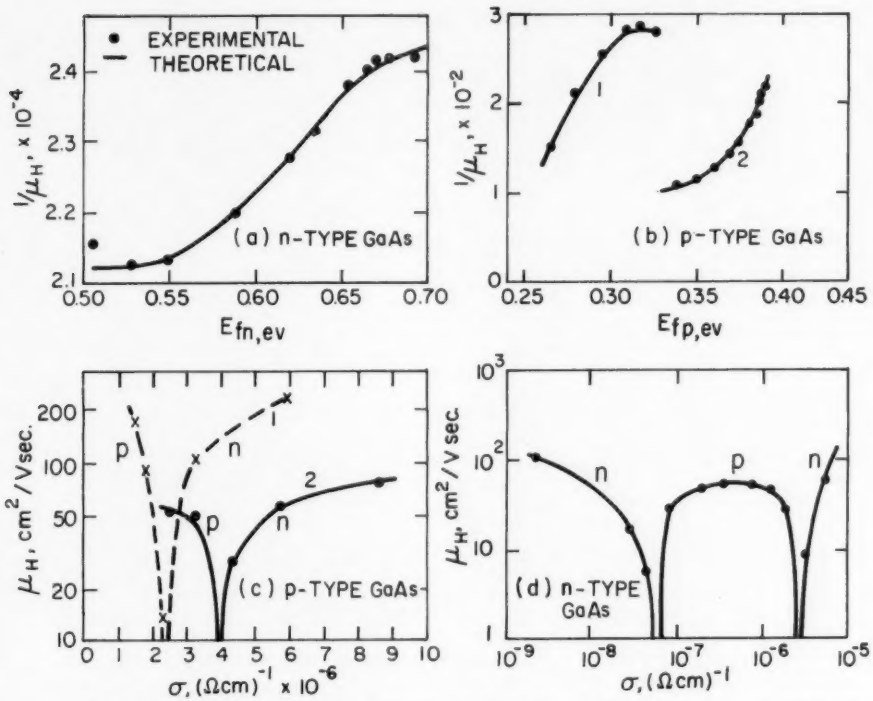

FIG. 1. Photo-Hall effects in GaAs crystals. (a) $1/\mu_H$ as a function of E_{fn}, as varied by photoexcitation, in n-type GaAs. Experimental points are compared with theoretical curve calculated from equations (3) and (4), with scattering cross-section of 3×10^{-11} cm^2. (b) $1/\mu_H$ as a function of E_{fp}, as varied by photoexcitation, in p-type GaAs containing a high density of electron traps. (c) Change in conductivity type caused by photoexcitation of p-type GaAs. (d) Double reversal of conductivity type caused by photoexcitation of n-type GaAs containing a high density of electron traps unfilled in the dark.

type are shown for two different crystals in Fig. 1(b). Finally, if a crystal of high-resistivity n-type GaAs has a high density of electron traps lying above the Fermi-level in the dark, band-gap photoexcitation first shifts the conductivity to p-type as photo-excited electrons are trapped but photoexcited holes are free to conduct; finally as the intensity is increased still further to provide approximately equal densities of electrons and holes, the conductivity once more becomes n-type. Such an effect is illustrated in Fig. 1(d).

PHOTO-HALL EFFECTS IN CADMIUM SULFIDE

Photo-Hall effects similar to those shown in Fig. 1(a) for GaAs, are also common in CdS crystals. Fig. 2(a) shows such an effect in a typical crystal with indications of the maximum spread in the data for the four possible ways of calculating μ_H from probe voltages V_{34} and V_{56}, and Hall voltages V_{35} and V_{46}. No obvious effects from inhomogeneities in the crystal are detected. The same data are replotted as $1/\mu_H$ v. E_{fn} in Fig. 2(b). The actual variation of photocurrent Δi, carrier density n, and Hall mobility μ_H, with light intensity are indicated in Fig. 2(c). The energy level E_+ associated with the mobility change shown in Fig. 2(b) is 0·34 eV. The location of the Fermi-level for the break in the curves of Δi and n v. L from slopes near 0·8 to slopes near 0·4 is 0·32 eV. The change in the role of centers with levels at 0·34 eV from trapping centers to recombination centers as the Fermi-level rises through them, can account for the observed change in slope. At low lights we have positively charged electron traps which

Table 1. Summary of variation of Hall mobility with photoexcitation

Material	Crystal no.	σ Type	Type of $\Delta(1/\mu)$ v. E_{fn}: Complete step	Partial step*	Anomalous	Energy level, eV: From $\Delta(1/\mu)$	From thermally stimulated current	$\mu_{H]L}/\mu_{H]d}$	N_tS, cm^{-1}	N_t, cm^{-3}	S, cm^2
CdS	A	n	X			0·35	0·40	{2·7}	8×10^5	10^{15}	8×10^{-10}
			X			0·46	0·46		6×10^5	3×10^{15}	2×10^{-10}
			X			0·54	0·55		5×10^5	3×10^{15}	2×10^{-10}
CdS	α	n	X			0·34		1·9	$1{\cdot}5\times10^6$		
CdS	EP	n	X			0·43		1·2	3×10^5		
CdS	β	n	X			0·35		3·3	$1{\cdot}4\times10^6$		
CdS	1121	n	X			0·47		{2·4}	4×10^5		
				X		~0·53			~3×10^6		
CdSe	A	n			X			16			
CdSe	65C	n			X			27			
GaAs	52T	n	X			0·51	0·56	{1·5}	2×10^5	10^{15}	2×10^{-10}
			X			0·61	0·65		6×10^4	10^{16}	5×10^{-12}
GaAs	52–2	n		X		~0·64	0·67	2·9	2×10^6	6×10^{16}	3×10^{-11}
GaAs	58	n	X			0·60	0·61	1·1	2×10^4	6×10^{14}	3×10^{-11}
GaAs	57–2	n		X		~0·53	0·51, 0·62	3·5	2×10^6	10^{16}	2×10^{-10}
GaAs:Cu	631–1	n			X			34			
GaAs:Cu	52–3A	p		X		~0·51		1·4	6×10^6		
GaAs:Cu	47	p		X		~0·27		1·8	10^7		
InP:Cu	340–1	n			X			13			

* In certain cases, the measured range was sufficient to reveal only part of the step. The N_tS product was estimated from the slope of the rising portion of the step.

scatter effectively, whereas at high lights we have neutral centers which act as efficient recombination centers, decreasing the photosensitivity.

A variation of μ_H with L has also been observed for a CdS sintered layer, as shown in Fig. 3(a). Here a monotonic variation of μ_H is found with varying light intensity, instead of a "steep" variation as in single crystals. This is consistent with the observation that trap densities in sintered layers of CdS and CdSe are monotonic functions of trap depth.[12, 13]

The results of a measurement of μ_H during the process of infrared quenching in CdS are shown in Fig. 3(b).[2] A much larger decrease in μ_H results when the conductivity of the crystal is decreased by incerasing the intensity of incident infrared radiation in the presence of a fixed intensity of 5170 Å radiation, than when the conductivity is decreased by decreasing the intensity of the 5170 Å radiation alone. The additional decrease in μ_H is attributed to the effect of the holes freed by the infrared in the quenching process[14] in initiating two-carrier conductivity.

Vol. 22
1961

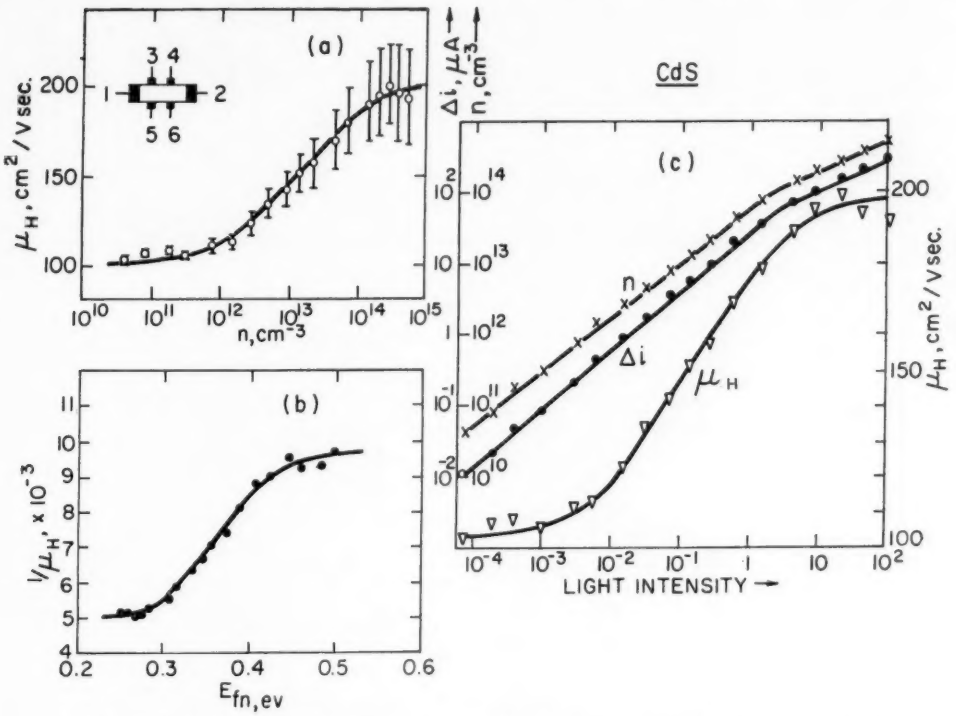

FIG. 2. Photo-Hall effects in CdS crystals. (a) Hall mobility as a function of electron density, as varied by photoexcitation. The dispersion around the indicated points shows the variation of the calculated μ_H depending on which set of probes are used to determine conductivity and Hall constant. (b) Data of (a) plotted as $1/\mu_H$ as a function of E_{fn}. (c) Dependence of photocurrent Δi, electron density n, and Hall mobility μ_H, on light intensity, for the same sample as (a) and (b).

PHOTO-HALL EFFECTS IN SILICON

Measurements on a high-resistivity p-type Si crystal at room temperature are summarized in Figs. 3(c) and 3(d). The contacts (indium) on the crystal were such that carrier injection occurred with one direction of applied field and therefore the sign of R changed with increasing field as electrons were injected, as shown in Fig. 3(c). On the other hand, if the applied field were kept small to minimize injection effects or if the field were applied in the opposite direction, the sign of R could be observed to change upon photo-excitation as shown in Fig. 3(d), because the electron mobility is higher than the hole mobility. A good fit can be made to the curve of Fig. 3(c) by combining the excess injected current data with the Hall data.

The value of μ_H in high-resistivity n-type Si crystals decreases under photoexcitation, as indicated in Fig. 3(e). This decrease probably results from the change of μ_H from μ_n in the dark to the intrinsic μ under equal electron and hole densities.

ANOMALOUS PHOTO-HALL EFFECTS

Figure 4 shows two cases of a much larger variation of Hall mobility with photoexcitation intensity, as has been occasionally measured. Whereas the variation in Hall mobility is generally not more than a factor of 3 for crystals exhibiting a single step in μ_H v. L, the Hall mobility in these crystals of CdSe and InP varies by factors as high as 30 with photoexcitation (see column 9 of Table 1). The data of Fig. 4 indicate that the variations observed are not particularly affected by

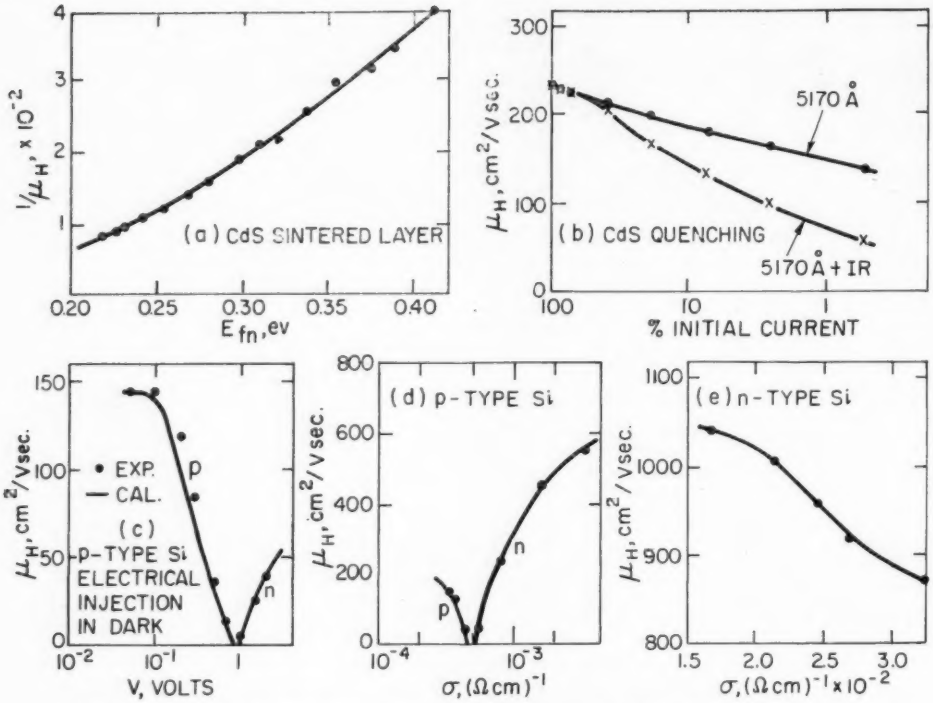

FIG. 3. (a) $1/\mu_H$ as a function of E_{fn}, as varied by photoexcitation, for a sintered layer of CdS. (b) Hall mobility as a function of the per cent of initial current remaining, both as the current is decreased by decreasing the intensity of 5170 Å radiation alone, and as the current is decreased by increasing the intensity of infrared radiation at fixed 5170 Å radiation. (c) Change in conductivity type caused in high-resistivity *p*-type Si by electrical injection of electrons in the dark; electrode spacing was 0·5 cm. (d) Change in conductivity type caused in high-resistivity *p*-type Si by optical excitation. (e) Dependence of μ_H on conductivity in high-resistivity *n*-type Si, as the conductivity is increased by photo-excitation, initiating two-carrier conductivity.

the wavelength of the light used, or by the particular portion of the crystal which is measured. It should be noted that measurements of Δi for the CdSe crystal of Fig. 4(a), for example, show a completely linear dependence on L over a whole range of the measurements, some five orders of magnitude of excitation intensity.

There is evidence of a correlation between crystal orientation in CdS and CdSe and the type of mobility variation with photoexcitation observed. For applied field perpendicular to the *c*-axis, a "step" variation is generally found; for applied field parallel to the *c*-axis an "anomalous" variation is generally found. It may be noted that the preferred orientation of dislocations in these materials is perpendicular to the *c*-axis.

DISCUSSION

The phenomena involving two-carrier conductivity effects seem to be reasonably well understood. On the other hand, for cases of single-carrier conductivity, the principal quantitative problem is the magnitude of the scattering cross-sections calculated from $\Delta(1/\mu_H)$ v. E_{fn} (see final column of Table 1), which is some two orders of magnitude greater than that expected for a Coulomb center with unit charge.

A number of consistent patterns in the data of Table 1 can be pointed out. (1) the mobility data point consistently to the same trap depths: 0·35, 0·45, and 0·54 eV in CdS; 0·51 and 0·61 eV in GaAs. These are the same levels which have been independently detected as donors, or as

Vol. 22
1961

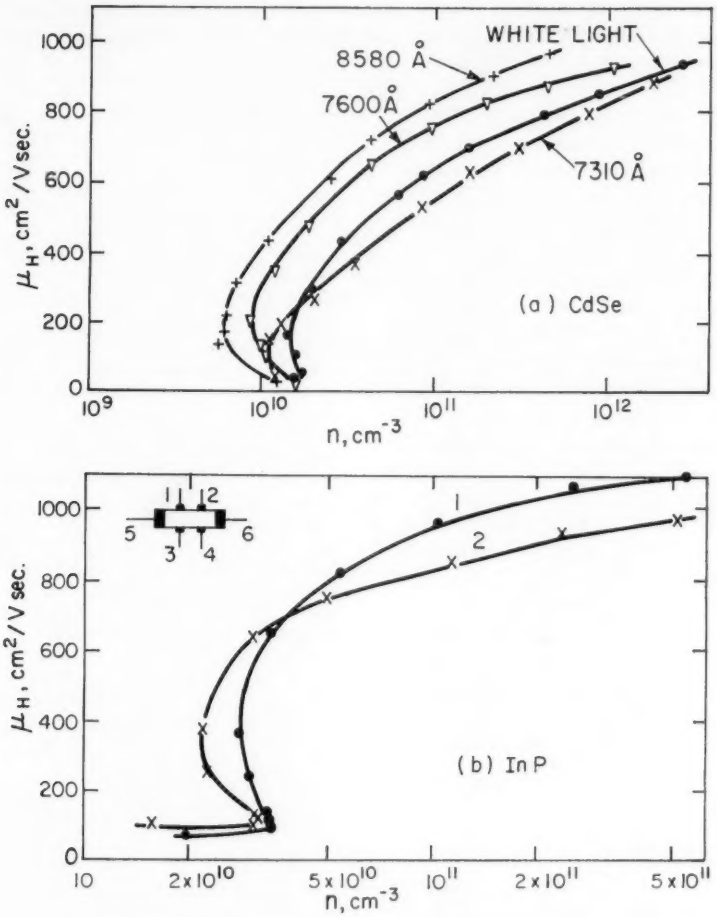

Fig. 4. Anomalously large variations of Hall mobility with photoexcitation. (a) Crystal of CdSe, excited with various wavelengths. (b) Crystal of InP, the two curves being for two ways of calculating the Hall mobility from the possible combinations of conductivity and Hall constant.

electron trapping centers when compensated. (2) Whenever check measurements on trap depth from thermally stimulated current have been possible, a close correlation has been found between the trap depth indicated by the mobility data and that indicated by the thermally stimulated current. (3) The product S_+N_+ lies between 10^5 to 10^7 cm^{-1}. For a Coulomb S_+ of 10^{-12} cm^2, this calls for values of N_+ between 10^{17} and 10^{19} cm^{-13}. Whenever the value of N_+ has been measured independently, it has been found to lie in the more reasonable range of 10^{15} to 10^{16} cm^{-3}. Such magnitudes of trap density have been confirmed by space-charge-limited current data on similar crystals. The evidence supports an effective S_+ of about 10^{-10} cm^2. (4) A comparison of data in Table 1 for crystals of GaAs, 52–2 and 58, show that measured trap densities and measured S_+N_+ products are exactly such as to give the same value for S_+, even though the trap densities are two orders of magnitude less in crystal 58 than in 52–2.

It has been shown experimentally that the effects observed are not detectably dependent upon wavelength of excitation, position of measuring contacts, surface effects, magnitude of applied electric field, or magnitude of applied magnetic field. The analysis of several models involving macroscopic inhomogeneities in the form of regions of different conductivity show that $\mu_H < \mu$ in the dark can be obtained only when the Hall constant is determined by measurement in a high-conductivity region and the conductivity is determined by current limitation by a low-conductivity region. In these cases, a variation of μ_H *and* R with L will occur only if the photosensitivity is somewhat higher in the high-conductivity regions than in the low, but by a factor less than the conductivity ratio. Even if this assumption is made, the shape of the resultant μ_H v. n curve calculated in a typical case does not give a "step" behavior.

The most likely explanation of the large scattering cross-sections observed is the existence of aggregates of charged centers, giving rise to space-charge regions in the crystal. The observation from Table 1 that $N_t S^{3/2} \geqslant 1$ in many cases indicates that such aggregates do not have spherical symmetry. This conclusion is consistent with the apparent effects of crystal orientation on the form of the mobility variation. Measurements of temperature dependence should provide critical data for further understanding of the phenomenon.

Acknowledgements—The authors are indebted to Drs. A. Rose, L. R. Weisberg and R. Williams for valuable discussions.

REFERENCES

1. Tyler W. W. and Woodbury H. H., *Phys. Rev.* **102,** 647 (1956).
2. Bube R. H. and MacDonald H. E., *Phys. Rev.* **121,** 473 (1961).
3. Blanc J., Bube R. H. and MacDonald H. E., *J. Appl. Phys.*, **32,** 1666 (1961).
4. Tyler W. W. and Newman R., *Phys. Rev.* **98,** 961 (1955).
5. Woodbury H. H. and Tyler W. W., *Phys. Rev.* **100,** 659 (1955).
6. Carlson R. O., *Phys. Rev.* **104,** 937 (1956).
7. Conwell E. and Weisskopf V. F., *Phys. Rev.* **77,** 388 (1950).
8. Brooks H. and Herring C., quoted by Debye P. P. and Conwell E. M., *Phys. Rev.* **93,** 693 (1953).
9. Johnson V. A. and Lark-Horovitz K., *Phys. Rev.* **82,** 977 (1951).
10. Debye P. P. and Conwell E. M., *Phys. Rev.* **93,** 693 (1953).
11. Bube R. H., *J. Appl. Phys.* **31,** 315 (1960).
12. DeVore H. B., *RCA Rev.* **20,** 79 (1959).
13. Bube R. H., *J. Appl. Phys.* **32,** 1621 (1961).
14. Bube R. H., *Phys. Rev.* **99,** 1105 (1955).

J. Phys. Chem. Solids Pergamon Press 1961. Vol. 22, pp. 181–188. Printed in Great Britain.

PHOTO-HALL EFFECT IN CdSe SINTERED PHOTOCONDUCTORS

A. B. FOWLER

IBM Research Center, Yorktown Heights, New York

Abstract.—Measurements of the photo-Hall effect in sintered layers of CdSe were made. The mobility was found to vary as the 0·15 to the 0·49 power of the density of carriers per unit area depending on the sample and the temperature. Measurements of the mobility as a function of wave length indicate that the carriers do not appreciably diffuse away from the surface and there is evidence that some of the decrease of the photoresponse on the short wave length side of the absorption edge is due to a change in mobility, possibly resulting from surface scattering.

INTRODUCTION

IT HAS been proposed in the past by many workers that the effective mobility of charge carriers in polycrystalline photoconductors may vary with illuminating intensity if the conductivity is limited by intergranular barriers and if the height of these barriers is modulated by the light. PETRITZ[1] has proposed a model in which the current through the barrier is treated as a diode current and after simplication for the case of small fields across the barrier the effective mobility is given by

$$\mu_b^* = \frac{M}{NkT} \exp\left(\frac{-e\phi}{kT}\right)$$

where M is a transmission parameter, N is the density of particles per unit length, and ϕ is the barrier height. Thus if illumination depresses the barrier, an increase in mobility could result up to the point that the barriers are completely depressed and the mobility limited only by scattering within the particles. The variation of ϕ with illumination might be expected to depend on the nature of the barrier—that is on whether it is an oxide layer or an inverted region resulting from a high density of acceptor or donor states at the particle interfaces. If the latter were the case, the light dependence of the barrier height would depend on the nature of the interface states and also on the kinetics of recombination within the particle. The electron and hole cross-sections, energy levels, and densities of both particle and interparticle states would govern the dependence of the barrier height in a rather complicated way.

The effect of barrier modulation might be expected to disappear in samples subjected to voltages high enough to "wash out" the barriers as in the case reported by BUBE[5] for powders. However, at such voltages where the true particle mobility might be expected to be seen, heating of the carriers and other thermal effects would complicate the results. In measurements, it is necessary to be careful that the applied voltages are low enough so that the current-voltage characteristics are linear.

In fact no dependence of mobility on illumination was found by WOODS[2] or by SNOWDEN and PORTIS[3] who confirmed Woods' result in PbS. Dependence of mobility on illumination has been found in several materials in single crystals including CdS and CdSe by BUBE and MACDONALD[4]. This effect results however from the filling of ionized impurity scattering centers. It is quite possible that such an effect could occur in sintered layers as well. However, if such were the case, a series of plateaus, perhaps smeared out, should be observed as they are in the single crystals.

EXPERIMENTAL TECHNIQUES

Hall measurements were carried out on sintered layers of CdSe deposited on alundum plates and doped with 100 p.p.m. of copper. The samples measured 8×3 mm and were about 60 μ thick.

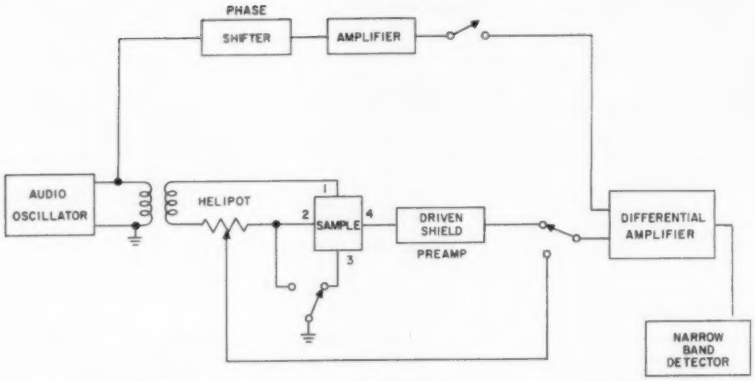

FIG. 1. Measuring circuit for a.c. Van der Pauw measurements. The circuit is shown for measurement of R_{1234}. The switches for R_{2314} and R_{1324} are not shown.

The particles were about 10–20 μ in their largest dimension. Four electrodes were made with an indium amalgam as near the center of each edge as possible. VAN DER PAUW[6] has shown that the resistivity of a sample of uniform thickness is given by

$$\rho = \frac{\pi(R_{1234}+R_{2341})df}{2 \ln 2}$$

where R_{1234} is the ratio of the voltage across terminals 3 and 4 to the current passed through terminals 1 and 2, R_{2341} is a similar ratio with the leads permuted, d is the thickness of the sample, and f is a correction factor equal to one if R_{1234} is equal to R_{2341}. The Hall mobility, $\mu_H = R\sigma$, is given by

$$\mu = \frac{2 \ln 2}{\pi} \frac{\Delta R_{1324} 10^8}{(R_{1234}+R_{2341})H}$$

where ΔR_{1324} is the change in R_{1324}, defined in a manner similar to the above when a magnetic field, H, is applied. As d is not known in general in photo-Hall effect measurements, the resistivity may not be determined but ρ/d or σd may. The latter is proportional to a surface density (charge density/unit area), of charge v, and because the mobility is known to within the factor of the ratio, r, of the Hall to the conductivity mobility v may be determined. Whether r is $3\pi/8$ or some other value is not known but it should be a constant at any given temperature and not vary much under any circumstances.

It was found convenient to use an a.c. variation of the Van der Pauw measurement although the results were checked with a d.c. technique. Most measurements were made at 20 c/s using the circuit shown in Fig. 1. The appropriate resistance, R_{ijkl}, was measured using a substitution method by setting the voltage drop across the Helipots equal to that across the appropriate electrodes. For Hall measurements, the IR drop across terminals 2 and 4 was bucked out using the phase shifter and amplifier. This system has the advantages of all a.c. Hall measurements, e.g. elimination of thermal effects and by use of a narrow band detector, reduction of noise—combined with rapidity of measurement, flexibility of electroding, and the possibility of the internal checks resulting from reciprocity relationships in the Van der Pauw method. It is however limited to samples with impedances of the order of 10^8 ohms or less by capacitive shorting of the sample.

The measurements were carried out in a Dewar under a vacuum of about 0·1 μ. Temperature was measured with a copper–constantan thermocouple pressed against the front face of the sample plate but not exposed to the illumination. The samples were illuminated with a tungsten source through a grating monochromator. No exact measurement of the light intensity was made but a rough calibration was made using a Hoffman silicon photocell. The light intensity was varied by using calibrated neutral screen filters.

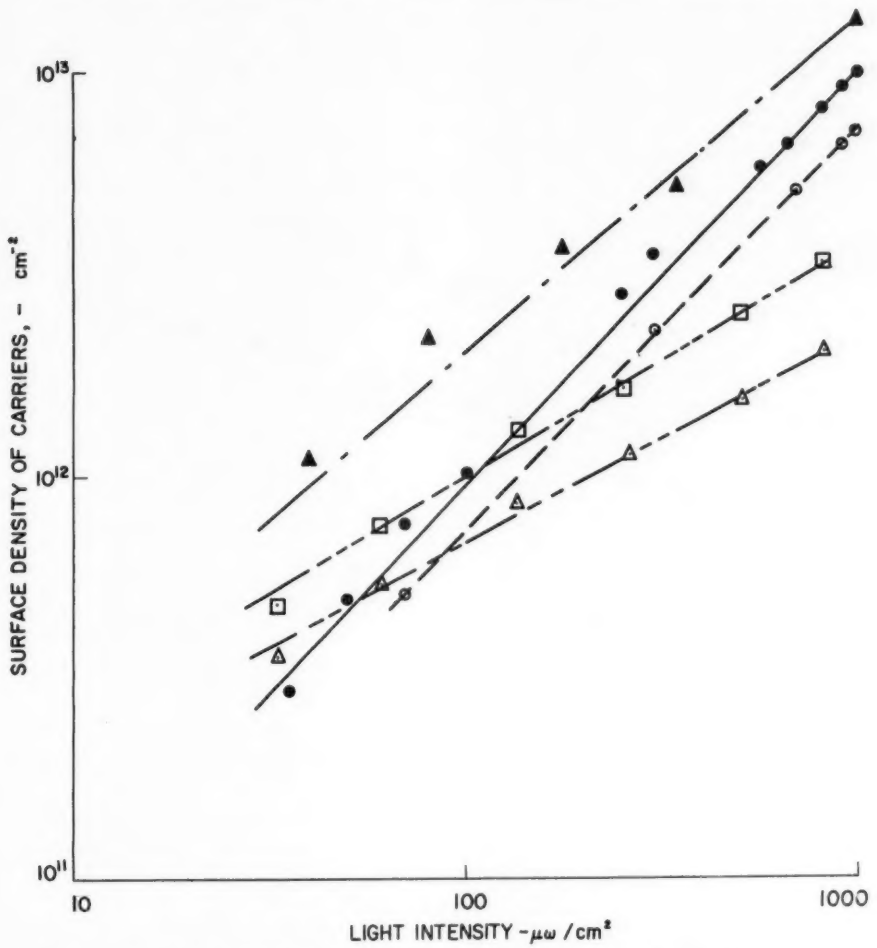

FIG. 2. Dependence of surface density of carriers on light intensity for sample 738–7 at different temperatures. ● 294°K, ○ 308°K, ▲ 208°K, △ 104°K, □ 165°K.

OBSERVATIONS

Measurements in each sample were found to be reproducible, but wide variation was found from sample to sample. In all measurements here described voltages were kept low enough so that no nonlinear effects were seen. Checks were made for the internal consistency of the Van der Pauw relationships and the data presented were satisfactory. Dependence on frequency within the range of 10 to 200 c/s was not found. In all samples studied the principal current carriers were electrons.

Of the samples studied two representative ones will be discussed in some detail. The first, 738–7, was studied in a region where the conductance depended in a superlinear fashion on the illuminating intensity. The second, 738–79, was sublinear.

In Figs. 2 and 3 the dependence of the surface density of carriers, v, on intensity, L, and of the Hall mobility on the carrier density are shown for sample 738–7. It may be seen that at room temperature the carrier density was directly proportional to the light intensity, which means that the free carrier lifetime, τ, was constant

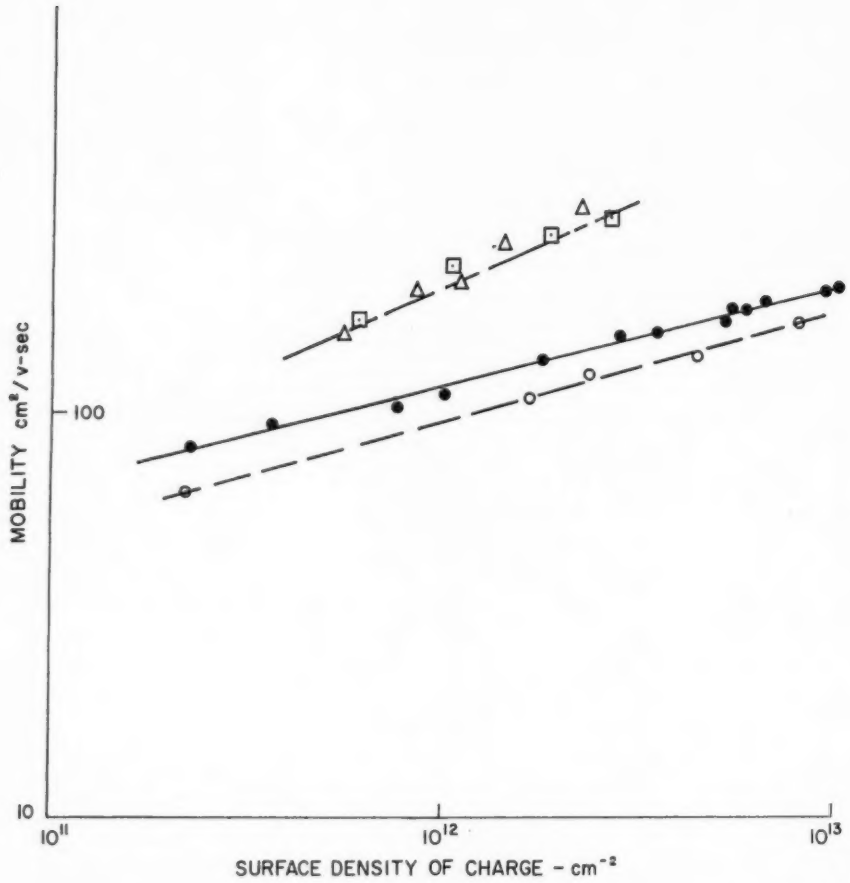

FIG. 3. Dependence of mobility on carrier density, sample 738–7. ● 294°K, ○ 308°K, △ 104°K, □ 165°K.

(about 3 msec). However, the mobility was proportional to the 0·15 power of the number of carriers. Therefore, the conductance varied as the 1·25 power of the intensity. In this sample the superlinear behaviour arose only from the mobility variation. At 308°K both the lifetime and mobility dropped by about 20 per cent but the dependences remained the same. At 208°K the dependences were still about the same but the lifetime was 2·5 times as large as at room temperature and the mobility was somewhat higher. In the range of temperatures from 104°K to 165°K the sample was no longer linear with intensity, at least at the higher light intensities. There is an indication that the response was becoming more linear in the lower intensity range at 165°K. The mobility was not temperature-dependent in this lower range but was higher than at room temperature and depended on carrier density as the 0·45 power rather than the 0·25 power.

The results on sample 738–79 are shown in Figs. 4 and 5. This sample was sublinear at room temperature. The carrier density varied as the 0·61 power of the light intensity in the temperature range 20–36°C. Little temperature dependence was observed in this sample. The mobility

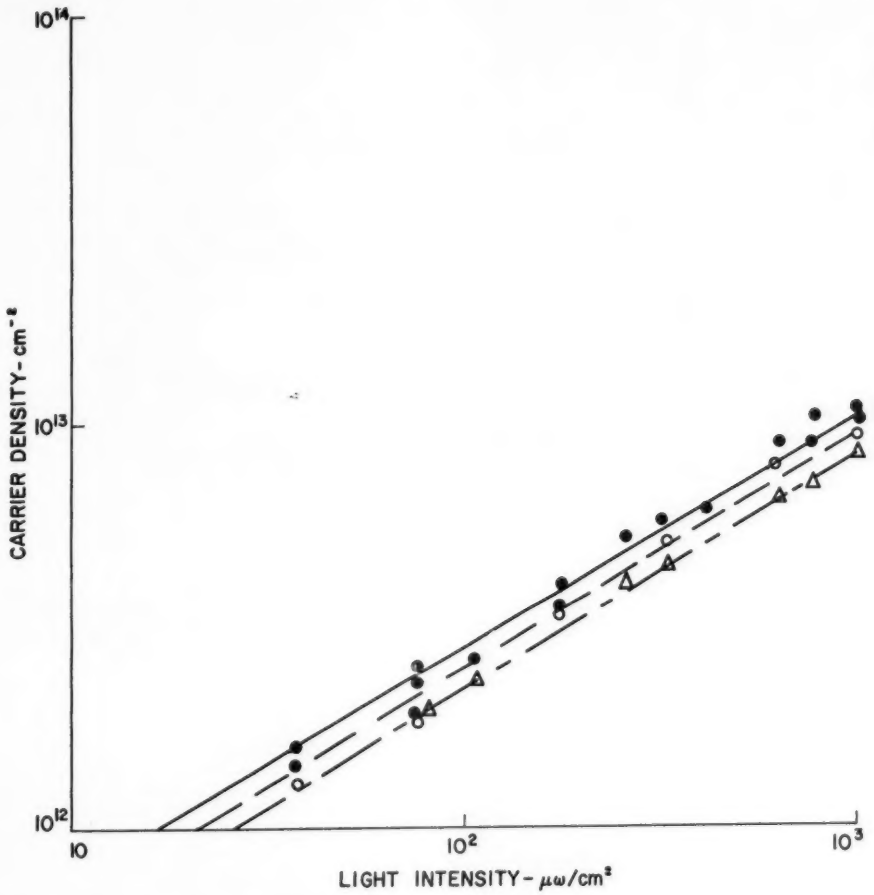

FIG. 4. Dependence of carrier density on light intensity, sample 738–79. ● 20·5°C, ○ 30°C, ▲ 36°C.

dependence was lower than in sample 738–7. The mobility depended on the 0·16 power of the carrier density so that the conductance depended on the 0·71 power of the light intensity.

In several samples where the lifetime was a constant the response went through a maximum somewhat below room temperature and fell by a factor of about 4 at 60°C. The mobility in general increased as the temperature was lowered and furthermore the dependence of mobility on carrier density increased at lower temperatures. For instance in one sample the mobility at a given carrier density decreased from 60 cm^2/V sec at 1°C to 35 at 21°C to 28 at 45°C. The dependence of the mobility went from the 0·49 power to the 0·32 power to the 0·16 power at the same temperatures. Thus the variation of mobility with temperature depended on the carrier density, so that no temperature curves are given.

A dependence of mobility on the wave length of the exciting light was observed. Because the absorption constant, α, of the light varies with wave length the effective thickness, d, of the samples changes, and for a given surface density of carriers the volume density changes if there is no diffusion away from the surface. The actual

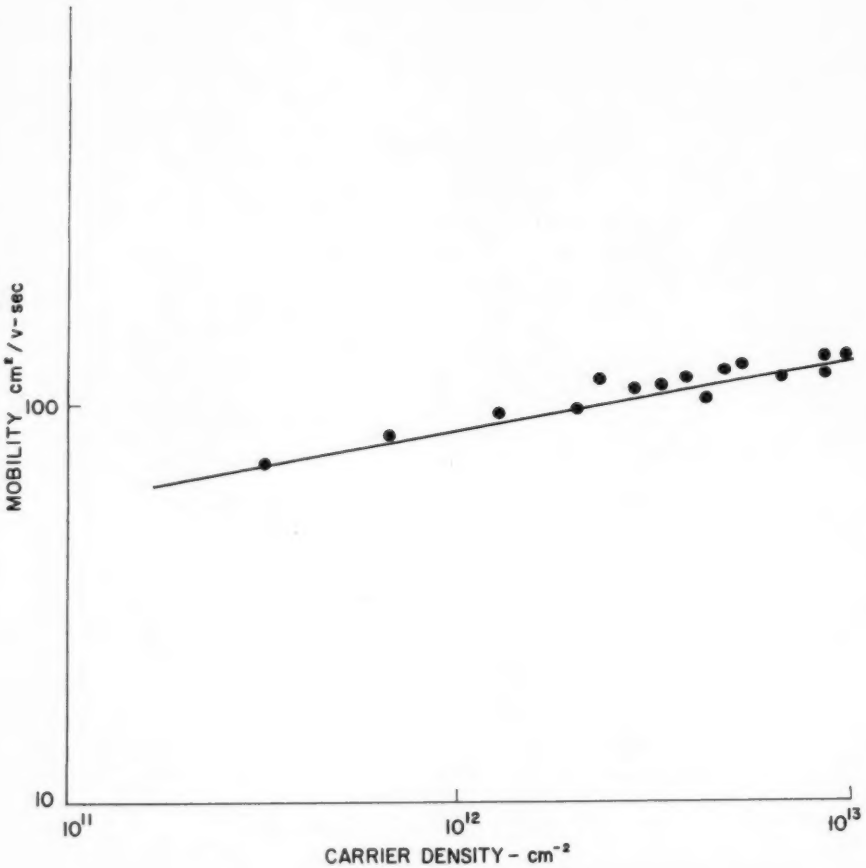

FIG. 5. Dependence of mobility on carrier density, sample 738–79. • 20·5°C.

relationship between the measured Hall voltage and the mobility is complex in such a case as the local Hall field varies from the front to the back of the sample and circulating currents must result. However, it may be argued that most of the Hall current is developed within an absorption length of the front surface so that the measured mobility should depend on the average bulk concentration in this region. Hence the mobility should vary as $(\alpha v)_p$, where p is the power of the dependence of mobility on density. Therefore for low values of α the measured mobility should be less than for high values. That this is the case may be seen in Fig. 6 where the mobility is plotted as a function of wave length in measurements where the conductance of the sample was held constant (μv = const.). The conclusions would be the same if the surface density had been held constant. The mobility may be seen to have decreased beyond the absorption edge as the above argument indicated it should. However, at short wave lengths there was also a decrease. This may have resulted from surface scattering. There there is little redistribution of the carriers away from the surface by diffusion is indicated, because if the diffusion length were of the order of the absorption length the above effects would disappear.

Vol. 22
1961

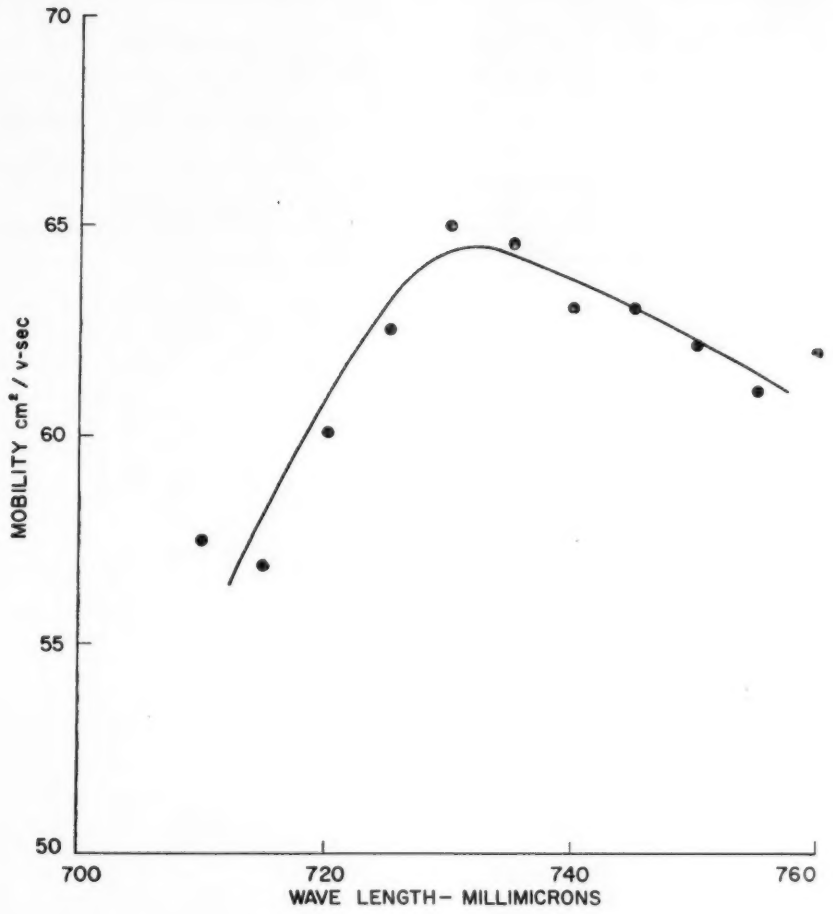

FIG. 6. Dependence of mobility on wave length for constant conductance ($v\eta$ = constant).

DISCUSSION

In all of the samples measured, the mobility was found to depend on carrier density. In sample 738–7 the response would have seemed super-linear if the conductance only had been measured. If an attempt had been made to interpret the recombination processes an error would have resulted. The generality of the finding of mobility variation calls into question any interpretation of the recombination kinetics in sintered layers in which the mobility has not been measured.

It has not been definitely established that the change in mobility results from barriers, but no other mechanism suggests itself. There is no evidence of plateaus in the variation of mobility with carrier density so a change of scattering by filling of ionized impurities does not seem likely. Petritz's factor, B, the ratio of the relative change in mobility to the change in carrier density took values from 0·15 to 0·49 in the samples studied. The mobility variation thus can represent a large contribution to photoconductive gain in some samples.

The significance of the measurement of mobility

as a function of wave length is that the observed variation offers an alternate cause of the decrease of photoconductivity on the short wave length side of the absorption edge to those previously proposed.

Acknowledgements—Finally, I should like to acknowledge the assistance of Mr. EUGENE TYNAN in these measurements, Mr. GEORGE CHEROFF *et al.* for providing samples, and Drs. E. STUPP, S. TRIEBWASSER, and S. P. KELLER for a critical reading of the manuscript and for helpful suggestions.

REFERENCES

1. PETRITZ R. L., *Phys. Rev.* **104,** 1508 (1956).
2. WOODS J. F., *Phys. Rev.* **106,** 235 (1957).
3. SNOWDEN D. P. and PORTIS A. M., *Phys. Rev.* **120,** 1983 (1960).
4. BUBE R. H. and MACDONALD H. E., *Phys. Rev.* **121,** 473 (1961).
5. BUBE R. H., *J. Appl. Phys.* **31,** 2239 (1960).
6. VAN DER PAUW L. J., *Philips Research Rpts.* **13,** 1 (1958).

Vol. 22
1961

J. Phys. Chem. Solids Pergamon Press 1961. Vol. 22, pp. 189–197. Printed in Great Britain.

THE ROLE OF INJECTING CONTACTS IN PHOTOCONDUCTORS

MURRAY A. LAMPERT

Radio Corporation of America, RCA Laboratories, Princeton, N. J.

Abstract—It is usually assumed that the only role of the "ohmic," i.e. injecting, contacts is that of supporting Ohm's law currents through the photoconductor. In actual fact the injecting contact plays a key role in limiting the available gain (G)–bandwidth ($1/\tau_0$) product of the photoconductor, through the agency of space-charge which is either injected and volume-distributed or spatially localized near the potential minimum at the contact. G/τ_0 has a limiting value M/τ_T where τ_T is the dielectric relaxation time under operating conditions and M is a dimensionless quantity determined by either the volume-distributed or contact-localized space charge.

Where the negative contact is injecting for electrons and the positive contact injecting for holes, two-carrier current flow in the insulator is supplied by the contacts. Double injection and photoconductivity are closely related in that the characteristics of both phenomena are governed by the same recombination centers. Double injection has been analyzed for an idealized insulator with a single set of recombination centers completely filled in thermal equilibrium. Outstanding results are: (i) a threshold voltage for the double injection, and (ii) a negative resistance associated with a hole lifetime which increases with injection level.

I. INTRODUCTION

AN OHMIC contact is by definition and tradition one that is experimentally invisible, i.e. one that plays no role in electrical measurements other than to permit the flow of Ohm's law currents corresponding to the *bulk* value of conductivity. On this account one might well wonder how there can be enough content in the subject to merit a published article. The point is that, in actuality, a so-called ohmic contact is generally an injecting contact, i.e. a contact which can inject excess carriers into the solid, thereby promoting non-ohmic current flow. Further, it is a remarkable fact that, even in the regime of (steady-state) Ohm's law currents, the ohmic contact can make itself felt experimentally, in transient phenomena, e.g. in the response time for photoconductivity.

In this paper we shall touch on two areas of problems. First we shall review earlier work by Dr. ROSE and the author, concerned with one-carrier or majority-carrier photocurrent flow. Here the significant physical parameter through which the injecting contact may exert an influence on photoconductivity is space charge. In steady-state photoconductivity the space charge in question is injected and volume distributed; in transient photoconductivity it may alternatively be spatially localized near the potential minimum at the contact. Then we shall discuss more recent work concerned with two-carrier, or double-injection, current flow in insulators. Here the important physical parameter is the free carrier lifetime—a parameter which is, of course, also central to photoconductivity.

The different kinds of contacts a metal can make to the conduction band of an insulator are illustrated by the schematic energy-band diagrams of Fig. 1. The left-hand diagrams correspond to thermal equilibrium. E_c denotes the bottom conduction band level, F the thermodynamic Fermi level. (There will also, of course, be numerous localized states in the forbidden gap. These are not shown on the diagrams.) The right-hand figures show the energy diagrams for the corresponding contacts with a voltage applied across the insulator, the polarity being such that the contact shown is negative. The top pair of diagrams represent the ohmic or injecting contact. At the contact, in the downward-bending region, is a reservoir of free electrons available for injection into the bulk

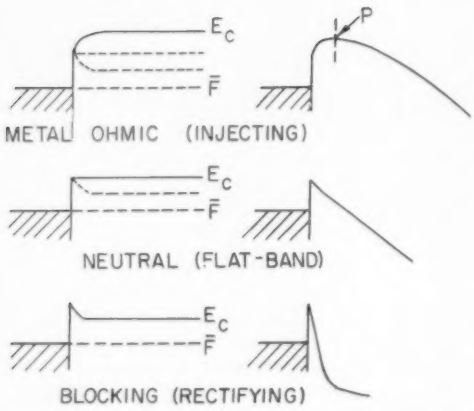

FIG. 1. Schematic energy-band diagrams illustrating the different types of contacts to the conduction band. The left-hand diagrams correspond to thermal equilibrium, the right-hand ones to an applied voltage.

of the insulator. At sufficient voltage this reservoir delivers a space-charge-limited, excess electron current into the conduction band—a fact of considerable importance for the later discussion. Under an applied voltage there is a potential minimum or energy maximum in the insulator near the contact interface, shown at position P in the upper-right figure. This is quite analogous to the famous potential minimum near the cathode of thermionic vacuum tubes operated under space-charge-limited conditions. For future reference we note that *all* excess electrons to the right of the energy maximum P, i.e. in the bulk of the insulator, are compensated by an equal number of positive charges on the anode contact, not shown in the figures. Also, when an electron leaves the insulator at the anode contact an electron will automatically enter the insulator at the cathode contact, a fact which makes possible high photoconductive gain. This last is also true of the neutral or flat-band contact, middle figures. With this kind of contact an applied voltage is ohmically distributed across the insulator, and only Ohm's law currents will flow—at least up to the point where temperature-limited, or saturated, current is drawn from the metal. This type of contact is not easy to come by experimentally. Finally, bottom figures, we have the blocking, or rectifying, contact. Here most of the applied voltage is localized at the contact. An electron leaving at the anode can no longer be replaced by injection at the cathode, and so, in the absence of contact breakdown, the photoconductive gain is limited to unity at most. It is important to recognize that under photoexcitation of the insulator the injecting contact may be converted into a neutral contact (straight dashed line in upper-left figure) or even a blocking contact (lower dashed line in upper-left figure); likewise the neutral contact may be converted into a blocking contact. Such effects have been observed experimentally.[1] Everything we have said about contacts to the conduction band applies equally well to contacts to the valence band, using the appropriate, complementary energy-band diagrams. For the remainder of this paper we restrict our discussion to injecting contacts.

II. MAJORITY-CARRIER PHOTOCONDUCTIVITY. THE GAIN-BANDWIDTH PRODUCT

In discussing one-carrier or majority-carrier photoconductivity we assume, for the sake of definiteness, that the current carriers are electrons. Photoconductive gain G is defined by: $G = \Delta I/eF$ where ΔI is the induced photocurrent and F is the absorbed light flux producing it. Since an electron leaving at the anode is replaced by an equivalent one entering at the cathode, G is also the number of transits a photo-excited electron makes in its lifetime, i.e.

$$G = \frac{\tau_l}{T'} \qquad \tau_l = \frac{\mathcal{N}}{F} \tag{1}$$

with τ_l the electron lifetime and T' its time of transit from cathode to anode. The second relation in (1) is the defining relation for $\tau_l, \mathcal{N}$ being the total number of photo-excited, free electrons.

There will generally be a much larger number of trapped electrons in quasi-thermal equilibrium with the free electrons. During the photoconductive rise the light must supply these trapped electrons as well as the free ones. Therefore the rise time τ_0 may be written as:

$$\tau_0 = \frac{\mathcal{N}_T}{F} \tag{2}$$

where $\mathcal{N}_T$ is the increment in the total number of photo-excited electrons, free plus trapped, accompanying an increase in the absorbed light flux

Vol. 2
1961

of amount F. Equation (2) may be regarded as a defining relation for $\mathcal{N}_T$. During the photoconductive decay the trapped, as well as free, electrons must get back to their states of origin. Therefore τ_0 is also the photoconductive decay time, and it is convenient to refer to τ_0 simply as the *response time*.

The computation of $\mathcal{N}_T$ is illustrated in the energy-band diagram of Fig. 2. F_n is the position of the steady-state, electron Fermi level corresponding to some definite light excitation (absorbed light flux F). Shown also are representative electron

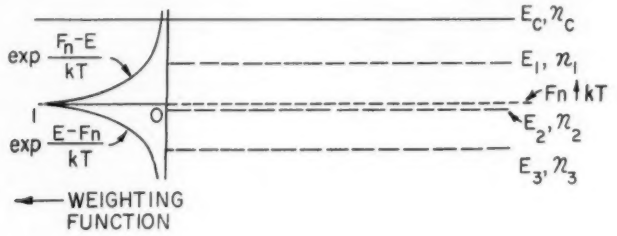

FIG. 2. Schematic diagram for the computation of $\mathcal{N}_T$.

trapping states of total number $\mathcal{N}_1$ at energy E_1 such that $E_1-F_n \gg$ kT, of number $\mathcal{N}_2$ at energy E_2 such that $|E_2-F_n| <$ kT, and of number $\mathcal{N}_3$ at energy E_3 such that $F_n-E_3 \gg$ kT. ($\mathcal{N}_c$ is the total effective number of conduction-band states.) All of these states are assumed to be in quasi-thermal equilibrium with the free electrons. $\mathcal{N}_T$, at the given level of photo-excitation, equals the change in the number of electrons in all of these states if we double the light excitation, and thereby move F_n up by approximately kT. The states at E_1, well above F_n, will double their occupancy. Hence their contribution to $\mathcal{N}_T$ equals $\mathcal{N}_1$ weighted by the Boltzmann factor $\exp(F_n-E_1)/kT$. States $\mathcal{N}_2$ at energy E_2 within kT of F_n change their occupancy from approximately empty to approximately full; hence they contribute approximately their full number $\mathcal{N}_2$ to $\mathcal{N}_T$. The only occupancy change possible in states $\mathcal{N}_3$ at energy E_3 well below F_n is that those few empty ones become filled with electrons. Hence their contribution to $\mathcal{N}_T$ equals $\mathcal{N}_3$ weighted by the hole-occupancy probability, again the Boltzmann factor $\exp(E_3-F_n)/kT$. Thus, to compute $\mathcal{N}_T$ we count up the number of electron traps, each set being multiplied by an appropriate weighting function which is strongly peaked at F_n, as illustrated by the plot at the left side of Fig. 2.

We proceed now to our goal, an evaluation of the gain-bandwidth product. The shortest time variation of excitation the photoconductor can follow is given by its response time τ_0. Correspondingly, the highest frequency of excitation it can follow is $1/\tau_0$, and it clearly can respond fully to all lower frequencies. Thus $1/\tau_0$ is also the bandwidth for the photoconductor response.

From (1) it then follows that the gain-bandwidth product may be written as: $G/\tau_0 = \tau_l/T'\tau_0$. From (1) and (2), $\tau_l/\tau_0 = \mathcal{N}/\mathcal{N}_T$. The transit time $T' = L^2/\mu V$, L being the cathode-anode spacing, μ the electron mobility and V the applied voltage. This is just distance divided by average drift velocity. Substituting these into the above relation for G/τ_0 and multiplying both numerator and denominator by eC, C being the capacitance of the photoconductor, we obtain:

$$G/\tau_0 = (e\mathcal{N}\mu/L^2C)(CV/e\mathcal{N}_T).$$

Finally, noting that $L^2/e\mathcal{N}\mu$ is the resistance R of the photoconductor at the operating point, and that CV/e is the total number of *excess* electrons in the bulk of the photoconductor and therefore also equals the total number $\mathcal{N}_A$ of positive charges on the anode, we obtain for the gain-bandwidth product:

$$G\frac{1}{\tau_0} = \frac{1}{\tau_r}M, \qquad \tau_r = RC, \qquad M = \frac{\mathcal{N}_A}{\mathcal{N}_T}$$

The time constant τ_T is the dielectric relaxation time for the photoconductor at the operating point.

Equation (3) represents a universal form for the gain-bandwidth product. It is a rather convenient form in which to express this product because of a very interesting property of M discovered several years ago by STÖCKMANN,[2] ROSE[3] and REDINGTON[4]: under a wide variety of circumstances M, as a function of the applied voltage V, has a maximum possible value of unity. The many injected, excess electrons as are excited by the light. This marks the onset of space-charge-limited current injection, which occurs then at $M = 1$. Beyond this voltage $\mathcal{N}(\mathcal{N}_T)$ increases together with $\mathcal{N}_A$ and $M = 1$ at all higher voltages. The origin of this maximum M-value of unity lies in the fact that the onset of space-charge-limited current flow occurs where $\mathcal{N}_A = \mathcal{N}_T$. This will be true for other, more complicated, models of photoconductors as well. A key to obtaining M-values exceeding unity is the invocation of

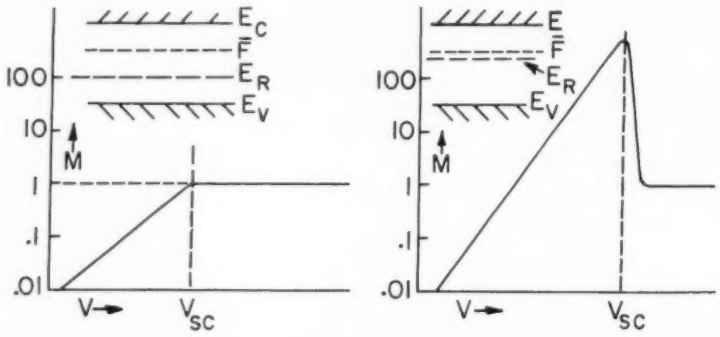

FIG. 3. Variation of $M = \mathcal{N}_A/\mathcal{N}_T$ with voltage V for two simple photoconductors: left, a trap-free photoconductor with deep-lying recombination centers, $(\bar{F}-E_R)/kT \gg 1$ and right a trap-free photoconductor with recombination centers near the Fermi level, $|\bar{F}-E_R|/kT < 1$.

reason why this is true can be seen by considering a simple photoconductor, namely the trap-free photoconductor with deep-lying recombination centers ($\bar{F}-F_R \gg kT$) illustrated in Fig. 3(a). In order to compute the variation of M with voltage it is necessary to know how $\mathcal{N}_A$ and $\mathcal{N}_T$ separately vary with voltage. The anode charge $\mathcal{N}_A$ simply varies linearly with voltage. On the other hand, so long as excess charge has not been injected into the insulator, $\mathcal{N}_T$ is a constant independent of voltage and dependent only on the electronic structure of the insulator and the light excitation level, as shown above. Thus, in the Ohm's law region of current flow M, hence G/τ_0 increases linearly with voltage. This result clearly holds for *any* photoconductor. For the particular case of Fig. 3(a) there are no trapped electrons, and so $\mathcal{N}_T = \mathcal{N}$ at all voltages. Now, at that voltage V_{sc} where $\mathcal{N}_A = \mathcal{N} = \mathcal{N}_T$ there are as localized states in the forbidden gap which influence space-charge-limited current flow but are *not* electron traps, i.e. are not in quasi-thermal equilibrium with the free electrons. Recombination centers are such states since they are in kinetic, rather than quasi-thermal, equilibrium with the free electrons. Consider, for example, a trap-free photoconductor where the recombination centers are located within kT of the Fermi level, illustrated in Fig. 3(b). In this case space-charge-limited current flow will set in at that voltage V_{sc} where $\mathcal{N}_A = \mathcal{N}_{p,R}$, the number of empty recombination centers. Since $\mathcal{N}_T = \mathcal{N}$ as previously, M will increase linearly with voltage up to its maximum value of $\mathcal{N}_{p,R}/\mathcal{N}$, attained at voltage V_{sc}. This ratio can, of course, be much greater than unity. Between V_{sc} and $2V_{sc}$, $\mathcal{N}$ increases up to $\mathcal{N}_A$ so that M drops to unity, and remains so at higher voltages. Detailed analysis of other

Vol. 2
1961

models of photoconductors including electron traps is given in an article by ROSE[5] and the author.

We next consider the influence of the injecting contact on the photoconductive transient, i.e., on the response time. Referring to Fig. 4, let there be a steady photocurrent J_0 flowing in response to some steady level of illumination. The corresponding potential minimum or energy maximum occurs at some position P_0 near the cathode interface. Let the level of incident light flux suddenly be doubled, the applied voltage being held fixed. The new, steady photocurrent will also be approximately doubled. In order to deliver the increased current the energy barrier must shift downwards, by an amount $e\Delta V$ and to the left from P_0 to P_1, a distance Λ. In a simplified diffusion model for the energy barrier,[6] $e\Delta V \simeq kT$ and Λ is a Debye length corresponding to the *total*, excess charge density N_T at the potential minimum (instead of just the *free*, excess charge density), $\Lambda = (\epsilon kT/e^2N_T)^{1/2}$, where ϵ is the static dielectric constant. The time $\tau_{0,c}$ it takes for the energy barrier to shift from P_0 to P_1 is the contact-controlled response time. It remains to compute $\tau_{0,c}$. Between P_0 and P_1 there are $\mathcal{N}_{T,c} = AN_T\Lambda$ negative charges, where A is the cross-sectional area of the photoconductor. At the lower current J_0 these negative charges are all compensated by positive charges to the *left*, at the cathode interface. At the higher current $2J_0$ they must be compensated by positive charges to the *right* of P_1. Since the applied voltage is unchanged, these positive charges can only be obtained through sweep-out of the additional photoelectrons excited by the increased light, the light-excited holes being trapped and left behind in the photoconductor. The time required to build up the necessary positive charges is $\tau_{0,c}$ and is given by:

$$\tau_{0,c} = \frac{\mathcal{N}_{T,c}}{F}, \qquad \mathcal{N}_{T,c} = \frac{A}{e}(\epsilon kTN_T)^{1/2} \quad (4)$$

with F the absorbed light flux. Correspondingly,

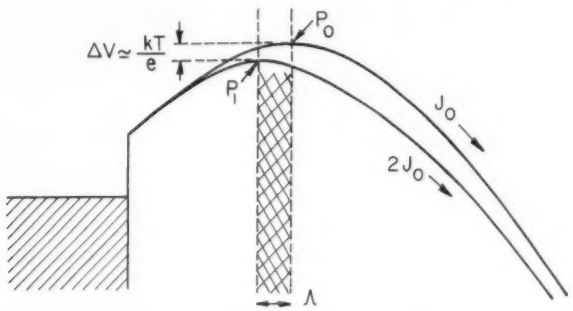

FIG. 4. Transient response of the ohmic (injecting) contact.

the contact-controlled gain–bandwidth product is:

$$G\frac{1}{\tau_{0,c}} = \frac{1}{\tau_r}M_c, \qquad M_c = \frac{\mathcal{N}_A}{\mathcal{N}_{T,c}} \quad (5)$$

with τ_r the same dielectric relaxation time at the operating point as in (3). Note that the above derivation is independent of the nature of the current J_0, i.e. whether it is an ohmic or a space-charge-limited current.

In any given photoconductor the controlling response time is obviously whichever is the longer time, τ_0 or $\tau_{0,c}$.

The corresponding response time also determines the gain–bandwidth product.

III. DOUBLE INJECTION IN INSULATORS

We turn now to the subject of two-carrier current flow in insulators, or double injection. The schematic energy-band diagram for the insulator is shown in Fig. 5. At the negative electrode, or cathode, there is an electron-injecting contact, as before. Now, at the positive electrode, or anode, there is a hole-injecting contact which,

of course, would not be used in one-carrier studies. (The fact that the contacts shown are of junction type rather than metal-insulator type, such as in Fig. 1, in no way alters our discussion.) With sufficient voltage applied across the insulator, electrons come pouring in from the cathode into the conduction band E_c and holes from the anode into the valence band E_v. This double injection of carriers under an applied voltage is closely analogous to photoconductivity induced by band-gap light excitation. In both cases, free carriers are directly injected into the conduction and valence bands, in the photo case usually near the surface of light incidence and in the voltage case from suitable contacts. In both cases the injected electrons and holes neutralize each other and in both cases it is the finite lifetimes of the electrons and holes against mutual recombination which limit the induced conductivity, hence the currents which can flow. Further comments on the interrelationships between double injection and photoconductivity are made below.

In any insulator there will be large densities of recombination centers, labelled N_R in Fig. 5, of electron traps N_{tn} and of hole traps, N_{tp} and comparatively very small densities of thermally generated free electrons n_0 and free holes p_0. Under double injection, as the injection level changes the occupancies of the recombination centers N_R will generally change, and so likewise will the electron and hole lifetimes. Further, these lifetime changes can be enormous. These features of double injection, which are characteristic of insulators as compared to semiconductors, can lead to very interesting current-voltage characteristics, as will be seen below.

Figure 5 corresponds to a "real" insulator in the sense that there are indicated a sufficient density and variety of localized states in the forbidden gap to correspond to reality. The behavior of this insulator under double injection is likely to be quite complicated and the theoretical analysis unduly involved. It is perhaps judicious to first gain an understanding of the double-injection behavior of a much simpler model of an insulator, such as shown in Fig. 6. Here there is just a single set of localized states in the forbidden gap, functioning as recombination centers and completely filled in thermal equilibrium. Simple as it is, this model nonetheless has built into it the

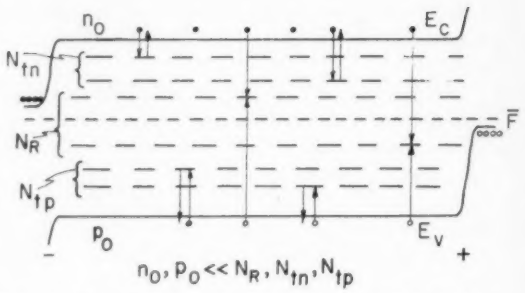

FIG. 5. Schematic energy-band diagram for double injection into an insulator (junction-type contacts). N_{tp} are electron traps, N_{tn} hole traps, and N_R recombination centers.

all-important feature of carrier lifetimes changing with injection level.

The lifetime τ of a free carrier is written, in the usual manner, as $\tau = 1/\bar{v}\sigma N_{\text{cap}}$, with $\bar{v}$ the average thermal velocity of the carrier, σ the cross-section for its capture by a recombination center, and N_{cap} the density of capturing centers. In the model of Fig. 6 the most interesting situation is that for which $\sigma_p \gg \sigma_n$ with $\sigma_p(\sigma_n)$ the cross-section for capture of a hole (electron) by a filled (empty) recombination center. This would be the case if the states N_R were acceptor-like, that is, negatively charged when occupied by an electron. We assume this inequality of the cross-sections for the remainder of our discussion.

At low injection levels, the electron occupancy of the recombination centers is very little disturbed. Therefore the density of hole-capturing centers to be inserted into the lifetime formula to obtain

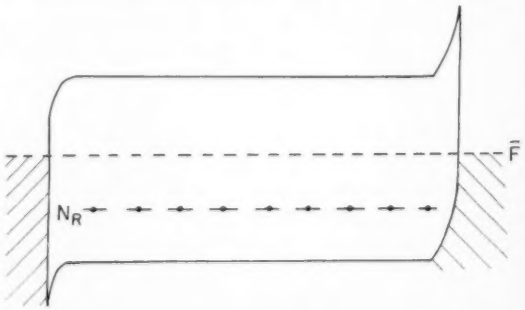

FIG. 6. Highly simplified model of an insulator; there are no traps and just a single set of recombination centers completely filled with electrons in thermal equilibrium.

Vol. 22
1961

the low-level hole lifetime $\tau_{p,\text{low}}$ is just N_R. At high injection levels, where $n \gg N_R$ and $p \gg N_R$, n and p being the injected free electrons and hole densities respectively, charge neutrality requires that $n \approx p$. With $\sigma_p \gg \sigma_n$ the electron and hole recombination rates can only be balanced if the recombination centers are largely empty. The electrons formerly in these centers have been transferred to the conduction band. Therefore, at high injection levels the density of electron-capturing centers to be inserted into the lifetime formula to obtain the high-level electron lifetime $\tau_{n,\text{high}}$ is again N_R. With $n \approx p$ it follows necessarily that $\tau_{n,\text{high}} \approx \tau_{p,\text{high}}$ the high-level hole lifetime. These results are summarized as follows:

$$\tau_{p,\text{low}} \approx \frac{1}{\bar{v}_p \sigma_p N_R}; \quad \tau_{n,\text{high}} \approx \tau_{p,\text{high}} \approx \frac{1}{\bar{v}_n \sigma_n N_R} \tag{6}$$

From (6) it follows, taking $\bar{v}_p/\bar{v}_n \approx 1$, that

$$\tau_{p,\text{high}}/\tau_{p,\text{low}} \approx \sigma_p/\sigma_n.$$

This drastic increase of hole lifetime with injection level between low and high levels means that, in this region of currents, the more holes that are injected the "easier" it is for them to get across the insulator (in the face of recombination). In fact, it is so much easier that the voltage required actually decreases as the current increases. The double-injection current-voltage characteristic for the model of Fig. 6 contains a regime of negative resistance.

Another extremely interesting feature of double injection in the model of Fig. 6 is the existence of a voltage threshold for two-carrier current flow. This result, which is contrary to previous speculation[7] on this question, can be obtained through a rather simple argument. At low injection levels the hole lifetime throughout the insulator has its low-lifetime value $\tau_{p,\text{low}}$. Define the drift length d as the distance a hole moves in one lifetime: $d = v_{p,\text{drift}}\tau_{p,\text{low}} = \mu_p \mathcal{E} \tau_{p,\text{low}}$, with $\mathcal{E}$ the applied field, which varies with position. As $\mathcal{E}$ increases, d increases proportionately. Let successive drift lengths be measured off, starting from the anode, as in Fig. 7. At the end of each drift length the free hole density p decreases by a factor of approximately two. Because of neutrality requirements the free electron density n does likewise. In order that the total current remain constant, the field $\mathcal{E}$ must increase by the same factor of approximately two over each drift length. (Variations of p, n and $\mathcal{E}$ with position are indicated in Fig. 7.) Thus each drift length is roughly twice

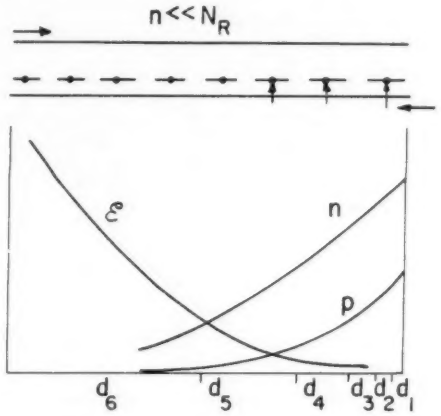

FIG. 7. Drift-length diagram illustrating the voltage threshold for double injection. The d_i denote successive drift lengths for holes.

as long as the preceding drift length: $d_2 \simeq 2d_1$ $d_3 \simeq 2d_2 \simeq 4d_1$, etc. Hence the final drift length d_f(d_6 in Fig. 7) $\simeq L/2$, where L is the cathode–anode spacing. Correspondingly, by definition of drift length, the hole transit-time across half of the insulator $= \tau_{p,\text{low}}$, so that we have finally the result:

$$t_{p,\text{th}} \simeq \frac{L^2}{\mu_p V_{\text{th}}} \simeq \tau_{p,\text{low}} \tag{7}$$

where subscript "th" denotes threshold and t_p is the hole transit time. Rigorous mathematical analysis[8] gives $L^2/\mu_p V_{\text{th}} = 2\tau_{p,\text{low}}$. The complete current–voltage characteristic for the model of Fig. 6 is shown on the log–log plot of Fig. 8. Three regimes are apparent: a steeply rising current near the voltage threshold, a negative resistance down to some minimum voltage V_M, and finally a square-law dependence of current on voltage at high currents. This last regime corresponds to injection levels sufficiently high that $n \approx p \gg N_R$ so that $\tau_n \approx \tau_p \approx \tau_{n,\text{high}} \approx \tau_{p,\text{high}}$ as given in (6). The transfer of electrons initially in the recombination centers N_R to the conduction band through double injection has been completed.

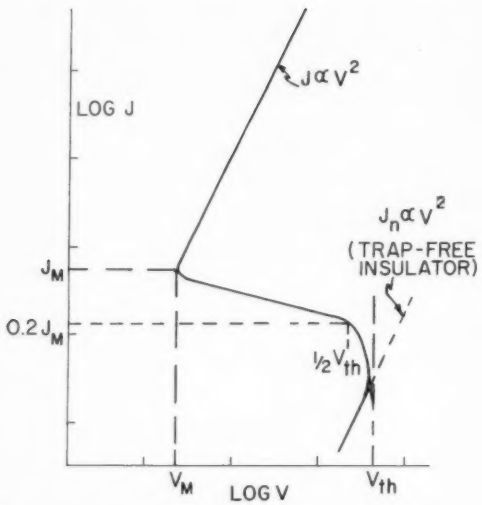

FIG. 8. Current (J)—voltage (V) characteristic, on log–log plot, for the model of Fig. 6.

As a result, at high injection levels the insulator behaves exactly like a semiconductor with an equivalent thermal free carrier density $n_0 = N_R$. The insulator has, in a manner of speaking, been electronically converted, through double injection, into a semiconductor. (The same effect could be produced by shining bandgap light on the insulator.) The square law shown in Fig. 8 is precisely that derived by ROSE and the author[9] for the equivalent semiconductor. At still higher injection levels, when injected space charge takes on importance, the square law goes over into a cube law, not shown in Fig. 8. The low current end of the square law in Fig. 8 is determined by the condition:[8] $t_{p,M} = L^2/\mu_p V_M \approx \tau_{p,\text{high}}$, a result essentially identical to that for the equivalent semiconductor problem.[9] Comparing this result with (7) we see that $V_{\text{th}}/V_M \approx \tau_{p,\text{high}}/\tau_{p,\text{low}} \approx \sigma_p/\sigma_n \gg 1$. A further feature to be noted in Fig. 8 is the relatively small variation of current with voltage over most of the negative-resistance regime. J increases by only a factor of five between $V_{\text{th}}/2$ and V_M.

Upon reflection it will be seen that the double-injection characteristic exhibited in Fig. 8, which was derived neglecting space charge, cannot possibly be valid down to arbitrarily low currents. For, corresponding to the threshold voltage there must be in the insulator a space charge $Q_{\text{th}} = CV_{\text{th}}$, where C is the capacitance of the insulator. The neutrality-based, double-injection solution cannot be valid until the injected electron charge exceeds Q_{th}. At lower injection levels the current in the idealized insulator of Fig. 6 is actually the one-carrier, space-charge-limited electron current for a trap-free insulator shown as the dashed line.

On the experimental side, a current-voltage characteristic such as exhibited in Fig. 8 might be expected to produce one of two striking effects: first, because of the negative resistance, spontaneous oscillations under d.c. applied voltage, or, if the oscillations are quenched by external circuit resistance, a marked hysteresis in the d.c. current-versus-voltage curve. Both effects have been reported for a number of insulators and high-resistance semiconductors: spontaneous oscillations in Au-doped Ge,[10] high-resistivity GaAs,[11] CdS[12] and ZnSe[13]; hysteresis in Fe-doped Ge,[14] CdSe[15] and CdS[16]. Almost certainly a lifetime increasing with injection level is the underlying cause in some, and perhaps all, of these observations.

It remains to establish quantitatively, both by experiment and theory, the relationships between photoconductivity and double injection. The basis for a close relationship has already been suggested —both depend profoundly on the behavior of the free carrier lifetimes. The correlations between infrared quenching excitation and double-injection "breakdown" observed earlier by TYLER[14] in his studies of Fe-doped Ge augur well for future studies of such relationships.

Acknowledgements—The work reported in Section II of this paper was initiated by Dr. A. ROSE and carried out jointly by Dr. ROSE and the author. The author is further pleased to acknowledge many conversations with Dr. ROSE which helped to clarify certain aspects of the double-injection studies reported in Section III of this paper.

REFERENCES

1. RUPPEL W., paper in these Proceedings.
2. STÖCKMANN F., *Z. Phys.* **147,** 544 (1957).
3. ROSE A., *Helv. Phys. Acta* **30,** 242 (1957).
4. REDINGTON R. W., *J. Appl. Phys.* **24,** 189 (1958).
5. ROSE A. and LAMPERT M. A., *Phys. Rev.* **113,** 1227 (1959).

6. LAMPERT M. A. and ROSE A., *Phys. Rev.* **113,** 1236 (1959).
7. BROSER I. and BROSER–WARMINSKY R., *J. Phys. Chem. Solids* **6,** 386 (1958).
8. LAMPERT M. A., to be published.
9. LAMPERT M. A. and ROSE A., *Phys. Rev.* **121,** 26 (1961).
10. LEBEDEV A. A., STAFEEV V. I. and TUCHKEVICH V. M., *Zh. Tekh. Fiz.* (SSSR) **26,** 1419 (1956) (translation: *Soviet Phys.—Technical Phys.* **1,** 2071 (1957).
11. BLANC J., BUBE R. H. and MACDONALD H. E., *J. Appl. Phys.* (in press).
12. LIEBSON S. H., *J. Electrochem. Soc.* **102,** 529 (1955); BUBE R. H. and BARTON L., *RCA Rev.* **20,** 564 (1959).
13. BUBE R. H. and LIND E. L., *Phys. Rev.* **110,** 1040 (1958).
14. TYLER W. W., *Phys. Rev.* **96,** 226 (1954).
15. NICOLL F. H., *RCA Review* **19,** 77 (1958); BUBE, R. H. *J. Appl. Phys.* **31,** 2239 (1960).
16. SMITH R. W., *Phys. Rev.* **105,** 900 (1957) and private communication.

DISCUSSION

L. HEYNE: In the derivation of $GB = M/\tau_{rel}$ you made use of the expression $\tau_0 = \tau_l(n_l/n)$ which is valid only when thermal equilibrium is maintained during the decay. For deep traps this is generally not the case. The decay then consists of a fast and slow part, the latter may be only a few per cent of the photocurrent. Can you tell how this effects the factor M?

M. A. LAMPERT: You are right that in the derivation of the gain–bandwidth product it is assumed that the traps are in quasi-thermal equilibrium with the free carriers. Although for deep traps this is *sometimes* not the case, I believe that it is overstating matters somewhat to say that it is then *generally* not the case. Deep traps out of quasi-thermal equilibrium with the free carriers simply make no contribution to n_t so that the measured M-value is correspondingly larger.

D. A. CUSANO: You have indicated the influence of illumination on the neutral ohmic contact. You also stated that the maximum quantum efficiency for the rectifying contact is $q = 1$. If, however, the illumination influences the rectifying contact at sufficiently high voltage—allows it to become injecting—is it not possible to observe $q > 1$, as in the case of the neutral ohmic contact? (One-carrier case).

M. A. LAMPERT: Yes, it is possible.

R. W. REDINGTON: I would like to comment on your M-value greater than unity. For the model you used, the gain itself increases monotonically until it saturates in the space-charge-limited region. M drops on the high voltage side of its maximum because the response time increases. For the maximum gain case one never needs M-values different from unity if the dielectric relaxation time is defined dynamically.

M. A. LAMPERT: In the model of Fig. 3 (right) the drop-off of M after the onset of space-charge-limited currents is due to the large increase of n_T, between V_{SC} and $2V_{SC}$. In this model $n_T = n$ at all voltages so that $\tau_0 = \tau_l$. Any change in τ_l, hence τ_0, in the voltage region between V_{SC} and $2V_{SC}$ has no bearing on the M-value the way we have defined it.

BLANK
PAGE

Vol. 2
1961

J. Phys. Chem. Solids Pergamon Press 1961. Vol. 22, pp. 199–206. Printed in Great Britain.

ELECTRON INJECTION AND EXTRACTION IN CdS CRYSTALS

W. RUPPEL

Laboratories RCA Ltd., Zurich, Switzerland

Abstract—The measurement of the total crystal charge of a CdS single crystal with pressed In contacts, as a function of voltage and light intensity, permits the determination of the transition from electron injection to extraction in the crystal. From the potential distribution in the vicinity of the contacts, inferred from the charge measurements in conjunction with the observation of current–voltage characteristics, the mechanism which limits the current flow through the crystal under the different experimental conditions is determined.

INTRODUCTION

THE mechanism which limits the current flow through an insulator is closely correlated with the potential distribution in the insulator in the vicinity of the contacts and hence, via Poisson's equation, with the total charge of the insulator. Space charge of the sign of the majority carriers indicates that the current flow is the space-charge-limited analog to current flow in a vacuum. Space charge of the opposite sign points to extraction of the majority carriers and limitation of the current flow by a limited supply of carriers from the electrodes. Of particular interest is the case of current flow far in excess of the ohmic current which cannot be ascribed to a change in mobility but is rather due to a change in the free carrier concentration. If substantial two-carrier conduction can be excluded, the determination of the total crystal charge permits the distinction between space-charge-limited majority excess carrier injection and an increase of the free carrier concentration by the extraction of majority carriers from traps through collision ionization or field emission in the interior of the crystal.

In order to demonstrate the mechanism of the increase in electron concentration in CdS under applied voltage the total crystal charge was measured in conjunction with current–voltage characteristics by SMITH and ROSE[1] and BÖER and KÜMMEL[2]. These measurements were, however, not in sufficient agreement to yield conclusive information about the current limiting mechanisms involved for a particular contact to the CdS crystal. The experimental results that will be outlined in the following suggest that by considering the influence of the applied voltage, as well as that of photoexcitation of free electrons in the interior of the crystal, a systematic picture including both injection and extraction of electrons for the case of pressed In contacts to the CdS crystal is obtained.

EXPERIMENTAL PROCEDURE

The CdS single crystals used were prepared by the FRERICHS method and not deliberately activated. They were platelets with an area of about $0{\cdot}15 \times 0{\cdot}15$ cm^2 and a thickness varying between $1{\cdot}0 \times 10^{-3}$ and $2{\cdot}5 \times 10^{-3}$ cm.

The crystals were clamped in between two In contacts with a contact area of about $2{\cdot}5 \times 10^{-3}$ cm^2. When the In contacts were removed for the detection of the total crystal charge the crystal dropped onto the pan of a one-string electrometer with a charge sensitivity of 3×10^{-13} C/div.

Photogeneration of free carriers was effected by white light. Its intensity was adjusted by means of chromium filters. As a criterion for uniform illumination zero photovoltage across the crystal and both contacts was used.

In order to ensure that the detected total crystal charge was not an irregular spurious charge the crystal charge was also measured for an equal potential applied to both contacts. The charge in this case was observed to be equal to the expected value of the product of the applied potential and the capacity of the crystal with respect to the electrometer ground. This demonstrates

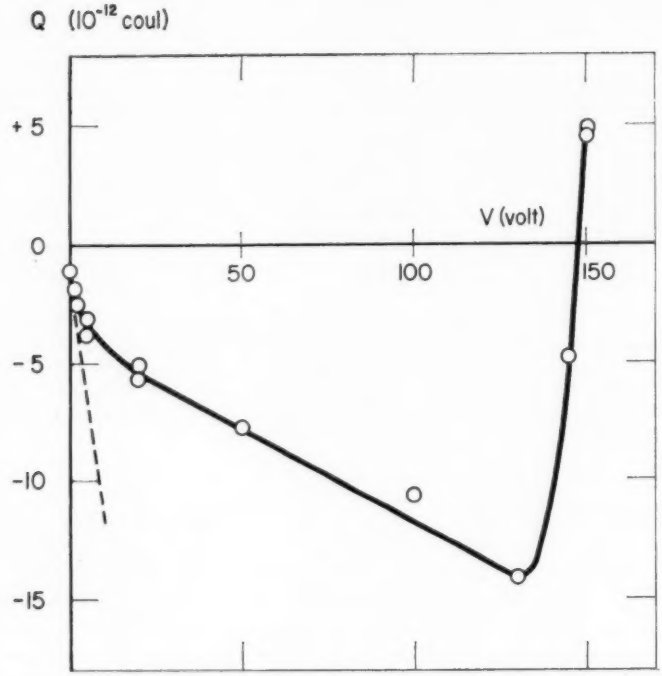

FIG. 1. Crystal charge in the dark as a function of voltage applied between pressed In contacts. Distance between contacts $2{\cdot}5 \times 10^{-3}$ cm. Contact area $2{\cdot}5 \times 10^{-3}$ cm^2. The dotted line represents the charge computed for an ohmic cathode and a blocking anode.

the absence of any essential spurious charge arising from the removal of the In contacts from the crystal.

EXPERIMENTAL RESULTS AND DISCUSSION

The total charge observed for a CdS crystal as a function of the applied voltage in the dark is shown in Fig. 1. Already at zero applied voltage a small negative charge is observed. This charge can be accounted for by the contact potential difference between the CdS crystal and the In contact. It presents a direct experimental evidence for the presence of a surface space charge layer in a semiconductor in contact with a metal. The negative sign of the charge indicates the presence of an electron accumulation layer in the *n*-type CdS and, therefore, that of an ohmic contact for electrons of the In to the CdS. Sign and magnitude of the observed charge permit the calculation of the internal field at the crystal surface in thermal equilibrium with the In contact (Fig. 2a).

With an applied voltage one expects, according to the ohmic contact for electrons, the occurrence of an additional negative space charge formed by injected excess electrons (Fig. 2c). For small applied voltages this additional charge should be equal to simply the applied voltage multiplied by the interelectrode capacitance (dotted line in Fig. 1). Experimentally, for voltages up to a few volts the observed charge values follow the dotted line. At higher voltage a smaller negative charge and finally a change to slight positive charges is observed.

The increasing lag of the magnitude of the negative charge behind the value computed for a cathode ohmic for electron flow and an anode blocking for hole flow could be due to either an

Vol. 2
1961

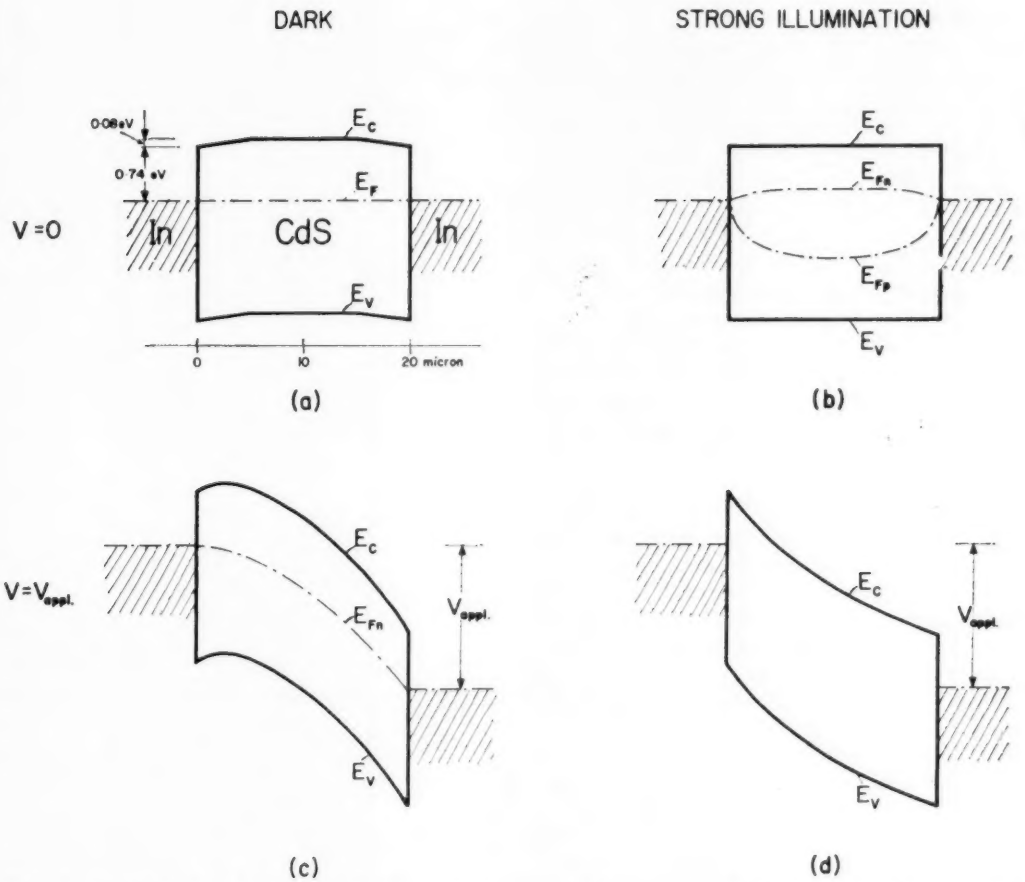

FIG. 2. Potential distribution in a CdS crystal with pressed In contacts. (a) In the dark without applied voltage; (b) under strong uniform illumination without applied voltage; (c) in the dark with applied voltage. Case of electron injection; (d) under strong illumination with applied voltage. Case of electron extraction.

increasing hole contribution or a saturation of the ohmic cathode.[3] The first possibility seems unlikely since a diffusive hole contribution across an ohmic anode would decrease with increasing total current and since no band gap light emission is observed as it would be in the case of hole injection.[4] On the other hand, saturation of the cathode would imply saturation of the current with increasing voltage unless tunneling at the cathode and extraction of electrons from traps by collision ionization or field emission occurs.

In Fig. 3 are plotted charge (bottom) and current (top) as functions of voltage. From the linear current portion at low voltage the thermal equilibrium electron concentration and the distance between conduction band and Fermi level in the interior of the crystal can be computed (Fig. 2a). At a critical voltage a steep current increase is observed. The maximum negative charge and the subsequent change to positive values fall within this range of current increase. This observation indicates that a transition from space-charge-limited injection of electrons to field induced extraction of electrons from traps occurs within a small voltage range.

The close coincidence of the voltages at which injection has reached the trap-filled-limit[5] but also gives rise to a field induced extraction of carriers from those traps[6] must probably be understood by the effect that at the trap-filled-limit of injection the quasi-Fermi level for electrons rises steeply and that therefore the voltage necessary for collision ionization of filled traps decreases correspondingly. Positive observed charge indicates that even traps in addition to those filled by previous injection must have been emptied. Quantitatively, an average field of 6×10^4 V/cm (Fig. 3) appears to be too low to account for the extraction of carriers from those traps but according to BÖER and KÜMMEL[6,7] local fields in the crystal can exceed the average field by orders of magnitude.

When the crystal is illuminated the free electron concentration in the interior of the crystal increases. At the surface a high recombination rate and hence a constant carrier concentration will be assumed. Under applied voltages exceeding the photovoltages set up between the surface and the interior of the crystal which tend to straighten the bands (Fig. 2b), the curvature of the bands will change its sign (Fig. 2d). The sign of the crystal charge will correspondingly change from negative to positive with increasing illumination.

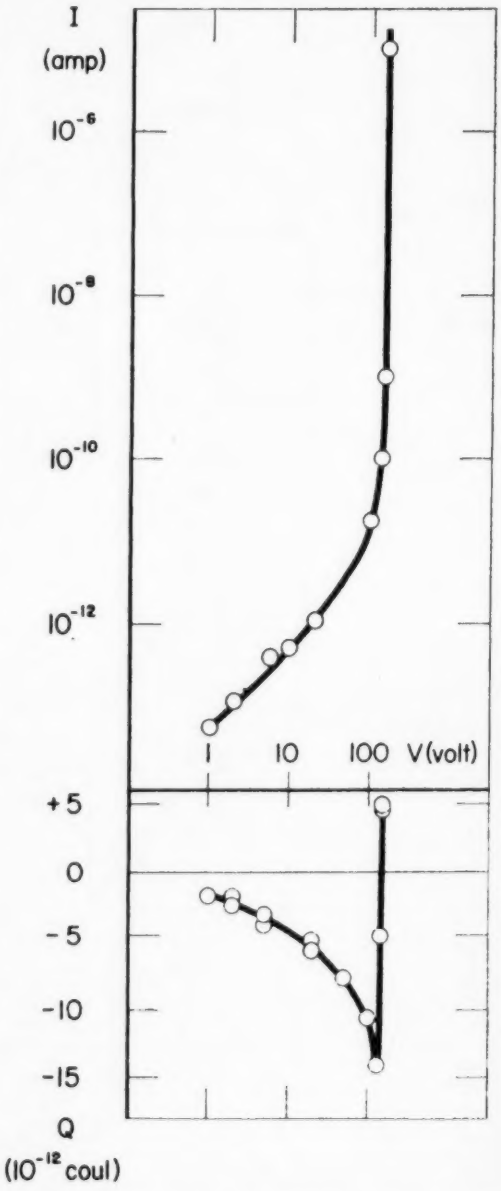

FIG. 3. Upper curve: I–V-characteristic of the crystal of Fig. 1. Lower curve: Crystal charge of Fig. 1 on a logarithmic voltage scale.

Vol. 2
196

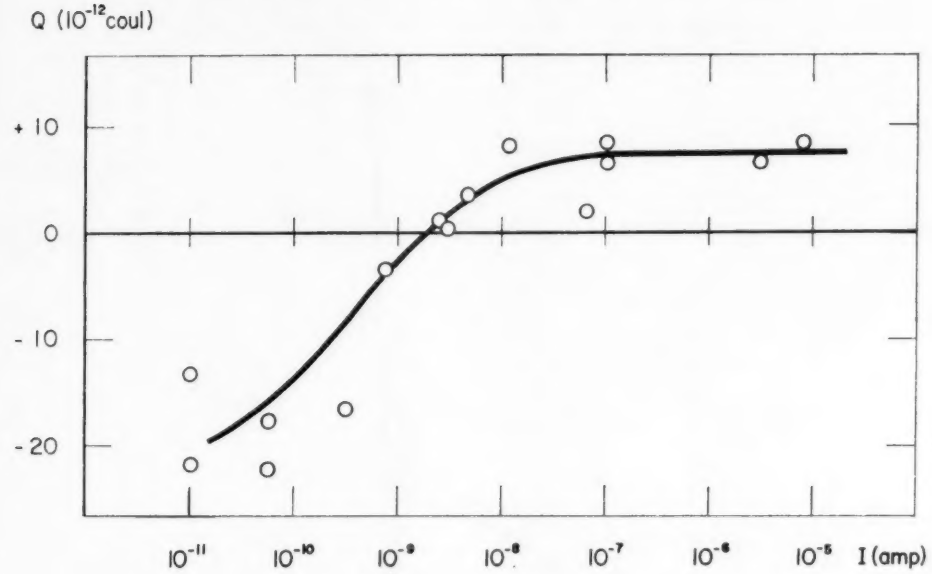

FIG. 4. Crystal charge as a function of photocurrent through the crystal at 100 V. Distance between contacts 2×10^{-3} cm. Contact area $2{\cdot}5 \times 10^{-3}$ cm^2.

ol. 22
1961

This expectation is borne out by the experimental results shown in Fig. 4. Here the crystal charge is measured at constant applied voltage as a function of illumination. The total charge zero corresponds to flat bands ("neutral" contact). From the magnitude of the current at zero charge the energy difference between conduction band and Fermi level at the surface can be computed, thus completing the quantitative picture of the CdS crystal in thermal equilibrium with an In contact (Fig. 2a).

The charge observations are corroborated by the measurement of current–voltage characteristics in the dark and under illumination (Fig. 5). The square-law portion in the dark points to space-charge-limited injection. Also, at low light intensities the current increases more than linearly as soon as the voltage generated excess electron concentration exceeds the photogenerated free carrier concentration. In the range of about 10^{-10} to 10^{-9} A the current increases linearly up to the steep rise, in accordance with the space-charge-free neutral contact observed in this photocurrent range (Fig. 4). At higher photocurrents for which positive crystal charge is found (Fig. 4), saturation is observed. This indicates saturation of the cathode without free carrier multiplication by extraction of electrons from traps.

In order to exclude other possible photocurrent saturation mechanisms such as extraction of photogenerated holes from the crystal or an increased recombination rate by injection of excess electrons the cathode saturation is demonstrated by the temperature dependence of the saturated photocurrent (Fig. 6a). The activation energy of the saturated current above room temperature is found to be 0·8 eV in agreement with the cathode barrier height determined from the crystal charge as a function of illumination (Fig. 2a). At about 60°C the current is no longer limited by saturation of the cathode but by the free carrier concentration in the volume of the crystal. By extrapolating the ohmic part of the current–voltage curve (Fig. 6b) to 10 V a current of about 3×10^{-9} A is expected while the temperature dependence of the saturation current is observed to disappear at about 2×10^{-9} A (Fig. 6a).

At high voltages the current increases steeply. For a photoinduced change in free carrier concentration the transition from injection to extraction was observed to take place at a current of

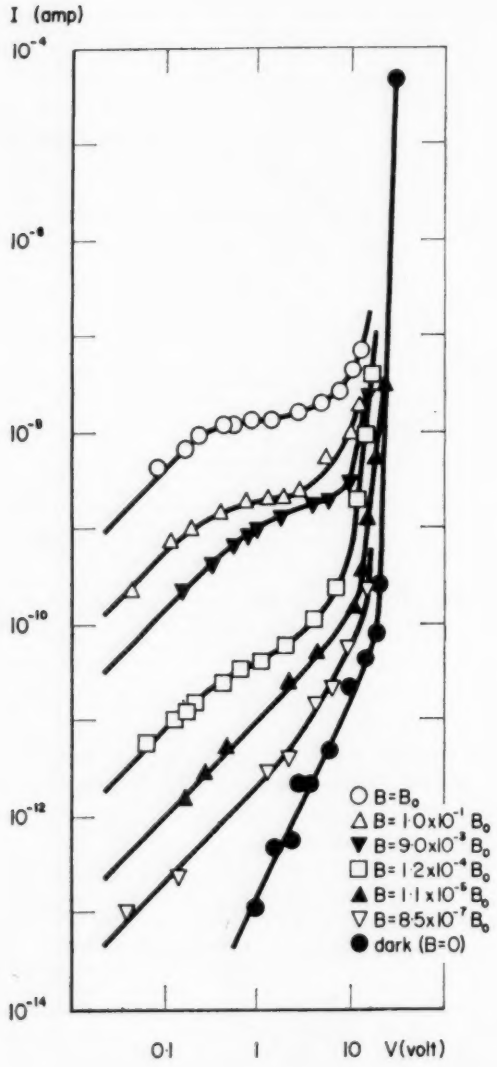

FIG. 5. I–V-characteristics at different light intensities of a CdS crystal with pressed In contacts. Distance between contacts 1×10^{-3} cm. Contact area $2{\cdot}5\times10^{-3}$ cm². Intensity B of white light in arbitrary units.

2×10^{-9} A (Fig. 4). If a similar transition point is assumed also for voltage-generated excess free carriers, the transition from space-charge-limited excess electron injection to a field induced extraction of electrons from traps in the steep part of the current–voltage characteristics occurs at a critical current density of about 1×10^{-6} A/cm².

Vol. 2
1961

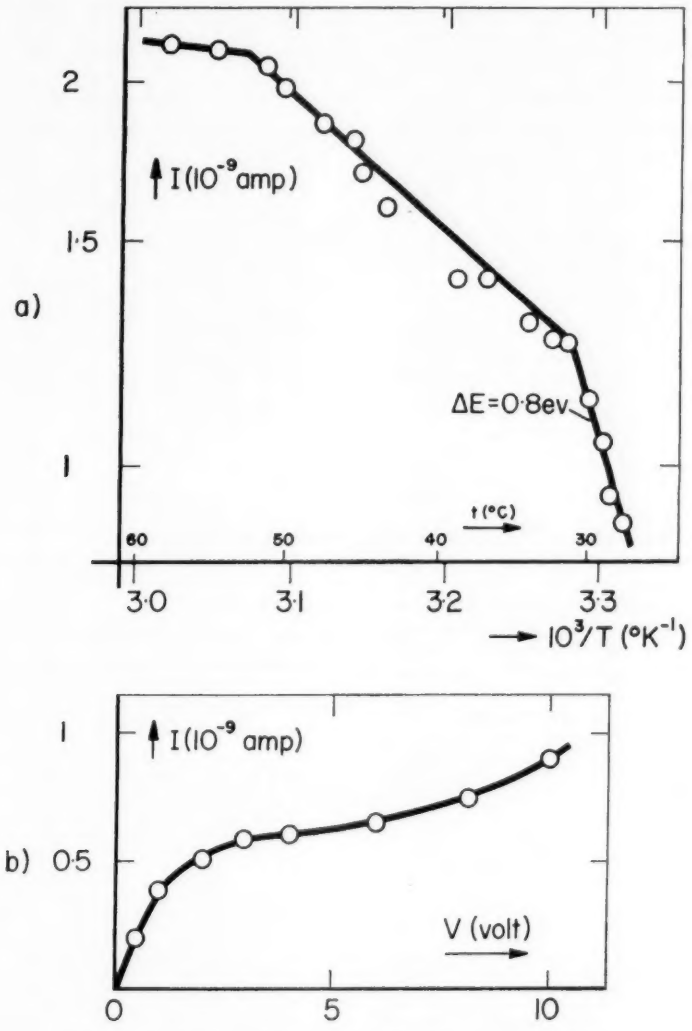

FIG. 6. (a) Temperature dependence of saturated photocurrent through a CdS crystal with pressed In contacts. Distance between contacts 2×10^{-3} cm². Contact area $2{\cdot}5\times10^{-3}$ cm². (b) *I–V* characteristic of the same crystal at room temperature.

CONCLUSIONS

The total crystal charge of a CdS crystal varies in a systematic way as a function of voltage and illumination. From the total crystal charge the potential distribution in the vicinity of the contacts can be inferred and with it the mechanism that limits the current flow through the crystal can be determined. For the particular case of pressed In contacts to CdS crystals one finds that below current densities of about 10^{-6} A/cm² space-charge-limited injection of electrons predominates while for larger currents extraction of electrons

sets in. Depending on whether the extraction of electrons from the crystal is accompanied by field induced extraction from traps and a tunnelling emission current at the cathode, the free electron concentration in the extraction range is found to be smaller or larger than the electron concentration in the ohmic range. The simultaneous determination of crystal charge and current as a function of voltage and illumination yields a consistent quantitative picture of a CdS crystal with a pressed In contact.

Acknowledgements—The author is indebted to Dr. A. ROSE, Mr. M. A. LAMPERT and Prof. F. STÖCKMANN for discussions on the subject. The CdS single crystals were prepared by Dr. R. NITSCHE and Mr. H. U. BOELSTERLI.

REFERENCES

1. SMITH R. W. and ROSE A., *Phys. Rev.* **97,** 1531 (1955).
2. BÖER K. W. and KÜMMEL U., *Z. Naturforsch.* **12a,** 667 (1957); *Ann. Phys.* (*Leipzig*) (7), **2,** 217 (1958).
3. PARMENTER R. H. and RUPPEL W., *J. Appl. Phys.* **30,** 1548 (1959).
4. SMITH R. W., *Phys. Rev.* **105,** 900 (1957).
5. LAMPERT M. A., *Phys. Rev.* **103,** 1648 (1956).
6. BÖER K. W. and KÜMMEL U., *Ann. Phys.* (*Leipzig*) (6), **14,** 341 (1954).
7. BÖER K. W., *Proc. Int. Conf. Semicond.* (*Prague*) p. 828 (1960).

DISCUSSION

R. H. BUBE (Comment): There have been a number of recent reports of unreasonably small trap densities resulting from the interpretation of a rapid rise in space-charge-limited current as the traps-filled limit. Recent experiments of ours are in agreement with those of this paper which indicate that their rapid rise may be caused not by filling of all traps present but by impact ionization of the shallower traps present. If trap densities are determined from the temperature dependence of a square-law portion of the SCLC curve *below* the rapid rise to the trap-free curve, these densities are in excellent agreement with densities determined from thermally stimulated current or photoresponse time data—and as much as 10^4 times larger than those calculated by assuming that the rapid increase in current corresponds to the filling of all traps.

A. ROSE: Am I right in understanding your argument that the crystal charge changes from negative to positive when the crystal current exceeds the temperature limited emission from the contact, independent of whether the crystal current is increased by light or by voltage?

W. RUPPEL: Yes.

J. Phys. Chem. Solids Pergamon Press 1961. Vol. 22, pp. 207–212. Printed in Great Britain.

CONTACT INFLUENCE ON THE PHOTOCONDUCTIVITY OF LEAD OXIDE

L. HEIJNE

Philips Research Laboratories, N.V. Philips' Gloeilampenfabrieken, Eindhoven-Netherlands

Abstract—Continuous primary photocurrents can be observed in PbO layers obtained by vapour deposition and sandwiched between Ag or Ag–SnO_2 contacts. When the dark conductance, which is determined by the deviation from stoichiometry, is strongly *p*-type, the following characteristics are found: saturating photocurrent–voltage dependence at unity quantum yield, linear photocurrent–intensity dependence, and localization of the photosensitivity near the anode. This indicates blocking contacts for holes. Layers made *n*-type by a treatment at low oxygen pressure show a gain factor exceeding unity, no saturation and high dark current. The photosensitivity is not confined to a particular electrode. Thus the same type of contacts can replenish conduction electrons in this case. Further information is obtained from "electrical" glow curves. The voltage dependence of currents generated by electrons when they are released from traps is markedly different from that occurring with holes. This enables the charge-carrier sign during the glow experiment to be determined. Transition from blocking to replenishing action of the contacts also for holes occurs, when the PbO is doped with *n*- and *p*-type impurities together. The photocurrent–light intensity characteristic becomes superlinear and the gain becomes higher than one, indicating an illumination-dependent replenishment.

INTRODUCTION

In samples of lead oxide obtained by an evaporation process in a low pressure oxygen atmosphere contacts can behave differently with respect to the replenishment of both types of charge carriers and under different circumstances.

The microcrystalline PbO layers were sandwiched between conducting tin oxide (in the form of a coating on a glass window) and evaporated silver contacts. The deviation from stoichiometry was established after the deposition of the lead oxide layer by a bake at 300°C in an oxygen atmosphere at a certain pressure. The sandwich cells were constructed in such a way that they formed part of an evacuated envelope, and during their preparation and processing any contact with the air was carefully avoided.[1]

DARK CURRENT CHARACTERISTICS

In contrast to the other lead salt photoconductors yellow lead oxide has an orthorhombic structure, and the photosensitivity has its maximum in the visible part of the spectrum instead of in the infra-red. The correspondingly high value of the band gap (about 2·7 eV) is the reason why the dark resistivity may be very high. Values of the order of $10^{14}\ \Omega$ cm can be found at room temperature. However, the actual resistivity depends strongly on the deviation from stoichiometry. From Fig. 1 we see that layers baked at a low oxygen pressure show highest conductivity. Thermoelectric voltage measurements revealed that the conductivity was *n*-type in that region. When the bake is carried out at a higher oxygen pressure, the *p*-type conductivity is not revealed by the expected drop in resistance, though its presence is indicated by the sign of the thermoelectric voltage. The increase in capacitance of the cells (see Fig. 1) at these pressures indicates that the hole current is blocked at a contact barrier on which the applied field is concentrated.

CONTACT MODEL

A model of the field distribution near the contacts to explain the above-mentioned results is represented in Fig. 2. It must be recognized that the width of the Schottky barriers as assumed in this model, especially of the one at the positive electrode, may be comparable to the electrode distance of the sandwich cells (10 μ). From the

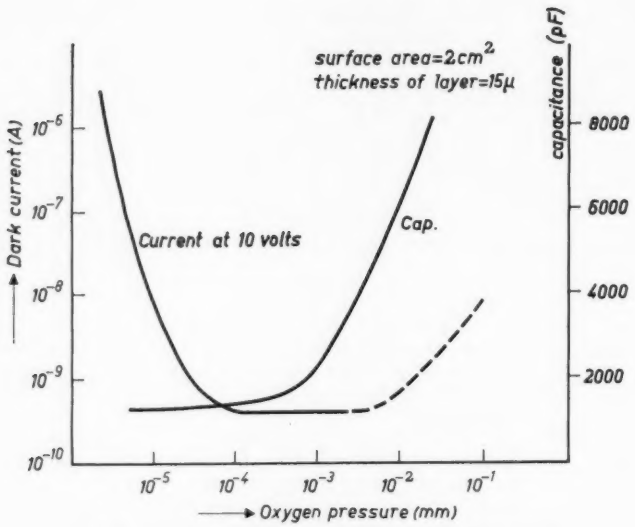

FIG. 1. Dependence of dark current and capacitance on the oxygen pressure used during a bake at 300°C. The dotted part of the curve corresponds to a region of partial breakdown at the voltage used.

expression for the thickness of the Schottky barrier[2]:

$$W = \left(\frac{2\epsilon\epsilon_0 V_t}{qN}\right)^{1/2} \qquad (1)$$

where: V_t is the total voltage across the barrier, equal to $V_{\text{applied}} + V_b$,
q the absolute value of the electronic charge,
N the impurity concentration and
$\epsilon\epsilon_0$ the dielectric constant,

we find under these conditions for the critical acceptor concentration a value of about 10^{14} cm^{-3}. At higher concentrations of acceptors (for example, lead vacancies introduced by a treatment at a high oxygen pressure) narrower space-charge regions are found at the contacts. Thus the measured capacitance is higher than that calculated from the thickness of the layer. When the acceptor concentration is lower than the critical concentration of 10^{14} cm^{-3}, the total negative space charge that can be built up inside the layer is insufficient to allow of a complete Schottky barrier to be developed. In that case, the negative space-charge maximum is so low that conduction electrons can enter the substance from the contacts and the sample becomes n-type conductive, although, by its composition alone, it should have been p-type. The dark current–voltage characteristic is superlinear in this case.

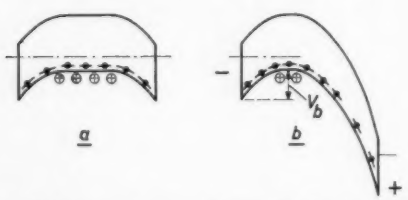

FIG. 2. Voltage and space-charge distribution near the contacts in a p-type PbO layer, (a) without applied voltage, (b) with applied voltage.

PHOTOCONDUCTIVE PROPERTIES

It appears that the photocurrent is proportional to the light intensity and that with increasing voltage it reaches a sharply marked saturation value at a quantum yield of almost unity. The sensitivity appears to be mainly localized near the anode. This is because the blocking barrier at which the field concentrates is situated at this electrode. The photocurrent resulting from illumination with strongly absorbed light must be carried predominantly by holes. It behaves as a purely primary current. This is in accordance with

Vol. 22
1961

the contact model of Fig. 2, where no replenishment of holes is possible at the anode.

On the other hand, the replenishment of conduction electrons in lead oxide having a lower oxygen content appears to be quite possible. This follows from the high dark current observed in that case. Moreover, the photocurrents observed in such samples lack the characteristics of a primary photocurrent mentioned above.

So far, only evidence has been presented that the contacts used behave *differently* with respect to electrons and holes in *different* samples. Results will now be shown, in which the replenishment of electrons and the blocking of the entry of holes is demonstrated in the *same* sample. This takes place during thermostimulated current experiments.

THERMOSTIMULATED CURRENTS

In these measurements the sample, which forms part of a circuit with a voltage source and a current measuring instrument, is cooled down to the temperature of liquid nitrogen in complete darkness. Then the substance is irradiated with a known amount of light and subsequently the temperature is again increased in the dark at a constant rate. The plot of the current against the time obtained experimentally during this heating up shows several maxima corresponding to the emptying of certain trapping levels (Fig. 3).

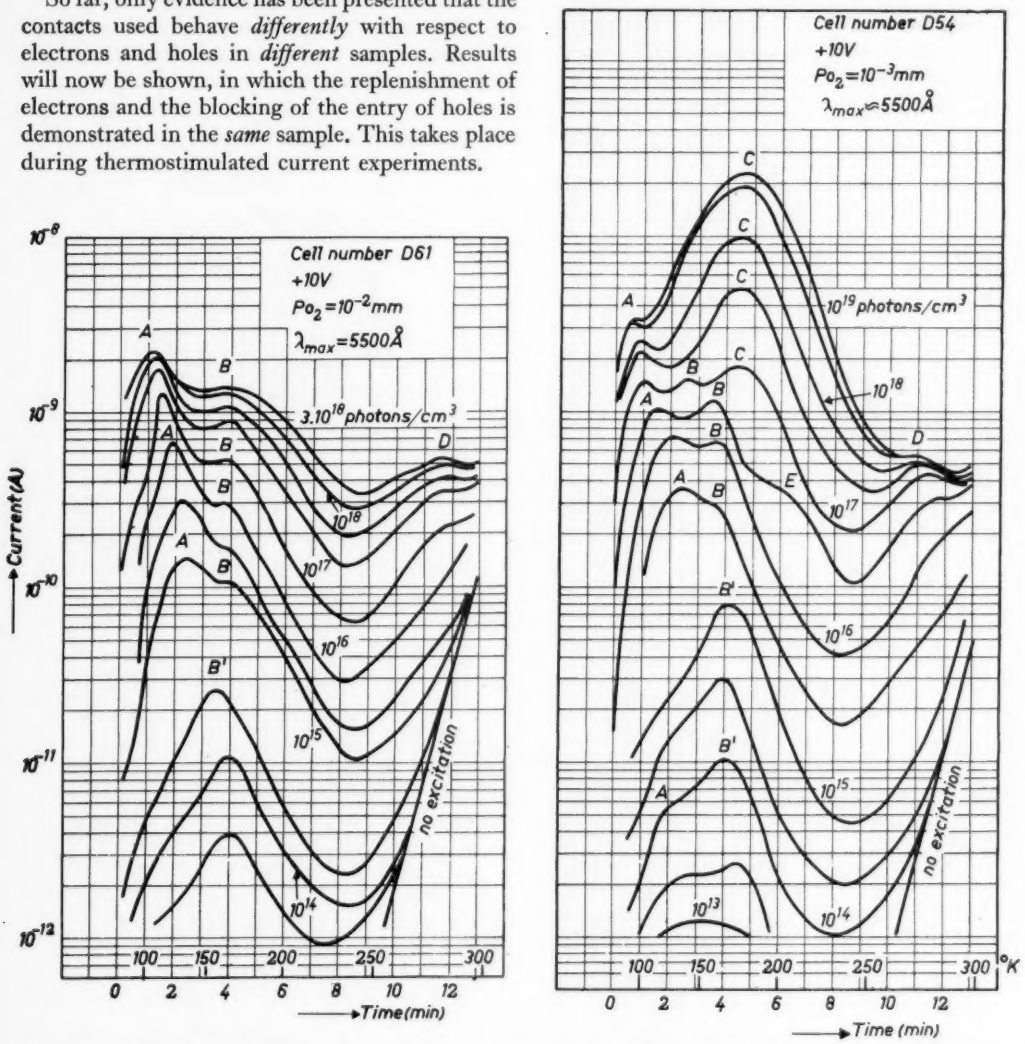

FIG. 3. Built-up thermostimulated current curves obtained at different levels of excitation for two samples baked at different partial oxygen pressures.

From thermostimulated current curves information about number, depth and capture cross-section of these levels can be obtained.[3] However, it is impossible to ascertain from the curves whether a certain peak corresponds to an electron or a hole trap. Now, when the voltage dependence of a particular curve obtained after excitation by a certain number of photons is considered (Fig. 4), we find that the peaks found may be divided into two classes. The height of the peaks belonging to the first is almost independent of the applied voltage or varies with the square root of it. On the other hand, peaks of the second class grow approximately quadratically with increasing voltage. In Fig. 4 examples of these behaviours are shown for peaks B and C of Fig. 3.

With the previous results in mind, it seems obvious to correlate the peaks with sublinear voltage dependence with hole traps and those with a superlinear dependence with electron traps.

The square-root dependence of hole peaks can be explained easily when it is taken into account that space-charge effects must accompany the displacement of the liberated holes.

The concentration of a level may be found from the amount of excitation at which a peak ceases to grow with increasing excitation. A value of the same order of magnitude is found for the concentration when the number of electronic charges crossing the layer during the occurrence of the peak is determined from the surface area under the peak (when the latter is plotted on a linear scale). But this is true only for hole peaks, which saturate with the applied voltage. Evidently, unity yield is obtained for the collection of the holes liberated from these traps.

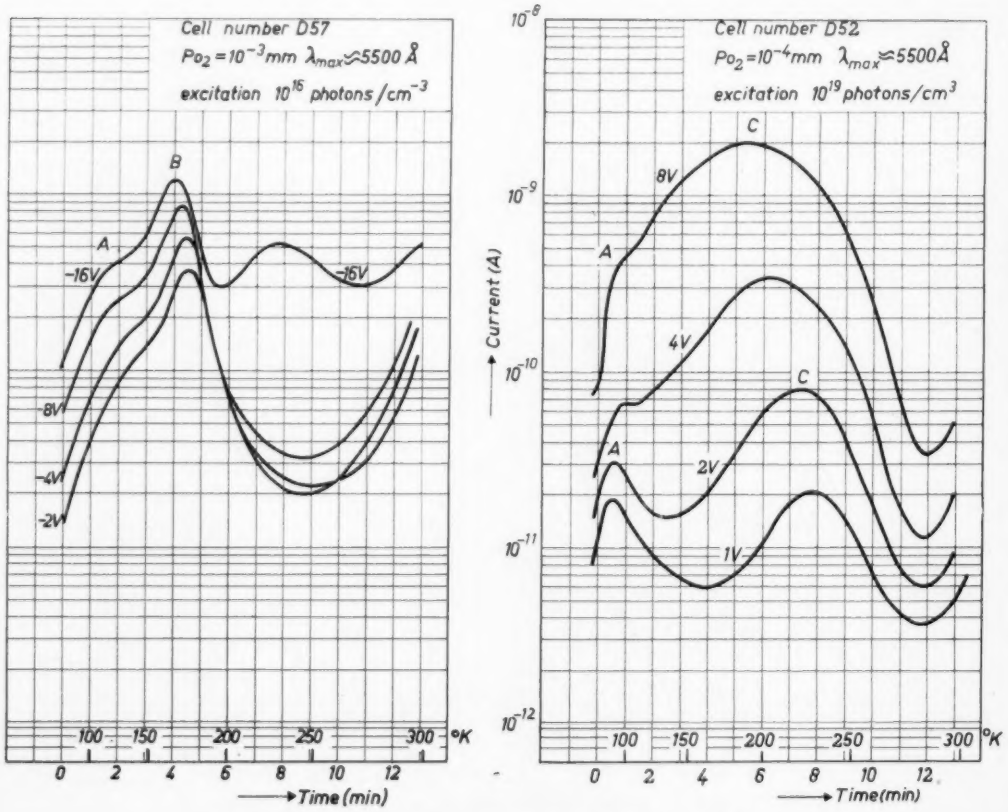

FIG. 4. Voltage dependence of peaks A, B and C of Fig. 3.

Vol. 22
1961

On the other hand, when the charge flowing through the layer during the emptying of electron traps is compared with the excitation used for the filling of it, a gain factor exceeding unity may be observed, depending on the applied voltage. This again confirms the idea that electrons can be easily replenished by the contacts.

ACTIVATED LAYERS

When trivalent impurity atoms, such as Sb or Bi, are added to the lead oxide it is found that they tend to make the layers more *n*-type, and consequently the curves of Fig. 1 shift to higher oxygen pressures. The opposite occurs when monovalent metals (Ag, Tl) are added. However, when two impurities of different type are introduced together in a rather high concentration like $1:10^3$, new effects appear that are not found in layers of pure lead oxide.

Firstly, when the capacitance of such a sandwich cell is measured by means of an a.c. bridge at a low frequency (10–1000 c/s), it is found that the capacitance has become strongly dependent on the illumination level. This is not the case with pure lead oxide layers possessing only a deviation from stoichiometry. So, for a particular layer, an increase from 4000 pF in the dark to 65,000 pF with an illumination level of approximately 20 lux was measured. At the same time the losses expressed as a tan δ, did not exceed 0·2 at 1000 c/s, and did not increase with a weak illumination.

From these observations, it must be concluded that the contact is separated from the relatively well conducting bulk by a narrow blocking layer, the width of which decreases strongly upon illumination.

The second way in which the properties of activated layers deviate from those made with pure PbO is represented in Fig. 5. The photocurrent grows linearly with the light intensity at low light levels, just as in pure layers. However, at a certain point, the photocurrent suddenly starts to grow more than linearly with the illumination level. The light intensity at which this happens depends on the temperature as well as on the concentration of the impurities present. As soon as the current–light curve becomes superlinear, the saturating current–voltage characteristic which exists at low light levels changes into a linear or, at high excitation levels, superlinear dependence.

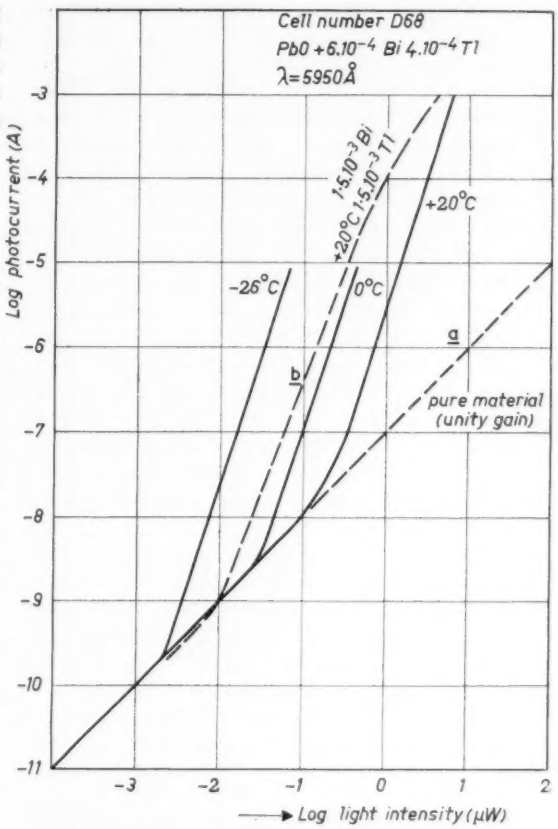

FIG. 5. Intensity dependence of photocurrent in activated layers at different temperatures, (a) curve for an unactivated layer, (b) curve for a highly activated layer.

In these regions the photocurrent gain factor may be as high as 1000.

Gain factors of this order of magnitudes are also found for the currents occurring during peaks in thermostimulated current curves. These curves show maxima corresponding to those of pure PbO. However, the peaks are higher and they grow much faster than proportional to the excitation. Furthermore, electron peaks as well as hole peaks grow superlinearly with the applied voltage. So the possibility of distinguishing between electron traps and hole traps by means of this voltage dependence does not exist here. Only by comparison with the behaviour of corresponding peaks in pure samples may a distinction sometimes be made.

These phenomena, which indicate that replenishment of holes has now become possible, can be explained from the narrowing of the blocking barrier, as was indicated by the capacitance measurements. It is assumed that, at a certain illumination density, the barrier becomes so narrow, and thus the field strength so high, that penetration of the barrier by means of a tunnel effect becomes possible. The "transparency" of a barrier with constant space-charge density is proportional to $\exp[-(a/QV)^{1/2}]$, where a is a constant, V the voltage difference across the barrier and Q the space-charge density inside it.[4] This function varies so steeply with QV that a critical value of this product may be considered to exist, above which tunnelling and thus replenishment of charge carriers takes place. If we assume that the amount of negative charge trapped in the contact region increases with the excitation density, a critical illumination level must also exist at which replenishment of holes just starts. If complete replenishment of all holes drawn by the field from the anode region were to take place, a higher illumination level would no longer result in a higher space-charge density, because in this case the increase in electron concentration (free and trapped) would equal the increase in hole concentration. Thus the superlinear part of the photocurrent–light characteristic must be considered as a transition from the blocking case to this situation. This region of very high light intensities and high photocurrents in which the latter would be controlled by the recombination lifetime could not be covered experimentally.

An indication of the depth of the level controlling the contact action is obtained by plotting against $1/T$ the current at the bend of the photocurrent light characteristic. In this way a slope of 0·5 eV is found. Approximately the same activation energy is found from plots of the decay time against $1/T$. So it seems that the response time of the photocurrent is determined mainly by the contact region.

REFERENCES

1. HEIJNE L., Thesis, Amsterdam (1960). To be published as a supplement to *Philips Res. Repts.* (1961).
2. SCHOTTKY W., *Z. Phys.* **113,** 367 (1939), **118,** 539 (1942).
3. RANDALL J. T. and WILKINS M. H. F., *Proc. Roy. Soc.* **A184,** 390 (1945); GARLICK G. F. J. and GIBSON A. F., *Proc. Phys. Soc.* **60,** 574 (1948); HOOGENSTRAATEN W., *Philips Res. Repts.* **13,** 515 (1958).; BUBE R. H. *Photoconductivity of Solids*, p. 292. John Wiley and Sons Inc., New York (1960).
4. ZALM P., *Philips Res. Repts.* **11,** 423 (1956).

DISCUSSION

D. R. FRANKL: In germanium and silicon, contact properties are primarily determined by surface states. Are similar effects found in CdS and other photoconductors?

W. RUPPEL: Surface states enter implicitly into the band picture in that they modify the amount of energy that appears as the difference in the effective work functions between the contact material and the photoconductor. The observation whether a contact appears ohmic or blocking is therefore affected by the presence of surface states. Only since the surfaces of crystals grown from the vapor phase usually do not receive any further treatment by grinding, etching, etc., surface states in these crystals are less extensively discussed explicitly than they are for germanium or silicon.

J. Phys. Chem. Solids Pergamon Press 1961. Vol. 22, pp. 213–222. Printed in Great Britain.

PHOTOLEITUNG UND LUMINESZENZ VON II–VI-VERBINDUNGEN BEI TIEFEN TEMPERATUREN

I. BROSER, R. BROSER-WARMINSKY, G. KLIPPING, R. RASS und H.-J. SCHULZ

Institut für Elektronenmikroskopie am Fritz-Haber-Institut der Max-Planck-Gesellschaft, Berlin-Dahlem

Abstract—Low temperature measurements are carried out on single crystals of ZnS, ZnSe, CdS, and CdSe in order to study the fine structure of some optical and electrical properties which are influenced by low energy effects. These include phonons, excitons, and valence band splitting.

From the investigation of infrared luminescence in ZnS : Cu it can be concluded that the emission is connected with electron transitions between two localized energy levels of the luminescent center. The structure of the emission spectrum can be explained on the assumption that the luminescence may take place with the simultaneous emission of one of several longitudinal optical phonons.

The mechanism of edge emission in CdS can be fully understood by comparison with photoconductivity. From this it follows that the emission is caused by the recombination of a free electron and a trapped hole on a level near the top of the valence band. This level is split into two sub-levels, according to the splitting of the valence band, so explaining the existence of two systems of small bands. The separation of the bands within each of these systems is equal to the energy of the longitudinal optical phonon.

The measurements of line spectra of CdS in the emission, absorption, and reflection add some new experimental data to those already existing in the literature. The multiplicity of the spectra can be explained by phonon interaction, band splitting, and by hydrogen-like series of excited states of excitons.

Zusammenfassung—Bie tiefen Temperaturen wurden an Einkristallen aus ZnS, ZnSe, CdS, und CdSe Messungen zum Studium der Feinstruktur einiger optischer und elektrischer Eigenschaften durchgeführt. Hierbei wurden Erscheinungen wie Phononenwechselwirkung, Exzitenen- und Valenzband-Aufspaltung untersucht, die durch das Auftreten sehr kleiner Energiewerte gekennzeichnet sind.

Untersuchungen der Ultrarot–Lumineszenz von ZnS:Cu zeigen, dass diese Emission mit Elektronenübergängen zwischen zwei lokalisierten Energieniveaus des Lumineszenzzentrums verknüpft ist. Die Struktur des Emissionsspektrums lässt sich durch die Annahme erklären, die Lumineszenz finde unter gleichzeitiger Emission eines oder mehrerer longitudinaler optischer Phononen statt.

Der Mechanismus der Kantenemission von CdS ist durch einen Vergleich mit der Photoleitung widerspruchsfrei zu deuten. Demnach entsteht die Emission bei der Rekombination eines freien Elektrons mit einem gebundenen Defektelektron an einem Term nahe der oberen Kante des Valenzbandes. Eine Aufspaltung dieses Terms in zwei Niveaus, die der Aufspaltung des Valenzbandes entspricht, erklärt das Auftreten von zwei Systemen schmaler Banden. Der Abstand der Banden innerhalb eines jeden dieser Systeme ist gleich der Energie eines longitudinalen optischen Phonons.

Die Messungen der Linienspektren von CdS in Emission, Absorption und Reflexion ergänzen die aus der Literatur bekannten experimentellen Daten. Die Multiplizität der Spektren kann durch Phononen–Wechselwirkung, Bandaufspaltung und durch eine wasserstoffähnliche Serie angeregter Exzitonenzustände erklärt werden.

EINLEITUNG UND ÜBERSICHT

NACHDEM es R. FRERICHS im Jahre 1945 gelungen war, Kadmiumsulfid-Kristalle synthetisch herzustellen,[1] sind Untersuchungen über die optischen und elektrischen Eigenschaften der II–VI-Verbindungen in ständig zunehmender Zahl durchgeführt worden. Besonders über Kadmiumsulfid, den Prototyp des Photohalbleiters, und

Zinksulfid, den Prototyp des Kristallphosphors, liegt heute ein umfangreiches experimentelles Material vor. Viele Messungen wurden von Zimmertemperatur bis herab zur Temperatur der flüssigen Luft ausgedehnt, jedoch gibt es bisher nur wenige Untersuchungen bei sehr tiefen Temperaturen, der Temperatur des flüssigen Heliums und darunter. Auf eine 1951 von C. C. KLICK[2] veröffentlichte Arbeit über die Lumineszenzeigenschaften verschiedener Phosphore bei 4°K folgten erst in den letzten Jahren mehrere weitere Untersuchungen bei Heliumtemperatur. Das Hauptinteresse galt der Feinstruktur von Elektronenniveaus nahe der Bandkante[3–6]; einige andere Arbeiten betrafen Probleme der Zyklotronresonanz[7], der Anti-Stokes-Lumineszenz[8], und des Leitungsmechanismus im Gebiet der Störstellenstreuung[9].

Die relativ kleine Zahl von Experimenten bei 4°K erklärt sich aus dem erheblichen apparativen Aufwand, mit dem das Arbeiten mit flüssigem Helium verbunden ist, besonders wenn man gezwungen ist, das verdampfende Helium in einem geschlossenen Kreislauf wieder aufzufangen. Die Einrichtung eines Tieftemperatur-Laboratoriums in unserem Institut hat es ermöglicht, eine Reihe von Untersuchungen der Photoleitung und verschiedener optischer Eigenschaften an von uns gezüchteten Kristallen aus ZnS, CdS, ZnSe und CdSe bei der Temperatur des flüssigen Heliums durchzuführen.

In der vorliegenden Arbeit behandeln wir die Ultrarot-Lumineszenz von ZnS, die Kantenemission von ZnS, CdSe, ZnSe und die Linienspektren von CdS.

Die im ersten Kapitel wiedergegebenen Messungen der Ultrarot-Lumineszenz von ZnS führen frühere Arbeiten zur Klärung der energetischen Struktur des Leuchtzentrums fort. Es zeigt sich, dass für das Störzentrum zwei verschiedene Energieniveaus anzunehmen sind und die UR-Emission Übergängen zwischen diesen beiden Niveaus zuzuordnen ist. Die Aufspaltung des Emissionsspektrums in verschiedene Teilbanden lässt sich durch Abgabe eines oder mehrerer Phononen deuten.

Die im zweiten Kapitel behandelten Messungen der Kantenemission führen zu einer Einordnung der hierbei auftretenden Elektronenübergänge in das Termschema der Kristallphosphore. Aus dem Vergleich der Lumineszenz mit der Photoleitung kann man schliessen, dass eine Rekombination von freien Elektronen mit gebundenen Defektelektronen stattfindet. Das Emissionsspektrum zeigt bei CdS nicht nur eine Vielfalt der Banden infolge Phononen–Wechselwirkung, sondern auch eine weitere Struktur, die der Aufspaltung des Valenzbandes entspricht. Bei CdSe und ZnSe konnte eine Struktur nicht nachgewiesen werden.

Die im dritten Kapitel behandelten Messungen der linienhaften Emission, Absorption und Reflexion an CdS im Bereich der Bandkante ergänzen das in der Literatur bereits vorliegende Material und ermöglichen eine sinnvolle Ordnung der zahlreichen Linien. Die Multiplizität der Spektren lässt sich gut erklären durch Phononen–Wechselwirkung, durch die Aufspaltung des Valenzbandes und durch eine wasserstoffähnliche Serie von Anregungszuständen der Exzitonen, deren Bindungsenergie mit der Energie des longitudinalen optischen Phonons übereinstimmt.

APPARATUR

Zur Messung der optischen und elektrischen Eigenschaften bei tiefen Temperaturen wurden die untersuchten Kristalle in einem mit zwei Quarzfenstern versehenen Metall–Dewargefäss derart angebracht, dass sie von zwei Seiten bestrahlt bzw. beobachtet werden konnten. Bei dem in Abb. 1 gezeigten Kryostaten befand sich der Kristall im Vakuum und hatte über eine Legierung von Indium und Quecksilber guten thermischen Kontakt mit dem von innen durch flüssiges Helium gekühlten Kristallhalter. Die genaue Angabe der Kristalltemperatur ist hier schwierig, jedoch dürfte bei der guten Wärmeleitfähigkeit der Kristalle kein allzu grosser Temperaturunterschied zwischen der Messstelle und dem Kristallhalter bestanden haben. Für Messungen, bei denen auf grössere Genauigkeit der Temperaturangabe Wert gelegt wurde, konnte der innere Behälter durch ein Glasgefäss ersetzt werden, in welchem sich der Kristall direkt in flüssigem Helium befand. Von Nachteil ist hier, dass ein Einfluss des Heliums auf die Eigenschaften der Kristalloberfläche nicht ausgeschlossen werden kann. Die Kontrolle des Heliumstandes erfolgte nach einer neuartigen Methode,[10] bie der die Widerstandsänderung einer stromdurchflossenen Wolframwendel beim Übergang vom flüssigen in gasförmiges Helium ausgenutzt wird.

Die Untersuchung der linienhaften Emissions-, Absorptions-und Reflexionsspektren des Kadiumsulfids erfolgte mit Hilfe eines Vierprismenspektrographen (R. Fuess, Berlin), der bei einer Wellenlänge von 5000 Å ein Auflösungsvermögen von 20 Å/mm hat. Angeregt wurden die Kristalle mit der von einem SCHOTT-Filter UG 11 durchgelassenen ultravioletten Strahlung einer Quecksilberdampflampe HBO 200 (Osram GmbH); für

Vol. 2
1961

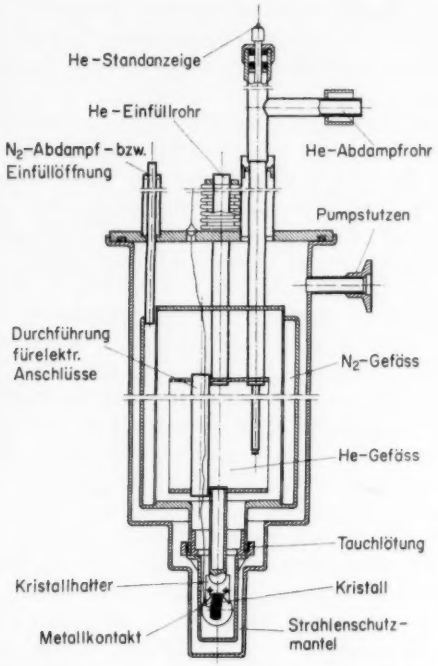

ABB. 1. Kryostat zur Messung der Photoleitung und der optischen Eigenschaften von Kristallen bei tiefen Temperaturen.

die Aufnahme der Absorptions- und der Reflexionsspektren verwendeten wir eine Projektionslampe. Zur besseren Lokalisierung von starken und schwachen Linien auf derselben Aufnahme setzten wir vor den Eingangsspalt des Spektrographen ein 6-Stufen-Filter, das die Lichtintensität im Verhältnis 100 : 3 : 6 : 12 : 25 : 50 : 100 variiert. Die wiedergegebenen Spektren zeigen daher eine dieser Abstufung entsprechende Struktur von 7 Streifen.

Wenn grössere Wellenlängen–Bereiche erfasst werden sollten, wurden die Emissionsspektren mit einem Doppel-Monochromator (Carl Leiss, Berlin) und einem rot- und ultrarotempfindlichen Photomultiplier (Fernseh-AG) aufgenommen. Zur Aussonderung von breiteren Spektralbereichen für die Anregung benutzten wir zum Teil auch Interferenzfilter. Die Spektren im Ultraroten wurden mit einer Wechsellicht-Methode unter Verwendung eines Einfach-Monochromators mit Quarzprisma und eines Bleisulfid-Photoleiters erhalten.

ULTRAROT–EMISSION VON ZINKSULFID

GARLICK und DUMBLETON[11] fanden 1954 an kupferaktiviertem Zinksulfid eine strukturierte Emission im Spektralgebiet zwischen 1,4 und 2,0 μ, die besonders bei der Temperatur des flüssigen Stickstoffs stark ausgeprägt war. BROWNE[12] führte 1956 eine ausführliche Untersuchung durch, bei der Emissions- und Anregungsspektren sowie Intensitäts- und Temperaturabhängigkeiten verschieden präparierter Zinksulfid- und Kadmiumsulfid-Phosphore gemessen wurden. Die drei von ihm gefundenen Teilbanden ordnete er verschiedenen Elektronenübergängen im Bändermodell einschliesslich zweier diskreter Niveaus zu. Den Einfluss der Präparationsbedingungen auf die UR-Emission verfolgten APPLE und PRENER[13]; ihre Ergebnisse bestätigten die Notwendigkeit der Anwesenheit von Kupfer für das Auftreten dieser Lumineszenz.

Messungen über Zusammenhänge zwischen der UR–Emission und anderen optischen Eigenschaften sowie der Photoleitung führten I. BROSER und H.-J. SCHULZ[14] zur Aufstellung eines Energiemodells des für die UR–Emission verantwortlichen Leuchtzentrums. Danach führt der Übergang von Elektronen zwischen zwei diskreten Energietermen, entsprechend einem Übergang im Innern des Zentrums, zur Aussendung der ultraroten Lumineszenz, während Übergänge aus dem Leitungsband in eines der beiden Energieniveaus die sichtbare Lumineszenz liefern. Die Absorption der die UR–Emission anregenden Strahlung erfolgt entweder durch Anregung eines Elektrons vom Valenzband in den oberen unbesetzten Term oder durch einen zur UR–Emission inversen Elektronenübergang zwischen den beiden Niveaus des Zentrums. Diesen Mechanismus erkennt man gut aus den bei 4°K und 80°K aufgenommenen Anregungsspektren der UR–Lumineszenz (Abb. 2). Das besonders bei 4°K stark ausgeprägte Maximum bei $\lambda = 1{,}35\ \mu$m entspricht dem Übergang innerhalb des Zentrums, das relativ breite Plateau in Bereich $0{,}8\ \mu\text{m} > \lambda > 0{,}5\ \mu$m dem Übergang aus dem Valenzband in den oberen Term.

Im Zusammenhang mit der Frage nach der Entstehung des Doppelterms war von verschiedenen Autoren vermutet worden, das als Akzeptor eingebaute Kupfer könne ausser dem Grundzustand auch noch angeregte Zustände für Defektelektronen besitzen und der Übergang zwischen diesen Zuständen führe zur Emission und Absorption von ultrarotem Licht. Wenn dies die Ursache für die beobachteten zwei Niveaus ist, sollten bei tiefen Temperaturen weitere, sonst durch die

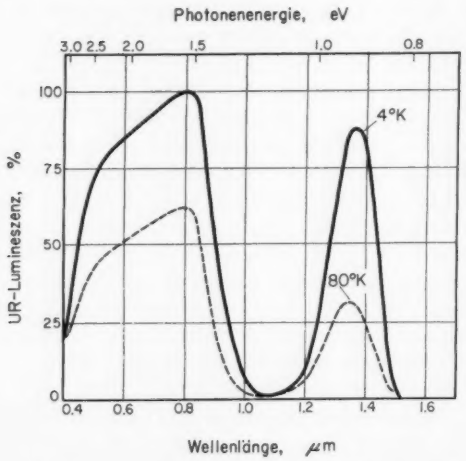

ABB. 2. Anregungsspektrum der Ultrarotlumineszenz eines ZnS-Kristalles bei gleichzeitiger Blaueinstrahlung ($\lambda = 436$ nm).

Nähe der Bandkante verdeckte, angeregte Terme auftreten. Man findet jedoch im Gebiet um $\lambda = 0{,}9\ \mu$m bei Abkühlung auf 4°K bis auf eine geringfügige Verschiebung nach langen Wellen hin keine merkliche Strukturänderung im Anregungsspektrum. Daher muss man annehmen, das nächste angeregte Niveau läge bereits im Valenzband oder ein anderer Mechanismus sei für das Auftreten des beobachteten Doppelterms verantwortlich.

Eine Schwierigkeit bei dem von uns vorgeschlagenen Modell des Leuchtzentrums bestand darin, dass die UR–Emission nur bei Übergängen zwischen den zwei diskreten Energieniveaus auftreten soll, dass aber mindestens drei Teilbanden beobachtet werden, deren Intensitätsverhältnisse von der Temperatur und den Anregungsbedingungen fast unabhängig sind. Um der Struktur der UR–Emission Rechnung zu tragen, haben wir eine Aufspaltung der Niveaus angenommen,[14] ohne aber eine physikalische Ursache hierfür angeben zu können. Die von BROWNE[12] ausgesprochene Vermutung, dass ähnlich wie bei der Kantenemission eine Phononen–Wechselwirkung vorliegen könne, schien sich nicht zu bestätigen, da die Abstände der drei Teilbanden dann gleich sein müssten, was offensichtlich nicht der Fall war. Bei einem genauen Studium des bei 4°K aufgenommenen Spektrums (Abb. 3) fiel uns jedoch auf, dass der Abstand zwischen den beiden gut ausgeprägten Maxima doppelt so gross wie der Abstand zwischen dem Haltepunkt bei 0,705 eV und dem Maximum bei 0,75 eV ist, dass die

Vol. 22
1961

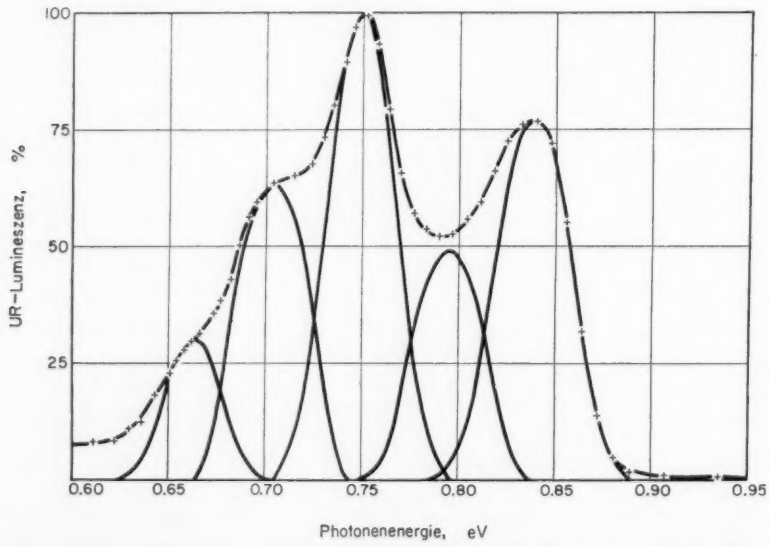

ABB. 3. Teilbandenzerlegung der Ultrarotlumineszenz eines ZnS-Kristalles bei 4°K.

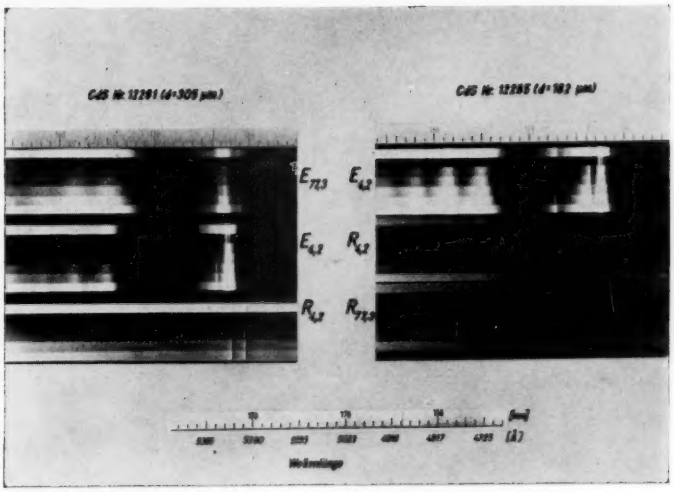

ABB. 4. Emissions- und Reflexionsspektren von CdS-Kristallen bei 4,2 und 77,3°K ($400\ \text{nm} > \lambda_{\text{Anregung}} > 300\ \text{nm}$).

BLANK
PAGE

Vol. 22
1961

Differenz aus den letzten beiden Werten, 0,045 eV, etwa der aus der Literatur[15] bekannten Energie des longitudinalen optischen Phonons des ZnS entspricht und dass die Banden unsymmetrisch sind. Eine Zerlegung des Spektrums in symmetrische Teilbanden von der Seite hoher Energien her liefert nun ein überraschendes Ergebnis : Das Spektrum enthält mindestens fünf äquidistante Banden, die alle etwa eine Halbwertsbreite von 0,04 eV und einen gegenseitigen Abstand von 0,045 eV haben. Zu klären bleibt noch die Frage, warum bei der UR–Emission keine gleichmässige Abnahme der Intensität der Maxima mit wachsender Zahl der beteiligten Phononen erfolgt, wie es z.B. bei der Kantenemission der Fall ist.

KANTENEMISSION VON CdS, CdSe UND ZnSE

Kadmiumsulfid hat eine besonders bei tiefen Temperaturen ausgeprägte Emission im Gebiet der Bandkante,[16] die aus einer Vielzahl von schmalen Banden und Linien besteht (Abb. 4). Man unterscheidet im Hinblick auf Struktur und Wellenlänge zwei Bereiche,[17] einen langwelligeren, grünen Teil, der aus Banden besteht, und einen kurzwelligeren blauen Bereich, der hauptsächlich Linien enthält. Während man die linienhafte blaue Emission mit Exzitonenzuständen in Verbindung gebracht hat,[4] wird für die grüne "Kantenemission" ein Zusammenhang mit Gitterfehlern[18] vermutet.

Viel diskutiert wurde die Frage, ob für diese Kantenemission freie Elektronen oder freie Defektelektronen verantwortlich sind. Lambe, Klick und Dexter[5] deuteten ihre auch die Photoleitung einschliessenden Versuche mit der Annahme, dass eine Rekombination von gebundenen Elektronen mit freien Defektelektronen stattfindet. Andere Autoren[19, 20] zeigten, dass das bekannte Schön–Klasensche Modell die Messungen besser wiedergibt. Pedrotti und Reynolds[21] untersuchten die Temperaturabhängigkeit des Emissionsspektrums im Gebiet zwischen 4°K und 77°K und beobachteten dabei zwei verschiedene um +0,016 eV bzw. −0,023 eV gegeneinander verschobene Bandensysteme, von denen eines bei höheren, das andere bei tieferen Temperaturen stärker ausgeprägt war ; die Frage nach der Beteiligung freier Elektronen oder freier Löcher am Leuchtprozess bleibt aber auch hiernach noch offen.

Eine Entscheidung hierüber sollte der Vergleich zwichen Lumineszenz und Photoleitung bringen ; wenn freie Elektronen — die Träger der Leitfähigkeit beim CdS — am Leuchtprozess beteiligt sind, müsste das Abklingen gleich schnell verlaufen. Abb. 5 zeigt einen Vergleich zwischen

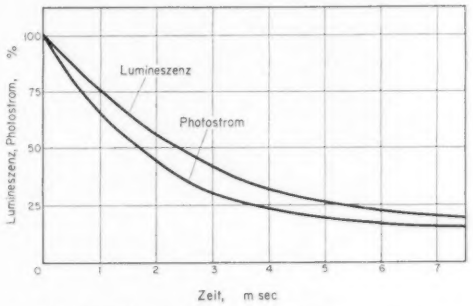

Abb. 5. Abklingen der roten Lumineszenz und des Photostromes eines CdS-Kristalles bei Zimmertemperatur ($\lambda_{\text{Anregung}} = 518$ nm).

der Photoleitung und der roten Emission ($\lambda =$ 7200 Å) bei Zimmertemperatur, Abb. 6 den Vergleich mit der grünen Kantenemission bei 4°K. Man erkennt die gute Übereinstimmung im Abklingen zwischen Photoleitung und roter Lumineszenz, obwohl durch die Temperaturänderung die Abklingzeit um zwei Grössenordnungen verändert wurde, und man sieht auf Abb. 6 ferner, dass auch die grüne Emission den gleichen zeitlichen Verlauf wie die Photoleitung aufweist. Hieraus kann geschlossen werden, dass es sich bei der Kantenemission von CdS um die Rekombination eines freien Elektrons mit einem gebundenen Loch handelt.

Nicht nur bei CdS, sondern auch an anderen II–VI-Verbindungen tritt eine Kantenemission auf. So berichtete Kröger[16] bereits 1940 über die Tieftemperaturlumineszenz von reinem ZnS und Andress und Mollwo[22] beobachteten eine entsprechende Emission beim ZnO. In allen Fällen wurde eine Aufspaltung in eine Reihe von schmalen Banden gleichen energetischen Abstandes gefunden, was sich durch eine Wechselwirkung der Leuchtzentren mit Phononen deuten lässt. Beim CdS beträgt diese Verschiebung 0,038 eV (vgl. Abb. 4) und ist identisch mit der im Ultrarot-Absorptionsspektrum gefundenen Energie des longitudinalen optischen Phonons.[19] Die Möglichkeit, diese Energie im sichtbaren

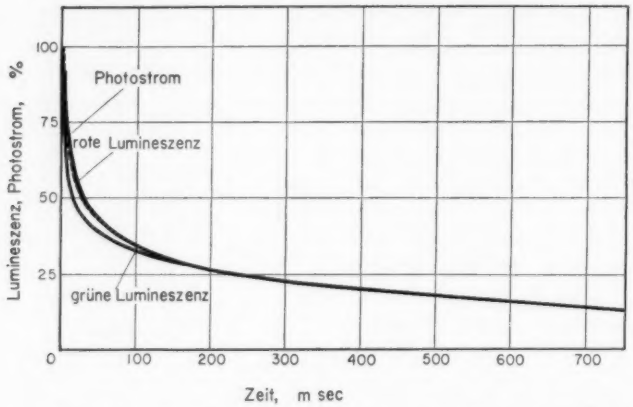

ABB. 6. Abklingen der roten und grünen Lumineszenz und des Photostromes eines CdS-Kristalles bei 4°K ($\lambda_{\text{Anregung}} = 489$ nm).

Spektralbereich vorzufinden, veranlasste uns, auch an anderen von uns gezüchteten Kristallen die Kantenemission zu studieren. Während wir an ZnS-Kristallen bisher keine derartige Lumineszenzerscheinung finden konnten, war sie bei ZnSe und CdSe leicht zu messen (Abb. 7). Die beiden Emissionsmaxima bei 4590 Å (ZnSe) und 6830 Å (CdSe) sind gegenüber CdS um +0,25 eV bzw. −0,63 eV verschoben, was relativ gut mit der Verschiebung der Bandkanten ($E_{CdS} \approx 2{,}55$ eV, $E_{ZnSe} \approx 2{,}75$ eV, $E_{CdSe} \approx 1{,}85$ eV) übereinstimmt.

Im Gegensatz zu CdS zeigen die in Durchstrahlung gemessenen Spektren von CdSe und ZnSe keinerlei Aufspaltung der Kantenemission in Teilbanden. Auch bei vergleichenden Untersuchungen mit dem höher auflösenden Spektrographen konnte nur eine relativ breite Bande gefunden werden. Beim ZnSe tritt aber bei etwa 4375 Å eine noch kurzwelligere schmale strukturierte Bande auf, die offensichtlich der blauen Fluoreszenz des CdS entspricht. Ob der Wert der Phononenenergie bei ZnSe und CdSe zu klein[31] ist, so dass die Aufspaltung der Kantenemission nicht mehr zu erkennen ist, oder ob dieser Effekt bei den Seleniden überhaupt fehlt, muss zunächst offen bleiben.*

* *Anmerkung bei der Korrektur.* HALSTED und Mitarbeitern (*J. Phys. Chem. Solids* **22**, 109 (1961) konnten die Phononenaufspaltung auch an den Seleniden und Telluriden des Zn und Cd nachweisen und zeigen, dass die Energiedifferenz zwischen den Banden gleich der jeweiligen aus dem Ultrarotspektrum bekannten Energie der longitudinalen optischen Phononen ist.

Die Kantenemission von CdS zeigt, wie schon erwähnt, neben der Aufspaltung durch Phononen-Wechselwirkung noch eine weitere Unterteilung in jeweils zwei Banden, wie sie auch in Abb. 4 erkennbar ist. Da die Energiedifferenz +0,016 eV beträgt[21] (vgl. Abb. 4, Kristall 12281) und damit gerade dem Abstand der beiden oberen Valenzbänder gleicht,[23] liegt es nahe, entsprechend der Bandaufspaltung auch eine Aufspaltung des Störterms anzunehmen.[24]

LINIENSPEKTRUM DES KADMIUMSULFIDS

Die Feinstruktur der Absorption, Emission und Reflexion von Kadmiumsulfid-Kristallen bei Wellenlängen nahe der Bandkante wurde bei tiefen Temperaturen von mehreren Autoren untersucht. GROSS und Mitarbeiter[3,6] studierten eingehend die linienhafte Struktur des Absorptionsspektrums und die Zusammenhänge mit den Anregungsspektren der Photoleitung, GRILLOT[4] berichtete über das Auftreten von schmalen Emissionslinien im Gebiet zwischen 4850 und 5000 Å und DUTTON[25] fand im Reflexionsspektrum zwei scharfe Minima bei 4840 und 4870 Å. In den Jahren 1959 und 1960 erschienen drei weitere Arbeiten über diese Probleme, in denen sehr genaue Angaben über Einzelheiten der Linienspektren gemacht wurden. GRILLOT, GROSS und Mitarbeiter[26] verglichen das Emissionsspektrum reiner Kristalle mit dem Absorptionsvermögen und steigerten die Messgenauigkeit bis

Vol. 22
1961

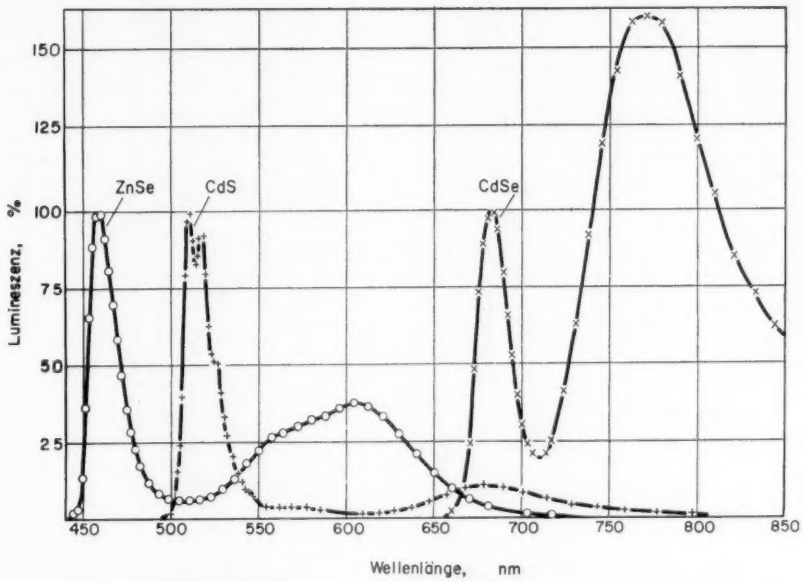

ABB. 7. Emissionsspektren eines ZnSe-, eines CdS-und eines CdSe-Kristalles bei 4°K. (Anregung jeweils in Grundgittergebiet nahe der Absorptionkante).

auf Bruchteile eines Ångström ; THOMAS und HOPFIELD[23] führten eine sorgfältige Analyse der von ihnen gefundenen Reflexionsspektren durch und verknüpften die auftretenden Strukturen mit drei Exzitonenserien, die sie der Aufspaltung des Valenzbandes zuordnen. Aus der Beobachtung angeregter Exzitonenzustände und deren Polarisationseigenschaften schlossen sie auf die Bindungsenergie der Exzitonen und auf die Symmetrieeigenschaften von Valenz-und Leitungsband. Korrelationen zwischen den Emissions- und den Reflexionseigenschaften bestanden bei ihnen nur bei 77°K. PEDROTTI und REYNOLDS[21] deuteten die von ihnen aufgenommenen Emissionsspektren auf Grund eines Energiemodells, das die Existenz von Störzentren voraussetzt. Sie weisen besonders darauf hin, dass die Vielzahl von Linien und Banden durch eine Wiederholung der primären Spektren im Abstand der Energie des longitudinalen optischen Phonons ($\sim$ 0,038 eV) hervorgerufen wird.

Vergleicht man die drei zuletzt genannten Untersuchungen, so findet man zwar in einigen Fällen eine überraschend gute Übereinstimmung der Resultate ; es bestehen aber teilweise auch erhebliche Unterschiede in den experimentellen Befunden und deren theoretischen Deutungen, so dass es gerechtfertigt erschien, weitere Messungen mit den uns zur Verfügung stehenden Kristallen durchzuführen. Insbesondere haben wir versucht, Reflexions-, Absorptions- und Emissionsspektren am gleichen Kristall in gleicher Anordnung aufzunehmen und die ganz offensichtlich vorhandenen Zusammenhänge zwischen ihren Strukturen deutlicher als bisher aufzuzeigen.

Emissions- und Reflexionsspektren wurden an einer Reihe von reinen und dotierten Kristallen verschiedener Schichtdicke aufgenommen. Es zeigte sich eine gute Übereinstimmung der Lage der auftretenden Linien bei allen untersuchten Kristallen ; dagegen traten erhebliche Abweichungen in den Intensitätsverhältnissen der Linien von Kristall zu Kristall auf.

Bei der Temperatur des flüssigen Stickstoffs zeigen hauptsächlich dicke und weniger reine Kristalle eine helle Lumineszenz in Form einer etwas verwaschenen Linienstruktur (Abb. 4, Kristall 12281). Es tritt eine schmale Bande bei 4843 Å, eine breitere bei 4870 Å und eine weitere Linie bei 4883 Å auf. Reinere Kristalle haben bei

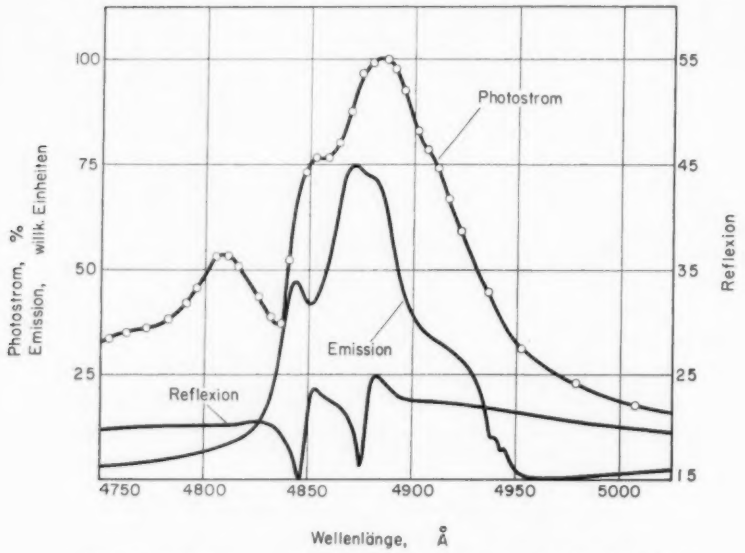

ABB. 8. Emissions- und Reflexionsspektrum eines CdS-Kristalles, aufgenommen mittels Mikrophotometer, und Anregungsspektrum der Photoleitung bei 77°K.

dieser Temperatur eine nur sehr schwache Emission. Zwischen den beiden kurzwelligen Emissionslinien und den Linien des Reflexionsspektrums (Abb. 4, Kristall 12285) besteht gute Übereinstimmung. Dies erkennt man auch gut aus Abb. 8, die ausserdem noch einen Vergleich mit der Photoleitung enthält, wo ebenfalls eine Feinstruktur gefunden wurde.[6,29,30] Wenn man die beiden steilen Flanken des Photoleitungsspektrums dem Minimum der Reflexion bzw. dem Maximum der Emission zuordnet, ist ein Zusammenhang deutlich sichtbar. Die Emissions- und Reflexionsmessungen entsprechen weitgehend den Resultaten von THOMAS und HOPFIELD[23] und von DUTTON[25] und LEMPICKI[27]. Neu erscheint lediglich die Tatsache, dass die Helligkeit der Linien bei unseren Kristallen relativ gross ist und bei Abkühlung auf 4°K nicht wesentlich steigt.

Bei 4°K beobachtet man gegenüber 77°K eine Verschiebung der drei Linien um ca. 20 Å ins kurzwellige Gebiet des Spektrums, zusätzlich erscheint jetzt aber noch eine grössere Zahl weiterer Linien, die vor allem im langwelligen Teil des Spektrums liegen. Bemerkenswert erscheint zunächst, dass die bei 77°K kurzwelligste Linie jetzt wieder mit der Linie des Reflexionsspektrums (4823 Å) übereinstimmt. Messungen mit zeigen, dass das Licht hier im Gegensatz zu allen übrigen Linien auch einen erheblichen polarisations filter mit E|| zur *c*-Achse polarisierten Anteil enthält. Dies unterstreicht die Zugehörigkeit zur kurzwelligen Reflexionslinie, die auch bei Polarisation des auffallenden Lichtes mit $E\|$ zu c vorhanden ist. Ferner fällt eine besonders im Reflexionsspektrum stark ausgeprägte Linie bei 4852 Å ins Auge, die bei der Emission mit $E \perp c$ polarisiert ist[23]. Bedeutsam erscheint uns ausserdem eine schwache Emissionslinie bei 4814 Å, die ebenfalls im Reflexionsspektrum vorhanden ist und an derselben Stelle wie das von THOMAS und HOPFIELD gefundene schwache Reflexionsminimum liegt. Diese Linie könnte, den Vorstellungen der eben genannten Autoren folgend, dem ersten angeregten Zustand eines Exzitons zugeordnet werden.

Versucht man, in dem Linienspektrum, das durch Phononen-Wechselwirkung noch vielfältiger gestaltet wird, eine Systematik zu finden, so erscheint es uns sinnvoll, bei der zuletzt genannten Linie 4814 Å zu beginnen. Handelt es

Vol. 2
1961

sich um den ersten angeregten Exzitonenterm, so wäre die Linie bei 4852 Å der dazugehörige Grundzustand. Nach höher angeregten Zuständen sucht man im kurzwelligen Teil des Spektrums aber wohl vergeblich, weil das starke Absorptionsvermögen des Kristalles für mit $E \parallel c$ polarisiertes Licht eine möglicherweise vorhandene Emission nicht nach aussen gelangen lässt. Nun kehrt aber das Spektrum infolge Phononen-Wechselwirkung noch mehrmals, um jeweils 0,038 eV nach längeren Wellenlängen hin verschoben, wieder, der Grundzustand ($\lambda = 4852$ Å) bei 4926 Å und 5003 Å, der erste angeregte Zustand ($\lambda = 4814$ Å) bei 4887 Å, 4960 Å und 5036 Å. Da die Intensitätsverhältnisse sich in den Spektren höherer Ordnung umkehren (die Linie des angeregten Zustandes ist jetzt intensiver als die des Grundzustandes), wird es möglich, auch noch weitere Linien einer Exzitonenserie zu finden. Auf Abb. 4 erkennt man im "Spektrum erster Ordnung" eine scharfe und starke Linie bei 4868 Å (mit korrespondierenden Linien bei 4940 Å und 5019 Å) und eine etwas verbreiterte Linie bei 4863 Å (hier sind die korrespondierenden Linien in den Spektren höherer Ordnung nicht mehr zu sehen). Beide Linien, die einem zweiten und dritten Anregungszustand des Exzitons zuzuordnen wären, sind stark mit $E \perp c$ polarisiert, die energieärmere aber schwächer als die energiereichere. Während die meisten Linien eine scharfe kurzwellige Grenze haben, scheint die 4863–Linie nach kurzen Wellenlängen hin verbreitert zu sein und enthält anscheinend noch eine weitere Feinstruktur[26]. Es liegt nahe, hier eine Überlagerung von Linien in der Nähe der Seriengrenze zu vermuten. Die Grenze selbst dürfte bei etwa 4858 Å liegen.

Damit haben wir ein Termschema gefunden, das grosse Ähnlichkeit mit den an anderen Stoffen gefundenen wasserstoffähnlichen Spektren von Exzitonen aufweist. Die gefundenen Energiewerte 2,511 eV, 2,531 eV, 2,541 eV und 2,545 eV rücken immer näher zusammen und konvergieren zu einer Seriengrenze bei 2,549 eV. Die Termfolge lässt sich allerdings nach einem Gesetz von der Form $E = A - (B/n^2)$ nur darstellen, wenn man den Wert für $n = 1$ ausnimmt (vgl. z.B. die entsprechende Beobachtung von NIKITINE[28] am Absorptionsspektrum des PbJ_2). Man erhält dann für B einen Wert von 0,07 eV, der sich erheblich von dem von THOMAS und HOPFIELD[23] angegebenen Wert von 0,028 eV unterscheidet. Die Bindungsenergie des Exzitons ergibt sich zu $E_1 - E_\infty = 0{,}038$ eV und stimmt mit der Energie des longitudinalen optischen Phonons überein. Das Ende einer Serie fällt mit dem Beginn der Serie niederer Ordnung zusammen.

Offen bleibt zunächst die Frage, aus welchem Grunde angeregte Zustände der mit dem kurzwelligen Reflexionsmaximum übereinstimmenden Linie bei 4823 Å nicht gut sichtbar in Erscheinung treten ; eine schwache Andeutung der Linien ist teilweise vorhanden.

Ein Problem bildet ferner die Deutung der ganz unsystematischen Intensitätsverhaltnisse der einzelnen Linien, die zudem von Kristall zu Kristall schwankt. Die dem Anregungszustand $n = 2$ entsprechende Linie ist z.B. bei einem in Abb. 9 wiedergegebenen Spektrum eines sehr dünnen Kristalles kaum vorhanden, während die übrigen Linien gut ausgebildet sind ; die von PEDROTTI und REYNOLDS vertretene Meinung, dass sie bei Kristallen, die keine grüne Kantenemission zeigen, stets fehlen sollte, konnten wir allerdings nicht bestätigen. Zu vermuten ist, dass die Intensitätsverhältnisse vom Störstellengehalt des Kristalles abhängen.

An einem dünnen Kristall ($d = 3\ \mu$m) wurde auch das Absorptions spektrum aufgenommen (Abb. 9). Man erkennt zunächst die gute Übereinstimmung der starken Banden mit den beiden Reflexionsminima, was noch besser mit polarisiertem Licht verdeutlicht wird. Zahlreiche Banden des Absorptionsspektrums erscheinen bei diesem dünnen Kristall nochmals im Reflexionsspektrum als helle Bereiche, was wohl daran liegt, dass bevorzugt solche Wellenlängen reflektiert werden, die der Kristal besonders stark absorbiert.

Die kurzwellige Grenze, bis zu der Licht durchgelassen wird, liegt bei 4782 Å und entspricht dem Übergang vom unteren Valenzband in den Exzitonenterm für $n = 2$. Den Wert des Abstandes zwischen oberstem Valenzband und Leitungsband erhält man, wenn man die für das Exzitonenspektrum 1. Ordnung gefundene Seriengrenze bei 2,549 eV um die Phononenenergie 0,038 eV verschiebt. Es ergeibt sich also der Bandabstand des CdS bei 4°K zu 2,587 eV für das oberste Valenzband bzw. 2,603 eV für das zweite Valenzband.

LITERATUR

1. FRERICHS R., *Naturwiss.* **33,** 281 (1946).
2. KLICK C. C., *J. Opt. Soc. Amer.* **41,** 816 (1951).
3. GROSS E. F. und JAKOBSON M. A., *Dokl. Akad. Nauk SSSR* **102,** 485 (1955).
4. GRILLOT E., *J. Phys. Radium* **17,** 822 (1956).
5. LAMBE J. J., KLICK C. C. und DEXTER D. L., *Phys. Rev.* **103,** 1715 (1956).
6. GROSS E. F., KAPLIANSKII A. A. und NOVIKOV B. V., *Dok. Akad. Nauk. SSSR* **111,** 761 (1956).
7. DEXTER R. N., *J. Phys. Chem. Solids* **8,** 494 (1959).
8. BROSER I., BROSER-WARMINSKY R. und SCHULZ H.-J., *Proc. Internat. Conf. on Semiconductor Physics, Prague* 1960, *Czech. J. Phys.* 771 (1961).
9. PIPER W. W. und HALSTED R. E., *Proc. Internat. Conf. on Semiconductor Physics, Prague* 1960, *Czech J. Phys.* 1046 (1961).
10. KLIPPING G. und RASS R. C. *Kältetechnik* **3,** 283 (1961).
11. GARLICK G. F. J. und DUMBLETON M. J., *Proc. Phys. Soc. Lond.* B**67,** 442 (1954).
12. BROWNE P. F., *J. Electron.* **2,** 1 (1956).
13. PRENER J. S. und APPLE E. F., *J. Phys. Chem. Solids* **13,** 81 (1960).
14. BROSER I. und SCHULZ H.-J., *J. Electrochem. Soc.* **108,** 545 (1961).
15. HAAS M. M. C. und MATHIEU J. P., *J. Phys. Radium* **15,** 492 (1954).
16. KRÖGER F. A., *Physica* **7,** 1 (1940).
17. FURLONG L. R. und RAVILIOUS C. F., *Phys. Rev.* **98,** 954 (1955).
18. KULP B. A. und KELLEY R. H., *J. Appl. Phys.* **31,** 1057 (1960).
19. COLLINS R. J., *J. Appl. Phys.* **30,** 1135 (1959).
20. BROSER I. und BROSER-WARMINSKY R., *Solid State Physics in Electronics and Telecommunications* Vol. 4, p. 680, Academic Press London (1960) (*Proc. Internat. Conf. Brussels*, June 2–7, 1958).
21. PEDROTTI L. S. und REYNOLDS D. C., *Phys. Rev.* **120,** 1664 (1960).
22. ANDRESS B. und MOLLWO E., *Naturwiss.* **46,** 623 1959).
23. THOMAS D. G. und HOPFIELD J. J., *Phys. Rev.* **116,** 573 (1959).
24. BIRMAN J. L., *J. Electrochem. Soc.* **107,** 409 (1960).
25. DUTTON D., *Phys. Rev.* **112,** 785 (1958).
26. BANCIE–GRILLOT M., GROSS E. F., GRILLOT E. und RAZBIRINE B. S., *C.R. Acad. Sci.* (*Paris*) **248,** 86 (1959).
27. LEMPICKI A., *Proc. Phys. Soc. Lond.* **74,** 138 (1959).
28. NIKITINE S., *Helv. Phys. Acta* **28,** 308 (1955).
29. BÖER K. W. und GUTJAHR N., *Z. Phys.* **152,** 203 (1958).
30. BROUDE V. L., FREMENKO V. V. und CHIKOVANI N. N. *Dokl. Akad. Nauk. SSSR* **119,** 911(1958).
31. MITSUISHI A., YOSHINAGA H., und FUJITA S., *J. Phys. Soc. Japan* **13,** 1235 (1958).

DISCUSSION

A. HALPERIN: The system of lines classified by the author as hydrogen-like series (for CdS) do not look to have shapes and intensity ratios as one would expect for such a series. I wonder how many lines were observed in a series, or what was the highest n of the observed lines.

I. BROSER: The shape of the exciton-series seems to be understandable if phonon-interactions are taken into account. The ratio of the intensities of the lines is indeed difficult to explain, as it varies from crystal to crystal. Defect or impurity states apparently control the brightness of the lines. The highest n of the lines, which could be observed, so far, was 4.

R. E. HALSTED: Do you find that the infrared emission attributed to Cu impurity in CdS can also be constructed from a series of emission lines separated by the longitudinal optical phonon energy?

I. BROSER: We have not yet measured the emission spectrum of CdS at low temperatures. From the similarity of emission spectra of ZnS–Cu and CdS–Cu at 77°K it might be expected that the construction of infrared emission by a series of equally spaced bands will also be possible with CdS. It seems, however, that the distance of the bands in this case is somewhat greater than the energy of the longitudinal optical phonon.

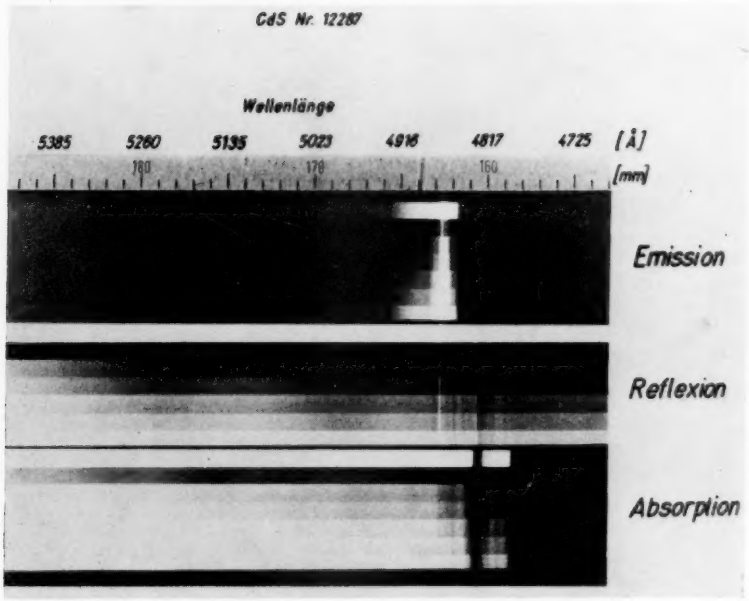

ABB. 9. Emissions-, Reflexions- und Absorptionsspektrum eines dünnen ($d = 3\mu$m) CdS–Kristalles bei 4°K (400 nm $> \lambda_{\text{Anregung}} >$ 300 nm).

BLANK
PAGE

Vol. 22
1961

J. Phys. Chem. Solids Pergamon Press 1961. Vol. 22, pp. 223–226. Printed in Great Britain.

STRUCTURES OF PHOTOCONDUCTIVITY SPECTRA AND RELATED PHENOMENA OF CADMIUM SULPHIDE

HIROJI MITSUHASHI

Technical Research Laboratories, Japan Broadcasting Corporation (NHK), Kinuta, Setagaya, Tokyo

Abstract—Single crystals of highly pure CdS show the structures of photoconductivity spectra near the absorption edge at liquid nitrogen temperature. For specimens of high photosensitivity, a prominent structure is observed on the longer wavelength side of the exciton band ($\lambda > 4870$ Å), which is presumably due to imperfections in crystals. Structure of this kind is different in nature from that appearing in the exciton band. The specimen giving pronounced peak at room temperature undergoes infra-red quenching of photoconductivity, indicating that there must be a certain correlation of the defect responsible for the quenching with that for the photoconductivity structure in the imperfection band.

INTRODUCTION

THE CdS crystal of high response has quite a sharp single peak of photoconductivity near the fundamental absorption edge at room temperature[1] and the peak gets fairly distinct structures at lower temperature.[2,3,4] Several investigators have reported that the crystal of high sensitivity shows the occurrence of infra-red quenching of photocurrent.[5,6]

One of the principal purposes of this paper is to study the origin of photoconductivity, especially of the peak on the longer wavelength side of the exciton band. Infra-red measurements are also provided to aid in correlating the experimental data with the properties associated with the crystal defect.

In a previous paper[7] the photoconductivity structures of highly pure single crystals near the absorption edge at 81°K were discussed to some degree. Measurements were made of spectral distribution of the structures and spectral dependence of decay time of the response as well. It was ascertained from data concerning exciton band[8,9] that the structures were classified into two groups. One, which occurred in the shorter wavelength range ($\lambda < 4870$ Å) was attributed to the photoconductivity due to excitons. The other, denoted as I band, was attributed to that from some crystal imperfections, which appeared on the longer wavelength side of the former. The I band generally emerged at the longer wave side of the exciton band where the absorption coefficient was considerably lower. Therefore the free carriers due to the I band were generated in the bulk and have a long lifetime. Thus the I band exerted an important bearing on the photosensitivity of the crystal. The peak of this band was generally more prominent for the more photosensitive material. The mechanism of I band photoconductivity could be inferred that the electrons excited from the filled band to the I band would be ionized into the conduction band through absorption of phonons.

Referring to the infra-red quenching, BUBE has made a detailed study according to a hypothesis advanced by ROSE[10]. He assumed two classes of recombination centers owing to crystal defects, class 1 and class 2. These could be associated on electrostatic grounds with the anion and cation vacancies respectively. Infra-red light excited the trapped holes in class 2 centers from their ground states to higher levels for holes lying close to the filled band. Here they could be ionized thermally into the filled band, with a resulting decrease of photoconductivity due to bias illumination.

EXPERIMENTAL

For measurement at low temperatures, a simple cryostat is designed to hold the crystals.[7] The cryostat is kept evacuated in order to avoid the influence of atmosphere. All of the crystals were grown by sublimation from pure CdS powder.

The monochromator used to measure the photoconductivity due to the I band is a modified Cary spectrophotometer Model 14. The resolution of the instrument is adjusted to be about 2 Å. In general a photoconductivity structure comes out at the longer wavelength side of the exciton band as illustrated in Fig. 1. Samples of

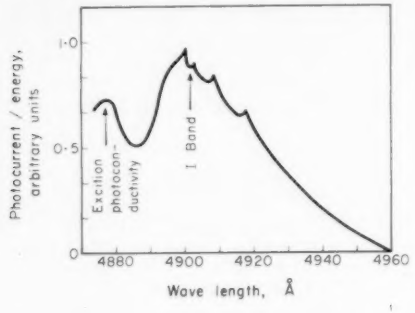

FIG. 1. The spectral structures of I band photoconductivity (specimen No. 7, 109°K, electric light vector $E \perp c$, 50 V/cm).

poor response do not exhibit well-defined I band structure. In addition the I band shows its peak at different wavelengths, depending on each sample, while the peak of some samples emerges in the long wavelength region in the exciton band. One of the remarkable properties of this band is that the peak is field dependent. The wavelength at which the maximum occurs shifts to longer wavelength as the applied field is increased as given in Fig. 2, while no shift of the peaks

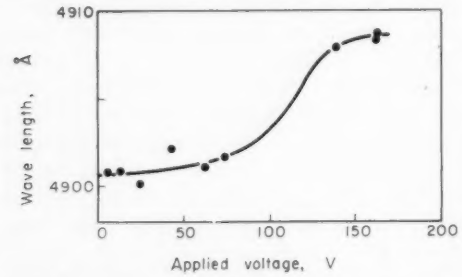

FIG. 2. Dependence of wavelength of the peak for I band on the electric field at 109°K (specimen No. 7, $E \perp c$ electrode distance 2·5 mm).

for exciton photoconductivity can be observed within the experimental errors. More careful spectral observation concerning the I band photoconductivity reveals that the sensitive specimens show very narrow but weak structures comprising several lines, each being about 2 Å or less wide as shown in Fig. 1. Wavelengths of the fine structures vary from one sample to another.

In order to get any relationship between the centers characteristic of I band photoconduction and infra-red quenching, the measurement described below was made at room temperature. At this temperature the augmented infra-red quenching is obtained at 1·4 microns. The spectral structure near the absorption edge is changed from its appearance at lower temperatures to a considerable degree. As the temperature of the sample is increased above 80°K the I band retains its shape, but is displaced to longer wavelength. The structure due to exciton formation is diminished. Thus the sensitivity of the crystal at room temperature is dominated by the response due to I band with a peak around 510 mμ, varying somewhat according to each sample. For primary infrared illumination a spectrophotometer is used with a rock salt prism. Bias irradiation from a tungsten lamp is introduced to the sample through an interference filter with transmission maximum at 5560 Å (halfwidth of

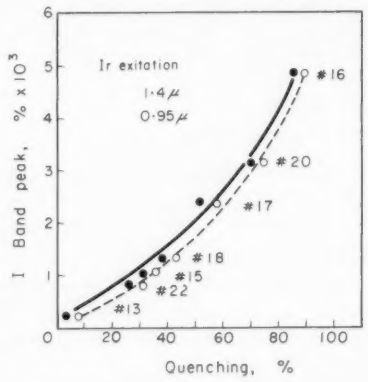

FIG. 3. The photoconductivity peak height due to I band as a function of infra-red quenching for different specimens.

about 100 Å). Figure 3 shows I band height versus the degree of infra-red quenching for different specimens. Standardization of both the I band value and infra-red quenching is arbitrarily made on the photocurrent at 4400 Å. That is, 100 per cent of the I band corresponds to the case where the photocurrent is equal for the I band, and 4400 Å-illumination. The quenching represents the ratio of the decrease in the bias photocurrent, due to infra-red irradiation of constant intensity, to the current due to bias illumination only. The strength of the bias photocurrent is so controlled as to make the bias photocurrent equal to the value of the current at 4400 Å. From Fig. 3 one can easily confirm a tendency that the crystals which show sharp I band are more infra-red sensitive.

DISCUSSION

Because all the specimens under investigation are highly pure, the centers causing I band

Vol. 22
1961

photoconductivity and infra-red quenching are probably due to stoichiometric imperfections.

Assignment of the photoconductivity spectra as due to I band can be given primarily on the basis of their different nature from exciton photoconductivity. As was stated earlier the peak of I band exhibits a field-dependent shift. This effect is presumably due to the strong local field strength near the imperfections involved in crystals where absorption of I band and generation of the free carriers occur. It is also reported by WILLIAMS[11] that the optical absorption edge tends to shift to longer wavelength with an increase of applied electric field on account of tunnel effect of optically excited electrons. Most of the I states fall within

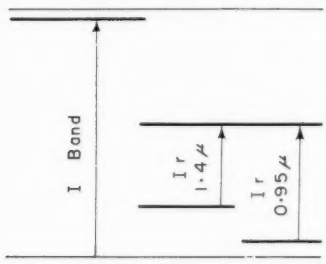

FIG. 4. A tentative energy diagram illustrating (a) the photoconductivity due to I band and (b) infra-red quenching.

about 0·02 eV of the exciton state at 80°K according to the present experiment. In the imperfection band several weak lines of photoconductivity about 2 Å are seen at irregular spacings. THOMAS and HOPFIELD[9] stressed that a favorable mechanism for the radiative decay of excitons could be provided by "impurity states" situated 0·015 eV lower than the main exciton band. They also noted that fluorescence spectra at liquid helium temperature consisted largely of the sharp lines. Most of them were narrow of half-widths of the order of 10^{-4} eV. By reflecting on the appearance of the fine structures and spectral range, a close correlation between the imperfection that gives rise to I band photoconductivity to the "impurity" state which takes part in the fluorescence is presumed. Considering that the crystal which exhibits photoconductivity peak is believed to involve a sulphur deficiency,[12] the defect responsible for I band seems to be associated with the same sulphur vacancy.

From the measurement of quenching strength as a function of temperature the thermal activation energies for infra-red quenching were estimated at about 0·6 and 0·20 eV for 0·95 and 1·4 micron band respectively in the temperature range lower than −40°C.[13] These energy values are considerably different from the activation energy of the I band which corresponds to the difference of I band from the conduction band (about 0·05 eV). Thus I band and infra-red quenching band can be thought of as occurring from centers which are different in physical nature. As stated in the introduction the defect levels responsible for the infra-red quenching can be assumed to be associated with the cation vacancy.

However, a close parallel exists between the two types of centers which cause I band photoconductivity and infra-red quenching as seen from Fig. 3. Such centers can be thought to arise from the groups which comprise cadmium and sulphur vacancies.

CONCLUSION

Certain conclusions can be drawn from the above-mentioned argument. The photoconductivity structures outside the exciton band will be due to the crystal imperfection, which may be associated with sulphur vacancies. The infra-red quenching is due to an imperfection presumably associated with cadmium vacancies. Yet a certain correlation exists between the two centers in physical respects. Further experimental investigations will be required in order to get direct identification of the imperfections causing a variety of the physical properties inherent to CdS.

Acknowledgements—The author is greatly indebted to Prof. MAKISHIMA, Drs. G. KUWABARA and S. SHIONOYA of Tokyo University and Dr. K. TSUSHIMA of his Laboratory for their helpful discussions, and to Mr. T. TAKAHASHI of Tokyo University for the measurement. He wishes to express his appreciation to Director S. SHIMA, Vice-director T. NOMURA and Dr. H. KURODA of the Laboratories for their continued encouragement.

REFERENCES

1. BUBE R. H., *Phys. Rev.* **101,** 1668 (1956).

2. Böer K. W. and Gutjahr H., *Z. Phys.* **152,** 208 (1958).
3. Gross E. F. *et al.*, *Dokl. Akad. Nauk SSSR* **110,** 761 (1956).
4. Winogradoff N. N., *J. Appl Phys.* **22,** 506 (1961).
5. Taft E. A. and Hebb M. H., *J. Opt. Soc. Amer.* **42,** 249 (1952).
6. Bube R. H., *Phys. Rev.* **99,** 1105 (1955).
7. Mitsuhashi H., *J. Phys. Soc. Japan* **16,** 989 (1961).
8. Dutton O., *Phys. Rev.* **112,** 785 (1958).
9. Thomas D. G. and Hopfield J. J., *Phys. Rev.* **116,** 573 (1959).
10. Rose A., *Phys. Rev.* **97,** 322 (1955).
11. Williams R., *Phys. Rev.* **117,** 1487 (1960).
12. Shivonen Y. T., Boyd D. R. and Woelke C. D., *Phys. Rev.* **113,** 965 (1959).
13. Mitsuhashi H. To be published.

DISCUSSION

R. E. Halsted: The quenching levels you describe have previously been correlated with the presence of Cu in CdS. Do you have any measurement of the residual Cu content of your crystals?

H. Mitsuhashi: I have not made any measurement on the crystal doped with Cu.

Vol. 22
1961

J. Phys. Chem. Solids Pergamon Press 1961. Vol. 22, pp. 227–234. Printed in Great Britain.

PHOTOCONDUCTIVITY OF ZINC OXIDE AS A SURFACE PHENOMENON

G. HEILAND

Universität Erlangen-Nürnberg, Germany

Abstract—Up to now photoconductivity of zinc oxide has not been reported as a bulk effect in single crystals. The most prominent feature of the photo-surface conductivity (single crystals and evaporated layers) is the increase with the surface conductivity in the dark through several orders of magnitude. At present it seems probable that this connection is caused by traps for the majority carriers (electrons), whereas the influence of light intensity is determined by trapping of minority carriers. This model is based upon measurements of field effect and photoconductivity at the same crystals. Some conclusions concerning the storage and the recombination of electrons and holes at the surface are drawn. Trap densities and lifetimes are estimated.

1. INTRODUCTION

ZINC OXIDE is now well known as an *n*-type semiconductor having a large band gap (about 3 eV).[1] Not only bulk but also surface properties of synthetic single crystals have been studied by several authors.[1,2,5–8] Whereas hydrogen or zinc vapor can produce surface donors, adsorbed oxygen has been found to bind electrons and to decrease the always *n*-type surface conductivity. This generation of surface states by adsorbed gases results in the formation of a space charge layer at the surface. An excess of donors at the surface is connected with an accumulation layer and the bands are bent down. On the contrary an excess of oxygen causes a depletion layer and the bands are curved upwards.

Photoconductivity of zinc oxide has been observed so far only as a surface phenomenon and, without sensitization by adsorbed foreign substances, merely with light in the spectral region of the fundamental absorption.[3–7] Mostly a wavelength of 3650 Å has been used having a penetration depth of about 2×10^{-5} cm. Therefore a great deal of the light energy is absorbed within the space charge region at the surface.

The bulk conductance of the single crystals at 90°K was immeasurably low and the dark conductance was located in an accumulation layer at the surface. All measurements of photoconductivity and field effect have been performed in a vacuum after a surface treatment by heating or by the action of gases to adjust the surface conductivity to the desired value. The photocurrent is carried by electrons.[16]

Figure 1 shows an example for the change of photoconductivity with time. Besides the fast and reversible increase of surface conductivity during irradiation there is also a slow rise which is irreversible in a vacuum. It is connected with the photodesorption of atomic oxygen[9] which was bound in the lattice or adsorbed at the surface.

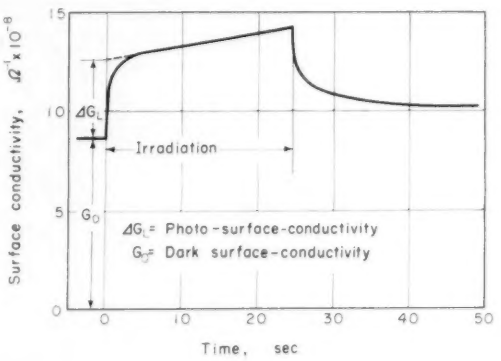

FIG. 1. Surface conductivity of a ZnO crystal as a function of time during irradiation with light. $h\nu = 3{\cdot}4$ eV, $T = 90°$K. Four-contact method.[7]

Also deep traps for holes may cause a slow process at low temperatures. In this paper the fast process will be treated.

2. DEPENDENCE OF PHOTOCONDUCTIVITY ON DARK CONDUCTIVITY

Figure 2a shows that the photoconductivity increases with the dark conductivity through several orders of magnitude (cf. Fig. 1). For low conductivities the rise is proportional, for higher conductivities the curve can be approximated by a 2/3 power law. This was found not only for single crystals, but also for evaporated layers.[3] The relation is not sensitive to the way the dark surface conductivity has been changed, by a short heat treatment in hydrogen, by the action of atomic hydrogen at low temperatures, or by electron bombardment (removal of oxygen from the surface). Also a stepwise oxygen adsorption has been used.

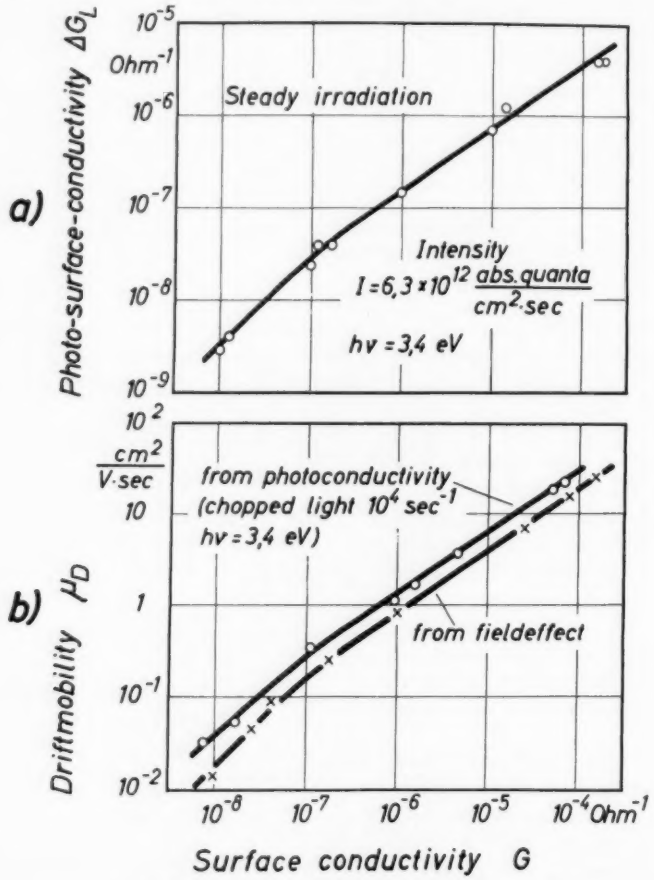

FIG. 2. (a) Photo-surface conductivity ΔG_L as a function of dark surface conductivity G_0. 90°K. (b) Drift mobility μ_D for the same crystal as a function of surface conductivity G. 90°K.[6]

According to Fig. 2a the lifetime of electrons in the conduction band increases with the electron density. The first models tried to explain this fact by the assumption that excess zinc atoms[4,11] or

Vol. 22
1961

the adsorbed oxygen[10] play a decisive role for the generation and recombination of carriers in the photoconductivity. New light was shed upon this problem by the field effect experiment, which allowed to study the change of surface conductivity by a known density of induced carriers without the complication of recombination processes.[6]

The surface conductivity G is connected with the micromobility μ_C and the surface density N_C (cm^{-2}) of conduction electrons in the accumulation layer by

$$G = e\mu_C N_C \tag{1}$$

From the observed change of surface conductivity ΔG_{Fd} by the induced electron density ΔN_{Fd} a field effect mobility μ_{Fd} can be derived for sufficient small changes:

$$\mu_{Fd} = \Delta G_{Fd}/e\Delta N_{Fd} \tag{2}$$

Figure 2b shows an increase with the surface conductivity through several orders of magnitude. Somewhat similar results have been obtained by KRUSEMEYER[8].

The only possible explanation is that merely a small fraction (ΔN_C) of the induced electrons (ΔN_{Fd}) contributes to the surface conductivity. The main part is trapped (ΔN_S). With increasing surface conductivity the conduction band at the surface approaches the Fermi level and a growing fraction of the induced charge appears in the conduction band. The derived mobility refers to the sum of mobile and trapped electrons and may be called a drift mobility. Using Boltzmann statistics and assuming a continuous energy distribution of traps S_n one can explain the observed dependence of drift mobility μ_D on surface conductivity:

$$\mu_D = \mu_C \frac{\Delta N_C}{\Delta N_C + \Delta N_S} \approx \mu_C \frac{\Delta N_C}{\Delta N_S} = \frac{G}{2eS_n kT} \tag{3}$$

With the exception of high conductivities ΔN_C in the denominator is negligible.

On some premises a drift mobility can also be derived from measurements of the photoconductivity with chopped light.[6] (Fig. 2b, upper curve.) Using eqn. (3) a trap spectrum has been calculated (Fig. 5a). The logarithmical plot of surface conductivity corresponds to a linear scale of electron energy as long as Boltzmann statistics are valid and the mobility μ_C is constant. The conduction band at the surfaces may reach the Fermi level for $G \approx 10^{-5}$ ohm^{-1}. Below that limit the spectrum is about $14\,kT$ wide (90°K). One has to regard that for an accumulation layer the electron concentration n_R at the very surface is proportional to N_C^2 and G^2.[12] For low conductivities the trap density is constant, for higher values the power law of Fig. 2b can be ascribed to an exponential energy distribution of traps[13]:

$$S_n \sim \exp[-(E_C - E)/E_n], \tag{4}$$

E_C = edge of the conduction band,

$$E_n \approx 6kT \approx 4{\cdot}6 \times 10^{-2}\ \text{eV}$$

From a comparison of the curves in Fig. 2b and 2a the conclusion results that also the dependence of photoconductivity on surface conductivity is caused by trapping of electrons and that recombination processes do not influence this relation.

3. DEPENDENCE OF PHOTOCONDUCTIVITY ON IRRADIATION INTENSITY

The photoconductivity increases with a low power of light intensity I, between 1/2 and 1/3, for thin layers as well as for single crystals (Fig. 3).

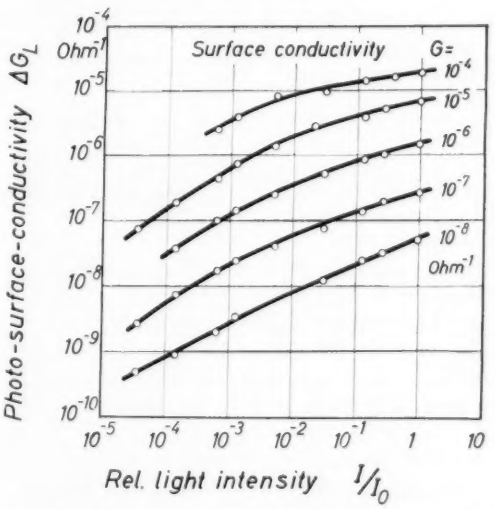

FIG. 3. Photo-surface conductivity ΔG_L as a function of irradiation intensity I for the same crystal as in Fig. 2, a and b. $I_0 = 4{\cdot}8 \times 10^{15}$ absorbed quanta/cm^2 sec. $h\nu = 3{\cdot}4$ eV. 90°K.[6]

The explanation takes into account the derived drift mobility. By combining parts *a* and *b* (upper curve) of Fig. 2 one obtains the density of excited electrons ΔN^*, including conduction band (ΔN_C) and traps (ΔN_S):

$$\frac{\Delta G_L}{e\mu_D} = \Delta N_C + \Delta N_S = \Delta N^* = I \times \tau^*. \quad (5)$$

Density ΔN^* and lifetime τ^* of the excited states are quite independent of dark conductivity, that is independent of electron density and excitation rate. Hence nearly all recombination centers must be occupied by electrons whereas the trapped holes are protected against recombination with electrons (see Section 4).

From Fig. 3 a continuous trap spectrum can be derived with the assumption that the distribution of holes between traps and valence band is given by a quasi Fermi level (Fig. 5b). The logarithmical plot of intensity, increasing downwards, corresponds then to a linear energy scale, increasing upwards. The distance from the valence band is not known. A reasonable description of the trap spectrum is given by

$$S_p \sim \exp[-(E-E_V)/E_p], \quad (6)$$

E_V = edge of the valence band, E_p changing from $2\,kT$ to $3\,kT$ (1·6 to $2{\cdot}3 \times 10^{-2}$ eV). The width of the spectrum amounts to about $10\,kT$. With increasing irradiation intensity the quasi Fermi level approaches the valence band and an increasing fraction of holes is free for recombination. That causes the decrease of the lifetime of excited states τ^*.

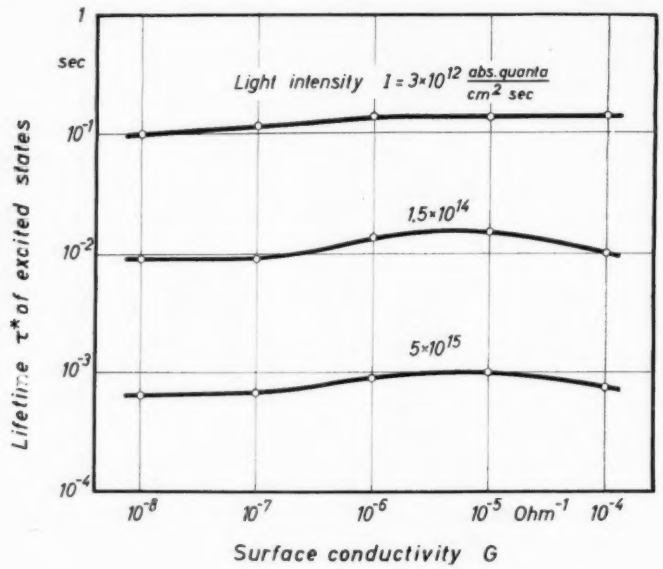

FIG. 4. Lifetime τ^* of excited states as a function of surface conductivity G, calculated from Figs. 2 and 3.

of electron density N_C in the conduction band and therewith of the bending of the bands at the surface. This is shown by Fig. 4 for several light intensities I. In spite of a variation of the surface conductivity through four orders of magnitude the lifetime of excited states changes only by a factor of 1·5. Therefore no free electrons should be involved in the recombination process.

For an explanation of this fact a model is proposed subsequently: the photoconduction is carried by electrons and the holes are mainly trapped. A small fraction of them is mobile for recombination with a constant lifetime τ_v, which is

Vol. 22
1961

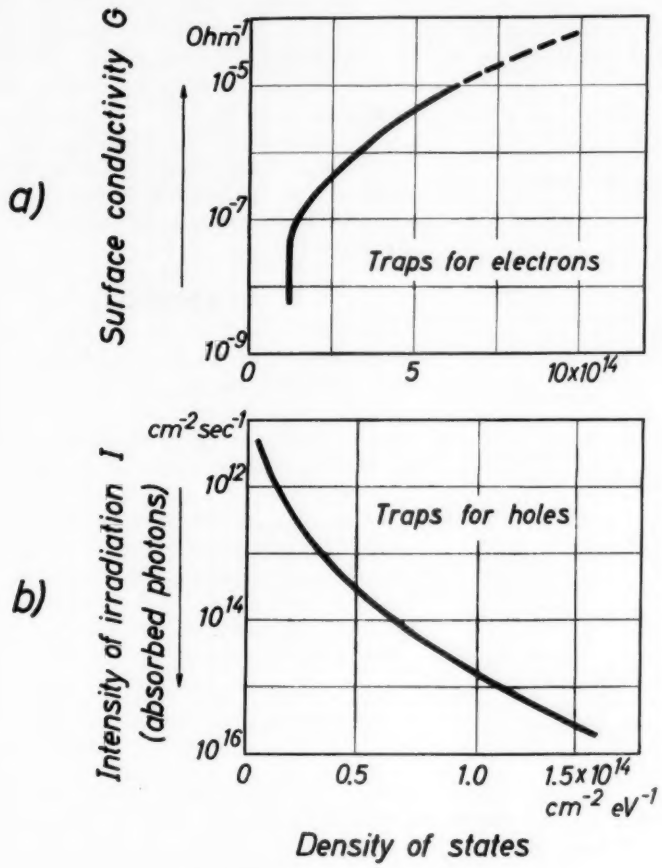

FIG. 5. (a) Density of trapping states for electrons S_n vs. surface conductivity G, calculated from Fig. 2b, upper curve. (b) Density of trapping states for holes S_p vs. light intensity I, calculated from Fig. 2b and Fig. 3.

4. NATURE OF THE TRAPS

It has been shown in the previous Sections, that both odd power dependences of photoconductivity, on dark conductivity and on irradiation intensity, can be referred to exponential energy distributions of trapping states for electrons respectively for holes. As a completion to Fig. 5 the distribution of traps through the energy gap can be seen in Fig. 6. The derived continuous distributions of states cover only a very small fraction of the wide gap.

The traps for electrons are located at the surface or in the space charge layer because of their action in the field effect. They are not effective for recombination. There may be a continuum of traps (total density about $10^{13}\,cm^{-2}$) in the range covered by the Fermi level during the change of the surface conductivity through four orders of magnitude. Also another possibility should be mentioned: with increasing surface conductivity a band of surface donors arises while the main charge transport still happens in the conduction band. The density of states at the Fermi level in this donor band is then found in Fig. 5a. The increase of trap density starts at about 0·05 eV below

the conduction band. This is the activation energy found by HUTSON for zinc and hydrogen donors at low concentrations in the bulk (Hall effect).[15]

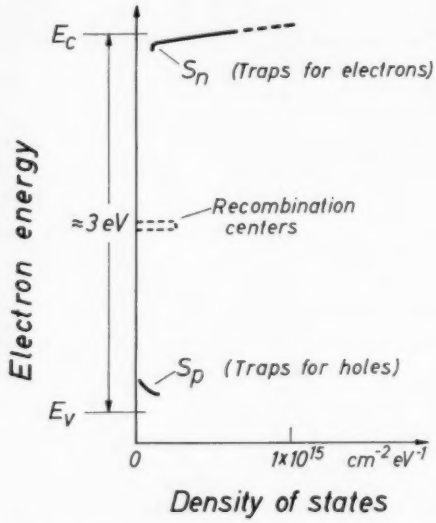

FIG. 6. Density of trapping states vs. electron energy. No density or energy is known for the recombination centers. Also the distance of the traps for holes from the valence band has not been estimated.

At higher conductivities the surface donor band may merge with the conduction band. A surface conductivity of 10^{-4} ohm^{-1} ($N_C \approx 6 \times 10^{12}$ cm^{-2}) is completely independent from temperature (300 – 60°K). Finally a continuum of surface states can also be found if a single level crosses the Fermi level inside the space charge layer.

The traps for holes must be located near the traps for electrons with regard to neutralization of charge. The density of trapped carriers can exceed the density of electrons in the conduction band by several orders of magnitude. At the highest irradiation intensity (Fig. 3) there are about 3×10^{12} trapped carriers per cm^2. The simultaneous increase of electron density in the conduction band can be as low as 10^{10} cm^{-2}. A spatial separation of the two kinds of traps would result in bending of the bands and great changes of surface conductivity, which are not observed. With regard to the recombination process, which is independent from the density of free electrons, the trapped holes are protected against recombination with electrons, e.g. the traps may have a double negative charge in the empty state. Oxygen ions at the surface can satisfy the requirement. However the trap spectrum for holes has been found to be independent of the dark conductivity, that is from the coverage of the surface with adsorbed oxygen. Therefore also the oxygen bound in the lattice may provide hole traps at the surface or additionally in the bulk.

5. LIFETIMES

The time dependence for field effect and photoconductivity at the same crystal is shown in Fig. 7. In both cases the dependence on surface conductivity is equal (Fig. 2,b,a), whereas the response times are different. They are determined in the first case by electron traps and in the second by hole traps.

Three different lifetimes are defined in the model. The lifetime τ^* of excited states decreases with increasing irradiation intensity from 4×10^{-1} to 8×10^{-4} sec (Figs. 3, 4), but it is independent surface conductivity. The lifetime τ_C of the photoelectrons in the conduction band is[14]

$$\tau_C = \tau^* \frac{\Delta N_C}{\Delta N^*} \approx \tau^* \frac{N_C}{2 S_n k T} \qquad (7)$$

It covers a range from 10^{-7} to 10^{-1} sec. The lifetime τ_V of free holes in the valence band is connected with τ^* in a corresponding way. No estimation can be given at present but $\tau_V \ll \tau^*$.

The diffusion of holes to the surface of a zinc oxide crystal under the influence of the field in the space charge layer has been theoretically treated in connection with the slow process.[8] According to this calculation the diffusion rate depends on the bending of the bands. In the case of an accumulation layer the field drives the holes back from the surface, but the highest excitation rate is just at the surface. According to the present experiments the lifetime of holes should be completely independent of the space charge layer. Perhaps the prevailing recombination takes place in the bulk. No specified considerations are given at present to the motion of holes. Nothing is known about the diffusion length. This is really an open question in connexion with the photoconductivity of zinc oxide.

Vol. 22
1961

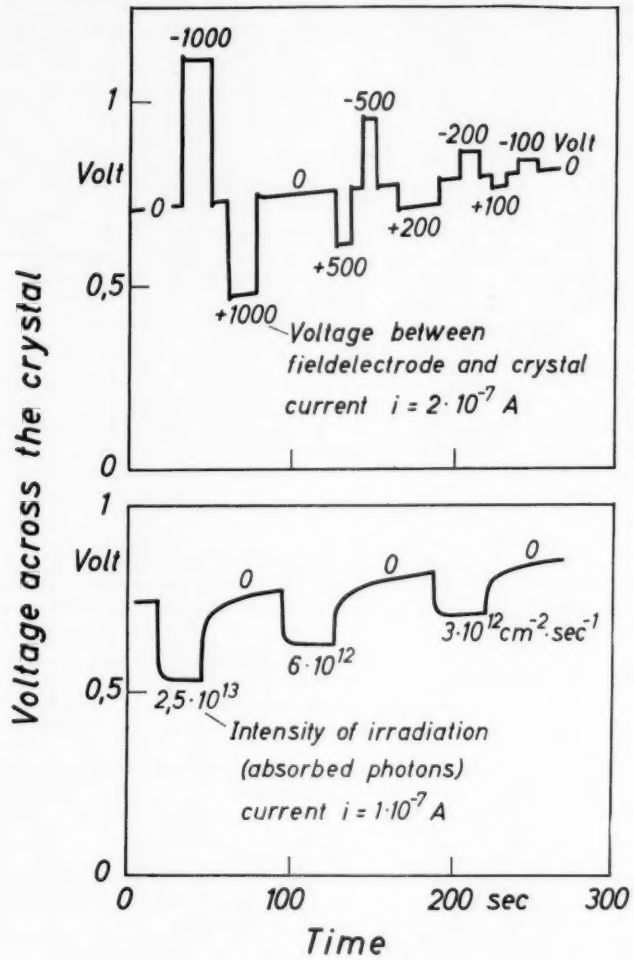

FIG. 7. Voltage across the crystal as a function of time during measurements of field effect and photoconductivity. Recorder trace. In both experiments the same crystal, amplifier and recorder was used. 90°K. $h\nu = 3{\cdot}4$ eV.

REFERENCES

1. HEILAND G., MOLLWO E. and STÖCKMANN F., *Solid State Phys.* **8,** 191 (1959).
2. LANDER J. J., *J. Phys. Chem. Solids* **14,** 137 (1960).
3. MOLLWO E., *Ann. Phys. Leipzig* **15,** 230 (1948).
4. MOLLWO E. and STÖCKMANN F., *Ann. Phys. Leipzig* **15,** 240 (1948).
5. COLLINS R. J. and THOMAS D. G., *Phys. Rev.* **112,** 388 (1958).
6. HEILAND G., *J. Phys. Chem. Solids* **6,** 155 (1958).
7. HEILAND G., *Z. Phys.* **142,** 415 (1955).
8. KRUSEMEYER H. J., *Phys. Rev.* **114,** 655 (1959).
9. HEINZEL W. and HEILAND G., unpublished.
10. STÖCKMANN F., *Z. Phys.* **146,** 407 (1956).
11. MOLLWO E., *Proceedings of the Conference on Photoconductivity, Atlantic City,* ed. R. G. BRECKENRIDGE *et al.*, Wiley, New York (1956).
12. HEILAND G., *Z. Phys.* **148,** 28 (1957).
13. ROSE A., *Proceedings of the International Conference*

on Semiconductor Physics, Prague, p. 458. *Czechoslovak Academy of Sciences.*
14. ROSE A., *RCA Rev.* **12,** 362 (1951).
15. HUTSON A. R., *Phys. Rev.* **108,** 222 (1957).
16. INTEMANN K. and STÖCKMANN F., *Z. Phys.* **131,** 10 (1951).

DISCUSSION

G. K. GAULÉ: Did you consider the possible influence of vacancies on these surface effects?

G. HEILAND: There is little information about imperfections in ZnO. An excess of zinc is connected with the presence of donors, which may be interstitial zinc atoms or oxygen vacancies occupied by electrons. A surface donor may also be created by atomic hydrogen:

$$O^{--}_{\text{lattice}} + H_{\text{gas}} \rightarrow OH^{-}_{\text{surface}} + e^{-}_{\text{crystal}}$$

F. A. HAMM: (1) Are you sure that the chemisorbed oxygen (a hole trap for photoholes) is doubly negatively charged or might it be singly charged? Also, why do you assume hole trapping by lattice O^{--}?

(2) Is the surface of your zinc oxide crystals really zinc oxide or some nebulous hydrate?

If you expose (photolyze) enough so as to consume all chemisorbed oxygen ions via photohole trapping, then if lattice oxygen ions become neutral through hole trapping they should escape into the vacuum and cause surface erosion. This erosion phenomenon has been shown for silver halides where the free halogen is the hole.

G. HEILAND: (1) I do not know if the adsorbed oxygen is doubly or singly charged. If the adsorbed oxygen provides mainly hole traps, the density of hole traps must depend on the coverage of the surface by adsorbed oxygen, but it is nearly completely independent of the dark surface conductivity, i.e. the density of adsorbed oxygen (see Fig. 4). Therefore one possible explanation may be the trapping of holes by lattice oxygen. This does not yet require photolysis.

(2) The observed dependence of photoconductivity on dark conductivity and irradiation intensity is nearly independent of the way the surface conductivity was produced. After heating in a vacuum of 10^{-7} Torr, the crystal, surrounded by a shield at liquid air temperature, shows the same effects. Also evaporated layers, just oxidized at 500°C, obey these laws. Experiments on the action of H, H_2 and H_2O have been carried out and were published several years ago.

Note added in proof:

There is some doubt if photolysis of ZnO does happen at all for quantum energies not much higher than those at the absorption edge. I refer to *Disc. Faraday Soc.* **28,** (1959), contributions by TERENIN and SOLONITZIN and by HEILAND, and discussion remarks by STONE, by TERENIN and by HEILAND, pp. 28, 168, 72, 74, 75, 211, 212.

F. BROWN: Why is it that photoconductivity cannot be observed for more penetrating light—or how about the use of penetrating ionizing radiation such as β-rays?

G. HEILAND: I would like to mention two possible reasons. The lifetime of excited states may be shorter in the bulk of the crystals, e.g. if the traps for holes exist only at the surface in a sufficient density. However, excitation in the bulk is a condition for bulk photoconductivity. The absorption edge of ZnO is very steep and does not show a tail like the absorption edge of CdS. By heating in zinc vapor the crystals turn yellow and there is a reasonable absorption coefficient in the blue region of the spectrum, but at the same time the dark conductivity in the bulk is increased. No photoconductivity was detected during preliminary experiments with excitation in this absorption region. But yesterday F. HAMM told me that β-ray excitation caused a transient increase of bulk conductivity.

J. Phys. Chem. Solids Pergamon Press 1961. Vol. 22, pp. 235–240. Printed in Great Britain.

USE OF PARAMAGNETIC RESONANCE TO DETECT OPTICAL PROCESSES IN PHOTOCONDUCTORS

REUBEN S. TITLE

International Business Machines Corporation, Thomas J. Watson Research Center
Yorktown, New York

Abstract—In photoconductivity the light induced transfer of charge from one impurity or defect site in the lattice to another is a common process. It is in fact while the charge is free that it contributes to the photocurrent. As a result the valence of the sites involved in the process will change by one. In principle this valence change should be observable using paramagnetic resonance absorption techniques because at each site we are going from a state with an even number of electrons to an odd number or vice versa. The use of paramagnetic resonance to detect light induced charge transfer will be illustrated by several experiments carried out on II–VI compounds doped with various impurities. In addition to the observed valence change, interaction between defects in the lattice has been detected. The resonance technique is useful in that it isolates a single microscopic process occurring during photoconductivity and hence is a definite aid in setting up a model for the photoconductive process. It will also be shown how the apparatus used to detect paramagnetic resonance can be used to measure microwave photoconductivity. The measurement does not require any electrodes on the sample.

THE effect of impurities on the photoconductivity of several materials has been known almost as long as photoconductivity itself. It is only in comparatively recent times, concurrent with the rise in understanding of the solid state, that a physical model has been advanced to explain the role of the impurities in the photoconductive process. The model involves charge transfer to and from the impurities which are assumed localized in the lattice. The charge transfer may result from such processes as excitation, both optical and thermal, from recombination with or without the emission of optical radiation, and from trapping.

The detection of optically induced charge transfer by the use of paramagnetic resonance techniques will be described in this paper. Charge transfer processes that have been detected by this technique are illustrated in Fig. 1. In Fig. 1(a) light of energy equal to or larger than the band gap of the host material causes the formation of an electron–hole pair. These carriers may wander through the lattice contributing to the conductivity. The carriers may however be trapped as shown at the levels due to added impurities or defects in the lattice. The impurity that gives rise to the hole trap is referred to as the activator and that producing an electron trap is referred to as the coactivator. The time a carrier remains in a trap will depend on the relative energy separation of the trap from the conduction or valence band compared to kT. A level with a trapped carrier may serve as a recombination center for a carrier of opposite sign. Figure 1(b) illustrates the direct ionization by optical radiation of an electron from an activator level to the conduction band. The electron remains free in the lattice until it either recombines at the site of an ionized activator giving off the energy in the form of luminescence or is trapped at the coactivator level. If the depth of the coactivator level is large compared to kT the time the electron spends at this level is long and one has in effect stored energy in the material. The situation in Fig. 1(c) is similar to that in 1(b) except that in this case an electron is optically excited from the valence band to an empty activator site, leaving a hole in the valence band as the charge carrier. A recombination of the hole at an occupied coactivator site is shown. In Fig. 1(d) the activator and coactivator are assumed close enough in the lattice, perhaps due to an interaction, that light may cause a direct transfer of charge between activator and coactivator. The charge is

not free in this transfer and thus does not contribute to the conductivity.

The net effect of all the processes illustrated in Fig. 1 is to change the number of electrons (or holes) at an impurity site. Whether a given site is paramagnetic or not depends on the pairing of electrons at that site. Alteration of the number of electrons will result in a change in the pairing and the change should therefore manifest itself as a change in the paramagnetism of the sample. Either d.c. magnetic susceptibility or resonance measurements may be used, both being of roughly comparable sensitivity. The resonance measurements are, however, more useful in that they may be used to identify the paramagnetic impurity and give information concerning the local symmetry at the impurity site as well as the number of such sites. Typical resonance spectrometers can detect on the order of 10^{14} paramagnetic centers. Since sample size is limited by cavity dimensions this represents a concentration of 10^{15} cm^{-3} or about a part in 10^7.

The optically induced change in paramagnetism may be observed in a double resonance experiment in which the sample present in the usual microwave and magnetic fields required for paramagnetic resonance measurements is simultaneously illuminated by monochromatic light (Fig. 2). The number of sites at which the charge has changed must at least be equal to the sensitivity of the resonance apparatus. This number is a function of the lifetime of the charge at the site and of the light intensity. The lifetime may be increased if necessary by lowering the temperature. High intensity lamps such as a high pressure xenon lamp or a high wattage tungsten filament lamp are used. With one kilowatt of power these lamps give about 5×10^{15} photons/cm^2/sec into a 10 millimicron bandwidth with the usual monochromators.

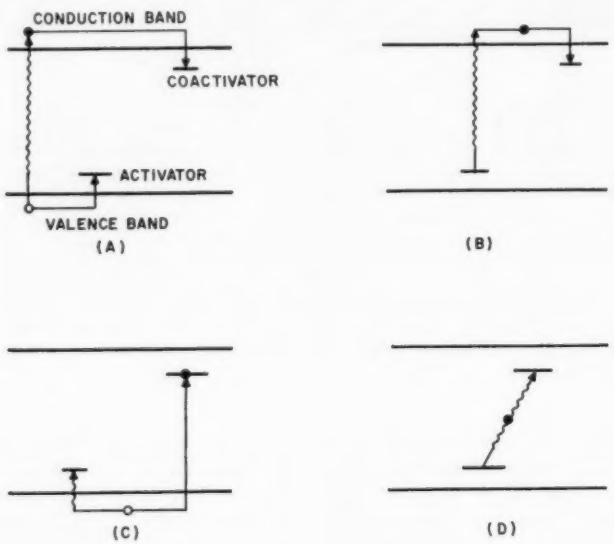

FIG. 1. Optically induced charge transfer processes.

Several unsuccessful attempts to observe optically induced changes in paramagnetism have been made.[1–3] The first successful measurements were reported simultaneously by LAMBE *et al.*[4] working with CdS:Fe and by the author[5] working with SrS:Eu, Sm.

Several experiments which have since been carried out will now be described. These were performed on ZnS both impurity doped and self-activated.

Vol. 22
1961

A sample of ZnS:Gd, Cl[6] was found to show little or no paramagnetic resonance absorption in the dark. When the sample is irradiated with light near 385 mμ a resonance attributed to Gd^{3+} is observed. (The samples were generally polycrystalline. However, there was sufficient alignment of the crystallites in one sample to permit an identification of the seven line fine structure of the Gd^{3+} ion.) When the irradiating light is removed the resonance decreases slowly in magnitude to half value in about one hour at room temperature. The magnitude of the resonance can, however, be quickly decreased by irradiating the sample with red or infra-red light.

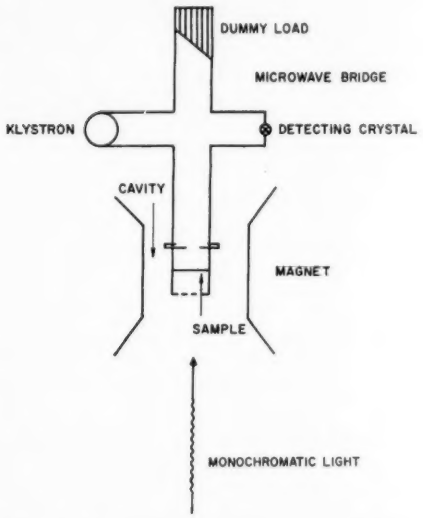

FIG. 2. The apparatus shown schematically.

A model capable of explaining the results is shown in Fig. 3 and Fig. 4. Gadolinium is assumed to enter the lattice as Gd^{2+}. Light near 385 mμ excites an electron from a Gd^{2+} ion to the conduction band. Some of these electrons may be trapped at some trap. This trap is presumably Cl^- since $GdCl_3$ was used in the preparation of the sample. The gadolinium is then present as Gd^{3+} which has a half filled *f* shell of electrons and an $^8S_{7/2}$ ground state. The paramagnetic resonance spectrum of such a state is easily observed at room temperature. The slow decrease in the intensity of the spectrum on removal of light is presumably due to the thermal release of electrons from the traps and their subsequent recapture at the Gd^{3+} sites.

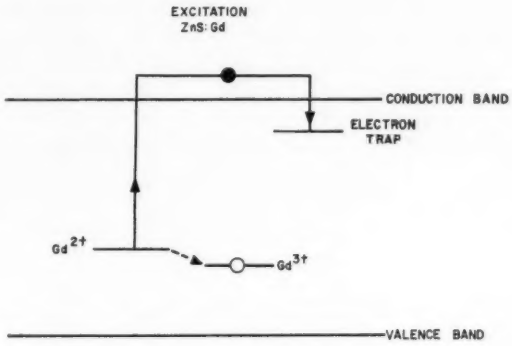

FIG. 3. Excitation of ZnS:Gd.

The rapid decrease in the magnitude of the resonance spectrum on shining red light on the sample is caused by the excitation of an electron from the valence band to a Gd^{3+} ion. The hole left in the valence band recombines with the trapped electron. The observed luminescence, phosphorescence and quenching of the phosphorescence are in agreement with this model.

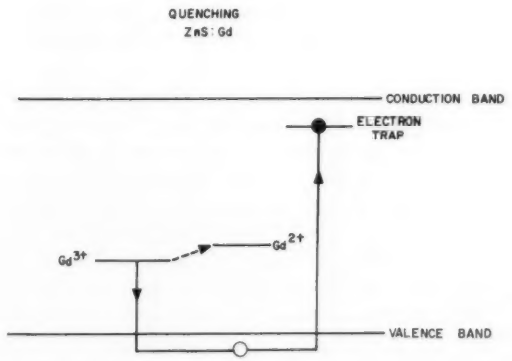

FIG. 4. Quenching of ZnS:Gd.

The model also predicts photoconductivity both during the excitation and quenching processes. The apparatus used to measure the paramagnetic resonance spectrum may also be used to detect photoconductivity. The apparatus as shown in

Fig. 2 that is used to measure paramagnetism consists of a microwave bridge that monitors the microwave impedance of the cavity normally balanced against a dummy load. With the sample placed in a region of the cavity with maximum microwave magnetic field (which is a region of zero electric field) the bridge may be used to detect changes in the magnetic impedance of the cavity caused by paramagnetic resonance absorption or dispersion. By moving the sample into a region of non-zero microwave electric field the bridge is also capable of detecting changes in the electrical impedance of the cavity. Photoconductivity manifests itself as a change in electrical resistance and may therefore be detected by this technique. It is often not necessary to move the sample in the cavity as the finite dimensions of the sample insure that some of the sample is in an electric field region. Either d.c. light may be used and the off balance condition detected by a meter in series with the monitoring crystal or else the light may be chopped so that a lock-in amplifier can be used. Variation in the frequency of the chopping light can be used to measure the kinetics of the photoconductivity. The magnetic field is of course not necessary during these measurements.

No electrodes are required on the sample. The method is best suited for relative measurements as for example in plotting the spectral dependence of photoconductivity. Absolute measurements are possible but require careful calibration.

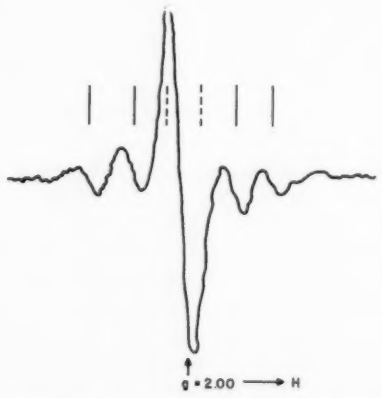

FIG. 5. Resonance spectrum of self-activated ZnS coactivated with Al under 360 mμ illumination.

Photoconductivity measurements were carried out on ZnS:Gd, Cl. A steady state photoconductivity was observed with 385 mμ on the sample in agreement with the model. With red light on the sample no photoconductivity was observed unless the sample had been first excited with 385 mμ. This conductivity was transient in character as one would expect from the model. It is due to holes in the valence band created by the excitation of electrons from the valence band into Gd^{3+} sites. As the number of Gd^{3+} sites decrease this current should decrease as was observed. The peak value

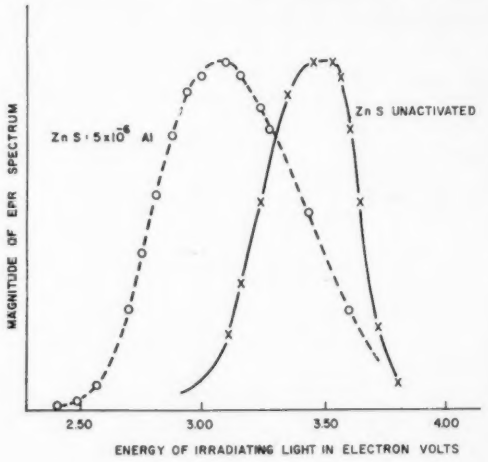

FIG. 6. The excitation spectrum for ZnS with zero added Al and 5 p.p.m. added Al.

was about one tenth of the steady state photoconductivity observed at 385 mμ.

Some measurements performed on self activated ZnS coactivated with aluminum will now be described.[7] The sample was prepared from R.C.A. luminescent grade ZnS fired at 1100°C for two hours in a flowing H_2S atmosphere. Spectroscopic analysis showed the sample to contain about one part per million by weight of Al. In the dark no resonances were observed. With 360 mμ on the sample the spectrum shown in Fig. 5 was observed. The spectrum was observed in crystals as well as powders and found to be isotropic. The spacing of the lines was such that the four resolvable outer lines were believed to be part of a six line structure with the two inner lines obscured

by the large central peak. If the six lines are attributed to hyperfine structure of a nucleus with spin 5/2, possible nuclei are Zn^{67} and Al^{27}. Naturally occurring zinc contains 4 per cent Zn^{67}. A sample enriched to 28 per cent in Zn^{67} showed no increase in the magnitude of the hyperfine structure. It was therefore inferred that Zn^{67} was not the nucleus giving rise to the observed hyperfine structure. Several samples with varying aluminum concentration up to fifty p.p.m. (0·02 molar per cent) were prepared. The resonance

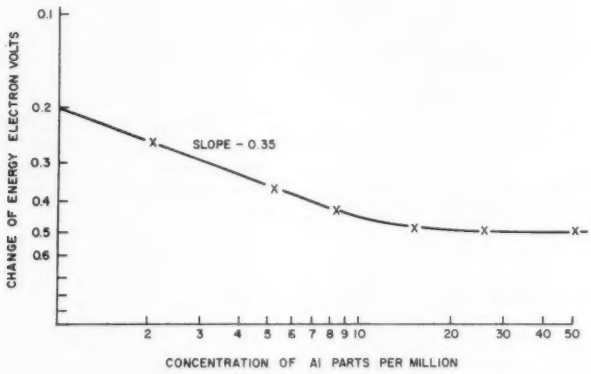

FIG. 7. The change in the energy of excitation as a function of aluminum concentration.

spectrum remained unchanged. However, the energy of light necessary to produce the spectrum changed. This is shown in Fig. 6 which compares the results for zero added Al and 5 parts per million Al. A definite shift to lower energies is observed for both the peak and the long wavelength cutoff of the excitation. (The high energy tail on the 5 p.p.m. Al sample is probably due to the fact that band gap light at 3·7 eV may also contribute to the process in this case.) The change in energy relative to the zero added Al sample is plotted as a function of added Al on a log–log scale in Fig. 7. There is a $-0{\cdot}35$ dependence on aluminum concentration at low concentrations with a levelling off at the high concentrations. To explain these results we use the model of Fig. 1(d). It is assumed that the excitation involves the transfer of an electron from a zinc vacancy to an Al^{+++} ion with which it is associated. Since the excitation energy is concentration dependent it is assumed that the excitation is direct. The zinc vacancy is doubly negatively charged with respect to the lattice and is compensated by two Al^{+++} ions each of which is singly positive with respect to the lattice. After the excitation the zinc vacancy has a single negative charge and one of the associated aluminum ions is present as Al^{++}. Both the singly charged zinc vacancy and Al^{++} are paramagnetic with a g value close to the free electron g value. It is therefore postulated that in the observed resonance (Fig. 5), the large central peak is due to the singly charged zinc vacancy and the six lines are hyperfine lines arising from the interaction of an electron at the aluminum site with an aluminum nucleus of spin 5/2. The observed A value is 12×10^{-4} cm^{-1}.

The variation in the energy necessary to excite the resonance with varying aluminum concentration is due to a variation in the aluminum zinc vacancy separation. For low concentrations this separation should vary as the 1/3 power of the aluminum concentration. The observed $-0{\cdot}35$ dependence indicates that the fall in energy necessary to excite the resonance is proportional to the reciprocal of the activator–coactivator separation.

Similar shifts have been observed in the excitation energy when either gallium or indium were

added. The hyperfine structure was, however, not observed. Because of the presence of two isotopes in each of these cases, the magnitude of the hyperfine lines would be below the level of the noise.

The excitation of Fe^{++} to Fe^{+++} has also been observed in ZnS both in powders and single crystal samples. These experiments will be reported on at a later date.

Acknowledgements—I wish to acknowledge the aid of J. A. KUCZA in the preparation of the samples and of E. E. TYNAN in performing some of the measurements.

REFERENCES

1. HERSHBERGER W. D. and LIEFER H. N., *Phys. Rev.* **88,** 714 (1952).
2. LOW W., *Phys. Rev.* **98,** 426 (1955).
3. MANENKOV A. A., PROKHOROV A. M., TRAPEZNIKOVA Z. A. and FOK M. V., *Optika i Spektroskopia (S.S.S.R.)* **2,** 470 (1957).
4. LAMBE J., BAKER J. and KIKUCHI C., *Phys. Rev. Letters* **3,** 270 (1959).
5. TITLE R. S., *Phys. Rev. Letters* **3,** 273 (1959).
6. TITLE R. S., *Phys. Rev. Letters* **4,** 502 (1960).
7. TITLE R. S., *Quantum Electronics*, 1961 (to be published by Columbia University Press).

DISCUSSION

G. F. J. GARLICK: (1) Are you certain that the six peak resonance in ZnS–Al is not due to Mn^{2+} traces?

(2) In the assumption of direct electron transitions between the cation vacancy and Al^{3+} there would appear to be difficulties as regards the high probability of the return transition.

R. TITLE: (1) Our samples contained no Mn^{2+} and we could see about one part in 10^7 if Mn^{2+} were present. Besides the A value (hyperfine structure) of Mn^{2+} is $65 \times 10^{-4}\,cm^{-1}$ whereas the A value of the reported hyperfine structure of this paper was $12 \times 10^{-4}\,cm^{-1}$.

(2) We are aware of this difficulty. One can, however, overcome it fairly easily. G. LASHER, of our laboratory, has suggested that the transfer of charge may be via the excited state of one site (V Zn) to an excited state of the other site (Al). The electron at the aluminum site can thus remain at that site in the absence of any radiation.

H. A. KLASENS (comment): SMITH (I.B.M.) has been trying to confirm the author's results on ZnS doped with Al. He was not successful. The only resonance peak he found at $g \approx 1{\cdot}995$ was due to a trace of Cr. On cooling below room temperature, however, he found in Al containing ZnS phosphors a resonance at $g = 1{\cdot}88$ after excitation. The fact that one has to cool to observe this is what one would expect, considering the shallow trap depth of Al.

R. TITLE: The absence of hyperfine structure on the $g = 1{\cdot}88$ line suggests it may be due to something else beside Al^{++}: Our samples were shown spectroscopically to contain less than one part per million of chromium. We would therefore not attribute our line near $g = 2{\cdot}0$ to chromium.

I. BROSER: Do you know the shape of the quenching spectra of your ZnS–Gd crystals? What was the concentration of copper in your crystal?

R. TITLE: The quenching spectrum is given in reference 6. It appears quite similar to that of Cu-doped ZnS. However, chemical analysis showed the Cu concentration to be less than three parts per million. The magnitude of the resonances we observed were more than an order of magnitude greater than what one would expect from this Cu concentration and besides could only be identified with Gd^{3+} and not Cu^{++}.

F. G. ULLMAN: At what temperature was the infrared photoconductivity in the Gd-doped ZnS observed?

Was this observed at all at low temperature?

R. TITLE: Measurements have thus far only been carried out at room temperature.

J. Phys. Chem. Solids Pergamon Press 1961. Vol. 22, pp. 241–247. Printed in Great Britain.

IMPURITY PHOTOCONDUCTIVITY IN *N*-TYPE InSb

E. H. PUTLEY

Royal Radar Establishment, Malvern, England

Abstract—Photoconductivity is observed when sufficiently pure *n*-type InSb is illuminated by radiation of wavelengths between 0·2 and 8·6 mm. The time constant of this effect has been found to be not greater than 1 μsec.

The electrical characteristics of the material showing this effect and the strong dependence of both the photoconductive and electrical properties upon a magnetic field are described.

INTRODUCTION

THIS paper describes a photoconductive effect in *n*-type InSb which has been observed at sub-mm and mm wavelengths.[1]

It has been found practicable to employ this effect to construct detectors for these wavelengths which have a sensitivity which compares favourably with that of the best thermal detectors but which have a much shorter time constant. This makes these detectors very suitable for studying radiation from pulsed sources such as plasma discharges* or shock tubes. In this paper, however, this aspect of the subject will not be pursued, but attention will be concentrated on the nature of the effect.

Measurement of the electrical properties of fairly pure *n*-type InSb indicated that shallow impurity levels ($\sim 5 \times 10^{-4}$ eV) appear in the presence of magnetic inductions of about 5000 G. This suggested that impurity photoconductivity could occur at wavelengths up to 2 to 3 mm. This effect was looked for and observed, but it was found that the effect could be detected at much longer wavelengths than expected (beyond 8 mm).

The results to be presented consist mainly of a study of the responsivity and the electrical properties of this material. We have not yet been able to measure the absorption coefficient, so that any deductions we can make from the results obtained so far may require modification in the light of further evidence.

* G. N. HARDING and V. ROBERTS, International Conference on Plasma Physics and Controlled Nuclear Fusion Research, Salzburg. September, 1961.

EXPERIMENTAL RESULTS

The material used to study this effect contains an excess electron concentration of about 5×10^{13} cm^{-3} (as determined by Hall effect measurements at 77°K). The electron mobility is greater than 5×10^5 cm^2 volt^{-1} cm^{-1} at 77°K and at 4·2°K it is between 5×10^4 and 10^5. Below 4·2°K the carrier freeze-out effect becomes quite marked in magnetic inductions as low as 3000 G in the best material. From these measurements the impurity ionization energy and the total impurity concentration may be calculated using a similar method to that used for normal impurity levels. (Figures (1) and (2) show Hall coefficient and conductivity results.) The total impurity concentration is found to be about 5×10^{14} cm^{-3}. This value is somewhat higher than might be expected but is not inconsistent with the comparatively low mobility at 4·2°K. At and below 4·2°K marked deviations from Ohm's law occur when quite small electric fields are applied. Ohm's law is not strictly obeyed at fields greater than 0·1 V/cm while breakdown occurs at fields of 1·0 V/cm or less. (Fig. (3)).

The photoconductive effect was studied at wavelengths between 0·2 and 2·0 mm using a mercury lamp source, suitable filters, and a grating spectrometer. Measurements at longer wavelengths up to 8·6 mm were made using klystron oscillators and crystal harmonic generators.

So far, the absorption coefficient has not been measured, but estimates using the expression given by FAN[2] for the absorption of an impurity centre indicated a value of about 50 cm^{-1}. Despite this, the first experiments were carried out on

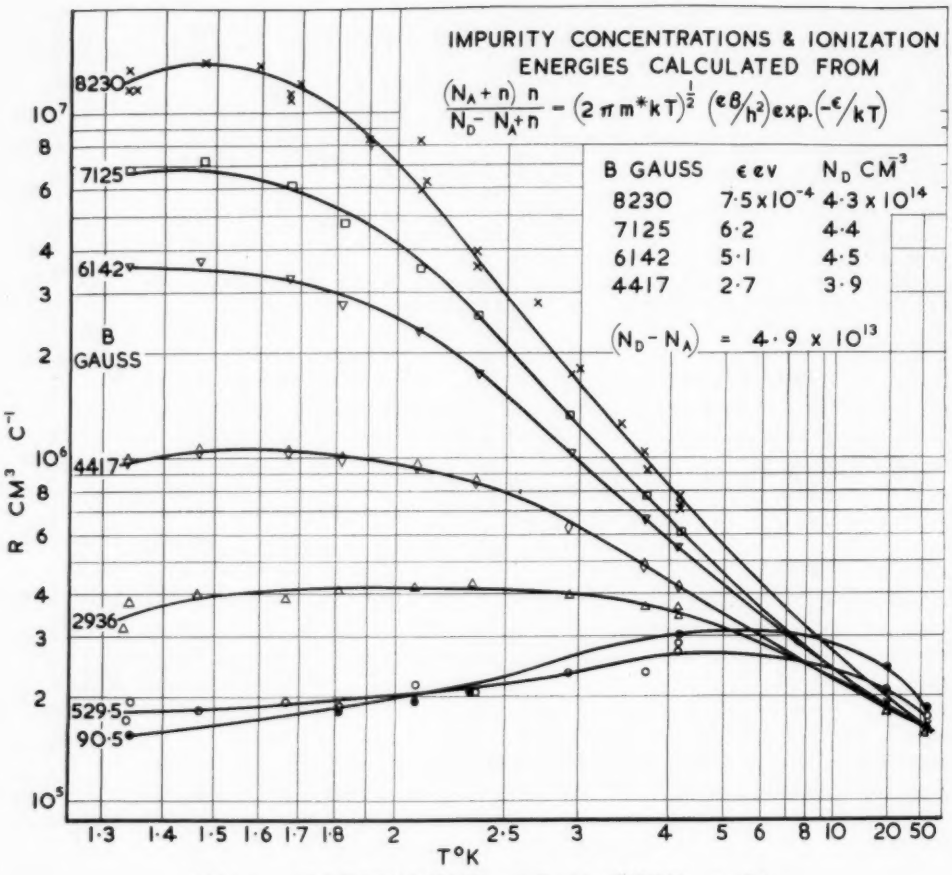

HALL COEFFICIENT OF N-TYPE InSb

(C158/84)

FIG. 1. Hall coefficient of *n*-type sample of InSb over temperature range 1·35°–77°K and at inductions from 90 to 8000 G. The impurity ionization energy and concentration can be calculated from these results using the relation:

$$(N_A+n)n/(N_D-N_A+n) = (2\pi mkT)^{1/2}(\epsilon B/h^2)\exp(1-\epsilon/kT)$$

with the following results:

$$(N_D-N_A) = 4{\cdot}9\times10^{13}\ \text{cm}^{-3}$$

B (gauss)	ϵ (eV)	N_D (cm^{-3})
8230	$7{\cdot}5\times10^{-4}$	$4{\cdot}3\times10^{14}$
7125	6·2	4·4
6142	5·1	4·5
4417	2·7	3·9

Vol. 22
1961

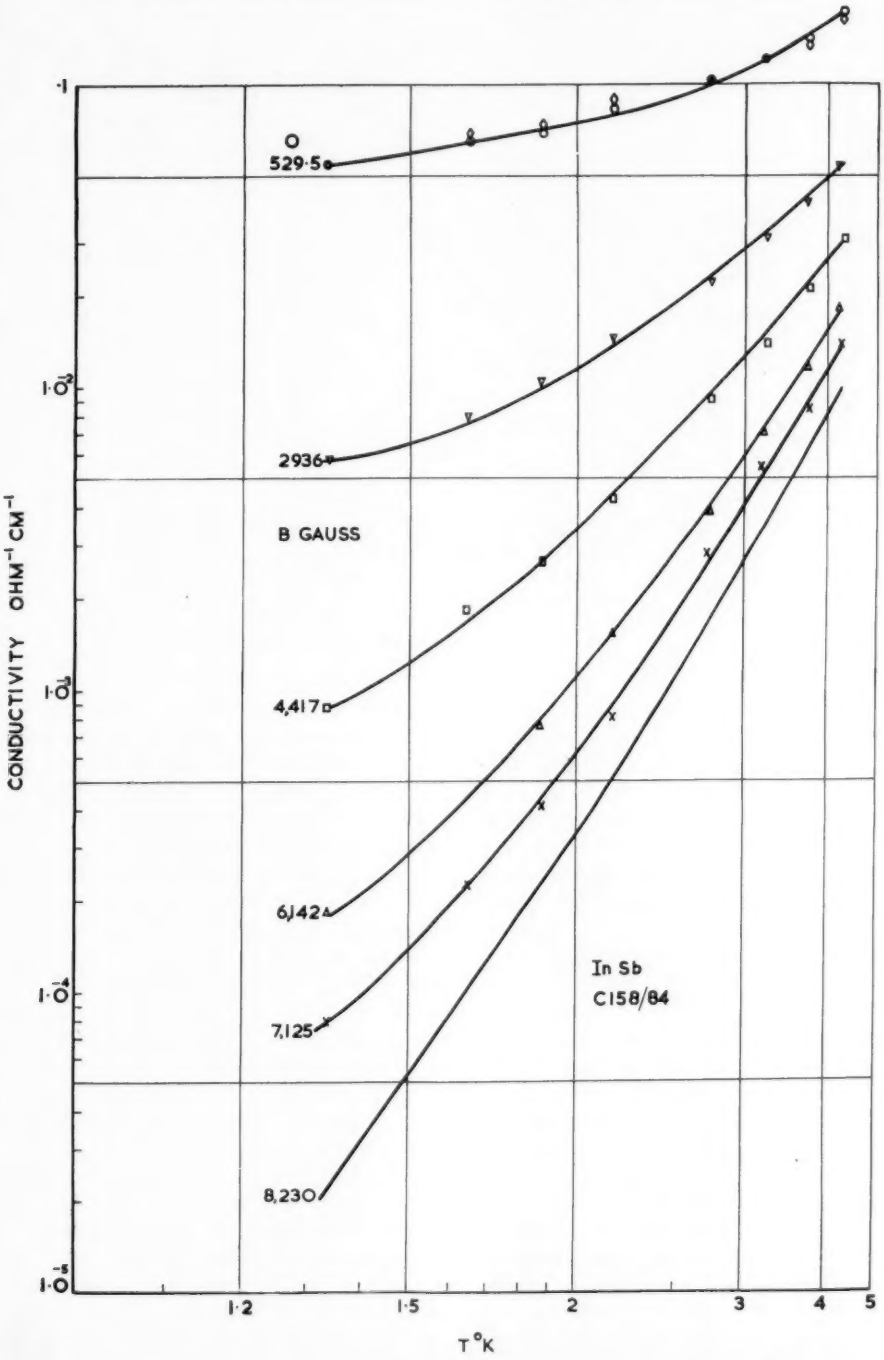

FIG. 2. Conductivity of *n*-type sample of InSb between 1·35 and 4·2°K and at induction 0 to 8000 G.

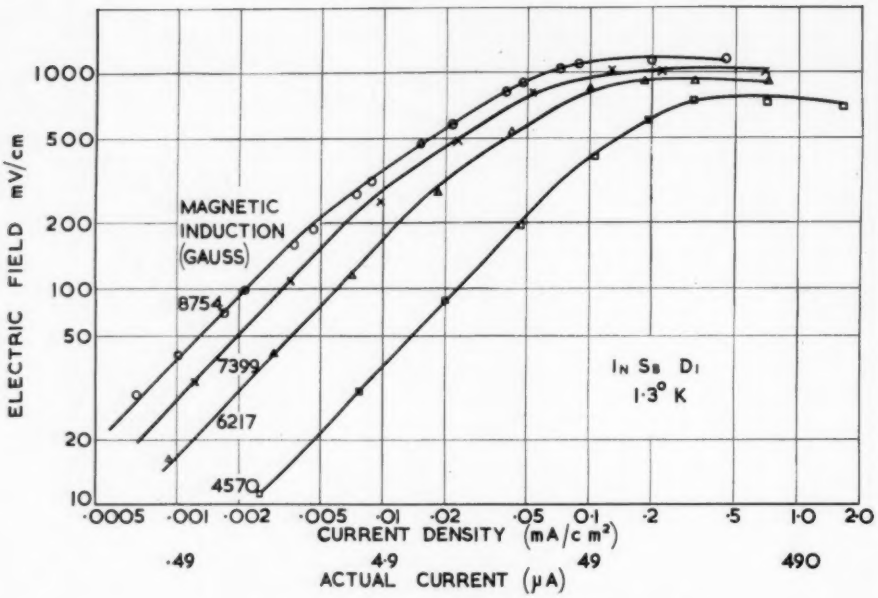

FIG. 3. Current–voltage characteristic of *n*-type InSb.

samples about 1 cm thick. The area exposed to radiation was about $0{\cdot}5 \times 0{\cdot}5$ cm square, designed to suit the optics of the spectrometer.

Although we have not been able as yet to measure the relevant optical properties, an experiment was made to determine whether or not the absorption coefficient was of the order of magnitude estimated. Two samples were mounted in the cryostat one above the other so that if an appreciable amount of radiation were transmitted through the upper specimen it would be detected by the lower one. It was then found that a sample 1 cm long transmitted less than 10 per cent of the incident radiation, and that the thickness of the upper sample could be reduced to about 3 mm before a significant amount of radiation was transmitted. These results indicate that the absorption coefficient is probably somewhat smaller than the value estimated.

The responsivity was measured at a number of wavelengths over the range covered as a function of current density and magnetic induction. Fig. (4) shows typical results. It is seen that at a constant induction the responsivity at first increases linearly with current density, but then passes through a maximum and falls at high current densities. The position of the maximum corresponds with the position of the shoulder on the current voltage characteristic. Thus as the magnetic induction is increased, the maximum occurs at lower current densities.

It will be noticed that an effect is observed even in the absence of a magnetic field, but that the responsivity increases rapidly as the magnetic induction increases. There is usually an optimum field, above which the responsivity falls.

These results are obtained at temperatures between 1·1 and 2°K. It is found that best results are obtained at about 1·5°K but the temperature is not very critical. The optimum magnetic induction depends upon temperature, falling as the temperature is reduced.

By making measurements of this sort at a number of wavelengths, Fig. (5) may be constructed. This shows the dependence upon wavelength of the maximum responsivity at various inductions. We see that for the higher values of the induction the responsivity increases linearly with wavelength up to about 1 mm. At longer wavelengths the responsivity appears to fall but

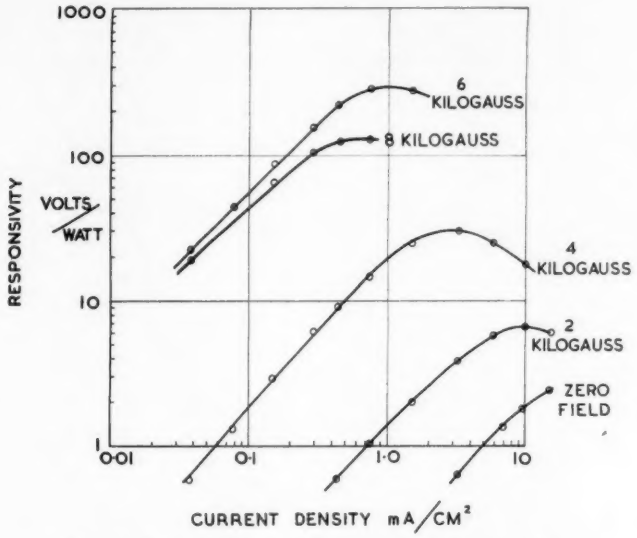

FIG. 4. Dependence of photoconductive responsivity of *n*-type InSb upon current density and magnetic induction. Wavelength of radiation 0·2 mm. Temperature 1·65°K.

this is probably due to instrumental errors associated with the spectrometer when used beyond 1 mm. The latest microwave measurements at 4·2 mm indicate that in the higher inductions the responsivity is about three times greater than the values shown at 1 mm. At zero induction and at 2000 G (which is too small to produce measureable carrier freeze-out) the responsivity increases at approximately the square of the wavelength up to 1 mm, and again falls off at longer wavelengths.

Before discussing these results, two further points should be mentioned. First, although the time-constant of the effect has not been measured, study of the time-resolution obtained when observing discharges from shock tubes has shown that the time-constant is not greater than 1 per cent. Secondly, the resistance of the samples used is usually not more than 10 KΩ. This has meant that the minimum detectable signal from detectors utilizing this effect has been determined by amplifier noise. Despite this, values of D^* (the detectivity[1] normalized to unit area and unit bandwidth) of 4×10^{10} at 0·2 mm and 2×10^{11} at 1·0 mm have been achieved.

* Detectivity of a detector is defined as the signal to noise ratio per watt incident power.

DISCUSSION

The first thing we can say about these results is that the behaviour up to 1 mm wavelength in magnetic inductions of 4000 G or greater is consistent with the supposition that we are dealing with a conventional photoconductive effect, the bulk of the radiation being absorbed. This simple model does not appear to account for the fact that an appreciable effect is observed in the absence of a magnetic field and at wavelengths much longer than would be expected from the ionization energies shown in Fig. (1). It might be argued that there could exist a small ionization energy ($\gtrsim 10^{-4}$ eV) in the absence of a magnetic field. This would not be detected by Hall effect measurements at the temperatures so far used but might be responsible for the small photoconductive effect. Even if this were so, one would still expect to see a long wave cut-off when a large magnetic induction is applied. Thus when $B \sim 8000$ G $\epsilon \sim 7\times10^{-4}$ eV, giving an expected cut-off at 1·8 mm. Yet Fig. (6) showing relative performance at 4·2 mm is of similar form to Fig. (4) which showed the behaviour at 0·2 mm.

A possible mechanism to account for these effects is the absorption by free carriers.[3] This

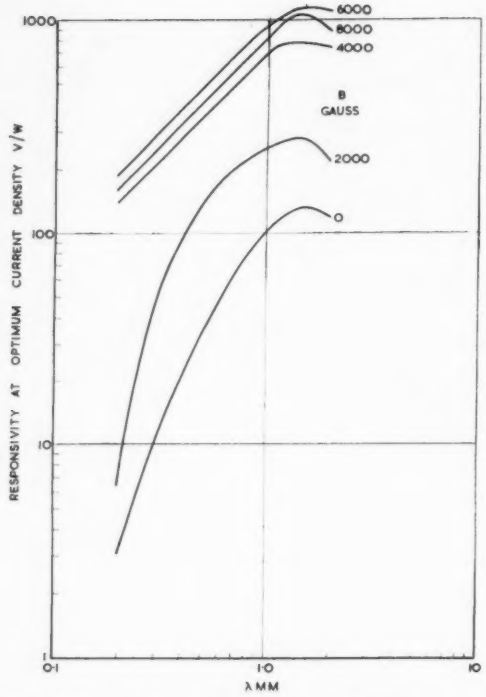

FIG. 5. Variation of responsivity with wavelength. Results at various magnetic inductions with the optimum current in each case.

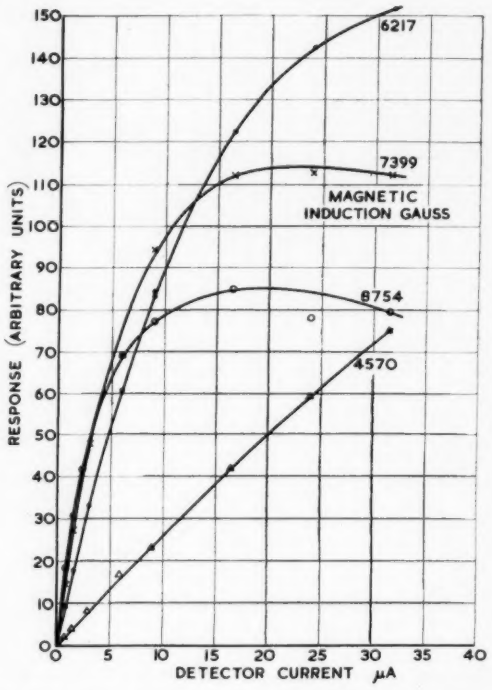

FIG. 6. Dependence of photoconductive effect upon magnetic induction and current density at 4·2 mm wavelength.

absorption could increase the effective electron temperature. Since impurity scattering is dominant, the mobility should increase. Hence the conductivity will increase, as with the conventional photoconductive effect. Also the time constant of this "electronic bolometer" should be less than 1 μsec. We would expect the free carrier absorption coefficient to be about 50 cm^{-1} at 1·0 mm but only 0·1 cm^{-1} at 0·2 mm. Thus the magnitude of this effect should fall more rapidly as the wavelength is reduced than the impurity photo-effect. On applying a magnetic field the free carrier absorption will be reduced due to the carrier freeze-out but the resistance of the sample will be increased. The observed responsivity is proportioned to the sample's resistance. Figures (1) and (2) show that while the carrier concentration can be reduced about two orders of magnitude, the resistance increases by three. Hence if free-carrier absorption were the dominant process we could expect about one order of magnitude increase in responsivity on applying a field. The results at 1 mm are consistent with this, but at 0·2 mm the field produces a larger increase.

It appears then that the two processes suggested can account for the observed behaviour, but more detailed study of the optical properties is required to confirm that this explanation is correct.

Acknowledgements—It is a pleasure to thank Dr A. F. GIBSON for the many discussions we have had on this subject and to thank Mr. V. ROBERTS and Mr. M. F. KIMMITT for their help with far-infrared techniques. British Crown Copyright Reserved.

REFERENCES

1. PUTLEY E. H., *Proc. Phys. Soc. Lond.* **73,** 280 (1959).
2. FAN H. Y., *Rep. Progr. Phys.* **19,** 107 (1956).
3. ROLLIN B. V., *Proc. Phys. Soc. Lond.* **77,** 1102 (1961)

Vol. 22
1961

DISCUSSION

D. W. GOODWIN (comment): PUTLEY's results on InSb at zero magnetic field can be interpreted as a change of mobility with electric field vector of the electromagnetic field. For wavelengths greater than 1 mm the energy relaxation time has a value of the order of 10^{-7} sec, which agrees with theory, assuming that energy loss occurs via acoustic phonons. A turnover at 1 mm could indicate a mobility of 6×10^4 cm/sec/V/cm. The effect of freeze out with a magnetic field is to leave the λ^2 region unmodified, provided that the same bias voltage is used but in the region of complete absorption for wavelengths greater than 1 mm the responsivity will be inversely proportional to the carrier concentration.

A similar effect using *n*-type germanium at 4·2°K has been used to produce a far infrared detector. A detector having high resolution has been achieved by operating well down the λ^2 region and increasing the absorption in a narrow spectral band by cyclotron resonance techniques. The specimen was lined up with the magnetic field in the $\langle 100 \rangle$ direction to give a single resonance band. The energy relaxation time at 4·2°K is approximately 5×10^{-9} sec, agreeing with an energy loss by acoustic phonons. At wavelengths of 8 mm the resolution of the detector is of the order of 20 and $D^* = 10^{12}$ cm/W. Further increase in absorption should raise this figure by two orders of magnitude. With the use of higher magnetic fields and suitable resonant structures a detector having a D^* of the order of 10^{14} cm/W at a wavelength of 1 cm should be possible with a resolution of the order of 10^3.

A. ROSE: Were any coherence effects observed when millimeter radiation from a Klystron was used?

E. H. PUTLEY: No.

E. BURSTEIN: For carrier concentrations of 10^{14}/cm^3 the plasma frequency should occur at about 1 mm. We would expect the absorption to become negligible at longer wavelengths due to the onset of metallic reflection. Is there any evidence for this in your zero magnetic field results?

E. H. PUTLEY: So far we have not seen evidence of plasma resonance but we have seen some indication of magneto-optical resonance effects in fields of 2000 G or greater. We have not yet been able to observe these effects sufficiently precisely to assign an exact interpretation.

J. S. BLAKEMORE: The magnetic freeze out of carriers is controlled by the contraction of the impurity wavefunction in the magnetic field. KEYES has suggested that this contraction is anisotropic, occurring mainly for directions perpendicular to that of the magnetic field. Thus it would be interesting to see the results of measurements on your samples for current both parallel to and perpendicular to the magnetic field.

E. H. PUTLEY: The increase in resistance in a strong magnetic field below 4°K is caused by two processes: (1) the freeze-out of carriers, (2) the reduction in mobility. I would not expect the freeze-out effect to depend on the orientation of the magnetic field, but the mobility change could. Some preliminary measurements of the variation of resistance upon rotating the magnetic field at 1·5°K with $B = 30$ kG showed that the resistance was practically constant as the magnetic field was rotated from a transverse direction to a direction parallel to the sample current.

E. BURSTEIN: A shift of the plasma frequency to longer wavelengths with decreasing carrier concentration would be an additional property which could be used to study the freeze-out of carriers with increasing magnetic field. One would carry out reflection measurements as a function of frequency to determine the plasma frequency and it would be necessary to apply corrections for magnetic plasma effects.

BLANK
PAGE

Vol. 22
1961

J. Phys. Chem. Solids Pergamon Press 1961. Vol. 22, pp. 249–254. Printed in Great Britain.

PHOTOCONDUCTIVITY IN *P*-TYPE INDIUM ANTIMONIDE WITH DEEP ACCEPTOR IMPURITIES*

W. ENGELER†, H. LEVINSTEIN and C. STANNARD, Jr.

Syracuse University, Syracuse, N.Y.

Abstract—The addition of Au, Ag or Cu impurities to InSb may be expected to produce two acceptor levels in InSb when these atoms with one valence electron replace In in the crystal lattice. The location of the energy levels has been determined by observing the extrinsic photoconductivity produced by the excitation of electrons from the valence band to the impurity levels and from the levels to the conduction band. The energy levels for Ag are in close agreement with those calculated by assuming a simple He atom model. The greater divergence for Au is attributed to the lattice distortion introduced when the larger Au atom replaces In in the crystal lattice. Oscillatory behavior of photoconductivity associated with charge carrier excitation to the lower level of all three impurities has been attributed to the successive emission of longitudinal optical phonons.

1. INTRODUCTION

IMPURITIES in Ge or Si produce a single energy level in the forbidden gap, if they have either one more or one less valence electron than the atoms they replace. The location of these levels as calculated by assuming a simple hydrogen-like impurity atom model is in close agreement with experiment. When lattice atoms are replaced by impurities with two less valence electrons, double acceptor levels are obtained. A helium-like impurity model does not, however, account for the 0·03 eV[1], 0·055 eV[1], and 0·087 eV[2] lower energy levels observed for Zn, Cd, and Hg in Ge. Ag, Au, and Cu impurities replacing In atoms in InSb also produce two acceptor levels. Calculations assuming a simple He-like impurity model yield 0·018 eV for the lower level and 0·04 eV for the upper level. BLUNT[3] has determined both levels for Cu using Hall measurements and a photoconductive quenching experiment on *n*-type InSb. His values of 0·023 eV and 0·056 eV for the lower and upper level respectively, are in fair agreement with expected values. Hall measurements on *p*-type InSb doped with Cu, Ag, and Au have recently been reported.[4] They confirmed BLUNT's value for Cu and in addition gave values of 0·022 eV for the lower level of Ag and 0·032 eV for Au. The activation energies of the upper levels, however, could not be uniquely determined from Hall measurements. Photoconductive response measurements have therefore been made to verify the lower and to determine the upper levels. The results of these measurements are reported here.

2. EXPERIMENTAL PROCEDURE

Indium and antimony in stoichiometric proportions were first reacted in a low pressure of hydrogen and heated for several hours to remove the volatile impurities. The compound was then zone refined by means of a zone heater assembly containing 3 heater elements. Hall measurements at liquid nitrogen temperatures indicated an impurity concentration no larger than 10^{14} cm^{-3} for the zone refined ingots. Single crystals were grown in the (211) direction by the zone leveling technique at rates between 0·5 and 1 cm per hour. Selected impurities were deposited at various points along the ingot. The systematic addition of these impurities permits the production of *p*-type crystals with various concentrations of impurities along their length. The first section of these crystals contained only the impurity whose energy levels were to be measured (Cu, Ag, Au)

* This work has been supported by the Air Research and Development Command, U.S. Air Force.

† Now at General Electric Research Laboratory, Schnectady, New York.

and trace impurities. Concentrations between 10^{14} and 10^{15} atoms per cm^3 were obtained. Beyond the first section, Se was added in various amounts (by means of an InSb–Se alloy). Se, replacing Sb in the crystal lattice, acts as a shallow donor impurity and its ionized electrons fill first the lower and then the upper level of the 2 level acceptor impurity. By properly compensating these levels, both energy levels can be measured on samples cut from various sections of the same crystal.

Crystals were cut and then etched in a 1 part HF, 4 parts HNO_3 solution to a size of approximately $2{\cdot}5 \times 2 \times 1{\cdot}5$ mm. In many cases, the samples cut for photoconductive measurements were sections from samples on which Hall measurements had previously been made. These samples were soldered to the cold finger of a conventional liquid helium dewar and to other electrical connections with an alloy of In, 2 per cent Cd. Photoconductive measurements were made on a Perkin Elmer Model 13 monochromator.

3. PHOTOCONDUCTIVE MECHANISM ASSOCIATED WITH ACCEPTOR LEVEL IMPURITIES

Several photoconductive mechanisms are possible in *p*-type material containing double acceptor level impurities depending on the degree of compensation of these levels. The transitions leading to photoconductivity are shown in Fig. 1.

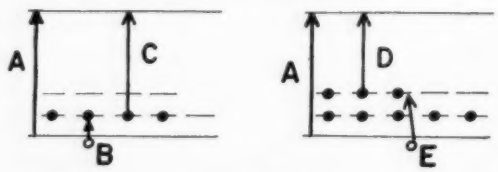

FIG. 1. Possible transitions of charge carriers to and from energy levels of Au, Ag or Cu in InSb with various degrees of compensation.

Excitation of electrons across the forbidden gap (transition A) leads to the production of electron hole pairs and is independent of the type of impurity. Its long wavelength photoconductive threshold corresponds to the intrinsic energy gap of InSb. If the lower level of the impurity is not entirely filled with electrons from the donor impurity, excitation of an electron to this level from the valence band may take place (transition B). If this level is not entirely empty, electrons from it may be excited to the conduction band (transition C). The location of the lower energy level of the impurity is then determined either by the energy corresponding to the long wavelength threshold of the former (transition B) or the difference between the energy gap and the threshold energy for the latter (transition C). If the upper level is not entirely filled, transitions to it from the valence band may take place (transition E); if it is not entirely empty, electrons from it may be excited to the conduction band (transition D). The location of this energy level may then be determined from the spectral response curves in the same manner as for the lower level. The magnitude of the extrinsic photoresponse depends on competitive absorption processes, the density of the impurity atoms, and the lifetime of the photoconductive carriers which in turn depends on the degree of compensation of these levels. The extrinsic photo-response may be many

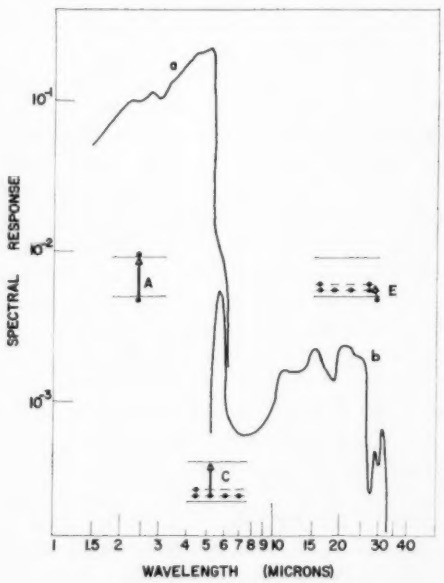

FIG. 2. Spectral response of InSb doped with Ag. (a) Intrinsic response and extrinsic response produced by excitation of electrons from lower level to conduction band. (b) Extrinsic response due to excitation from Ag lower level to conduction band and from valence band to upper Ag level.

Vol. 22
1961

orders of magnitude smaller than the intrinsic photoconductivity.

4. EXPERIMENTS RESULTS

A. *Crystals with a filled lower level*

Measurements were made first on samples which had a filled lower level. Fig. 2(a) shows the spectral response due to Ag whose upper level was nearly empty. The first sharp drop at 5·3 μ corresponds to the minimum energy for the intrinsic transition and yields the well known band gap of 0·23 eV at 5°K. The second sharp drop at about 6 μ (0·2 eV) corresponds to electron excitation from the lower level to the valence band (transition C). Fig. 2(b) shows the spectral response of a similar sample with a cooled InSb filter. The intrinsic region is now suppressed because of the high absorbtion of InSb in its intrinsic region (below 5·3 μ). This suppression reduces noise and makes possible the observation of the smaller extrinsic response. The sharp peak between 5 and 6 μ can be attributed to transition C, Fig. 1.

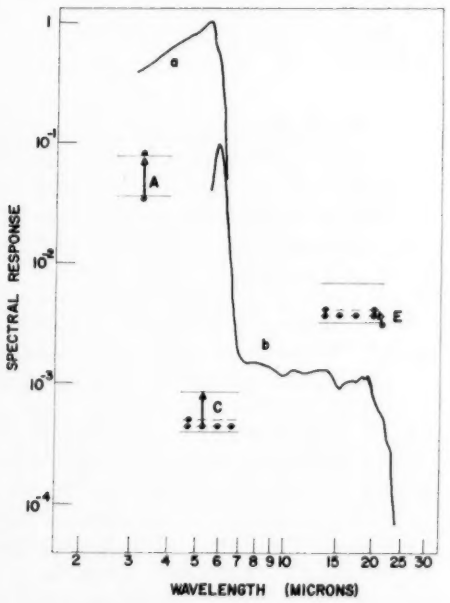

FIG. 3. Spectral response of InSb doped with Cu. (a) Intrinsic response and extrinsic response produced by excitation of electrons from lower level to conduction band. (b) Extrinsic response due to excitation from lower Cu level to conduction band and from valence band to upper Cu level.

The remaining spectral response is due to the electron transition from valence band to the upper level (E, Fig. 1), the long wavelength threshold yielding a value of 0·039 eV for the energy of the upper level. Figures 3(a) and 3(b) show the results on samples of InSb doped with Cu, giving an energy of 0·056 eV for the upper level. Figure 4(a) shows the spectral response of a gold sample

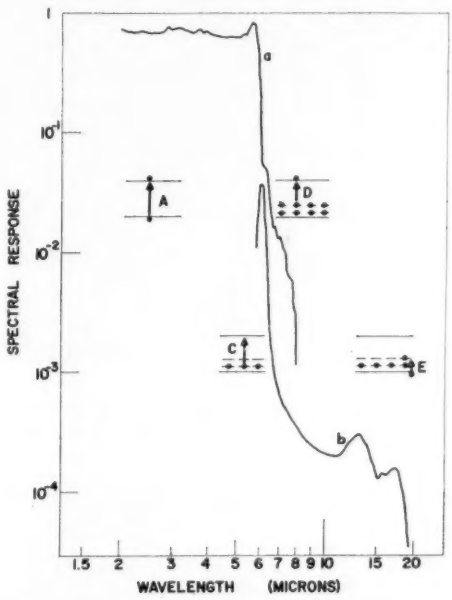

FIG. 4. Spectral response of InSb doped with Au. (a) Intrinsic response and extrinsic response produced by excitation from lower and upper Au levels to conduction band. (b) Extrinsic response due to excitation from lower Au level to conduction band and from valence band to upper Au level.

whose upper level is 75 per cent filled. This sample then shows, in addition to the intrinsic process and the excitation from the lower level, excitation from the upper level to the conduction band (D, Fig. 1). The energy of 0·16 eV corresponding to the cutoff at 7·6 μ when subtracted from the band gap (0·23 eV) yields an energy in agreement with that obtained (0·066 eV) from the long wavelength threshold of the spectral curve in Fig. 4(b). This curve shows the photoconductivity due to transitions from the valence band to the upper levels (E, Fig. 1) of a sample with nearly

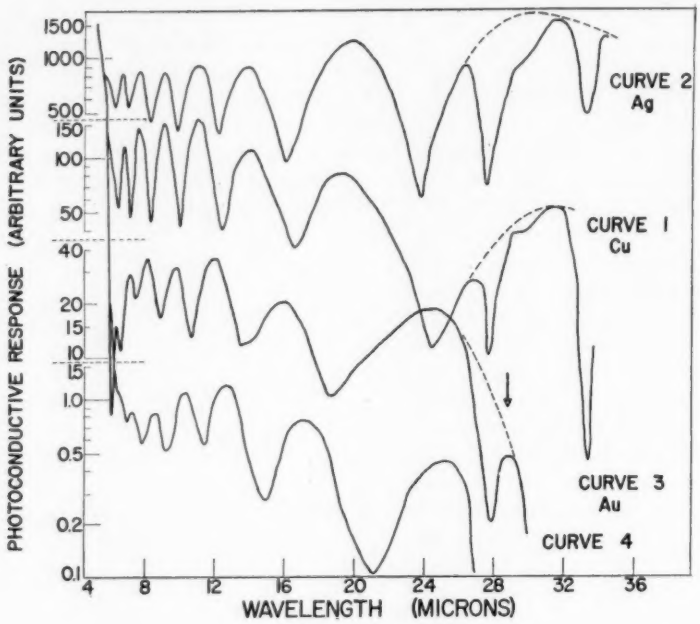

FIG. 5. Oscillatory photoresponse associated with the lower level of Ag, Au, Cu and an unknown impurity in InSb.

Vol. 22
1961

empty upper levels, provided with a cooled InSb filter.

B. *Crystals with partially filled lower levels*

Figure 5 shows the spectral response due to Ag, Au, Cu and an unknown impurity in InSb when only small compensation is used in crystal growth (near first section of the crystal). Measurements were made at liquid He temperature. The curves are composites, using data obtained with a NaCl and a CsBr prism. Intrinsic response was suppressed through the use of a cooled InSb filter. The rise near 6 microns is again presumed due to photoconductivity produced by the transition between the lower impurity level and the conduction band. The ratio of the magnitude of the spike to the photoconductivity produced through excitation from the valence band to the lower level depends upon the degree to which the lower level is filled by donor electrons. The greater its occupation the larger the magnitude of the spike compared with the photoconductivity beyond it. The oscillating behavior, also observed by BLUNT[5] for InSb doped with Cu, has recently been explained[6]. The interpretation is based on observations from the spectral curves and from their more graphical presentation in Fig. 6 where the number of each minimum has been plotted as a function of the energy at which it occurs. The slopes of these lines, representing the energy difference between successive minima, as calculated by the least squares fit of the data, are identical within experimental error. The location of the minima depends on the type of impurity in contrast to the location of lattice absorptions at 27·5 and 33·5 μ which are independent of impurity. In the case of gold where a cutoff is observed in the spectral response, this cutoff agrees with the energy intercept of the straight line (Fig. 6). Since the threshold for Cu and Ag was not in the range of the optical equipment, the assignment of the number of the minima was based on the estimate of the position of the threshold energy by Hall measurements.

The explanation assumes that the oscillations are due to the superpositions of a series of spectral

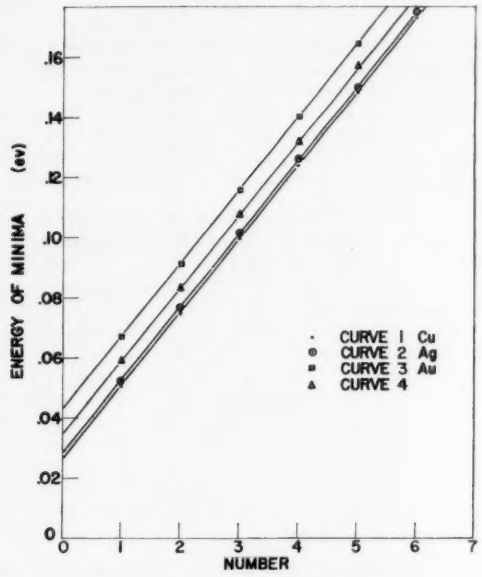

FIG. 6. Location of spectral response energy minima vs. their number for various impurities in InSb.

curves. The long wavelength threshold corresponds to the excitation of an electron from the valence band to the lower impurity level. The next threshold corresponds to the same process accompanied by the emission of a longitudinal optical phonon, succeeding thresholds at shorter wavelengths to the emission of 2, 3, 4, etc. phonons, respectively. This process appears reasonable since the transition probability starting at $\boldsymbol{k} = 0$, corresponding to the long wavelength threshold, at first increases, then decreases for increasing photon energies. When a photon energy is reached where a longitudinal optical phonon may be emitted, the process repeats itself, excitation again occurring at $\boldsymbol{k} = 0$ and proceeding to higher $\boldsymbol{k}$ values. The slope of all 4 lines of Fig. 6 is 0·0244 eV and represents the energy of the longitudinal optical phonon. This number is in good agreement with a value of 0·024 eV obtained by HALL, RACETTE and EHRENREICH[7] from tunneling experiments and 0·0244 eV recently reported by FRAY, JOHNSON and JONES[8]. Little can be inferred from the relative magnitude of these oscillations since they are not directly related to transition probabilities, depending in addition on other as yet undetermined competing processes.

5. DISCUSSION OF RESULTS

Table 1 represents a summary of the results. The energy intercept of the lines in Fig. 6 may be considered an optical activation energy. In the case of Au, where the long wavelength threshold was obtained, this value agrees well with the energy intercept. In all cases, Hall measurements, however, give somewhat lower values for the activation energy. This may be attributed to a systematic error in Hall measurements, produced by a certain amount of impurity band conduction, or perhaps merely due to the differences between thermal and optical activation energies. The experimentally determined values of lower and upper Ag levels agree most closely with the He atom model. This seems reasonable since the Ag atom has the same inner shell configuration as In, the atom it replaces. The values for Au show the largest discrepancy, again as expected, since Au, because of its large size, probably produces some distortion of the crystal lattice when it replaces In.

Table 1. *Summary of results*

Impurity	Upper level (eV) Photocond. data	Lower level (eV) Hall data	Lower level (eV) Energy intercept
Cu	0·056	0·023	0·026
Ag	0·039	0·023	0·028
Au	0·066	0·032	0·043
He atom model	0·040	0·018	

REFERENCES

1. NEWMAN R., WOODBURY H. H. and TYLER W. W., *Phys. Rev.* **102,** 613 (1956).
2. BORRELLO S. and LEVINSTEIN H., Report 104–5, Syracuse University Research Institute, February 1, 1961.
3. BLUNT R. F., *Bull. Am. Phys. Soc. II,* **3,** 115 (1958).
4. ENGELER W. and LEVINSTEIN H., *Bull. Am. Phys. Soc.* **6,** 156 (1961).
5. BLUNT R. F., *Bull. Am. Phys. Soc.* **3,** 115 (1958).
6. ENGELER W., LEVINSTEIN H. and STANNARD, Jr.,C. *Phys. Rev. Letters* **7,** No. 2 (1961).
7. HALL R. N., RACETTE J. H. and EHRENREICH H., *Phys. Rev. Letters* **4,** 456 (1960).
8. FRAY S. J., JOHNSON F. A. and JONES R. H., *Proc. Phys. Soc.* (*London*) **76,** 939 (1960).

DISCUSSION

M. A. LAMPERT: Your series of "high-energy" photoconductivity peaks (which you interpret as photon absorption with simultaneous emission of 0, 1, 2, 3, 4, ... etc., longitudinal optical phonons), *if taken at face value*, lead to the striking conclusion that absorption with emission of say 4 phonons is just as probable as absorption with emission of 1 phonon. The question is: Can the data be taken at face value (in this sense)? If the sample is essentially transparent over the range of wavelengths in question, and simultaneously any optical interference effects can be ruled out, then it is difficult to see how this "face value" interpretation can be avoided. On the other hand, if the sample is largely opaque over all or parts of the wavelengths region, the situation is considerably more complicated, and very likely, alternatives can be found to the "face value" interpretation. Measurement of the absorption constant over the wavelength region concerned would prove most helpful in resolving this matter.

W. ENGELER: The sample to be measured was placed in the standard integrating cavity used for IR detectors of this type. In such a cavity the incoming photon can make many transitions through the generally transparent sample until it is finally absorbed either by a photoconductive transition or by some other competitive process. The response of the detector is then determined by the relative magnitude of these two types of processes. The face value interpretation of the spectral response data, which shows a decrease of only a factor of three, can therefore be very misleading unless the magnitude of the competitive process is known, as the variation with wavelength of these processes can be quite large. For example, the general background absorption of the InSb lattice has been shown by S. J. FRAY, F. A. JOHNSON and R. H. JONES[8] to vary by two orders of magnitude between 17 and 30 μ. Absorption measurements are currently planned and should illuminate this problem.

E. BURSTEIN: These results are particularly interesting as similar structure in impurity photoionization spectra is not found for the case of impurities in homopolar semiconductors such as silicon and germanium. It may be associated with the fact that the host lattice InSb is polar and moreover piezoelectric. This would imply a strong coupling of longitudinal optical vibrations. The mechanism may very well involve a multiple phonon Franck–Condon effect in which the electronic energy of the ground state of the impurity is strongly dependent on the nuclear "configuration" and in particular a longitudinal optical mode type configuration. That the matrix elements do not decrease rapidly with increase in the number of phonons is not inconsistent with a Franck–Condon effect.

M. G. BERNARD: (1) We have shown at the Prague Conference that in Ge the simultaneous emission of n phonons is actually possible. (2) The use of LAX's calculations for these processes requires the knowledge of both the deep level state and the phonon spectrum in the vicinity of the center; generally both of them are unknown.

Vol. 22
1961

J. Phys. Chem. Solids Pergamon Press 1961. Vol. 22, pp. 255–259. Printed in Great Britain.

THE CAPTURE OF HOLES IN DEEP-LYING ACCEPTOR LEVELS IN GOLD-DOPED GERMANIUM

G. RUPPRECHT

Research Division, Raytheon Company, Waltham 54, Massachusetts

Abstract—The capture cross-section for holes and its temperature dependence have been measured on gold-doped germanium for the 0·145 eV acceptor level by pulsed field effect in the temperature range from 50°K to 100°K. The result: $\bar{\sigma}_p = 7 \times 10^{-13}(T/100)^{-n}$ cm^2 with a value for n between $\frac{1}{2}$ and 1. Effective cross-sections of the first acceptor level for gold, nickel and manganese in germanium show a correlation with maximum solubility and segregation constant indicating that these impurities may introduce an appreciable perturbation in the homopolar germanium host lattice, the geometrical extension of which may be responsible for the observed large capture cross-sections.

INTRODUCTION

One of the basic problems in photoconductivity is the capture of free-charge carriers in localized states. For attractive centers large capture cross-sections have been observed.[1,2] An explanation of their size and a prediction of their temperature dependence have been given by Lax in his theory of giant traps.[3] Experimental observations on shallow impurities seem to be in fair agreement with this theory.[4] It has been noticed, however, that this is not the case for deep lying impurity levels.[5] Here, a different explanation, which provides for the possibility of efficiently dissipating enough of the energy of a free carrier in the surrounding of an impurity center during the capture process, seems necessary.

The following investigation consists mainly of a careful study of the temperature dependence of the 0·145 eV acceptor level in gold-doped p-type germanium. In addition to its other advantages, p-type germanium was chosen for the simplicity of its band structure for holes, which excludes the possibility of intervalley scattering. The tool of investigation is pulsed field effect.

PULSED FIELD EFFECT EXPERIMENT

It has been shown previously[5] that under suitable experimental conditions, the capture cross-section of an impurity level may be obtained by pulsed field effect experiment. Accordingly, for an impurity level (E_T) which is in interaction with the valence band (E_V) the temperature dependent cross-section $\sigma(T)$ is given by the relation

$$\frac{1}{\tau N_V v_T} = \frac{\sigma(T)}{\gamma} \exp\left(\frac{E_V - E_T}{kT}\right). \qquad (1)$$

The quantity procured from pulsed field effect is $\tau(T)$, the time constant for thermal generation of holes out of the impurity level. γ is the statistical weight factor of this level.[6] Since N_V and v_T are readily known, the cross-section and its temperature dependence are determined as soon as a sufficiently accurate value of $(E_T - E_V)$ is available and if the additional assumption is made that γ is temperature independent.

Figure 1 shows the sample holder and the measuring circuit. It can be seen from equation (1) that the requirements for an accurate temperature measurement are quite stringent in this experiment. Great care has, therefore, been taken to ensure that the temperature which is recorded with a thermocouple on the back side of the sapphire indicates the sample temperature. Heating of the sample was eliminated by sufficiently low d.c. currents. The radiation shields around the sample holder are not shown. The time constant τ is extracted from an evaluation of the time dependence of the sample conductivity after a step voltage has been applied to the field plate. It has been checked that τ is

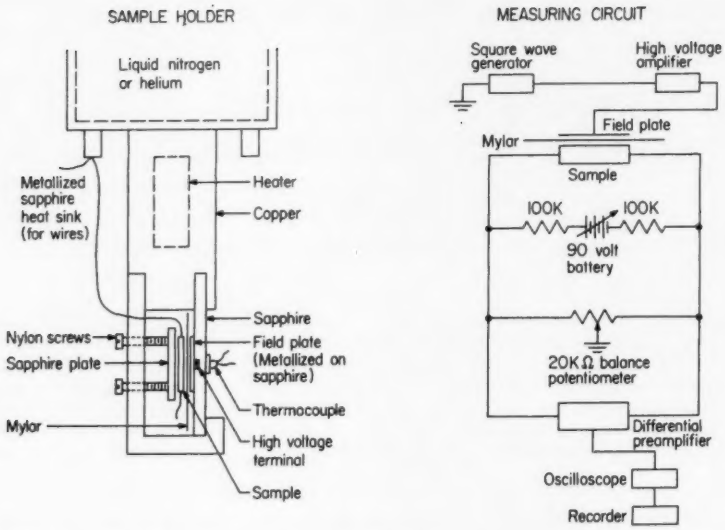

FIG. 1. Sample holder and measuring circuit for pulsed field effect experiment.

independent of pulse height for sufficiently small pulses.

EXPERIMENTAL RESULTS

Measurements of the time constant τ for hole generation are summarized in Fig. 2. The germanium samples were doped with gold, nickel and manganese. The quantity $1/\tau N_V v_T$ is plotted vs. $1000/T$ on a semi-logarithmic scale and yields fairly straight lines for all three dopings. An evaluation of these slopes leads to energy values 0·141 eV, 0·216 eV, 0·145 eV for gold, nickel, and manganese respectively. These energies though somewhat smaller, are in close agreement with the known values for the energy position of these three acceptor levels above the valence band. From such data the conclusion has been drawn that the temperature dependence of the cross-section is quite weak.[5] In the case of gold-doped germanium a determination of the temperature dependence of the cross-section is possible, since as accurate value for the energy position of the acceptor level is known. It is $E_T - E_V = 0{\cdot}145$ eV.[6] It seems worthwhile mentioning that this energy value and the pulsed field effect data, presented here, are both obtained from the same sample GT 17–4.

To evaluate equation (1) the cross-section $\sigma(T)$ has been introduced as:

$$\sigma(T) = \sigma_o \cdot (T/T_o)^{-n}. \tag{2}$$

Equation (1) may then be written in the form:

$$\log\left(\frac{1}{\tau N_V v_T}\right) + \frac{0{\cdot}4343 \times 0{\cdot}145\ (\text{eV})}{kT\ (\text{eV})} = \log\left(\frac{\sigma_o}{\gamma}\right) - n \log(T/T_o). \tag{3}$$

Fig. 3 shows the data calculated from the left hand side of equation (3) plotted vs. $\log(T/T_o)$. T_o is chosen to be 100°K. For this temperature $\sigma_o/\gamma = 9 \times 10^{-14}$ cm^2. To make comparison convenient, the right hand side of equation (3) is drawn in Fig. 3 for values $n = \frac{1}{2}$ and $n = 1$. The experimental points fall between these two limits. It does not seem justified, however, to deduce a more accurate value for n with the present data. Using the value $\gamma = 8{\cdot}5$ the capture cross-section becomes

$$\bar{\sigma}_p = 7 \times 10^{-13}\ \text{cm}^2 \text{ at } 100°\text{K}.$$

This is in fair agreement with the value $\sigma = 1{\cdot}55 \times 10^{-12}$ cm^2 which NEURINGER and

Vol. 22
1961

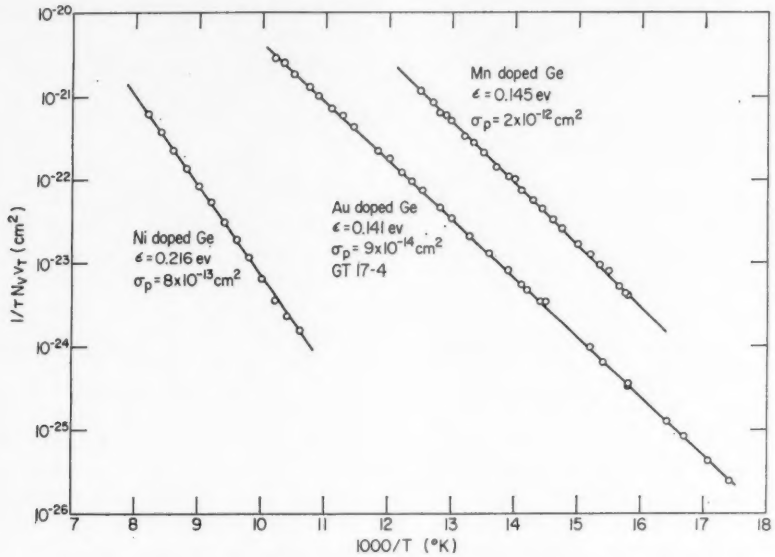

FIG. 2. $1/\tau N_V v_T$ vs. $1000/T$ for gold, nickel and manganese in germanium.

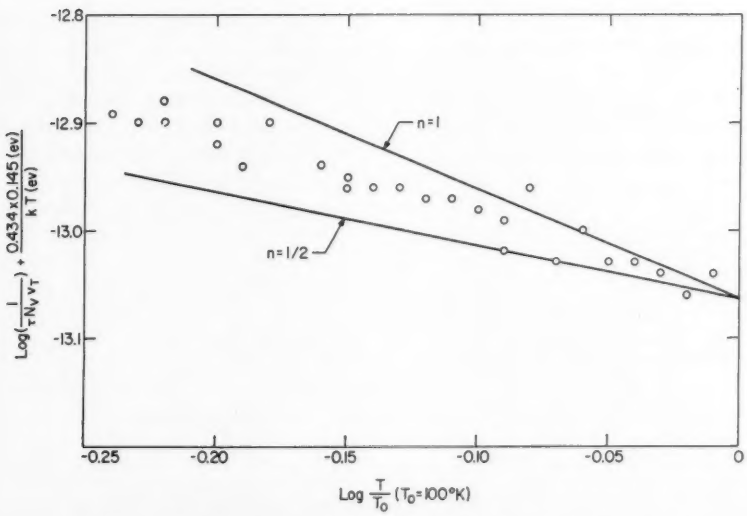

FIG. 3. Temperature dependence of the 0·145 eV gold acceptor level.

BERNARD[7] obtained from noise measurements on the same sample (GT 17–4). JOHNSON and LEVINSTEIN found $\sigma \approx 10^{-13}\text{cm}^2$ from measurement of the photoresponse for this level.[2]

In order to compare cross-sections for different dopings, the data in Fig. 2 have been evaluated to yield effective cross section σ_o/γ, under the assumption that the temperature dependence of the capture cross-section is described by equation (2) with $n = \frac{1}{2}$ for nickel and manganese also. One finds then σ_o/γ and a corrected value for $(E_T - E_V)$ simultaneously:

Ni: $\sigma_{\text{eff}}(\text{Ni}) = \sigma_o/\gamma = 8 \times 10^{-13}\,\text{cm}^2$ at 100°K and $E_T - E_V = 0{\cdot}220$ eV.

Mn: $\sigma_{\text{eff}}(\text{Mn}) = \sigma_o/\gamma = 2 \times 10^{-12}\,\text{cm}^2$ at 100°K and $E_T - E_V = 0{\cdot}149$ eV.

The effective cross-sections at 100°K are therefore substantially different. The corrected values for the energy position of nickel and manganese are in good agreement with values in the literature.[8,9]

DISCUSSION

It has been well established that the investigated acceptor levels of gold, nickel, and manganese in germanium are single-negatively charged when empty. The capture of a hole into an empty level is therefore assisted by Coulomb attraction. The extremely large cross-section suggests that this attraction is the important feature for the capture mechanism. The cascade theory[3] can explain the order of magnitude of such attractive cross-sections, suggesting a capture mechanism via excited states with large hydrogen-like orbits. The necessary dissipation of energy during the capture process is achieved by interaction of the carrier in orbit with accoustical and optical phonons.

1. According to this theory the capture cross-section should not depend upon the particular kind of impurity as long as the charge character is the same. The measurements, however, yield effective cross-sections which vary substantially in size.

2. Assuming that in the vicinity of an impurity center bulk properties can be used, LAX has shown that his theory predicts a temperature dependence of the cross-section with T^{-4}. The experimental results, however, show that this capture mechanism does not seem to apply here. The temperature dependence of the cross-section somewhere between $T^{-1/2}$ and T^{-1} suggests that the thermal energy of the incoming hole alone may be held responsible for this exponent.

Present results seem to indicate that it is necessary to postulate a more efficient way to dissipate energy in the surrounding of an impurity atom. In this context it might be interesting to consider how an impurity atom influences the lattice. Shallow acceptors and donors, such as As and Sb, are soluble in the germanium lattice in high concentrations. The relatively large segregation constant k indicates that they build fairly easily into the lattice. It is further well established that such shallow impurities occupy regular germanium sites. Maximum solubility and segregation constant may be considered measures of the misfit of the impurity in the host lattice.

In the case of gold, nickel, and manganese, these impurities are still assumed to occupy regular sites. However, their low solubility and small segregation constant suggest that they do not fit into the lattice too well. It is therefore quite possible that the host lattice is severely disturbed in the surrounding of such an impurity atom.

Following this concept one might expect that

Table 1

Substance	k Segregation constant	S Maximum solubility (cm^2)	σ Capture cross-section (cm^2)
As	0·02	$\approx 10^{20}$	2×10^{-12} (4°K)
Sb	0·003	$\approx 1 \times 10^{19}$	2×10^{-11} (4°K)
Au	$1{\cdot}3 \times 10^{-5}$	$> 2 \times 10^{6}$	9×10^{-14} (100°K)
Ni	3×10^{-6}	8×10^{15}	8×10^{-13} (100°K)
Mn	$\simeq 10^{-6}$	$\approx 10^{15}$	2×10^{-12} (100°K)

Vol. 22
1961

the capture cross-section for a carrier is connected with the geometrical extension of such a lattice perturbation. In Table 1 the values for maximum solubility S and segregation constant k are listed, together with effective cross-sections for Au, Ni, Mn at 100°K, and ASCARELLI and BROWN's cross-section values at 4°K for Sb and As impurities.[4]

It is apparent from Table 1 that as expected the cross-sections for Au, Ni, Mn are increasing, whereas solubility and segregation constant are decreasing. This correlation seems to hold even for the shallow donors As and Sb.

From the described behavior of capture cross-sections in germanium one might draw the tentative conclusion that the homopolar germanium host lattice no longer has the properties of the undisturbed lattice. It may show an appreciable change of the interaction with a free-charge carrier in the surrounding of an impurity.

Acknowledgement—The author is indebted to P. SMAKULA for his help and great care in obtaining the data.

REFERENCES

1. KOENIG S., *J. Phys. Chem. Solids* **8,** 227 (1959).
2. JOHNSON L. and LEVINSTEIN H., *Phys. Rev.* **117,** 1191 (1960).
3. LAX M., *J. Phys. Chem. Solids* **8,** 66 (1959).
4. ASCARELLI G. and BROWN S. C., *Proceedings of the International Conference on Semiconductor Physics, Prague* (1960), p. 271.
5. RUPPRECHT G., *Proceedings of the International Conference on Semiconductor Physics,* Prague (1960), p. 282.
6. KLEIN C. A. and DEBYE P. P., *Proceedings of the International Conference on Semiconductor Physics, Prague* (1960), p. 278.
7. NEURINGER L. F. and BERNARD W., *Phys. Rev. Letters* **6,** 455 (1961).
8. TYLER W. W., NEWMAN R. and WOODBURY H. H., *Phys. Rev.* **98,** 461 (1955).
9. WOODBURY H. H. and TYLER W. W., *Phys. Rev.* **100,** 659 (1955).

DISCUSSION

G. HEILAND: If one studies a discrete level at the very surface by field effect, there is a single well defined distance from the Fermi level. But in studying a bulk level one faces a more complicated situation, for the distance from the Fermi level varies as a function of the distance from the surface within the space charge layer. In many respects one may then observe results as for a continuous distribution of levels at the very surface, e.g. the number of states changing the occupation during a pulse may show no saturation with increasing field. How are your results influenced by these facts?

G. RUPPRECHT: The results are not influenced by these facts, since they have been taken into account for the evaluation of $\tau = (gN_V)^{-1}$. In the case of bulk states the time dependence of the conductance after pulsing is indeed no longer a simple exponential function, as is the case with surface states. It becomes dependent upon parameters like surface potential, temperature, concentration of impurities and pulse height. The time dependence of the redistribution of charges in the space charge region has been calculated by solving a partial differential equation, in part through the help of a computer. From the obtained general solution a simple method has been derived for the determination, of τ from the observed conductance change.

M. A. LAMPERT (comment): Your temperature region 50°–100°K, is, I believe, an inappropriate one for comparison with LAX's theory. In Ge, the entire "hydrogenic" series of levels covers only about 0·01 eV, and this spread is much too close to kT to apply LAX's mechanism of a "random walk" up and down the energy scale. The probable energy step of a single "random walk", at your temperatures, is much too big. Consistent with this remark, is the fact that your observed cross-sections differ greatly from Au to Ni to Mn impurity, indicating that the deep-lying non-hydrogenic ground state is playing a key role in the capture process. Accepting this, plus the supposition that non-radiative capture is strongly favored over radiative capture (pointed out by AIGRAIN), your interpretation of the correlation between observed capture cross-sections and known solubilities (or segregation coefficients) seem quite reasonable. Low solubilities are presumably associated with strong local strains, and these would, in turn, certainly play a strong role in multi-phonon emission processes.

G. RUPPRECHT: Your proposal of a capture via a multi-phonon emission process is an interesting possibility provided that such a process can account for the observed large capture cross-sections.

To satisfy this condition it has been proposed here that through introduction of the impurities the lattice scattering via optical phonons, for instance, might be largely enhanced in the surrounding of an impurity center.

BLANK
PAGE

Vol. 22
1961

J. Phys. Chem. Solids Pergamon Press 1961. Vol. 22, pp. 261–267. Printed in Great Britain.

CARRIER LIFETIMES IN *n*-TYPE GOLD-DOPED GERMANIUM

R. L. WILLIAMS*

Canadian Armament Research and Development Establishment, Valcartier, Quebec, Canada

Abstract—Minority and majority carrier lifetimes in *n*-type gold-doped germanium have been evaluated by means of the combined photoconductive and photoelectromagnetic effects. The room temperature capture cross-section of the upper gold level for electrons is evaluated to be $1{\cdot}0\ (\pm\ 0{\cdot}3) \times 10^{-16}$ cm^2 and for holes $1{\cdot}5\ (\pm\ 1{\cdot}0) \times 10^{-12}$ cm^2. These values agree with the order of magnitude values found by JOHNSON and LEVINSTEIN[3].

Between 150° and 60°K an exponential temperature dependence is found for the electron capture cross-section with an activation energy of 0·01 eV. Between room temperature and 400°K, surface recombination effects are important, but the PC/PEM ratio method permits the evaluation of the now nearly equal electron and hole lifetimes.

Equations are derived for the electron carrier concentration temperature dependence, with partial compensation of the gold level 0·20 eV from the conduction band. The expression is used to evaluate the donor and acceptor concentrations: $N_d = 4{\cdot}7 \times 10^{15}$/cm^3 and $N_a = 2{\cdot}9 \times 10^{15}$/cm^3. In analysing the data, a mobility ratio of 1·2 at 370°K is required to make the observed data agree with the calculations.

LIST OF SYMBOLS

n_0, p_0	Equilibrium concentration of electrons and holes
n_1, p_1	Value of n_0 and p_0 when the Fermi level lies at the energy E_1
n_2, p_2	Value of n_0 and p_0 when the Fermi level lies at the energy E_2
n_i	Intrinsic carrier concentration
n_{ex}	Extrinsic electron concentration
c_{n_2}, c_{p_2}	Capture probabilities for electrons and holes at a level with energy E_2
A_{n_2}, A_{p_2}	Cross-section for recombination of electrons and holes of centers at the energy level E_2
v_n, v_p	Thermal velocity of electrons and holes
τn_2, τ_{p_2}	Electron, hole lifetime for energy levels at E_2
μ_n, μ_p	Electron, hole mobility
D_n, D_p	Electron and hole diffusion coefficient
ϕ	Light flux—quanta/sec.
E	Electric field
H	Magnetic field
N_a	Acceptor impurity concentration
N_d	Donor impurity concentration
M_1, M_2	Electron density for the level E_1, E_2
E_1	Energy level of the lower gold site 0·015 eV from valence band
E_2	Energy level of the upper gold site 0·20 eV from conduction band
k	Boltzman's constant
T	Absolute temperature
L_D	Hole diffusion length
s	Surface recombination velocity

* Present address: RCA Victor Research Laboratories, 1001 Lenoir Street, Montreal 30, Quebec, Canada.

INTRODUCTION

THE EXISTENCE of multiple energy levels for impurity atoms in semiconductors is now well established.[1] Energy levels which are doubly charged are expected to have very different capture probabilities for electrons and holes. The results of experiments by TYLER and WOODBURY[2] with *n*-type manganese-doped Ge suggested that such a large difference in capture cross-sections exists for doubly charged Mn sites. Measurements were made of majority but not minority carrier lifetimes, so the relative magnitude of the hole and electron capture cross-section could not be calculated.

Extensive measurements made on *n*- and *p*-type gold-doped germanium by JOHNSON and LEVINSTEIN[3] confirmed that gold capture cross-sections can be very different for electrons and holes. In this work photoconductive phenomena were observed in *n*- and *p*-material and the results indicated that the capture cross-section for holes was 6000 times larger than for electrons.

RECOMBINATION THEORY

The existence of separate lifetimes for electrons and holes was predicted by SHOCKLEY and READ[4]. More complete theoretical descriptions of recombination phenomena including two separate time constants have been calculated by SANDIFORD[5], CLARKE[6] and WERTHEIM[7].

BERNARD[8] has developed the equations for recombination through double energy level impurities and the results may be summarized as follows. If the Fermi level remains between the two energy levels in question, the lifetime of the electrons and holes are a factor of 2 greater than the value predicted for the single level theory of SHOCKLEY and READ. Although only shown to be correct for low impurity concentration, it is here assumed to be true generally; thus the electron lifetime is:

$$\tau_{n_2} = 2\frac{C_{p_2}[p_0+p_2+N_a(p_2/p_0+p_2)]+C_{n_2}(n_0+n_2)}{C_{p_2}C_{n_2}N_a[n_0+p_0+(N_an_2n_0/n_0+n_2)^2]}. \tag{1}$$

The value for holes is:

$$\tau_{p_2} = 2\frac{C_{n_2}[n_0+n_2+N_a(n_2/n_0+n_2)]+C_{p_2}(p_0+p_2)}{C_{p_2}C_{n_2}N_a[n_0+p_0+(N_an_2n_0/n_0+n_2)^2]}. \tag{2}$$

The subscript 2 refers to the second ionization level for gold in germanium which is 0·20 eV from the conduction band. The symbols are defined in the "list of symbols". From the analysis which follows, recombination in the n-type gold-doped germanium crystals examined is adequately described by neglecting recombination through the lower level 0·15 eV from the valence band.

LIFETIME MEASUREMENT METHODS

The lifetime of electrons and holes are usually different in the heavily doped materials used in the study of charged centres. Photoconductivity is then primarily a majority carrier phenomena and unless additional information is available it is difficult to determine both electron and hole capture cross-sections from this one type of measurement. ZITTER[9] has shown that for the condition of different electron and hole lifetimes that the photoelectromagnetic (PEM) effect depends on the magnitude of the minority carrier lifetime. AMITH[10] emphasizes the fact that the PEM effect is entirely a minority carrier phenomena.

Following the analysis of ZITTER[9], with different electron and hole lifetimes in n-type Au-doped Ge, the photoconductive (PC) short circuit current is given by the expression:

$$i_{PC} = \phi e\mu_n\tau n_2 E, \tag{3}$$

and the PEM short circuit current is

$$i_{PEM} = (1+1/b)\phi e\mu_n H(D_p\tau_{p_2}). \tag{4}$$

The data to be presented is based on the above two equations being valid over the temperature range investigated. As will be apparent later, at high temperature the value of τ_{p_2} approaches τ_{n_2} (thus $\tau_{p_2} = \tau_{n_2} = \tau_2$) and surface recombination becomes important. The corresponding set of equations for this region are:[11]

$$i_{PC} = (1+1/b)\cdot\frac{\phi e\mu_n\tau_2 E}{1+L_D{}^{s}/_{D}}, \tag{5}$$

and

$$i_{PEM} = (1+1/b)\cdot\frac{\phi e\mu_n H\sqrt{D_p\tau_2}}{1+L_D{}^{s}/_{D}}. \tag{6}$$

Hall effect determination of impurity concentrations

The charge in the gold impurity sites can be calculated using the results of CHAMPNESS[12] or BERNARD[8]. If M_1 is the density of sites with one electron and M_2 the density with two electrons, then the density of electrons on gold sites is given by (BERNARD):

$$M_1+2M_2 = \frac{2N_an_0(n_0+n_2)}{n_0(n_0+n_2)+n_2(n_0+n_1)}.$$

For an n-type sample with E_2 0·20 eV from the conduction band and E_1 0·15 eV from the valence band $n_o \gg n_1$ for temperatures of interest. Thus, approximately:

$$M_1+2M_2 \doteq 2N_a\left(\frac{n_0+n_2}{n_0+2n_2}\right).$$

For the material used the donor levels are ionized over the temperature range investigated so the charge balance equation can be written for the extrinsic range:

$$n_0+2N_a\cdot\left(\frac{n_0+n_2}{n_0+2n_2}\right) = N_d,$$

Vol. 22
1961

or

$$n_{ex} = n_0 = \frac{2n_2+2N_a-N_d}{2} \times \left[\left\{1+\frac{8n_2(N_d-N_a)}{(2n_2+2N_a-N_d)^2}\right\}^{1/2}-1\right], \quad (7)$$

which is defined as n_{ex}, the extrinsic carrier concentration.

When the hole density becomes non-negligible at high temperatures it has been allowed for by using the form:

$$n_0-n_i^2/n_0 = N_d-N_a. \quad (8)$$

This involves a small error since the acceptor sites are not completely ionized at the temperatures when the hole density begins to make a significant contribution to the conductivity.

Sample Material. The material used in the experiments, n-type gold-doped germanium, was kindly supplied by M. LASSER of the Philco Corporation. The material was single crystal germanium with the second gold level (0·20 eV) partially compensated. The material is described briefly in the article by LASSER *et al.*[13] which discusses the n-type gold-doped germanium infrared detector for which it was prepared.

Samples shaped into bridges were used for Hall and conductivity measurements as well as PC and PEM measurements.

Hall and conductivity measurements

Conventional cryostat arrangements were used for the temperature control of the sample. The Hall and conductivity measurements were made using a DAUPHINEE and MOOSER[14] system and a potentiometer for high resistance work.

The carrier concentrations have been calculated from the Hall coefficient $R = \gamma 1/ne$ with the factor γ assumed equal to $3\pi/8$. Impurity scattering is important even near room temperature, since the mobilities are smaller than the values given by MORIN[15] (Fig. 2). The value of γ can be calculated on the basis of the ratio of the accepted to the observed mobilities and then the correct mobilities[16] recalculated. Using $\gamma = 3\pi/8$ the maximum error, which occurs at low temperature, is not more than 50 per cent.

The effective mass of electrons and holes used in the carrier concentration expressions and the equation for n_i were taken from CONWELL[17].

The variation of carrier concentration with inverse temperature is shown in Fig. 1. Using the analysis procedure of LEE[18] on the experimental points of Fig. 1, values of N_a and N_d are obtained. These values $N_a = 2{\cdot}9\times10^{15}$ per cm^3 and $N_d = 4{\cdot}7\times10^{15}$ per cm^3) were used in equations (7) and (8) to evaluate the solid line curve of Fig. 1.

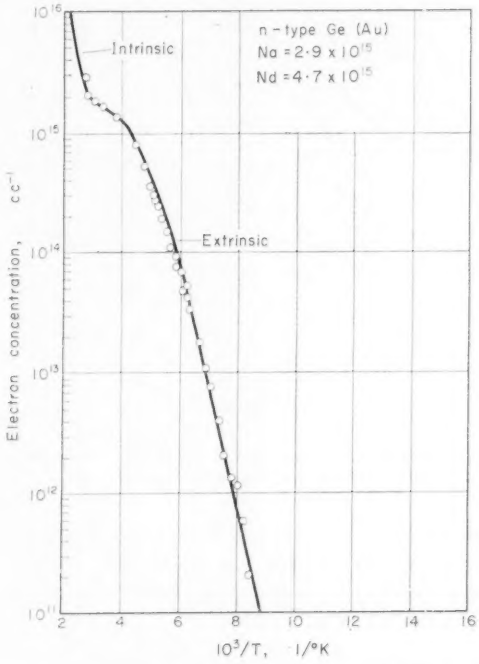

FIG. 1. Variation of carrier concentration with reciprocal temperature. From the shape of the curve both N_a and N_d were evaluated.

In the intrinsic conductivity region a mobility ratio of 1·2 resulted in the best fit of theory to the experimental points. As the choice of n_i values effects the choice of b the value of 1·2 is not highly accurate.

Mobility Data. The values of μ_n shown in Fig. 2 were calculated using values of n shown in Fig. 1 along with conductivity measurements. The μ_n line represents the value of μ_n used in the work to be quoted. The lines labelled μ_{Ln} and μ_{Lp} are the mobility data of MORIN[15] for high purity Ge.

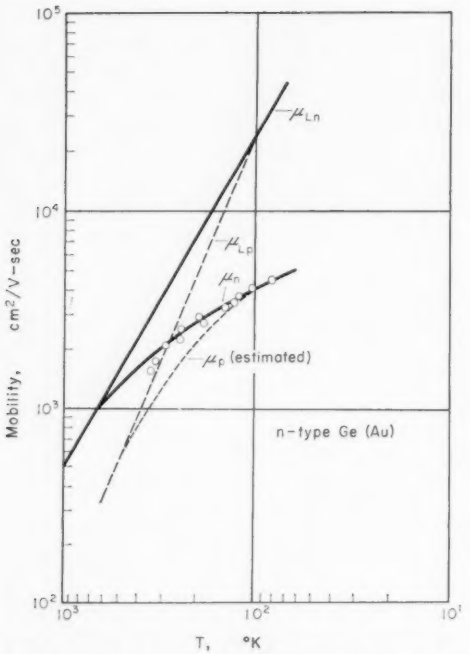

FIG. 2. Mobility data of MORIN (μL_n and μL_p) with electron mobilities deduced from Hall and conductivity measurements. The hole mobility was estimated using a mobility ratio deduced from MORIN's data.

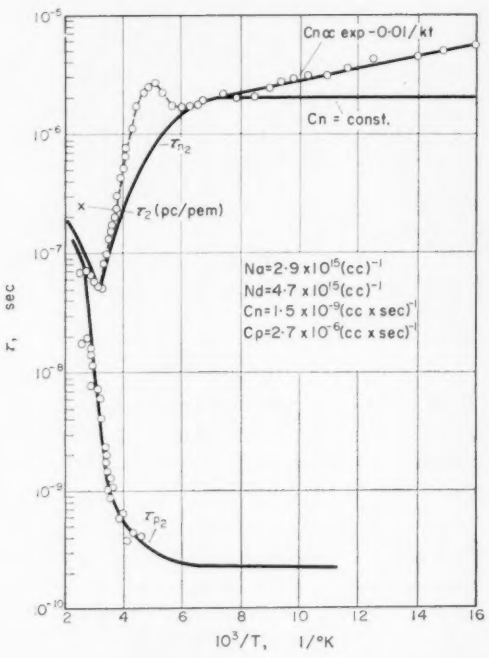

FIG. 3. Measurements of the lifetimes of electrons τ_{n_2} and holes τ_{p_2}. At high temperatures surface recombination effects dominate the recombination process. In spite of this the ratio of PC and PEM signals has been used to evaluate the now equal lifetimes. (x-point at 400°K).

Because of the uncertainty of the b-value deduced from the electron concentration data, a μ_n/μ_p ratio equal to the value for high purity germanium was used to calculate μ_p.

PC–PEM Data

Using a calibrated light source restricted to the wavelength interval 1·2–1·4 microns, the data of Fig. 3 were obtained. The solid line curve has been calculated using equations (1), (2), (3) and (4), with the following data. $N_a = 2{\cdot}9\times10^{15}$ cm^{-3}, $N_d = 4{\cdot}7\times10^{15}$ cm^{-3}, $C_{p_2} = 2{\cdot}7\times10^{-6}$ cm^3 sec^{-1} and $C_{n_2} = 1{\cdot}5\times10^{-9}$ cm^3 sec^{-1}. The cross-sections of recombination, using a value of $v_p = 1{\cdot}8\times10^7$ cm sec^{-1} and $v_n = 1{\cdot}5\times10^7$ cm sec^{-1} ($T = 300$°K), are $A_{p_2} = 1{\cdot}5\times10^{-13}$ cm^2 and $A_{n_2} = 1{\cdot}0\times10^{-16}$ cm^2. The ratio of $A_p/A_n = 1500$ is very large, but somewhat smaller than the value of 6000 obtained by JOHNSON and LEVINSTEIN. Their A-values are $A_{p_2} \sim 10^{-13}$ cm^2 and $A_{n_2} \sim 10^{-17}$ cm^2.

Although there is general agreement between the experimental points and the theoretical curve, the deviations are such that detailed discussion must be given of the three temperature regions: below 120°K, above 350°K, and near 200°K. In analysing the data, recombination through the lower gold level could not be used to explain any of the discrepancies.

Low Temperatures. The lack of points at low temperatures for τ_{p_2} is a consequence of the reduced PEM signal which was lost in noise.

Below 125°K the lifetime curve rises having an energy slope of 0·01 eV. The theoretical (solid line) lifetime is based on a temperature insensitive cross-section and the rising curves suggest that C_{n_2} is proportional to $\exp(-0{\cdot}01/kT)$. JOHNSON and LEVINSTEIN also observed such a region but their slope indicated an energy of 0·018 eV.

Vol. 22
1961

Other Lifetime Values. Above 350°K the deviation of the experimental points from the calculated curve can be explained in terms of surface recombination.

At 400°K the electron and hole lifetimes are nearly equal and equations (5) and (6) are applicable. It can be shown simply that if the τ_{p_2} and τ_{n_2} are reinterpreted in terms of these equations, that $\tau_{n_2}^2/\tau_{p_2} = \tau_2$, the now equal value of electron and hole lifetimes for recombination through the upper gold level. The "x"-point marked on the graph at $10^3/T = 2{\cdot}5$/°K is a point so calculated. The discrepancy between this point and the calculated curve embodies all the errors in calibrating of the intensity of the radiation used to determine the magnitude of τ_{p_2} and τ_{n_2}, as well as errors in measurement and the mobility assumption. The value of the x-point should be more accurate in magnitude than the rest of the experimental points as it is an evaluation of lifetime based on the ratio method (ratio of equations (5) and (6)) eliminating light calibration errors.

Measurements of photoconductive response times were made using a frequency response technique.[19] This method was preferred to a spark-gap pulse technique because the $\Delta R/R$ changes could be kept much smaller. In the temperature range 90°–145°K the PC response time values deduced were a factor of 2 larger than the value based on the magnitude of the photoconductivity. This result combined with the PC/PEM ratio lifetime indicates that the values of A_p and A_n are too large by a factor of 30–50 per cent.

Surface Recombination. Accepting the calculated values of lifetime as correct, the value of the hole diffusion length has been evaluated over most of the temperature region (Fig. 4). The points are data used in calculating τ_{p_2}. With these values of L_D, equation (6) and the value of τ_{p_2} a value of s can be determined for 400°K. The value obtained is $2{\cdot}4 \times 10^4$ cm/sec. With L_D falling rapidly at low temperatures it can be said only that s does not increase rapidly with decreasing temperatures.

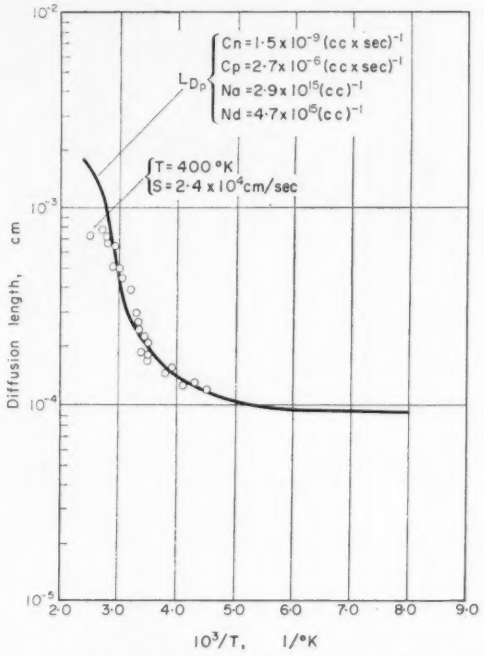

FIG. 4. Calculated diffusion length data compared to length deduced from PEM measurements. A surface recombination velocity has been deduced for 400°K.

Inhomogenieties

Near 120°K the Fermi level crosses the upper gold level and the factor of 2 in front of the Shockley–Read equations (1) and (2) has a value of 1·3 for lower temperatures. Such a change would result in a less round lifetime curve in this temperature region but not a maximum–minimum curve. This shape of the experimental curve is associated with inhomogeneities in the distribution of gold or the compensating impurity in the crystal. The acceptor concentration of $2{\cdot}9 \times 10^{15}$ is at least as large as is obtained in pulled crystals. Since the crystals were doped by zone levelling it is quite conceivable that the Au concentration was sufficiently high to produce some segregation. A second crystal with nearly equal gold and donor concentrations showed even more pronounced effects in this same temperature region. However, above 200°K the lifetime values as well as their dependence on temperature paralleled closely the results of Fig. 2. TWEET[20] has observed conductivity irregularities which he has been able to associate with segregation.

Some long wavelength measurements confirm that the peculiarities found near 160°K are not a

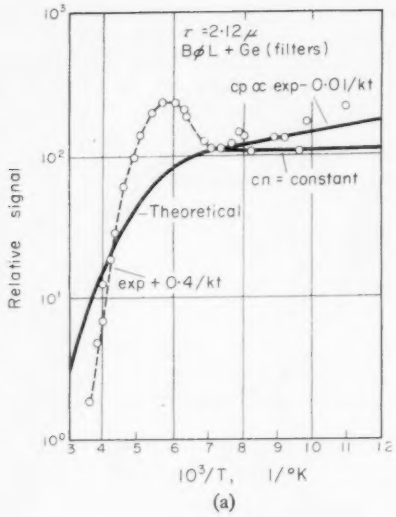

FIG. 5. (a) Irregularities near 200°K are shown to be bulk effects rather than surface effects by using penetrating radiation ($\lambda = 2{\cdot}12\ \mu$). (b) Using a higher intensity of light the irregularities near 200°K are essentially removed.

feature of the short wavelength highly absorbing light. Fig. 5(a) shows the results of measurements made with radiation of $2{\cdot}12\ \mu$ which would be nearly uniformly absorbed through the crystal. The same maximum–minimum behaviour is observed. Curve (b) of Fig. 5 was obtained at short wavelengths using a high light intensity level. The irregularities disappear with this high level of illumination, but such a level was not used at it was in general attempted to keep the change of conductance less than one part per thousand. Since a synchronous detector was employed for all the measurements this was accomplished.

The fall-off of the long wavelength photoconductivity at high temperatures does so proportional to $\exp(+0{\cdot}4/kT)$. This results from the combination of a decreasing lifetime and a decreasing population of E_2 states the latter of which determines the fraction of the radiation absorbed. As both factors have very nearly a 0·2 eV exponential exponent, the 0·4 eV slope is expected.

DISCUSSION

Table 1 summarizes the measurements of recombination cross-sections of gold in germanium. The errors indicated for the results herein presented are based on estimated errors of the various measured parameters, and assuming the theory utilized is correct. There are apparent discrepancies in some of the values of cross-sections. Having analysed the impurity concentration temperature dependence and used more recent lifetime theory, the data presented is felt to be more reliable than that of JOHNSON and LEVINSTEIN. The measurements were performed at sufficiently short wavelengths that quenching effects should be absent.

JOHNSTON and LEVINSTEIN interpret their exponential temperature dependent cross-section in a way which is believed difficult to substantiate. Using their equation $A_{n_2} = A'_{n_2} \exp(-\Delta E/kT)$ implies that A'_{n_2} is about equal to A_{n_2} at $T = 400°\text{K}$. $[\exp(-0{\cdot}01/kT) \doteqdot 0{\cdot}7)]$. It is difficult on this basis to call $A'_{n_2} = A_{n_1}$ as A_{n_1} and A_{n_2} would have a different charge state, thus a different cross-section is expected. Additional measurements are required to resolve these points.

Acknowledgements—The author wishes to acknowledge the assistance of Messrs. G. I. TURNER and J. MORAZIAN who performed many of the measurements.

Vol. 22
1961

Table 1. *Recombination cross-sections of the various levels of gold in germanium*

Cross-section (cm^2)	Johnson & Levinstein, 90°K	Williams 300°K	Williams 90°K
A_{p_1}	$\doteq 1\times10^{-13}$		
A_{n_2}	$\sim 10^{-17}$	$1{\cdot}0\,(\pm\,0{\cdot}3)\times10^{-16}$	$1{\cdot}6\,(\pm\,0{\cdot}5)\times10^{-16}$
A_{p_2}	$> 10^{-13}$	$1{\cdot}5\,(\pm\,1{\cdot}0)\times10^{-13}$	
A_{n_2}*	$\doteq 6\times10^{-16}$	$4{\cdot}2\,(\pm\,1{\cdot}3)\times10^{-15}$	

*$A_{n_2} = A'_{n_2}\exp(-\Delta E/kT)$.

REFERENCES

1. Tyler W. W., *J. Phys. Chem. Solids* **8,** 59 (1959).
2. Tyler W. W. and Woodbury H. H., *Phys. Rev.* **102,** 647 (1955).
3. Johnson L. and Levinstein H., *Phys. Rev.* **117,** 1191 (1960).
4. Shockley W. and Read W. T., *Phys. Rev.* **87,** 835 (1952).
5. Sandiford D. J., *Phys. Rev.* **105,** 524 (1957).
6. Clarke D. H., *J. Electron. Contr.* **3,** 375 (1957).
7. Wertheim G. K., *Phys. Rev.* **109,** 1086 (1958).
8. Bernard M., *J. Electron. Contr.* **5,** 15 (1958). For a more general analysis see: Sah G. T. and Shockley W., *Phys. Rev.* **109,** 1103 (1958) and Kalashnikov S. G. and Tissen K. P., *Sov. Phys. Sol. St.* **2,** 2443 (1961).
9. Zitter R. N., *Phys. Rev.* **112,** 852 (1958).
10. Amith A., *Phys. Rev.* **116,** 793 (1959). For other methods of determining minority carrier lifetime see: Bemski G., *Phys. Rev.* **111,** 1515 (1958); Das M. B. and Boothroyd A. R., *J. Electron. Contr.* **7,** 534 (1950) and Davis W. D., *Phys. Rev.* **114,** 1006 (1959).
11. Kurnick S. W. and Zitter R. N., *J. Appl. Phys.* **27,** 278 (1956).
12. Champness C. H., *Proc. Phys. Soc. Lond.* **B69,** 1335 (1956).
13. Lasser M. E., Cholet P. and Wurst E. C., *J. Opt. Soc. Amer.* **48,** 468 (1958).
14. Dauphinee T. M. and Mooser E., *Rev. Sci. Instrum.* **26,** 660 (1955).
15. Morin F. T., *Phys. Rev.* **93,** 62 (1954).
16. Dunlap W. C., *An Introduction to Semiconductors*, p. 122. Wiley, New York (1957).
17. Conwell E. M., *Proc. Inst. Radio Engrs.* **46,** 1282 (1958).
18. Lee P. A., *Brit. J. Appl. Phys.* **8,** 340 (1957).
19. Williams R. L., *J. Sci. Instrum.* **37,** 205 (1960).
20. Tweet A. G., *J. Appl. Phys.* **30,** 1319 (1959); this is the discussion on a paper by Sanders E., *J. Appl. Phys.* **30,** 1186 (1959).

DISCUSSION

van der Maesen: In using the ratio PC/PEM, did you assume beforehand that $\Delta n = \Delta p$?

R. L. Williams: I assumed that Δn was not equal to Δp, which is the case if equations (1) and (2) are used. However, based on the measured low temperature recombination cross-sections it was calculated that τ_{n_2} was equal to τ_{p_2} above room temperature. Thus for these temperatures Δn equals Δp and the PC/PEM ratio method can be used to evaluate the electron and hole lifetime.

BLANK
PAGE

Vol. 22
1961

J. Phys. Chem. Solids Pergamon Press 1961. Vol. 22, pp. 269–284. Printed in Great Britain.

LOW TEMPERATURE ELECTRON TRAPPING LIFETIMES AND EXTRINSIC PHOTOCONDUCTIVITY IN *n*-TYPE SILICON DOPED WITH SHALLOW IMPURITIES*

R. S. LEVITT† and A. HONIG

Syracuse University, Syracuse, New York

Abstract—The trapping lifetimes of conduction electrons photoexcited from shallow impurities have been measured in the liquid helium temperature range for samples of *n*-type silicon whose donor and compensating acceptor concentrations vary from 10^{13} to 10^{16} impurities/cm^3. A steady state method was employed, in which the conduction electron lifetime t_L is equal to $n_e\tau^i/N_D^0$. n_e is the conduction electron concentration which is determined from low temperature photo-Hall measurements, and $N_D^0\tau^i$ is the electron generation rate. The neutral donor concentration N_D^0 is measured by the Hall effect and τ^i, the lifetime against photoionization of a neutral donor, is obtained directly by an electron spin resonance technique. The trapping lifetimes t_L are generally independent of temperature between 4·2°K and 1·2°K, and are inversely proportional to the compensating acceptor concentration. This latter was determined using a recently developed combined infrared radiation and spin resonance method. The trapping cross-section result for phosphorus donors is about 5×10^{-12} cm^2 at 3°K. This is about an order of magnitude larger than the value obtained from the giant trap theory of LAX. Also, the concentration independence of the cross-section in the region of temperature independent t_L is not easily accounted for. The mobility of electrons photoexcited with 2 micron radiation considerably exceeds the mobility of electrons photoexcited with 8–25 micron radiation. This suggests the possibility of excitation to another band or minimum by the 2 micron radiation, as is also suggested by the free carrier absorption peak near 2 microns found in *n*-type silicon by SPITZER and FAN.

1. INTRODUCTION

ELECTRON spin resonance experiments at liquid helium temperatures on donor electrons bound to phosphorus impurities in silicon have yielded a method of measuring the conduction electron generation rate under extrinsic radiation.[1] The electron generation rate is proportional to the rate at which the donor electrons are photo-ionized by the extrinsic radiation, and this was shown to be equal to the rate at which the electron magnetizations associated with the two hyperfine components of the bound electron spin system approach equilibrium via an electron interchange mechanism.[1] Combined with experimentally obtained knowledge of the photo-carrier concentration by conventional photo-Hall and photoconductivity measurements, the determination of the generation rate enables one to measure the lifetime of the photoexcited electrons against trapping by the charged shallow impurities. One can also calculate the capture cross-section of these trapping centres if the ionized impurity concentration, or compensation, is known. This latter was determined accurately by employing a recently developed spin resonance technique.[2,3]

There have been several previous investigations of the capture cross-sections due to shallow impurities in silicon and germanium at liquid helium temperatures. SCLAR and BURSTEIN[4], using a steady state method, obtained a rough magnitude for the capture cross-section, and its very large value prompted the theoretical study of the problem by LAX, who showed that capture in highly excited states could yield the required large cross-sections.[5] A quantitative study of the concentration and temperature dependence was not possible in the SCLAR and BURSTEIN experiment because the concentrations and compensations

* Supported in part by the Air Force Office of Scientific Research.

† Now at I.B.M. Thomas J. Watson Research Center, Yorktown Heights, New York.

were not known accurately and because it was difficult to know the electron generation rate with any precision. KOENIG[6] has used a transient method to determine the trapping cross-section of Sb ions in germanium as a function of temperature. ASCARELLI and BROWN[7] employed a different transient technique on similar material. They both obtained large cross-sections of comparable magnitude, but their temperature dependences differed, and concentration dependence was not studied over an appreciable range. Recently, RODRIGUEZ and ASCARELLI[8] have proposed a theory which differs in some essential respects from that of LAX, and which gives cross-sections of the required magnitude.

In this paper, our steady state method for determining cross-sections is described and our cross-section determinations over the temperature range of 4·2°–1·2°K on silicon samples varying in phosphorus ion concentration from 10^{13} to $10^{16}/cm^3$ are given. These results are discussed in connection with the existing theories. In addition, measurements of the mobilities of photo-excited carriers were made at various temperatures, under radiation of different wavelength, and on samples covering a wide concentration range. Results of these studies are presented and discussed in the context of available theory. Evidence for the existence in silicon of conduction band minima having higher energy and smaller effective mass than the minima along the [100] direction is also presented.

2. GENERAL PRINCIPLES

(1) *Paramagnetic resonance*

Since the major feature of our method for obtaining lifetimes involves paramagnetic resonance techniques, we describe these first. Electron spin resonance on phosphorus donors in silicon was first reported by FLETCHER *et al.*[9], who observed two well-resolved hyperfine components associated with the $m_I = +1/2$ and $m_I = -1/2$ orientations of the phosphorus nuclei. Subsequently, the thermal electron spin-lattice relaxation processes were studied in considerable detail.[10,11] It was found that for phosphorus concentrations below about $10^{16}/cm^3$, the thermal spin-lattice relaxation time varied from minutes to many hours in the liquid helium temperature region for moderate magnetic field strengths. Additional bound electron spin-lattice relaxation under sample illumination by intrinsic radiation was observed by FEHER and FLETCHER[12], and PINES *et al.*[13] proposed that it was due to electron exchange between the bound electrons and conduction electrons which were presumed to relax rapidly while in the conduction band. ANDERSON[11] pointed out that exchange of bound electrons with conduction electrons could lead to an observable relaxation mechanism even if the conduction electrons did not relax to a Boltzmann distribution in the conduction band, provided the electron spin populations associated with the two hyperfine components differed. A similar relaxation mechanism was shown by HONIG[1] to occur under interchange of bound electrons via extrinsic photoexcitation to the conduction band. These latter exchange and interchange processes are the ones which are important for our present purposes, and because the times for these processes can be made considerably shorter than the spin-lattice relaxation time of the bound electrons due to all processes, the spin-lattice interactions can be neglected* in our discussion. The interchange relaxation process is illustrated in Fig. 1. The magnetization associated with the electron spins is proportional to the difference in population of electrons in the $m_S = -1/2$ and $m_S = +1/2$ states, which is denoted by Δn. Δn_L is thus proportional to the electron magnetization for the $m_I = +1/2$ hyperfine component, and Δn_H for the $m_I = -1/2$ hyperfine component. The system is initially allowed to come to equilibrium via the spin-lattice relaxation processes, providing approximately equal magnetization for both hyperfine components. Then the magnetization of one of the lines (in this case the one with $m_I = 1/2$, denoted by L) is reduced to zero by resonating that line alone. Extrinsic light is next allowed to ionize the neutral phosphorus impurities without regard to the magnetic energy state so that the electron magnetization per carrier of the resulting conduction electrons, $\Delta n_e/n_e$, is just the average value of the electron magnetization per impurity of the bound electron system, $(\Delta n_L + \Delta n_H)/N_D^0$,

* For some samples, the illumination introduces spin-lattice and spin heating effects which cannot be neglected in the evaluation of τ^i and τ_c^{ex}. In these cases, it has nevertheless been possible to interpret the data in a satisfactory manner.

Vol. 22
1961

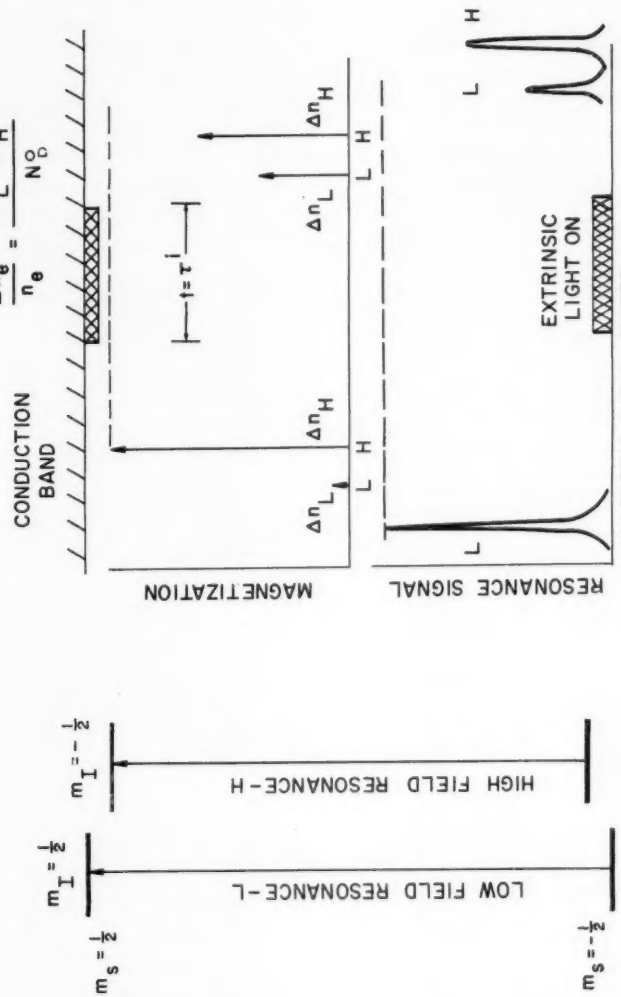

FIG. 1. Electron interchange relaxation mechanism in phosphorus-doped silicon. At the left are shown the magnetic energy levels of the neutral phosphorus impurities in an applied magnetic field, which give rise to two resonance lines. At the right, the upper plot shows the state of the electron magnetizations, and the lower plot illustrates the observed resonance signals. Starting with Boltzmann equilibrium for all the levels, the electron magnetization associated with line L is reduced to zero by resonating L. Upon application of extrinsic radiation for a time τ', electrons are interchanged via the conduction band between the $m_I = 1/2$ and $m_I = -1/2$ phosphorus nuclei, producing the observed relaxation effect. Spin-lattice ralaxation effects are not included.

where N_D^0 is the neutral impurity concentration. Subsequent recapture of these electrons impartially by phosphorus nuclei of both $m_I = -1/2$ and $m_I = +1/2$ leads to relaxation of the magnetization per impurity associated with both hyperfine lines to the average magnetization per carrier held by the conduction electrons. It is easy to show that the relaxation rate $(\tau^i)^{-1}$ is just the rate of ionization of a neutral donor, which is denoted by S. As mentioned above, exchange would produce a similar experimental effect. One must know the singlet exchange cross-section for a conduction electron and bound electron, the neutral phosphorus impurity concentration N_D^0 and the conduction electron lifetime t_L to determine whether exchange or interchange will be the dominant process. This can be easily understood because the interchange rate $(\tau^i)^{-1} = S$, which depends only on the magnitude Q of the absorbed light flux, while the conduction electron exchange rate $(\tau_C^{ex})^{-1}$ depends on the singlet exchange cross-section and on the conduction electron concentration, which is equal to $SN_D^0 t_L$. We have also observed another mechanism which produces the same experimental effect as τ^i and τ_C^{ex}, but which is strongly concentration dependent. We attribute this to exchange between bound electrons in their ground state and bound electrons which have just been trapped in highly excited states, so that overlap occurs during part of the time in which they cascade down to the ground state. The relaxation probability for this process

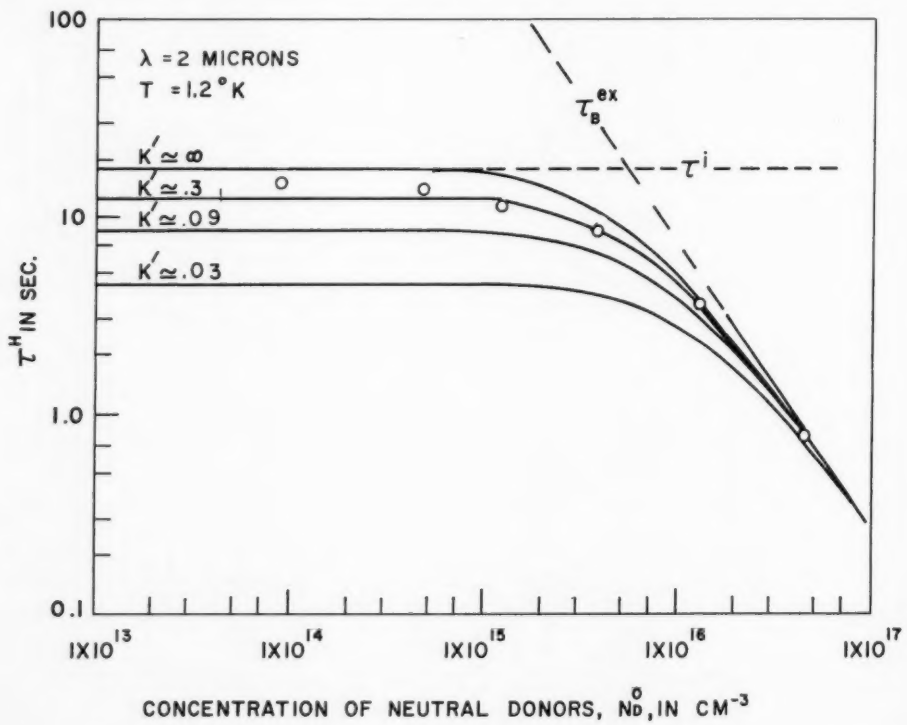

FIG. 2. Experimental "hyperfine" relaxation time τ^H induced by a constant extrinsic light flux plotted against neutral donor concentration. $(\tau^H)^{-1}$ is equal to $(\tau^i)^{-1}+(\tau_C^{ex})^{-1}+(\tau_B^{ex})^{-1}$, i.e. the sum of the interchange rate, the conduction electron exchange rate and the excited state bound electron exchange rate. τ_U^{ex}/τ^i was experimentally determined to be equal to about 11 K', where $K' = N_A/N_D^0$. $(\tau_B^{ex})^{-1}$ becomes important at high neutral donor concentrations. Samples are phosphorus-doped silicon compensated with boron.

Vol. 22
1961

is denoted by $(\tau_B^{ex})^{-1}$. We can express the experimental relaxation process seen in Fig. 1 in terms of a total "hyperfine" relaxation rate $(\tau^H)^{-1}$ which equals $(\tau^i)^{-1}+(\tau_C^{ex})^{-1}+(\tau_B^{ex})^{-1}$. In an earlier work,[1] it was suggested that $(\tau^i)^{-1}$ dominates for most samples. Since then, we have verified this utilizing a technique by means of which the conduction electron lifetime in a single sample can be varied over a factor of 10 by controlling the number of *ionized* impurities with intrinsic light irradiation.[2,3] This has made it possible to determine separately τ^i and τ_C^{ex}. τ_B^{ex} is obtained from measurements at constant light flux Q on higher concentration samples. In Fig. 2, the results of these investigations are plotted. It is seen that for dilute samples with greater than 8 per cent compensation,† interchange dominates and τ^i can be measured quite accurately. As stated before, this is the basis of our accurate determination of the conduction electron generation rate.

2. *Electron trapping lifetime and capture cross-sections*

The energy band scheme for n-type compensated silicon is illustrated in Fig. 3. At low temperatures, the neutral donor concentration N_D^O equals N_D-N_A, where N_D is the donor concentration and N_A is the compensating acceptor concentration. Extrinsic radiation ($1{\cdot}1$ eV $> E >$ $0{\cdot}044$ eV or $1{\cdot}1\ \mu < \lambda < 28\ \mu$) photo-ionizes these neutrals and generates conduction electrons per unit volume at a rate $G = SN_D^O$. The conduction electrons are captured predominantly by the positively charged donor ions (whose concentration $N_D^+ = N_A$) at a rate $1/t_L$ per electron so that the rate equation for the conduction electron concentration n_e is

$$dn_e/dt = SN_D^O - n_e/t_L. \qquad (1)$$

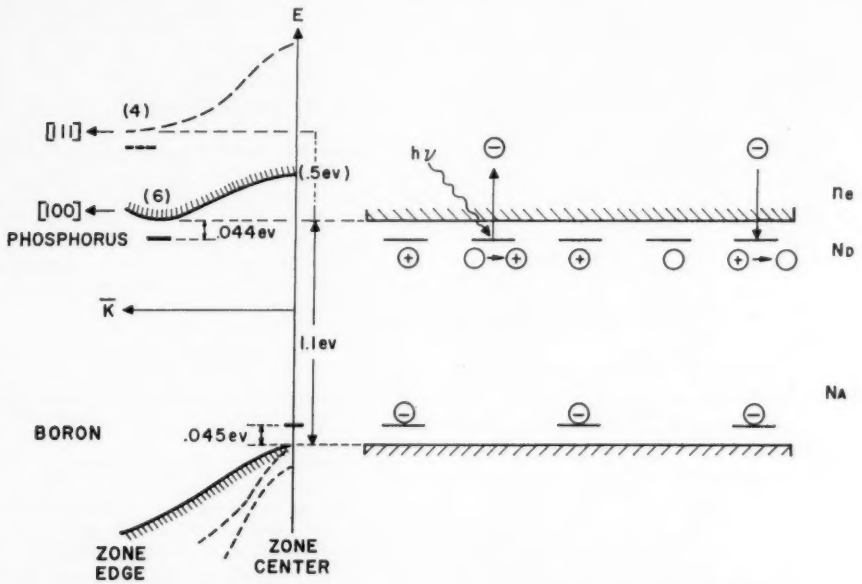

FIG. 3. Energy band scheme for n-type compensated silicon at low temperatures, and illustration of the dynamics under extrinsic photo-ionization. The $0{\cdot}5$ eV suggested energy difference between the 4-fold minima in the [111] directions and the 6-fold minima along the [100] directions comes from the $\lambda \simeq 2\ \mu$ absorption peak observed by SPITZER and FAN[18].

† The reason the relative importance of exchange and interchange relaxation can be expressed in terms of the compensation is as follows: $(\tau^i)^{-1}=S$, $(\tau_C^{ex})^{-1}\propto SN_D^O t_L$, and therefore $(\tau_C^{ex}/\tau^i)\propto 1/N_D^O t_L$. We have determined that $t_L\propto(N_A)^{-1}$ (see Section 4), and therefore $(\tau_C^{ex}/\tau^i)\propto N_A/N_D^O$, or K'.

In the steady state

$$t_L = n_e/SN_D^O. \tag{2}$$

The rate of capture per trap is

$$\alpha = (t_L N_A)^{-1}, \tag{3}$$

where α is defined as the capture rate constant and is related to the energy dependent capture cross-section $\sigma(E_o)$ by

$$\alpha = \langle \sigma(E_o) v_e \rangle, \tag{4}$$

where v_e is the velocity of carriers with energy E_o. $\langle \sigma(E_o) v_e \rangle$ represents a Boltzmann average over the actual electron energy distribution. One can define a capture cross-section as

$$\sigma_c = \langle \sigma(E_o) v_e \rangle / \langle v_e \rangle. \tag{5}$$

Then

$$\sigma_c = \alpha (8kT/\pi m^*)^{-1/2}, \tag{6}$$

where m^* is the effective mass of the carriers and k is the Boltzmann constant.

To determine t_L from equation (2) one evaluates n_e from a low temperature measurement of the photo-carrier mobility μ and resistivity ρ. Substituting $n_e = (e\rho\mu)^{-1}$ in equation (2) and replacing S by $(\tau^f)^{-1}$, as was shown in the previous Section, we obtain

$$t_L = \frac{\tau^f}{e\rho\mu N_D^O}. \tag{7}$$

It is convenient to express ρ in terms of the photocurrent i and the temperature independent factor $R/\rho V$, where R is the sample resistance and V is the applied voltage. This yields for t_L the expression from which our lifetimes are directly derived:

$$t_L = \frac{i}{V} \frac{R}{\rho} \frac{\tau^f}{e\mu N_D^O}. \tag{8}$$

Generally one does not measure μ directly. In the case of a photo-Hall experiment, the Hall mobility μ_H is obtained. It is related to μ by the Hall factor r_H through $\mu = \mu_H/r_H$. Photo-magneto-resistivity yields a mobility given by the relation

$$(\Delta\rho/\rho_o B^2)^{1/2} \times 10^8 = \mu_B, \tag{9}$$

where $\Delta\rho = (\rho_B - \rho_o)$ is the change in the photo-resistivity observed when the magnetic field is changed from 0 to B. μ_B is related to μ by the factor r_B through $\mu = \mu_B/r_B$. There is no reason to suppose $r_B = r_H$ or that either is equal to unity since they are affected by non-spherical energy surfaces, scattering anisotropies, and energy weighting factors which may differ according to how the mobility is measured. It is known,[14] however, that for ionized impurity scattering in the concentration and temperature range of most of our experiments, $\sim 1 < r_H < 2$, so that using μ_H in place of μ ought not to introduce an error larger than a factor of 2.‡

3. APPARATUS AND SAMPLE PROPERTIES

A standard X-band (~ 9 kMc/s) low temperature spectrometer was used in performing the electron spin resonance measurements. The sample is illuminated via an optical system composed of a source, prism monochrometer, light-pipe, cold filters and reflector. This system is illustrated schematically in Figs. 4 and 5. Fig. 4 also shows the components used to measure the magnetic field, photocurrent, photo-Hall coefficient, and to detect the resonance and calibrate the monochrometer. The design of the low temperature assembly is shown in Fig. 5. The mirror is mounted on a sliding block which when pulled up shields the sample from all illumination. Various combinations of filters and reflectors allow us to restrict the illumination to the desired wavelength region and to eliminate unwanted wavelengths from room temperature sources such as the top of the light pipe. For the long wavelength experiments the top of the light-pipe at room temperature served as the source, and a CaF_2 reflector was used which passed only wavelengths longer than 20 μ.

Two types of samples were used. One type is bridge shaped with six arms on which the room temperature resistivity ρ and low temperature photo-Hall mobility μ_H were measured. The other is a more or less rectangular slab on which the relaxation rates and low temperature photo-resistivity were measured. These two sample shapes were shown to be electrically identical by noting that the ratio $R(300°)/R(\text{photo}, 4°)$ on each sample shape was the same and was equal to $\rho(300°)/\rho(\text{photo}, 4°)$ on the bridge shaped sample. R is the ohmic resistance of the sample. Electrical contacts were made by alloying 0·005 in. diameter, 0·6 per cent antimony–doped gold wire onto the sample by a technique similar to welding. No anomalous effects usually attributed to contacts were observed at the low electric fields (~ 1 V/cm) used: Ohm's law was obeyed at all temperatures.

Some of the characteristics of the seven samples studied are presented in Table 1. The donor and compensating acceptor concentrations varied over three orders of magnitude. The compensating acceptor concentration was determined by employing a newly

‡ For the high concentration samples at low temperatures, the theory partially breaks down. It seems plausible, however, that $\sim 1 < r_H < 2$ is still true.

Vol. 22
1961

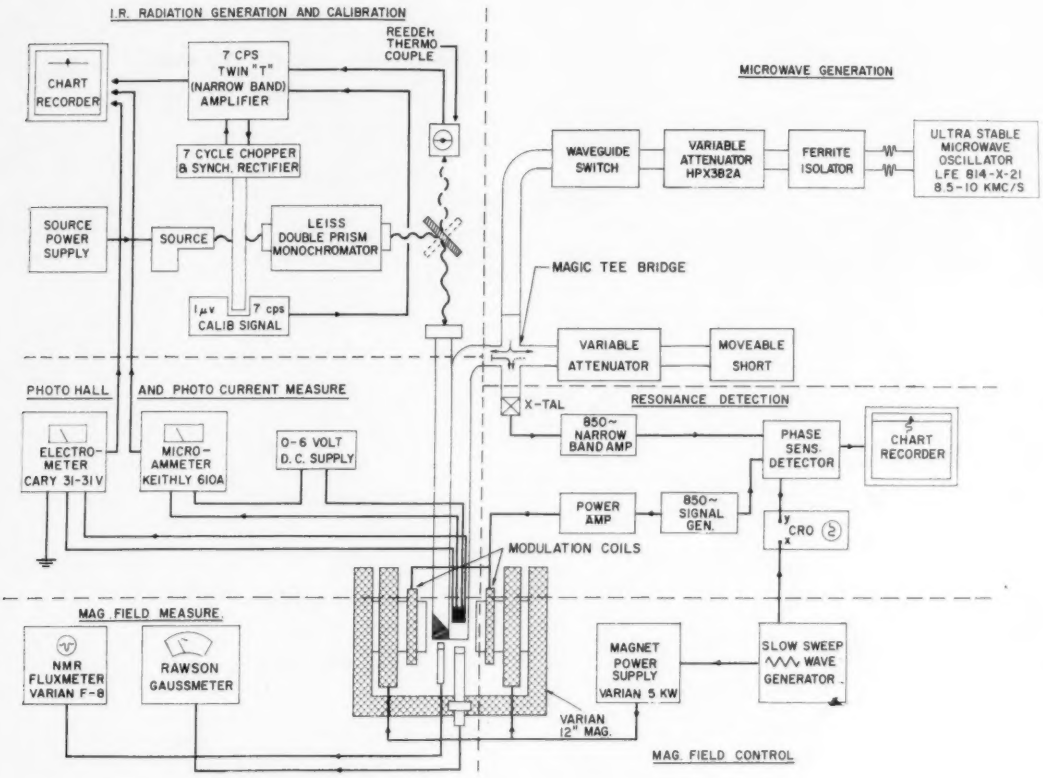

FIG. 4. Schematic of equipment used to determine the photo-carrier generation rate with paramagnetic resonance techniques and to measure the photo-carrier transport parameters.

developed resonance technique[2,3] in which the increase in the concentration of neutral donors resulting from the neutralization of donor ions upon illumination with intrinsic light is determined from the resulting increase in the paramagnetic resonance signal. Since the minimum concentration of neutral donors is $(N_D - N_A)$ while the maximum concentration is N_D, the ratio $(N_D - N_A)/N_D$ can be determined. By measuring the concentration of neutral donors from the room temperature Hall coefficient, the value of N_A can be separately obtained. This method was checked against the more conventional one in which N_A is deduced from the temperature dependence of the Hall coefficient and agrees well.

4. RESULTS AND DISCUSSION

Lifetime and capture cross-sections

τ^i was measured for three samples in which interchange is the dominant relaxation mechanism. We were able to ascertain the consistency of the photon flux over many runs. The value of τ^i so obtained and the photo-current measured in the same photon flux for all the samples were inserted into equation (8). The results for the trapping lifetime vs. the acceptor concentration are plotted in Fig. 6. The solid line represents a capture rate constant $\alpha = (t_L N_A)^{-1}$ of $1{\cdot}15 \times 10^{-5}$ cm^3/sec. Since the photo-Hall mobility was used to determine t_L, the lifetime values could conceivably be as much as a factor of 2 too small corresponding to $r_H = 2$. Aside from this possible but unlikely systematic error, the values of t_L given in Fig. 6 are good to within 20 per cent. Under long wavelength radiation ($\lambda > 20\,\mu$), α agrees within a factor of 2 with the α measured under $2\,\mu$ wavelength radiation. The $\lambda > 20\,\mu$ data is not as reliable as the $2\,\mu$ data, however.

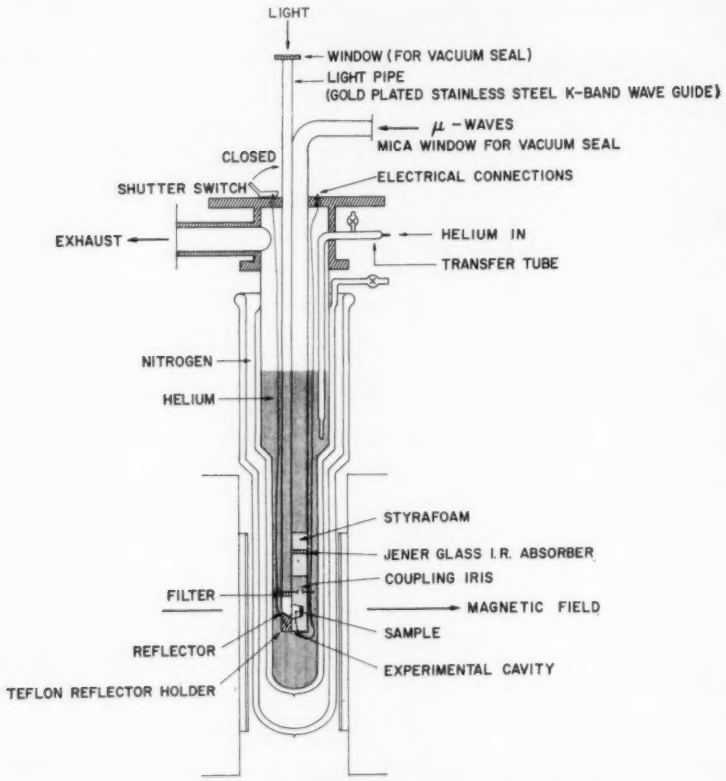

FIG. 5. Low temperature assembly for simultaneous microwave and infrared irradiation. Infrared radiation reaches the sample via a light-pipe and reflector. The reflector is movable and also serves as a shutter. Suitable choices of filters and reflectors permit various narrow-band wavelength regions to be employed. The sample, equipped with leads for measuring the photocurrent, is located in the center of a full wave X-band microwave cavity.

All of our samples except 4·5–0·15–16 exhibit a temperature independent t_L, so that from equation (6), σ_c is proportional to $T^{-1/2}$. This is seen in Fig. 7, as well as the temperature dependence of sample 4·5–0·15–16. The theoretical curve obtained from the giant trap theory of LAX[5] is also shown. A similar reservation to that mentioned above regarding the reliability of t_L applies to our σ_c values; namely, they could be as much as a factor of 2 too large corresponding to $r_H = 2$.

The large value of σ_c obtained in the temperature independent region of the capture rate constant α is consistent with the model[5,8] of capture into an excited bound state of the donor impurity ion. For comparison, the geometrical cross-section of the ground state of the impurity, given by

$$\sigma_0^* = \pi[(K/m^*)a_0]^2,$$

is 100 times smaller than σ_c at 1°K. In this equation, K is the dielectric constant (12 for silicon) and a_0 is the Bohr radius.

We now review briefly the present state of the relevant theory. LAX[5] has suggested that the large capture cross-section is due to the capture of the electron in a highly excited state of the ionized donor with the simultaneous emission of either a photon or phonon. Subsequently the

Vol. 22
1961

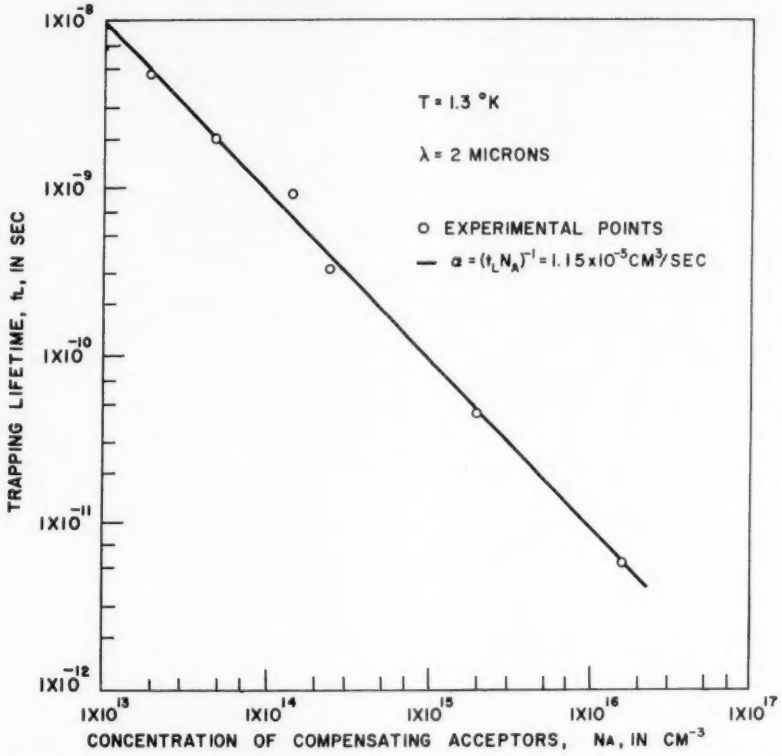

FIG. 6. Electron trapping lifetime dependence on compensating acceptor concentration in phosphorus-doped silicon. Experimental points are determined from the quantities τ^t, ρ and μ_H measured in a fixed light flux. For the experimental point at each extreme of the curve, the mobility was extrapolated rather than measured.

electron either emits additional phonons and cascades to smaller and more tightly bound orbits or is thermally re-ionized into the conduction band. When the electron reaches an orbit which is more than kT in energy below the conduction band the electron can be considered trapped and eventually enters the ground state. If, however, the highest energy thermally stable orbit overlaps a lower energy orbit of a neighboring ionized donor, this is not a localized orbit. One cannot count the electron as trapped in this orbit when in fact it is more suitably described as being trapped in the orbit of the neighbouring donor ion to which it is closer. This results in a cut-off to the cross-section, since the maximum value of σ_c will correspond to the maximum localized trapping orbit. Until the temperature is lowered to the point T_o where the highest energy thermally stable orbit has a radius equal to that of the maximum localized orbit, σ_c would have a strong temperature dependence ($\sim T^{-4}$). Below T_o, which we call the cut-off temperature, σ_c should have only the $T^{-1/2}$ dependence associated with the velocity of the electrons. The radius r_o of the highest energy thermally stable orbit at T_o is found by setting kT_o equal to the binding energy of the orbit, i.e.

$$kT_o = e^2/Kr_o. \tag{10}$$

The most probable separation of donor ions is r_s, which based upon a random distribution[15] of

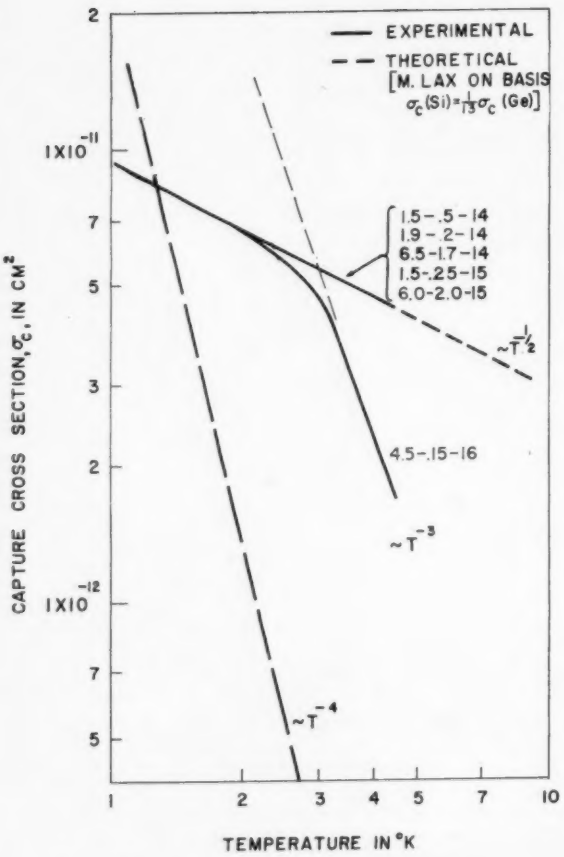

FIG. 7. Temperature dependence of the capture cross-section of 2 μ photoexcited carriers in phosphorus-doped silicon. The $T^{-1/2}$ dependence of the upper curve corresponds to a temperature independent lifetime t_L, and is the observed dependence for most of the samples. The sample with a $\sim T^{-3}$ dependence above 3°K is also shown. The dashed curve corresponds to the capture cross-section for silicon based on LAX's theory.

Table 1. Characteristics of phosphorus-doped silicon samples used in this investigation

Sample	N_D (cm^{-3})	N_A (cm^{-3})*	N_B^0 (cm^{-3})†	N_A/N_D	ρ(300°K) (Ω−cm)	ρ(1·2°K, 2μ)‡ (Ω−cm)	ρ(1·2°K, > 20 μ)§ (Ω−cm)	R/ρ (cm^{-1})‖
1·5–0·5–14	$1{\cdot}5\times10^{14}$	$0{\cdot}5\times10^{14}$	$1{\cdot}0\times10^{14}$	0·035	42	$1{\cdot}16\times10^{10}$		160
1·9–0·2–14	$1{\cdot}9\times10^{14}$	$0{\cdot}2\times10^{14}$	$1{\cdot}7\times10^{14}$	0·10	25	$1{\cdot}9\times10^{9}$	$6{\cdot}6\times10^{9}$	35
6·5–1·7–14	$6{\cdot}5\times10^{14}$	$1{\cdot}7\times10^{14}$	$4{\cdot}8\times10^{14}$	0·23	10·5	$7{\cdot}0\times10^{9}$	$7{\cdot}4\times10^{10}$	49·5
1·5–0·25–15	$1{\cdot}5\times10^{15}$	$0{\cdot}25\times10^{15}$	$1{\cdot}2\times10^{15}$	0·17	4·15	$1{\cdot}0\times10^{10}$	$2{\cdot}0\times10^{11}$	20
6·0–2·0–15	$6{\cdot}0\times10^{15}$	$2{\cdot}0\times10^{15}$	$4{\cdot}0\times10^{15}$	0·33	1·15	$3{\cdot}8\times10^{10}$	$1{\cdot}4\times10^{12}$	23
5·0–2·0–16	$5{\cdot}0\times10^{16}$	$2{\cdot}0\times10^{16}$	$3{\cdot}0\times10^{16}$	0·40	0·23	$8{\cdot}0\times10^{10}$		34
4·5–0·15–16	$4{\cdot}5\times10^{16}$	$0{\cdot}15\times10^{16}$	$4{\cdot}4\times10^{16}$	0·03	0·14	$6{\cdot}5\times10^{9}$	$2{\cdot}1\times10^{11}$	30

* Determined by resonance technique (see text).
† Determined from room temperature Hall coefficient.
‡ Reduced to fixed flux at $\lambda = 2\ \mu$.
§ Reduced to fixed flux at $\lambda > 20\ \mu$.
‖ R and ρ measured at room temperature and 77°K on the rectangular shaped sample used in the resonance and photoresistivity experiments.

N_L^+, is given by

$$r_s = (2\pi N_D^+)^{-1/3}. \qquad (11)$$

T_0 is thus determined by setting r_0 equal to $(1/2)r_s$. Because of the dependence of r_s on $N_D^+(=N_A)$ we would expect T_0 to be proportional to $N_A^{1/3}$ and σ_c(max) to be greater the purer the material. Referring to Fig. 7, this is not observed.

The cut-off radius can also arise in a different way. It is necessary to introduce either a cut-off or a screening to the long range Coulomb potentials of the donor ions to prevent divergences in ionized impurity scattering theory.[14] One generally uses a potential of the form

$$\phi(r) = (-e^2/Kr)\exp(-r/R_0), \qquad (12)$$

Vol. 22
1961

where R_0 is the screening radius beyond which $\phi(r) \to 0$ rapidly. This can be interpreted as meaning bound states cease to exist beyond a few R_0. DINGLE[16] has shown that R_0 depends on temperature and concentration according to

$$R_0 = (1/e)(KkT/4\pi n')^{1/2}, \tag{13}$$

where $n' = n_e + (N_A + n_e)N_D^0/N_D$. If the maximum σ_C is limited by R_0 then the cut-off temperature is obtained from equation (10) by setting r_0 equal to R_0. One obtains

$$T_0 = e^2/Kk(4\pi n')^{1/3}. \tag{14}$$

Again T_0 should decrease and $\sigma_C(\max)$ increase for purer material, which is contrary to what is observed.

Table 2 summarizes pertinent information concerning the cut-off radius based upon the two models just discussed. The geometrical radius of the ground state, a_0^*, is also listed. For the excited state of quantum number n, $a_n^* = n^2 a_0$. We note from the Table that both the overlap and screening cases yield a T_0 at least an order of magnitude larger than observed on the 4·5–0·15–16 sample. Because of the restricted temperature range used, no temperature cut-offs were observed on our other samples. We can say from the date only that $T_0 > 6°K$ for these samples. The situation regarding the above cut-off procedures is quite unsatisfactory in that no explanation of our results on samples 4·5–0·15–16 and 6–2–15 (which have approximately the same acceptor concentration but very different T_0) appears in a natural way, and because of the absence of observed variation of $\sigma_C(\max)$ in samples of markedly different concentrations.

Experimental investigations of trapping cross-sections of shallow impurities in germanium have been made by several workers. A summary of the results is presented in Fig. 8(a). The transient technique used by ASCARELLI and BROWN[7] and KOENIG[6] can result in serious systematic errors[8] and certain of the data presented in Fig. (8a) must be considered with caution. A measurement by a different technique on fairly pure germanium has recently been made by MICHEL and ROSENBLUM[17], who apparently obtain a temperature independent lifetime in their purest sample.

Table 2. Summary of data pertinent to cut-off radii of excited states of impurities in silicon and germanium

Material	$a_0^* = (K/m^*)a_0$† (cm)	$r_0 = e^2/KkT_0$‡ (cm)	$\frac{1}{2}r_s = \frac{1}{2}(2\pi N_A)^{1/3}$¶ (cm)	$R_0 = (1/e)(KkT/4\pi n')^{1/2}$§ (cm)
Ge	$3·5\times10^{-7}$	$2·5\times10^{-5}$	$2·7\times10^{-6}(T_0' = 37°K)$‖	$1·85\times10^{-6}(T_0' = 22°K)$
Si	$2·0\times10^{-7}$	$3·5\times10^{-5}$	$2·7\times10^{-6}(T_0' = 52°K)$	$1·6\times10^{-6}(T_0' = 31°K)$

† Radius of ground state in a medium with dielectric constant K and effective mass m^*. a_0 is the Bohr radius.
‡ r_0 is the radius of the orbit which characterizes $\sigma_C(\max)$.
§ R_0 is the cut-off radius for screening of the coulomb potential as derived by DINGLE. See Ref. 16.
$n' = n + (N_A + n)N_D^0/N_D$.
‖ T'_0 is the temperature at which $r_0 = r_s/2$ or $r_s = R_0$.
¶ r_s is the most probable separation of acceptor impurities and is obtained by maximizing the distribution function for neighboring centers: $\omega(r) = 4\pi r_i^2 N_i \exp[(4\pi/3)r_i^3 N_i]$.
See Ref. 15.

Recently, RODRIGUEZ[8], and ASCARELLI and RODRIGUEZ[8] have proposed a theory for trapping in which lower-lying excited states, e.g. third or fourth excited states of the principal quantum number n in the liquid helium temperature range for germanium, play a dominant role in the capture process, as compared with somewhat higher excited states which would be mostly involved in LAX's theory. It is easy to see how such a theory leads to a lower cut-off temperature T_0, since more excited states of radii smaller than the cut-off radii discussed above become available

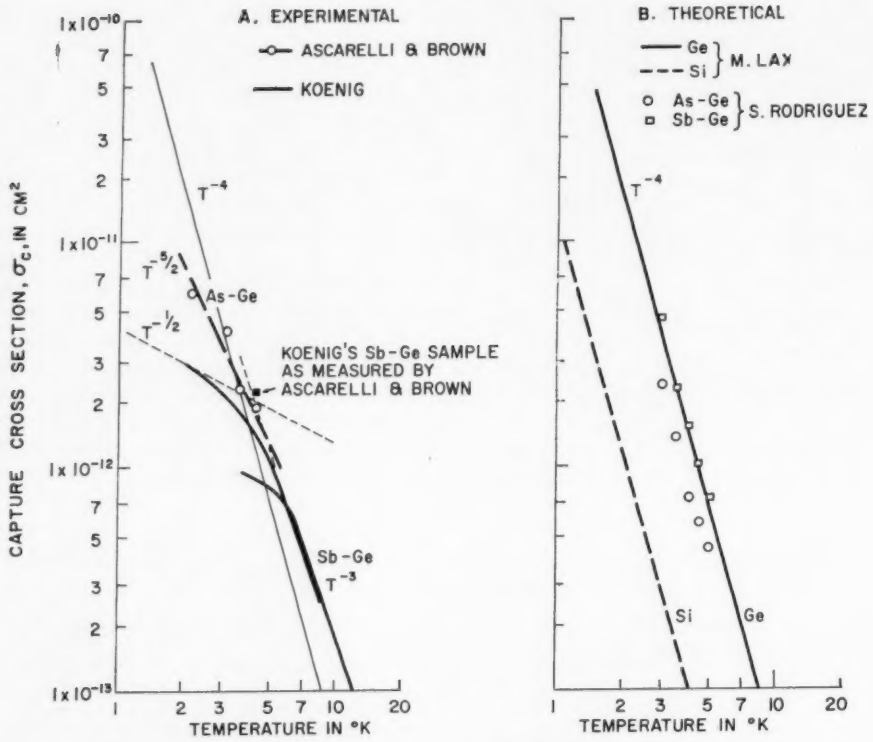

FIG. 8. (a) Experimental values of the cross-section of shallow traps in germanium. (b) Calculated values of the cross-section of shallow traps in germanium and silicon based on the theory of LAX and that of RODRIGUEZ.

for capture as the temperature is decreased. Their calculations have been made for germanium [see Fig. 8(b)], but unfortunately not yet for silicon. Nevertheless, it does not seem that their theory solves the difficulties inherent in our results.

By way of summary, we call attention to a few features of the results on low temperature electron trapping by shallow impurities. The experimental cross-sections exhibit close to a T^{-3} dependence at higher temperature and a $T^{-1/2}$ dependence at lower temperatures corresponding to a temperature independent capture probability of maximum value. The presence of a large excess of neutral donors may be the important parameter which reduces the cross-section in the T^{-3} region and reduces the cut-off temperature. The magnitude in the T^{-3} region of the cross-section of shallow donors in silicon appears to be an order of magnitude larger than predicted on the basis of currently available theories and comparable to the cross-sections observed in germanium doped with shallow donors. None of the existing theories adequately accounts for the temperature independent capture probability.

A final remark about the general question of capture into excited states seems appropriate here. There can be little doubt concerning the importance of the excited states in order to obtain the large σ_c's observed and their temperature dependence. We believe additional evidence regarding these excited capture states exists in the $(\tau_B^{ex})^{-1}$ relaxation mechanism briefly mentioned in Section 2(1), and exhibited in Fig. 2. The relaxation is attributed to overlap between excited state bound electrons and neighboring ground state

Vol. 22
1961

bound electrons. The temperature and concentration dependence of the $(\tau_B^{ex})^{-1}$ mechanism are in qualitative agreement with this interpretation.

Mobility

In order to determine the temperature and concentration dependence of t_L from measurements of the photo-current by use of equation (8) it is necessary to know how the mobility depends upon these parameters. This and other considerations motivated us to make a careful investigation of the mobility using several techniques.

The results of the photo-Hall experiments are given in Fig. 9 and those of the photo-magneto

The photo-magneto-resistivity mobility, μ_B, was calculated from equation (9). The photo-magneto-resistance exhibited a deviation from the expected[14] B^2 dependence at high fields for all samples and at lower fields for the more dilute samples where the field dependence is more like $B^{3/2}$.

The photo-Hall mobility was also measured under longer wavelength radiation (8–10 μ and $> 20\,\mu$) and found to be 7–10 times smaller than under $2\,\mu$ photo-excitation. If we accept the proposal of SPITZER and FAN[18] which suggests that the $2\,\mu$ free carrier absorption peak in n-type silicon is probably due to excitation to a higher lying energy band or minimum, then the larger

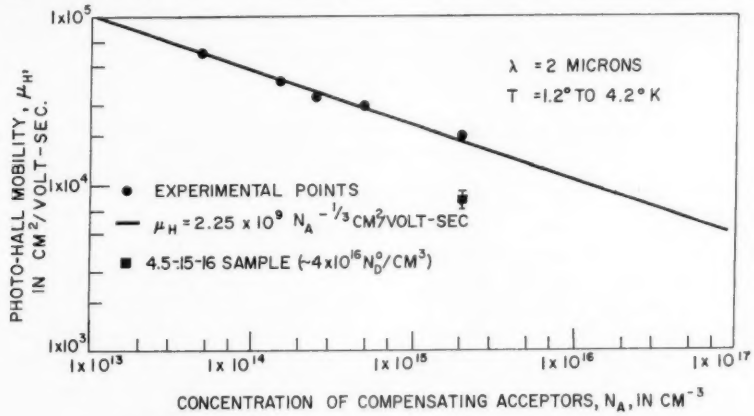

FIG. 9. Low temperature extrinsic photo-Hall mobility of phosphorus-doped silicon under $2\,\mu$ photoexcitation as a function of compensating acceptor concentration.

resistivity experiments in Fig. 10. The same light intensity and wavelength ($2\,\mu$) and applied potential (1 V) was used as in the photo-current measurements. The solid curve in both figures represents a temperature independent (4·2°–1·2°K) mobility which varies as the $-1/3$ power of the acceptor concentration. The points represent the experimentally determined values which exhibited no temperature dependence within the $\pm$ 10 per cent experimental error encountered. The solid square represents the experimental value for the 4·5–0·15–16 sample in which neutral impurity scattering is expected to dominate due to the relatively large ratio of neutral to ionized impurities.

mobility under $2\,\mu$ radiation could be due to carriers in this band or minimum with a smaller effective mass than carriers in the 6-fold degenerate minimum 85 per cent out along the [100] axis. As suggested by Fig. 3, if this minimum is the one at the edge of the Brillouin zone along the [111] axis it should be 4-fold degenerate. The lifetime of the photo-carrier in these minima would be determined by capture into the bound states of an ionized donor whose bound state wave functions must be made up of wave functions of the free electron states of these minima. Because all donors are essentially equivalent, the captured electrons can cascade to the donor states associated with the [100] minima, the excess energy being carried off

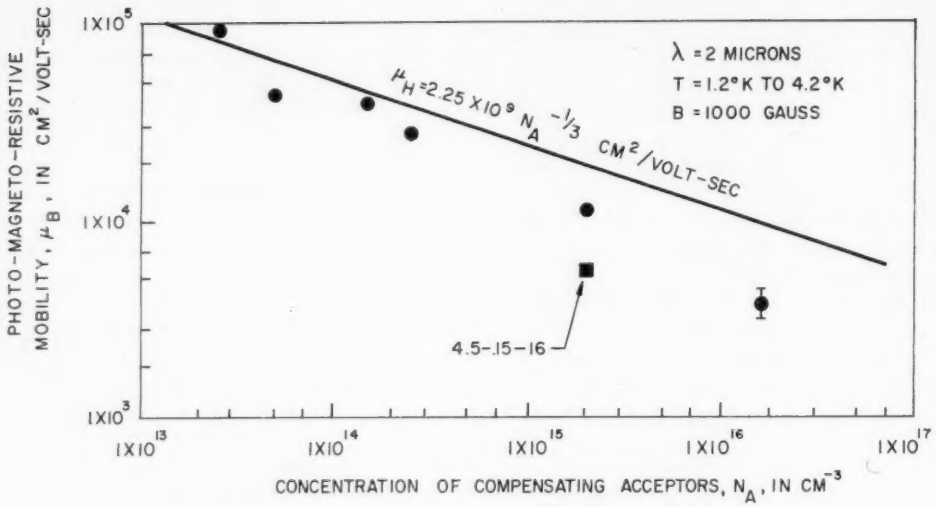

FIG. 10. Low temperature photo-magneto-resistivity mobility of phosphorus-doped silicon under 2 μ photo-excitation as a function of compensating acceptor concentration.

by phonons. If this model is correct then the lifetime of the 2 μ photo-excited electrons in the [111] minima must be limited by the capture lifetime and not by a shorter lifetime against decay to the [100] minima or else the mobility of the photo-excited carrier would be independent of wavelength. Heating of the carriers by the 2 μ excitation has been considered but is not believed to make any important contribution to the larger mobility observed under 2 μ radiation.

It is not possible to predict theoretically the photo-carrier mobility throughout this temperature and concentration region. The most rigorous and generally accepted method of calculating mobilities in the ionized impurity scattering region is that of BROOKS and HERRING[19]. One of the requirements of their theory is that the Born approximation be used, i.e. the motion of the carrier is only slightly perturbed by the scattering potential. This results in the restriction $b \equiv \langle 2\bar{k}R_0 \rangle^2 \gg 1$ where $\bar{k}$ is the wave number of the carrier and R_0 is the range of the scattering potential given by equation (13). If we attempt to calculate the mobility assuming the Born approximation to be valid for $b \geqslant 10$ the resulting values agree within factors of 2 with that observed when carriers are excited with long wavelength radiation, or thermally at $T > 20°$K. The 2 μ photo-excited carrier mobility is accounted for on the dilute samples if we assume an effective mass $\sim 0{\cdot}1\, m_e$ and assume that the Brooks–Herring formulation can be used with $b \sim 5$. For these low concentration samples for which $b \geqslant 5$ in the temperature range employed, the mobility so calculated also seems to approach temperature independence, in agreement with our observations. For the higher concentration samples the approximations are no longer valid at low temperature so that the temperature independence, concentration dependence and effective mass dependence of the photo-carrier mobility for these samples cannot be predicted with any of the presently available treatments of impurity scattering mobility.

Other evidence exists to support this model in which carriers with a reduced effective mass exist for an appreciable time in a higher energy band or minimum when photo-generated with radiation in the 2 μ region. We refer to Section 2(1), where it was pointed out that the exchange relaxation rate $(\tau_C^{ex})^{-1}$ could be measured independently and was proportional to the singlet exchange cross-section for a conduction electron and a bound electron. This exchange cross-section contains an $(m^*)^{-2}$ dependence. Preliminary

Vol. 22
1961

analysis of the data leads to an effective mass of conduction electrons photoexcited with $2\,\mu$ radiation of roughly $0{\cdot}15\,m_e$.

A cyclotron resonance experiment under $2\,\mu$ radiation seems definitely feasible, and would provide the most direct evidence for the existence of conduction electrons in these higher energy minima.

Acknowledgements—We would like to thank Mr. A. S. RUGARE of G.E. and Dr. B. ROSENBLUM of RCA for kindly supplying the samples used in this investigation. Appreciation is also due to Dr. J. WOODS and Mr. E. GOREY at I.B.M. Research Labs. for performing some of the Hall coefficients vs. temperature measurements. One of us (R.S.L.) would also like to thank Dr. S. KOENIG, Dr. R. LAFF and Dr. R. W. KEYES of I.B.M. Research Labs. for informative discussions.

REFERENCES

1. HONIG A., *Quantum Electronics Conference*, 1959, p. 450. Columbia University Press, New York (1959).
2. HONIG A., *Proceedings of the International Conference on Semiconductor Physics, Prague*, 1960, p. 610. Special publication of the *Czech. J. Phys.*, Prague (1961).
3. HONIG A. and LEVITT R., *Phys. Rev. Letters* **5,** 93 (1960).
4. SELAR N. and BURSTEIN E., *Phys. Rev.* **98,** 1757 (1955).
5. LAX M., *Phys. Rev.* **119,** 1502 (1960).
6. KOENIG S. N., *Phys. Rev.* **110,** 988 (1958).
7. ASCARELLI G. and BROWN S. C., *Phys. Rev.* **120,** 1615 (1960).
8. RODRIGUEZ S., unpublished report; ASCARELLI G. and RODRIGUEZ S., unpublished report.
9. FLETCHER R. C., YAGER W. A., PEARSON, G. L. HOLDEN A. N., READ W. T. and MERRITT F. R., *Phys. Rev.* **94,** 1392 (1954).
10. HONIG A. and STUPP E., *Phys. Rev. Letters* **1,** 275 (1958); HONIG A. and STUPP E., *Phys. Rev.* **117,** 69 (1960).
11. FEHER G. and GERE E. A., *Phys. Rev.* **114,** 1245 (1959).
12. FEHER G. and FLETCHER R. C., *Bull. Amer. Phys. Soc.* **1,** 125 (1956).
13. PINES D., BARDEEN J. and SLICHTER C. P. *Phys. Rev.* **106,** 489 (1957).
14. See, for example, BLATT F., *Solid State Physics*, Vol. 4, pp. 199–366. Academic Press, New York (1957).
15. CHANDRASEKHAR S., *Rev. Mod. Phys.* **15,** 1 (1943).
16. DINGLE R. B., *Phil. Mag.* **46,** 831 (1955).
17. MICHEL R. E. and ROSENBLUM B., *Bull. Amer. Phys. Soc.* **6,** 115 (1961).
18. SPITZER W. and FAN H. Y., *Phys. Rev.* **108,** 268 (1957).
19. BROOKS H., *Phys. Rev.* **83,** 870 (1951); HERRING C., unpublished.

DISCUSSION

G. ASCARELLI: Would it be possible that the "hot" carriers excited by light excite electrons out of excited states of the donors?

R. S. LEVITT: It is possible, but the short lifetime of the excited states of the donors results in only a small concentration of these excited states, typically about $10^6/\text{cm}^3$ in our experiments, and the effect of electron excitation from these excited states should be negligible.

T. S. MOSS: Have you measured the spectral dependence of the high mobility carriers and is there evidence of a threshold energy for the production of these carriers?

R. S. LEVITT: We have only measured the spectral dependence of mobility using broad band illumination at $> 20\,\mu$ and at ~ 6–$12\,\mu$, and using narrow band illumination at $\sim 2\,\mu$. The results are consistent with the existence of a threshold, but are not extensive enough for a conclusive statement.

M. A. LAMPERT: You have interpreted the increase of photo-excited electron mobility at $2\,\mu$ exciting light as excitation to a new, higher conduction band minimum. How certain are you that you are not simply dealing with "hot" electrons in the normal, lowest minimum? Assuming the dominance of ionized impurity scattering in your samples, the mobility change is certainly in the right direction just from the hot carrier effect.

It has seemed worthwhile to raise this question because your trapping (recombination) times are certainly very short (10^{-10}–10^{-12} sec)—perhaps substantially shorter than the thermalization time for a 1/2 eV electron in the normal minimum. Indeed GOODWIN reports a thermalization time for slightly excited electrons (free carrier absorption at 8 mm wavelengths) in Ge at $4{\cdot}2°\text{K}$ of 5×10^{-9} sec. In your case (much hotter electrons) optical phonon emission may substantially shorten this time—but only down to a Debye temperature roughly of the electrons, at which point only acoustic phonons will be effective in further cooling.

R. S. LEVITT: It is possible that "hot" electrons in the normal minimum are responsible for the increased mobility. Such an explanation would be similar to that given by ROLLIN and ROWELL for their low temperature mobility study in *p*-type germanium.* However, we prefer the interpretation of excitation to another

* *Proc. Phys. Soc. Lond.* **76,** 1001 (1960). ROLLIN B. V. and ROWELL J. M.

minimum for the following reasons. (1) The spectral dependence of the excitation of high mobility carriers corresponds roughly to that of the free carrier absorption peak measured by SPITZER and FAN (Ref. 18) in n-type silicon (see reply to above question by T. S. Moss). (2) The trapping lifetimes of our samples varied from $\sim 5\times10^{-9}$ sec to $\sim 5\times10^{-12}$ sec. Also, by neutralizing donor ions by means of intrinsic excitation, the lifetime could be increased to about 5×10^{-8} sec in our purest sample. Over this entire range of lifetimes, the ratio of mobility of $\sim 2\,\mu$ excited carriers to the mobility of $> 20\,\mu$ excited carriers remains approximately constant. If "hot" carriers were responsible for the mobility increase, they would have to thermalize in a time of the order of 5×10^{-12} sec to a particular low temperature, and then "stick" there for a time at least equal to 5×10^{-8} sec to account for our results. Though not impossible, this situation would be surprising. Also, the particular low temperature would be $\sim 30°$K to account for the magnitude of the mobility observed, and the observed spectral dependence of mobility is incompatible with a "sticking" temperature below $\sim 500°$K.

Vol. 22
1961

J. Phys. Chem. Solids Pergamon Press 1961. Vol. 22, pp. 285–292. Printed in Great Britain.

STUDIES OF PHOTOCONDUCTIVITY IN IODINE SINGLE CRYSTALS

A. MANY, M. SIMHONY, S. Z. WEISZ and J. LEVINSON

Department of Physics, The Hebrew University, Jerusalem, Israel

Abstract—Photoconductivity studies in iodine show it to possess unique properties. Sustained space-charge-limited photo-currents (SCLPC) generated at the positive electrode are obtained even for samples over 1 mm thick. Hole conduction is predominant over electron conduction. The dominant hole traps are found to be shallow, lying 0·4–0·5 eV above the valence-band edge, and to have a density of 10^{13}–10^{15}. The ratio of free to trapped hole concentration θ is $\sim 0{\cdot}02$ at room temperature. The slow trapping permits a detailed study of transient SCLPC with conventional circuitry. A theory, of which a simplified version is presented here, accounts satisfactorily for the observed transient characteristics. The hole drift mobility is determined to be 0·7 cm²/V sec, and is temperature-independent between 200 and 320°K. The spectral photoresponse consists of two sensitivity bands, a main band centered around 0·45μ and a much weaker one around 0·8μ. The response to polarized light is anisotropic.

INTRODUCTION

IODINE forms molecular crystals which belong to the base-centered orthorhombic system. The crystal faces have a bright metallic lustre. The material has a low melting point (114°C) and a high vapour pressure at room temperature (0·2 mm Hg). Little information has appeared in the literature concerning either the conductivity or the photoconductivity of iodine. Such work as has been published[1] was carried out on melted or evaporated layers.

The interest in iodine in this laboratory stems from the molecular nature of its crystal binding. In many respects iodine affords a more convenient medium than other molecular solids (such as organic materials) for a study of electronic processes. As far as transport, recombination and trapping processes are concerned, it is found that the phenomenological behaviour of iodine is not fundamentally different from that of other covalent or ionic crystals. For convenience, the experimental results will accordingly be discussed in terms of the band model, even though the band approximation is probably a poor one in such a molecular crystal.

EXPERIMENTAL TECHNIQUE

The samples studied were commercial, resublimated iodine (A.C.S. specifications). The material comes in the form of thin (0·1–2 mm) flakes from which it was possible to select single crystal wafers. These are all oriented parallel to the *ac* plane. From them samples were prepared either in sandwich-type or in surface-type cells. In the former the crystal is hermetically sealed between two transparent electrodes of conducting glass, one of which is provided with a guard ring. In the surface cell, two closely-spaced parallel lead contacts are applied on the crystal surface.

In the transient measurements, voltage pulses (amplitudes 0–1000 V, duration 0·1–30 msec) are applied to the sample in series with a 15 kΩ cathode-follower grid resistor. A light flash (duration $\sim 0{\cdot}2$ μsec) from a xenon discharge tube, triggered by each voltage pulse, is focused on the sample. The resulting transient photocurrent is amplified and displayed on a Tektronix CRO. The overall circuit response time is ~ 1 μsec, and the smallest observable photocurrent is 10^{-8} A.

The steady-state photocurrent is directly recorded as a function of applied d.c. voltage on a log–log scale. The photosignal obtained from chopped light (75 r.p.s.) is fed via a tuned amplifier to a logarithmic recorder. The applied voltage V varies exponentially with time, so that the uniform motion of the chart transforms the time axis into a log V axis. The smallest observable photocurrent is 10^{-11} A.

EXPERIMENTAL RESULTS

General. The dark conductivity is difficult to measure because of the large surface leakage, usually 2–3 orders of magnitude greater than the

bulk current. By use of a guard ring the bulk resistivity perpendicular to the *ac* plane of the crystal is estimated to be 10^{10}–$10^{11}\,\Omega$/cm at room temperature. It increases exponentially with temperature with an activation energy somewhere between 0·8 and 1 eV. The absence of both rectification and photovoltage, and the characteristics of the current response to pulses indicate

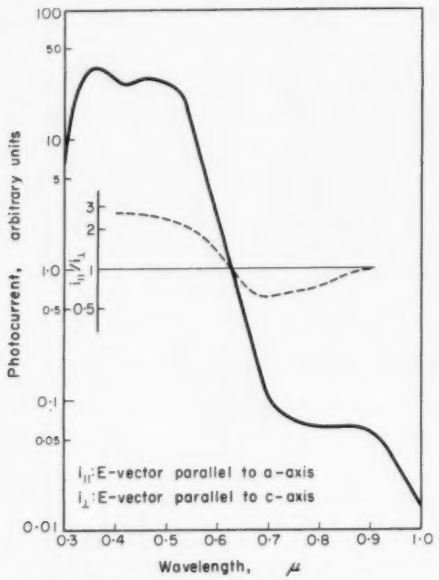

FIG. 1. Relative spectral response of iodine single crystals at 300°K (solid curve). The dotted curve gives the ratio of the spectral response for light polarized parallel to the *a*-axis to that parallel to the *c*-axis of the crystal.

that the contacts are effectively neutral (i.e. bands at interface remain flat at least to within a tunneling distance). Thermoelectric power measurements suggest that the samples are *p*-type. The dielectric constant in the range 1 kc–1 Mc is found to be 2.

The relative spectral photosensitivity of iodine single crystals at constant photon flux density as derived from both transient and steady-state measurements on sandwich and surface cells is shown in Fig. 1 (solid curve). The general shape agrees with previously reported measurements on polycrystalline films.[1] Two photosensitive bands are apparent, a main one between 0·35 and 0·55μ and a much weaker one in the vicinity of 0·8μ. The absorption coefficient of iodine[1] is sufficiently large throughout the photosensitive spectral range, so that for the sample thicknesses used (0·3–1·2 mm), the non-reflected light is in effect fully absorbed. The response to polarized light is anisotropic, the main band being favoured by light polarized parallel to the *a* axis and the weak band by light parallel to the *c* axis. The ratio of the responses for light polarized along these two directions in a sandwich cell is shown by the dotted curve in Fig. 1.

Transient measurements. Typical oscillograms of transient photocurrent in a sandwich cell following an intense flash illumination of the positive electrode are shown in Fig. 2 for various applied voltages. The spectral composition of the light flash corresponds to the main sensitivity band (absorption coefficient 10^5 cm^{-1}). All traces are on a common time base (1·5 μsec/cm) but with different amplifier gains. The photosignal for the illuminated electrode negative is smaller by a factor of at least 10^3, indicating that hole conduction is predominant over electron conduction. It is seen that at the onset of the flash, the photocurrent rises abruptly (disregarding the circuit response-time) to an initial value. Thereafter it varies slowly, decreasing for low applied voltages (not shown here) and increasing for large voltages, up to a sharp inflection point corresponding to the transit time, whence it decays to zero. Fig. 3(a) represents log–log plots of the *initial* photocurrent density versus applied voltage for various light-flash intensities. For strong light and low applied voltages the current varies as V^2 and is insensitive to light intensity, whereas for large voltages and decreasing intensity the slope departs from 2 and approaches unity. The V^2 dependence is characteristic of space-charge-limited photocurrents (SCLPC). Indeed, the theory of SCLPC under transient conditions, to be outlined below, accounts satisfactorily for the V^2 dependence of the initial photocurrent as well as for the general form of the subsequent variation with time. According to this theory the initial photocurrent density for strong flash illumination (corresponding to an effectively infinite reservoir of holes at the anode) is given by

$$j(0) = 4{\cdot}4 \times 10^{-14}\,\epsilon\mu V^2/L^3\ \text{A/cm}^2, \qquad (1)$$

where ϵ is the dielectric constant, μ the hole mobility, L the sample thickness and V the applied

Vol. 22
1961

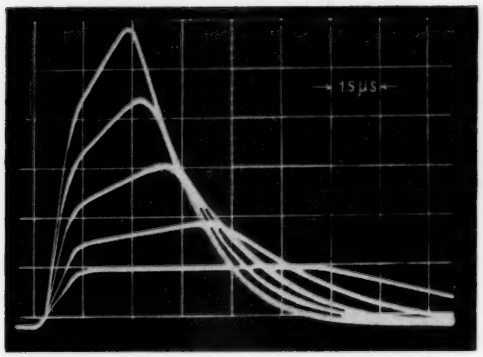

FIG. 2. Oscillograms of transient photocurrent in a sandwich cell following flash illumination, for various applied voltages, at 300°K. The time base is the same (1·5 μsec/div.), the *y*-amplifier gain is different for the various traces.

voltage. The transit time is given by

$$t_1 = 2(1-e^{-1/2})\,(L^2/\mu V) \approx 0{\cdot}8t_0, \qquad (2)$$

where $t_0 = L^2/\mu V$ is the transit time for space-charge *free* flow. Equation (1) is represented in Fig. 3(a) by the upper curve. It is seen to agree well with the experimental points at full light intensity. As the light is decreased and the voltage increased, the anode reservoir can no longer supply the full value prescribed by Eq. (1), and the photocurrent approaches the value corresponding to space-charge free flow. The transit time should then approach t_0. This is demonstrated in Fig. 3(b), where the measured transit time is plotted against $1000/V$ for strong (squares) and weak (circles) incident light intensities. It is seen that indeed the ratio of the slopes of the two lines is 0·8, i.e. $t_1 \approx 0{\cdot}8t_0$ as required by eqn. (2). Both curves yield the value 0·7 cm²/V sec for the hole mobility. From the current at very low light intensities, the lower limit of the quantum efficiency (in the main sensitivity band) is estimated to be 0·02. Obviously the actual value may be higher if an appreciable number of optically-excited carriers are rapidly (faster than ~ 1 μsec) trapped at the illuminated surface.

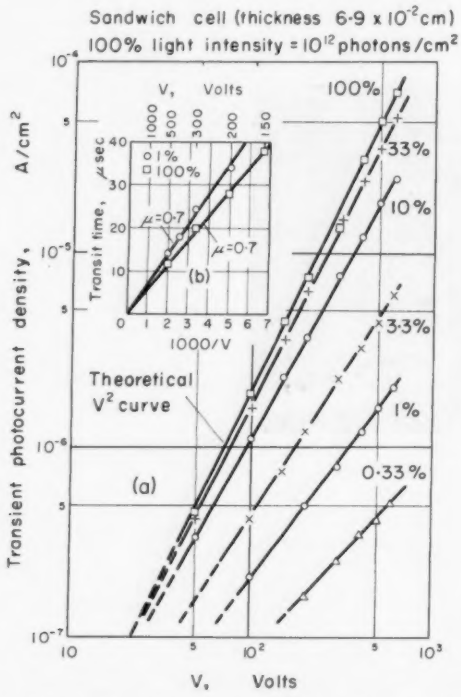

FIG. 3(a). Initial transient photocurrent density in a sandwich cell plotted against applied voltage for various light flash intensities. $T = 300°$K. The heavy dotted curve is calculated from equation (1) using the values $\mu = 0{\cdot}7$ cm²/V sec and $\epsilon = 2$.

(b) Transit time *versus* applied voltage for strong (squares) and weak (circles) incident light intensities. $T = 300°$K.

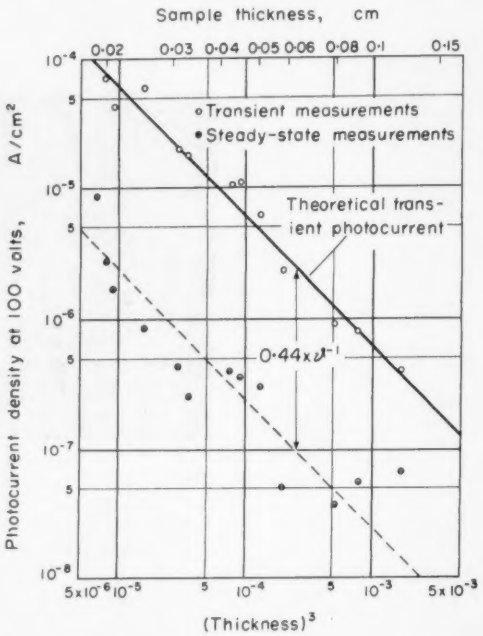

FIG. 4. Transient (circles) and steady-state (bisected circles) SCLPC density at 100 V applied voltage for different samples plotted against the third power of their thickness. The solid line is computed from equation (1) ($\mu = 0{\cdot}7$, $\epsilon = 2$). $T = 300°$K.

The mobility, as measured from both the transit time and the initial photocurrent, does not vary with temperature over the range 200–320°K, within the experimental accuracy ($\sim$ 5 per cent).

A striking demonstration of the space-charge-limited nature of the transient photocurrent is given in Fig. 4. Here the initial values of photocurrent density following an intense light flash for *different* sandwich cells (measured at 100 V) are

Vol. 22
1961

plotted (circles) against the third power of their thickness L on a log–log scale. The solid curve is a plot of equation (1) using the independently determined values of μ and ϵ. It is seen that the agreement between the experimental points and the theoretical curve is very good, as regards both slope (-1) and absolute magnitude.

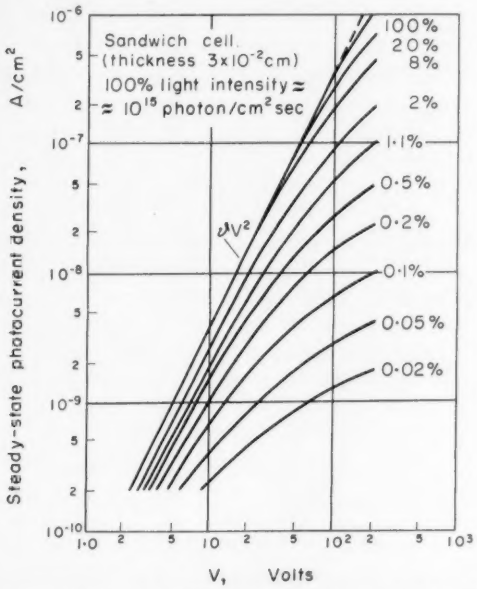

FIG. 5. Steady-state SCLPC density in a sandwich cell plotted against applied voltage for various incident-light intensities. $T = 300°K$.

Steady-state measurements. Light corresponding to the main sensitivity band is focused on one surface of the sandwich cell. As in the case of the transient measurements, the photosignal is very small for the illuminated electrode negative. With the reverse polarity, on the other hand, large sustained photocurrents are obtained even for samples over 1 mm thick. Conduction is again seen to be predominantly by holes, and these have an exceedingly large range. Plots of steady-state photocurrent density versus applied voltage for different incident light intensities, reproduced directly from the recorder traces, are shown in Fig. 5. For strong light intensities and low voltages ("infinite reservoir" conditions) the photosignal saturates with light and varies with voltage very nearly as V^2. This behaviour is characteristic of SCLPC in crystals having shallow traps.[2, 3] The SCLPC is then given by[2, 3]

$$j_{ss} = 10^{-13}\,\theta\epsilon\mu V^2/L^3 \text{ A/cm}^2, \qquad (3)$$

where θ is the fraction of the total injected space-charge that is free. For the case of hole trapping

$$\theta \approx p/p_t = (N_v/N_t)\exp(-\Delta E/kT), \qquad (4)$$

N_v being the effective density of states in the valence band, N_t the concentration of traps and ΔE their energy position above the valence-band edge. For diminishing light intensities and increasing voltages, the photocurrent tends to saturate with voltage, space-charge effects becoming increasingly insignificant. The quantum efficiency as computed from the saturated value is $\sim 0{\cdot}1$, but it is not clear what is the role, if any, played by secondary photocurrents.

Figure 4, referred to previously, shows values of transient SCLPC plotted against L^3 for a number of different samples. Measurements of *steady-state* SCLPC (i.e. corresponding to intense constant illumination) were carried out on the *same* samples and are represented by the bisected circles. Although the scatter of the points is large (due to some variation in trap content from sample to sample), they are seen to conform well to the L^3 dependence law (dotted curve). Inspection of equations (1) and (3) shows that the distance between the solid and dotted curves should give the value of $0{\cdot}44\,\theta^{-1}$ averaged over the samples studied. At room temperature, where these measurements were carried out, the average value of θ is found to be $\sim 0{\cdot}02$.

The temperature dependence of the steady-state SCLPC measured on one sample and converted into θ values, is shown in Fig. 6. The slope yields the value of 0·46 eV for the position of the shallow hole traps above the valence band. Making use of equation (4), one obtains $N_t/N_v \approx 10^{-6}$. Taking 10^{19}–10^{21} for N_v (the higher value is probably nearer the truth, iodine being a molecular crystal), one obtains $N_t \approx 10^{13}$–$10^{15}\,\text{cm}^{-3}$.

Measurements on surface cells. In iodine, where any light giving rise to appreciable photocurrents is strongly absorbed, surface cells afford practically the only configuration for studying carrier recombination *per se*, as distinct from majority-carrier trapping. Even though generally the surface layer may be quite different from the underlying bulk,

the measurements indicate that in iodine much the same traps are involved in both regions. In particular, the steady-state photocurrent is found to vary as the square root of the light intensity and is strongly temperature dependent. Here, again,

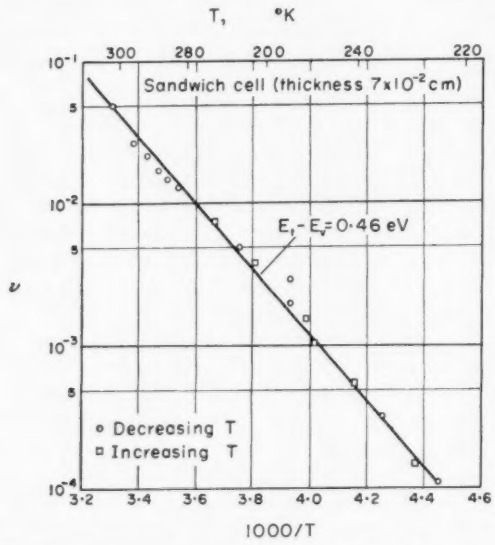

FIG. 6. Temperature dependence of θ derived from that of steady-state SCLPC in a sandwich cell.

shallow levels seem[4, 5, 6] to be the dominant hole traps. An interesting feature of the photocurrent is its saturation with applied voltage at very low incident light intensities. The range of holes is then believed to be governed by[7] $\tau_R\,\theta$, where τ_R is the relaxation time associated with the surface layer. The product $\eta\tau$ (where η is the quantum efficiency and τ the free carrier lifetime) at the sensitivity peak ($\sim 0{\cdot}45\mu$) as determined from either the linear or saturation values is $\sim 5\times10^{-6}$ sec. For $\eta = 1$, one obtains $\tau = 5$ μsec, a value not inconsistent with measurements of transient response to flash illumination carried out on the same cells.

Theory of transient SCLPC. In this Section the simplest case, that of a perfect insulator, will be treated in order to bring out the main features of the problem. The detailed theory, taking into account trapping and the dark conductance, will be published elsewhere. Consider an insulator sample of thickness L, across which a constant voltage V is maintained. At time $t = 0$ the anode ($x = 0$) is illuminated by an intense highly absorbed light flash of infinitely short duration. As a result, photoexcited holes drift towards the cathode. The current density at any point x is given by the sum of the conduction and displacement current densities:

$$j(t) = (\epsilon/4\pi)\partial E(x,t)/\partial t + q\mu p(x,t)E(x,t), \quad (5)$$

where $p(x,t)$ is the hole density and $E(x,t)$ the electric field intensity (cgs units). The diffusive contribution to the current is being neglected. In the absence of trapping, Poisson's equation assumes the form:

$$\partial E(x,t)/\partial x = (4\pi q/\epsilon)p(x,t). \quad (6)$$

The light flash is assumed to be sufficiently intense and the life of holes at the surface sufficiently long to achieve effectively the condition of an infinite hole reservoir at the anode throughout the period of interest. Consequently, one obtains the boundary conditions at the anode:

$$E(O,t) = 0, \quad t \geqslant 0. \quad (7)$$

Elimination of p by the use of equations (5) and (6) gives

$$j(t) = (\epsilon/4\pi)[\partial E/\partial t + \tfrac{1}{2}\mu(\partial E^2/\partial x)]. \quad (8)$$

By integrating equation (8), using the boundary conditions equation (7) and the fact that

$$\int_0^L E\,dx = V = \text{const.},$$

one obtains

$$j(t) = (\epsilon/4\pi)[\partial E/\partial t + \tfrac{1}{2}\mu(\partial E^2/\partial x)] = (\epsilon\mu/8\pi L)E^2(L,t) \quad (9)$$

where $E(L,t)$ is the field at the cathode. Before the arrival of the leading front of carriers at the cathode, $\partial E/\partial x = 0$ at $x = L$ [equation (6)], and hence equation (9) reduces to an ordinary differential equation in $E(L,t)$ whose solution yields for the current density

$$j(t) = (\epsilon\mu V^2/8\pi L^3)\,(1 - t/2t_0)^{-2}; \quad t \leqslant t_1, \quad (10)$$

where $t_0 = L^2/\mu V$ and t_1 is the transit time of the leading front of carriers. This front moves towards

Vol. 22
1961

the cathode under a field of magnitude $E(L, t)$ just calculated. Hence t_1 may be computed from the relation

$$L = \int_0^{t_1} \mu E(L,t)\, dt,$$

and is given in equation (2). The initial value $j(0)$ of $j(t)$, as given by equation (1), follows from equation (10). Thereafter, $j(t)$ increases towards its peak value of $\sim 2{\cdot}718j(0)$ at $t = t_1$. The calculation of $j(t)$ for $t > t_1$ is more complicated and will not be presented here. From physical considerations it can be seen that $j(t)$ should decay in this region to its steady-state value[8] of $(9\epsilon\mu V^2/32\pi L^3) = 2{\cdot}25\, j(0)$, as the space-charge distribution at $t = t_1$ relaxes towards its steady-state configuration. The relaxation time is that associated with the conductance of the injected space-charge and is therefore proportional to $1/V$, i.e. to t_1.

The oscillograms in Fig. 2 show the experimental behaviour to follow the general pattern predicted above. The decay of the photocurrent to zero instead of to the value $2{\cdot}25j(0)$ is due to the progressive processes of charge accumulation in traps and of the dwindling of the hole reservoir at the anode by recombination, both factors not having been allowed for in the simplified treatment presented above.

DISCUSSION

Iodine affords an excellent medium for a quantitative study of SCLPC under both transient and steady-state conditions. The low effective majority-carrier trapping found in iodine sets it apart from any other known insulator. This is particularly notable in view of the fact that the samples employed were of commercial origin with no additional purification. Their large value of θ ($\sim 10^{-2}$ at room temperatures) is to be contrasted with, e.g. the 10^{-9} quoted[9] for carefully grown CdS. The experimental evidence points to the following conclusions. The samples studied are p-type with the Fermi level in the dark lying in an essentially trap-free void at about 1 eV above the valence-band edge. Upon illumination, the electrons are rapidly trapped in recombination levels while the holes are distributed among the valence band and trapping levels.[4, 5] Dominant among the latter are traps of density 10^{13}–10^{15} cm^{-3} situated 0·4–0·5 eV above the valence-band edge. They are shallow in the sense that they lie below the steady-state Fermi limit for all excitation levels achieved in practice.

The general characteristics of transient SCLPC are satisfactorily accounted for by the simple theory presented here. The hole mobility as derived from transit-time measurements has the low value of 0·7 cm^2/V sec and is independent of temperature between 200 and 320°K. It is hard to comment on these observations, as little is known to date about the transport mechanism in molecular crystals. The lack of temperature dependence strongly indicates, however, that the value quoted is the true free-hole mobility and not an effective mobility due to some fast trapping process at shallow levels.

Although the transport, trapping and recombination processes are phenomenologically similar to those in covalent and ionic insulators, the spectral response is markedly different. As in other molecular crystals[10] the sensitivity bands are broad and there is no sharp absorption edge. Even though the quantum efficiency in the main sensitivity band may well approach unity (the experimental evidence sets its lower limit at 0·02), that in the weak band is definitely 2 to 3 orders of magnitude lower. The anisotropic response to polarized light suggests that both sensitivity bands arise from intrinsic processes. It may therefore be inferred that in addition to carrier generation some other mechanism is operative in the energy dissipation of absorbed radiation.

Acknowledgements—The authors wish to express their gratitude to Dr. H. S. Sommers, Jr., for many stimulating and helpful discussions during his stay in this laboratory.

Thanks are due to various members of this Department for their help, and in particular to Mr. I. Weisman for preparing the samples, to the personnel of the Fine Mechanics Workshop under the direction of Mr. B. Loewenson for building the mechanical parts and to Mr. D. Freihan for constructing the electronic apparatus.

REFERENCES

1. Moss T. S., *Photoconductivity in the Elements* Butterworths Scientific Publications, London (1952); references.
2. Rose A., *Phys. Rev.* **97,** 1538 (1955).

3. LAMPERT M. A., *Phys. Rev.* **103,** 1648 (1956).
4. ROSE A., *RCA Rev.* **12,** 362 (1951).
5. ROSE A., paper in *Photoconductivity Conference*, p. 3. John Wiley, New York (1956).
6. BUBE R. H., *Photoconductivity of Solids.* John Wiley, New York (1960).
7. STÖCKMAN F., paper in *Photoconductivity Conference*, p. 269 John Wiley, New York (1956).
8. MOTT N. F. and GURNEY R. W., *Electronic Processes in Ionic Crystals.* Clarendon Press, Oxford (1957).
9. SMITH R. W., *RCA Rev.* **20,** 69 (1959).
10. See, for example, *Proceedings of the Conference on Electronic Conductivity in Organic Solids.* Interscience, New York (1960).

J. Phys. Chem. Solids Pergamon Press 1961. Vol. 22, pp. 293–298. Printed in Great Britain.

OPTICAL ABSORPTION AND PHOTOCONDUCTIVITY IN GERMANIUM SELENIDE*

C. R. KANNEWURF and R. J. CASHMAN

Technological Institute, Northwestern University, Evanston, Illinois

Abstract—Optical absorption was investigated in extremely thin single crystal specimens of GeSe. Absorption data at 300°K cover a wavelength range of 1·20 to 0·45 microns with the absorption coefficient changing from 30 to $1{\cdot}2\times10^5$ cm^{-1}. An analysis of the absorption edge for direct and indirect transitions is described. In the high absorption region a direct transition photon energy dependence of $(h\nu-E_g)^{3/2}$ with $E_g = 1{\cdot}53$ eV was shown to give a good fit to the data over a considerably greater energy range than was found for $(h\nu-E_g)^{1/2}$. The spectral response curve for an evaporated film type photoconductive layer was obtained for the same wavelength range. This curve shows two bands of responsivity with the threshold energies corresponding closely to the energy gap values that were determined for the direct and indirect band transitions.

INTRODUCTION

A CONSIDERABLE amount of information concerning the optical properties of lead salt crystals and films is available in the literature, but hardly any optical data have been reported for other IV_b–VI_b compounds. In particular very little information is available concerning the optical properties of the chalcogenides of germanium. The preparation at this laboratory of extremely thin single crystal specimens of germanium sulfide and germanium selenide has made it possible to investigate optical absorption in these materials to an order of magnitude in absorption coefficient slightly greater than 10^5 cm^{-1}. Therefore an analysis of the absorption edge to establish evidence for direct band transitions is possible. Further information has also been gained from a study of the photoconductivity in thin film-type samples of germanium selenide, GeSe.

A complete crystal structure analysis for GeSe was first reported by OKAZAKI[1] and was confirmed by KANNEWURF *et al.*[2] The crystal system is primitive orthorhombic; the lattice values are $a = 4{\cdot}40$, $b = 10{\cdot}82$, and $c = 3{\cdot}85$ Å. ASANABE and OKAZAKI[3] have studied some of the electrical properties and indicate that the material is a semiconductor. They estimate an energy gap to be nearly 1·0 eV from the slope of resistivity curves at high temperatures. Most of their measurements were made on a variety of *p*-type polycrystalline samples. Thermal probe tests indicate that all single crystal samples employed in the present optical investigation were also *p*-type. For the purpose of optical absorption measurements the grown single crystals were found to be superior in all respects to single crystal fragments cleaved from polycrystalline ingots.

PREPARATION OF CRYSTALS

Selenium was obtained from the American Smelting and Refining Company with a rated chemical purity of 99·999 per cent. Germanium was prepared by reduction of the best grade of Eagle Pitcher germanium dioxide. Polycrystalline ingots of GeSe are first obtained by heating to 790°C in a muffle furnace a mixture of stoichiometric proportions of germanium and selenium which have been sealed in a evacuated quartz tube. The polycrystalline ingots are placed in a quartz boat which is then positioned in a Vycor gas flow tube. The Vycor tube is centered horizontally in a glass oven such that a controlled temperature gradient can be maintained along its length. As the

* Supported in part by the Department of the Navy, Bureau of Ships, Washington, D.C. and in part by the Advanced Research Projects Agency of the United States Department of Defense.

temperature of the oven is increased, the polycrystalline pieces begin to sublime at 540°C. The GeSe vapor flows into a cooler region and begins to condense on the walls of the tube forming a great variety of crystalline shapes. Throughout the process a hydrogen gas flow is maintained in the tube to reduce any oxide contamination on the surface of the ingots and to prevent the formation of germanium diselenide. When the oven has cooled, the crystals are easily dislodged from the walls of the Vycor tube.

The single crystals generally grow in one of two principal forms. Many grow as thin filaments with parallel edges and faces but irregular ends, the approximate dimensions of the largest being 1 cm by 1 mm with a few exceeding 0·2 mm in thickness. Most are considerably thinner, being 20 to 50 microns thick. Others grow in the form of extremely thin plates with irregular edges; the effective diameters range from 5 mm to fractions of a millimeter. The crystals cleave quite readily in planes which are perpendicular to the largest lattice cell dimension. They are quite soft, probably not exceeding a hardness of 2 on Moh's scale. Microscopic examination showed that nearly all specimens of any appreciable thickness greater than 20 microns were hollow or had indications of other internal imperfections. As will be shown in the next section, GeSe transmits infrared radiation, and therefore the internal condition of a particular sample could be determined, without possible damage by cleaving, by viewing the sample with an infrared image converter (a metascope). One of the more noteworthy properties that was observed for the single crystals was their apparent plasticity. GeSe crystals bend easily in air and liquids, and with sufficiently thin samples the bending process can be repeated several times.

OPTICAL ABSORPTION

The optical system employed to measure the percent transmission of the crystals as a function of radiation wavelength was designed around the sample in, sample out, technique. A van Cittert double prism type monochromator with glass optics was used with a tungsten filament lamp as source. The monochromatic radiation is focused on the plane of the sample mount and the transmitted intensity is detected by a cooled lead sulfide cell. The sample mounts were brass plates with two precision drilled circular apertures in each. The diameters of the apertures ranged from 6 to 40 mils.

The single crystal specimens selected for transmission measurements were those without internal defects and having excellent surfaces. Both the natural and cleaved surfaces appear light gray metallic with a high reflective luster. The thinnest crystals were found by visual examination to transmit light in the deep red region of the visible spectrum. To investigate the high absorption region, extremely thin samples were prepared. Such samples may be peeled off the crystals by using transparent adhesive tape. These single crystal fragments showed a variety of color transmission in the visible spectrum. The thicker samples showed red to red-orange, the thinner ones yellow to pale yellow-green. Most of the cleaved fragments were not self supporting and were left attached to the cleaving tape for transmission measurements. The thinnest fragments were less than 10 mils in effective diameter. For crystals thicker than 10 microns the sample thickness was determined from displacement data taken either from edge measurements under a 500 power microscope or from the contact thickness as registered by a Federal Surface Gauge.

The reflection coefficient R was obtained by two methods. In the first method a comparison system was devised using a vertical illuminating microscope with a photovoltaic cell located at the eyepiece position. The incident radiation was monochromatic, and data were obtained at various wavelengths in the visible spectrum. Samples from many preparation trials with both cleaved and uncleaved surfaces were examined. For those with the better quality surfaces an average R of $0{\cdot}42 \pm 0{\cdot}01$ was obtained. In the second method a procedure devised by FAN and BECKER[4] to obtain R by an extrapolation plot was followed. Fig. 1 gives sample transmission as a function of sample thickness for various wavelengths. The extrapolation point at zero thickness is $(1-R)^2$ which can be read directly. From Fig. 1 R is 0·43 which is in agreement with the first method. With $R = 0{\cdot}42$, the index of refraction is calculated to be 4·7 and was found to be approximately constant for wavelengths less than 1·0 microns.

Figure 2 is the optical absorption curve for GeSe with all radiation at normal incidence along

Vol. 22
1961

the crystallographic direction of the b axis. This curve represents the accumulation of data from many samples. On the scale for which the plot is made the individual data points could not be resolved; thus the curve is drawn for the most part as continuous. At the onset of the edge the data $K \sim 5 \times 10^3\,\text{cm}^{-1}$ at $\lambda = 0{\cdot}80\mu$. Above $K = 10^4\,\text{cm}^{-1}$ both R and the sample thickness had to be calculated from the normalization of the data in the overlap regions where the curve had already been established from thicker samples. The ranges in sample thickness d for the various regions of the

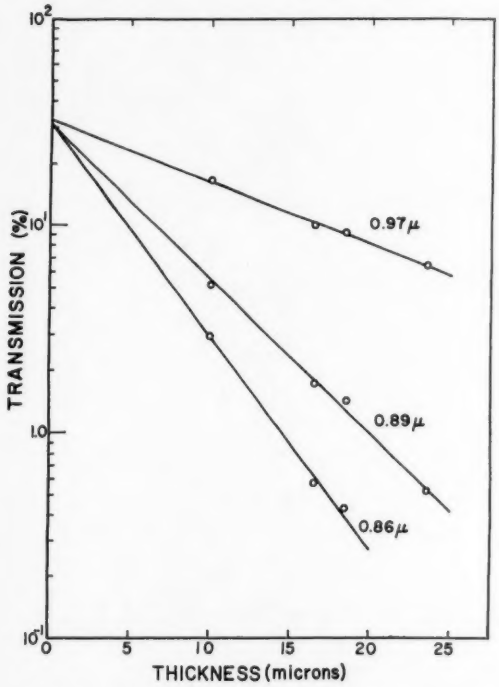

FIG. 1. Transmission through GeSe as a function of sample thickness.

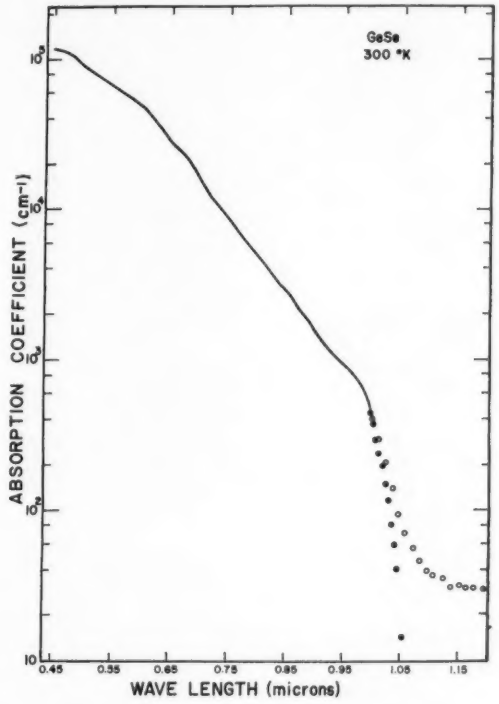

FIG. 2. Optical absorption coefficient for GeSe as a function of wavelength.

points are separated into two branches showing the extremes in absorption coefficient, K, caused by the variation of R throughout the samples. The nearly vertical drop in K of the one branch for K less than $100\,\text{cm}^{-1}$ is probably due to some interference effects in that particular sample. The K values for all other samples tested in the low absorption region were located between these two branches. Out to $1{\cdot}80\mu$ in the high transmission region K did not show any appreciable increase above $30\,\text{cm}^{-1}$.

Independent reflection coefficient and thickness measurements were made on most samples up to absorption curve are as follows: Below $K = 5 \times 10^3$ cm^{-1}, $d = 10$–25 microns; from $K = 5 \times 10^3$–$2 \times 10^4\,\text{cm}^{-1}$ $d = 5$–2 microns; from $K = 2 \times 10^4$–$9 \times 10^4\,\text{cm}^{-1}$, $d = 0{\cdot}7$–$0{\cdot}35$ microns; above $K = 9 \times 10^4$ d is less than $0{\cdot}17$ microns. A crystal $0{\cdot}15$ microns thick is 139 unit cells in width or in terms of atomic positions approximately 550 atoms in width along the crystallographic direction of the b axis. In the thinnest sample fragments tiny surface and thickness irregularities were known to exist in the area covering the transmission aperture, but these defects did not appreciably effect the final K values.

The absorption edge for GeSe shifts toward shorter wavelengths as the temperature of the sample is decreased. This shift in wavelength was not investigated quantitatively. All GeSe optical data presented in this paper are for 300°K.

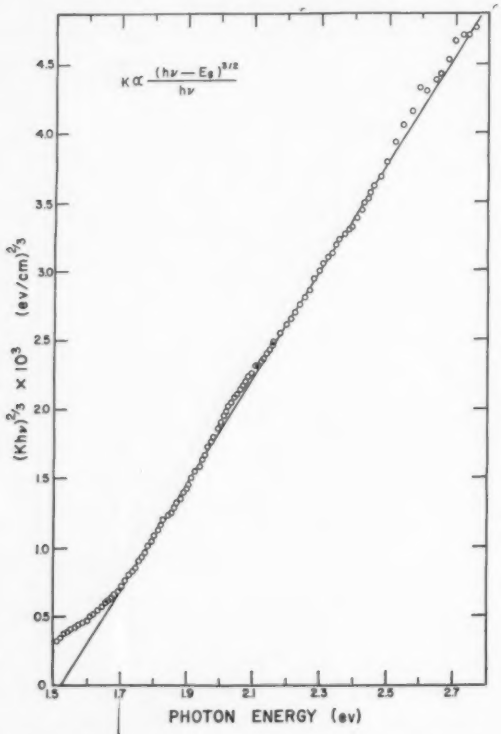

FIG. 3. Evidence for direct transitions where the absorption coefficient is a function of photon energy to the three-halves power.

DIRECT AND INDIRECT TRANSITION ENERGIES

Detailed discussions of the various possible expressions giving the absorption coefficient as a function of photon energy for both the direct and indirect band transitions are available in the literature.[5–8] According to DRESSELHAUS[9] an energy dependence of either $(h\nu - E_g)^{1/2}$ or $(h\nu - E_g)^{3/2}$ is possible for the mechanism of direct transitions in anisotropic materials depending on whether the band transition in momentum space at $\boldsymbol{k} = 0$ is allowed or forbidden. The photon energy is $h\nu$ and E_g is the energy gap value. The entire absorption curve was examined for evidence of direct transitions. With $E_g = 1{\cdot}83$ eV in the energy range of $h\nu = 1{\cdot}9$ to $2{\cdot}2$ eV the absorption coefficient was found to be nearly proportional to $(h\nu - E_g)^{1/2}$.

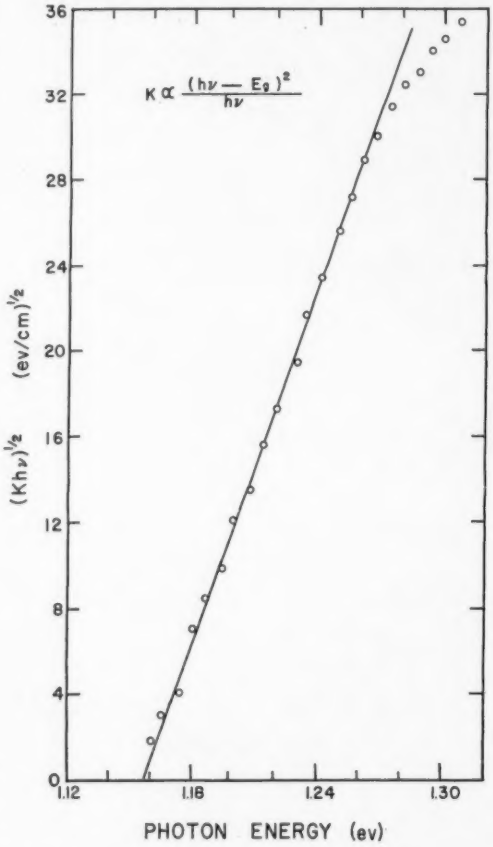

FIG. 4. The square root of the absorption coefficient as a function of photon energy indicating evidence for indirect transitions.

However, if $Kh\nu$ is plotted as a function of $(h\nu - E_g)^{3/2}$ as shown in Fig. 3, a remarkably close fit to the experimental absorption curve is obtained throughout the entire high absorption region. The extrapolated E_g value is 1·53 eV. The linear region in Fig. 3 covers nearly the entire wavelength range of the visible spectrum. Thus in the direct transition region the dependence of K is best represented by the expressions with $(h\nu - E_g)^{3/2}$ where $E_g = 1{\cdot}53$ eV.

Vol. 22
1961

For photon energies less than 1·3 eV K was found to be proportional to $(h\nu - E_g)^2$ as shown in Fig. 4, thus possibly indicating evidence for the mechanism of indirect transitions. From BARDEEN *et al.*[6] it would appear that it is preferable to plot $Kh\nu$ as a function of photon energy. The extrapolated E_g value for indirect transitions is 1·16 eV. To establish the indirect transition region with more certainty, thicker homogeneous samples of higher semi-conductor purity are needed to obtain more complete absorption data in the neighborhood of $K = 10\ \text{cm}^{-1}$. Between 1·4 and 1·6 eV K is again proportional to $(h\nu - E_g)^2$. In the intermediate energy ranges none of the individual energy laws give a good fit to the experimental data.

PHOTOCONDUCTIVITY

To investigate the responsivity of GeSe, a Hilger–Muller monochromator with rock salt optics was used in conjunction with a Nernst glower and a Schwarz thermopile. Single crystal filament type samples gave only a very slight indication of a photocurrent; the effect was too small to permit any quantitative measurements. However, with a film type sample a spectral distribution curve could be easily obtained. A polycrystalline film of GeSe was deposited by evaporation between two colloidal graphite electrodes in an evacuated glass cell. Fig. 5 is the spectral response curve for this cell. The spectral response is plotted here as a function of energy rather than wavelength since the exponential fall at long wavelengths is slightly more linear with energy.

Two bands of responsivity are clearly indicated. The maximum response is seen to occur at 1·7 eV. In order to find the activation energies, the observed results were separated into two component bands to find the point where the response has fallen to half value for each component band. Such a procedure has been described by MOSS.[10] The activation energy was found to be 1·51 eV for the main band and 1·17 eV for the secondary band. These values are seen to correspond closely to the energy gap values that were deduced for the direct and indirect band transitions in the analysis of the single crystal absorption data. However, in the case of the secondary band the magnitude of the response at the extrapolated peak is seen to be nearly one half that of the main band. This result is difficult to reconcile with the low absorption of the crystal in this wavelength region, unless the absorption of the polycrystalline film is much greater than that of the single crystal of equal thickness. There is a possibility that the photoconductivity and the absorption in this region are associated with another principal band gap in the complete band structure of the crystal.

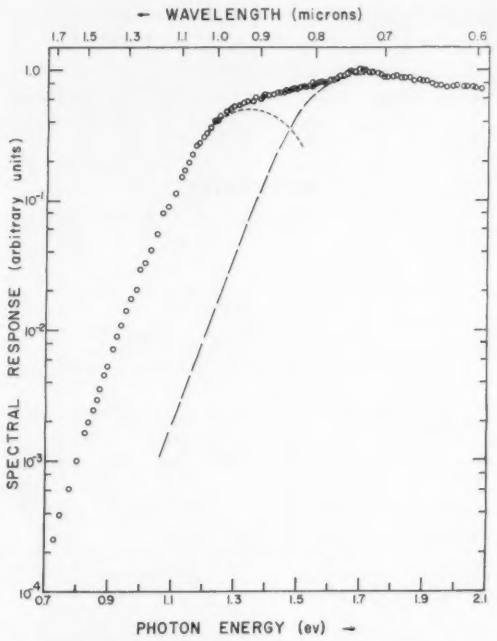

FIG. 5. Photoconductive spectral response as a function of photon energy for an evaporated film of GeSe with the two bands of responsivity indicated by the dashed lines.

CONCLUSIONS

The shape of the optical absorption edge in GeSe has been determined experimentally by transmission measurements between 0·449 and 1·20 microns. A detailed analysis of the absorption edge in the high absorption region shows that the absorption coefficient is proportional to $(h\nu - 1{\cdot}53)^{3/2}$ for direct band transitions over a remarkably large range in photon energy. Possible evidence for indirect transitions has also been shown. The analysis of the photoconductive spectral response curve for a thin film of GeSe also indicates that the principal band gap for the

material is in the neighborhood of 1·5 eV. It is interesting to note that the activation energy for the secondary band of responsivity agrees with the band gap indicated for indirect transitions.

Samples thin enough to investigate optical absorption in either of the other two principal crystallographic directions have not been successfully prepared. The fact that the thicker crystals are inhomogeneous has made it impossible to obtain any reliable conductivity or Hall measurements on the single crystal material. Crystal growth and optical absorption in GeSe are quite similar to the corresponding properties exhibited by germanium sulfide.[11]

REFERENCES

1. Okazaki A., *J. Phys. Soc. Japan* **13,** 1151 (1958).
2. Kannewurf C. R., Kelly A. and Cashman R. J., *Acta Cryst.* **13,** 449 (1960).
3. Asanabe S. and Okazaki A., *J. Phys. Soc. Japan* **15,** 989 (1960).
4. Fan H. Y. and Becker M., *Semiconducting Materials* (edited by Henish H. K.) p. 132. Butterworths, London (1951).
5. Brooks H., *Advances in Electronics and Electron Physics*, Vol. VII. Academic Press, New York (1955).
6. Bardeen J., Blatt F. J. and Hall L. N., *Photoconductivity Conference*, (edited by Breckenridge R. G., Russell B. R. and Hahn E. E.) p. 146, John Wiley New York (1956).
7. Dexter D. L., *Phys. Rev.* **101,** 48 (1956).
8. Fan H. Y., *Rep. Progr. Phys.* **19,** 107 (1956).
9. Dresselhaus G., *Phys. Rev.* **105,** 136 (1957).
10. Moss T. S., *Photoconductivity in the Elements*. Butterworths, London (1952).
11. Betz C. R., thesis, Northwestern University (1958).

DISCUSSION

R. H. Bube: There is a striking similarity between the crystallographic, optical, and electrical properties of GeSe and those of GaSe and GaS. This similarity extends to the layer-type structure, the multiple photoexcitation peaks, and the preponderance of *p*-type conductivity in the selenide.

G. K. Gaule: (1). Could you give an estimate of rise and decay times? (2) Could you give an estimate of the dark conductivity?

C. R. Kannewurf: (1). The rise and decay times are equal, about 3 milliseconds. (2). Preliminary work on the single crystal material indicates an electrical conductivity of approximately 1·2 $(\Omega\text{-cm})^{-1}$ (see Ref. 3).

D. L. Mitchell: Measurements of the optical absorption of the related compound SnSe were performed at Syracuse University and they do exhibit a polarization dependence. SnSe is birefringent over a wide range of wavelengths, and is dichroic from the absorption edge (0·86 eV) to a value of the absorption coefficient $\alpha = 1{\cdot}5 \times 10^4\ \text{cm}^{-1}$ (1·2 eV).

Only *p*-type conductivity has been observed in SnSe. What type of conductivity do you observe in GeSe?

C. R. Kannewurf: Optical measurements on GeSe discussed in this paper did not employ polarized incident radiation. All material prepared thus far has been *p*-type.

Vol. 22
1961

J. Phys. Chem. Solids Pergamon Press 1961, Vol. 22, pp. 299–307. Printed in Great Britain.

A COMPREHENSIVE STUDY OF A SIMPLE PHOTOCONDUCTIVE PHOSPHOR

H. FEDDERS, M. HUNGER and F. LÜTY

II. Physikalisches Institut der Technischen Hochschule Stuttgart, Germany

ALKALI halide crystals, containing *F*-centers as the only (additionally added) point imperfections, have been known for a long time to be a very simple and clear example of an extrinsic photoconductor.[1,2] There have been several attempts[3–5] to correlate the photoconductivity measurements with the electron transitions observed in absorption,[6,7] which lead at least to a qualitative understanding of the processes involved.

In the last few years a characteristic emission of *F*-centers was discovered,[8,9] which recently was shown to be divided into two limiting cases: *F*-center fluorescence and *F*-center phosphorescence.[10] These emission results and new photoconductivity data presented here now establish—together with the older center conversion experiments (which were carefully repeated)—a wide range of experimental data which make it possible to approach a *quantitative* description of the system by a model of a simple photoconductive phosphor. As experiments towards this aim are still under way, this report is still of an intermediate nature.

The system described here is KCl, in which by additive coloration[11] some 10^{16} cm^{-3} *F*-centers were introduced. These *F*-centers can either—by light absorption—lose an electron, leaving behind an empty anion vacancy, the so called α-center, or capture a second electron, forming the so called *F'*-center. The models of these three centers involved, their characteristic absorption bands and their possible reactions with light and electrons are illustrated in Fig. 1. All measurements are restricted to temperatures lower than -100°C, where thermal instability of *F'*-centers and secondary ionic processes are avoided.

All electrons being located first as *F*-electrons in the vacancies the first step is the optical excitation by irradiation in the *F*-band. Figure 2 shows in curve *A* the temperature dependence of the initial quantum yield η for *F*-center ionization under *F*-light irradiation, first measured by PICK[6]. This process reaches full efficiency at about -100°C. It can quantitatively be understood by the assumption that *F*-light irradiation raises the *F*-electron into an excited bound state *F**, from where it can either be thermally released to the conduction band (the probability being given by an Arrhenius type equation), or with constant probability fall back into the ground state F_o. Our measured $\eta(T)$ should be the ratio of transitions to the conduction band to the sum of all transitions, which leads to equation (1) in Fig. 2. A plot of $1/\eta - 1$ logarithmically over the inverse temperature produces—as expected from equation (1)—a straight line whose slope gives the value *U* for the distance of the *F**-level from the conduction band for thermal excitation.

Investigating the *F*-emission in the first moment of the optical excitation of the pure *F*-center system, we find a dependence of its initial quantum efficiency on temperature plotted in curve *B*, Fig. 2. This observed emission must be ascribed to a radiative back process of the excited *F*-electron, that means a pure *F-center fluorescence*. Its temperature dependence can quantitatively be accounted for by the assumption that the number of radiative transitions is determined by the number of *F**-electrons not thermally released into the conduction band. This means that $\eta_{fluor} = 1 - \eta$, which is well confirmed by the analysis in Fig. 2b.*

The electron, optically released from the *F*-center, can be captured by other *F*-centers, forming an *F'*-center (see Fig. 1). Under best conditions, one can convert a pure *F*-center system into about

* See, however, discussion at the end of the paper.

40 per cent F', 40 per cent α and 20 per cent remaining F-centers. In such an optically converted system, light irradiation into the F'-band releases easily one of the weakly bound F'-electrons, the quantum efficiency for the electron freeing being unity in all temperature ranges.[6] Three processes can be observed together with this F'-irradiation.

(3) Irradiation into the F'-band is accompanied by a photocurrent first measured by DOMANIC[12]. In Fig. 4(b) is illustrated what we expect for this photocurrent under the assumption that the released photo-electrons are only captured by either α-centers (with the capture probability (a) or by F-centers (with the capture probability f). Our measurements [Fig. 4(a)] confirm what is

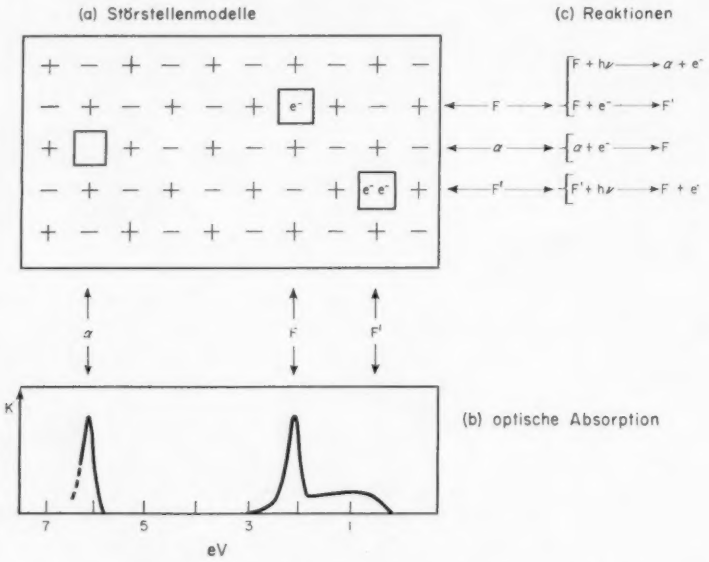

FIG. 1. Microscopic models, absorption bands and reactions of the three point imperfections treated here: F, F' and α-centers.

(1) The optically released electrons can be captured by empty anion vacancies and form F-centers again as one can see from the change in the absorption spectra. The initial quantum efficiency for this process $\eta_{F'-F}$ (first measured by PICK[7]) is shown in its temperature dependence in Fig. 3a.

(2) The capture process of an electron into an empty anion vacancy is accompanied by the emission of a light quantum[10] as shown in Fig. 3(b). The quantum yield of this emission, which we call *F-center phosphorescence*, runs exactly parallel to the capturing process [Fig. 3(a)], the spectral distribution of it being the same as that of the F-fluorescence, treated before (Fig. 2).

expected from the model: the inverse photocurrent varies at fixed temperatures linearly with the ratio of F/F' concentration, demonstrating that only the two traps, F and α, are limiting the schubwege. Taking from the measurements the intercept A of our curves with the ordinate and the slope B of the curves, the ratio A/B gives us directly the ratio of capture cross-sections a/f of the α- and F-traps as one can see from equations 4 and 5, Fig. 4(b).

This result can be used now to analyze the measured $F'-F$ and F' phosphorescence quantum yield (Fig. 3). Writing down the expected relative probability for an electron optically released from F' to be captured in an anion vacancy, $W_{F'-F_0}$,

Vol. 22
1961

(which is half the quantum efficiency $\eta_{F'-F}$), we find that this probability should depend only on the ratio of trap concentrations and the ratio of capture cross-sections a/f, [Fig. 5(a) equation 6].

Before making this analysis we try to understand first more about the mechanism of the capture process. It was assumed already in several papers,[3,4] that the capture process of an electron into the empty vacancy is going via an excited state of the F-center. Our observation that the phosphorescence connected with this capture process is spectrally the same as the F-fluorescence

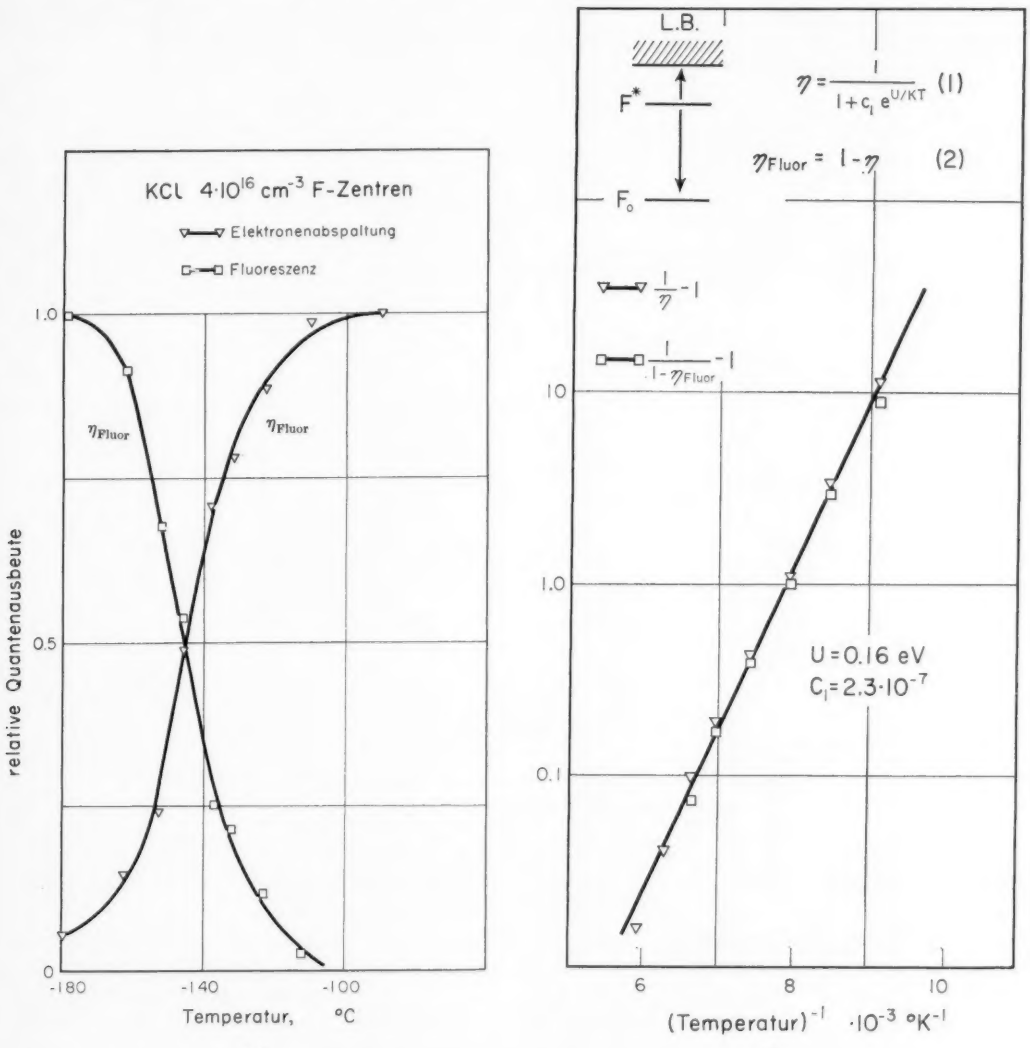

FIG. 2. (a) Relative quantum efficiency of F-center ionization (η) and of F-center fluorescence η_{Fluor} under F-light irradiation in dependence on temperature.
(b) Plot of the measured η and η_{Fluor} in such a way as to produce straight lines according to equations (1) and (2).

[occuring between the F^*- and F_o-levels (Fig. 2)] confirms this assumption experimentally. So instead of a capture probability "a" into the F_o ground state we better define a capture probability "a^*" of the electron into the excited state F^*. The relative probability $W_{F'-F^*}$ that this process occurs λ probability it goes into an F^*-level, from here with $1-\eta$ under irradiation into the ground state. That part $\eta \cdot \lambda$ which was thermally re-emitted has again a chance of $\lambda(1-\eta)$ to be trapped into another F^* and to go now to the F ground state—and so on. Summing up these probabilities we

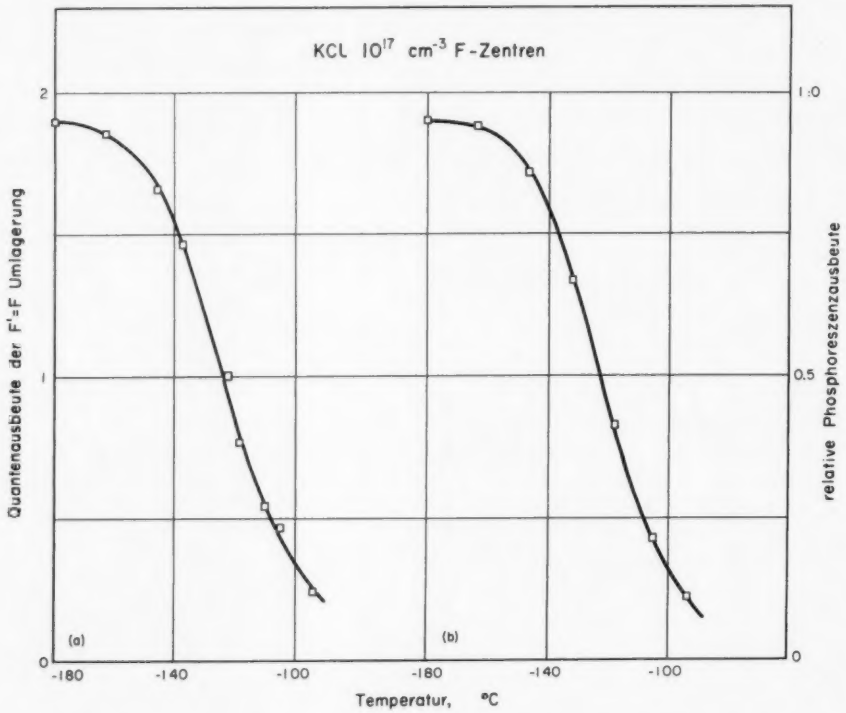

FIG. 3. Temperature dependence of the quantum yield for (a) $F'-F$ conversion under F'-light irradiation; (b) F-phosphorescence under F'-light irradiation.

after F'-irradiation is written down in Fig. 5(b), equation (7), and called λ. From the measurement and analysis in Fig. 2, we know what happens to an electron in the excited F-state F^*: with $\eta(T)$ relative probability it is thermally emitted, with $1-\eta(T)$ it returns under light emission to the ground state. Assuming that the same probabilities hold for a conduction electron which became captured into the F^*- state, it is easy now to sum up the total probability of an ionized F'-electron to be really captured into a vacancy [equation (8)]: with end up with an expression for $\eta_{F'-F}$ [equation (9)] which compared with equation (6) shows that the former effective capture probability "a" into the F ground state is to be replaced by the probability "a^*" for the real present capture process into the F^*-level times a function $1-\eta(T)$ which accounts for the temperature dependent re-emission properties out of this state.

Figure 6(a) shows (circles) our measured a/f ratio from Fig. 4 plotted against temperature. This a/f should be replaced now by an expression

Vol. 22
1961

$a^*(1-\eta)/f$. [equation 10]. Comparing the measured a/f values with a function const. $(1-\eta)$—obtained from our measured $\eta(T)$ in Fig. 2—we find that $a/f \approx$ const. $(1-\eta)$ if we choose const. = 6. So we end up with a very clear result: the strong temperature dependence of our measured a/f is explained in the new description quantitatively by the function $1-\eta$, which accounts for the re-emission properties after the capture process into the excited F^*-state. *The ratio of capture cross sections of the two really effective shallow trap levels F^* and F' is independent of temperature and has the value of* 6.

We have now to check if our measured $a/f = a^*(1-\eta)f$ can explain the observed $F'-F$ conversion and F-phosphorescence. Taking the expected function for $\eta_{F'-F}$ [equation (9) from Fig. 5], putting in $a^*/f = 6$ and $F'/F = 2$ (which was used in our measurement), we end up with equation (11), Fig. 6(b), which as shown in the diagram below fits very well the measured quantum yield $\eta_{F'-F}$. The same considerations hold for the F-phosphorescence [Fig. 6(c)] and here too the measured values are in good agreement with the expected curve.

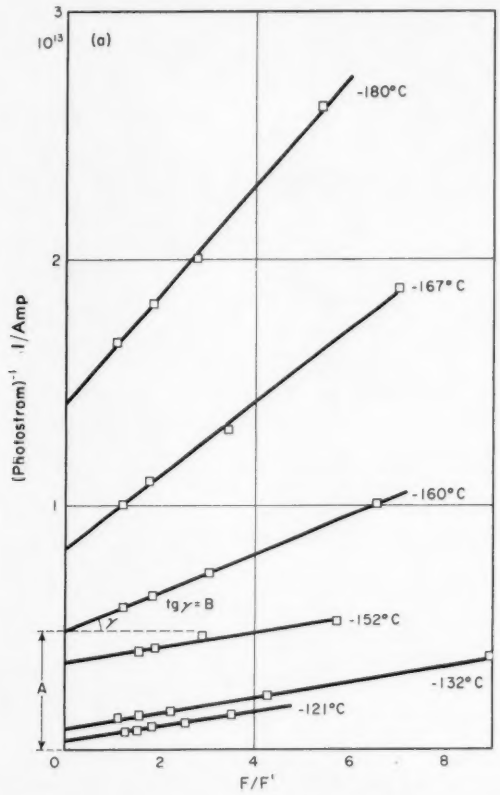

FIG. 4. (a) Inverse transient photocurrent under F' irradiation in dependence on the ratio of concentration of F to F'-centers for different temperatures.

Summarizing we can say that the capture process of electrons into the empty vacancy, as we measure it in a highly temperature dependent $F'-F$ conversion, F-phosphorescence and F'-

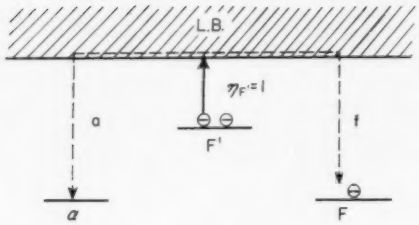

$$i_F = c_1 \cdot \mu\ (T)\ \frac{I_0 - I}{F \cdot f + \alpha \cdot a} \tag{3}$$

$$\alpha = F'$$

$$(I_0 - I) \approx c_2 \cdot F'$$

$$i_{F'} = c_3\ \mu\ (T)\ \frac{F'}{F\ f + F'\ a}$$

$$\boxed{\frac{I}{i_{F'}} = \frac{C}{\mu(T)} \cdot \left(a + \frac{F}{F'} \cdot f\right)} \tag{4}$$

$$= \quad A \quad + \quad \frac{F}{F'} \cdot B$$

$$\boxed{\frac{a}{f}\ (T) = \frac{A\,(T)}{B\,(T)}} \tag{5}$$

FIG. 4. (b) Expected behavior of the F-photocurrent under the assumption of full efficient optical electron release from F'-centers ($\eta_{F'} = 1$) and capture processes in F- and α-centers only.

α, F, F' denote concentrations of the corresponding centers
μ electron mobility
a capture probability into the α-center.
f capture probability into the F-center
$I_0 - I$ absorbed light energy (which for small optical densities is proportional to the F'-center concentration).

Vol. 22
1961

photocurrent, can be quantitatively understood by a model implying:

(1) "pre-capture" of the electron in the excited state F^* with following thermal re-emission or radiative transition $F^* - F_0$;

(2) temperature independent ratio of capture cross sections of the F^*- and F'-levels $a^*/f = 6$.

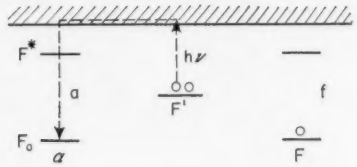

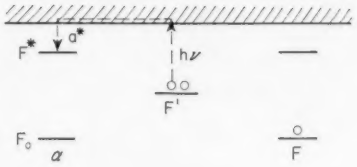

$$W_{F'\to F_0} = \frac{F'a}{F'a + Ff} = \frac{1}{1 + Ff/F'a} \qquad (6)$$

$$= \frac{1}{2}\eta_{F'\to F}$$

$$W_{F'\to F^*} = \frac{1}{1 + Ff/F'a^*} = \lambda \qquad (7)$$

$$\frac{1}{2}\eta_{F'\to F} = \lambda(1-\eta) + \eta\lambda^2(1-\eta) + \eta^2\lambda^3(1-\eta) + \cdots \qquad (8)$$

$$= \lambda(1-\eta)\left[1 + \lambda\eta + (\lambda\eta)^2 + (\lambda\eta) + \cdots\right]$$

$$= \frac{\lambda(1-\eta)}{1-\lambda\eta}$$

$$= \frac{1}{1 - \frac{Ff}{F'a^*(1-\eta)}} \qquad (9)$$

$$a(T) = a^*(1-\eta) \qquad (10)$$
$$f/a^* = \text{const}$$

FIG. 5. (a) Description of the $F'-F$ conversion using an effective capture probability "a" into the F ground state. (Other letters used as in Fig. 4.) (b) Description of the $F'-F$ conversion by a capture probability a^* into the excited state F^*, followed by transition probabilities η and $1-\eta$ analyzed in Fig. 2.

It was shown several years ago[13] that the excited F-electron can cross the energy gap between the F^*-level and the conduction band not only by thermal emission processes but by electric field emission too. So instead of $\eta(T)$ one can measure a function $\eta(E)$ which now according to the above considerations should effect *all* electron transitions of our system. A thorough investigation of the influence of high electric fields on all electron transitions has just been finished[14] and confirms strongly the model described above.

REFERENCES

1. GUDDEN B. and POHL R. W., *Z. Phys.* **31,** 651 (1925).
2. GLASER G., *Nachr. Ges. Wiss. Göttingen* **3,** 31 (1937).
3. MOTT N. F. and GUERNEY R. W., *Electronic Processes in Ionic Crystals.* Oxford University Press (1940).
4. MARKHAM J. J., *Phys. Rev.* **88,** 500 (1952).
5. SEITZ F., *Rev. Mod. Phys.* **18,** 392 (1946).
6. PICK H., *Ann. Phys.* **31,** 365 (1938).
7. PICK H., *Ann. Phys.* **37,** 421 (1940).
8. BOTDEN TH., VAN DOORN C. Z. and HAVEN Y., *Philips Res. Rep.* **9,** 469 (1954).
9. BECKER K. H. and PICK H., *Nachr. Akad. Wiss., Göttingen* **7,** 167 (1956).
10. LÜTY F., *Elektronenübergange in Farbzentren, Halbleiterprobleme VI.* Vieweg, Braunschweig (1961).
11. RÖGENER H., *Ann. Phys.* **29,** 386 (1937).
12. DOMANIC F., *Ann. Phys.* **43,** 187 (1943).
13. LÜTY F., *Z. Phys.* **153,** 247 (1958).
14. FEDDERS H. and LÜTY F., *Z. Phys.* (to be published).

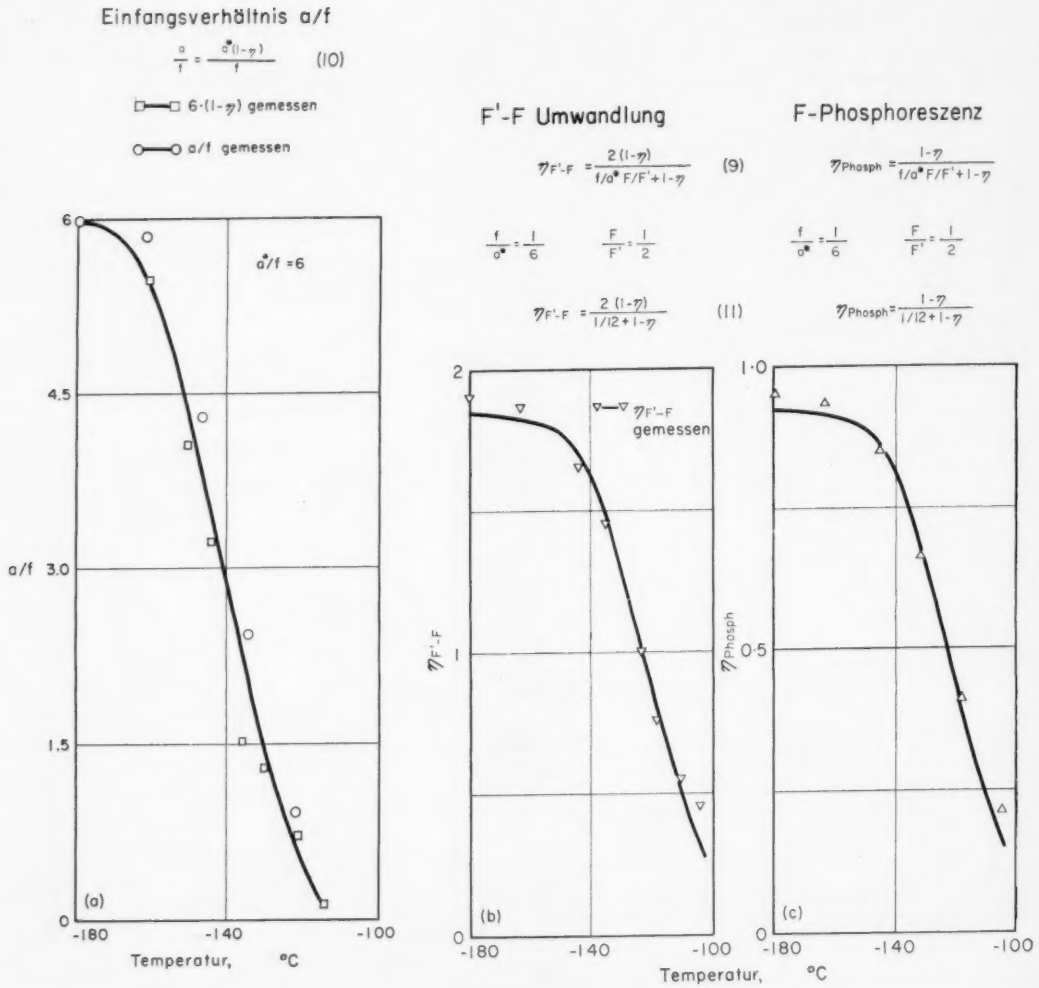

FIG. 6. (a) Comparison of the measured ratio a/f (from Fig. 4) with the values of $6 \cdot (1-\eta)$ in dependence on temperature. (b) Comparison of the measured $F'-F$ conversion with the expected curve [equation (9) from Fig. 5] using $a/f = 6\,(1-\eta)$. (c) The same as in (b) for F-phosphorescence. In all three cases $\eta(T)$ was obtained from the measurement in Fig. 2.

Vol. 22
1961

DISCUSSION

A. ROSE: (1) Are any of the transitions into the α-centers radiation-less? (2) What is the estimated capture cross section of electrons into the F^*-state?

F. LÜTY: (1) Firstly, the transition of a conduction electron into the F^*-state is—from all that we know and expect—radiation-less. For the transition $F^* - F_0$ it is a question of F center concentration. In very dilute systems ($< 10^{16}$ cm^{-3})—treated in this paper—practically all F^* electrons are either thermally released or make a radiative $F^* - F_0$ transition. Towards higher center concentrations more and more radiation-less transitions occur (e.g. at 10^{18} cm^{-3} F-centers about 80 per cent of all $F^* - F_0$ transitions are radiation-less[10]). The presence of radiation-less transitions seems so to be bound to some interaction effect between nearby centers.

(2) After absolute calibration of our equipment for absorbed light energy and taking the data of BROWN for the mobility $\mu(T)$, we can from Fig. 4 derive the absolute values and temperature dependence of both capture cross sections. This has not yet been done; from rough estimates we expect values of the order of 10^{-14} cm^2.

D. KAHN: (1) I would like to ask whether your curves of photocurrent contain the product of the carrier concentration and the schubweg, and have you been able to measure the efficiency of electron excitations of carriers into the conduction band?

(2) What voltage did you apply to your crystals?

F. LÜTY: (1) The curves in Fig. 4 are measured tranisent photocurrents, so containing the product of quantum yield η times schubweg w. We used, for the optical electron release, F'-centers which are known to have a value of $\eta_{F'} = 1$ for all temperatures, so we can easily determine the schubweg alone. These are, however, not primary ones but—as was shown—thermally prolonged by re-emission out of the F^*-state.

(2) We applied about 1000 V/cm.

BLANK
PAGE

Vol. 22
1961

J. Phys. Chem. Solids Pergamon Press 1961. Vol. 22, pp. 309–315. Printed in Great Britain.

PHOTOCONDUCTIVITY IN ZONE-REFINED KCl

H. KANZAKI, T. NINOMIYA and K. KIDO

The Institute for Solid State Physics, The University of Tokyo

Abstract—Photoconductivity measurements utilizing electrons excited from F centers have been performed on zone-refined KCl crystals containing various amounts of divalent impurity ions. At liquid nitrogen temperature, the electron range is determined by trapping by F centers in annealed crystals containing less than 1×10^{14} cm^{-3} of divalent impurities. Divalent ions of 10^{17} cm^{-3} produce additional electron traps equivalent to 1×10^{16} cm^{-3} of F centers, and dislocations produce traps equivalent to 1 to 2×10^{16} cm^{-3} F centers at this temperature. At -120°C, however, the electron range is exclusively determined by F centers alone, irrespective of divalent impurities or dislocations. Dependence of photoresponse with temperature and high electric field strength was also studied by excitation of light in the F and K bands. Both types of dependence are different for the two bands and it is concluded that the excited level corresponding to F excitation has a lower energy than that associated with K excitation.

1. INTRODUCTION

EXPERIMENTAL studies on alkali halide crystals of the highest purity are in progress in our group in order to clarify the fundamental properties of ionic crystals, especially those related to various types of lattice imperfections. Photoconductivity experiments on zone-refined KCl will be reported in this paper and the main emphasis will be placed on the following two lines of study. The first is the nature of electron traps at various temperatures. It is known that the range of conduction electrons in alkali halides is several orders of magnitude shorter than in other ionic crystals—silver and thallous halides, for example. It is still an open question to what extent such a short range of electrons and holes is an intrinsic property of alkali halides and how the value is influenced by lattice imperfections. The photoconductivity measurements on alkali halides of high purity containing F centers to be described here will be a first step in the solution of the problem. The second problem is the nature of the optical transitions associated with color centers. It is well known that the photoconductivity experiments due to excitation of F centers carried out at Göttingen[1] were experiments in determining the electronic structures of F and F' centers. There are several companion bands due to trapped electrons other than F centers—K, R, M and L bands—whose electronic structures are not yet fully understood. Photoconductivity experiments on F and K bands will be reported here as one of the studies to clarify the nature of optical excitation of these color centers.

2. OUTLINE OF EXPERIMENTS

Single crystal ingots of KCl have been obtained by successive application of chemical purification, vacuum distillation, and zone refining.

Original material was prepared from reagent grade $KHCO_3$ and purified HCl. KOBAYASHI and TOMIKI[2] discovered that this procedure is very effective for removing bromine impurity in KCl. According to measurements of fundamental absorption by Dr. TOMIKI, concentration of bromine impurity in our best crystal is as low as their best crystal [KCl–ak–1 in Ref. (2)]. Next step of purification by vacuum distillation was reported previously.[3] In this experiment, KCl powder was melted in a purified chlorine atmosphere before distillation. The distilled product was sealed in a purified chlorine atmosphere of about 300 mm Hg and transferred to a zone refining apparatus. Zone melting was performed in a two-zone furnace moving at 6 mm/hr. By a suitable choice of temperature gradient and also by adopting two final zone passes with the very low speed of 2 mm/hr, entire ingots turned out successfully to be single crystals.

The value of ionic conductivity in the extrinsic range of temperature varies by a factor of 10^4 along the ingot axis. The residual content of divalent

ions can be estimated to be at most 1×10^{14} cm^{-3} for half of the ingot (1 cm in width and 15 cm in length) subjected to 25 zone passes.[4] Specimens of about $4 \times 4 \times 1$ mm were cleaved from various locations along the ingot and used for photoconductivity and optical absorption experiments.

Photoconductivity experiments utilizing electrons excited from F centers have been performed in order to clarify the nature of electron traps in these highly purified crystals. Various amounts of F centers were introduced either by additive coloration or by irradiation of penetrating X-ray at room temperature (40 kV, 10 mA, tungsten target with aluminum filter 1 mm thick and exposed from both sides). Primary photoconductivity has been measured by using monochromatic light pulses of 0·1 sec from a Hitachi spectrophotometer and a vibrating reed electrometer (Model 31, Appl. Physics Co.). The amount of induced charge per light pulse is at most 10^{-14} to 10^{-13} coulombs cm^{-2} at a field strength of 0·5 to 1×10^3 V/cm^{-1}. Evaluation of ηw_0 (quantum yield times unit range) from the measured value of induced charge was done in the manner described in the paper by VAN HEYNINGEN and BROWN.[5] Optical absorption measurements were made at room temperature and at liquid nitrogen temperature soon after the photoconductivity measurements.

The cryostat and sample holder are nearly the same as those used by INCHAUSPÉ[6] except that a NESA coated quartz plate was used as one of the electrodes and Mylar films were used to block both electrodes. The absolute value of light intensity was measured directly by a Bi–Ag thermopile (Eppley Lab.) calibrated by NBS.

In the first series of experiments to be described in 3a, dependence of ηw_0 upon temperature (78°K to 220°K) for excitation at the F band peak has been studied as a function of F center concentration (2×10^{15}–1×10^{17} cm^{-3}). The main problem in this case is to study the dependence of w_0 upon F center concentration at a fixed temperature where η is fixed in order to clarify the nature of the electron traps.

In the second series of experiments to be given in 3*b*, dependence of ηw_0 upon temperature has been studied for excitation at various wavelengths corresponding to F and K bands. The main interest here is to study the dependence of η upon exciting wavelengths in the same specimen where w_0 is fixed. The results are discussed in relation to the nature of the optical transitions associated with the F and K bands. The field ionization effect previously studied by LÜTY[7] for bleaching and luminescence of F centers is also studied by measuring the photoresponse at high electric fields. The difference of the high field effects between F and K bands is also discussed from the same standpoint.

3. RESULTS AND DISCUSSIONS

3a. *Photoconductivity due to F bands*

The general behavior of ηw_0 with temperature for excitation by light in the F band peak (550 mμ) is the same as the Göttingen results.[1] Fig. 1

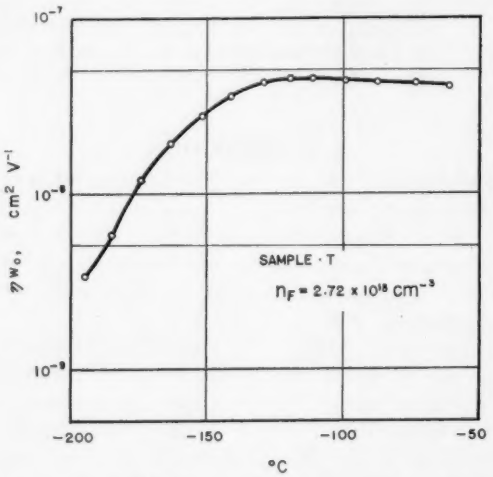

FIG. 1. ηw_0 against temperature for X-rayed crystal T from purest part of the ingot. Excitation by F band peak.

shows the results for a specimen taken from the purest part of the zone-refined ingots (containing divalent ions less than 1×10^{14} cm^{-3}, called "pure specimens" in the following) and Fig. 2 is for a specimen taken from an impure part of the ingot (divalent ions 10^{17} cm^{-3}, called "impure specimen"). Specimen T of Fig. 1 and specimen R of Fig. 2 were exposed to X-rays under exactly the same condition and amount of exposure. Different concentrations of F centers of $2{\cdot}7_2 \times 10^{15}$ cm^{-3} of T and $3{\cdot}2_5 \times 10^{15}$ cm^{-3} of R show the difference of X-ray darkenability at room temperature.

In the earlier stages of the experiments, it was found that the electron range at liquid nitrogen

Vol. 22
1961

temperature is very sensitive to the density of dislocations. Figure 3 shows an example which illustrates the remarkable decrease of ηw_0 below -150°C. The F center density $9{\cdot}1 \times 10^{15}$ cm^{-3} of this sample P is to be compared with those of the T and R samples described above. Such a parallelism of high darkenability at room temperature and short

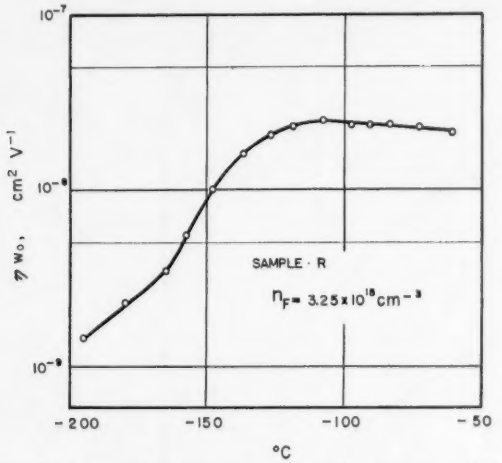

FIG. 2. ηw_0 against temperature for X-rayed crystal R from the impure part of the ingot. Excitation by F band peak.

electron range at liquid nitrogen temperature is a definite feature of X-rayed KCl crystals with a high density of dislocations. All of the specimens, except otherwise stated, to be described below, including specimens T and R of Figs. 1 and 2, have been annealed at 450°C in a purified nitrogen atmosphere after being cleaved from the ingots, cooled to room temperature at a rate of 10–20°C/hr and then X-rayed.

Figure 4 shows ηw_0 against F center concentration on various crystals studied at -120°C and -180°C.

(1) Values of ηw_0 at -120°C are inversely proportional to the F center concentration, irrespective of impurities and dislocations. Even the sample P of Fig. 3 fits on the straight line. Electron traps at -120°C are exclusively F centers.

(2) The situation is different at -180°C. Various kinds of electron traps are operative in addition to F centers. They are related to divalent ions and dislocations and will be discussed one by one in the following. It is clearly seen that these various traps are masked completely by F centers at -120°C. In other words, it is important to notice that changes in the nature of the electron traps can occur in the temperature range between -180°C and -120°C where the quantum yield η for producing conduction electrons from the excited state of the F centers also changes.

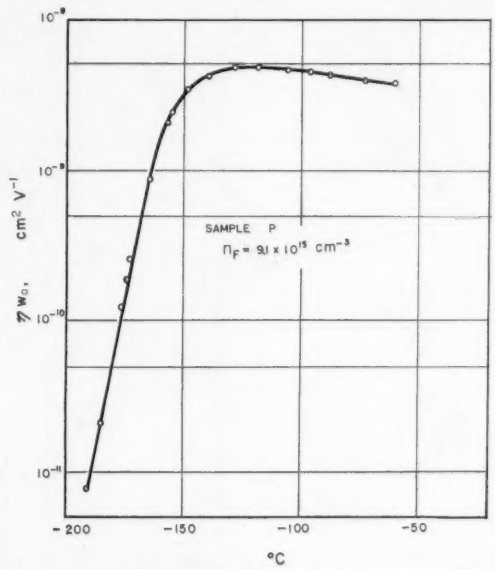

FIG. 3. ηw_0 against temperature for X-rayed crystal P containing a high density of dislocations.

Proportionality between ηw_0 and $1/n_F$ holds, however, in the case of *annealed* "pure" crystals (T_1b, X, T, N, T_1a, θ_1) at -180°C. The electron traps at -180°C are F centers only in these relatively perfect crystals.

(3) In the case of annealed "impure" specimens (R_1b, R, R_1a, θ_2), the following relation holds approximately

$$\eta w_0 \propto 1/n_F^{0.67}$$

at -180°C.

This result can be understood by assuming that divalent impurity ions of 10^{17} cm^{-3} produce electron traps in addition to F centers. This type of trap associated with divalent ions is equivalent to F centers of 1×10^{16} cm^{-3} at -180°C. This means that the value of trapping cross section per divalent ion is at most one-tenth that of an F center at this temperature.

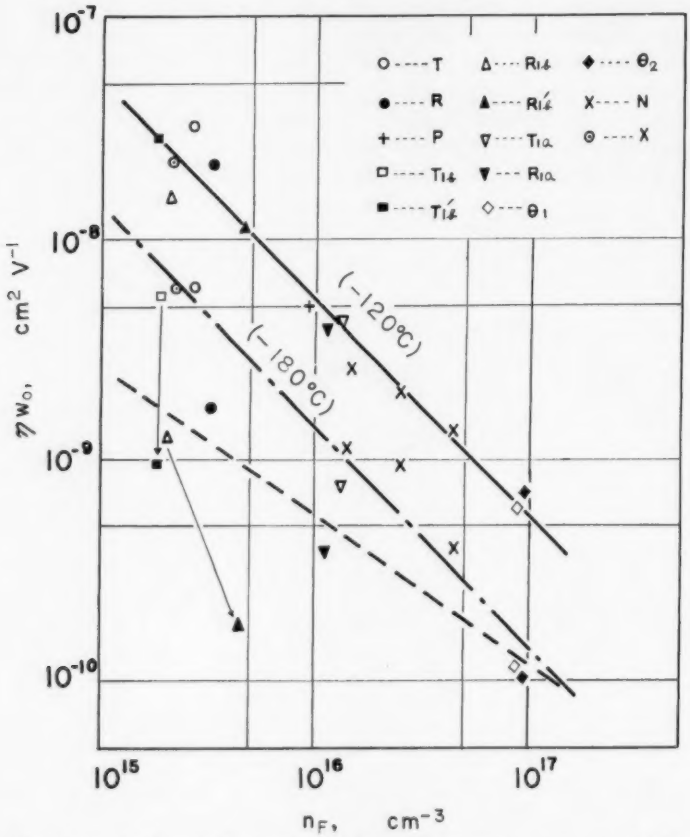

FIG. 4. $\eta\omega_0$ for F excitation against F center concentration n_F at −120°C (upper group) and −180°C (lower group).
Specimens T, T$_I$b, T$_I$a, and N are annealed pure crystals X-rayed. θ_1 and X are annealed pure crystals colored additively.
R, R$_I$b and Ra are annealed impure X-rayed. θ_2 is annealed impure colored additively.
Specimens T$_I$b′ is deform-and-annealed T$_I$b and X-rayed. R$_I$b′ is deform-and-annealed R$_I$b and X-rayed. P is pure crystal with high dislocation density and X-rayed.

(4) Results for specimen T$_I$b′ and R$_I$b′ in Fig. 4 are those of control experiments for examining effects of dislocation densities upon electron range. Specimens T$_I$b ("pure") and R$_I$b ("impure") were subjected to plastic deformation by 20 per cent compression at room temperature, then annealed in a purified nitrogen atmosphere at 410°C for 10 hr, and slowly cooled to room temperature. The density of dislocations in specimens thus treated* is estimated to be 1×10^7 lines cm^{-2} for both T$_I$b′ and R$_I$b′ from etch pit countings. This value is almost ten times larger than that for T$_I$b and R$_I$b of 2–3×10^6 lines cm^{-2}.[4]

Comparison of T$_I$b and T$_I$b′, and also R$_I$b and R$_I$b′ will give the effect of dislocations of 10^7 lines cm^{-2} with the impurity content fixed. It is clearly seen from Fig. 4 that the electron range at −180°C has been greatly reduced by increasing the dislocation density. Comparing T$_I$b with T$_I$b′, the

* Effects of this treatment upon ionic conductivity are to be published elsewhere.[4]

Vol. 22
1961

additional traps by dislocations are estimated to be equivalent to F centers of 1×10^{16} cm^{-3}. In R$_{\|}$b and R$_{\|}$b′, additional traps are equivalent to F centers of 2–$2{\cdot}5\times10^{16}$ cm^{-3}. Equivalence of dislocations of 10^7 lines cm^{-2} with F centers of 10^{16} cm^{-3} corresponds to a trapping cross section

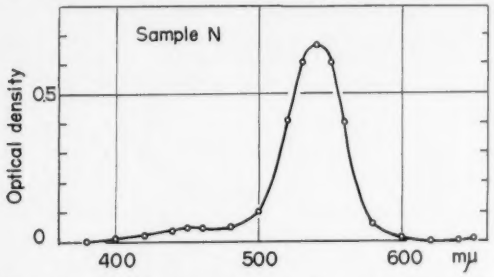

FIG. 5. Optical absorption of X-rayed sample N measured at liquid nitrogen temperature.

per atom along a dislocation line ten times larger than the cross section of an F center. This seems to suggest that the origin of dislocation trapping is a field around the dislocation line somewhat long-range in nature rather than jogs along dislocation lines. This type of trapping mechanism was first proposed by KAWAMURA and OHKURA[8].

Enhancement of darkenability due to dislocations is more pronounced in "impure" specimens (F center concentrations, R$_{\|}$b: 2×10^{16} cm^{-3} and R$_{\|}$b′: $4{\cdot}5\times10^{16}$ cm^{-3}) than in "pure" specimens (T$_{\|}$b : 2×10^{16} cm^{-3} and T$_{\|}$b′ : 2×10^{16} cm^{-3}), all of which were subjected to the same X-ray exposure. Taking these results into account, we might guess that effects of divalent ions upon electron range at -180°C and X-ray darkenability at room temperature is, to some extent, due to the indirect effect of divalent ions upon dislocation structure. Some of these results may be related to charged dislocations which are believed to exist in this crystal.[4,9]

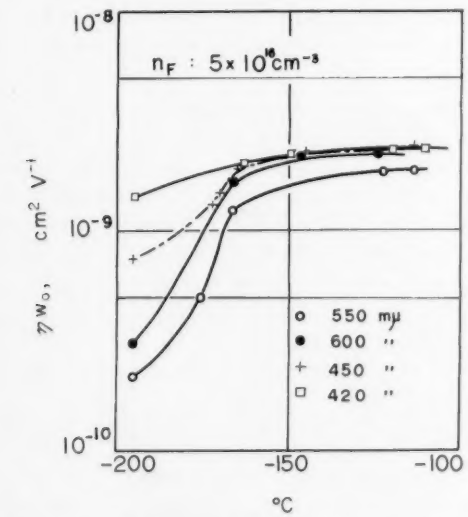

FIG. 6. ηw_0 for X-rayed sample N by excitation at various wavelengths: 600 and 550 mμ in F band, 450 and 420 mμ in K band.

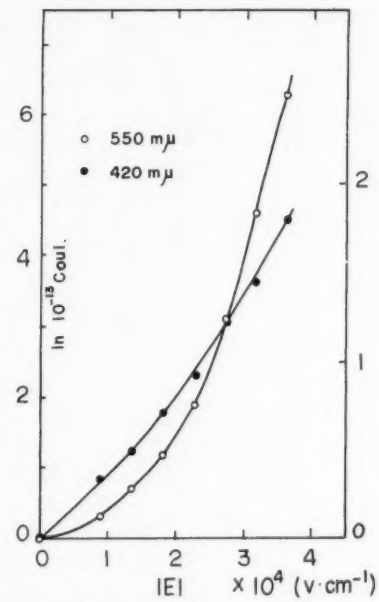

FIG. 7. Examples of induced charge per pulse against applied electric field. Right-hand ordinate is for 420 mμ and left-hand is for 550 mμ. Measured at liquid nitrogen temperature.

3b. *Photoconductivity due to F and K bands*

Figure 5 shows the optical absorption at liquid nitrogen temperature of "pure" crystal N X-rayed rather heavily (n_F: 5×10^{16} cm^{-3}). Photoconductivity of this specimen was measured as a function of temperature by exciting monochromatic light at various wavelengths, which are:

600 mμ (F band)
550 mμ (F band)
450 mμ (K band)
420 mμ (K band).

ηw_0 against temperature of these measurements are shown in Fig. 6. The results can be understood by assuming that the energy ΔE necessary for thermal excitation from the excited state to the conduction band is lower in the transition corresponding to K band than that in the F band transition. The value of ΔE for the F band transition can be estimated as about 0·06 eV from Fig. 6.

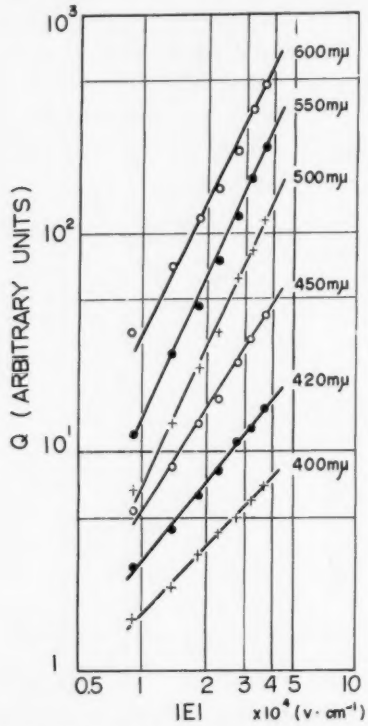

FIG. 8. Induced charge Q against field strength $|E|$ for excitation at various wavelengths in F and K bands. The scale of Q is changed for each curve.

In some of the experiments described above in Fig. 4 the temperature dependence of photoresponse was measured by excitation both at 550 mμ and 450 mμ for the same specimen. This confirmed that the observed temperature dependence of photoresponse below −150°C is partly due to change of electron range with temperature in addition to change of quantum yield, because the contribution from change of w_0 should be common to the measured value of ηw_0 for different exciting wavelengths.

If the value of ΔE is different between the F and K bands, the high field effect of the type studied by LÜTY[7] should be different. Fig. 7 shows one of the results for high field effect upon photoresponse. An annealed pure sample, 0·2 mm thick, subjected to weak X-ray irradiation was used in this experiment and voltages up to 800 V were applied at liquid nitrogen temperature.

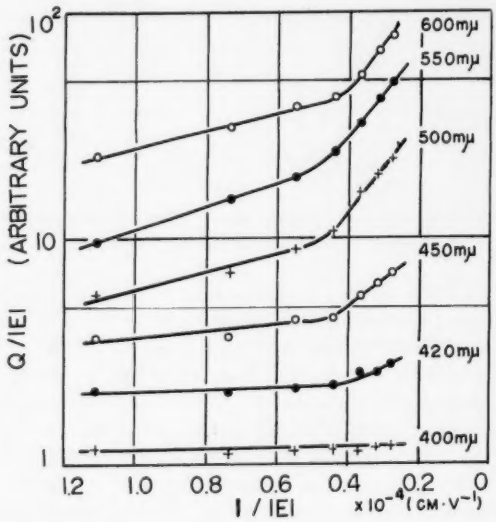

FIG. 9. $Q/|E|$ against $1/|E|$ for the data in Fig. 8. The scale for $Q/|E|$ is changed for each curve.

Experimental results for various exciting wavelengths on the same specimen are summarized in Fig. 8. It is seen that the induced charge Q per light pulse is proportional to $|E|^n$ where $|E|$ is the field strength. The value of n depends upon the exciting wavelength as follows:

wavelength (mμ)	600	550	500	450	420	400
n	2·02	2·17	2·17	1·54	1·19	1·02

In the F band region, n is close to 2 and decreases to 1 towards the K band.

According to the theory for field ionization by FRANZ[7a], the probability w of field ionization varies with field strength as follows,

$$w \approx \exp\left[-\text{const.}\,(\Delta E)^{3/2}/|E|\right] \qquad (1)$$

In photoconductivity measurements, neglecting

Vol. 22
1961

saturation effect, the number of conduction electrons produced is expressed as,

$$n \propto [Q/|E| \qquad (2)$$

Figure 9 shows the plot of $Q/|E|$ against $1/|E|$ for the results of Fig. 8. It is understood that the high field part in Fig. 9 corresponds to the type of field ionization expressed in equation (1) and the low field part is mainly governed by thermal ionization. In the F band region (600, 550 and 500 mμ), ΔE has a certain constant value and gradually decreases towards the K band region (450, 420 and 400 mμ). These results support the explanation for high field effect by field ionization, on the one hand, and the explanation for the K band transition as a transition to a higher excited state than the F band transition, on the other hand. Work is in progress for extending these observations to lower temperatures and also to other color centers.

Acknowledgements—The writers thanks are to Dr. T. TOMIKI for examining fundamental absorption of zone-refined KCl, to Dr. S. TAMURA for instruction in chemical purification and to Miss S. OHZORA for etch pit countings of specimens. It is our pleasure to record the value of co-operation with Professor K. KOBAYASHI.

REFERENCES

1. POHL R. W., *Proc. Phys. Soc.* (Suppl.) **49** 13 (1937).
2. KOBAYASHI K. and TOMIKI T., *J. Phys. Soc. Japan*, **15,** 1982 (1960).
3. KANZAKI H. and KIDO K., *J. Phys. Soc. Japan*, **15,** 529 (1960).
4. KANZAKI H., presented at the *International Conference on Chemical Physics of Nonmetallic Crystals*, Evanston, Illinois, September, 1961 (to be published).
5. VAN HEYNINGEN R. S. and BROWN F. C., *Phys. Rev.*, **111,** 462 (1958).
6. INCHAUSPÉ N., *Phys. Rev.* **106,** 898 (1957).
7. LÜTY F., *Z. Phys.*, **153,** 247 (1958).
7a. FRANZ W., *Handbuch der Physik* Band 7, S.155 Springer, Berlin.
8. KAWAMURA H. and OHKURA H., *J. Phys. Chem. Solids* **8,** 161 (1959).
9. ESHELBY J. D., NEWEY C. W. A., PRATT P. L. and LIDIARD A. B., *Phil. Mag.* **3,** 75 (1958).

BLANK
PAGE

Vol. 22
1961

J. Phys. Chem. Solids Pergamon Press 1961. Vol. 22, pp. 317–322. Printed in Great Britain.

PULSE AND STEADY PHOTOCONDUCTIVITIES OF COLORED ALKALI HALIDES

M. ONUKI* and H. OHKURA

Department of Applied Physics, Osaka City University, Osaka, Japan

Abstract—Measurements of pulse and steady photoconductivity were made on colored KBr and KCl in an attempt to investigate various kinds of electron traps in colored alkali halides. To investigate the space charge polarization effect which makes it difficult to measure the true photoconductivity of specimens, photocurrents produced by repeated light pulses under various conditions were observed. The frequency dependence of a.c. photocurrents under steady illumination was also investigated. From the above results, the condition of space charge free was found. The temperature dependence of the pulse photocurrent, the time constants of current-decay, and the a.c. photoconductivity under steady *F*-light illumination vs. its illumination level were measured under this condition. By applying trapping kinetics to the above results, three kinds of electron traps were found in colored KBr, one corresponding to *F*-centers and the other two to unknown centers. In KCl traps produced by photo-chemical reaction were found in addition to *F*-centers.

ALTHOUGH the photoconductivity in colored alkali halides has been investigated extensively by a number of workers, there seems to be few papers which deal with the trapping kinetics of photoelectrons in detail. This fact may be due to the difficulty in measuring an intrinsic bulk photoconductivity without any effects due to a space charge polarization. In the present work we made experiments on the pulse and steady photoconductivities of colored KBr and KCl under the condition of space charge free in the temperature range between −180°C and room temperature. This condition was realized by applying to the crystal an a.c. field and pulse illumination synchronized to the plus and minus peaks of the a.c. field. On the other hand the same condition also seems to be satisfied by using an a.c. field and steady illumination, when the frequency of the a.c. field is not too low. Using the above two methods, we measured pulse photocurrents with *F*-band light pulse of various conditions, and a.c. photocurrents under steady illumination of *F*-band light. The decay currents, after switching off the illumination, and the illumination level dependence of the steady a.c. photocurrent, were also studied at each temperature. From these results several kinds of electron traps were found in colored alkali halides. Crystals purified by a recrystallization technique and colored additively were used in this work.

Space charge formation occurs whenever charge carriers or vacancies accumulate near one or both electrodes. In the case of alkali halides, we can neglect the ionic space charge effect due to mobile ions because their mobility is lower than that of electrons at low temperatures. To investigate the electronic space charge effect, the variation of photocurrents in colored KBr with time caused by repeated pulse illumination were measured under the conditions of applying a.c. and d.c. fields. The a.c. field synchronized to the repeated light pulse led to constant magnitude of pulse photocurrents after applying the a.c. field. On the contrary, the pulse photocurrent decayed with time when the d.c. field was applied. From the observed decay time, it was concluded that the pulse photocurrent was decreased by the presence of the space charge field due to a charge of about $1{\cdot}5\times10^{-10}$ C/cm^2 flowing in one direction when a d.c. field of 10^3V/cm was applied.[1] Further, we measured the temperature dependence of pulse photocurrents in colored KBr under the following conditions; (1) the light pulses of 90 μsec duration and 30 rps were synchronized to both plus and minus peaks of the applied a.c. field (Case I), and (2) the light pulses of 90 μsec in duration and 30 rps were synchronized to either plus or minus peaks of the a.c. field (Case II). Figure 1 shows the results and the relations between the a.c. field and light pulses in the above cases. In the temperature region

* Now at the Tokyo Laboratories, Matsushita Electric Co., Tsunashima, Yokohama-City, Japan.

below −80°C the photocurrent in Case II was much smaller than that in Case I. This result indicates that at low temperatures the free charges swept to one direction become immobile and are accumulated near one of the electrodes, neither being drawn backward nor

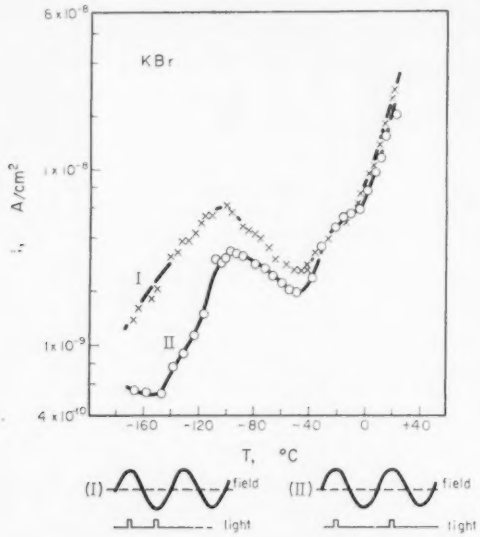

FIG. 1. The temperature dependence of pulse photocurrent. The conditions of synchronization between the periods of illuminations and the electric fields are different in the two curves. The relation of the position of the light pulses to the a.c. fields are shown in each case.

spread uniformly over the specimen by the a.c. field. The charge carriers may be trapped at a surface state near the electrode, the thermal depth of its level being estimated to be about 0·3 eV.[2]

In the a.c. measurement of photocurrents, the above trapping effect due to the surface state may be unimportant, because the steady illumination is applied in both plus and minus cycles of the a.c. field. Electrons which approach the anode surface in a half cycle of the a.c. field may fill the ionized F-centers (negative ion vacancies) which were formed near the surface in the previous half cycle, without filling the surface state. Thereby the surface regions of the specimen tend to be neutralized. However, it has been found that there are non-photoconducting layers between the electrodes and the specimen.[3] To investigate the property of these layers, the steady a.c. photoconductivity and the phase angle between the photocurrent and the applied voltage were measured, the frequency being varied from 20 c/s to 1000 c/s. Figure 2 shows the results, where $|G|$ is the absolute value of photoconductance and ϕ the phase angle. We can describe the equivalent circuit of the specimen as the one shown in Fig. 3, where G_∞ represents the conductance of the photoconducting region in the specimen, C_0 the geometrical capacity defined by the dimensions of the specimen, and C_1 and C_2 the capacities of the charge-free layers near the electrodes. From the values of C_1 and C_2, the thickness of the layer was estimated to be about 2×10^{-3} cm. The thickness of the layers was observed to change with time very slowly. For instance, the thickness of the layer was found to increase to about four times as large as the

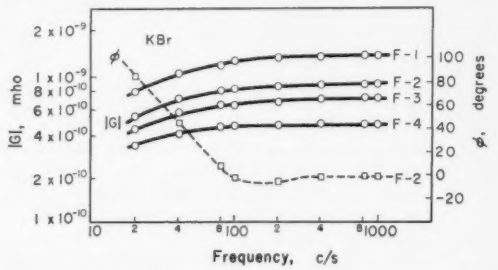

FIG. 2. The absolute value of photoconductance, $|G|$, and the phase angle, ϕ, between photocurrent and applied field vs. frequency in various illumination levels.

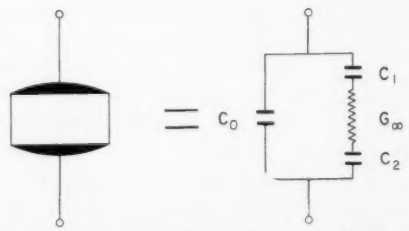

FIG. 3. The equivalent circuit of the specimen in the photoconducting state. In the circuit diagram, C_0 represents the capacity between the electrodes, G_∞ the conductance of the photoconducting region in the specimen and C_1 and C_2 the capacities of the charge-free regions near the electrodes.

initial value in a week after cleaving a bulk to a small specimen for use, while the value of G_∞ was decreased by as much as 10 per cent. The increase of the thickness of the layer is probably due to the creation of various traps near the surface introduced by the thermal bleaching of F-centers in the layer. An a.c. field whose frequency is at least higher than 200 c/s must be used in this case, in order to detect the true a.c. photoconductivity G_∞.

The pulse and steady photocurrents measured by the above methods were proved to be linearly dependent on the applied fields.

Generally speaking, the pulse photocurrents in colored alkali halides as a function of temperature

Vol. 22
1961

have been known to have the character shown in Fig. 4. The characteristic in the range β–γ in the figure is explained in terms of the quantum efficiency of excitation of F-center electrons to the conduction band. The temperature corresponding to point δ is described in terms of the thermal release of F'-center electrons created during the F-

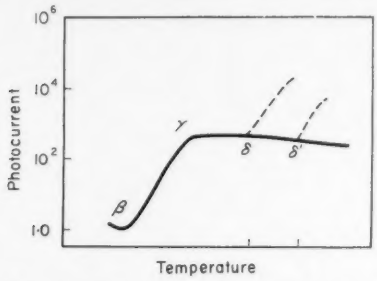

FIG. 4. The pulse photocurrent vs. temperature in the typical form.

band pulse illumination. Point δ shifts to the lower temperature side as the duration of the light pulse is increased, since the F'-electrons have more chance to be released thermally to the conduction band when pulsed illumination of longer duration is applied. This effect has been found by VON GERICKE for colored KCl.[4] We made experiments on this problem in detail for KBr by the methods of (1) a.c. field and pulse light and (2) a.c. field and steady light. The results are shown in Fig. 5. In the figure, Curves I, II and III are photocurrent vs. temperature curves for 30 μsec, 90 μsec and 800 μsec light pulse durations, respectively. The scale relationship among the different curves in the figure is arbitrary, and only their slopes are meaningful. The cusps at -32°C and $+2$°C in Curve 1 correspond to those at -50°C and -8°C in Curve II and to -74°C and -30°C in Curve III. On the other hand, the temperature-dependence of the 330 c/s a.c. photocurrent under steady illumination shown in Curve IV does not show a definite cusp.

A fast current-decay ($\leqslant 10^{-3}$ sec) after the pulsed illumination near the temperatures of O_2 and O_3 was observed in the measurement of pulse photocurrents. A slow current decay ($\geqslant 10^{-2}$ sec) after switching off the steady illumination above the temperature of O_1, was observed in the measurement of steady a.c. photocurrents. The time constants of the decays were decreased as the temperature was increased. This fact suggests that the current decays should be due to the thermal release of electrons trapped in various kinds of imperfection in the crystals. The observed time constant of the decay may be expressed in an approximation after HORNBECK and HAYNES as follows:[5]

$$\tau_\infty \simeq \tau_g\,(1+\tau_r/\tau_t), \qquad (1)$$

where $1/\tau_r$ is a rate of recombination of excess electrons in the conduction band or a rate of

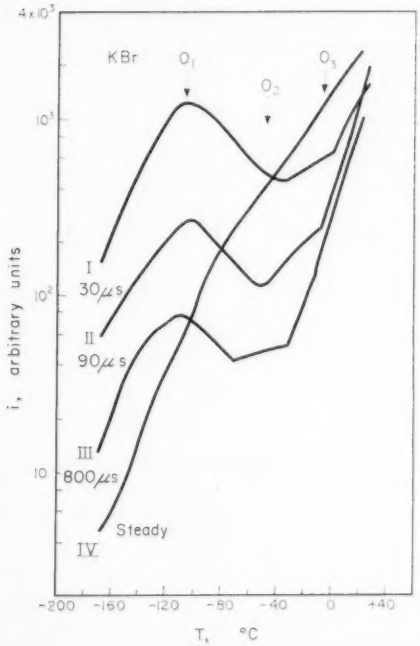

FIG. 5. The temperature-dependence of pulse photocurrent in various light durations (Curves I, II, and III), and that of steady a.c. photocurrent (Curve IV).

trapping by very deep traps, $1/\tau_g$ a rate of generation of electrons from the traps in question and $1/\tau_t$ a rate of trapping of electrons when all traps are empty. For example, the observed time constant of the slow decay τ_s as a function of the reciprocal of absolute temperature is shown in Fig. 6. The temperature dependence of the observed time constant τ_∞ may be mainly due to

τ_g in equation (1). We conclude that the slow decay-current can be explained by the thermal release of electrons in F'-centers, from the results of the experiment on the thermal life of electrons in F'-centers after PICK (see the dashed line in Fig. 6) and of the different behavior of Curve IV from Curves I, II and III in Fig. 5. From the observed temperature dependence of the slow decay current in Fig. 6 we found that the thermal activation energy of τ_s is 0·44 eV and the time factor of τ_s is 10^{-9} sec. In the present case τ_r is due to unknown centers, the density of which may be the order of $10^{15}/cm^3$. τ_t is due to the F-centers, the density of which is nearly $10^{17}/cm^2$. The factor τ_t/τ_t in equation (1) should be the order of 10^2 if we assume the cross section for trapping of unknown

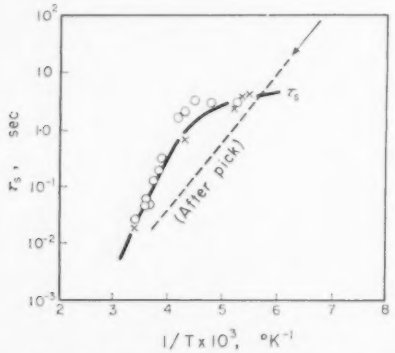

FIG. 6. The time constant of the slow decay, τ_s, as a function of $1/T$. The solid line shows the time constant of the slow decay, and dashed line the thermal life of F'-electrons after PICK.

centers to be equal to that of F-centers. From the above consideration, the time factor τ_{g0}, which is the reciprocal of the frequency factor of F'-electrons, is estimated to be 10^{-11} sec. For the traps related to the two fast decay currents around O_2 and O_3 temperatures, the activation energies were obtained as 0·35 and 0·43 eV respectively, assuming that their frequency factors are 10^{11}/sec. Little information concerning the origin of the fast decay currents is known at present. They are probably due to thermal treatment or unknown impurities.

Now, we shall discuss the illumination level dependence of the steady a.c. photoconductivity, G_∞, of colored KBr and KCl at several different temperatures. As is seen in Fig. 7, the photoconductivity G_∞ as a function of illumination level, I, could be approximately expressed as follows:

$$G_\infty = AI^p. \qquad (2)$$

In colored KBr, the magnitude of p is nearly equal to unity below -110°C, and it decreases to about 0·5 with the increase of temperature. Curve I in Fig. 8 shows the temperature dependence of the

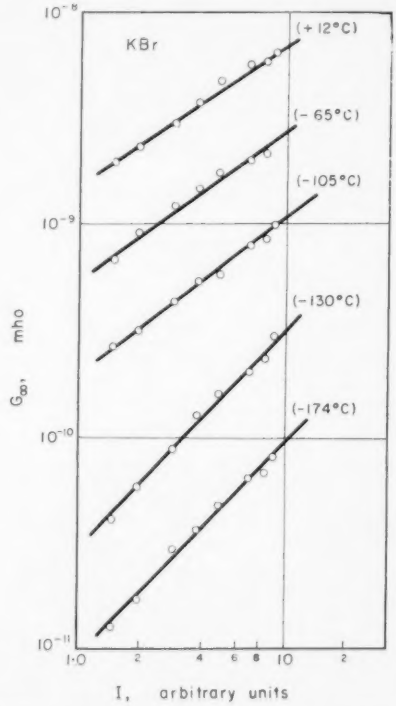

FIG. 7. The true photoconductivity G_∞ as a function of illumination level, I, at each temperature.

a.c. photoconductivity in colored KBr under steady F-band light illumination. The value of p at each temperature is indicated along the curve in this figure. Curve II in the figure shows one of the 90 μsec pulse photoconductivity, where Curve II is normalized to Curve I in G_∞ at -170°C. Considering the difference of two curve shapes and the value of p in each temperature region, it is concluded that the most dominant traps may be F-centers in the temperature range below -110°C, where the carrier density is determined by the

Vol. 22
1961

monomolecular process ($p = 1$). At high temperatures, vacant F-centers (or negative ion vacancies produced during illumination) may play effective roles for trapping the conduction electrons, where the bimolecular process becomes effective to determine the carrier density ($p \simeq 0{\cdot}5$), while F'-electrons tend to be released thermally.

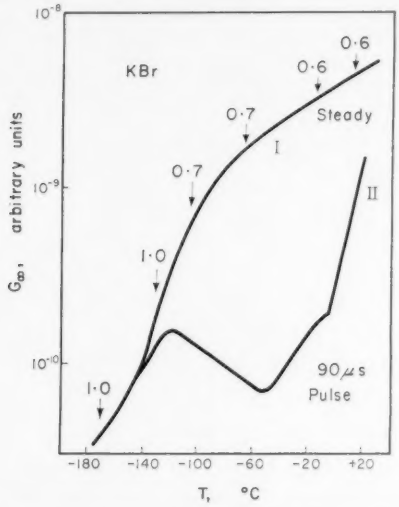

FIG. 8. The temperature dependence of the steady a.c. photoconductance G_∞ in colored KBr (Curve I). The value of p in equation (2) is shown along Curve I. Curve II, which corresponds to the 90 μsec pulse photoconductivity, is shown for reference.

In this case the unknown deep traps should be filled by the steady illumination. According to PICK's optical experiment, the quantum efficiency of $F' \rightarrow F$ conversion is known to be decreased as temperature is raised.[6] This fact seems to be inconsistent to our results at first sight. But there is no contradiction between them, because all of the F'-electrons produced by illumination should be released thermally at high temperatures and only vacant F-centers should be effective to trap electrons even if the cross section for trapping is small at high temperatures.

The results of the similar kind of experiment in colored KCl are shown in Fig. 9. In the figure, are shown the temperature dependences of the pulse photoconductivity, the pulse durations of which are 800 μsec, 90 μsec, and 30 μsec respectively. The temperature at which F'-electrons in KCl are released thermally may be expected to be about −80°C, considering the curve shapes in Fig. 9. On the other hand the value of p is nearly equal to 1·0 between −180°C and about −20°C. The bimolecular process becomes effective around +20°C. Some traps were observed to be produced by the photochemical reaction under a long time

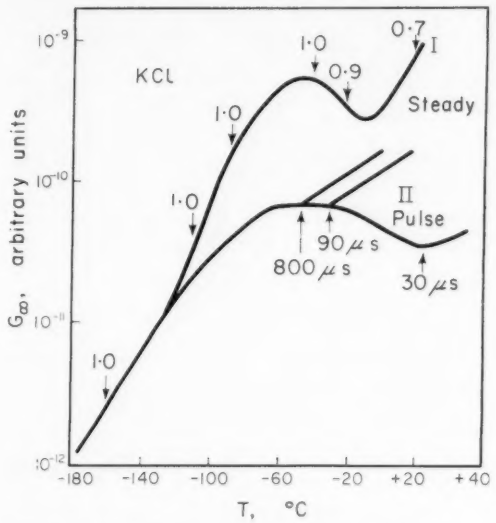

FIG. 9. The similar curves for colored KCl as those in Fig. 8.

illumination. These traps became less effective to trap electrons above +20°C, while F-centers themselves were bleached under illumination. The traps whose thermally releasing temperature of electrons is about 0°C should be produced by F-band light irradiation. The results of the steady photoconductivity in KCl cannot be analyzed so well as in KBr. This seems to be deeply concerned with the fact that A, M, and R centers are able to be produced more easily in colored KCl than in KBr by an illumination at room temperature.

Acknowledgements—We wish to express our thanks t Professors H. KAWAMURA, M. TOMURA and K. KOBA YASHI for their interest and valuable discussions.

REFERENCES

1. KITTEL C., *Solid State Physics* (2nd Ed.). p. 521. John Wiley, New York (1956).
2. GROSSWEINER L. I., *J. Appl. Phys.* **24**, 1306 (1953).

3. MACDONALD J. R., *J. Chem. Phys.* **23,** 275 (1955).
4. VON GERICKE V. O., *Nachr. Akad. Wiss. Göttingen,* 1 (1955).
5. HORNBECK J. A. and HAYNES J. R., *Phys. Rev.* **97,** 311 (1955).
6. PICK H., *Ann. Phys., Paris* **31,** 365 (1938).

DISCUSSION

D. KAHN: Did you use an a.c. field with steady illumination? Why should a.c. voltage and d.c. illumination give a different effect than d.c. voltage and pulse illumination?

M. ONUKI: Yes, I did. In the case of d.c. voltage and pulse illumination of long duration, space charge polarization results. On the other hand, for a.c. voltage and d.c. illumination the space charge effect is eliminated. Electrons that approach the anode surface in a half cycle of the a.c. field may fill the ionized F-centers which were formed near the surface during the previous half cycle; thereby the surface regions tend to be neutralized.

Vol. 22
1961

J. Phys. Chem. Solids Pergamon Press 1961. Vol. 22, pp. 323–325. Printed in Great Britain.

HOLE PHOTOCONDUCTIVITY IN KBr CRYSTALS CONTAINING Br^- MOLECULE IONS*

C. J. DELBECQ†

Argonne National Laboratory, Argonne, Illinois

Abstract—After X-ray irradiation at liquid nitrogen temperature, holes are trapped by forming Br_2^- molecule ions in KBr containing one of the impurities Ag^+, Tl^+, Pb^{++}, or NO_2^-. The Br_2^- molecule ions are oriented along ⟨110⟩ directions in the crystal and have two principal absorption bands at 385 mμ and 750 mμ, both of which show anisotropic properties. Irradiation into either one of these bands with [0$\bar{1}$1] polarized light causes a redistribution of the ions among the six ⟨110⟩ directions in the crystal so that the population in [011] is considerably enhanced. Photoconductivity has been observed upon bleaching with light of 750 mμ wavelength. The bleaching light used was polarized along either [0$\bar{1}$1] or [011]. Since continued bleaching at 750 mμ with [0$\bar{1}$1] light causes a decrease in the absorption of [0$\bar{1}$1] light, the observed photoconductivity decreases. If the plane of polarization of the bleaching light is rotated to [011], the photoconductivity rises and then decays to an equilibrium value. These changes in photoconductivity have been correlated with changes produced in the optical absorption spectra of Br_2^-.

INTRODUCTION

EARLIER work[1] has proven the existence of F_2^-, Cl_2^-, and Br_2^- molecule ions which are oriented in the six ⟨110⟩ directions in the alkali halides. Subsequently the optical transitions[2, 3] of these molecule ions, and also I_2^-, have been identified and studied. This latter work has shown that certain of these optical transitions are anisotropic, that is, the transition probability depends on the angle between the molecular axis and the electric vector of the exciting light, and that by excitation of these anisotropic transitions with plane-polarized light the population distribution in the six ⟨110⟩ orientations can be radically changed. It was believed that this reorientation of the molecule ion must involve the transport of a positive hole a few lattice distances through the crystal, and as a result might give rise to a measurable hole photoconductivity.

In order to obtain sufficiently high molecule ion concentrations and a minimum of interference caused by the presence of other color centers in the crystal, it was found desirable to use KBr–NO_2^- crystals for this work. Although other impurities act as efficient electron traps and thus promote the formation of X_2^- molecule ions, the optical excitation of the trapped electron, and consequent electronic photoconduction, appears to be a minimum, in the region of the X_2^- molecule ion absorption, for a crystal containing NO_2^-. KBr was chosen principally because the Br_2^- ion has an anisotropic absorption at 750 mμ (well displaced from the absorption of the trapped electron), as well as the principal anisotropic absorption at 385 mμ.

EXPERIMENTAL PROCEDURE

The single crystals used in these experiments were grown in this laboratory by the Kyropoulos method from a melt of KBr to which had been added 1 per cent of KNO_2. The crystals measured about 12 × 10 × 6 mm and were mounted in a Dewar flask so that both photoconductivity and optical absorption spectra could be measured on the same crystal. The electrodes were painted on the crystal using silver paint and the photoconductivity was measured using an Applied Physics Model 30 vibrating reed electrometer with a 10^{11} Ω load resistor and 1000 or 2000 V across the 6 mm dimension of the crystal. Color centers were produced by X-ray irradiation from a Machlett tube with a tungsten target operating at 50 kV and 50 mA, and filtered through 1 mm of quartz, or by γ-ray irradiation from a 4000 c Co^{60} source.

Optical absorption spectra were taken with a Cary Model 14*R* spectrophotometer. Polarized light for both

* Based on work performed under the auspices of the U.S. Atomic Energy Commission.

† Presented by P. H. YUSTER.

optical absorption and photoconductivity measurements was obtained by using an Ahrens prism. A 500 W filament lamp in conjunction with a 740 mμ interference filter and a #3387 Corning filter, and an *AH*–6 mercury lamp in conjunction with a 470 mμ interference filter and #308 and #3391 Corning filters were used in the photoconductivity measurements to excite the 750 mμ and 385 mμ Br_2^- transitions, respectively.

EXPERIMENTAL RESULTS

In Fig. 1 is shown the anisotropic absorption spectrum of Br_2^- in KBr which can be obtained as follows: expose a KBr–NO_2^- crystal at 77°K to

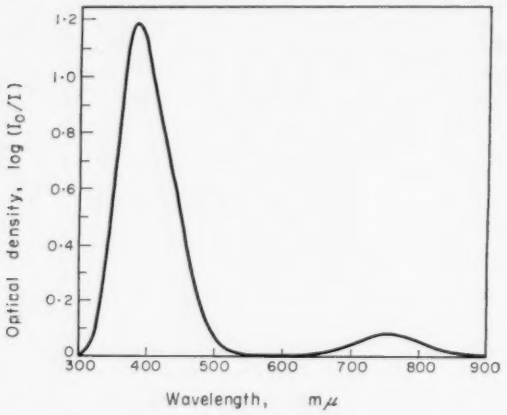

FIG. 1. The anisotropic absorption spectrum of the Br_2^- molecule ion in KBr–NO_2^-.

X-rays or Co^{60} γ-rays and then excite the crystal with [0$\bar{1}$1] polarized light in the 385 mμ or 750 mμ Br_2^- bands; this excitation reorients the Br_2^- preferentially into the [011] orientation causing an anisotropy in the absorption spectrum, and the anisotropic absorption spectrum is obtained by subtracting the [0$\bar{1}$1] spectrum from the [011] spectrum.

Figure 2 shows the photoconductivity at 77°K of a KBr–NO_2^- crystal, which had been exposed at 77°K to Co^{60} γ-rays for 15 min, upon excitation with [0$\bar{1}$1] polarized light in the 750 mμ band (before these photoconductivity curves were taken the crystal had also been exposed to 600 mμ light to remove the *F* band, and then with [011] light at 740 mμ to orient preferentially the Br_2^-). Before beginning the excitation with [0$\bar{1}$1] 740 mμ light, at $t = 1$ min in Fig. 2, the optical density at 740 mμ with [0$\bar{1}$1] light was 0·46 (65 per cent of incident light absorbed) and at the end of the excitation the optical density (740 mμ, [0$\bar{1}$1]) was 0·16 (31 per cent absorbed); during this excitation, the photocurrent decreased from an extrapolated initial value of $4{\cdot}2\times10^{-14}$ A to a final value of $1{\cdot}9\times10^{-14}$ A. Thus the ratio of the fraction of light absorbed at $t = 1$ min to that at $t = 4$ min is $L_1/L_4 = 2{\cdot}1$, and the ratio of the photocurrent at $t = 1$ to that at $t = 4$ is $I_1/I_4 = 2{\cdot}2$. It is apparent that the photocurrent remains proportional to the intensity of light absorbed by the Br_2^- ions during their reorientation.

At time $t = 4$, the crystal was shielded from the exciting light and the polarizing prism rotated by 90° and at time $t = 6$ the crystal was excited with [011] light at 740 mμ. The values $L_6/L_9 = 2{\cdot}2$ and $I_6/I_9 = 2{\cdot}3$ were obtained and the same general

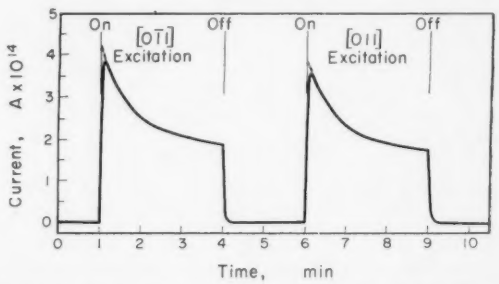

FIG. 2. Photocurrent measured at 77°K of a KBr–NO_2^- crystal, which had been exposed at 77°K to Co^{60} γ-rays for 15 min, upon excitation with ⟨110⟩ polarized light of wavelength 740 mμ.

behavior is observed as in the case of excitation with [0$\bar{1}$1] light. A series of such measurements can be carried out in which the photocurrent is found to be proportional to the intensity of light absorbed; however, the intensity of the photocurrent and the intensity of the 750 mμ band are observed to decrease. These decreases result from the migration of the Br_2^- ions through the lattice and a recombination with trapped electrons.

Experiments have also been carried out in which the crystal is excited in the 385 mμ band of Br_2^-. In this case, too, a photocurrent is observed which behaves qualitatively as that shown in Fig. 2; however, the current in this case is not proportional to the intensity of light absorbed (the decrease in the current with increasing time is less than would be observed if the current were proportional to the intensity of light absorbed).

Vol. 22
1961

DISCUSSION

The time dependence of the photoconductivity of a KBr–NO_2^- crystal containing Br_2^-, which is observed upon excitation of the crystal with ⟨110⟩ polarized light of wavelength 740 mμ (Fig. 2), can be readily understood both qualitatively and quantitatively on the basis that excitation of the 750 mμ transition of Br_2^- results in the motion of a hole for a short distance through the lattice and that it is this hole motion which gives rise to the observed photocurrent. It is well established[2, 3] that optical excitation of the X_2^- molecule ions causes a change in the orientation of the molecule ions in the lattice; a change in orientation requires at least a small translation of charge. And, in fact, it has been shown in the case of KCl–Ag^+ crystals containing Cl_2^- that excitation of the Cl_2^- causes the formation of the $(AgCl_4)^=$ molecule ion[4] which shows that after a number of excitations the Cl_2^- has moved a sufficient distance to encounter an Ag^+ at which it is then trapped. Therefore, one should, in principle, expect a hole photocurrent upon optical excitation of Br_2^-. The fact that the observed photocurrent is proportional to the rate of excitation of the Br_2^-, as the Br_2^- reorient and cause a decrease in the absorption of the exciting light,* is a very strong indication that the photocurrent observed is a hole photocurrent.

In the case of excitation in the 385 mμ band of Br_2^- with light of wavelength 470 mμ, it is believed that the photocurrent consists of two components: one component being electronic and arising from excitation of trapped electrons whose absorption overlaps the 385 mμ band and the other component being a hole current arising from optical excitation of Br_2^-.

The hole photocurrent which has been observed cannot be considered to result from the motion of a "free" hole through the lattice. On the basis of a simple molecular orbital model of the X_2^- molecule ions,[3] excitation of the high energy transition results in an antibonding state of the molecule ion and its dissociation; and excitation of the low energy transition results in a weakly bonding state which is believed to be too weak to overcome the high vibrational energy, so that in this case, too, the molecule ion dissociates. The hole then migrates through the crystal until the initially high local vibrational energy of the lattice has been sufficiently dissipated to allow the formation of a stable X_2^- molecule ion; however, during this period in which it moves through the lattice, the hole probably experiences some degree of molecular binding with a neighboring bromide ion.

Acknowledgements—I would like to thank P. H. YUSTER for many helpful discussions. I am also indebted to E. HUTCHINSON for growing the crystals used in these experiments.

* The Br_2^- transition giving rise to the 750 mμ band is not strongly anisotropic[3] and so the absorption, and therefore the photocurrent, do not change by a very large factor.

REFERENCES

1. CASTNER T. G. and KANZIG W., *J. Phys. Chem. Solids* **3,** 178 (1957).
2. DELBECQ C. J., SMALLER B. and YUSTER P. H., *Phys. Rev.* **111,** 1235 (1958).
3. DELBECQ C. J., HAYES W. and YUSTER P. H., *Phys. Rev.* **121,** 1043 (1961).
4. DELBECQ C. J., HAYES W. and YUSTER P. H., to be published.

BLANK
PAGE

Vol. 22
1961

J. Phys. Chem. Solids Pergamon Press 1961. Vol. 22, pp. 327–331. Printed in Great Britain.

PHOTOCONDUCTIVITY IN RbI AND KI*

Y. NAKAI† and K. TEEGARDEN‡

Institute of Optics, University of Rochester

Abstract—A threshold for intrinsic photoconductivity has been observed in RbI and KI at room temperature and lower temperatures. These experiments were carried out with an electrode arrangement quite different from that employed previously by TEEGARDEN and in a considerably cleaner vacuum. Photoconductivity occurs on the short wavelength side of the first exciton band in the region of the shoulder previously ascribed to the onset of band-to-band transitions. Photoconductivity also can occur on the long wavelength side of the first exciton peak when *F*-centers or other kinds of electron-surplus centers, formed by irradiation with ultraviolet light, are present in the crystals.

1. INTRODUCTION

THE PURPOSE of this experiment was to determine the band gap of KI and RbI by measuring the threshold for intrinsic photoconductivity. There are several reasons why this experiment is of interest.

(1) The relationship of the bandgap to the various features of the optical absorption spectrum of the alkali halides, i.e. the "exciton" bands, is of importance in determining the true nature of these features.

(2) The question of whether or not photoconductivity occurs at the position of the first exciton band cannot be answered unless the threshold for photoconductivity is actually determined. That is, one cannot say that the absence of photoconductivity in the exciton band is significant unless one demonstrates that photoconductivity in other regions can actually be detected.

(3) Energy transfer mechanisms, such as those thought to be responsible for host-sensitized luminescence in the alkali halides, include the production of free holes and electrons and the transfer of energy cannot be attributed to other mechanisms until photoconductivity has been ruled out.

Several attempts have been made during the past twenty years to detect intrinsic photoconductivity in the alkali halides.[1] Three years have passed since one of the authors started preliminary experiments on this subject.[2] Subsequent work has been devoted to extensive improvement of the experimental technique and reliability of the data. The results described in this paper are in good agreement with the results of the preliminary work.

2. EXPERIMENTAL

Crystals used in this experiment were cleaved from boules grown by Dr. K. KORTH of Kiel, Germany, by the Kyropoulos technique. The crystals were mounted in a cryostat so that they could be cooled to low temperature. The cryostat was provided with an evaporator so that films of KCl could be deposited on to the iodide crystals and electrodes after they had been mounted in the crystal holder. Several electrode arrangements were used in the experiment. Two of these are shown in Fig. 1. The second arrangement provided the most homogeneous electric field distribution in the crystal and therefore provided the most quantitative information. Thin sheets of Mylar were placed between the crystal and the electrodes to prevent charge from entering or leaving the crystal. A film of KCl approximately 1000 Å thick was evaporated on to the crystal and electrodes to prevent photoemission from these surfaces. Currents were measured with an Applied Physics Laboratory vibrating reed electrometer. The "rate of charge" method was used in detecting the small currents involved. Dry cells were used to produce the required fields in the crystals.

A Bausch and Lomb quartz prism monochromator was used with a hot-cathode low-pressure hydrogen discharge tube as a source. The light from the monochromator was focussed on to the crystal with a quartz lens. The intensity of the light was monitored by means of

* Work supported in part by the U.S. Air Force through the Office of Scientific Research of the Air Research and Development Command.

† On leave of absence from the University of Kyoto, Kyoto, Japan.

‡ Alfred P. Sloan Foundation Research Fellow.

a 1P21 photomultiplier and a sodium salycilate phosphor. An absolute measure of the light intensity was obtained with a previously calibrated 6199 end-on photomultiplier with sodium salycilate on the outside of the end window. The end-on tube was used in order to insure that all the light incident on the crystals was intercepted by the detector. It is estimated that absolute measurements of the light intensity could be made to about 10 per cent.

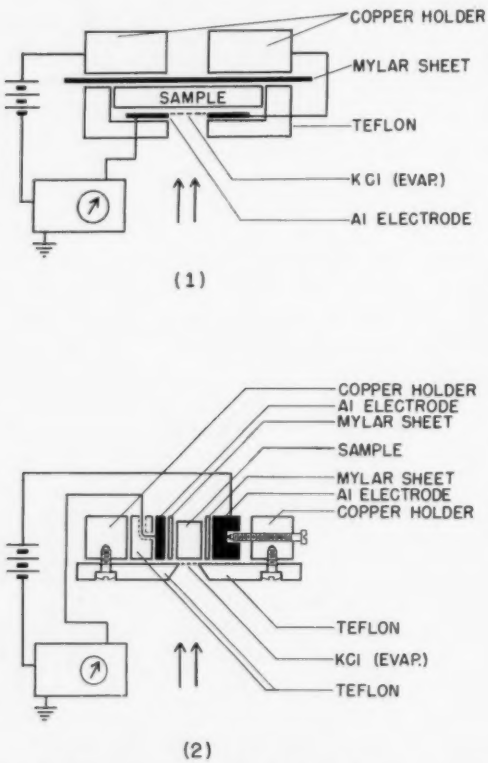

FIG. 1. Schematic diagrams of the electrode arrangement. The copper holder was attached to the bottom of the inner Dewar of a cryostat.

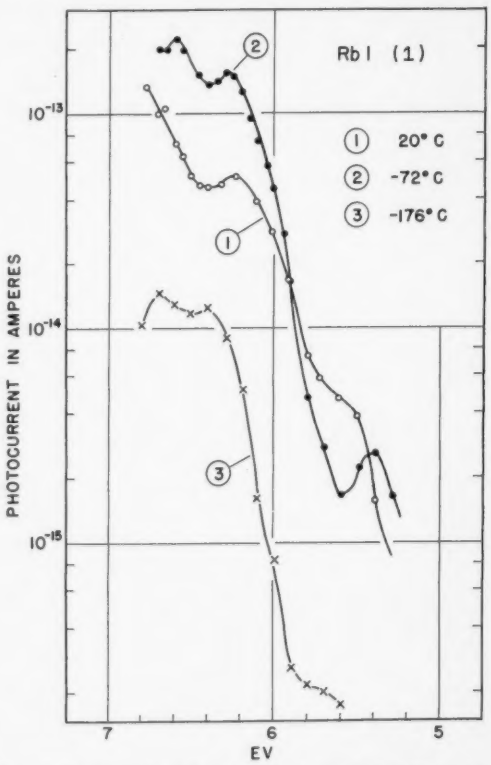

FIG. 2. Photoconductivity in a single crystal of RbI with the electrode arrangement shown in (1) of Fig. 1. (1). At 20°C. (2). At −72°C. (3). At −176°C.

It was found that a very clean vacuum was necessary to avoid contamination of the crystal surfaces at low temperature. A Varian Vac-Ion pump was finally used to evacuate the cryostat used in this experiment. If an oil-diffusion pump was used, the crystals became contaminated to the extent that photoemission could not be observed at low temperature.

The greatest experimental difficulties encountered in this work were photoemission from the crystal and surrounding surfaces and polarization of the crystals due to the motion of the electrons.[3] Great care was taken to minimize both these effects. It was found that a film of KCl on the crystal and electrodes greatly suppressed photoemission. The spectral distribution of the photoemission from the crystal and electrodes was actually measured so that this phenomenon could be recognized if it occurred during the course of the photoconductivity measurements. Blank experiments, in which the KI or RbI crystals were replaced with KCl, were performed to be sure that the currents observed were not due to some extraneous source. It was found that it was necessary to use very low intensities of light to avoid polarization of the crystals and the build-up of various types of color centers. Also, a certain relaxation cycle was used at room temperature to reduce further the effects of polarization. The crystals were exposed to ultraviolet radiation with the field in one direction and the current measured. Subsequently they were irradiated with both visible and ultraviolet light with the field reduced to zero. Then the current was measured at the same wavelength with the field in the opposite direction. This

Vol. 22
1961

cycle gave very reproducible results and the currents with both field directions were identical within a very small error. Curves 1 and 2 of Fig. 4 show the difference in photoconductivity which occurred when the crystal was not irradiated at zero field.

3. DISCUSSION OF RESULTS

The primary results of this experiment are shown in Figs. 2, 3 and 4. Fig. 2 shows the spectral distribution of the photocurrent in a crystal of

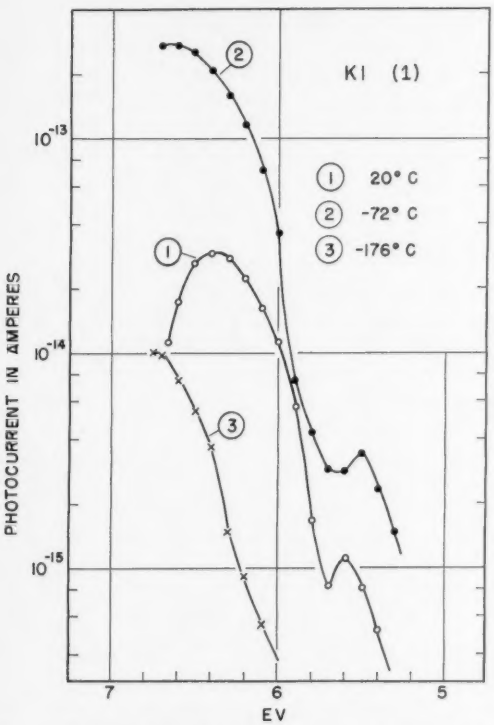

FIG. 3. Photoconductivity in a single crystal of KI with the electrode arrangement shown in (1) of Fig. 1.
(1). At 20°C. (2) At −72°C. (3). At −176°C.

RbI at three temperatures. This data was obtained using the electrode arrangement number 1 in Fig. 1. It should be remembered that these curves have been corrected for changes in incident light intensity. They are not corrected for changes in the reflectivity of the crystals. In all cases the main feature of the curves is the relatively abrupt increase in the photocurrent in the vicinity of 6·0 eV. Either small minima or inflection points occur at photon energies near the position of the first and second exciton bands in RbI.[4] These features are shifted to somewhat higher photon energies in KI, as would be expected.

The temperature dependence of the photocurrents shown in Figs. 2 and 3 has not been satisfactorily explained as yet, although it appears to be reproducible with a given electrode arrangement.

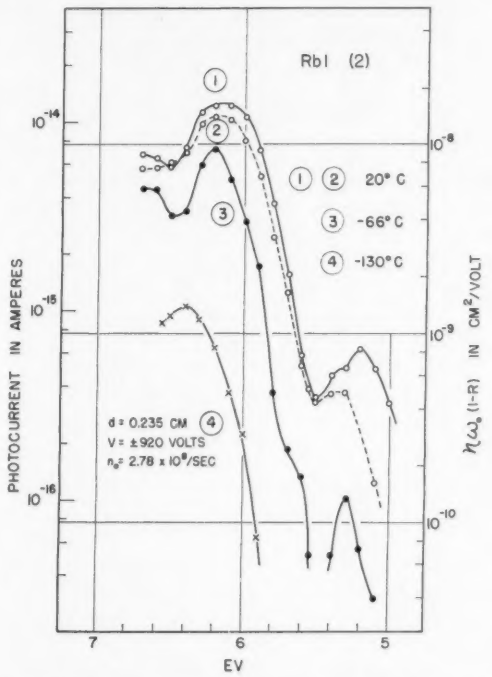

FIG. 4. Photoconductivity in a single crystal of RbI with the electrode arrangement shown in (2) of Fig. 1.
(1). At 20°C. The crystal was irradiated with both unfiltered tungsten light and ultraviolet light of the wavelength used for the measurement with the electric field reduced to zero after every single reading for both polarities of electric field.
(2). At 20°C. No irradiation at zero field.
(3). At −66°C. No irradiation at zero field.
(4). At −130°C. No irradiation at zero field.

With the electrodes arranged as in part (2) of Fig. 1, the dependence on temperature was somewhat different, as can be seen from Fig. 4.

It was found that the photocurrents increased linearly with increasing field at a photon energy of

6·2 eV, for both KI and RbI. This was true for both directions of applied field and the slope of the straight line was the same for both field directions. No saturation was observed for either field direction up to fields of approximately 6000 V/cm. The currents also increased linearly with increasing light intensity at 6·2 eV.

Figure 4 shows the results obtained with a crystal of RbI using the second electrode arrangement shown in Fig. 1. In this case the electric field was probably quite homogeneous in the crystal and an attempt has been made to give the results in terms of $\eta\omega_0\ (1-R)$, where η is the quantum efficiency, ω_0 is the range in unit field, and R is the reflectivity of the crystal. The value of $\eta\omega_0\ (1-R)$ was obtained by using the formula: $\eta\omega_0\ (1-R) = i(d)^2/en_0V$, where e is the charge of an electron, n_0 the number of photons incident per second, V the applied voltage, i the photocurrent, and d the effective electrode distance or the actual distance corrected for the presence of the two Mylar sheets. Values of these parameters are shown in Fig. 4.

4. CONCLUSIONS

The results presented above indicate a value of about 6·0 eV for the band gap of RbI and KI. The threshold for photoconductivity seems to correspond to the shoulder appearing in the optical absorption spectrum of these crystals which has been previously attributed to the onset of band-to-band transitions.[5]

Photocurrents were found to be smaller by a factor of at least 30 at photon energies corresponding to the peak of the first fundamental band, relative to the maximum photocurrents in KI and RbI. There are two explanations for this result. The one generally accepted is that the first absorption peak is due to the excitation of a non-photoconducting bound state of holes and electrons. Another is that the holes and electrons produced by photons of energy corresponding to the peak of the first fundamental band are created near the surface because of the high absorption coefficient in this region. It is to be noted that the absorption coefficient at the band peak is of the order of 10^6 per cm, while it is of the order of 10^5 per cm at 6·2 eV. The data indicate only a reduction by a factor of about 2 or 3 near the peak of the second exciton band where the absorption coefficient is also of the order of 10^6 per cm. This result means that the yield for free holes and electrons is indeed smaller at photon energies near the peak of the first fundamental band and supports the hypothesis that the band is due to a non-photoconducting transition. It is to be noted, however, that photoconductivity does appear at the position of the second exciton peak at about 6·5 eV in RbI and about 6·7 eV in KI. This seems to indicate that these bands lie about 0·5 eV above the bottom of the conduction band.

It still has not been demonstrated to the satisfaction of either of the authors that light absorbed in the first fundamental band gives rise to mobile excitons, however. In this regard the small but measureable yield for photoconductivity at photon energies lower than the position of the first fundamental band is of significance. While it was found that the currents stimulated with 6·2 eV photons increased linearly with increasing light intensity, no such relationship was found for the currents stimulated with photons of 5·6 eV and lower energies. There was some indication that these rise as the square of the intensity. Therefore it is believed that these currents may depend upon the photoproduction and destruction of color centers in the crystals. The fact that F-centers can be ionized with photons of these energies has been demonstrated by INCHAUSPÉ[6].

Because of this result, recent experiments which interpret host-sensitized impurity luminescence produced in alkali halide crystals by irradiation in the long wavelength tail of the first fundamental band as being due to the diffusion of excitons are open to criticism. Excitons are only one of the energy transfer mechanisms which can give rise to such luminescence. Another is the holes and electrons which are produced by irradiation in the fundamental band tail. It has been demonstrated that free-charge carriers can indeed cause luminescence of impurities in the crystals.[7]

Future experiments will be devoted to a study of the photoconductivity of these and other alkali halides at lower temperatures and higher photon energies. Since these materials have such a high absorption coefficient, the state of the crystal surfaces may play an important role in the photoconductive process. It would therefore be interesting to study the effect of different surface treatments on the photoconductivity.

Vol. 22
1961

Acknowledgements—The authors wish to thank Professor D. B. DUTTON for his extremely helpful criticism and advice during the course of this work. We also wish to thank Professor D. L. DEXTER for his many helpful suggestions and support.

REFERENCES

1. FERGUSON J. N., *Phys. Rev.* **66,** 220 (1944); TAYLOR J. W. and HARTMAN P. L., *Phys. Rev.* **113,** 1421 (1959).
2. TEEGARDEN K., *AFOSR* TN-59303, *ASTIA* Document No. A.D.-213087.
3. APKER L. and TAFT E., *Phys. Rev.* **79,** 964 (1950); **81,** 698 (1951); **82,** 814 (1951); PHILIPP H. R. and TAFT E. A., *Phys. Rev.* **106,** 671 (1957).
4. MARTIENSSEN W., *J. Phys. Chem. Solids* **2,** 257 (1957); EBY J. E., TEEGARDEN K. J. and DUTTON D. B., *Phys. Rev.* **116,** 1099 (1959); MARTIENSSEN W., *J. Phys. Chem. Solids* **8,** 294 (1959); HARTMAN P. L., SIEGFRIED J. G. and NELSON J. R., *Phys. Rev.* **105,** 23 (1957).
5. TAFT E. A. and PHILIPP H. R., *J. Phys. Chem. Solids* **3,** 1 (1957); PHILIPP H., TAFT E. A. and APKER L., *Phys. Rev.* **120,** 49 (1960).
6. INCHAUSPÉ N., *Phys. Rev.* **106,** 898 (1957).
7. TEEGARDEN K. and WEEKS R., *J. Phys. Chem. Solids* **10,** 211 (1959); TEEGARDEN K. and EDGERTON R. to be published.

DISCUSSION

A. ROSE: What is the response time (i.e. rise and decay time) for the photocurrents?

Y. NAKAI: In the intrinsic region, i.e. in the region of photon energy above 5·8 eV, we did not observe any delay in response as far as the detector could follow. In other words, both the rise and the decay times are smaller than 0·5 sec. However, in the region of lower photon energy, we observed that photocurrents increased with time of irradiation, starting from a very small initial value. With the u.v. light turned off, photocurrents decrease abruptly, that is, the decay time was shorter than 0·5 sec. If we repeated the same measurement without irradiating the crystal with visible light, the photocurrents started with an initial value approximately the same as the final value of the previous measurement. We believe that this type of response was due to the build-up of color centers produced by ultraviolet light in the region of photon energy lower than 5·8 eV.

BLANK
PAGE

Vol. 22
1961

J. Phys. Chem. Solids Pergamon Press 1961. Vol. 22, pp. 333–338. Printed in Great Britain.

PHOTOCONDUCTIVITY OF SOME ALKALI HALIDE CRYSTALS IN THE FUNDAMENTAL ABSORPTION RANGE

G. KUWABARA* and K. AOYAGI

Department of Physics, University of Tokyo, Tokyo, Japan

Abstract—The photoconductivity of KI, KBr and KCl in the fundamental absorption range was studied between −70° and 110°C. The spectral response curve consists of three characteristic regions. The first is a bell-shaped structure in the low energy tail of the intrinsic absorption band, which is temperature sensitive and presumed to be due to imperfections; the second is a very faint photoconduction at the first exciton peak, and the third is the temperature-insensitive photoconduction above the higher energy tail of the first absorption peak due to direct photoionization in the undisturbed crystal. The direct ionization starts at ca. 5·8, 6·8 and 7·5 eV in photon energy for KI KBr and KCl, respectively.

1. INTRODUCTION

THERE are several structures in the fundamental absorption range of alkali halide crystals. One group in the lower energy side has been interpreted as transitions creating electron–hole pairs coupled with each other, and another in the higher energy side as those creating free carriers.

Recent experiments[1, 2] have shown that there are much more complicated structures than those expected by simple considerations, especially in crystals composed of heavy halogens. Excitons do not cause conductivity unless they dissociate by absorbing thermal energy or ionize other impurity centers by transfering their energy. Therefore the study of the photoconductivity in this region may afford an important clue to the interpretation of the absorption band or behavior of excitons in these crystals. The external photoelectric effect has been measured,[3, 4] while the detection of the internal photoelectric effect has been unsuccessful as far as we know.[4, 5] In this paper the spectral response of the photoconductivity and some discussions thereof are given.

2. EXPERIMENTAL PROCEDURES

The vacuum monochromator used is the same as that reported previously.[5] The light intensity in the photoconductivity measurement was about 10^{10} photons/cm^2 sec for the pass band of 3 mμ at 200 mμ. The current was measured with a d.c. amplifier by the charging-up method or with a vibrating-reed electrometer. The noise level of the former is 10^{-15} C, and that of the latter is 2×10^{-16} A in the measuring condition.

In this experiment, it is essential to reduce the external photoelectric current as far as possible, because most of the ordinary materials emit photoelectrons below 200 mμ, and the internal photocurrent will be completely masked.[4, 5] In order to reduce the external photocurrent from the electrode or from the crystal, various electrode arrangements and materials were tested. The best one so far obtained is shown in Fig. 1(a). The crystal is pressed between two electrodes, on which LiF films are carefully evaporated. The light falls on the crystal through many fine holes drilled on the front electrode, i. e. the incident light is parallel to the applied electric field. In this arrangement the forward or reverse direction denotes the case in which the negative or positive potential is applied to the front electrode. The photoconductivity was measured with the forward direction, in which the created photoelectrons are drawn into the interior of the crystal. In some cases a third positive grid is placed before the front electrode to draw up the external photoelectrons from the front electrode. Another arrangement, as in Fig.

* Now at Argonne National Laboratory, Argonne, Illinois, on leave from the University of Tokyo.

1(b) was also tested, in which the background current due to the external photoeffect of the crystal was larger than that in the former, especially below 200 mμ in KI.

The crystals used were those purchased from Harshaw and grown in our Laboratory by the Bridgeman method. They were cleaved to about 10×10×1·3 mm. The voltage applied was 450 V, i.e. the electric field was ca. 3500 V/cm.

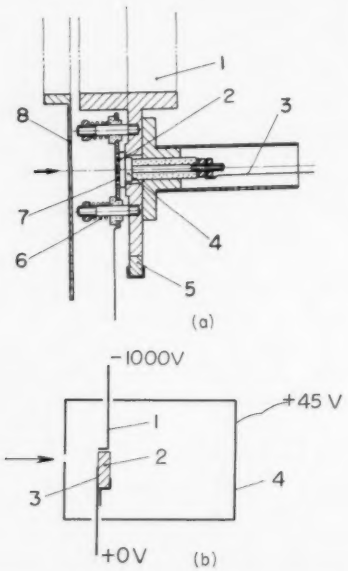

FIG. 1. Electrode arrangements. Electric field is parallel (a) and perpendicular (b) to the incident light.
(a) 1. Dewar, 2. crystal, 3. lead to the electrometer, 4. rear electrode, 5. heater, 6. spring, 7. front electrode and 8. radiation shield.
(b) 1. electrode, 2. crystal, 3. electrode and 4. shielding case.

In the measurements above room temperature, the detection chamber was filled with dry nitrogen of 0·8 atmospheric pressure. With these procedures, the background current or the external photoelectric current for the forward direction could be reduced below the noise level for light above 160 mμ.

The current was kept small as far as possible, i.e. order of 10^{-15} A. Even with this small current the space charge effect appeared for light below 220 mμ in the case of KI, because of small light penetration depth.

3. RESULTS AND DISCUSSIONS

The spectral response of the photocurrent in KI for the forward direction at room temperature is shown in Fig. 2(a). The ordinate is a photocurrent normalized to incident photon numbers. The curve consists of three regions. One is a sharp

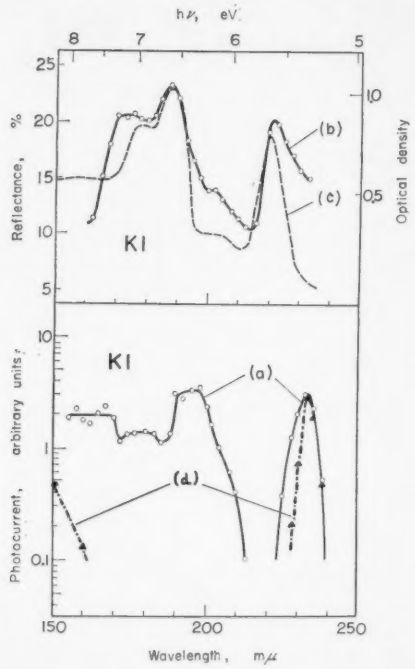

FIG. 2. Photocurrent and reflectivity of KI at room temperature: electrode arrangement (a), forward direction.
(a) photocurrent of KI in 0·8 atm N_2,
(b) reflectance of KI single crystal,
(c) absorption of KI film (after EBY *et al.*),
(d) photocurrent of mechanically treated KI, i.e. the surface was rubbed with emery paper and polished.

structure of a bell shape, whose maximum lies at about 234 mμ extending between 210 and 225 mμ (denoted as the first peak). The second is a very faint photoconduction* around the first absorption band (denoted as the second region). There is a sharp dip between these two regions. The third is

* This is just a little above the noise level and is not shown in the figure. A detailed study of this region with higher sensitivity is in progress and will be reported in another paper.

Vol. 22
1961

the broad structure which rises from the higher energy side of the first absorption band (third region). In the case of the forward direction an almost linear relation existed between the applied voltage and the amount of photocurrent for light of 185 mμ as well as that of 230 mμ up to a field of 6,000 V/cm. This result shows that the photocurrent is due to the internal photoeffect. The curves (a) and (b) in Fig. 3 are the photoresponses

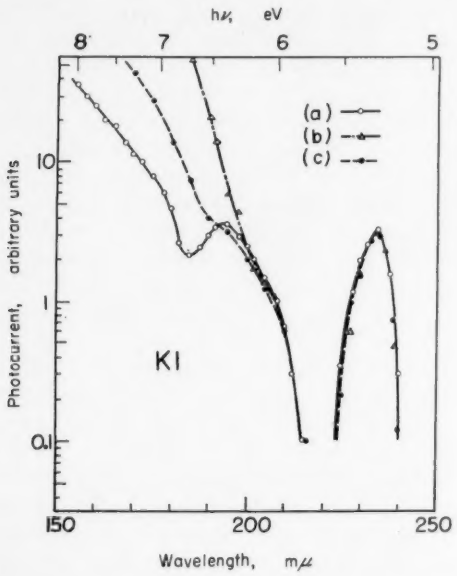

FIG. 3. Photocurrent of KI at room temperature, reverse direction.
(a) reverse direction in 0·8 atm N_2,
(b) in vacuum,
(c) electrode arrangement (b) in 0·8 atm N_2.

for the reverse direction obtained in N_2 of 0·8 atm and in vacuum, respectively, and (c) is for the electrode arrangement (b). These curves show that the external photocurrent from the crystal rapidly increases below 200 mμ.

The temperature dependence of the photoresponse between 110° and −70°C is shown in Fig. 4. As the temperature is decreased, the height of the first peak decreases remarkably compared with that of the third region, and its peak position shifts towards higher energy with a rate of $1{\cdot}0\times10^{-3}$ eV/deg, which is almost the same rate as that of the exciton peak.

Curve (d) in Fig. 1 is the response of a mechanically treated crystal, i.e. the surface is rubbed with emery paper and then polished with a fine cloth to reduce the light scattering. With this procedure, which is supposed to cause a large amount of strain or imperfections near the surface, the current in the third region decreased to less than one-tenth of its original value, while that in the first peak remains almost the same except for a slight

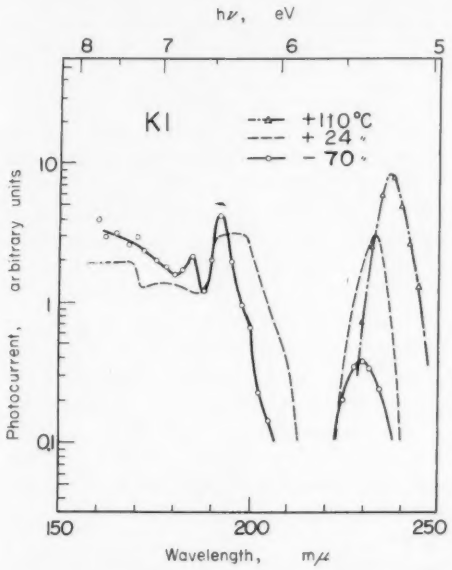

FIG. 4. Temperature dependence of photocurrent of KI.

change in the form of the higher energy side cut-off. By dissolving the surface layer with water, the photocurrent recovered almost the same value as that before treatment. The vacuum evaporation of a LiF film on to the surface also caused a similar effect.

The current in the third region also decreases conspicuously with continuous irradiation by light in this band, while that of the first peak remains almost unchanged by irradiation with light in the first peak or in the third region. This is because in the former case a higher local space charge builds up near the surface than in the latter for an equal amount of current in the outer circuit. The above two facts show that the photoeffect in the first peak occurs almost uniformly

throughout the crystal, while that in the third region occurs within a quite thin layer near the surface, owing to the extremely small penetration depth of light, and is liable to be affected greatly by the crystal imperfection near the surface.

After irradiation in the first peak for several minutes, the light above 600 mμ (designated as infrared light) causes the photocurrent, which decreases to zero with time. Moreover, the first peak almost coincides with the absorption peak of the β-band. Accordingly, it may be suggested that the peak is correlated with the *F*-center which is formed by an exciton and successively ionized by another exciton or directly by absorbing light in the β-band. This mechanism, however, is denied by the following reasons. The first peak appears even in the freshly cleaved crystal and the amount of current neither increases by prolonged irradiation with ultraviolet light nor decreases after sufficient irradiation with infrared light which includes the *F*-band of KI. If the α- or β-band is the origin of the photocurrent, we expect a large amount of negative-ion vacancies and accordingly a higher first peak for the quenched crystal. However, the peak height is nearly the same irrespective of the various treatments. If we assume that the creation and successive ionization of the *F*-center is the origin of the photocurrent, we should have a superlinear relation between the amount of current and the light intensity. This also contradicts the experiment.

There are two possible mechanisms which cause the first peak:

(1) Localized exciton absorption, i.e. the excitation of the halogen ion near an imperfection, or the absorption band due to an impurity is hidden under the tail of the first absorption band.

(2) Excitons created by light at normal lattice points transfer their energy to the electron trapping impurity centers, ionizing them.

At the first peak, 2×10^9 photons/sec are absorbed by the crystal, and we get 10^{-9} cm^2/V as $\eta\omega$ at room temperature, where η is the quantum efficiency per incident photon and ω the schubweg per unit applied voltage. If we assume 2 per cent of the 234 mμ light is directly absorbed by the hidden band or 2 per cent of created excitons transfer their energy to impurities, the above value of ω seems to be reasonable. In the former, the spectral sensitivity curve at around 234 mμ is interpreted to correspond to the shape of the impurity absorption affected by the tail of the fundamental absorption band, and the impurity concentration is estimated as 10^{16} cm^{-3} assuming the absorption coefficient of 0·8 cm^{-1} (ca. 2 per cent absorption at 234 mμ). In the latter, the decrease of the higher energy side may be interpreted to arise because excitons are formed too densely near the surface so that the most of them annihilate before transferring their energy effectively to the uniformly distributed impurity centers of low concentration. The building up of the infrared photoconductivity by u.v. radiation shows that the original impurity centers are destroyed and that ejected electrons are trapped by shallow traps. Nevertheless, the peak height remains unaltered. This seems to favor mechanism (2) because newly developed centers may also be ionized by excitons. The hidden impurity absorption band is not the β-band, because the peak height does not decrease even after photoconduction by i.r. light has completely disappeared.

It cannot be decided at present which of the two mechanisms is responsible for the first region. This will be discussed in another paper together with the photocurrent at the exciton peak.

The temperature dependence of the photoconductivity in the additively colored KI[7] shows that the schubweg is nearly constant between −60° and 110°C. Therefore, the strong temperature dependence of the current in the first peak might be ascribed to the change of ionizing efficiency. Assuming the temperature dependence to have the form $\exp(-E/kT)$, we get $E = 0{\cdot}11$eV.

Comparing the photoconductivity below 220 mμ with the reflection spectra, it may be seen that the photoconductivity arises from the high energy tail of the first absorption band or near the absorption shoulder and shows a peak around the low energy side of the second absorption band. The decrease at the second peak is not as steep as that at the first absorption peak and the structure below 200 mμ corresponds well with the reflection curve. The slight temperature dependence of the photocurrent in this region is mainly due to that of the schubweg, and ionization occurs with almost constant quantum efficiency irrespective of photon energy or temperature. These features show that above around 5·8 eV, the free carriers are directly

Vol. 22
1961

created by photons contrary to the region below 5·8 eV.

Figure 5 and Fig. 6 are the photoresponses for KBr and KCl, respectively. The main features are nearly the same with those of KI, i.e. a bell-shape peak, which is probably due to imperfections,

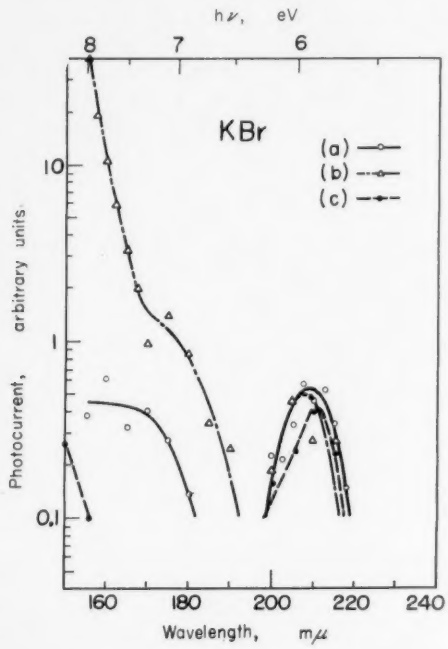

FIG. 5. Photocurrent of KBr at room temperature.
(a) forward direction in 0·8 atm N_2,
(b) reverse direction in vacuum,
(c) mechanically treated, forward direction in 0·8 atm N_2.

appears in the low energy tail of the first absorption band, the current drops sharply or is hardly detectable at the absorption peak and again increases as the photon energy exceeds the higher energy tail of the first peak. However, there are some differences in the details, the study of which are now in progress. The approximate photon energy for the onset of direct photoionization in the undisturbed lattices of KI, KBr and KCl at room temperature are listed in Table 1.

4. CONCLUSIONS

The photoconductivity of KI, KBr and KCl were studied in the fundamental absorption range. The spectral responses consist of three characteristic regions: a bell-shaped peak in the low energy side of the fundamental absorption band which is probably caused by impurities, a faint photoconduction at the first absorption peak and a tempera-

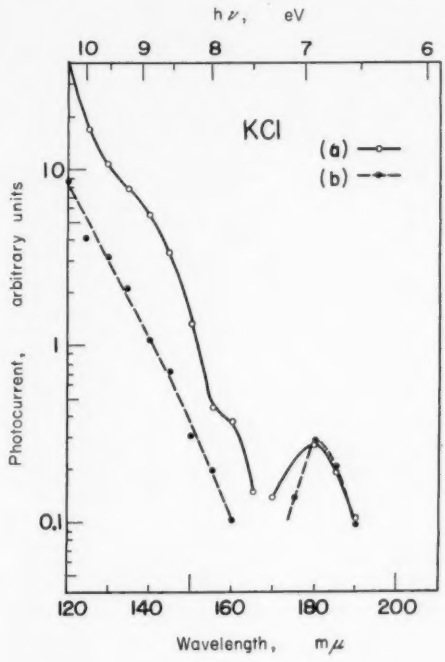

FIG. 6. Photocurrent of KCl at room temperature.
(a) forward direction in 0·8 atm N_2,
(b) mechanically treated, forward direction in 0·8 atm N_2.

Table 1

Crystal	Onset of direct photo-ionization (eV), room temperature	The first peak of photocurrent (eV), room temperature
KI	5·8	5·25
KBr	6·8	5·85
KCl	7·5	6·81

ture-insensitive photoconduction due to direct photoionization in the undisturbed lattice which occurs above the high energy tail of the first peak with nearly constant quantum efficiency irrespective of the photon energy.

REFERENCES

1. EBY J. E., TEEGARDEN K. J. and DUTTON D. B., *Phys. Rev.* **116,** 1099 (1959).
2. FISCHER F. and HILSCH R., *Nachr. Akad. Wiss. Göttingen* **8,** 241 (1959).
3. TAFT E. A. and PHILIPP H. R., *J. Phys. Chem. Solids* **3,** 1 (1957).
4. TAYLOR W. J. and HARTMAN P. L., *Phys. Rev.* **113,** 1421 (1959).
5. FERGUSON J. N., *Phys. Rev.* **66,** 220 (1944).
6. AOYAGI K. and KUWABARA G., *J. Phys. Soc. Japan* **15,** 2334 (1960).
7. GLASER G., *Nachr. Math-Phys. Göttingen* **3,** 31 (1937).

DISCUSSION

A. ROSE: If you assume that each photon excites one free electron, can you estimate the lifetime of a free electron?

G. KUWABARA: No, we cannot, because the mobility of an electron in KI has not been determined.

Vol. 22
1961

J. Phys. Chem. Solids Pergamon Press 1961. Vol. 22, pp. 339–349. Printed in Great Britain.

PHOTOCONDUCTIVITY IN ORGANIC SINGLE CRYSTALS

J. KOMMANDEUR*

Parma Research Laboratory, Union Carbide Corporation, Parma 30, Ohio

Abstract—In general, it is very difficult to define a "band gap" in organic materials. The ultraviolet spectrum of the solid is almost identical to that of the molecules in the vapor phase. Therefore, light absorption is essentially determined by the single molecules. Thus, no relation between thermal and optical band gap is to be expected or found.

Phenomenologically, anthracene can be used for an illustration of most of the properties encountered. Surface currents and bulk currents have been observed and separated experimentally. Under inhomogeneous illumination, space charge effects, the Dember effect, and many other related phenomena have been detected. The photoresponse is closely related to the absorption spectrum and depends critically on the geometrical arrangement. The material is exceedingly sensitive to neutron irradiation. The high impedance of the material precludes measurements of the Hall or photoelectromagnetic effect, but recently the hole and electron mobilities have been measured by a pulsed photoconductivity technique. It was found that the mobilities are of the order of 1 cm^2/V-sec and anisotropic. A theoretical calculation of this anisotropy has been successful.

The magnitude of the photocurrents and their spectral sensitivity can be changed markedly by absorption of electron acceptors, or donors, on the surface of the crystals. This leads to the conclusion, already inferred from other work, that most of the charge carriers are generated in the surface layer.

INTRODUCTION

PHOTOCONDUCTIVITY is a feature common to many organic materials. Particularly in compounds containing π-electrons, i.e. possessing conjugated double or triple bonds or some aromatic ring system, photoconductivity has been found to occur. Historically, the phenomenon has been known to exist since the first decade of the century, but only recently have experiments been carried out which produced detailed information on the photocurrents.

A previous review of the subject was given by GARRETT[1], but recent developments in the field appear to warrant a renewed effort. An endeavour will be made to discuss the subject from a mechanistic as well as from a phenomenological point of view. The molecular nature of the solids must be taken into account and this prohibits the blanket application of the theory of the solid state as it was developed for inorganic semiconductors. Therefore, a discussion of the mechanism of the photoconductivity of organic solids seems to be in order. Since the latter subject is still rather underdeveloped, a large number of experiments have been carried out, which are more or less phenomenological in nature. They have generally been interpreted on the assumption that charge carriers are formed in some way or other at, or close to, the region where light is being absorbed.

To acquaint the reader with the subject matter, a very short review will be given of the chemical nature of the various materials studied. This section will be followed by a few paragraphs outlining the experimental problems and techniques. Since no striking differences between organic compounds have been found, anthracene will be used as the compound with which to illustrate conveniently the mechanistic and phenomenological points of interest.

THE MATERIALS

As mentioned above, almost any organic containing a π-electron system exhibits some photoconductivity. These materials fall largely into two classes. The aromatic hydrocarbons have been

* Present address: Laboratorium voor fysische chemie, Rijksuniversiteit te Groningen, Bloemsingel 10, Groningen, The Netherlands.

studied because theoretical knowledge about the molecules making up the crystal is well developed. The other well studied group is the organic dyes. A large number of them have the property of "sensitizing" inorganic photoconductors. For instance, the spectral response of the photoconductivity of zinc oxide can be shifted towards the visible by absorbing dyes on the surface. This has led to a great amount of interest and many studies on the photoconductivity of dye films are available.[2] In a review of this nature, however, it appears to be sensible to limit the subject. Since the field is relatively new, most information will be gleaned from single crystal studies, and this limits the discussion almost entirely to the aromatic hydrocarbons.

EXPERIMENTAL

Purification of organic materials presents a problem at the present time, since no criteria are yet available to assess the purity. Three methods have been used. Sublimation can eliminate adsorbed gases, chromatography[3] is an excellent tool for removing similar hydrocarbon impurities, and zone-refining[4] has been used by a number of workers to obtain highly purified materials. Crystals have been grown in three different ways. Sublimation[5] leads to thin flakes, which are difficult to handle, but easy to grow. Growing crystals from solution[6] is a little harder, but it has been carried out successfully and it yields larger, less fragile samples. Most widely used is the Bridgman furnace technique.[7] Single crystals up to three feet long have been grown in this manner.

Contacts to samples have been made by silver paint, Aquadag, silver or platinum (pressed on, melted on, or evaporated), and recently by electrolytic solutions.[8] For photoconductivity measurements, evaporated silver has found the widest application, but the electrolytic solutions have led to more intriguing discoveries. The contact problem has not been solved at all, and in the discussion there shall be need to return to this subject.

The photocurrents studied are usually extremely small, in the order of 10^{-10} to 10^{-14} A. This necessitates the use of high input impedance d.c. amplifiers or even vibrating-reed electrometers, together with strong light sources. For the latter, the high-pressure mercury arc and the xenon lamp have found wide application, while recently the tungsten–iodine lamp has provided a very easy and cheap source of light. In addition to d.c. measurements, techniques have been developed using pulsed and modulated light sources.[9] With appropriately tuned amplifiers, very high sensitivities can be obtained.

PHENOMENOLOGICAL ASPECTS

The earlier work on the photoconductivity of anthracene, which will be used as a model to illustrate the properties of organic photoconductors, was mainly concerned with the behavior of

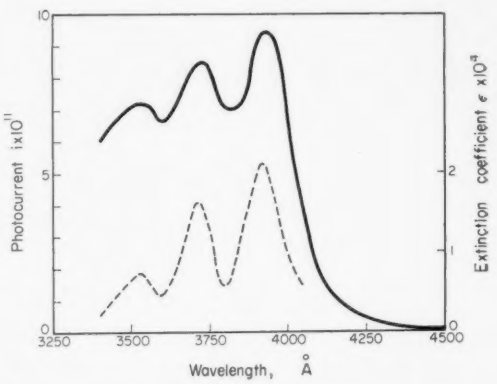

FIG. 1. ———— Spectral response of the surface photocurrent of anthracene. - - - - - - - - - *b*-polarized absorption spectrum of crystalline anthracene.

charge carriers after they had been produced by the light in the material. A distinction must be made between charges traveling across the surface or through the bulk of the material. The surface currents have a spectral response, which is practically identical with the absorption spectrum (Fig. 1). First, this was taken as a point of fundamental interest, but LYONS[10] showed that it could be explained on one of two assumptions: (a) the mobility of charge carriers on the surface is much higher than of those in the bulk, or (b) the charge carriers are formed by excitons, which have to reach the surface first. In both cases, a high absorption coefficient will produce a high number of carriers participating in the transport of charge. It was shown later[11] that the spectral response of the bulk currents was quite different.

Vol. 22
1961

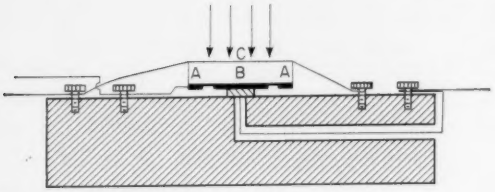

FIG. 2. Sandwich cell:
A—guard ring.
B—solid back electrode.
C—transparent electrode.
(After KOMMANDEUR and SCHNEIDER[12].)

For very pure crystals it could actually be exactly the opposite, i.e. at points of high absorption low currents were obtained.[12]

The bulk currents—separated from the surface currents by guard rings (Fig. 2)—present the most interesting phenomenological problems. One of the most intriguing effects is what is commonly called in this field, the "rectifying effect." If the positive electrode of a crystal is illuminated, the bulk current is substantially higher than when the negative electrode is illuminated. The dependence on the applied voltage is also different in those cases, as is the dependence on the light intensity. This is illustrated in Fig. 3. The positive current usually varies as the square root of the intensity,

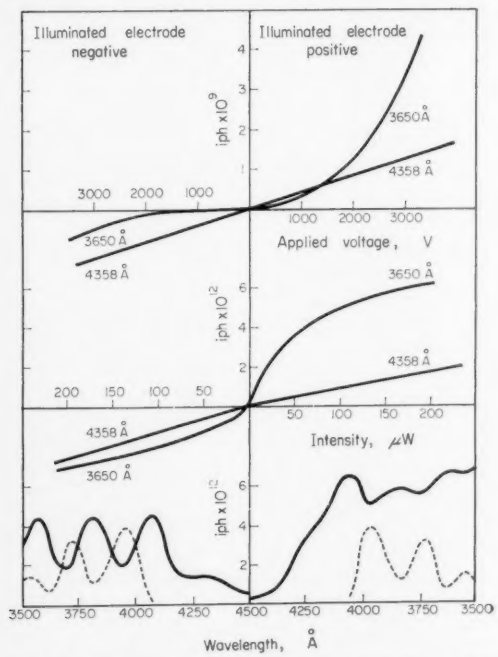

FIG. 3. Differences between positive and negative bulk photocurrents in anthracene. Light of $\lambda > 4000$ Å is weakly absorbed, while light of $\lambda < 4000$ Å is very strongly absorbed.

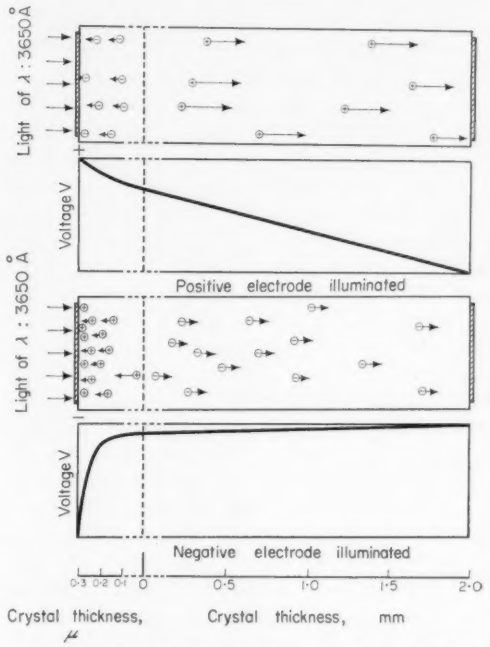
Light of λ : 3650 Å
Voltage V
Positive electrode illuminated
Negative electrode illuminated
0·3 0·2 0·1 0 0·5 1·0 1·5 2·0
Crystal thickness, μ
Crystal thickness, mm

FIG. 4. Charge and field distributions in the sandwich cell for the two directions of field. (After KOMMANDEUR and SCHNEIDER[12].)

the negative as some power closer to one. Also, as can be seen from Fig. 3, the spectral responses are quite different. Then, polarization effects are quite marked. KALLMANN[13] showed that the polarization of a crystal by means of light and applied voltage will persist for many days if thereafter it is kept in the dark. Most of these phenomena were explained on three assumptions.[12]

(a) When suitable energy is absorbed by the crystal, charge carriers are formed in, or close to, the region where this absorption takes place.

(b) Carriers of either sign are discharged at the electrodes but are not freely replenished there.

(c) The positive charge carriers are more mobile.

This then leads to a field and carrier distribution as shown in Fig. 4. With the illuminated electrode positive, the current is recombination limited. It varies as the square root of the intensity and high absorption leads to low currents. With the illuminated electrode negative, a space charge region with a dominance of positive carriers is created, marked polarization effects occur, the recombination becomes more unimolecular, and the spectral response will be a complicated function of the absorption coefficient. Since the slower negative carriers now travel in a region of low field, the negative current is substantially lower than the positive current, where the faster positive carriers are traveling through a field which has not been reduced quite as much. It should be pointed out that a fairly small difference in mobility can thus lead to rather a large "rectifying effect". Similar experiments with inhomogeneous illumination were reported by ZINSZER[14] for the surface cell. Illuminating mainly the positive electrode, he obtained higher currents than when illuminating the negative electrode. When no electrodes are attached to a crystal, a transient is observed upon illumination, which is highest with the applied field in the positive direction, if the positive charge carriers are more mobile. PUTSEIKO[15] used this technique to determine the sign of the majority charge carriers.

When homogeneous illumination is applied in either a surface or a bulk current experiment (in the latter case by using light which is weakly absorbed), the nonlinearities are not present. This is illustrated in Fig. 3 by the curves for light of wavelength 4358 Å impinging on a sandwich cell. The literature contains many references to nonlinear voltage dependences of the photocurrents, but from these experiments it seems that most of these nonlinearities must be related to inhomogeneous illumination andsub sequently developing space charges. MURRELL[16] has given a careful algebraic analysis of the phenomena observed in the sandwich cell. SILVER and MOORE[17] devised a technique for the investigation of the space charge distribution in anthracene sandwich cells. They come to the conclusion that carries are, at least to some extent, injected at the illuminated electrode.

Inhomogeneous illumination will also give rise to a photovoltaic effect. In a sandwich cell arrangement as depicted in Fig. 2, strong illumination will give rise to a Dember photovoltaic effect[18] of up to one volt.[19] The power conversion achieved, however, is extremely small in view of the high impedance over which the voltages are developed.

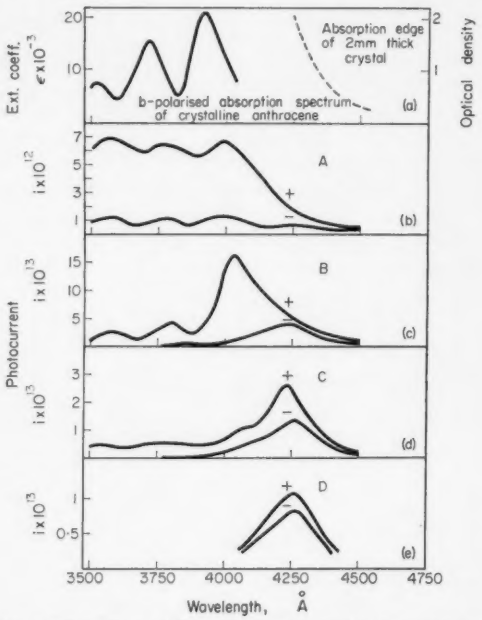

FIG. 5. The effect of damage on the spectral response of bulk photocurrents in anthracene.

A—Very pure, carefully grown crystal.
B—Commercial crystal.
C—Crystal irradiated with neutrons for 20 sec.
D—Crystal irradiated with neutrons for 90 sec.

The sign refers to the polarity of the illuminated electrode. (After KOMMANDEUR and SCHNEIDER[22].)

The magnitude of the photocurrent is anisotropic. Anthracene is a monoclinic crystal with the long axis of the molecules almost parallel to the *c*-axis.[20] It turns out that in this direction the currents are smaller by an order of magnitude than in the *ab*-plane where they are isotropic to within 10 per cent.[21]

The bulk currents in anthracene are extremely sensitive to trapping. The dependence of these currents on wavelength, voltage, and light intensity can be changed completely by irradiating the crystals for a very short time (30 sec at a flux of

Vol. 22
1961

$0{\cdot}2 \times 10^{13}$ cm^{-2} sec^{-1}) with thermal neutrons.[22] Even bulk currents in crystals grown less carefully, and probably containing more defects and impurities, have properties which are quite different from others which have been prepared with great care. Fig. 5 shows the change in the spectral response of the bulk photocurrent in going to progressively more impure and defect-containing crystals. KOMMANDEUR and SCHNEIDER[22], and later BRYANT *et al.*[23], proved the existence of these traps by performing a series of experiments called the conductivity analogue of a thermoluminescent "glow" curve. Crystals are illuminated at low temperatures (77°K), the light is shut off, and they are then heated rapidly. At some temperature, the trapped carriers will be released and an anomalous increase in the dark current occurs. After all the traps are emptied, the dark current returns to its normal value. From the position of the current peak on the temperature scale, the depth of the traps can be inferred—for anthracene about 0·8 eV.[23]

The experiments discussed so far can be explained mainly on the basis of geometrical considerations, recombination, trapping, etc., but they yield little information on the basic process of creation of the carriers and the manner in which they move through the crystal lattice. The next section will be devoted to the information available on these subjects.

THE MECHANISMS OF CREATION AND TRANSPORT OF CARRIERS

The ultraviolet spectrum of crystalline anthracene is very much like the ultraviolet spectrum of the molecule in the vapor phase. Fig. 6 gives the spectra for vapor, solution, and solid, and it is clear that only small red shifts occur in going from the vapor via the solution to the solid. At least, the electronic spectrum of the crystal then is best discussed in terms of discrete energy levels. These arise from the electronic structure of the separate molecule and its various vibrational modes, and they are only weakly perturbed by the environment. A very adequate discussion of these spectra has been given by WOLF[24]. This situation is quite different from that in nonmolecular crystals where band-to-band transitions, or transitions related to these, are the dominant phenomena. It is not certain, therefore, that a linear combination of, for example, the first excited states of the molecules will lead to a band of adequate width to allow appreciable conduction. There is, for instance, no simple relation between the energy of the threshold

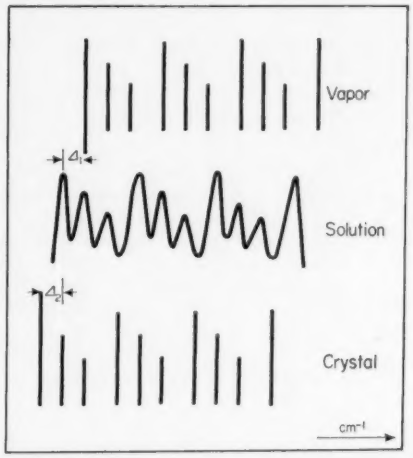

FIG. 6. The change of the ultraviolet spectrum of anthracene for the transition from the vapor, via the solution, to the solid phase. The last two refer to low temperature measurements. (After WOLF[24].)

for photoconduction and the activation energy for dark conductivity. Table 1 compares these numbers for a variety of substances, and it will be obvious that the activation energy for dark conductivity

Table 1. *Dark current activation energies and photoconduction threshold*

Compound	Ref.	E_{dark} (eV)	E_{ph} (eV)
Naphthalene	(a) (d)	0·75	3·7
Anthracene	(b) (d)	0·98	3·0
Tetracene	(b) (e)	0·82	2·4
Pyrene	(b) (d)	1·03	3·2

(a) PICK H. and WIESSMANN W., *Z. Phys.* **138,** 436 (1954).
(b) NORTHROP D. C., *Proc. Phys. Soc. Lond.* **74,** 756 (1959).
(c) NORTHROP D. C. and SIMPSON O., *Proc. Roy. Soc.* **234,** 124 (1956).
(d) KOMMANDEUR J., KORINEK G. J. and SCHNEIDER W. G., *Canad. J. Chem.* **36,** 607 (1958).
(e) BREE A. and LYONS L. E., *J. Chem. Phys.* **22,** 1630 (1954).

Table 2. Dark current activation energy for anthracene

Author	Ref.	Aggregate state	E_{dark} (eV)	Electrode
NORTHROP	(a)	single crystal	0·98	transparent conducting glass
NORTHROP	(b)	film	0·97	lead
SCHIELER	(c)	powder	1·07	"platinum paint"
METTE	(d)	single crystal	0·83	mercury
RIEHL	(e)	film	0·75	mercury
INOKUCHI	(f)	single crystal	1·35	aluminum
ELEY	(g)	powder	0·82	platinum

(a) NORTHROP D. C., *Proc. Phys. Soc. Lond.* **74,** 756 (1959).
(b) NORTHROP D. C. and SIMPSON O., *Proc. Roy. Soc.* **234,** 124 (1956).
(c) SCHIELER L., ANDERSON H. R. and NICHOLS P. L., Jr., *California Institute of Technology Memo Report* 20–162 on Contract DA–04–495.
(d) METTE H. and PICK H., *Z. Phys.* **134,** 566 (1953).
(e) RIEHL N. V., *Zh. Fiz. Kim.* **9,** 1537 (1955).
(f) INOKUCHI H., *Bull. Chem. Soc. Japan* **29,** 131 (1956).
(g) ELEY D. D., PARFITT G. D., PERRY M. J. and TAYSUM D. H., *Trans. Faraday Soc.* **49,** 79 (1953).

is at least not directly related to what would normally be called "half the band gap". Actually, as should be clear from Table 2, there is no hard and fast number known for "half the band gap" in anthracene—the substance most carefully studied. No number, however, comes close to the 1·5 eV required by the threshold for photoconductivity at about 3·0 eV.

A rather extensive search has been made to determine what states could possibly be involved in the conductivity. A likely candidate appears to be the ground triplet state, which lies below the first excited singlet state and has an energy somewhat close to double the dark current activation energy. Experiments on doped hydrocarbons by NORTHRUP and SIMPSON[25] appeared to indicate this state. They found that at low temperatures the activation energy for conduction corresponded to the triplet state of the dopant, while at higher temperatures an energy not related to the triplet state, but characteristic of the host hydrocarbon, was found. In a study of the spectral response of other hydrocarbons than anthracene, KOMMANDEUR *et al.*[26] found that transitions just below the absorption edge were very efficient in promoting photoconductivity. Most spectral responses are plotted at equal incident energy, but if curves at equal absorbed energies are drawn, results as depicted in Fig. 7 are obtained. The photocurrent shows a number of peaks in a region where the crystal hardly absorbs. They suggested that a charge-transfer state might be involved as it is, for instance, in the fluorescence of pyrene.

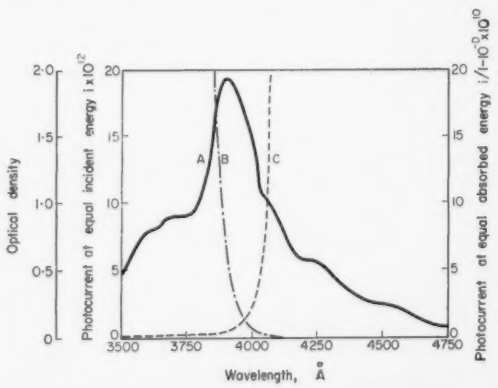

FIG. 7. The spectral response of the photocurrent in pyrene plotted at equal incident energy (A) and at equal absorbed energy (C). The absorption edge of the crystal is indicated by B. (After KOMMANDEUR *et al.*[26].)

ROSENBERG[27] did a similar study on anthracene and found some peaks in the region where one expects the triplet state to absorb. Fig. 8 gives his photoresponse for anthracene. All the experiments, however, seem to reduce to the fact that the

conductivity of the crystal will increase when it absorbs energy, and no final conclusion can be drawn about which state is indeed involved.

In all materials studied the photocurrent depends exponentially on temperature according to the relation:

$$i_{ph} = i_{0ph} \exp(-E/kT).$$

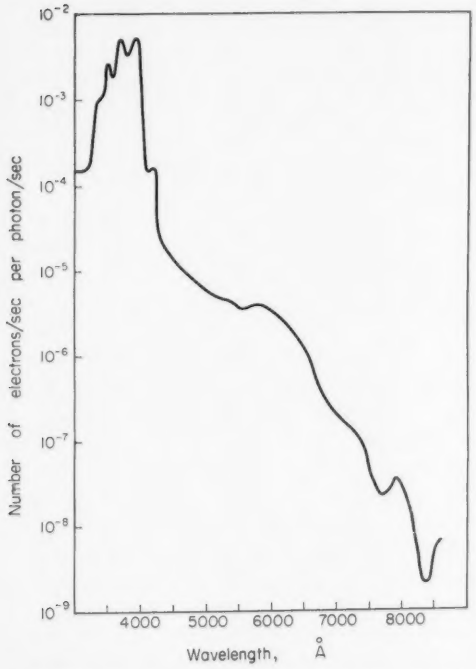

FIG. 8. The spectral response of the photocurrent in anthracene far below the absorption edge (4000 Å). (After ROSENBERG[27].)

Table 3 gives an accumulation of the energies. ROSENBERG[27] has attempted to interpret these numbers in relation to the vibrational states of the molecules. He noticed that they all correspond to one or two vibrational quanta of some vibrational mode of the molecules. It should be noted, of course, that there are many such modes in a large molecule and the correspondence might be coincidental. ROSENBERG cites it as proof for the involvement of the triplet state in the conductivity, but that is an unwarranted speculation, since every state would have these vibrational modes superimposed.

Table 3. The activation energy of the photocurrent[a]

Compound	E (eV)
anthracene	0·18
β-methyl-anthracene	0·17
pyrene	0·35
stilbene	0·082
terphenyl	0·14
biphenyl	0·087
naphthalene	0·078
azulene	0·24

The photosensitivity at room temperature decreases in the downward direction.

(a) KOMMANDEUR J., KORINEK G. J. and SCHNEIDER W. G., *Canad. J. Chem.* **35,** 998 (1957).

More recently evidence appears to be accumulating for the generation of charge carriers on the surface. KALLMANN and POPE[28] studied anthracene crystals with electrolyte contacts. When 0·1N NaCl solution is used as electrolyte, the behavior of the anthracene is not much different from its behavior with metal electrodes. If, however, iodine is dissolved in the electrolyte, the photocurrents are several orders of magnitude higher and the spectral response is extended considerably into the visible part of the spectrum.

BOROFFKA[29] compared crystals with CuI electrodes with excess iodine to aluminum electrodes. He also finds a large increase in the photoconductivity with the iodine-containing electrode. These observations are in agreement with earlier results obtained by WADDINGTON and SCHNEIDER[30] who studied the effects of absorbed gases on the surface photoconductivity of anthracene. They found that electron accepting molecules, such as NO_2, Cl_2 and to a lesser degree O_2, alcohol, ether, etc., increased the photocurrents, while electron donating molecules, such as NH_3, amines, etc., effected a decrease. All these phenomena point to the surface of the crystal as an important source of the carriers.

In this context the experiments of CALVIN and KEARNS[31] on the photoconductivity of phthalocyanine are of interest. They showed that they could increase the photoconductivity of phthalocyanine by a factor of 10^6 by subliming a layer of the electron acceptor chloranil onto the surface

of the phthalocyanine film. This photoconductivity was accompanied by a decrease in the spin resonance signal they found to be present in this lamellar cell. Later they also showed similar effects for other hydrocarbons, such as tetracene and perylene.[32]

It took till 1960 before some quantitative work was reported on the photoconductivity of anthracene. KEPLER[9] and later LEBLANC[33] measured the mobility of the charge carriers in anthracene.

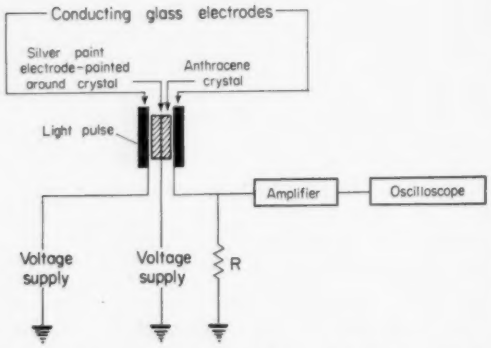

FIG. 9. Apparatus for measuring mobilities by a flash technique. (After KEPLER[9].)

The technique used is similar to a method employed by BROWN and DART[34] for inorganic photoconductors. Using the apparatus sketched in Fig. 9 and pulsed light, KEPLER showed that in a "good" crystal he could generate a pulse of charge carriers at one electrode, which under the applied field migrates to the other. The resulting displacement current pulse can be measured on an oscilloscope. From this one obtains the transit time of the charge carriers and thus their mobility. KEPLER found anisotropy in the mobility. In the cleavage (*ab*) plane the mobilities for holes and electrons were 1·3 and 2·0 $cm^2\ V^{-1}\ sec^{-1}$ respectively, while at right angles to this plane the mobilities were, respectively, 0·4 and 0·3 $cm^2\ V^{-1}\ sec^{-1}$. This is in complete agreement with the previous observations of the anisotropy in the photocurrent by METTE and PICK[21], but only partially with the general conclusions from the rectifying phenomena that the positive charge carriers are most mobile. KEPLER also found a marked dependence of the current pulses on the types of crystals used. Only in the very purest and most perfect were the full transient pulses observed. From the shape of the spectral response for the generation of charge carriers, and from the marked effects that surface treatments had on the production of charge carriers, KEPLER was also forced to the conclusion that the main source of charge carriers is the surface.

The temperature dependence of the mobility was a normal T^{-1} dependence, and the exponential dependence of the photocurrent on temperature can, therefore, not be due to a thermally activated "hopping" process. It must have its source in the generation of the carriers, and ROSENBERG's[27] suggestion of the involvement of a vibrational state becomes rather attractive.

A very intriguing theoretical calculation on the band structure and transport properties of anthracene has been made by LEBLANC[35]. His treatment differs from conventional band theory in that he uses a linear combination of ionic wave functions rather than a linear combination of wave functions for the ground and excited states. Therefore, he derives transport properties only for excess holes or electrons, in a "hole" or "electron band," respectively. These bands are different from the conventional valence and conduction bands, since they do not give any information on transitions yielding an electron and a hole directly. From his calculations, using simple ionic Slater wave functions, LEBLANC obtains a bandwidth of 0·56 kT and an anisotropy for the mobilities, which is roughly equal to that measured by KEPLER. From the absolute experimental values of the mobilities LEBLANC obtains scattering parameters, which indicate that an electron or a hole can travel at least a few lattice parameters before it is scattered, indicating that it still makes sense to talk in terms of band structure for the transport mechanism.[36] This theoretical treatment then does not yield any information on the band gap, or on the states, which should be combined to give an intrinsic valence and conduction band. It only deals with the excess electrons or holes which in some fashion enter into the crystal.

LYONS[37] has endeavored to estimate the band gap, or at least the energy required to obtain a separated electron and hole, by an essentially thermodynamical argument. With slight modifications it can be reproduced as follows:

Consider a solid made up of molecules A and B (Fig. 10).

1. Remove a molecule A to vacuum. Energy involved $+S_A$.
2. Remove a molecule B to vacuum. Energy involved $+S_B$.
3. Ionize molecule A. Energy involved $+I$.
4. Put electron on molecule B. Energy involved $-E_a$.

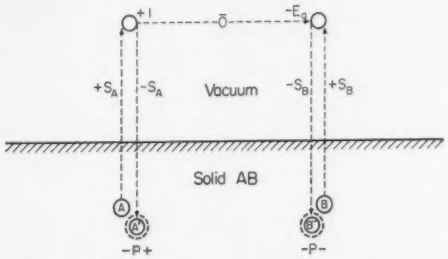

FIG. 10. Diagram for the calculation of the energy for charge separation.

5. Put positive ion A^+ back in the solid, but keep all the electrons in place. Energy involved $-S_A$.
6. Put negative ion B^- back in the solid, and keep all the electrons in place. Energy involved $-S_B$.
7. Let electrons relax in and around A^+. Energy involved $-P_+$.
8. Let electrons relax in and around B^-. Energy involved $-P_+$.
9. Let A^+ and B^- interact Coulombically. Energy involved $-Q$.

When these energies are summed, the energy involved in creating a separated hole and electron is obtained:

$$E_{c.s.} = I - E_a - P_+ - P_- - Q.$$

When $A = B$ this holds for a pure molecular solid and

$$E_{c.s.} = I - E_a - 2P - Q.$$

By estimating the various quantities involved, LYONS found for anthracene $E_{c.s.} = 5{\cdot}2$ eV. FOX[38], who considered next nearest neighbor interactions in the polarization energy, revised this number downward somewhat, but it has not yielded a satisfactory value for the dark current activation energy of about 1·6 eV. Of course, if the surface or impurities are the source of carriers, then it becomes considerably harder to make any calculations with this scheme. If carriers are injected by a metal electrode, then for positive hole injection $E_{c.s.}$ becomes:

$$E_{c.s.} = I - W - P_+,$$

where W is the work function of the metal. (Q is usually too small at these carrier concentrations to play a role.) This would explain Table 2 with the many different values obtained for the dark current activation energy. The numerous experimenters used different electrodes! The effects of electron accepting molecules adsorbed on the surface, or used as electrodes (iodine!), can also be understood on this scheme. Since they all have high electron affinities (E_a), they will tend to decrease $E_{c.s.}$, thus make more carriers available and increase the semi- or photoconductivity. The recently obtained high conductivities in organic materials consisting of donor–acceptor complexes[39, 41] also point in this direction.

In summary, it can be stated that although many organic materials exhibit photoconductivity, even for the most carefully studied compound—anthracene—the mechanism by which the charge carriers are formed is not completely understood. All evidence seems to point in the direction of extrinsic photoconductivity with impurities, or the surface of the crystal as the main source of supply.

The high impedances involved have so far precluded any technical use of organic photoconductors, but as the role of specific impurities is better understood, some applications not needing high mobilities may yet come about. Of further academic interest is the question whether photoconductivity may be involved in some biological processes, such as vision or photosynthesis. Some authors[42] have tried to find some correlation, but so far without much success.

REFERENCES

1. GARRETT C. G. B. and HANNAY H. B., *Semiconductors*, p. 634. Reinhold, New York (1959).
2. VARTANYAN A. T., *Izv. Akad. Nauk. SSSR. (fiz. ser.)* **20**, 1541 (1956).

3. SANGSTER R. C. and IRVINE J. W., *J. Chem. Phys.* **24,** 670 (1956).
4. BEYNON J. H. and SAUNDERS R. A., *Brit. J. Appl. Phys.* **11,** 128 (1960).
5. FERGUSON J., *Aust. J. Chem.* **9,** 160 (1956).
6. KALLMANN H. and POPE M., *Rev. Sci. Instrum.* **29,** 993 (1958).
7. LIPPSETT F. R., *Rev. Sci. Instrum.* **29,** 423 (1958).
8. KALLMANN H. and POPE M., *Rev. Sci. Instrum.* **30,** 44 (1959).
9. KEPLER R. G., *Phys. Rev.* **119,** 1226 (1960).
10. LYONS L. E., *J. Chem. Phys.* **23,** 220 (1955).
11. LYONS L. E. and MACKIE J. C., *J. Chem. Soc.* 5186 (1960).
12. KOMMANDEUR J. and SCHNEIDER W. G., *J. Chem. Phys.* **28,** 582 (1958).
13. KALLMANN H. and ROSENBERG B., *Phys. Rev.* **97,** 1596 (1955).
14. ZINSZER H. J., *Z. Naturf.* **11A,** 306 (1956).
15. PUTSEIKO E. K., *Dokl. Akad. Nauk. SSSR* **67,** 1009 (1954).
16. MURRELL J. N., *Disc. Faraday Soc.* **28,** 36 (1959).
17. MOORE W. and SILVER M., *J. Chem. Phys.* **33,** 1671 (1960).
18. KALLMANN H. and POPE M., *J. Chem. Phys.* **30,** 585 (1959).
19. KOMMANDEUR J., unpublished work.
20. MONTEATH ROBERTSON J., *Organic Crystals and Molecules*, p. 187. Cornell University Press, New York (1953).
21. METTE H. and PICK H., *Z. Phys.* **134,** 566 (1953).
22. KOMMANDEUR J. and SCHNEIDER W. G., *J. Chem. Phys.* **28,** 590 (1958).
23. BRYANT F. J., BREE A., FIELDING, P. A. and SCHNEIDER W. G., *Disc. Faraday Soc.* **28,** 48 (1959).
24. WOLF H., *Solid-State Physics* (edited by SEITZ F. and TURNBULL J.) Vol. 9, p. 1. Academic Press, New York (1959).
25. NORTHRUP D. C. and SIMPSON O., *Proc. Roy. Soc.* **234,** 124 (1956).
26. KOMMANDEUR J., KORINEK G. J. and SCHNEIDER W. G., *Canad. J. Chem.* **36,** 607 (1958).
27. ROSENBERG B., *J. Chem. Phys.* **29,** 1108 (1958).
28. KALLMANN H. and POPE M., *J. Chem. Phys.* **32,** 300 (1960).
29. BOROFFKA H., *Z. Phys.* **160,** 93 (1960).
30. WADDINGTON T. C. and SCHNEIDER W. G., *Canad. J. Chem.* **36,** 789 (1958).
31. KEARNS D. R., TOLLIN G. and CALVIN M., *J. Chem. Phys.* **32,** 1020 (1960).
32. KEARNS D. R. and CALVIN M., *J. Amer. Chem. Soc.* **83,** 2110 (1961).
33. LEBLANC O. H., *J. Chem. Phys.* **33,** 626 (1960).
34. BROWN F. C. and DART F. E., *Phys. Rev.* **108,** 281 (1957).
35. LEBLANC O. H., to be published.
36. FRÖLICH H. and SEWELL G. C., *Proc. Phys. Soc. Lond.* **74,** 643 (1959).
37. LYONS L. E., *J. Chem. Soc.* 5001 (1957).
38. FOX D., *J. Phys. Chem. Solids* **8,** 439 (1959).
39. KOMMANDEUR J. and HALL F. R., *J. Chem. Phys.* **34,** 129 (1961).
40. LABES M. M., SEHR R. and BOSE M., *J. Chem. Phys.* **32,** 1570 (1960).
41. KEPLER R. G., BIERSTEDT P. E. and MERRIFIELD R. E., *Phys. Rev. Letters* **5,** 503 (1960).
42. ROSENBERG B. *J. Opt. Soc. Amer.* **51,** 238 (1961).

DISCUSSION

MILTON GREEN: Has anyone ever detected a Hall voltage on organic materials?

J. KOMMANDEUR: No. It would be extremely difficult to detect a Hall voltage because the purer crystals are essentially insulators. In semiconducting compounds of organics various attempts have been made, but no positive results have been reported. It would seem as if the extremely low mobility in addition to a possible lowering of the Hall effect due to a high degree of carrier localization would make the effect very hard to measure.

A. ROSE: While you put emphasis on the generation of free carriers at the surfaces, it seemed to me that your own data showed good evidence of volume generation of carriers.

J. KOMMANDEUR: Bulk generation is only marked when weakly absorbed radiation is used. Then the photocurrents are considerably lower. One would immediately suspect impurities to be responsible in this case. Since the light now penetrates the whole crystal, all impurities can take part in the generation.

G. K. GAULÉ: You mentioned that μ_p is always greater than μ_n. Is this characteristic of all anthracenes and other organic crystals?

J. KOMMANDEUR: The literature mentions only one example of *n*-type conductivity in the case of an amonic dye. Dr. M. KLEINERMAN from Louisiana State University mentioned that phenazine also shows *n*-type conductivity.

D. L. DEXTER: Can you estimate the highest purity now obtainable in bulk anthracene?

J. KOMMANDEUR: This is a hard question to answer since at present no criteria are available for assessing the purity of anthracene. KEPLER's work was carried out on "very pure" crystals, containing less than 2 p.p.m. of radioactively tagged materials. Experiments on the elimination of tetracene from anthracene (which is easily detectable to 1 p.p.m. because at that point the anthracene fluorescence returns and the tetracene fluorescence disappears) indicate that one chromatography run eliminates this impurity to less than 1 p.p.m.

D. KAHN: (1) What is the specific resistivity of an anthracene crystal illuminated with 4025 Å light?

(2) Are the surface effects important because of absorbed impurities or are they caused by disarranged electron bonds due to surface forces?

J. KOMMANDEUR: (1) With an illumination of about 100 μW/cm^2 of 4000 Å light, the bulk conductivity of anthracene is about $10^{-12}\ \Omega^{-1}\ \text{cm}^{-1}$.

(2) Anthracene in the vapor phase has no disarranged bonds and it should therefore not have any on the surface of a crystal. It would take about 80 kcal to disarrange such a bond and since no obvious compensation for this energy is present, the broken bonds should probably be relegated to the realms of the imagination, at least in the case of organic solids.

A. M. GOODMAN: Do you have any measurements of the time constants associated with the photocurrents (i.e. rise and decay times)?

J. KOMMANDEUR: They are being measured at present and are quite fast.

M. SILVER: (comment) Rise times are much faster than a μsec. Decay times are slower and dependent upon trapping (surface and bulk). In the S.C.L. region, decay times are $\sim$ 100 μsec and in the non-S.C.L. region they are $\sim$ 10 μsec or less.

G. ONEAL, Jr.: In anthracene crystals does increasing purity lead to lower dark currents and higher photocurrents?

J. KOMMANDEUR: Increasing purity does reduce dark current. Some impurity additives increase the photocurrent considerably, but on the other hand, as impurities and traps are eliminated, the steady-state photocurrents may be increased in some cases. It depends, as usual, on the impurities under consideration.

R. K. SWANK: What is the range of excitations in a typical case?

J. KOMMANDEUR: 500–600 Å as found from the interpretation of the photoresponse, from studies of the impurity fluorescence and from experiments by NORTHRUP and SIMPSON on the excitation transfer through thin layers of anthracene on to luminescing cadmium sulfide.

T. S. MOSS: To study the bulk photoconductivity it would be advisable to mount electrodes close together in the middle of the crystal (if necessary growing the crystal around them) and then focus long wavelength light between the electrodes.

J. KOMMANDEUR: Although this might preclude effects of ambient gases, it will not eliminate the most troublesome impurity of all—the electrode. It looks, for instance, as if recombination effects are much more pronounced at metallic electrodes than at electrolytic contacts. Also, the long wavelength light which will have to be used to obtain sufficient penetration will not allow studies of charges traveling through the dark bulk of the material which was the primary consideration for the use of the sandwich cell.

22
61

BLANK
PAGE

Vol. 22
1961

J. Phys. Chem. Solids Pergamon Press 1961. Vol. 22, pp. 351–363. Printed in Great Britain.

PHOTOCONDUCTIVITY AND THE EXTERNAL PHOTOELECTRIC EFFECT IN PbS*†

A. SMITH and D. DUTTON

Institute of Optics, University of Rochester, Rochester, N.Y.

Abstract—We have measured the yields for photoconductivity and external photoemission in the vacuum ultraviolet spectral region, 584–3000 Å, using polycrystalline layers and natural crystals. The photoconductive yield in PbS layers rises approximately linearly with incident photon energy $h\nu$ up to 7·5 eV; further extension of the measurement was thwarted by the magnitude of the external photocurrent. The rise in yield, as previously reported by us, is attributed to collision multiplication beginning at $h\nu_t = 2$ eV. The observed photoelectric threshold for galena crystals was ~ 5 eV, and for layers ~ 6 eV. Both kinds of specimen exhibit very large external photoyields at high $h\nu$: 10–20 per cent at $h\nu = 14{\cdot}5$ eV. The energy distribution of emitted electrons was examined using retarding-potential methods. The high photoelectric thresholds imply that any electron with sufficient energy to escape would be subject to scattering due to collision multiplication, an effect expected normally to limit the attainable photoelectric yield. From the high ultimate yields that were observed, and from the changes in the energy distribution of the emerging electrons with increasing $h\nu$, we infer that scattering by collision multiplication, considered as a function of $h\nu$, is not a monotonically rising function, but has a maximum. The data suggest strongly that this occurs for incident photon energies of slightly more than 9 eV.

THIS paper describes an exploratory investigation of photoconductivity and external photoemission of lead sulfide in the vacuum ultraviolet spectral region, in the range $h\nu = 4{\cdot}5$–$21{\cdot}2$ eV. We had previously reported[1] a rise in the relative quantum yield of photosensitive PbS layers, with increasing incident photon energy, beginning at $h\nu = 2$ eV and continuing monotonically to 6 eV, the limit of the measurements. (See Fig. 1.) This rise was attributed to the onset of collision multiplication, as observed in other photoconductors by KOC[2], TAUC[3], VAVILOV[4] and others. The original aim of the present investigation was an attempt to extend such spectral response measurements in PbS layers to higher photon energies, in the expectation that such measurements might provide further information or insight about the collision multiplication process in this material.

* Research supported by the Office of Scientific Research, U.S. Air Force, and by the National Aeronautics and Space Administration, Goddard Space Flight Center.

† Based on the Ph.D. dissertation of ABBOTT SMITH, University of Rochester, 1961.

EXPERIMENTAL METHODS

The monochromator used is a normal-incidence instrument which employs a concave grating constrained to move on a 40-cm Rowland circle. The grating is used in first order, and is blazed for 1500 Å. The light source is a high-voltage capillary discharge in hydrogen (or helium). The discharge gas enters the lamp continuously through a capillary leak and is exhausted by the main pumping system of the monochromator. There are no windows in the system, so the sample chamber contains hydrogen, at a pressure of from 1 to 10 μ. To eliminate overlapping orders, filters of fused silica or Vycor glass can be inserted before the exit slit; these permit an upper limit of about 7·5 eV and 5·6 eV, respectively, in the transmitted radiation. The useful spectral range of the monochromator is from 4·5 to 14·5 eV, with one additional point at the He 584 Å line, 21·2 eV.

Attached after the exit slit is a brass chamber containing a probe reflectometer.[5] (See Fig. 2.) The reflectometer probe consists of a bent Pyrex rod, coated with aluminum, with a polished face normal to the incident beam. This face is coated with sodium salicylate, applied by spraying with a

solution of sodium salicylate in alcohol. Light from the phosphor is conducted through the Pyrex rod to a photomultiplier located outside the vacuum system. The housing of the reflectometer served as the sample chamber for all measurements, and the probe was used as the primary monitor of the intensity of radiation on the sample.

the monochromator vacuum. The thermocouple was introduced at frequent intervals in order to maintain an absolute calibration of the phosphor–probe–photomultiplier system.

Outside the 7–14 eV spectral region, available beam intensities were too low to obtain accurate readings with the radiation thermocouple, and

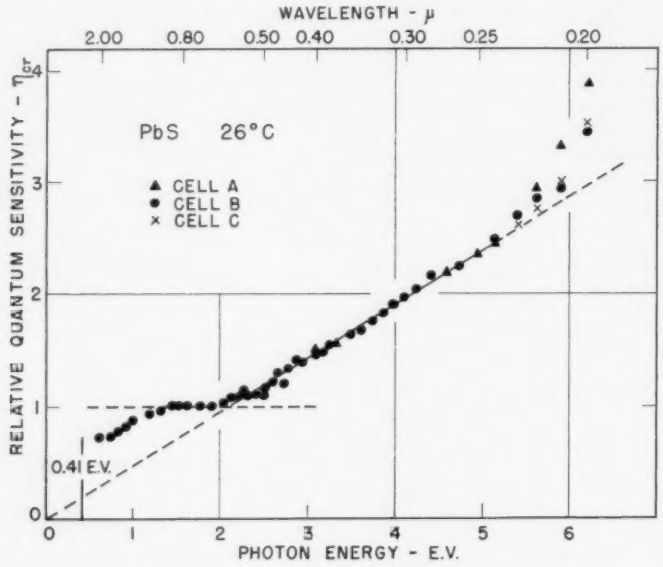

FIG. 1. The relative quantum yield of photoconductivity for three chemically deposited PbS layers. The ordinate is interpreted as being proportional to the number of electron–hole pairs created per absorbed photon, and the absolute value of this number is approximately that given by the ordinate scale. (After SMITH and DUTTON[1].)

Figure 2 shows the arrangement for reflectance measurements. For measurements of photoconductivity or photoemission, the samples were supported from a brass cylinder coaxial with the beam and entering the chamber through the "accessory port" shown in the Figure. This sample mount could be moved in toward the exit slit or back without breaking the vacuum. A compatible mount holding a radiation thermocouple could be introduced instead of the sample mount; the sample chamber could be sealed off from the monochromator by a compact ball-valve arrangement, so that the interchange of sample and thermocouple could be made without breaking the absolute radiometry depends on the assumption of a constant quantum yield for the sodium salicylate phosphor.[6, 7]

The electrode geometry and circuitry are illustrated schematically in Fig. 3. For photoconductivity measurements, the beam was mechanically modulated at 15 c/s and the signal measured with a tuned amplifier system having an input noise threshold of 0·2 μV. In every case the practical threshold of signal detection was limited by the noise of the photocell. For measurements of external currents, in most cases a vibrating-reed electrometer was used, and the current measured in the emitter circuit.

Vol. 22
1961

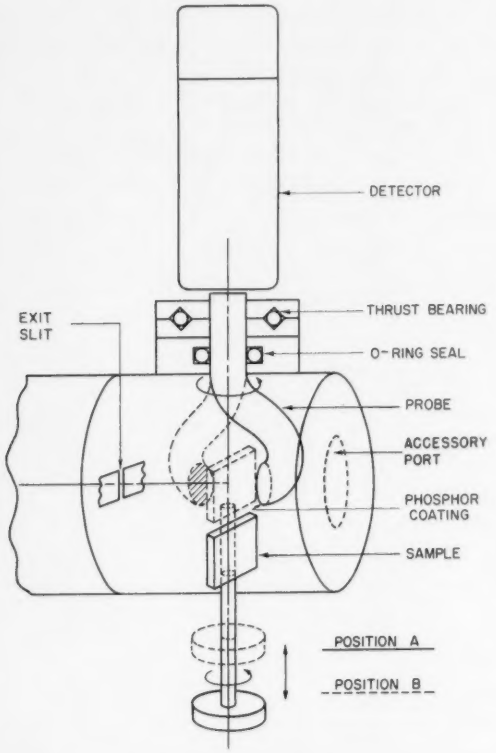

FIG. 2. The probe reflectometer, as used for reflectance measurements. For electrical measurements, the samples were mounted on a tube (not shown) which enters at the "accessory port" through an arrangement of O-ring seals which permits the sample to be moved towards the slit and back without breaking the vacuum.

PHOTOCONDUCTIVITY

Photoconductivity samples were chemically deposited layers, 4 mm square, with electrodes of evaporated gold. They were typical Kodak Ektron "Type *N*" detectors, except for the absence of a protective coating. Reflectance measurements were made on similar films on which, for convenience, the electrodes were omitted.

The absolute reflectance spectra for three such layers are shown in Fig. 4. The low values of reflectance (1–7 per cent) are probably due to the three-dimensional structure of such coatings, which contain crystallites in various orientations, many of which have dimensions approaching the average thickness of the film.

The determination of photoconductivity spectra proved extremely difficult. The photocells were not only unstable in the environment of the monochromator (this instability was chiefly evident as a drastic increase in resistance), but were also extremely sensitive to irradiation fatigue effects, for incident quantum energies greater than about 6 eV. Even the minimal exposure intensities necessary to detect internal photocurrents resulted in appreciable loss of sensitivity, and intense irradiation caused a drastic increase in the dark noise, almost total loss of sensitivity, a temporary drop in resistance (followed by a four- or five-fold increase on cessation of the irradiation), and an obvious discoloration of the specimen.

Figure 5 shows typical results of a photoconductivity spectrum measurement. The uppermost curve in this figure was obtained on a previously unexposed cell (curve 1A). (The spectral dependence of the external yield on the same current scale is shown as curve 1B.) Curve 2 was obtained immediately afterwards, and shows an overall reduction in the internal yield resulting from the

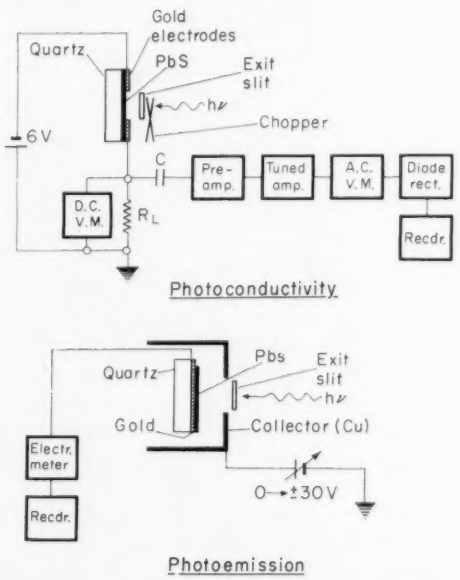

FIG. 3. Schematic illustration of electrode arrangements and circuitry. All metal parts near the beam were coated with polystyrene to prevent spurious photoemission effects.

relatively small exposure required for the previous runs. The internal yield after exposure to an estimated 3×10^{16} photons using the monochromator's zero-order beam filtered by fused silica ($h\nu$ limited to $< 7{\cdot}5$ eV) is shown in curve 4, and after a comparable irradiation dose using the full zero-order beam (most of the radiation in the 1600 Å and 1200 Å regions), the internal current could not be detected at all.

by HAMANN[7] in sodium salicylate phosphor coatings at the corresponding wavelength.

In sum, the present attempt to extend photoconductivity spectra in PbS has not yielded any new detailed information relevant to the collision multiplication process; the most apt description of the behavior, from these measurements, is that of a continued monotonic rise in the yield at least to $h\nu = 7{\cdot}5$ eV.

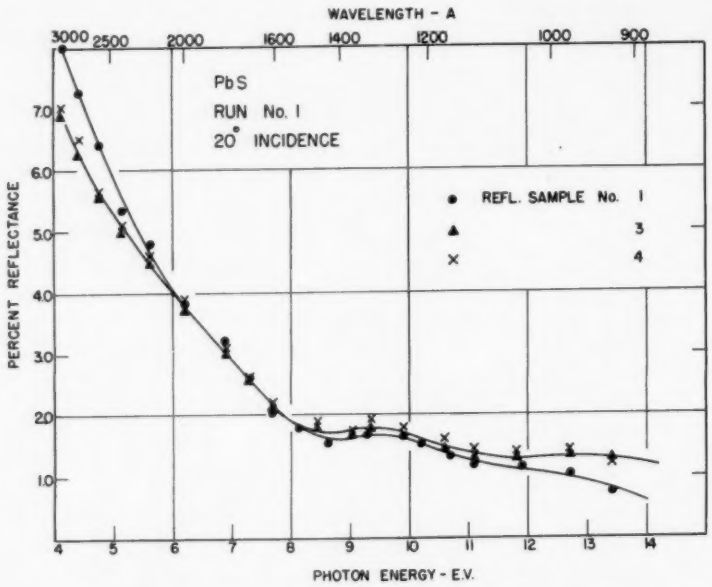

FIG. 4. Reflectance spectrum for polycrystalline, chemically deposited PbS layers. Three samples are shown.

All the photoconductivity data taken with minimal exposure show a continued increase in the yield, approximately linear with $h\nu$, out to $7{\cdot}5$ eV, beyond which external currents were so large that observation of internal currents was impossible. All the data show an apparent peak in the internal yield, near $h\nu = 4{\cdot}5$ eV. This region had been covered in our earlier study, and measurements were made during the present study using a different apparatus, in air; in neither case was this structure observed. We believe it to be merely an artifact of the radiometry. In all cases it is traceable to an anomalous dip in the incident-light spectrum, probably associated with a transmission window observed

PHOTOEMISSION

The spectral dependence of the external photoelectric yield, on an absolute scale, for three different PbS films, is shown in Fig. 6. The photoelectric threshold invariably shifted slightly to higher energies, after the first exposure of the specimen, after which the yield curve was stable and could be repeated several times without further change; it is the stabilized yield curve that is shown in Fig. 6. The yield curve was, somewhat surprisingly, quite reproducible from sample to sample, for samples subjected to the same irradiation history.

The significant point of these data is the ultimate high value of the external yield—15–20 per cent

Vol. 22
1961

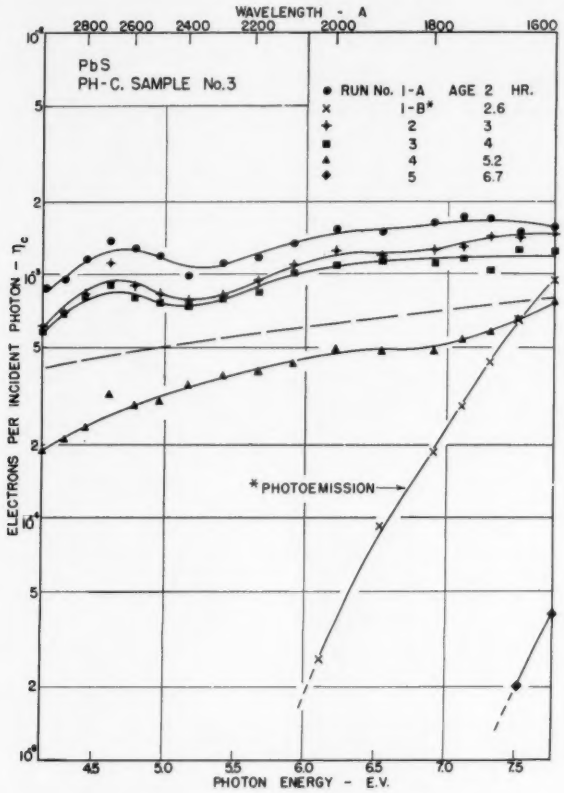

FIG. 5. Typical photoconductivity spectral data for a PbS layer. The resistance of the sample was changing throughout the measurements, so the response is reduced to electrons passing through the external circuit, per incident quantum, per unit electric field in the sample. Run 1–A was measured on a previously unexposed sample, and Run 2 immediately following Run 1–B, the latter being an observation of the total external photocurrent. Run 2 illustrates the irradiation "fatigue" due only to the exposure received during monochromatic illumination while taking the data of 1A and 1B. Curve 4 shows the marked reduction of sensitivity by exposure to the zero-order beam filtered by quartz (passing only photon energies $h\nu < 7{\cdot}5$ eV). Curve 5 was obtained after irradiation by a comparable number of higher-energy photons ($\sim 3\times10^{16}$) using the unfiltered zero-order beam. The peak at 4·5 eV is an artifact of the radiometry. The dashed curve is the plot of a linear function having the same slope as that observed in similar measurements (see Fig. 1) at the threshold for collision multiplication near 2 eV.

at $h\nu = 14{\cdot}5$ eV. (Assuming that the sensitivity of the radiometric phosphor was still unchanged at 21·2 eV, the yield at 21·2 eV was of the same order, 15–30 per cent.)

Retarding-potential measurements were made for various incident photon energies. Although with the electrode geometry used here such curves cannot be interpreted quantitatively in terms of the external electron energy distribution, we expect that any gross features of a dependence on $h\nu$ would still be preserved. Fig. 7 shows retarding-potential curves for a layer specimen for

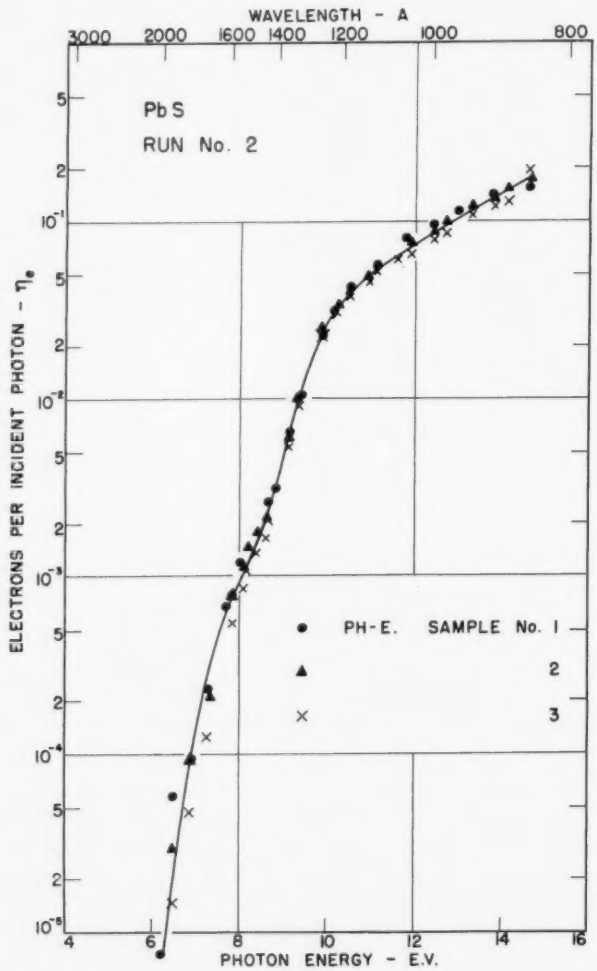

FIG. 6. External photoelectric yield data for three different PbS layers, plotted on the same absolute scale. Plotted here is the stable form of the yield curve, always obtained as the second repetition of the measurement procedure on a previously unexposed sample. Further repetitions of the measurement do not affect the yield curve.

Vol. 22
1961

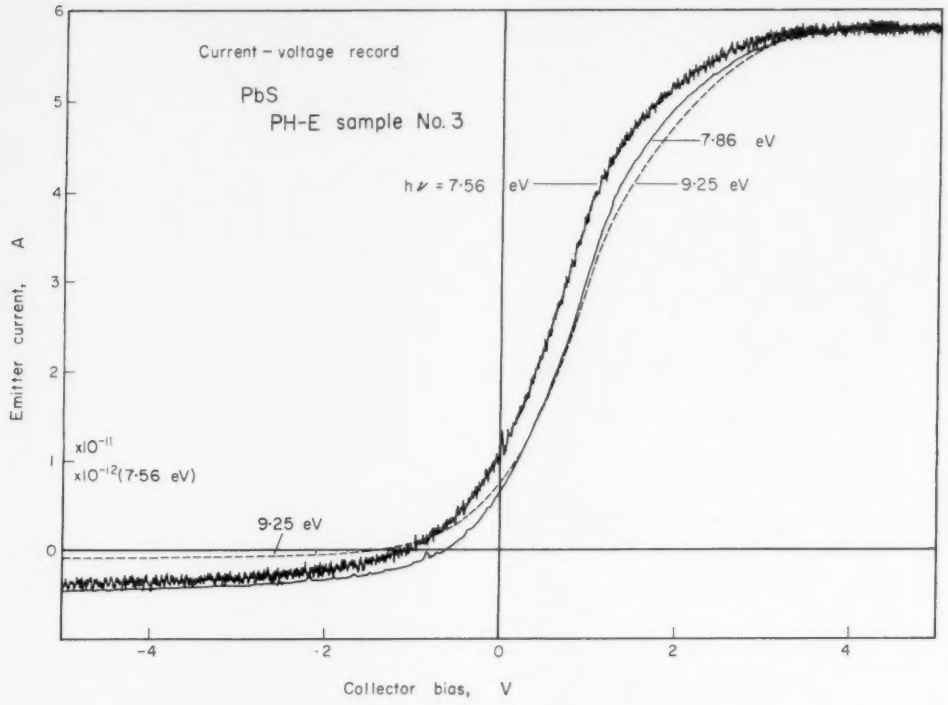

FIG. 7. Reproduction of retarding-potential data obtained by an automatic curve-plotting method. The emitter is a PbS layer. Note the slight shift of the curves toward lower collector voltages, as the incident photon energy increases.

incident photon energies ranging from 7·7 to 9·25 eV. As the photon energy increases, there is a slight shift toward lower kinetic energies of the emerging electrons. As $h\nu$ is increased above 9·25 eV (see Fig. 8), the shift of the external-electron energy distribution reverses and moves toward higher energies, with an increasing fraction of higher energy electrons. The energy distributions obtained by graphical differentiation of retarding-potential curves are given in Fig. 9.

For comparison, similar data were taken using natural crystal specimens from Kansas, Wisconsin and Peru. The Peruvian galena crystals were markedly more perfect in crystal habit than the others and were especially easy to cleave, with almost mirror-like cleavage planes. Fig. 10 shows the reflectance of a cleaved surface of Peruvian galena. The structure shown is significant, and could be seen in the Kansas and Wisconsin specimens, in somewhat poorer detail in the latter cases.

It was possible to cleave the Peruvian crystals in the vacuum system, and the photoelectric yield data obtained on such surfaces for several specimens are shown in Fig. 11. (Crystals cleaved in air and placed immediately in the sample chamber displayed very nearly the same yield curves.) Data for Kansas and Wisconsin specimens were quite similar.

Typical retarding-potential curves, using a crystal specimen, are shown in Fig. 12, and the (qualitative) electron energy distributions in Fig. 13. The gross features of the dependence on incident $h\nu$ are the same as that observed for polycrystalline samples, except that two reversals in the

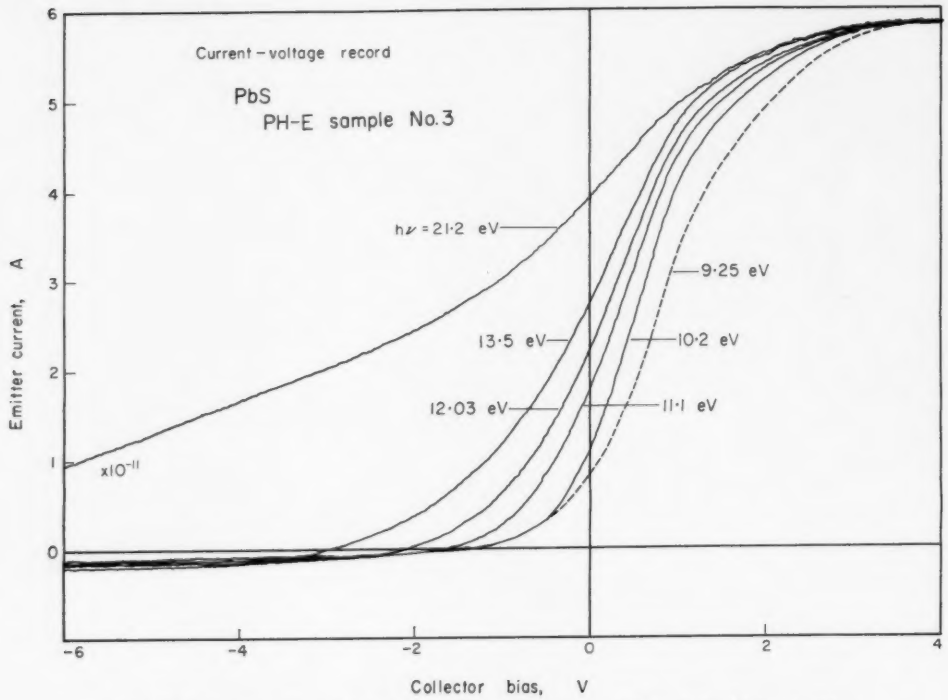

FIG. 8. Retarding-potential data for the same emitter as in Fig. 7 for higher incident photon energies. Note that the curves now shift toward higher collector voltages with increasing $h\nu$.

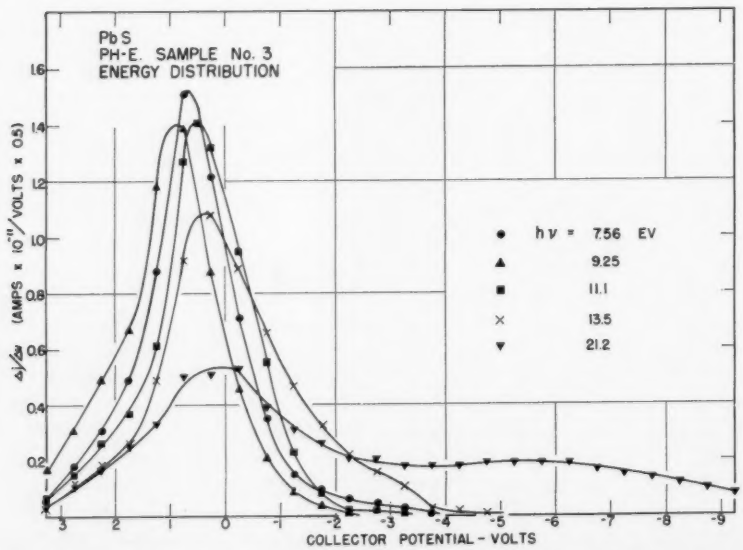

FIG. 9. Plots of the derivatives of the curves in Figs. 7 and 8, showing qualitative energy distribution of emitted electrons (energy increasing toward the right).

trend of the external electron energy distribution are now apparent.

The rather complex behavior has recently been studied more extensively by recording a great many retarding-potential curves using small increments in $h\nu$. The peak of the energy distribution curves first shifts slightly toward higher energies, in the range $h\nu = 7{\cdot}5$–$8{\cdot}6$ eV; there is then a rapid shift toward lower energies, with a sharp "minimum" at $h\nu = 9{\cdot}13$ eV, after which, as $h\nu$ increases, the peak moves steadily toward higher energies; and the fraction of higher energy electrons also steadily increases. Fig. 14 shows the detailed dependence of the peak of the energy distribution curves on the incident photon energy.

DISCUSSION

If the electron affinity of a crystal (defined as the distance from the vacuum level to the bottom of the conduction band) is larger than the threshold energy for collision multiplication, multiplication provides a dominant scattering mechanism for any electron which has enough internal kinetic energy to escape from the crystal; such a material, as pointed out by TAFT *et al.*[8], would be expected to have a low photoelectric yield since the escape depth of strongly scattered electrons would be very small. In the case of PbS, the observed photoelectric thresholds ($\sim$ 5 eV for crystal surfaces, $\sim$ 6 eV for polycrystalline layers) are substantially larger than the band gap, 0·41 eV, and well above the apparent incident photon energy threshold for collision multiplication, which as inferred from the photoconductivity spectra occurs at $h\nu = 2$ eV. The ultimate yield observed, at very large photon energies, is nevertheless quite large, comparable to that observed in materials of very small electron affinity. The emerging electrons excited by energetic quanta have a different energy distribution, a more marked high-energy "tail",

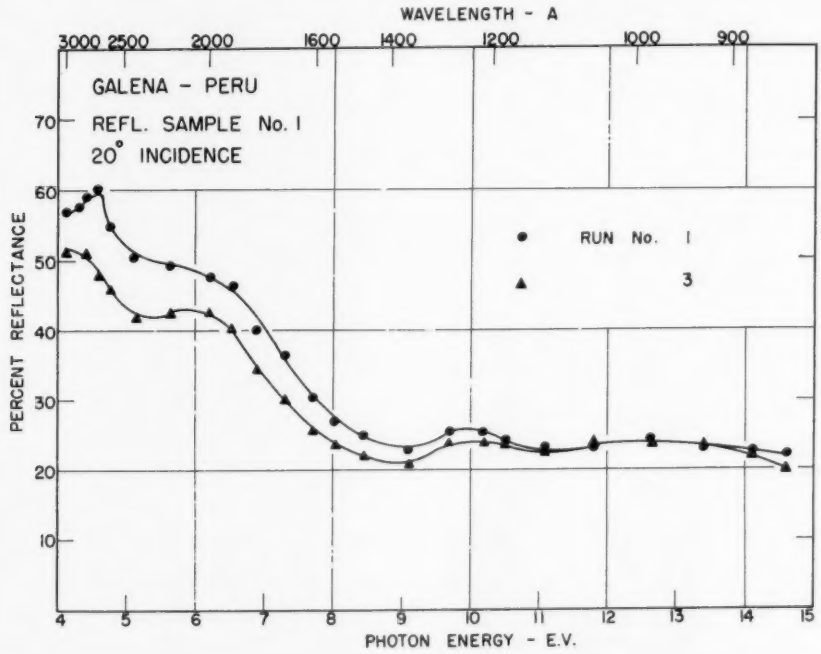

FIG. 10. Reflectance of cleaved surface of a crystal of Peruvian galena. Run No. 1 was made on a surface freshly cleaved in air and placed immediately in the vacuum system. Run No. 3 was measured on the same surface after exposure to the zero-order beam for a total irradiation of the order of 10^{18} photons/cm^2.

than those excited at lower $h\nu$; this change in distribution is quite marked for $h\nu = 21$ eV.

The inference we wish to make, and the significant point of this paper, is that the cross-section for scattering of the excited electrons, as the incident photon energy increases, must pass through a maximum; and thus that the criteria which apply to materials which show a high external yield very near the photoelectric threshold[9, 10] do not necessarily distinguish such materials (which are characterized by an electron affinity small compared to the band gap) entirely in terms of the ultimate photoelectric yield. Rather, if the multiplication scattering process becomes less effective upon excitation with light of very high $h\nu$—the interpretation for these observations in PbS proposed above—materials of high electron affinity might still show high yields, at large enough photon energies.

It is difficult to infer the location of such a

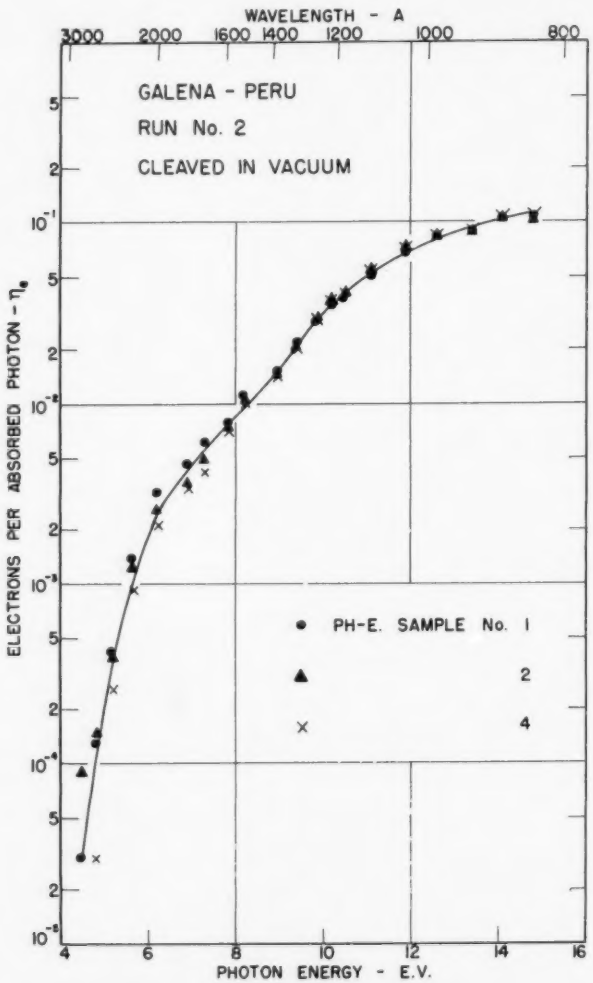

FIG. 11. External photoelectric yields for three specimens of Peruvian galena, measured on surfaces cleaved while the crystal was in vacuum. The data for all specimens are plotted on the same absolute scale.

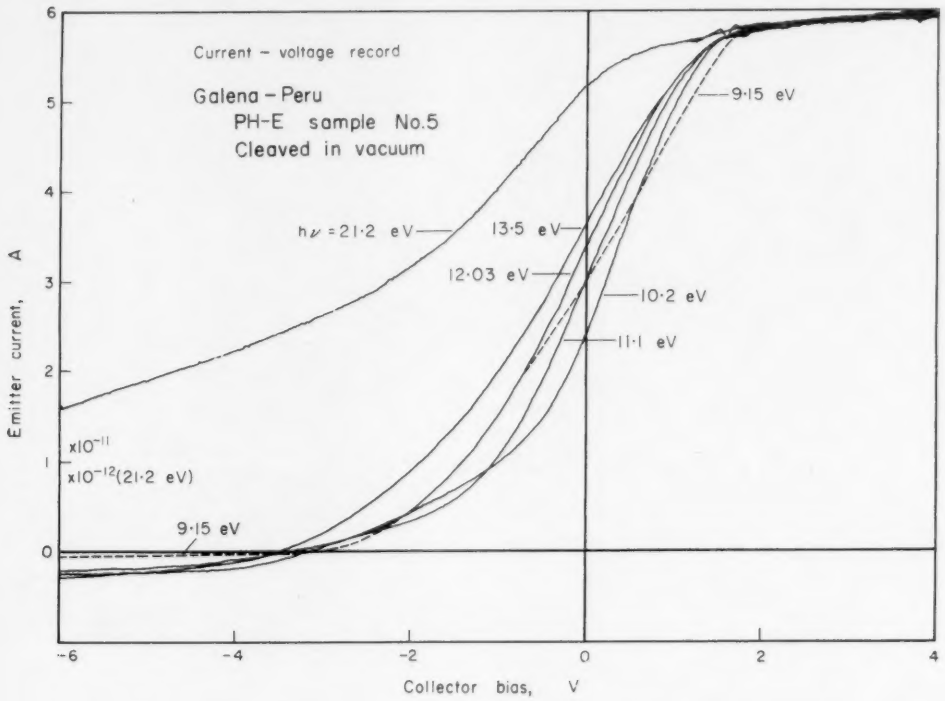

FIG. 12. Retarding-potential curves typical of those obtained using Peruvian galena specimens.

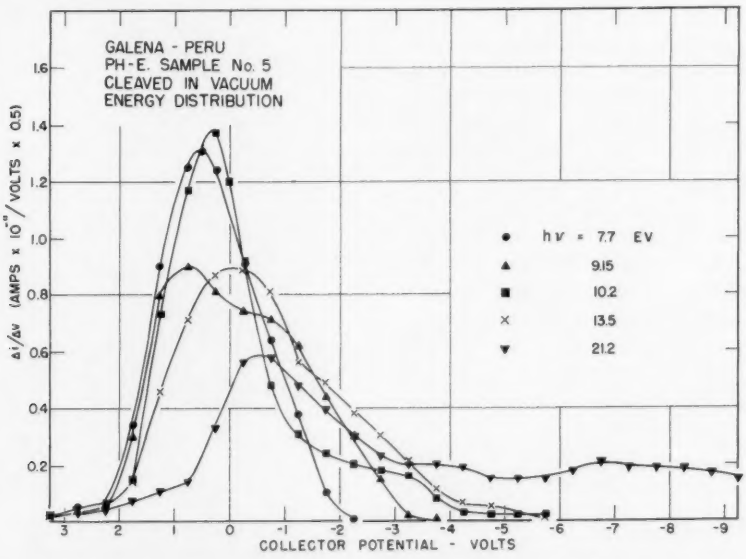

FIG. 13. Energy distribution curves obtained by graphical differentiation of the data of Fig. 12.

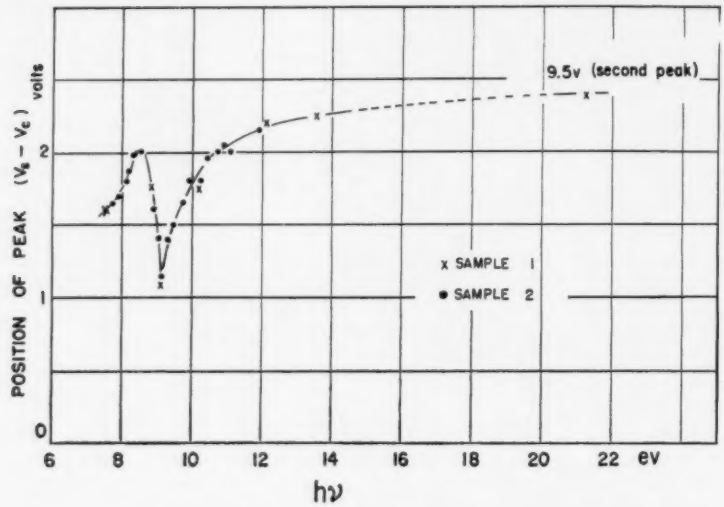

FIG. 14. Position of the peak of the energy-distribution curve as a function of incident photon energy $h\nu$. V_c is the collector potential, $V_s = 2{\cdot}0$ V is the potential at which the current saturates.

scattering "maximum", in terms of incident photon energy, from the data presented here. The median energy of the emerging electrons is lowest for $h\nu = 9{\cdot}1$–$9{\cdot}2$ eV; the spread in energies of the emerging electrons is least at $h\nu = 10{\cdot}2$ eV. One might infer that the collision scattering "maximum", considered as a function of incident photon energy, occurs at $h\nu = 9{\cdot}1$ eV. A slight inflection in the yield curves, in both films and crystals, occurs near 8·5–9 eV, where the increase in yield becomes slightly more rapid. However, variations of the optical absorption coefficient might also conceivably influence the energy distribution of the emerging electrons in such a way as to produce the curious anomaly illustrated in Fig. 14, and there is evidence for some structure in the absorption spectrum in this region in the reflectance data of Fig. 10.

More detailed knowledge of the absorption spectrum and a better understanding of the distribution in energy of the electrons excited by a given $h\nu$ before escape from the crystal are needed to arrive at a more quantitative conclusion than the general trend we have outlined above.

Acknowledgements—We are indebted to the Eastman Kodak Company for preparing the special PbS layers required, and to P. NATALE, F. BENNETT and H. E. SPENCER for a number of helpful discussions. We have also profited from the comments of L. APKER and W. E. SPICER. Finally we wish to thank R. A. KNAPP of this laboratory for his assistance, especially for much of the detailed data of Fig. 14.

REFERENCES

1. SMITH A. and DUTTON D., *J. Opt. Soc. Amer.* **48,** 1007 (1958).
2. KOC S., *Czech J. Phys.* **7,** 91 (1957).
3. TAUC J., *J. Phys. Chem. Solids* **8,** 219 (1959).
4. VAVILOV V. S., *J. Phys. Chem. Solids* **8,** 223 (1959).
5. SMITH A., *J. Opt. Soc. Amer.* **50,** 862 (1960).
6. WATANABE K. and INN C. Y., *J. Opt. Soc. Amer.* **43,** 32 (1953).
7. HAMMANN J. F., *Z. Angew. Phys.* **10,** 187 (1958).
8. TAFT E. A., PHILIPP H. R. and APKER L., *Phys. Rev.* **110,** 876 (1958).
9. APKER L., TAFT E. and DICKEY J., *J. Opt. Soc. Amer.* **43,** 78 (1953).
10. SPICER W. E., *Phys. Rev.* **112,** 114 (1958).

DISCUSSION

W. E. SPICER: Would you comment on the possibility of surface contamination affecting the photoemissive quantum yield curve?

D. DUTTON: The vacuum conditions in our system are certainly very far from ideal for determining truly intrinsic properties of a clean surface, and we cannot tell whether the threshold data either for films or for crystals cleaved inside the system is affected by contamination. There are no indications of changes in the yield curves associated with the time (within a few minutes) after cleaving. There is, in the polycrystalline samples, a shift toward a higher threshold upon first exposure of the sample to mild radiation, no doubt due to a change of some sort in the surface condition.

Y. MARFAING: Do you observe, in the curve of internal photoelectric effect, a second break corresponding to the onset of multiplication by holes?

D. DUTTON: No, there is no indication of a second threshold observable within the limits of accuracy of the photoconductivity data. The rate of rise in yield appears to be slightly less at the upper energy limit of the observations, $h\nu = 7{\cdot}5$ eV.

J. J. BROPHY: Can you comment on the nature of fatigue effects?

D. DUTTON: Irradiation effects are immediately apparent as a drop in the photosensitivity, very likely associated with a decrease in time constant. Strong irradiation results in a drastic increase in noise, a reduction in resistance and virtually complete loss of photoconductivity signal.

J. ZEMEL: The fatigue effects noted here are not overly surprising. Heating to 125°C can radically and irreversably change the properties of PbS photodetectors. We have assumed these to be due to changes in the structure of the oxide states responsible for photoconductivity. A hydrogen discharge producing hydrogen ions could certainly attack or alter these states. In addition, ambients will affect the time constant and noise level of the cells. Hydrogen ions from the discharge will undoubtedly change the surface potential radically leading to major changes in the photoconductivity and dark resistance.

D. DUTTON: The effect of hydrogen ions is quite apparent. The resistance begins to rise very rapidly when the discharge is turned on, even though the cell is shielded from the optical beam.

D. W. GOODWIN (comment): There is evidence in InSb at 77°K that fatigue effects are associated with transfer of carriers between the oxide surface layer and the bulk. This effect increases rapidly for wavelengths shorter than $0{\cdot}5\ \mu$, and has long time constants associated with it. Equivalent effects may be even more important in layer photoconductors.

BLANK
PAGE

Vol. 22
1961

J. Phys. Chem. Solids Pergamon Press 1961. Vol. 22, pp. 365–370. Printed in Great Britain.

THE PRODUCTION OF PAIRS IN SEMICONDUCTORS BY LOW ENERGY ELECTRONS

W. E. SPICER

RCA Laboratories, Princeton, N.J.

Abstract—The minimum electron energy necessary to produce a hole–electron pair has been measured in a number of materials by means of the velocity distribution of photoelectrons. For [Cs]Na_2KSb, Na_2KSb, Rb_3Sb, K_3Sb and $Cs_3Bi(Ag)$, this energy is between three and four times the band gap energy. Cs_3Sb and Cs_3Bi have thresholds of less than twice the band gap energy. A correlation between crystallographic order and the threshold for pair production is noted.

The mean free path for pair production has been found to decrease from a few hundred angstroms for electrons with energies close to the threshold energy to about 15 Å for electrons with energies one or two electron volts above the threshold energy.

1. INTRODUCTION

In studying the velocity distribution of photoelectrons from Cs_3Sb, Apker *et al.*[1] in 1952 found evidence for the production of hole–electron pairs by energetic electrons. Using the same techniques, Taft and Philipp[2] have recently obtained additional data on this process. After 1952, data were also obtained on pair production through the theoretical[3] and experimental[4, 5] studies of avalanche breakdown and from the study of the quantum efficiency of the photoconductive and photovoltaic effects. From the avalanche breakdown work (principally in silicon), a threshold energy for pair production of about twice the band gap energy[5] and a mean free path for pair production of about 15 Å[3] (for electrons with energies 0·5 eV above threshold) were inferred. The threshold is larger than the band gap because of the necessity to conserve k.[3] From the photoconductivity work, the threshold for pair production was obtained in terms of the energy of the incident photons. There is usually an ambiguity in these threshold determinations because of the lack of knowledge of the division of a photon's energy between the hole and electron which are *excited* by it.* Values of threshold varying between two and four times the band gap energy have been obtained by this method for Ge[6], [7], Si[7], InSb[6], and PbS[8]. Dexter has shown that such values are reasonable.[9]

It has been the purpose of this work to determine the thresholds and the mean free paths for pair production in the alkali antimonide[10] and Cs_3Bi[11] systems through the use of the velocity distribution of photoemission. This method has the advantage over those above mentioned in that the energy distributions of the electrons are obtained so that there is no ambiguity in the electron energy at the threshold of pair production. Knowledge of the energy distribution of the photoelectrons also allows the determination of the mean free path for pair production. Disadvantages of the method are that it can only be used for electrons and not for holes, and that it depends, in most cases, on the escape of the electrons from the material.

It is our purpose in this paper to report preliminary results of this investigation. Space limitations do not allow a complete description of the methods used and the results obtained. These will be reported fully when complete reports of this work are published.

2. EXPERIMENTAL DETAILS

The phototubes used to measure the velocity distributions were of the simple cylindrical type described by Apker and his co-workers.[1,2] As Taft and Philipp

* In the case of germanium and silicon, it appears that this ambiguity is being lifted by the knowledge of the optical absorption process.

have pointed out,[2] these tubes give surprisingly good results despite their departure from ideal geometry. However, it is clear that more accurate data would be obtained from tubes with superior geometry.

An a.c. method was used to obtain the velocity distribution curves. A small (0·05 V or less) 24 c/s voltage was superimposed on the retarding potential voltage and the retarding potential was varied at a rate of about 1V/min. Thus a 24 c/s signal was generated which was proportional to the derivative of the retarding potential characteristic.* This signal was amplified, synchronously rectified, and placed on the vertical drive of an X–Y recorder whose horizontal deflection was proportional to the retarding potential. This method requires a much less stable light source and amplifier than the usual d.c. method.†

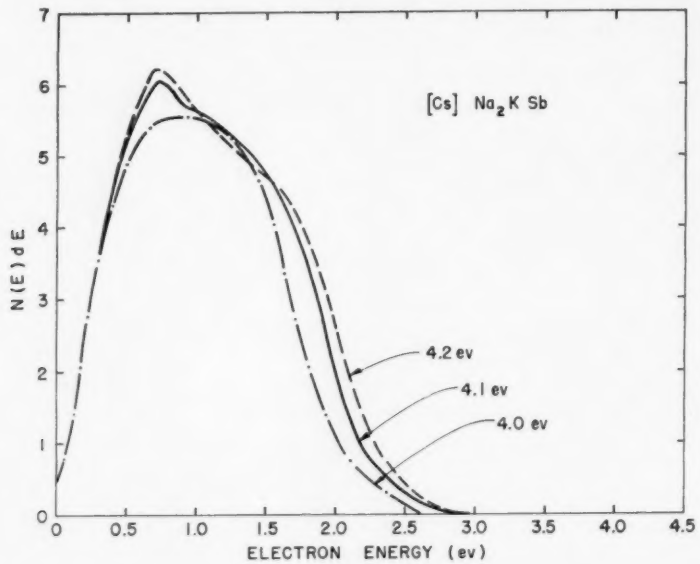

FIG. 1. Velocity distribution curves for [Cs]Na_2KSb for photon energies near the threshold for pair production. The exciting photon energies are indicated on each curve by means of the arrows. The 4·0 eV curve does not have the slow peak characteristic of pair production, but it appears with excitation by 4·1 and 4·2 eV photons.

3. RESULTS AND INTERPRETATIONS

(A). *Comments on interpretation of the data*

As was pointed out by APKER *et al.*[1] the onset of pair production can be detected by the appearance of a group of low energy electrons.‡ In the alkali-antimonide and Cs_3Bi systems, the energy of these electrons seem to be independent of the exciting photons.§ It is important to know whether the pair production is due to electrons or to holes and whether or not the electrons involved in pair production escape. It appears that these questions can be answered by examining the spectral distribution of the quantum yield from these materials. The quantum efficiency of most of the materials studied here reach a plateau for photon energies about 0·5 eV below the threshold for pair production and remains constant from this point to the limit of measurement (about 5·7 eV). This behavior indicates that the observed

* The capacitive component of the output signal was removed by a proper selection of phase.

† The a.c. method was suggested by L. LEDER and is similar to a system developed for other purposes.[12]

‡ For convenience, this group of electrons will be termed the "slow group".

§ An alternate explanation for the "slow group" would involve preferential optical absorption into states just above the vacuum level. Such an explanation seems to be ruled out by the fact that the "slow group" has a threshold energy below which it does not appear.

Vol. 22
1961

pair production is due to electrons and not holes.* The constancy of the quantum yield also indicates that, on the average, one of the two electrons involved in pair production escapes.

(B). *Threshold for pair production*

The threshold for pair production is taken as the maximum electron energy at which the "slow group" of electrons is first observed (see Figs. 1 and 2).† The thresholds for pair production for a number of materials are given in Table 1. For the materials which have an ordered crystal structure,[13] the threshold for pair production is approximately three times the band gap. This is in general agreement with theory[3], [9] and with experimental results from other materials such as Si[5, 7], InSb[6], and PbS[8]. However, for the materials which have a partially disordered lattice, Cs_3Sb[16] and Cs_3Bi[17], the threshold energies seem to approach the band gap energy. This strongly supports and extends the suggestion of TAFT and PHILIPP[2] that the disorder in the Cs_3Sb lattice may lead to a relaxation of the conditions on conservation of $\bar{k}$. After the addition of a small quantity of silver to Cs_3Bi to form $Cs_3Bi(Ag)$,[11] the threshold for pair production occurs at about four times the band gap energy. Thus, the effect of the silver seems to be to increase the crystallographic order.‡ It is hoped that X-ray studies now under way will clear up this point.

Table 1. *Threshold for pair production. The threshold energy given is the electron energy measured from the bottom of the conduction band.*

Material	Threshold for pair production E_{Th} (eV)	Band gap E_g(eV)	$\frac{E_{Th}}{E_G}$	Crystal structure
K_3Sb	$\leqslant 3{\cdot}7$	1·1	$\leqslant 3{\cdot}3$	hexagonal (ordered)
Rb_3Sb	3·0	1·0	3·0	hexagonal (ordered)
[Cs]Na_3KSb and Na_2KSb	3·0	1·0	3·0	cubic (ordered)
Cs_3Sb	2·0	1·6*	1·25	cubic (partially disordered)
Cs_3Bi	$< 1{\cdot}3$	0·7	$< 1{\cdot}8$	cubic (partially disordered)
$Cs_3Bi(Ag)$	2·9	0·7	4·1	unmeasured

* There is some uncertainty about the band gap of Cs_3Sb. See Ref. 10.
† This threshold value has been inferred from photo-emission data. See Ref. 11.

(C). *Mean free path for pair production*

If one knows the threshold for pair production, it is possible to determine the number of electrons, $N(E > E_{Th}, h\nu)$, which had sufficient energy to produce a pair, but which escaped without doing so. Because of the characteristic shape and position of the "slow group", it is also possible to determine the number of primary electrons producing pairs $N_S(h\nu)$. Thus, the probability for an electron

* At 5·7 eV the "slow group" contains over 75 per cent of the emitted electrons. If the slow peak were due to pair production by holes, this should result in a rise in yield by a factor of about 3 between the threshold and 5·7 eV.

† This threshold corresponds to a mean free path $\bar{l}(h\nu)$ [see equation (2)] of about 250 Å or an integrated mean free path of about 750 Å. Pair production with longer mean free paths could not be detected by this method.

‡ It is interesting to note that large changes can be induced in evaporated films of CdS by the addition of a small amount of Ag.[14]

with $E > E_{Th}$ escaping without producing a pair can be determined from the experimental data. This is given by:

$$P_e(E > E_{Th}, h\nu) = \frac{N(E > E_{Th}, h\nu)}{N(E > E_{Th}, h\nu) + N_s(h\nu)}. \quad (1)$$

Theoretically, the expression:

$$P_T(E > E_{Th}, h\nu, \chi) = \exp[-(\chi/\bar{l}(h\nu)] \quad (2)$$

may be written for the probability of escape from a depth χ without pair production. The quantity $\bar{l}(h\nu)$ will be termed the mean free path for escape.* The probability of a photon being absorbed at a depth x is given by:

$$P_a(h\nu,\chi)\, d\chi = \alpha(h\nu) \exp[-\alpha(h\nu)\chi]\, dx, \quad (3)$$

where $\alpha(h\nu)$ is the optical absorption coefficient.† Taking the product of (2) and (3) and integrating from ϕ zero to infinity the expression:

$$P_T(E > E_{Th}, h\nu) = \frac{\alpha(h\nu)}{\alpha(h\nu) + [1/\bar{l}(h\nu)]} \quad (4)$$

is obtained. From equations (1) and (4) one obtains:

$$\bar{l}(h\nu) = \frac{N(E > E_{Th}, h\nu)}{\alpha(h\nu) N_s(h\nu)}. \quad (5)$$

Typical results obtained from [Cs] Na_2KSb[10] are shown in curve 1 of Fig. 3.‡ For values of $(h\nu - h\nu_0)$ of only a few tenths of a volt, $\bar{l}(h\nu)$ is about 100 Å. It drops to less than about 20 Å for $(h\nu - h\nu_0)$ above 0·8 eV. Within experimental error, the results from [Cs] Na_2KSb and Na_2KSb were the same. Although Rb_3Sb and Cs_3Sb have not yet been studied as thoroughly as the Na_2KSb system, preliminary results indicate a mean free path of about 15 Å for electrons with energies 2·0 eV above the threshold energy.

It is possible to transform the distribution from $\bar{l}(h\nu)$ to $\bar{l}(E)$, i.e. to one dependent on the electron energy, by making certain approximations. The results of such a transformation are also given in Fig. 3. As should be expected, $\bar{l}(E)$ decreases much faster with increasing energy than $\bar{l}(h\nu)$. It reaches a value of 15 Å at about 0·5 eV above threshold and within the accuracy of the measurement is constant to 2·0 eV above threshold.

The mean free paths with which we have been dealing are defined by equation 2 and related to the distance traveled in a *direction perpendicular to the surface*. Although this is the quantity of most immediate interest in many problems, the mean free path defined in terms of the integrated path length traversed by the electron is perhaps of more fundamental interest. Rough estimate for these are 20 Å and 750 Å for electrons with energies in excess of the threshold energy of 0·5 eV and 0·1 eV respectively.

4. CONCLUSIONS

Thresholds for pair production of about three times the band gap have been found for Na_2KSb, [Cs] Na_2KSb, Rb_3Sb, K_3Sb and $Cs_3Bi(Ag)$. This indicates that conservation of $\bar{k}$ is required in pair production. For Cs_3Sb and Cs_3Bi the threshold for pair production seems to be much closer to the band gap. This indicates that the requirement for conservation of $\bar{k}$ may be relaxed because of the partial disorder of the Cs_3Sb and Cs_3Bi lattices.[18] In [Cs] Na_2KSb and Na_2KSb the mean free path for pair production has been found to be about 15 Å for electrons with energies 0·5–2 V in excess of the threshold energy. This is in surprisingly good agreement with WOLFF's theoretical estimate[3] of 15 Å for electrons with energies 0·5 eV above threshold. For the other materials studied preliminary results indicate a mean free path of about 15 Å for electrons with energies 2·0 eV above threshold.§

Because of space limitations, we have not discussed such interesting points as the conservation of $\bar{k}$ in the optical absorption process as opposed to its conservation in the pair production process,

* $\bar{l}(h\nu)$ is rigorously defined by the relation:

$$\exp[-\chi/\bar{l}(h\nu)] = \frac{\int_{E_{Th}}^{\infty} \exp[-x/\bar{l}(E)]\, n(E, h\nu)\, dE}{\int_{E_{Th}}^{\infty} n(E, h\nu)\, dE},$$

$n(E,h\nu)$ is the original energy distribution and $\bar{l}(E)$ is the mean free path for an electron of energy E.

† Values of $\alpha(h\nu)$ have been determined.[15]

‡ These values are probably only accurate within a factor of 2. The values for $h\nu - h\nu_0 > 0{\cdot}4$ eV should be more accurate than those for lower values of $(h\nu - h\nu_0)$. $h\nu_0$ is the photon energy at the threshold for pair production.

§ The quantum yield of about 0·1 electron/photon obtained for PbS[19] and metals[20] in the vacuum u.v., seem to suggest that the mean free path for pair production may increase as the electron energy is increased.

Vol. 22
1961

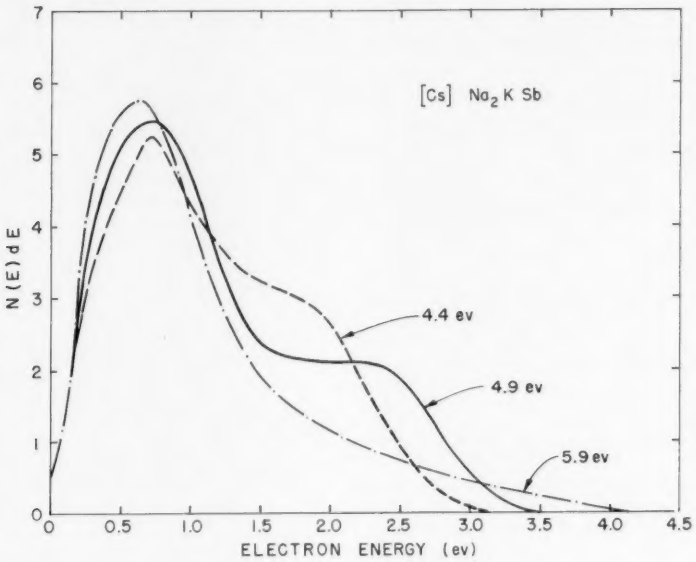

FIG. 2. Velocity distribution curves for [Cs]Na_2KSb for photon energies of 4·4, 4·9 and 5·9 eV. The increase in the relative number of electrons involved in pair production can clearly be seen.

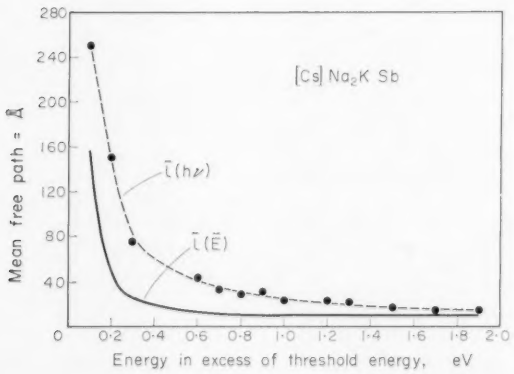

FIG. 3. The mean free paths for pair production as a function of the energy above the threshold energy. $\bar{l}(h\nu)$ is the mean free path for the electrons excited by a photon of energy $h\nu$ with energy $(h\nu - h\nu_0)$ above threshold; $\bar{l}(E)$ is the mean free path in terms of electron energy.

the peculiarities in band structure which would result in the energy of the "slow group" being independent of the energy of the electron producing the hole–electron pair, and the effect of band bending on pair production. More detailed studies of the mean free path for pair production as a function of energy should be particularly fruitful for those materials where the condition on the conservation of $\bar{k}$ seems to be relaxed.

Acknowledgements—The author is greatly indebted to A. H. SOMMER for preparation of the samples and for many valuable discussions. He is also indebted to L. LEDER, R. SIMON, M. LAMPERT and many other members of RCA Laboratories for valuable discussions.

REFERENCES

1. APKER L., TAFT E. A. and DICKEY J., *J. Opt. Soc. Amer.* **43,** 78 (1953).
2. TAFT E. A. and PHILIPP H. R., *Phys. Rev.* **115,** 1583 (1959).
3. WOLFF P. A., *Phys. Rev.* **95,** 1415 (1954); *J. Phys. Chem. Solids* **16,** 184 (1960).
4. MCKAY K. G., *Phys. Rev.* **94,** 877 (1954); CHYNOWETH A. G. and MCKAY K. G., *Ibid.* **102,** 369 (1956); **106,** 418 (1957); *J. Appl. Phys.* **30,** 1811 (1959); CHYNOWETH A. G. and GUMMEL H. K., *J. Phys. Chem. Solids* **16,** 191 (1960) and the references given in these papers.
5. CHYNOWETH A. G. and MCKAY K. G., *Phys. Rev.* **108,** 29 (1957).
6. TAUC J., *J. Phys. Chem. Solids* **8,** 219 (1959).
7. VAVILOV V., *J. Phys. Chem. Solids* **8,** 223 (1959).
8. SMITH A. and DUTTON D., *J. Opt. Soc. Amer.* **48,** 1007 (1958).
9. DEXTER D., *Proceedings of the International Conference on Semiconductors,* 1960, to be published.
10. SPICER W. E., *J. Appl. Phys.* **31,** 2077 (1960) and the references cited there.
11. SOMMER A. H. and SPICER W. E., *J. Appl. Phys.* **32,** 1036 (1961).
12. LEDER L. and SIMPSON J. A., *Rev. Sci. Instrum.* **29,** 571 (1958).
13. BRAUER G. and ZINTL E., *Z. Phys. Chem.* **37B,** 323 (1937); SCHEER J. J. and ZALM P., *Philips Res. Rep.* **14,** 143 (1959); MCCARROLL W. H., *J. Phys. Chem. Solids* **16,** 31 (1960); GNUTZMANN G., DORN F. W. and KLEMM W., *Z. Anorg. Chem.* **309,** 210 (1961); CHIKAWA J., IMAMURA S., TANAKE K. and SHIOJIRI M., *J. Phys. Soc. Japan* **16,** 1175 (1961).
14. GILLES J. M. and VAN CAKENBERGHER J., *Nature, Lond.* **182,** 862 (1958); *Solid-State Physics in Electronics and Telecommunications,* Vol. 2, p. 900. Academic Press, New York (1960).
15. SPICER W. E. and SOMMER A. H., to be published.
16. JACK K. H. and WACHTEL M. M., *Proc. Roy. Soc.* **239A,** 46 (1957); GNUTZMANN G., DORN F. W. and KLEMM W., *Z. Anorg. Chem.* **309,** 210 (1961).
17. ZHORALEV N. N. and SMIRNOV V. A., *Sov. Phys. Cryst. Phys.* **4,** 503 (1960); GNUTZMANN G., DORN F. W. and KLEMM W., *Z. Anorg. Chem.* **309,** 210 (1961).
18. PARMENTER R. H., *Phys. Rev.* **104,** 22 (1960).
19. SMITH A. and DUTTON D., preceding paper.
20. WALKER W. C., RUSTGI O. P. and WEISSLER G. L., *J. Opt. Soc. Amer.* **49,** 471 (1959) and the references cited there.

DISCUSSION

R. J. ZOLLWEG: Can you comment on how the density of states variation in the valence band and conduction band and variation in transition probabilities effect your results.

W. E. SPICER: It is the author's belief that any variations not accounted for by this treatment will not lead to serious errors.

Z. SZEPESI: Does CdS show the external emission effect?

W. E. SPICER: Yes, any material should show it if the photon energy is high enough. The threshold energy for CdS could be between 5·5 and 5 eV.

J. Phys. Chem. Solids Pergamon Press 1961. Vol. 22, pp. 371–377. Printed in Great Britain.

SOME TOPICS IN THE FLUCTUATIONS OF PHOTO-PROCESSES IN SOLIDS

R. E. BURGESS

Department of Physics, University of British Columbia, Vancouver, Canada

Abstract—Photons and electrons in solids can undergo the stochastic processes of generation, absorption and multiplication. A general analysis of the steady-state mean value and variance due to these processes is applied to consideration of imperfect photon absorbers, and of photon and electron multipliers. The fluctuations of photon flux interacting with perturbed populations in a pair of electron levels are shown to be consistent with boson statistics at an effective temperature determined by the temperature of the input photons and the temperature of the level populations; the results are valid even if the latter temperature is negative and thus apply to amplifying as well as to attenuating systems.

Fluctuations of carrier numbers in a non-stationary system are considered and the difficulties of formulating their spectral distribution are indicated.

Carriers in a photoconductor produced by energetic photons have excess energy which is rapidly lost by phonon scattering or by further ionization and these hot carriers therefore introduce additional noise components.

1. INTRODUCTION

THE FLUCTUATIONS in population of electronic levels in a semiconductor exposed to radiation depends on the statistical formulation of the photon–electron and electron–electron interactions. The analytical methods for discussing these problems are largely already familiar in the theory of Markov processes in which the behaviour of a discrete variable (number of particles) in continuous time is governed by the transition probabilities to a neighbouring state. Such processes are known as birth-and-death processes in biological statistics. They are termed homogeneous when the transition probabilities depend on the particle numbers and not explicitly on time. However in some situations these probabilities are age-dependent in a manner which is non-Markovian (i.e. not exponential) e.g. the probability of ionization by an energetic carrier which is losing energy to the lattice.[1]

Since the numbers of particles (electrons, photons) involved are usually large we are fortunately not concerned with finding their probability distribution functions since (except in the case of a critical state) these may be taken as Gaussian. Then only the mean values, the variances and the covariances are needed to specify the system statistically.

In certain special cases very near to thermal equilibrium the fluctuations may also be calculated thermodynamically. Then although temperature T is involved explicitly in the analysis the variances can nevertheless always be expressed in terms of mean values without reference to T.

Previous work[2] on univariate systems has yielded simple results for the mean and variance of the number variable n in terms of the generation and recombination rates g_n and r_n which are functions of n but not of time. The relaxation time and the spectral density of the number fluctuations are also easily found.

For the special circumstances in which g_n and r_n are equal and have equal derivatives at the same value of n the case of a "critical state" arises and the distribution function is no longer Gaussian. The fluctuations are then relatively large and can be interpreted as a macroscopic instability of the system.

In the present paper some extensions of previous work are made. Consideration is given to processes in which multiplication and absorption of particles play an important part and the results are applied to both photons and electrons. The fluctuations of the output variable always contain parts attributable to the input fluctuations and to

the fluctuations of the transformation (multiplication or absorption). An invariant property of the latter part of the fluctuations is found.

Non-stationary systems are of interest in photon detectors which use pumping (or a strong electric field) to establish an inversion of population and a negative temperature between certain levels since it is common to make the operating phase follow the pumping phase after a lapse permitting rapid downward transitions to be completed. Then during the operating phase the system relaxes back to equilibrium and is not in a steady state. The fluctuations of the state of the system during this period require a different approach from that developed for the steady-state g–r theorem and some results are given for the case of linear kinetics.

In processes involving photon absorption in a semiconductor the possibility of producing energetic carriers always arises whether from an ionization process[3] (where $h\nu > \epsilon_i$) or by free carrier absorption[4] (when $h\nu > kT$). The creation of such energetic carriers and their subsequent thermalization are statistical processes which contribute to the observable fluctuations in the semiconductor. We give some consideration to these effects and note that the fluctuations of the energy of free carriers may be significant.

2. MULTIPLICATION AND ABSORPTION PROCESSES

2.1. *General*

There are several instances of phenomena in a system in which the "input" particles are transformed into a different number of "output" particles by some statistical process. For instance the input may consist of photons and the output of photoelectrons with a certain probability that an electron will emerge when a photon is incident. The process of impact ionization in a semiconductor by energetic carriers is another example in which there is a set of probabilities that a carrier will give rise to 0, 1, 2, . . . ionizing collisions.

Some general results can be simply derived as follows. Let x input particles arrive in a time t and let y be the number of output particles. Then

$$y = \sum_{i=1}^{x} m_i, \tag{2.1}$$

where m_i is the multiplication ratio for the ith input particle. Then for a stationary system with the outcome of the events statistically independent

$$\langle y \rangle = \langle x \rangle \langle m \rangle \tag{2.2}$$

$$\text{var } y = \langle x \rangle \text{ var } m + \langle m \rangle^2 \text{ var } x. \tag{2.3}$$

The two terms in the variance of output number are due respectively to fluctuations in m and to those in x. If the input process x is Poisson

$$\text{var } y = \langle y \rangle \langle m^2 \rangle / \langle m \rangle. \tag{2.4}$$

2.2. *Examples*

(i). *Photoelectric emission.* If p is the probability of a photoelectron being emitted when a photon is absorbed: $\langle m \rangle = \langle m^2 \rangle = p$ and var $m = p(1-p)$, whence

$$\begin{aligned} \text{var } y &= p(1-p)\langle x \rangle + p^2 \text{var } x \\ &= \langle y \rangle (1-p+p \text{ var } x/\langle x \rangle). \end{aligned} \tag{2.5}$$

If the incident photons $h\nu$ are derived from thermal radiation at temperature T then var $x/\langle x \rangle = 1+b$ where b is the boson factor

$$b = \frac{1}{\exp(h\nu/kT)-1}, \tag{2.6}$$

whence

$$\text{var } y/\langle y \rangle = 1+pb. \tag{2.7}$$

The shot noise of a vacuum photo-diode would be greater than the standard value $2eI$ by this factor.

The photoelectron statistics are Poisson if p or $kT/h\nu$ is sufficiently small. On the other hand for high radiation temperatures or low energy photons

$$\text{var } y \sim p^2 b \langle x \rangle \tag{2.8}$$

and the fluctuations are greatly in excess of the Poisson value.

(ii). *Imperfect photon absorber.* The energy fluctuations of an imperfect absorber coupled to its environment by radiation can be calculated in the same way. If η is the emissivity of the body for photons of frequency ν then in a thermal radiation field of temperature T the number of incident photons in unit time in the interval ν to $\nu+d\nu$ has the mean value:

$$\langle x \rangle = 2\pi A b \nu^2 c^{-2} \cdot d\nu$$

and we identify the parameter p of the previous

Vol. 22
1961

section with η. Thus the variance of the number of photons absorbed in unit time is

$$\text{var } a_1 = 2\pi Ab\nu^2\eta(1+b\eta)c^{-2}\cdot d\nu. \quad (2.9)$$

It might be thought that the variance of the number of photons emitted by the body per unit time would have the same value but this is not the case. Certainly for equilibrium the mean numbers of absorbed and emitted photons are equal but their variances will differ; the principle of detailed balance requires that the reflected r_1 and emitted e_1 photons must recreate in both the mean and the variance the values expected for black-body radiation outside the body.

This leads to

$$\langle e_1\rangle = \langle a_1\rangle = \eta\langle x_1\rangle$$
$$\text{var } e_1 = \langle x_1\rangle\eta[1+b(2-\eta)]$$
$$\text{var } a_1 + \text{var } e_1 = 4\pi Ab\nu^2\eta(1+b)c^{-2}\cdot d\nu. \quad (2.10)$$

From these results it is found using Campbell's Theorem that the total energy fluctuations due to photon absorption and emission are

$$\text{var } E = 2\pi h^2 A\tau c^{-2}\int_0^\infty \nu^4 b(1+b)\eta\cdot d\nu, \quad (2.11)$$

where τ is the thermal relaxation time of the body given by the ratio of the differential heat capacity ($K = d\langle E\rangle/dT$) to the radiation conductance G. Now

$$G = 2\pi hAc^{-2}\int_0^\infty \eta\nu^3(db/dT)\cdot d\nu. \quad (2.12)$$

Since

$$db/dT = h\nu b(1+b)/kT^2,$$
$$\text{var } E = kT^2 K, \quad (2.13)$$

exactly as required, independently of the temperature and frequency dependence of the emissivity. Similarly the spectral density of the fluctuations of radiative power flow to and from the body is

$$S_p(f) = 4kT^2G \quad (2.14)$$

and the spectral density of the fluctuations of energy is

$$S_E(f) = \frac{K^2S_p(f)}{\omega^2K^2+G^2} = \frac{4kT^2G}{\omega^2+\tau^{-2}} \quad (2.15)$$

which integrates to give (2.13).

(iii). *Imperfect transmission.* When radiation passes through a medium with transmission of less than unity, the fluctuations of photon flux are modified. If for photons of frequency ν the transmission is p then the variance of the number of transmitted photons in a given time interval is

$$\text{var } n = p^2 \text{ var } m + \langle m\rangle p(1-p),$$

where m is the number of incident photons. If the radiation temperature is T then

$$\text{var } n = \langle n\rangle(1+pb),$$

where b is the boson factor. The fluctuations are thus the more nearly Poisson in character the smaller the transmission.

When these results are applied to a filter the total radiation emerging also contains the component radiated by the filter itself. If the filter and incident radiation are at the same temperature the sum of the transmitted and emitted fluxes must reconstruct both the mean and variance of the incident flux. However, for different temperatures no general result is possible since Kirchhoff's Law is no longer applicable.

A non-reciprocal filter (e.g. using the Faraday effect in a magnetically active medium) can be used in conjuntion with polarizers to provide one-way transmission. It might be thought that two bodies in radiative contact through such a filter would violate the second law of thermodynamics. However all such filters are *essentially* lossy and it may readily be shown that if the bodies and the filter are at the same temperature, the photon fluxes in the two directions exactly balance by virtue of the absorption and emission by the filter exactly compensating for the asymmetry of transmission of the radiation from the two bodies.

(iv). *Cascade multiplication.* A number of possible multiplication processes can occur in a photoconductor: e.g. photocarriers either under the influence of a strong electrical field or by virtue of the excess energy derived from an energetic photon may create further free carriers by impact ionization. We can also consider photon multiplication processes such as occur when radiation is transmitted through a medium having a negative temperature between suitably spaced energy levels.

Let the multiplication process be regarded as taking place in a sequence of N stages where m is

the multiplication of each stage. By iteration of (2.2) and (2.3) for an input of x particles to the first stage, the output y from the Nth stage has a mean value:

$$\langle y\rangle = \langle x\rangle\,\langle m\rangle^N = M_o\langle x\rangle,$$

where $M_o = \langle m\rangle^N$ is the average overall multiplication.

The variance of the output is

$$\operatorname{var} y = M_o^2 \operatorname{var} x + \frac{M_o(M_o-1)}{\langle m\rangle(\langle m\rangle-1)} \operatorname{var} m\cdot\langle x\rangle. \tag{2.16}$$

Now if the input x is Poisson and the overall multiplication M_o is large compared with unity,

$$\operatorname{var} y \simeq M_o^2\langle x\rangle[1+\operatorname{var} m/\langle m\rangle(\langle m\rangle-1)]. \tag{2.17}$$

Thus the ratio var $m/[\langle m\rangle\,(\langle m\rangle-1)]$ determines whether the fluctuations of the input or of the multiplication process govern the output fluctuations.

These results may now be generalized by going to the continuous case in which the N stages are regarded as N steps of length Δz along the path of the particles with $z = N\cdot\Delta z$ as the overall path length. Furthermore we may consider that particles disappear as well as multiply such that in Δz the probability of a particle creating a secondary is $A\cdot\Delta z$ and the probability of disappearance is $B\cdot\Delta z$ while the probability of spontaneous creation is $C\cdot\Delta z$. The fluctuations of output are found from the differential-difference equation for this Markov process:

$$dP_n/dz = [C+(n-1)A]P_{n-1} - [C+n(A+B)P_n + (n+1)BP_{n+1}.$$

Hence if $n(0)$ particles are the input at $z = 0$,

$$\langle n(z)\rangle = \left[\langle n(0)\rangle + \frac{C}{A-B}\right] M_o - \frac{C}{A-B},$$

$$\operatorname{var} n(z) = M_o^2 \operatorname{var} n(0) + \langle n(0)\rangle \frac{A+B}{A-B} M_o(M_o-1) + \frac{C(M_o-1)(AM_o-B)}{(A-B)^2}, \tag{2.18}$$

where $M_o = \exp(A-B)z$ is the macroscopic multiplication per particle. The three terms in the variance are due respectively to: (i) the variance of the input, (ii) the variance of the multiplication and (iii) the fluctuations of the spontaneous emission.

The multiplication fluctuation has a property that the quantity

$$\frac{\operatorname{var} M}{M_o(M_o-1)} = \frac{A+B}{A-B} = \text{const.}$$

independently of z.

The validity of this relation for an infinitesimal path Δz is readily seen since the response to a single input particle has mean value $1+(A-B)\Delta z$ and variance $(A+B)\Delta z$.

These results can be applied to the transmission of photons through a medium with appropriately spaced levels exhibiting stimulated emission (A), absorption (B) and spontaneous emission (C). If energy levels 1 and 2 in a crystal have occupation numbers n_1 and n_2 and separation E then in thermal equilibrium with the lattice temperature T_L the ratio $n_1^0/n_2^0 = \exp E/kT_L$. If the populations are disturbed, e.g. by some ionizing agency or by a pumping field, the ratio will be disturbed but may be used to define an effective temperature T between the levels:

$$n_1/n_2 = \exp E/kT$$

If now photons of energy $E = h\nu$ traverse the crystal in the z-direction and their flux at z is $\phi(z)$ then

$$d\phi/dz = n_2(K+\phi L) - n_1\phi L,$$

where the three terms correspond to spontaneous and stimulated emission and to absorption of the photons. Thus for comparison with the previous notation: $A = n_2L$, $B = n_1L$ and $C = n_2K$, giving

$$\langle\phi(z)\rangle = M_o[\langle\phi(0)\rangle - Kb/L] + Kb/L,$$

where $b = n_2/(n_1-n_2)$ is the boson factor $(\exp E/kT-1)^{-1}$.

The fluctuations in the photon flux at z are:

$$\operatorname{var}\phi(z) = M_o^2 \operatorname{var}\phi(0) - \langle\phi(0)\rangle(1+2b)M_o(M_o-1) + (K/L)b(M_o-1)[b(M_o-1)-1]. \tag{2.19}$$

Despite appearances, the second and third terms are always non-negative whether the temperature T between the levels is positive or negative:

if $T > 0$, $n_1 > n_2$, $M_0 < 1$, $b > 0$ (attenuation)

$T < 0$, $n_1 < n_2$, $M_0 > 1$, $b < -1$ (amplification).

Vol. 22
1961

If the system is in equilibrium with the input photon flux, then $\langle\phi(z)\rangle = \langle\phi(0)\rangle$ and var $\phi(z) =$ var $\phi(0)$ for all z, and hence for any M_o. This requires

$$\langle\phi\rangle = Kb/L \text{ and var } \phi = Kb(1+b)/L$$
$$= \langle\phi\rangle(1+b)$$

in conformity with the boson fluctuation property associated with the kinetics of absorption and stimulated emission. It should be noted that the consistency of the relations for the variance requires the inclusion of the gain fluctuation (second term) as well as the additive noise due to spontaneous emission (last term).

The general situation occurs when the source is at a temperature T_i different from that of the system T; the mean flux of emergent photons is

$$\langle\phi(z)\rangle = (K/L)[(b_s-b)M_o+b] \equiv (K/L)b_e,$$

where b_s is the boson factor for T_s, and b_e is the effective factor for the mean output flux. Now the important point is that the variances of the output flux is also given exactly by the boson fluctuations using the same factor b_e:

$$\text{var } \phi(z) = K/L[M_o^2 b_s(1+b_s)$$
$$-b_s(1+2b)M_o(M_o-1)+b(M_o-1)(bM_o-b-1)]$$
$$= (K/L)b_e(1+b_e). \qquad (2.20)$$

From the point of view of an observer at the output the emergent photons have a variance and mean consistent with a temperature

$$T_e = h\nu/k \ \ln(1+1/b_e).$$

If now $h\nu/k$ is small compared with all the temperatures involved

$$T_e = (T_s-T)M_o+T,$$

whence the effective noise temperature T_n defined by $T_e = M_o(T_s+T_n)$ is given by:

$$T_n = -T(1-1/M_o). \qquad (2.21)$$

3. NON-STATIONARY SYSTEMS

3.1. *Fluctuations in relaxing systems*

In previous discussions of fluctuations of numbers due to competing stochastic processes (e.g. generation and recombination) we have dealt with the steady state in which time and ensemble averages are identical.

More recently there has arisen interest in non-stationary systems such as those involving negative temperatures or pumped systems to obtain electron distributions strongly disturbed from thermal equilibrium.[5] Commonly such systems operate on a time-division basis such that the time interval for useful operation follows the pumping or excitation phase after a sufficient pause to permit any rapid and undesirable transitions to be completed.

Take for simplicity a univariate system with a single number variable n governed by the rate equation:

$$\frac{dn}{dt} = g_n - r_n$$

and consider the fluctuations in n when the system is relaxing to the steady state from some initial value $n(0)$.

In view of the need to take into account initial conditions in computing the moments under non-stationary conditions, the analysis is more elaborate than for the steady state. Starting from the stochastic equation

$$\frac{\partial P_n}{\partial t} = g_{n-1}P_{n-1} - (g_n+r_n)P_n + r_{n+1}P_{n+1},$$

it is found that

$$\frac{\partial\langle n\rangle}{\partial t} = \langle g_n\rangle - \langle r_n\rangle$$

and

$$\frac{\partial\langle n^2\rangle}{\partial t} = \langle(2n+1)g_n\rangle - \langle(2n-1)r_n\rangle,$$

whence

$$\frac{\partial \text{ var } n}{\partial t} = \langle g_n\rangle + \langle r_n\rangle + 2[\langle ng_n\rangle$$
$$-\langle n\rangle\langle g_n\rangle - \langle nr_n\rangle + \langle n\rangle\langle r_n\rangle]. \qquad (3.1)$$

These results which give the rate of change of the moments can be considered to apply to the situation where an ensemble of systems all start with $n = n(0)$ at $t = 0$ and whose subsequent evolution is observed.

If we now assume that at any given t the P_n over the ensemble is a sharp function peaked at n we may write to a good approximation:

$$\frac{d}{dt}\text{var } n = g(\langle n\rangle)+r(\langle n\rangle)+2[g'(\langle n\rangle) -r'(\langle n\rangle)]\text{ var } n. \tag{3.2}$$

The mean and variance for linear kinetics are analogous in form to those derived earlier for spatially varying systems. We put $g = (C+An)$ and $r = Bn$ with $(B-A) = a > 0$. If $n = n(0)$ at $t = 0$,

$$\langle n(t)\rangle = [\langle n(0)\rangle - C/(B-A)]\, e^{-at} + C/(B-A)$$

$$\text{var } n(t) = \frac{CB}{(B-A)^2} + \left[\langle n(0)\rangle - \frac{C}{B-A}\right]\frac{B+A}{B-A}e^{-at} + \left[\text{var } n(0) - \langle n(0)\rangle\frac{B+A}{B-A} + \frac{AC}{(B-A)^2}\right]e^{-2at} \tag{3.3}$$

For small values of t the variance increases as

$$\text{var } n(t) - \text{var } n(0) = [C + \langle n(0)\rangle(A+B) - 2a\text{ var } n(0)]t, \tag{3.4}$$

which is of a diffusional character.

If an "aged" system is considered which at t has come to a given $\langle n(t)\rangle$, we can eliminate the initial conditions by taking $(B-A)t \gg 1$ and re-writing the variance as

$$\text{var } n(t) = \frac{B+A}{B-A}\langle n(t)\rangle - \frac{AC}{(B-A)^2} \tag{3.5}$$

which does not contain $n(0)$ or var $n(0)$ and involves t only implicitly through $\langle n(t)\rangle$.

There are difficulties in attempting to formulate the autocorrelation or spectral density of the fluctuations in a non-stationary system. The relaxation rate of the system is also the characteristic frequency involved in the spectrum and a "local" spectrum over any short interval of time cannot be considered to extend to low frequencies. Correspondingly, the autocorrelation function of $n(t)$ depends on the two moments of time considered and not only on their separation.

In considering the fluctuation spectrum in a non-stationary system it is therefore essential to formulate a precise observational procedure such as the passage of $n(t)$ through a linear filter of specified frequency response. Even in this situation not all ambiguity is removed since a realizable filter will have a finite delay and hence the spectral data it provides refer to the fluctuations in the system at some earlier time.

An attempt to derive an instantaneous power spectrum of $n(t)$ in the manner discussed by TURNER[6] has not been satisfactory. The question of the noise of a negative temperature system relaxing back to equilibrium is therefore not yet resolved.

3.2. *Energetic carriers and thermalization*

Energetic or "hot" carriers may be created in a semiconductor by irradiation with photons or particles having energy appreciably in excess of the ionization process involved or by the application of a sufficiently strong electric field.

The energetic photocarrier will thermalize to equilibrium with the lattice and the carriers heated by a field will do the same when the field is removed. In assessing the fluctuations in systems involving hot carriers it is necessary to know the rate of thermalization. If scattering is by acoustic phonons and the mean free path and effective mass of the carriers are assumed to be constant, then for an initial energy greatly in excess of the final energy it is the latter which determines the decay time. For decay to thermal energies we find to a good approximation

$$t_\theta \sim D_0/S^2, \tag{3.6}$$

where D_0 is the diffusivity of the thermal carriers and S the speed of sound. For typical cases t_θ lies in the range 10^{-11}–10^{-8} sec.

Here it was assumed that optical phonon scattering and inelastic collisions are unimportant. Also the assumed constancy of m^* may not be reasonable even when the excess energy is as small as 0·2 eV. Thus the result should be taken as a rough estimate and probably as an upper bound to the relaxation time. If the carrier initially was sufficiently energetic to lose energy to the optical modes, this part of the loss mechanism would be relatively so rapid as to increase the thermalization time only

Vol. 22
1961

slightly above the value estimated for acoustical modes.

The Johnson noise due to the photocarriers can be expressed in terms of an effective temperature derived from the average energy during the lifetime τ; if the initial carrier temperature was T_0

$$T_{eff} = T_L + (t_\theta/\tau)(T_0 T_L)^{1/2}. \qquad (3.7)$$

Thus if $T_L = 4°K$ and $T_0 = 900°K$ while $t_\theta = 10^{-9}$ sec and $\tau = 10^{-7}$ sec, the effective elevation of temperature during the lifetime is only $0{\cdot}6°K$. In typical circumstances therefore the Johnson noise of hot photocarriers would be negligible.

3.3. *Photo-mobility*

When a semiconductor is illuminated by photons of energy too small to cause ionization they may nevertheless produce transitions of free carriers. ROLLIN[4] has shown that this gives rise to a type of photoconductivity in which the carrier density is unchanged but the absorption of photons modifies the energy distribution and thereby changes the carrier mobility, especially at low temperatures.

The fundamental sources of noise associated with this effect are enhanced Johnson noise, as discussed in the previous section, and the mobility fluctuations due to the greater energy variance of the carriers which are subjected to gain of energy from the photons and subsequent loss to phonons.

If the band is non-degenerate and scattering is by acoustic phonons and the photon energy $h\nu$ large compared with kT_L the stimulated emission will be negligible compared with absorption. If a given carrier has probability p per unit time of absorbing a photon the mean carrier energy is increased by

$$\Delta E = h\nu p t_\theta$$

over the thermal value $3kT_L/2$. The variance of the carrier energy is increased by approximately

$$\text{var } E = \tfrac{1}{2}(h\nu)^2 p t_\theta$$

over the thermal value of $3k^2T_L^2/2$.

If for instance $T_L = 2°K$ and $h\nu = 4\times10^{-3}$ eV with $t_\theta = 10^{-8}$ sec and $p = 10^5\,\text{sec}^{-1}$ then the power absorbed per carrier is 6×10^{-17} W. The mean carrier energy is increased by 1·6 per cent whereas the energy variance is increased by 18 per cent and is therefore a significant contributor to the noise of this photoconductive process.

REFERENCES

1. YAMASHITA J., *Progress in Semiconductors*, Vol. 4. Heywood, London (1960).
2. BURGESS R. E., *Physica* **20,** 1007 (1954); *Proc. Phys. Soc. Lond.* B**68,** 661 (1955); **69,** 1020 (1956). *Canad. J. Phys.* **36,** 1569 (1958); *Disc. Faraday Soc.* **28,** 151 (1959).
3. TAUC J., *J. Phys. Chem. Solids* **8,** 219 (1959).
4. ROLLIN B. V., *Proc. Phys. Soc. Lond.* **77,** 1102 (1961).
5. BASOV N. G., KROKHIN O. N. and POPOV YU M., *Usp. Fiz. Nauk.* **72,** 161 (1960).
6. TURNER C. H. M., *J. Appl. Phys.* **25,** 1347 (1954).

BLANK
PAGE

Vol. 22
1961

J. Phys. Chem. Solids Pergamon Press 1961. Vol. 22, pp. 379–383. Printed in Great Britain.

A UNIFIED STATISTICAL APPROACH TO RECOMBINATION–GENERATION NOISE IN SEMICONDUCTORS

P. T. LANDSBERG and D. A. EVANS

Department of Applied Mathematics, University College, Cathays Park, Cardiff, Wales

Abstract—This paper outlines a unified discussion of equilibrium recombination–generation noise in semiconductors. It extends existing results in order to cover situations where certain types of Auger (electron collision) processes, as well as one-electron transitions, contribute to the noise. In order to achieve this, irreversible thermodynamics is used. The kinetic equations are written in a form involving generalized resistance and capacitance matrices. An admittance matrix and a lifetime matrix are also introduced. Results from semiconductor statistics are applied to evaluate these matrices in terms of the equilibrium electron numbers in, and equilibrium transition rates between, the various groups of states (bands and localized levels). The spectral densities and variances of the fluctuating electron numbers are related to the admittance matrix, and so finally to the equilibrium numbers and the transition rates, by means of the fluctuation–dissipation theorem. The spectral densities are in all cases superpositions of familiar terms of the form $A_k/(1+\omega^2\tau_k^2)$, and the paper outlines a general method of obtaining the coefficients A_k and the transient lifetimes τ_k.

INTRODUCTION

THE ELECTRONS in a semiconductor fall naturally into a number of groups (conduction and valence bands, trapped electrons) each group being assumed to have a quasi-Fermi level. If α_1,α_2 are the excess electron numbers in two such groups in fluctuations from an equilibrium state, one is interested in the mean value and the spectral density of the product $\alpha_1\alpha_2$. These are related by

$$\langle\alpha_1\alpha_2\rangle = \frac{1}{2\pi}\int_0^\infty G_{12}(\omega)\,d\omega. \qquad (1)$$

To find the spectral density $G_{12}(\omega)$, one may appeal to the fluctuation–dissipation theorem. This is a generalization of the Nyquist relation, and is given by

$$G_{12}(\omega) = \frac{4kT}{\omega^2}\mathrm{Re}\{Y_{12}(\omega)\}. \qquad (2)$$

$Y_{12}(\omega)$ is an admittance. The problem is therefore to express the admittance matrix Y in terms of more familiar quantities.

For the simplest case of a non-degenerate semiconductor without traps the results are well known and given by:

$$G_{nn}(\omega) = \frac{4n_0p_0}{n_0+p_0}\cdot\frac{\tau}{1+\omega^2\tau^2};\quad \tau = \frac{1}{p_{12}^o}\cdot\frac{n_0p_0}{n_0+p_0}$$

and

$$\langle(n-n_0)^2\rangle = \frac{1}{2\pi}\int_0^\infty G(\omega)\,d\omega = \frac{n_0p_0}{n_0+p_0}.$$

Here n_0,p_0 are equilibrium electron and hole numbers, and p_{12}^o is the equilibrium recombination rate. In obtaining such results, one uses the mass-action laws appropriate to one-electron generation and recombination processes. In the simplest case these refer to transitions of a single electron across the forbidden gap.

The question arises as to the extent to which the standard results of the theory remain valid in the presence of two-electron processes, such as electron–electron collisions. The change in the mass-action laws from being quadratic in the concentrations, to a cubic form, means that a great

deal of current theoretical work, including the basic papers by BURGESS and VAN VLIET[1,2] and collaborators, cannot be used unamended. Many additional processes which involve collisions ought to be considered. Thus if one confines oneself to processes in which no traps participate, there are three basic types, illustrated in the Figure, of which two involve electron–electron collisions. If a single set of traps participate in the typical recombination transition, one has a further

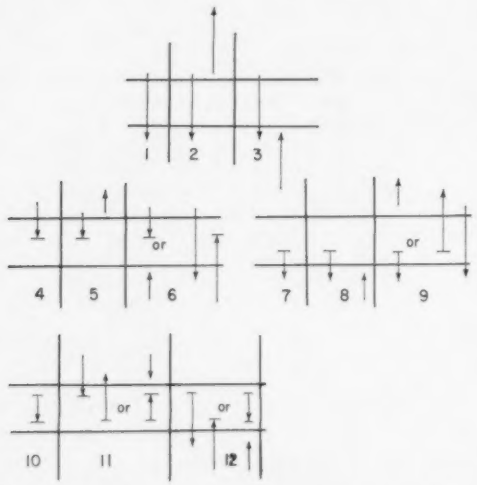

FIGS. 1–12. Main processes covered by the theory described in this paper.

six distinct processes, four of which are of the collision-type. With two sets of traps involved in a transition seven additional distinct processes occur, six of which are of the collision-type. Only three of these are shown as they are likely to be most important. To cover these sixteen types of transition it is desirable to get away from mass-action laws, and to proceed in a more general manner.

A paper by VAN VLIET[1] was found most suitable for this purpose. Its generalization proved possible by extending his use of irreversible thermodynamics. A uniform theory resulted which assumes as given: the equilibrium electron or hole numbers in the various groups of levels which are of interest (bands, or sets of traps) and the equilibrium transition rates between these groups. Expressions can then be given in terms of these quantities for the spectra $G_{ij}(\omega)$, the variances $\langle \alpha_1 \alpha_j \rangle$, and the transient as well as the steady-state lifetimes. Many of these turn out to be of the standard form already familiar from more special cases, provided they are expressed in terms of appropriate variables (equilibrium concentrations and transition rates). The theory is restricted by the assumption of small departures from equilibrium and the existence of quasi-Fermi levels. A minor restriction is that it can handle only elementary transitions the net result of which is that not more than one electron changes its quasi-Fermi level. This condition is clearly fulfilled by the fourteen processes shown, but it is not fulfilled by other rather less important processes. The work can, however, be extended to cover these cases, at the cost of increased complexity in the formulae, so that this restriction need not concern us here. In all cases the spectral densities turn out to be of the form

$$\Sigma A_k/(1+\omega^2\tau_k^2),$$

where the constants A_k and the transient lifetimes τ_k can be obtained in terms of concentrations and transition rates by the methods to be outlined.

2. THERMOSTATIC PRINCIPLES

It is not possible to present the results systematically in the space available, so that only general principles and suggestive rough arguments can be given here. These are intended to serve as an introduction to the full paper which will appear in the *Proceedings of the Royal Society*.

The thermodynamic situation can be made clear by considering a general class of systems. It is supposed that such a system exhibits extensive variables $Q_1, \ldots Q_s$ which vary under the constraint that their sum is constant. Thus if α_i denotes the departure from equilibrium of Q_i,

$$\sum_{i=1}^{s} \alpha_i = 0. \qquad (3)$$

It is assumed further that variables independent of the Q's are kept constant, and that under these conditions some thermodynamic function D has an extreme value in equilibrium. Thus if heat flows between two parts of a system, Q_1 and Q_2 represent the heat energy in the parts, Q_1+Q_2 is constant, and the entropy attains a maximum in

Vol. 22
1961

equilibrium. In this typical situation of irreversible thermodynamics all our assumptions are therefore satisfied. Returning to the general case, thermostatic forces $E_i = \partial D^{(s)}/\partial \alpha_i$ can be defined and turn out to be $1/T_i$ in the heat conduction case. $D^{(s)}$ means here that D is still expressed in terms of all s α's. Actually one of these, α_s say, can be eliminated by (3), and when this has been done, we write D instead of $D^{(s)}$. An increment of D is therefore of the form

$$dD = \sum_{i=1}^{s-1} (E_i - E_s)\, d\alpha_i$$

also

$$D = D_0 + \tfrac{1}{2}\eta_D \sum_{i,j=1}^{s-1} d_{ij}\alpha_i\alpha_j. \tag{4}$$

The last expression assumes small departures from equilibrium. In it $\eta_D = \pm 1$, depending whether D_0 is a minimum or maximum. η_D is introduced in order to give the matrix d always non-negative elements. Equation (4) leads to two alternative ways of defining the thermodynamic forces X_i which correspond to the displacement α_i

$$X_i = -\eta_D \frac{\partial D}{\partial \alpha_i}$$

$$= \begin{Bmatrix} \eta_D(E_s - E_i) \\ -\sum_{j=1}^{s-1} d_{ij}\alpha_j, \quad \text{i.e.} \boldsymbol{X} = -d\boldsymbol{\alpha} \end{Bmatrix}. \tag{5}$$

In the simple heat conduction case considered above there is only one such force, which is $X = 1/T_1 - 1/T_2$ – effectively a temperature difference.

The case of interest here occurs when the Q_i are the numbers n_i of electrons in the various groups. As the temperature is fixed, the free energy attains a minimum value, and one has $D \to F$, $\eta_D \to +1$, $E_i \to \partial F/\partial n_i = \mu_i$, $X_i = \mu_s - \mu_i$. Thus the chemical potentials (for quasi-Fermi levels) are the driving forces for our system which is at least roughly homogeneous in space. The heat conduction problem, though not homogeneous in space, serves however as a suggestive analogy.

3. KINETICS

For a discussion of the development of the system in time, a linear relation will be assumed between the forces X_i and the velocities $\dot{\alpha}_i$, as is appropriate for small departures from equilibrium:

$$\boldsymbol{X} = R\dot{\boldsymbol{\alpha}}. \tag{6}$$

From (5) and (6)

$$R\dot{\boldsymbol{\alpha}} + d\boldsymbol{\alpha} = \boldsymbol{O} \text{ or } \boldsymbol{V}(t), \tag{7}$$

depending on whether or not outside forces $V_i(t)$ are present. The introduction of the impedance and admittance matrices requires some care, but can be made plausible by appeal to an electrical analogy:

$$R\dot{Q} + (1/C)Q = 0 \text{ implies } Z = R + 1/i\omega C.$$

Hence (7) leads to

$$Z = R + d/i\omega = R(I - A/i\omega), \quad A \equiv -R^{-1}d.$$

The admittance matrix is

$$Y = Z^{-1} = (I - A/i\omega)^{-1}R^{-1}. \tag{8}$$

For the simple example of Section 1, matrices become numbers, and $R = kT/p_{12}^{o}$, $d = kT(1/n_{10} + 1/n_{20})$.

In order to make progress, observe that A can normally be diagonalized by choosing new variables (α_i') which are linear combinations of the given α_i. This representation will be denoted by primes, and the diagonal elements of A' (the eigenvalues of A) will be denoted by $-1/\tau_i$. Equation (7) yields:

$$\dot{\alpha}_i' = -(1/\tau_i)\alpha_i', \quad \text{i.e. } \alpha_i' = C_i \exp(-t/\tau_i).$$

The τ_i are thus seen to be lifetimes which characterize the return to equilibrium of the system. A may be called a lifetime matrix. The change in the variables may be achieved by multiplying the vector $\boldsymbol{\alpha}$ by a suitably chosen transformation matrix, whose elements can be expressed in terms of the elements of A. But the new representation is not the natural one which corresponds to the α's which are actually observed. It corresponds roughly to the choice of normal coordinates in dynamical problems.

Let the A-diagonal representation be adopted. Equation (8) then yields

$$Y'_{pq} = \frac{\omega^2\tau_p^2 + i\omega\tau_p}{1+\omega^2\tau_p^2}(R^{-1})'_{pq}. \qquad (9)$$

Thus one has the frequency dependence of the admittance matrix elements as needed in (2).

The problem is now formally solved. The solution is, however, not yet useful, as one needs to know the lifetimes and the resistances (i.e. the matrices d and R^{-1}) in terms of the parameters of the model: the equilibrium numbers and transition rates. These parameters are treated as known.

4. EQUATIONS FROM THE SEMICONDUCTOR MODEL

It turns out that nothing as specialized as mass-action laws has to be injected into the framework described so far. Two simple sets of equations are sufficient.

$$\text{(A)} \qquad \alpha_i = \xi_i n_{i0}(\mu_i - \mu_o)/kT. \qquad (10)$$

This result is straightforward for the electrons of conduction or valence bands. It merely needs a Taylor expansion of the non-equilibrium concentrations about the equilibrium Fermi level μ_o. ξ_i is a ratio of Fermi integrals, and is unity for non-degenerate bands. For localized levels a summation over the different charge conditions of a centre is involved. But a suitable ξ_i can be defined also in this case, and this removes the need to distinguish between bands and localized levels in the formal part of the theory. This device simplifies the final formulae considerably. Equation (10) relates thermodynamic forces and displacements, and can be combined with $\boldsymbol{X} = -d\boldsymbol{\alpha}$ [equation (5)] to yield the matrix d in terms of equilibrium numbers and the ξ_i.

$$\text{(B)} \qquad \dot{\alpha}_i = \sum_{k=1}^{s} p^o_{ik}(\mu_k - \mu_i)/kT. \qquad (11)$$

In this equation p^o_{ik} is the total equilibrium transition rate for the processes under consideration in each of which one electron moves from the group of quasi-Fermi level μ_i to the group of quasi-Fermi level μ_k. It takes a little manipulation to show that (11) is valid generally for all processes considered. The equation relates thermodynamic forces and velocities, just like $\boldsymbol{X} = R\dot{\boldsymbol{\alpha}}$ [equation (6)], and hence can be used to identify the resistance matrix in terms of the transition rates p^o_{ij}.

From d and R, the matrix $A \equiv -R^{-1}d$ and its eigenvalues can be obtained. The lifetimes τ_i follow in terms of the equilibrium numbers and transition rates. The formal solution (9) of the main problem can thus be linked to the model.

5. CONCLUDING REMARKS

The above approach is also suitable for discussing in a rather general framework the relation between transient and steady-state lifetimes. The equations for lifetimes and noise can be worked out in detail and, if the distinct groups of levels are not too numerous, all the matrices involved can be exhibited explicitly. This has been done for two and three groups of levels ($s = 2,3$) in the full paper in which the results obtained are also compared in detail with previous work.

Acknowledgement—One of us (D. A. EVANS) is grateful to the Department of Scientific and Industrial Research for the award of a N.A.T.O. studentship.

REFERENCES

1. VAN VLIET K. M., *Phys. Rev.* **110,** 50 (1958).
2. BURGESS R. E., *Proc. Phys. Soc. Lond.* **B68,** 661 (1955); **B69,** 1020 (1956).

DISCUSSION

P. J. PRICE: I believe that the condition for validity of such calculations is as follows:* after an electron makes a transition to a particular group of states, the time for it to "settle down" so that the probabilities of transitions to the other groups have reached their steady-state values must be small compared to the lifetime for the electron to remain in the group.

P. T. LANDSBERG: I think this condition is equivalent to the stated assumption stipulating the existence of quasi-Fermi levels.

K. M. VAN VLIET: If your condition is not satisfied *a priori* one may satisfy this by introducing more groups

* PRICE P. J., *J. Appl. Phys.* **31,** No. 69, 49–53 (June 1960).

of states, e.g. if carriers in the conduction band are not thermalized sufficiently fast, this band has to be represented by a group of states with different quasi-Fermi levels.

P. T. LANDSBERG: The situation just described by Dr. VAN VLIET can in principle be handled by the approach discussed here since the number of levels is left general in the formal part of the theory. When it comes to the evaluation of the formulae, however, the complexities go up rapidly with the number of levels.

K. M. VAN VLIET: It was pointed out that the free energy determines the carrier fluctuations. The only constraint is Σn_i = constant, but the energy is never constrained. In fact, as shown by BURGESS, the carrier variances can be adequately found from the energy fluctuations in a grand canonical ensemble. Thus, the derivation of Fermi–Dirac statistics for electrons in solids using carrier and energy constraint, as given in most solid-state textbooks, should be considered erroneous—or at least over simplified.

P. T. LANDSBERG: I agree that the grand canonical ensemble provides a very desirable approach to many statistical mechanical questions. In fact, I have recently had occasion to emphasize its usefulness.* The other methods quoted by the speaker should, however, give similar results whenever the fluctuations are small. The investigations of current carrier fluctuations mentioned by the speaker probably furnish examples of this general principle.

A. R. BEATTIE: Can this method be applied to the case of large departures from equilibrium provided the system may still be described by quasi-Fermi levels?

P. T. LANDSBERG: The method is limited to the neighborhood of equilibrium because the fluctuation–dissipation theorem is subject to this restriction.

R. LANDAUER: Modulated light techniques as described by CHEROFF and TRIEBWASSER are equivalent to generation–recombination noise techniques in terms of the information they yield. The equivalence is *exact* in the case of systems close to equilibrium, involving one-carrier transitions. The noise experiments are physically represented by the equivalent network given in VAN DER ZIEL's book. The same network with a constant current generator connected between the levels being "pumped" represents the response to the a.c. light flux. Since modulated light is now available even at microwave frequencies, it is hard to understand the reasons for the continuing predominant interest in the noise methods.

K. M. VAN VLIET: It is well known that the response to a.c. modulated light can be described by the same kinetic equations as the noise and consequently—if one desires so—the response can also be represented by an equivalent electrical network. Thus, if one is not interested in the noise characteristics of semiconductors as such—either to check the theory of equilibrium fluctuations or to find the practical radiation detection limit—but only in the determination of lifetimes, etc., one may employ a.c. light techniques as well. However, the methods are not completely equivalent. In the case of a multilevel semiconductor the noise spectrum may yield more information at once. When dealing with spontaneous fluctuations one measures the response to carrier population disturbances in *all* the levels and accordingly the spectra may reveal all the relaxation times of the system. In the photoconductive response, usually only specific transitions are induced and as a rule only one lifetime is observable. Thus the photoconductive response vs. a.c. chopping frequency is not completely proportional to the r.m.s. noise.† Furthermore, in the case of the spontaneous fluctuations, one can be sure that the disturbances are always small enough to linearize the kinetic equations.

P. T. LANDSBERG (Comment): The importance of noise in device work must also not be overlooked.

---

* *Thermodynamics with Quantum Statistical Illustrations.* Interscience, New York (1961).

† Compare VAN VLIET K. M. and BLOK J., *Physica* **22**, 525, 723 (1956).

BLANK
PAGE

Vol. 22
1961

J. Phys. Chem. Solids Pergamon Press 1961. Vol. 22, pp. 385–390. Printed in Great Britain.

GENERATION-RECOMBINATION NOISE AND CAPTURE CROSS-SECTIONS IN *p*-TYPE GOLD-DOPED GERMANIUM

L. J. NEURINGER and W. BERNARD

Research Division, Raytheon Company, Waltham, Massachusetts

Abstract—Generation–recombination noise in semiconductors arises from a modulation of the conductivity by random thermal fluctuations of the charge carriers between the valence (or conduction) band and the impurity levels. With certain impurities, such as gold in germanium, it is possible to have two interacting levels simultaneously contributing to the noise. We have studied two samples of gold-doped germanium in the temperature range 90°–100°K. In one sample, the Fermi level lies midway between the 0·041 eV donor level and the 0·145 eV acceptor level, so that the noise spectrum simultaneously exhibits relaxation times characteristic of both levels. In the second sample, the Fermi level is locked on the gold acceptor level. A straight-forward theory has been developed, capable of satisfactorily accounting, in general, for all of the observed noise in interacting two-impurity level systems of this type. Estimates of the total capture cross-sections of free holes by the 0·041 eV donor level and the 0·145 eV acceptor level in *p*-type gold-doped germanium of $\sigma_D = 3{\cdot}7 \times 10^{-18}$ cm^{-2} and $\sigma_A = 1{\cdot}5 \times 10^{-12}$ cm^2 have been obtained, in qualitative agreement with other independent measurements. Further, the results indicate some interesting possibilities regarding the existence of excited gold center states and their effect on the generation–recombination process.

WE HAVE previously reported[1] estimates of the capture cross-sections of free holes by the 0·041 eV donor level and the 0·145 eV acceptor level in *p*-type gold-doped germanium obtained from measurements of the generation–recombination noise spectrum. At 97°K the Fermi level of the sample studied earlier was located midway between the two gold levels, so that the noise spectrum simultaneously exhibited relaxation times characteristic of both levels. In this paper we report on additional measurements of the generation–recombination noise in this sample at 92°K and 100°K, and in a sample where the Fermi level lies close to the 0·145 eV acceptor level over the same temperature range. In general the experimental results further verify the theory developed to predict generation–recombination noise in interacting two-impurity level systems in terms of the capture cross-sections. However, it appears that transit time effects may appreciably modify the low frequency portion of the spectrum under certain conditions. Furthermore, the new results raise some question as to the conditions under which the 0·145 eV acceptor level can exhibit the strikingly large capture cross-sections previously reported.

Generation–recombination noise in semiconductors arises from the modulation of the conductivity by the random thermal fluctuations of charge carriers between the valence (or conduction) band and the impurity levels. Thus, for an extrinsic semiconductor, the time-dependent second moment $\langle \Delta J(0)\Delta J(t)\rangle$ of the current fluctuations is simply related to the corresponding moment $\langle \Delta p_V(0)\Delta p_V(t)\rangle$ of the fluctuations in the valence band population.

$$\langle \Delta J(0)\Delta J(t)\rangle = \frac{J^2}{p_V^2}\langle \Delta p_V(0)\Delta p_V(t)\rangle, \qquad (1)$$

where J is the average current and p_V the equilibrium valence band population. The generation–recombination noise spectrum $G(f)$ is the Fourier transform of equation (1).

VAN VLIET[2] has developed a general prescription for obtaining the free carrier fluctuations in multi-level systems by computing the linear response of the various level populations to the

thermodynamically conjugate applied Fermi potentials and has applied this technique to several simple systems and to the Shockley–Read model. More recently KLAASSEN[3] has studied generation–recombination noise in p-type nickel-doped germanium. However, the impurity level scheme for this system is such that only one nickel level need be considered at any given temperature. On the other hand, in the p-type gold-doped germanium system considered here, the 0·041 eV donor level and 0·145 eV acceptor level lie sufficiently close in energy that under appropriate conditions both levels are active simultaneously.

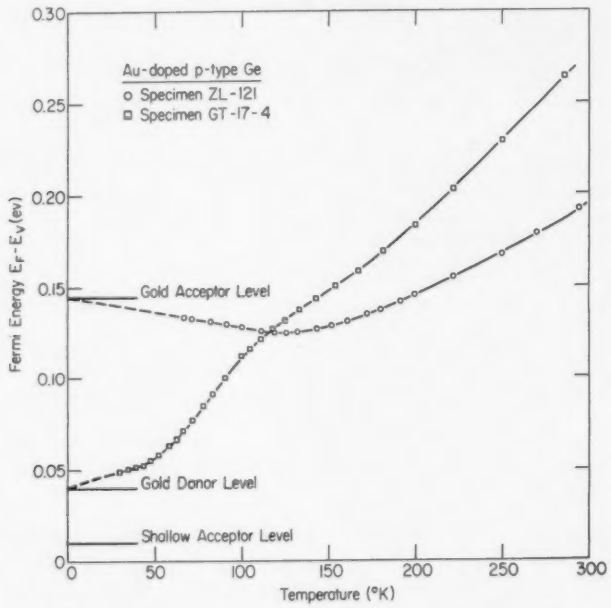

FIG. 1. Energy level scheme for p-type Au-doped germanium.

The model of p-type gold-doped germanium we consider is indicated in Fig. 1, which shows the impurity level scheme, and also the Fermi level as a function of temperature for the two samples studied, as given by KLEIN and DEBYE[4]. In the temperature range of interest the shallow acceptor level is assumed to be completely ionized, so that only two independent variables need be considered. The customary assumption is made regarding the interaction of the gold levels, wherein the number N_{Au}^0 of neutral gold atoms corresponds simultaneously to the number of ionized donor states and the number of filled acceptor states.

In order to distinguish clearly the principal features of the proper derivation we momentarily neglect *any* interaction between the two gold impurity levels. Under these conditions the instantaneous displacements from equilibrium Δp_A and Δp_D of the hole populations of the acceptor level and donor level, respectively, decay according to the simple scheme:

$$\Delta p_A(t) = \Delta p_A(0) \exp(-t/\tau_A) \qquad (2)$$

$$\Delta p_D(t) = \Delta p_D(0) \exp(-t/\tau_D), \qquad (3)$$

where $\Delta p_A(0)$ and $\Delta p_D(0)$ are the initial displacements. The decay of the valence band population, invoking charge neutrality, is therefore

$$\Delta p_V(t) = -\Delta p_A(0) \exp(t/\tau_A) - \Delta p_D(0) \exp(-t/\tau_D). \qquad (4)$$

Multiplying equation (4) by $\Delta p_V(0)$ and averaging over the equilibrium system yields the desired

Vol. 22
1961

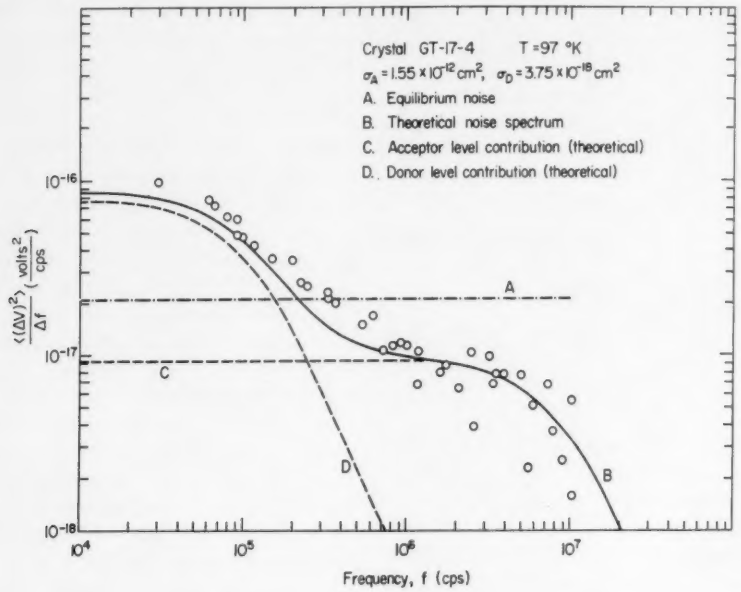
Crystal GT-17-4 T=97 °K
$\sigma_A = 1.55 \times 10^{-12}$ cm^2, $\sigma_D = 3.75 \times 10^{-18}$ cm^2
A. Equilibrium noise
B. Theoretical noise spectrum
C. Acceptor level contribution (theoretical)
D. Donor level contribution (theoretical)
$\frac{\langle(\Delta V)^2\rangle}{\Delta f}$ (volts^2/cps)
Frequency, f (cps)

FIG. 2. Generation–recombination noise spectrum at 97°K.

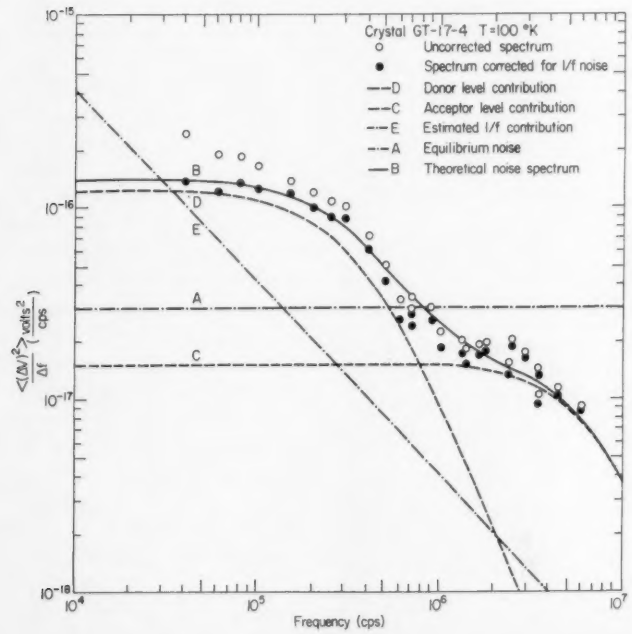

FIG. 3. Generation–recombination noise spectrum at 100°K.

second moment of the valence band fluctuations:

$$\langle \Delta p_V(0)\Delta p_V(t)\rangle = [\langle(\Delta p_V)^2\rangle + \langle \Delta p_V \Delta p_D\rangle]\exp(-t/\tau_A) - \langle \Delta p_V \Delta p_D\rangle \exp(-t/\tau_D) \tag{5}$$

From equation (1) the resulting generation–recombination noise spectrum is

$$G(f) = \frac{4J^2}{p_V^2} \times \left\{ \frac{[\langle(\Delta p_V)^2\rangle + \langle \Delta p_V \Delta p_D\rangle]\tau_A}{1+(2\pi f\tau_A)^2} - \frac{[\langle \Delta p_V \Delta p_D\rangle]\tau_D}{1+(2\pi f\tau_D)^2} \right\} \tag{6}$$

Equation (6), while representing a useful approximation in certain situations, is incorrect in two important respects: (a) the direct interaction arising from the fact that a neutral gold atom corresponds simultaneously to a filled acceptor and ionized donor has been neglected; (b) the indirect interaction between the two levels via the valence band has not been taken into account.

When the above modifications are properly introduced, the exact expression for the noise spectrum, as rerived in our earlier work[1], is

$$G(f) = \frac{4J^2}{p_V^2(\tau_D-\tau_A)} \times \left\{ \frac{\tau_D^2[(1-\tau_A A_{VV})\langle(\Delta p_V)^2\rangle - \tau_A A_{VD}\langle \Delta p_V \Delta p_D\rangle]}{1+(2\pi f\tau_D)^2} - \frac{\tau_A^2[(1-\tau_D A_{VV})\langle(\Delta p_V)^2\rangle - \tau_D A_{VD}\langle \Delta p_V \Delta p_D\rangle]}{1+(2\pi f\tau_A)^2} \right\}. \tag{7}$$

The A_{ij} are the coefficients of the coupled kinetic equations and are functions of the equilibrium statistics and the capture cross-sections σ_A and σ_D. The lifetimes τ_A and τ_D are the usual roots of the secular determinant obtained from the kinetic equations. The fluctuation moments $\langle(\Delta p_V)^2\rangle$ and $\langle \Delta p_V \Delta p_D\rangle$ are computed from the free energy according to the equilibrium fluctuation theory of GREENE and CALLEN[5], by solving the equations

$$\sum_k \frac{\partial^2 F}{\partial p_i \partial p_k}\langle \Delta p_k \Delta p_j\rangle = kT\delta_{ij}. \tag{8}$$

We note that it is also possible to obtain the equilibrium fluctuation moments following the method of LAX[6], which is based on the generalized Einstein mobility–diffusion relation.

The experimental noise spectra for the two samples studied are shown in Figs. 2–5. Fig. 2 exhibits a noise spectrum which is typical of crystal GT–17–4 in the temperature range over which the experiments were performed. These data have been corrected for the equlibrium noise. indicated by curve A. Two characteristic relaxation times, corresponding roughly to the two gold levels, are clearly evident as might be expected from the position of the Fermi level shown in Fig. 1. The best fit of equation (7) to the experimental points, corresponding to the total hole capture cross-sections $\sigma_A = 1{\cdot}5\times10^{-12}\,\mathrm{cm}^2$ and $\sigma_D = 3{\cdot}7\times10^{-18}\,\mathrm{cm}^2$, is shown by solid curve B. These values for the cross-sections are used in analyzing the data in Figs. 3–5.

Figure 3 presents the noise spectrum of crystal GT–17–4 at 100°K. These data have been corrected for an estimated $1/f$ contribution, curve E, as well as for the equilibrium noise, curve A. The two relaxation times are still clearly discernible. The relaxation time of the donor level has decreased in accordance with the theory. Using the previously obtained values for the cross-sections, good agreement between the theoretical prediction (solid curve B) and experimental data is obtained.

The generation–recombination noise spectrum of the same sample at 92°K appears in Fig. 4. The acceptor level contribution is readily observed and remains essentially unchanged. However, at this temperature any donor level contribution present is dominated by the $1/f$ noise, which amounts to $3\times10^{-16}\,\mathrm{V}^2/\mathrm{c/s}$ at 10^4 c/s. We note that the same $1/f$ component is present in Fig. 3. The theoretical spectrum, shown by the dotted line, agrees with the experimental acceptor level contribution, but requires a donor level contribution which should be readily observable. We suggest that the donor level contribution may be suppressed when the donor relaxation time becomes longer than the transit time. We intend to consider this possibility quantitatively in the future.

For the second sample studied the generation–recombination noise spectrum at 90°K is shown

Vol. 22
1961

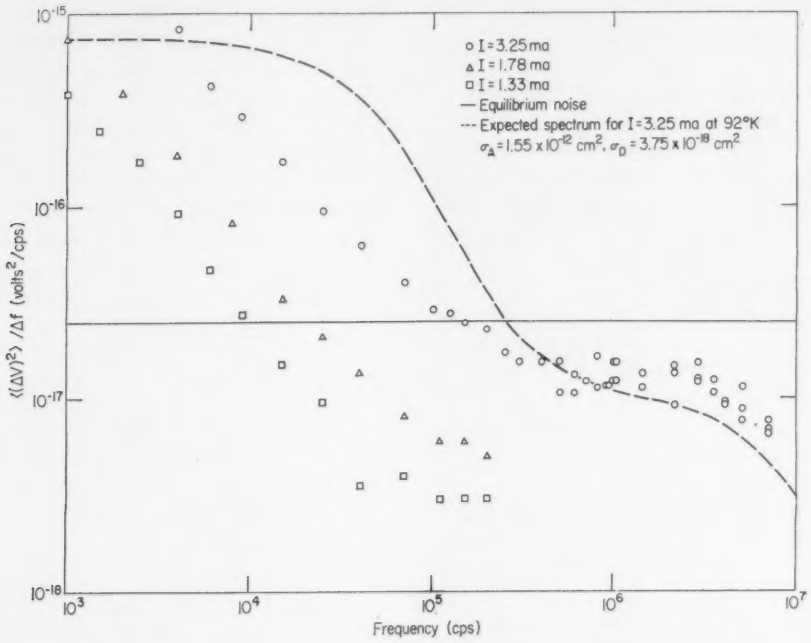
o I=3.25 ma
Δ I=1.78 ma
□ I=1.33 ma
— Equilibrium noise
--- Expected spectrum for I=3.25 ma at 92°K
$\sigma_A = 1.55 \times 10^{-12}$ cm², $\sigma_D = 3.75 \times 10^{-18}$ cm²
$\langle(\Delta V)^2\rangle / \Delta f$ (volts²/cps)
Frequency (cps)

FIG. 4. Generation–recombination noise spectrum at 92°K.

in Fig. 5. We recall from Fig. 1 that the Fermi level for this sample lies close to the 0·145 eV acceptor level, so that one might expect the noise to exhibit a contribution solely from this level. The two curves correspond to the noise measured with the current flowing through the sample in opposite directions. Using the values of the cross-sections, $\sigma_D = 3{\cdot}7 \times 10^{-18}$ cm² and $\sigma_A = 1{\cdot}5 \times 10^{-12}$ cm², obtained from analysis of the previous sample, the theory predicts a noise level of 5×10^{-16} V²/c/s and a generation–recombination frequency of 9×10^7 c/s arising from the acceptor and essentially no contribution from the donor. Although the theory predicts the correct integrated noise, it appears to be in serious error in other respects. The excessively short relaxation

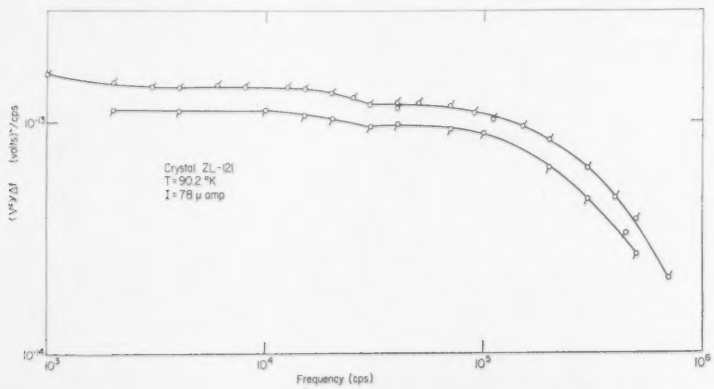

FIG. 5. Generation–recombination noise spectrum at 90°K.

time predicted is due to the presence of a large number of negatively ionized gold acceptor states. If the assumption is made that only a small fraction of these states is available for recombination, it is possible to predict the observed noise satisfactorily. To account for this apparent discrepancy we suggest the following mechanism. We suppose that the negative gold center can exist in either a ground state or an excited state. The excited state presents the large capture cross-section normally attributed to the negative gold center, whereas the ion in the ground state exhibits a more modest cross-section. Only those centers which actively engage in the thermal generation–recombination process exist in the excited state. The large percentage of negative gold centers, having lost a hole to the shallow Column V donor (arsenic), are present in the ground state.

To summarize, we assert that the general aspects of the theory developed to predict generation–recombination noise in interacting two-impurity level systems are correct and may be used to obtain reliable estimates of capture cross-sections. Our values for the total cross-sections, for example, are in fair agreement with those determined using field effect techniques by RUPPRECHT[7], who has found total cross-sections of $\sigma_A = 2{\cdot}5 \times 10^{-12}$ cm^2 and $\sigma_D = 6{\cdot}7 \times 10^{-19}$ cm^2. The experimental results reveal several interesting possibilities which could lead to a more detailed description of deep-lying impurity centers and their interaction with conducting states. We intend to pursue these matters both theoretically and experimentally in the future.

REFERENCES

1. NEURINGER L. J. and BERNARD W., *Phys. Rev. Letters* **6,** 455 (1961).
2. VAN VLIET K. M., *Phys. Rev.* **110,** 50 (1958).
3. KLASSEN F. M., Doctoral Thesis, Vrije Universiteit, Amsterdam, Netherlands (1961).
4. KLEIN C. A. and DEBYE P. P., *Proceedings of the International Conference on Semiconductors, Prague* (1960) p. 278. Czechoslovak Academy of Sciences, Prague (1961)
5. GREENE R. F. and CALLEN H. B., *Phys. Rev.* **83,** 1231 (1951).
6. LAX M., *Rev. Mod. Phys.* **32,** 25 (1960).
7. RUPPRECHT G., *Proceedings of the International Conference on Semiconductors, Prague,* (1960) p. 282. Czechoslovak Academy of Sciences, Prague (1961).

Vol. 22
1961

DISCUSSION

A. ROSE: Have you considered the contribution of a small fraction of doubly charged gold centers?

L. J. NEURINGER: We have assumed that the doubly charged gold centers do not contribute in any observable way to the noise spectrum since they are so far removed from the valence band. It is difficult to see how they could be important in the temperature range considered.

J. J. BROPHY: If the existence of excited and ground states of the negative gold ion is relevant to the generation–recombination process, why doesn't RUPPRECHT observe them in his field effect experiments?

L. J. NEURINGER: I believe that in his experiment RUPPRECHT bends the bands (by applying an electric field) in such a direction that he observes only the generation process, which should be essentially unaffected by the relatively few excited states postulated here. Under appropriate conditions it might be possible for him to observe the effects we describe if he would deform the bands in the opposite direction.

J. Phys. Chem. Solids Pergamon Press 1961. Vol. 22, pp. 391–399. Printed in Great Britain.

GENERATION-RECOMBINATION NOISE IN VARIOUS PHOTOCONDUCTIVE SEMICONDUCTORS

F. M. KLAASSEN*

Department of Physics, Free University of Amsterdam, The Netherlands

and

K. M. VAN VLIET and J. R. FASSETT

Department of Electrical Engineering, University of Minnesota, Minneapolis, Minnesota, U.S.A.

Abstract—Noise measurements are reported for nickel-doped germanium, manganese-doped germanium, gold-doped germanium, indium antimonide and tellurium. For nickel-doped germanium the noise spectra are found to be consistent with the *g–r* noise theory for double acceptor systems. The various capture cross-sections have been determined. At low temperatures the upper nickel level acts as a recombination center (hole trap).

The noise spectra for manganese-doped germanium are complex at temperatures close to 77°K. The noise is extremely low and consequently a large detectivity as a radiation detector is to be expected.

For gold-doped germanium, spectra were observed which are not of the usual form for multi-step relaxation processes. An explanation is suggested by noticing that the dielectric relaxation time for these samples is larger than the lifetime so that space charge transients can exist.

Some noise data are given for indium antimonide together with an estimate for the noise equivalent power.

Finally some features of noise in tellurium single crystals are reported.

1. INTRODUCTION

GENERATION–RECOMBINATION noise refers to carrier density fluctuations caused by spontaneous fluctuations in generation, recombination or trapping rates, including that part which is due to photon noise of the (background) radiation field.[1] The theory for *g–r* noise has been well confirmed in the last few years, particularly for intrinsic or near intrinsic materials or for simple photoconductors in which excitation takes place across the band gap like PbS.[2–5] Presently, in various institutions more complicated materials which contain various trapping levels, double acceptors, etc., are being studied. As illustrative examples we mention the studies of gold-doped germanium[6,7] and of cadmium sulfide, reported in the literature.[8,9] Generally, the noise spectra for these materials are complex, thereby reflecting the complexity of the energy level system involved. Roughly speaking, the spectral intensity of the noise is the Fourier transform of the current reponse $\Delta i(t)$ caused by the decay of excess carrier population of the various electronic energy states. As a consequence, the spectra reveal turnover (angular) frequencies equal to the reciprocals of the corresponding transition relaxation times which are also observed in other transient phenomena. Lifetimes as short as 10^{-8} sec can be determined by measuring the spectrum up to 16 Mc/s.

In this paper we shall report various measurements on nickel, manganese and gold-doped germanium, indium antimonide and tellurium.

Rather than presenting detailed mathematical calculations [for methods, compare Refs. (1), (10–14)], we shall present here the experimentally observed spectra for the various materials and discuss the main features of them.

2. NICKEL-DOPED GERMANIUM

The incorporation of nickel in germanium provides acceptor states 0·23 and 0·44 eV above

* Now at N. V. Philips Gloeilampenfabrieken, Eindhoven, The Netherlands.

the valence band. In samples which are partially counterdoped the noise spectra should be simple since in a wide temperature range (77°–180°K) the Fermi level is clamped at the lower acceptor sites. In that case there is only one dominant

$$\sigma_p^- = 3{\cdot}5 \times 10^{-14}\ \text{cm}^2 \text{ at } 200°\text{K}$$

and at other temperatures: $\sigma_p^- \sim T^{-1{\cdot}5}$.

Since the noise satisfied the theoretical expressions and was consistent with the Hall data,

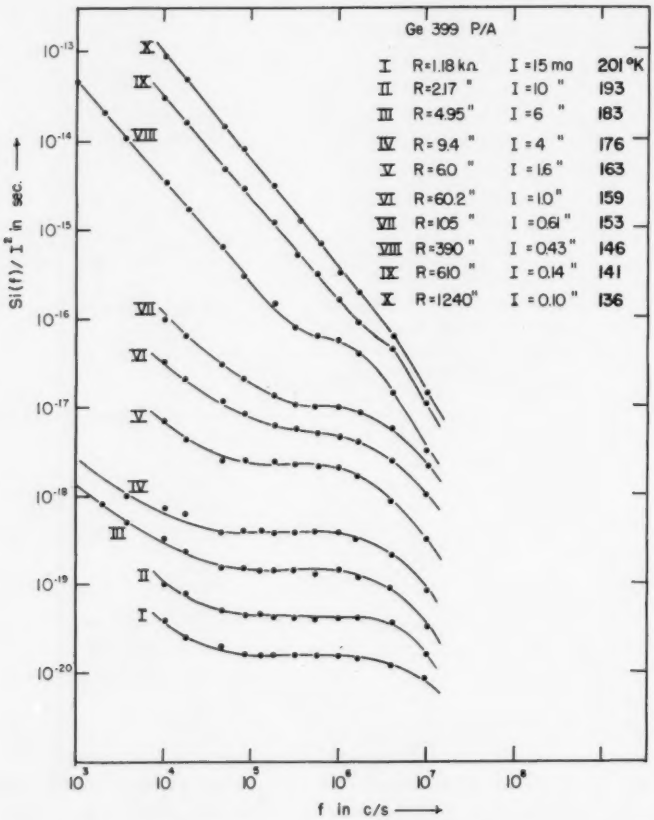

FIG. 1. Noise spectra at low temperatures for a compensated nickel-doped germanium p-type sample.

lifetime due to transitions between the valence band and the lower acceptor levels:

$$\tau = 1/\sigma_p^- \langle v_p \rangle n_c.$$

σ_p^- is the capture cross-section of singly ionized acceptors (lower levels) for holes, $\langle v_p \rangle$ is the mean hole velocity and n_c is the number of compensation centers. The observed spectra are shown in Fig. 1. From the turnover frequencies it follows:

it is not necessary to measure the photoconductive responsivity in order to determine the noise equivalent power; it is adequate to calculate the noise equivalent power from the simple expression:

$$P_{eq} = \frac{h\nu}{\eta}\left(\frac{4p_0 d}{\tau}\right)^{1/2}, \qquad (1)$$

where $h\nu$ is the optical energy (0·23 eV), η is the

Vol. 22
1961

quantum efficiency, p_o is the equilibrium hole density, d is the thickness of the crystal, τ is the observed lifetime (3×10^{-8} sec). For the sample shown at 150°K, $P_{eq}\approx 6\times10^{-10}$ W. This could go down by several orders of magnitude, if normal g–r noise of the form $C/(1+\omega^2\tau^2)$ would prevail at lower temperatures. However, Fig. 1 shows that below 150°K $1/f$ noise dominates. The difficulty here is that contact noise cannot be eliminated properly by probe techniques when the crystal resistance becomes extremely large ($\gtrsim$ 1MΩ). Also, a space-charge effect may modify the noise; compare for gold-doped germanium below.

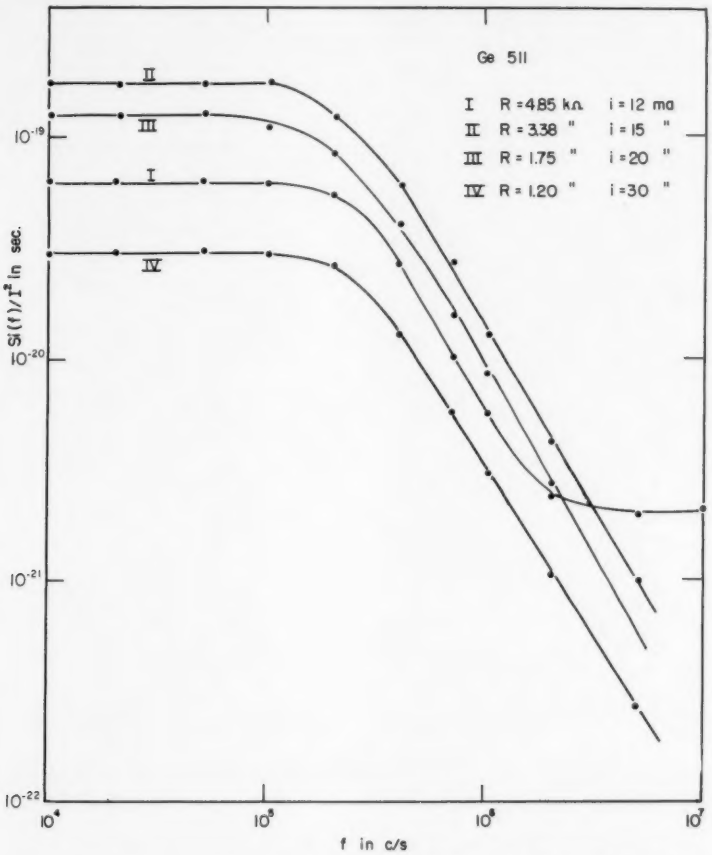

FIG. 2. Noise spectra in the intrinsic range for a 40 Ω cm nickel-doped germanium crystal.

At room temperature the spectra look quite different as demonstrated by Fig. 2. An analysis was undertaken under the assumption that the upper nickel center in this case acts as a recombination center (hole trap). This provided consistent results. The two possible bumps yielded: $\sigma_n^- = 2{\cdot}3\times10^{-16}$ cm^2 (capture cross-section of simply ionized states for electrons) and

$$\sigma_p^{=} \gtrsim 5\times10^{-14}\,\text{cm}^2$$

(capture cross-section of double ionized states for holes). The values of the various cross-sections are in agreement with the relation[15];

$$\sigma_p^{=} > \sigma_p^{-} > \sigma_n^{o} > \sigma_n^{-} \qquad (2)$$

which accounts for the electrostatic interaction.

3. MANGANESE-DOPED GERMANIUM

Manganese provides acceptor levels at 0·16 eV and 0·38 eV above the valence band. The crystals were counterdoped in order to fill up the low-lying acceptor levels ($\approx$0·05 eV) of unknown origin in these materials. Some noise curves for temperatures between 78° and 120°K are given in Fig. 3.

$\tau = 1/\sigma_p^- \langle v_p \rangle n_c$ should be practically independent of temperature. Curves 4, 5 and 6 seem to fit this formula, assuming $\tau \approx 10^{-8}$; however at lower temperatures the time constant increases, and the level of the noise is two orders of magnitude *lower* than expected from (3).

From the log R vs. $1/T$ curve, which is a straight

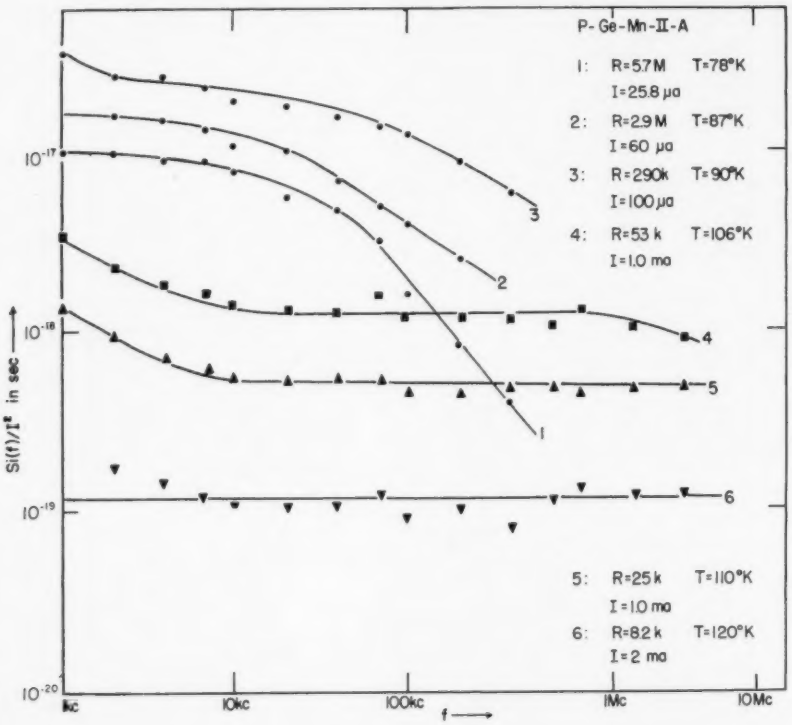

FIG. 3. Noise spectra for manganese-doped germanium at low temperatures.

The spectra are quite different from those for nickel-doped germanium. At first sight, the complexity of the spectra is not clear. If one could assume—as for nickel-doped germanium—that the noise is caused only by transitions between the valence band and the lower manganese levels, of which a number n_c is filled due to counterdoping, then, since $n_c \approx 10^{13} \gg p_0$ for the temperatures considered, one expects the noise to be given by the simple formula:

$$S_i(f) = 4I^2\tau/p_0V(1+\omega^2\tau^2), \qquad (3)$$

where V is the volume and τ is the relaxation time: line of slope 0·16 eV down to 77°K, one concludes that the holes did come from the lower acceptor levels and consequently one would expect g–r noise from these transitions. Applying equation (3) this would result in a noise level as large as the plateau in curve 1 but extending to 10 Mc/s as for curves (3), (4) and (5). Apparently the observed noise at 77°K is of different origin and the regular g–r noise from the acceptor levels is apparently *suppressed*, unless the time constant is of order 10^{-10} sec, i.e. the capture cross-section for holes is a factor 100 less than for nickel-doped germanium. The low-frequency turnover at

Vol. 22
1961

30 kc/s might arise from hole trapping by the low-lying acceptors of unknown origin. Also, a possible space-charge effect as will be discussed below for gold-doped germanium may effect the shape of the spectra.

The noise equivalent power for the reported crystal is very low, viz. of the order 5×10^{-13} W for

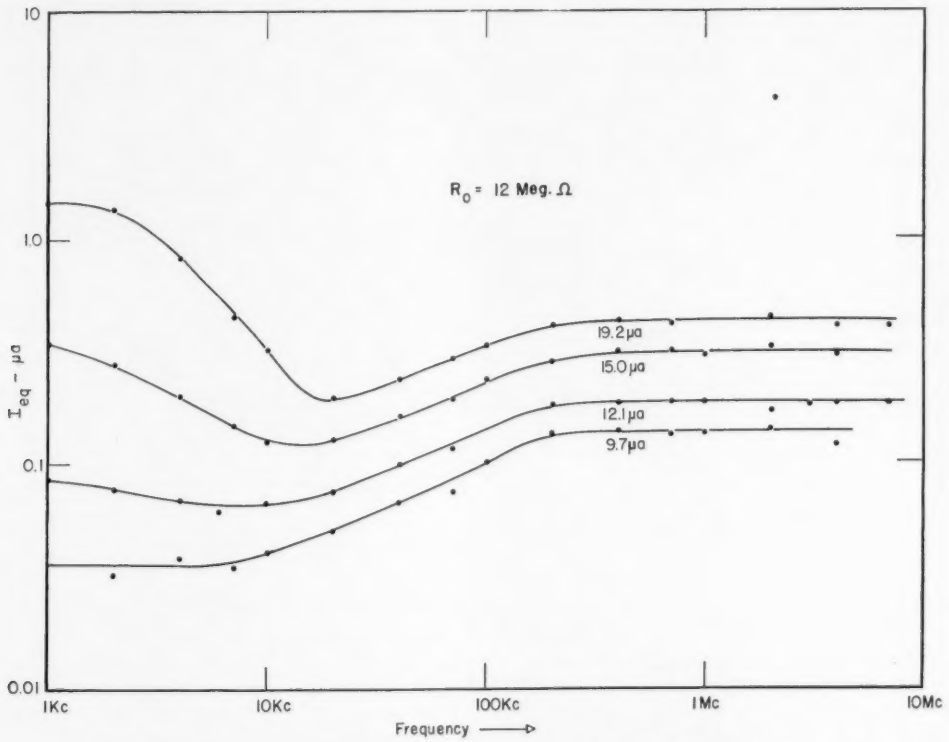

FIG. 4. Noise spectra for a gold-doped germanium sample at 88°K.

$h\nu = 0{\cdot}16$ eV and at 77°K. Noise spectra have also been measured under infrared irradiation thereby exciting electrons to the lower manganese levels. The results will be reported elsewhere.

4. GOLD-DOPED GERMANIUM

For practical infrared detectors gold-doped germanium is a useful material. Noise was measured before by JOHNSON and LEVINSTEIN[6] and by NEURINGER and BERNARD[7]; the first investigators measured only up to 10 kc/s and observed regular g–r noise. Some peculiarities in the noise spectra were recently observed at the University of Minnesota and will be briefly reported here. The crystals investigated were provided with alloyed contacts and were well-behaved. The I–V characteristics were reversible and linear. The samples were high-ohmic at liquid nitrogen temperature and showed the usual photoconductive response. At 77°K breakdown could be observed for voltages of the order of 1000 V/cm which has also been found by others.

Some noise spectra for 88°K, $R = 12$ MΩ are shown in Fig. 4. Below 10 kc/s the spectra are flat except for extra noise at higher currents. The noise spectra then rise till another plateau is reached. The falling-off of this noise is not observable anymore in the measured range (up to 10 Mc/s). At higher temperatures a similar

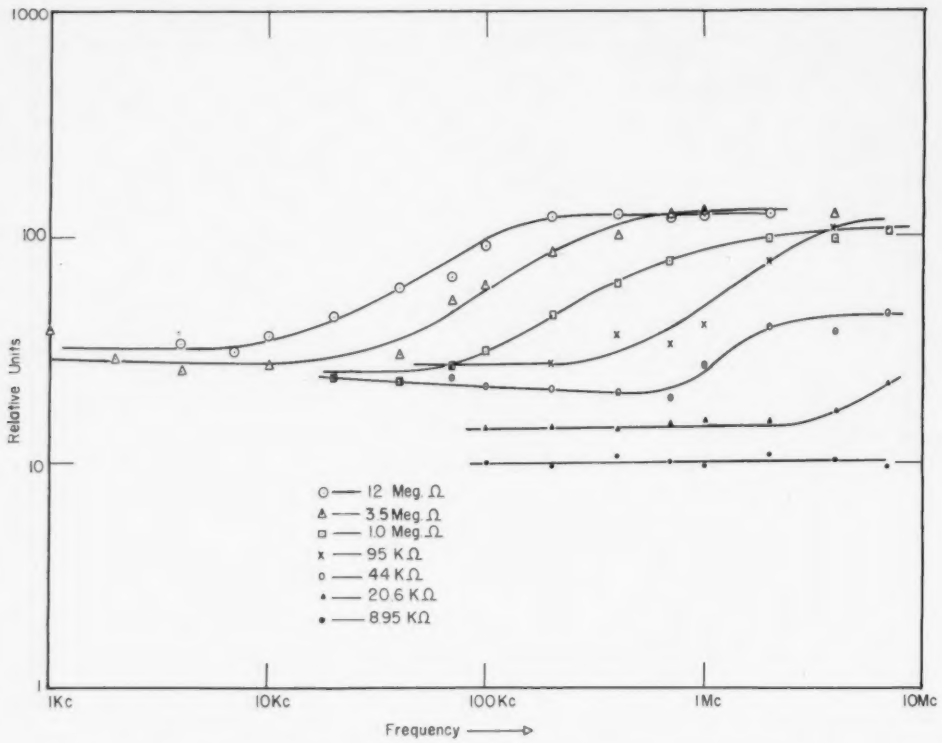

FIG. 5. Noise spectra for a gold-doped germanium sample at low temperatures.

pattern is found but the rising of the noise moves out to higher frequencies.* A summary of the data taken for various resistance values at temperatures above 77°K is presented in Fig. 5. At the highest temperature measured (141°K) the spectrum remains flat up to 10 Mc/s.

Spectra of the observed nature cannot be explained from the general theory of *g–r* noise which predicts a spectrum of the form:

$$S_i(f) = I^2 \sum_k A_k \tau_k (1+\omega^2\tau_k^2) \qquad (4)$$

with all A_ks positive. This is a consequence of the monotonic decrease of the correlation function of the equilibrium fluctuations. Apparently, the basic assumptions of regular *g–r* noise, viz. that the fluctuations are independent of position and that charge neutrality is maintained at any instant, are not satisfied. This is certainly probable in high ohmic materials. For the curve at 12 MΩ the lifetime is $\approx 10^{-8}$ sec, the dielectric relaxation time is $\epsilon\epsilon_0/\sigma \approx 2\cdot10^{-6}$ sec and the hole transit time is of order 10^{-6} sec. For variations faster than ≈ 100 kc/s no space charge neutrality can be maintained, which may cause the rising of the noise. The fact that at higher conductivities the enhancement of the noise finally moves out to frequencies larger than the reciprocal lifetime supports this idea. Also, anomalies have been observed in the impedance for frequencies larger than $1/\tau_{diel}$. A more detailed study of noise under space-charge limited flow or space-charge transients is under way.

5. INDIUM ANTIMONIDE

Two unsuccessful attempts to measure *g–r* noise in InSb have been reported in the

* If similar effects would be present in nickel-doped germanium it could not have been observed in our crystals, of Fig. 1, since at 77°K the crystals showed too much $1/f$ noise.

Vol. 22
1961

literature.[16,17] However, for rather pure p-type samples g–r noise can be observed in a small temperature interval around the temperature where the Hall coefficient has its maximum before it changes sign. The noise spectra were found to be flat. The noise level as a function of temperature is given in Fig. 6. The data can be explained with a tropic electrical properties. Noise measurements were made on samples with a triangular cross-section cleaved in liquid air. The current flow was in the direction of the hexagonal axis. g–r noise was measureable in the knee of the Hall curve and in the intrinsic region up to 250°K. In the extrinsic region no noise was observed except in

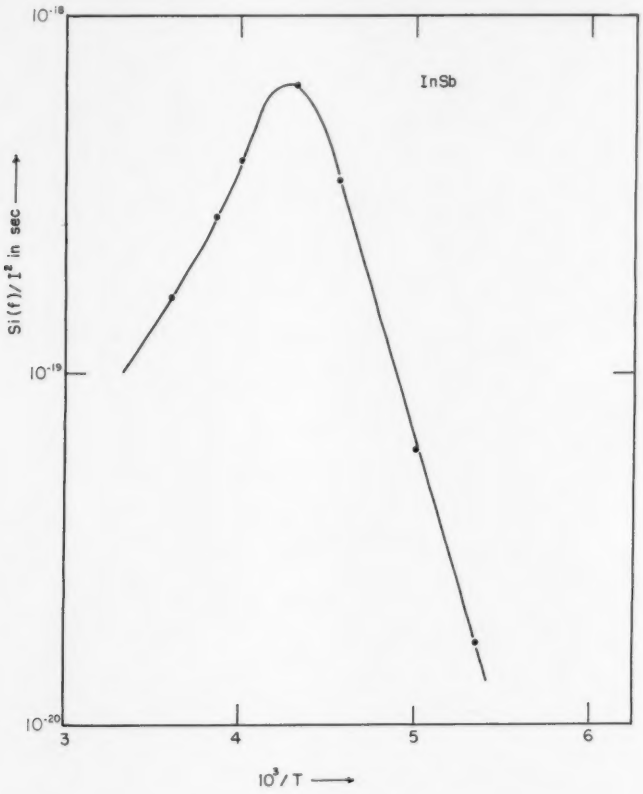

FIG. 6. Noise level for InSb as a function of temperature.

Shockley–Read model. The noise equivalent power was found to be $1{\cdot}0 \times 10^{-9}$ W at $T = 220$°K and $h\nu = 0{\cdot}18$ eV. This is an order of magnitude higher than present calculations[18] which neglect g–r noise predict. A fuller account will be published elsewhere.

6. TELLURIUM

Tellurium is a semiconductor with a bandgap of approximately 0·34 eV and with strong anisotropic electrical properties. Noise measurements were made on samples with a triangular cross-section cleaved in liquid air. The current flow was in the direction of the hexagonal axis. g–r noise was measureable in the knee of the Hall curve and in the intrinsic region up to 250°K. In the extrinsic region no noise was observed except in one out of twelve measured samples which exhibited large $1/f^3$ noise.

Some typical g–r noise curves are given in Fig. 7. The crystal was heated by the passage of the current up to 235°K; the ambient temperature was about 195°K. Though there is some inhomogeneity in the temperature of the sample, it has been shown before that for the set-up used most of the temperature gradient occurs outside the crystal.[19]

The spectra of Fig. 7 are constant for $f \gtrsim 10$ kc/s and have a high frequency slope close to 1·5 (i.e. $S(f) \propto 1/f^{3/2}$). We believe these spectra—which were observed in many more samples under similar conditions—are the first clear evidence usually a different spectral component of the form $1/f^{\alpha}$ with $\alpha \simeq 0{\cdot}5$ below 50 kc/s and $\alpha = 2$ for high frequencies was dominant. This noise, which could be greatly effected by etching, was attributed to the surface. Clearly the spectrum turns over for

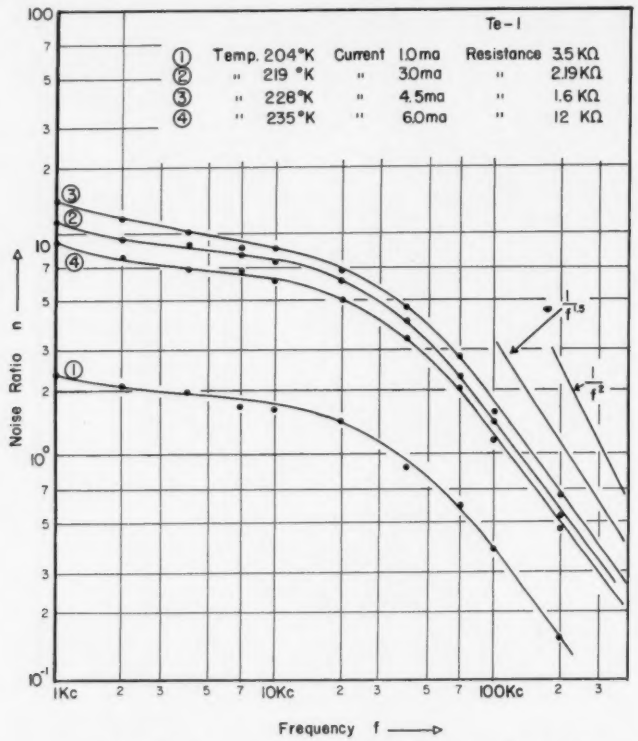

FIG. 7. Typical noise spectra for tellurium single crystals.

for "diffusion limited g–r noise" as was predicted by CHAMPLIN[20]. Such a noise spectrum occurs if the diffusion time for carriers from the bulk to the surface is larger than the lifetime associated with the surface generation–recombination process and shorter than the bulk lifetime; in our case $\tau_{diff} = (2/5)(3/56)a^2/D_a$, where a is the edge of the triangular cross-section and where D_a is the ambipolar diffusion constant. For the curves of Fig. 7 τ_{diff} observed is 4·3 μsec and the calculated value is 4·52 μsec. Also the magnitude of the noise is close to the expected values.

When higher currents were passed through the samples (the ambient temperature being 77°K), $\omega\tau_s \gg 1$. Present surface noise theories are incomplete in predicting the high-frequency behavior. Also, a correlation with the g–r noise component was apparent. A more detailed analysis will be reported elsewhere. Attempts to measure bulk g–r noise in tellurium crystals are in progress.

Acknowledgements—One of us (F.M.K.) wishes to express his gratitude for valuable discussions with Professor J. BLOK of the Free University, and with Professor D. POLDER, Ir. P. PENNING and Dr. B. H. SCHULTZ of the Physics Laboratory of N. V. Philips. K. M. v.V. and J. R. F. acknowledge discussions with Professor A. VAN DER ZIEL and the support of part of

Vol. 22
1961

this work by the U.S. Signal Corps. They thank Mr. D. PAI for taking the measurements on tellurium.

The crystals were provided by Ir. P. PENNING of the Philips Laboratories, Dr. J. H. DIRKSEN of the R.V.O.–T.N.O., The Hague, Dr. W. W. TYLER of General Electric Research Laboratory, Dr. J. S. BLAKEMORE of Minneapolis Honeywell Regulator Company, by Mullard Laboratories, England and by Sylvania Electrical Products Company.

REFERENCES

1. VAN VLIET K. M., *Proc. Inst. Radio Engrs.* **46,** 1004 (1958).
2. HILL J. E. and VAN VLIET K. M., *J. Appl. Phys.* **29,** 177 (1958).
3. SAUTER D. and SEILER K., *Z. Naturf.* (6) **12a,** 490 (1957).
4. PETRITZ R. L., *Phys. Rev.* **104,** 1508 (1956).
5. KLAASSEN F. M. and BLOK J., *Physica* **24,** 975 (1958).
6. JOHNSON L. and LEVINSTEIN H., *Phys. Rev.* **117,** 1191 (1960).
7. NEURINGER J. and BERNARD W., private communication.
8. VAN VLIET K. M., BLOK J., RIS C. and STEKETEE J., *Physica* **22,** 723 (1956).
9. BROPHY J. J. and ROBINSON R. J., *Phys. Rev.* **118,** 959 (1960).
10. VAN VLIET K. M. and BLOK J., *Physica* **22,** 231 (1956).
11. KLAASSEN F. M., VAN VLIET K. M. and BLOK J., *Physica* **26,** 605 (1960).
12. VAN VLIET K. M., *Phys. Rev.* **110,** 50 (1958).
13. LAX M., *Rev. Mod. Phys.* **32,** 25 (1960).
14. KLAASSEN F. M., Ph.D. Thesis, Free University of Amsterdam (1960).
15. LAX M., *J. Phys. Chem. Solids* **8,** 66 (1959); *Phys. Rev.* **119,** 1502 (1960).
16. OLIVER D. J., *Proc. Phys. Soc.* Lond. **B70,** 244, 331 (1957).
17. SMITS G. H., *J. Appl. Phys.* **27,** 1385 (1956).
18. MOSS T. S., *Photoconductivity Conference,* p. 426. Wiley, New York (1956).
19. KLAASSEN F. M., BLOK J. and DE HOOG F. J., *Physica* **27,** 187 (1961).
20. CHAMPLIN K. S., *Physica* **26,** 751 (1960).

. 22
61

BLANK
PAGE

Vol. 22
1961

J. Phys. Chem. Solids Pergamon Press 1961. Vol. 22, pp. 401–407. Printed in Great Britain.

THE NOISE POWER SPECTRUM OF p-TYPE INDIUM ANTIMONIDE

D. W. GOODWIN

Royal Radar Establishment, Great Malvern, Worcs. England

Abstract—The noise power spectrum of p-type indium antimonide has been measured in the extrinsic region for hole concentrations between 10^{12} and 10^{15} per cm^3. For frequencies greater than 1kc/s generation–recombination noise is dominant in all but very high resistivity specimens. Carrier lifetime determinations from these measurements are in agreement with those by photoconductive decay methods and indicate majority carrier photoconduction. For frequencies less than 1kc/s the noise power increases rapidly with decreasing frequency and with decreasing hole concentration. For very high resistivity material the noise power spectrum is dependent on the surface properties. The results which are presented are not inconsistent with the statistical theory of queuing.

1. INTRODUCTION

THE NOISE power spectrum of many semiconducting materials exhibits an inverse frequency characteristic at low frequencies extending down to 6×10^{-5} c/s.[1] Although the exact physical origin of this effect is very much in doubt its source has been associated with various effects such as the potential barriers existing at a p–n junction, around lattice dislocations and at the surface barrier of a semiconductor.[2] The majority of these effects have been studied using single crystals of germanium, usually at room temperature.

Because of the importance of p-type indium antimonide as an infra-red photoconductive detector[3] the noise power spectrum has been investigated in the extrinsic carrier region in order to determine the sources of noise and if at all possible reduce their magnitude. The use of semiconducting material other than germanium might reveal other noise characteristics likely to elucidate the source of low frequency noise.

In order to remove certain known sources of noise high purity p-type indium antimonide single crystals were used of high crystalline perfection. A detailed analysis of generation–recombination has been carried out in order to elucidate the photoconductive process in the extrinsic region. The effects of temperature and both surface treatment and field effect have been studied as a function of hole concentration.

2. EXPERIMENTAL PROCEDURE

Noise studies have been made on single crystal InSb doped with germanium and zinc having resistivities at 77°K between 0·1 and 1000 Ω cm. Slices of crystal revealed that the resistivity was uniform across the slice to better than 5 per cent and that the dislocation density on the ⟨111⟩ axis was less than 1000/cm^2. Filamentary specimens of 10 mm × 1 mm × 0·1 mm were produced by lapping and contacts made by diffusion of 95 per cent indium, 5 per cent lead alloy. Specimens were either mounted on a glass substrate, having the same expansion co-efficient as InSb, using a pressure sensitive silicone adhesive or else hung freely in the refrigerant.

A block diagram of the measuring equipment together with the specimen input circuit is shown in Fig. 1. A constant current source is provided for the filament by a smoothed battery supply and series resistor R. A noise voltage is measured on the inner contacts by amplification with a low-noise transformer and wide-band amplifier. This is followed by a harmonic analyser tunable over the range 20–2×10^4 c/s. The r.m.s. voltage is determined using a thermocouple detector and pen recording voltmeter. As the resistance of InSb filaments in the extrinsic region lies in the range 100–1000 Ω the noise voltage was transformed in order to be greater than the noise of the inputs stage of the wide-band amplifier. Extraneous noise due to voltage fluctuations in the battery supplies and contacts is eliminated by increasing the value of the series resistance R until no further increase in noise if observed. The equipment is calibrated after each noise measurement by injection of a known voltage at the operating frequency across a very low resistance placed in series with the specimen.

3. NOISE POWER SPECTRUM

The typical noise power spectrum of a p-type InSb filament at 77°K, as shown in Fig. 2,

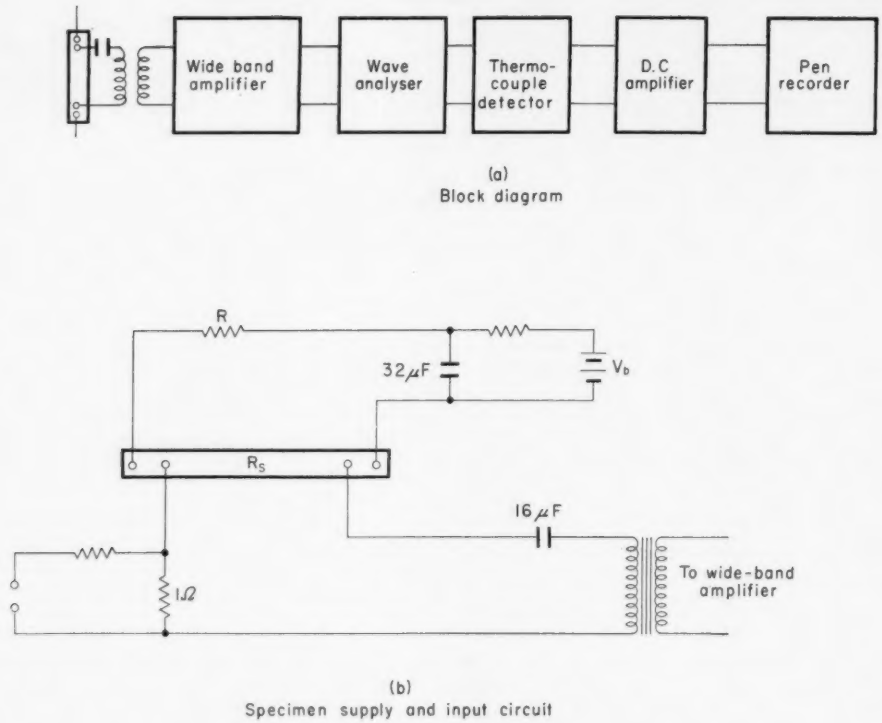

FIG. 1. Apparatus for electrical noise measurement.

consists of two components greater in magnitude than Johnson noise. At low frequencies the noise power is an inverse function of the frequency whilst at higher frequencies it is frequency independent indicative of generation–recombination noise. At still higher frequencies the noise power decreases rapidly with increasing frequency.

Measurements made on a large number of filaments of widely differing resistivities in the region where generation–recombination noise dominates are shown in Fig. 3.

For temperatures below 170°K electron trapping occurs at localized centres in p-type InSb. Determinations of minority and majority carrier lifetimes from the magnitude of the photoconductive and photomagnetic currents and from the decay of photoconductive current indicate that at 77°K the majority carrier lifetime (τ_p) is approximately four orders of magnitude greater than that of the minority carriers and that it is inversely proportional to the extrinsic carrier concentration (p_e) as given by:

$$\tau_p \cdot p_e = 4 \times 10^8 \text{ cm}^{-3} \text{ sec} \qquad (1)$$

a value slightly less than that obtained in other laboratories of $1{\cdot}5 \times 10^9$.[4] Because the hole mobility at 77°K is limited only by lattice scattering the majority carrier lifetime is proportional to the resistivity. The results shown in Fig. 3 are thus consistent with the general form of generation–recombination noise given by:

$$\bar{i}^2 = \alpha e^2 I^2 \frac{\tau_p}{p_e} \cdot \frac{1}{1+\omega^2\tau_p^2}, \qquad (2)$$

where e is the electronic charge, I the bias current, ω the angular frequency and α a constant. The value of α deduced from the results is $1{\cdot}9 \pm 0{\cdot}1$. The variation of noise power with frequency at high frequencies is consistent with a single lifetime whose value is given by equation (1).

Vol. 22
1961

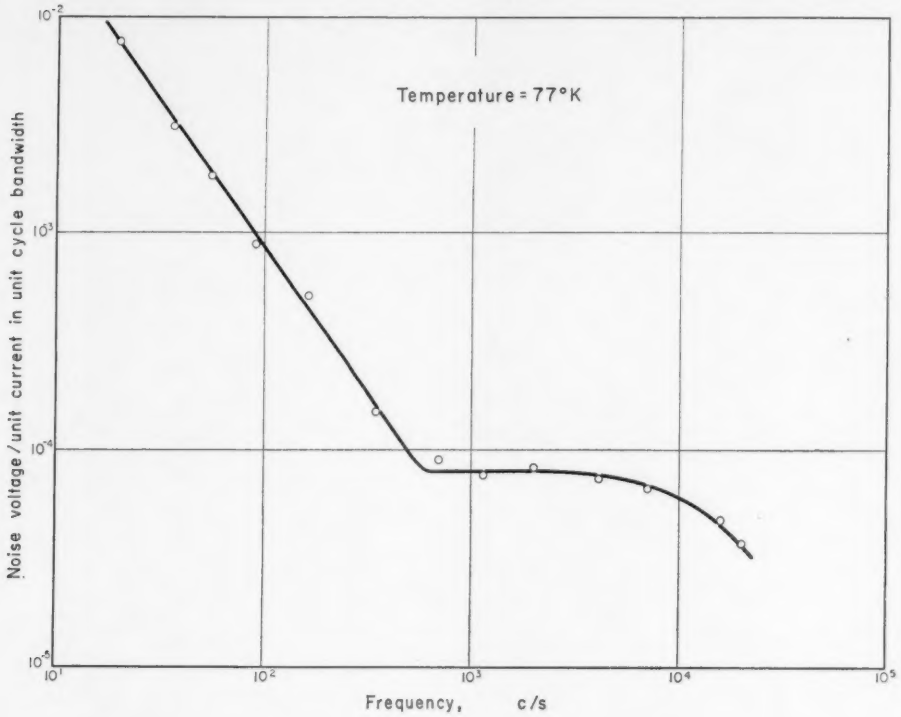

FIG. 2. Noise power spectrum of a p-type InSb filament.

VAN VLIET and BLOK[5] have considered generation–recombination noise associated with trapping processes and have shown that the noise power spectrum can be expressed in the form:

$$S(f) = \frac{4I^2}{N}\left[\frac{\lambda^2\tau_1}{\tau_a}\cdot\frac{\tau_1}{1+\omega^2\tau^2} + \frac{(1-\lambda^2+\alpha)\tau_2}{\tau_a}\cdot\frac{\tau_2}{1+\omega^2\tau_2^2}\right]. \quad (3)$$

Here N is the total number of carriers in the system, τ_1 is the relaxation time corresponding to recombination between traps and the ground state, roughly corresponding to the majority carrier lifetime, τ_2 corresponds to the minority carrier lifetime. τ_a is the apparent lifetime as determined by photoconductive decay, λ is a function of the carrier densities very close to unity and α an excitation function.

For p-type InSb at 77°K τ_2 is lower than 10^{-10} sec as determined by the photomagnetic effect whilst τ_1 is greater than 10^{-6} sec. Hence the results shown in Fig. 3 can be interpreted in terms of the first term in equation (3) assuming that λ is very close to unity, that τ_1 is equal to τ_a both being given by equation (1).

4. FACTORS AFFECTING LOW FREQUENCY NOISE

(a) *Carrier concentration*

The low frequency noise in InSb filaments at 77°K can be expressed in the usual form:

$$i^2 = \frac{AI^2\,df}{f^\alpha}, \quad (4)$$

where A and α are both constants.

Previous measurements of noise in InSb photo-diodes has shown that α is approximately 3

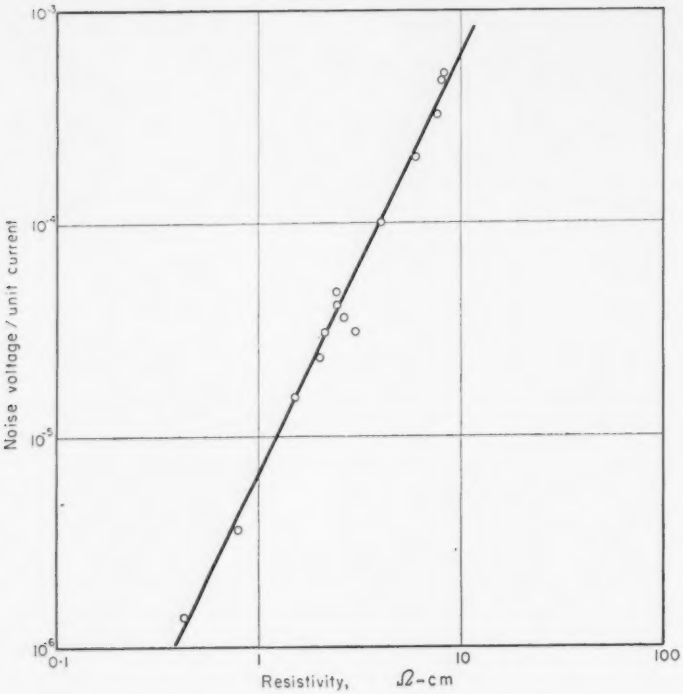

FIG. 3. Variation of g–r noise in InSb at 77°K with resistivity for $\omega\tau < 1$.

when the diode is illuminated with 300°K background radiation but that α decreases on cooling that background; however, these measurements made on filaments show that α is equal to 3 even for backgrounds as low as 77°K.

The variation of noise power with both carrier concentration and temperature has been measured in the extrinsic region. The results given in Fig. 4 show that A is proportional to the square of the resistivity and hence inversely proportional to the square of the extrinsic carrier concentration. The temperature variation of the noise power spectrum also supports this.

(b) *Surface effects*

The magnitude of $1/f$ noise in germanium is dependent on the surface potential.[6] A theory based on surface state relaxation times has been proposed but this can account for $1/f$ noise only. Experiments have been carried out therefore to determine the effect of surface potential on low frequency noise in InSb. Prior to carrying out noise measurements, the effect of surface charge on the conductivity of an InSb filament was investigated. Previous experience has shown that a suitable surface of low surface recombination rate can be produced by electrolytic polishing in either glycol–nitric acid mixtures or in KOH solution; such surfaces tend to have low surface resistances in the region of 10,000 Ω/cm^2. Filaments were prepared therefore having bulk-resistance much greater than that of the surface and a suitable field plate fitted for normal field effect experiments. Measurements have been made both in a suitable vacuum cell and by direct immersion in liquid coolant. D.C. field effect experiments show that the surface normally produced by electrolytic polishing is slightly p-type and that inversion occurs with approximately $1{\cdot}5 \times 10^{-8}$ C of induced charge. From a detailed analysis of the field

Vol. 22
1961

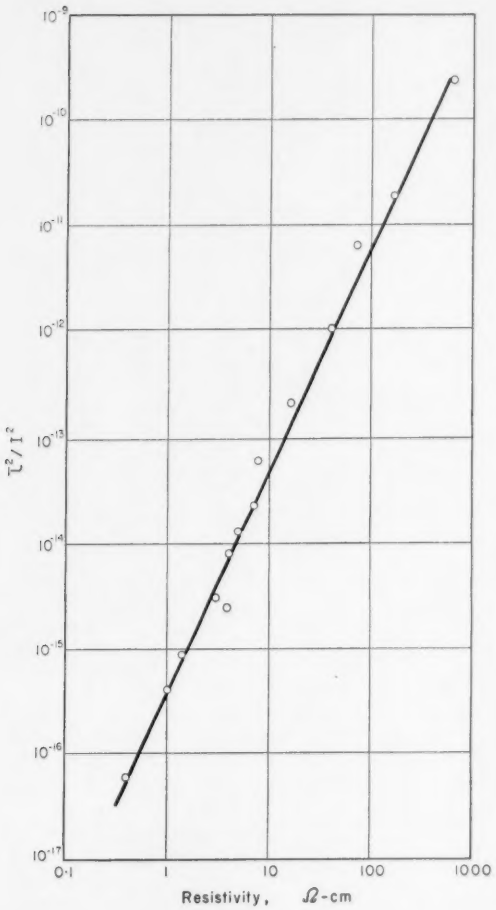

FIG. 4. Variation of noise power at low frequencies with resistivity.

effect, results could be explained in terms of a surface state 0·07 eV above the Fermi level for intrinsic material and of density 2×10^{11} charges/cm^2. Changes in surface potential can be obtained also by chemical treatment. The surface of a freshly etched p-type specimen is normally excess p-type because of the presence of water in the etch. The effect of halide vapour (bromine for example) is to make the surface invert and become excessively n-type. Thus by careful exposure to vapour the surface resistivity can be made as high as 10^7 Ω/cm^2. Measurements of photoconductive decay indicate that the surface recombination velocity at 77°K reaches a maximum value for zero surface potential. Measurements of relaxation time show that the fast states decay with roughly the same time constant as the majority carriers but that the time constant of the slow state is greater than 10^4 sec.

The effect of various surface treatments is shown in Fig. 5, for a specimen of bulk resistivity 500 Ω cm at 77°K. The effect of surface treatment both chemical and electrical is to change both A and α as given in equation (4). The variation of these constants with surface potential is shown in Fig. 6 where the surface potential is expressed in units of kT.

5. DISCUSSION

Previous investigations of noise power spectra of semiconductors may be summarized as follows.[17] The importance of conductivity modulations caused by charged carrier modulations at potential barriers both within the semiconductor and more especially at its surface has been demonstrated. Surface effects are attractive in explaining $1/f$ noise because of the long time constants associated with the surface states; however if queuing theory is incorporated there is no need to account for long relaxation times. However, no theory is at present able to explain power laws as high as 3 as have been obtained here and previously on InSb photo-voltaic devices exposed to ambient radiation and on germanium filaments exposed to CCl_4 vapour.

Queuing theory[8] gives a noise power spectrum for an expotential distribution of lifetime of

$$W(\omega) = \frac{1}{\omega} \cdot \log (1+\omega^2\tau^2), \qquad (5)$$

whilst if the distribution is terminated at a particular time τ

$$W(\omega) = \frac{4A^2}{\omega^2} \log (\gamma\omega\tau), \qquad (6)$$

where A is a constant close to unity and γ is Euler's constant. The dependence of the termination of the distribution on surface potential would account for some variation in the power law but not of the correct magnitude to account for the experimental results.

The variation of noise power magnitude with

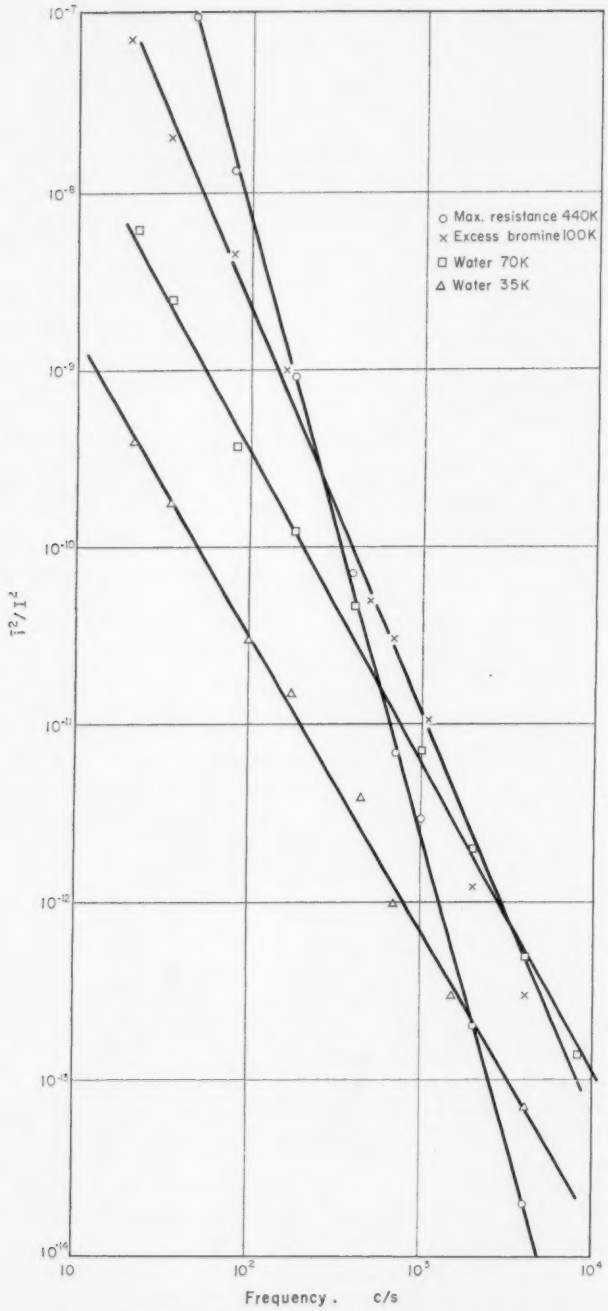

FIG. 5. Effect of surface treatment on the noise power spectrum of high resistivity material.

Vol. 22
1961

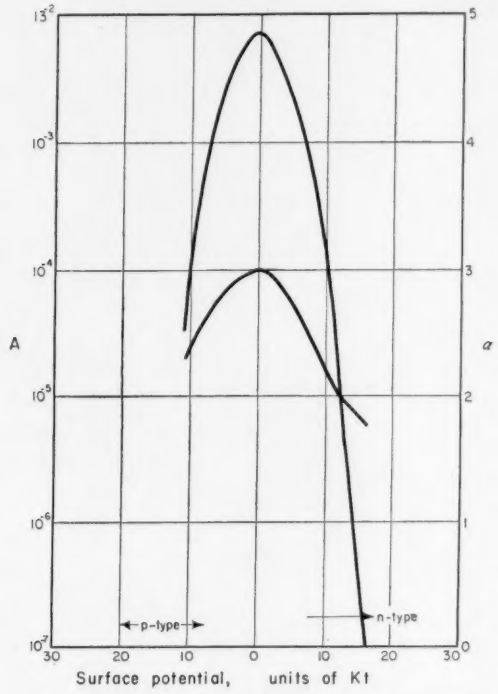

FIG. 6. Variation of A and α [equation (4)] with surface potential.

surface potential is very different from that observed on germanium where an increase in magnitude was observed only in the inversion region.

6. SUMMARY

The effect of minority carrier trapping in p-type on generation–recombination noise has been accounted for. The low frequency noise power spectrum normally obeys a $1/f^3$ law, the magnitude being a function of the majority carrier concentration. The index of the power spectrum depends on the surface potential decreasing rapidly with increase in surface potential of both sign. More detailed experimental work is necessary in order to give a clear understanding of the effects of the surface barrier.

Acknowledgement—The author wishes to acknowledge the assistance of Mr. R. A. BALE in this work. British Crown copyright reserved.

REFERENCES

1. ROLLIN B. V. and TEMPLETON I. M., *Proc. Phys. Soc. Lond.* **B66,** 259 (1953).
2. VAN VLIET K. M., *Proc. Inst. Radio Engrs.* **46,** 1004 (1958).
3. GOODWIN D. W., *J. Sci. Instrum.* **34,** 367 (1957).
4. LAFF R. A. and FAN H. Y., *Phys. Rev.* **121,** 53 (1961).
5. VAN VLIET K. M. and BLOK J., *Physica* **22,** 525 (1956).
6. MACRAE A. U. and LEVINSTEIN H., *Phys. Rev.* **119,** 62 (1960).
7. BROPHY J. J., *Solid-State Physics*, Vol. 1, pt. 1. Academic Press, New York (1960).
8. BELL D. A., *Electrical Noise*. Van Nostrand, New York (1960).

DISCUSSION

K. M. VAN VLIET: Could you comment on the nature of the trapping g–r noise with turnover frequency with about 20 kc/s?

D. W. GOODWIN: This is associated with the fluctuations in majority carriers which at 77°K have lifetimes greater than several microseconds. Minority carriers are trapped in times of the order of 10^{-10} sec and their contribution to the noise would appear to be negligible. The majority carrier lifetime as determined from the relaxing of g–r noise in the region of 20 kc/s agrees with those values obtained by analysis of photoconductive and photoelectromagnetic effects and by photoconductive decay determinations.

R. W. CUNNINGHAM: What is the magnitude of the slow state decay time?

D. W. GOODWIN: Measurements of the slow state decay time indicate that at 77°K it is greater than 10^4 sec.